O,O' CHELATED TITANIUM(IV) COMPLEXES.

A synthetic, kinetic, electrochemical and structural study

ANNEMARIE KUHN

O,O'-CHELATED TITANIUM(IV) COMPLEXES.

A synthetic, kinetic, electrochemical and structural study.

A dissertation submitted in accordance with the requirements of the degree

Philosophiae Doctor

Department of Chemistry
Faculty of Natural and Agricultural Sciences

University of the Free State

Promoter
Dr. J Conradie

ANNEMARIE KUHN

November 2008

I would like to thank all my friends, family and colleagues for their support, friendship and guidance throughout the, sometimes, very trying period of my studies. Special appreciation must be made to the following people:

My promotor, Dr. Jeanet Conradie, for your dedication, enthusiasm and for the many hours and late nights spent running NMR. I especially appreciate your energy in keeping me focused when the road ahead was unclear and in times when there were many other demands distracting me.

Prof. Jannie Swarts and fellow group members for your valuable input and discussions. Your experience and willingness to share knowledge has played a very influential part in my education.

My extraordinary mother and my sister and her family, you have all made many sacrifices and without your support this would not have been possible.

My children, Mia, John, Lawrence and Mikhail, you withstood the hardships with me and we made it. I hope that you all feel the benefit in the future.

My friend, Ronnie, although you only entered our lives near the end, you brought laughter and sunshine. Thank you for your love, support and prayers.

I wish to acknowledge Dr. A.J. Muller for the data collection and refinement of the crystal structures, Katherin Hopmann for the Gaussian calculations, Dr. Jeanet Conradie for the ADF calculation and the NRF and Chemistry Department for their financial support.

Thank you.
Annemarie Kuhn.

CONTENTS

LIST OF ABBREVIATIONS

Ligands

(a) β-Diketones

Hacac	2,4-pentanedione (acetylacetone)
Hba	1-phenyl-1,3-butanedione (benzoylacetone)
Hbfcm	1-ferrocenyl-3-phenyl-1,3-propanedione (benzoylferrocenoylmethane)
Hdbm	1,3-diphenyl-1,3-propanedione (dibenzoylmethane)
Hdpm	2,2,6,6-tetramethyl-3,5-heptanedione (dipivaloylmethane)
Hdfcm	1,3-diferrocenyl-1,3-propanedione (diferrocenoylmethane)
Hfca	1-ferrocenyl-1,3-butanedione (ferrocenoylacetone)
Hfctfa	1-ferrocenyl-4,4,4,-trifluoro-1,3-butanedione (ferrocenoyltrifluoroacetone)
Hhfaa	1,1,1,5,5,5-hexafluoro-2,4-pentanedione (hexafluoroacetylacetone)
Hmaa	1-methoxy-1,3-butanedione (methylacetylacetone)
Hnba	1-phenyl-3-(4-nitrophenyl)-1,3-propanedione (nitrophenoylbenzoylacetone)
Hpvac	5,5-dimethyl-2,3-hexanedione (pivaloylacetone)
Htfaa	1,1,1-trifluoro-2,4-pentanedione (trifluoroacetylacetone)
Htfba	4,4,4-trifluoro-1-(phenyl)-1,3-butanedione (trifluorobenzoylacetone)
Htfdma	1,1,1-trifluoro-5-methyl-2,4-hexanedione (trifluorodimethylacetylacetone)
Htffu	4,4,4-trifluoro-1-(2-furoyl)-1,3-butanedione (trifluorofuroylacetone)
Htfma	1,1,1-trifluoro-2,4-hexanedione (trifluoromethylacetylacetone)
Htfnb	4,4,4-trifluoro-1-(4-nitrophenyl)-1,3-butanedione (trifluoronitrophenoylacetone)
Htfth	4,4,4-trifluoro-1-(2-thenoyl)-1,3-butanedione (trifluorothenoylacetone)
Htftma	1,1,1-trifluoro-5,5-dimethyl-2,4-hexanedione (trifluorotrimethylacetylacetone)
Hthba	1-phenyl-3-(2-thenoyl)-1,3-propanedione (thenoylbenzoylacetone)

*The removal of H in the above abbreviations represents the anion (enolate) of the β-diketone.

(b) Dihydroxy-aryls

H_2binaph	2,2'-dihydroxybinaphthyl; 2,2'-binaphthol; 2,2'-binaphthyldiol	(binaphthol)
H_2biphen	2,2'-dihydroxybiphenyl; 2,2'-biphenol; 2,2'-biphenyldiol	(biphenol)
H_2cat	1,2-dihydroxybenzene; 1,2-benzyldiol	(catechol)
H_2mbinaph	2,2'-dihydroxy-methylene-binaphthyl; 1,1'-methylene-bis(2-naphthol)	(methylenebinaphthol)
H_2mbiphen	2,2'-dihydroxy-methylene-biphenyl; 1,1'-methylene-biphenyldiol	(methylenebiphenol)
H_2naph	2,3-dihydroxynaphthalene; 2,3-naphthyldiol.	(naphthol)

*The removal of 2H in the above abbreviations represents the dianion of the dihydroxy-aryls

(c) General Groups

^{t}Bu	tertiary butyl
bipy	2,2-bipyridine
β	β-diketonato ligand or β-diketone anion (β^-)
cisplatin	*cis*-diamminedichloro-platinum(II)
Cp	cyclopentadienyl ring (η^5-C_5H_5)$^-$
CO	carbonyl
diars	*o*-phenulene-bis(dimethylarsine)
Et	ethyl
Et_3N	triethylammine
Hβ	β-diketone
H_2L	dihydroxy-aryls
H_2G	glycols
H_2mal*	malonic (malonoic) acid; mal = malonoato ligand
H_2mal*	maltol; mal = maltolato ligand
L	bidentate ligand or dihydroxy-aryl dianion (L^{2-})
LDA	lithium diisopropylamide
Me	methyl
Me_2dtc	NN'-dimethyl-dithiocarbamate
OR	alkoxide
OPh	phenoxide
ox	oxiquine ($C_{10}H_7ON$)
Ph	phenyl (C_6H_5)
^{i}Pr	isopropyl
ROH	linear alcohols

*The same abbreviation used for different compounds in different journal articles.

Solvents

acetone-d_6	deuterated acetone (CD_3COCD_3)
chloroform-*d*	deuterated chloroform ($CDCl_3$)
DCE	dichloroethane ($C_2H_4Cl_2$)
DCM	dichloromethane (CH_2Cl_2)
DCM-d_2	deuterated dichloromethane (CD_2Cl_2)
DMF	dimethylformamide (C_3H_7ON)
DMSO	dimethylsulfoxide (C_2H_6OS)
EtOH	ethanol (C_2H_5OH)
MeOH	methanol (CH_3OH)
THF	tetrahydrofuran (C_4H_4O)

Other

α, β, γ	unit cell angles
a, b, c	unit cell lengths
Φ	centroid; centre of gravity of Cp ring, also represented by • in 
ε	dielectric constant
ω	dihedral angle between ligand and O-Ti-O plane
χ_R	group electronegativity (Gordy scale) of R group
DFT	Density Functional Theory
HOMO	highest occupied molecular orbital
IR	infrared spectroscopy
LUMO	lowest unoccupied molecular orbital
M	central metal atom
M.p.	melting point
pK_a	-log $[H^+]$, K_a = acid dissociation constant
RT	room temperature
T	temperature
ν_{CO}	infrared carbonyl stretching frequency
Δ	change in
NMR	nuclear magnetic resonance
^{1}H NMR	proton nuclear magnetic resonance spectroscopy
^{19}F NMR	fluorine nuclear magnetic resonance spectroscopy
δ	chemical shift
ppm	parts per million

Reaction Kinetics

A	absorbance
[A]	complex A or concentration of A
ε	molar extinction coefficient
E_a	energy of activation
$\Delta G^{\#}$	free energy of activation
$\Delta H^{\#}$	enthalpy of activation
k	general rate constant
k_2	second-order rate constant
K_c	equilibrium constant
k_{obs}	observed rate constant
$k_{(A)obs}$, $k_{(B)obs}$	observed rate constant for reaction A and B.
k_s	rate constant of solvation
l	path length in UV/vis spectroscopy

λ_{exp}	experimental wavelength
λ_{max}	wavelength at maximum absorbance
solv	solvent
$\Delta S^{\#}$	entropy of activation
UV/vis	ultraviolet/visible spectroscopy
$\Delta V^{\#}$	volume of activation
X	leaving ligand
Y	incoming ligand

Cyclic voltammetry

CV	cyclic voltammetry/cyclic voltammogram
E	applied potential
$E^{0'}$	formal reduction potential
E_{pa}	anodic peak potential
E_{pc}	cathodic peak potential
ΔE_p	separation of anodic and cathodic peak potentials
Fc	ferrocene or ferrocenyl
Fc^+	ferrocenium
i_{pa}	anodic peak current
i_{pc}	cathodic peak current
i_{fwd}	peak current of forward scan
i_{rev}	peak current of reverse scan
$TBAPF_6$	tetrabutylammonium hexafluorophosphate $[NBu_4][PF_6]$ or $[NBu_4]^+[PF_6]^-$
NHE (SHE)	normal (standard) hydrogen electrode
SCE	saturated calomel electrode
v	scan rate

Constants

F	Faraday Constant	$= 9.6487 \times 10^4$ C mol^{-1}
h	Planck's Constant	$= 6.6256 \times 10^{-34}$ J s
k_B	Boltzmann Constant	$= 1.3805 \times 10^{-23}$ J K^{-1}
R	Gas Constant	$= 8.134$ J K^{-1} mol^{-1}

LIST OF LIGANDS AND COMPLEXES

	O,O'-Ligands		Tetrahedral Complexes	Octahedral Complexes	
	β-Diketones		$[Cp_2Ti(\beta)]^+$	$Ti(\beta)_2Cl_2$	$Ti(\beta)_2$biphen
CF_3COCH_2COR	Hβ	R			
Series 1	Htfaa	CH_3	$[Cp_2Ti(tfaa)]^+$ [3][i]	$Ti(tfaa)_2Cl_2$ [13]	$Ti(tfaa)_2$biphen [24]
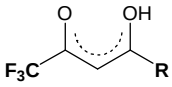	Hhfaa	CF_3	--	$Ti(hfaa)_2Cl_2$ [14]	$Ti(hfaa)_2$biphen [25]
	Htfth	C_4H_3S	$[Cp_2Ti(tfth)]^+$ [4]	$Ti(tfth)_2Cl_2$ [15]	$Ti(tfth)_2$biphen [26]
	Htffu	C_4H_3O	$[Cp_2Ti(tffu)]^+$ [5]	$Ti(tffu)_2Cl_2$ [16]	$Ti(tffu)_2$biphen [27]
	Htfba	Ph	$[Cp_2Ti(tfba)]^+$ [6]	$Ti(tfba)_2Cl_2$ [17]	$Ti(tfba)_2$biphen [28]
Series 2	Htfaa	CH_3	--	$Ti(tfaa)_2Cl_2$ [13]	$Ti(tfaa)_2$biphen [24]
	Htfma	$CH_2(CH_3)$	--	$Ti(tfma)_2Cl_2$ [18]	$Ti(tfma)_2$biphen [29]
	Htfdma	$CH(CH_3)_2$	--	$Ti(tfdma)_2Cl_2$ [19]	$Ti(tfdma)_2$biphen [30]
	Htftma	$C(CH_3)_3$	--	$Ti(tftma)_2Cl_2$ [20]	$Ti(tftma)_2$biphen [31]
$PhCOCH_2COR$	Hba	CH_3	$[Cp_2Ti(ba)]^+$ [7][ii]	$Ti(ba)_2Cl_2$ [21][iii]	$Ti(ba)_2$biphen [32]
	Htfba	CF_3	$[Cp_2Ti(tfba)]^+$ [6]	$Ti(tfba)_2Cl_2$ [17]	$Ti(tfba)_2$biphen [28]
	Hthba	C_4H_3S	$[Cp_2Ti(thba)]^+$ [8]	--	--
	Hdbm	Ph	$[Cp_2Ti(dbm)]^+$ [9][ii]	$Ti(dbm)_2Cl_2$ [22][iii]	$Ti(dbm)_2$biphen [33]
	Hnba [2][v]	$PhNO_2$	--	--	--
CH_3COCH_2COR	Hacac	CH_3	$[Cp_2Ti(acac)]^+$ [10][ii]	$Ti(acac)_2Cl_2$ [23][vi]	$Ti(acac)_2$biphen [36]
	Hmaa	OCH_3	$[Cp_2Ti(maa)]^+$ [11][i]	--	--
	Dihydroxy-aryls H_2L		**$Cp_2Ti(L)$**	**$Ti(acac)_2L$**	
	H_2cat	$H_2L^{5,1}$	--	$Ti(acac)_2$cat [34]	
	H_2naph	$H_2L^{5,2}$	--	$Ti(acac)_2$naph [35]	
	H_2biphen	$H_2L^{7,1}$	Cp_2Ti(biphen)[vii]	$Ti(acac)_2$biphen [36]	
	H_2binaph	$H_2L^{7,2}$	--	$Ti(acac)_2$binaph [37][viii]	
	H_2mbiphen	$H_2L^{8,1}$	--	$Ti(acac)_2$mbiphen [38]	
	H_2mbinaph	$H_2L^{8,2}$	--	acac: $Ti(acac)_2$mbinaph [39][ix]	
				tfaa: $Ti(tfaa)_2$mbinaph [40]	
				hfaa: $Ti(hfaa)_2$mbinaph [41]	

*red = synthesis of new compounds

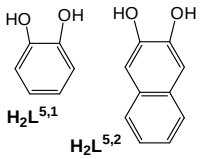

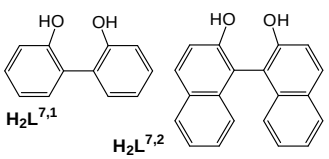

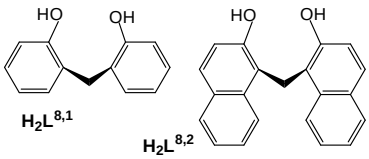

[i] E. Erasmus, J. Conradie, A. Muller and J.C. Swarts, *Inorg. Chim. Acta*, **360** (2006) 2277.
[ii] G. Doyle and R.S. Tobias, *Ionrg. Chem*., **6** (1967) 1111.
[iii] N. Serpone and R.C. Fay, *Inorg. Chem*., **6** (1967) 1836.
[iv] M.M. Conradie, A.J. Muller and J. Conradie, *S. Afr. J. Chem*., **61** (2008) 13.
[v] V. Bertolasi, P. Gilli, V. Ferretti and G. Gilli, *J. Am. Chem. Soc*., **113** (1991) 4917.
[vi] R.C. Fay and R.N. Lowry, *Inorg. Chem*., **6** (1967) 1512.
[vii] K. Andrä, *J Organmetal. Chem*., **11** (1968) 567.
[viii] S.N. Brown, E.T. Chu, M.W. Hull and B.C. Noll, *J. Am. Chem. Soc*., **127** (2005) 16010.
[ix] P.V. Rao, C.P. Rao, E.K. Wegelius, E. Kolehmainen and K. Rissanen, *J. Chem. Soc., Dalton Trans*., (1999) 4469.

LIST OF STRUCTURES

β-Diketones: Hβ

Hthba

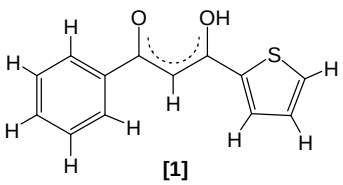

[1]

Hnba

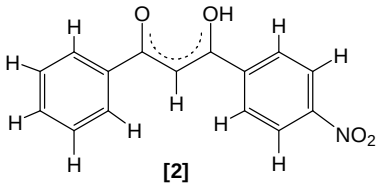

[2]

Mono(β-diketonato) Ti(IV) Complexes: $[Cp_2Ti(\beta)]^+$

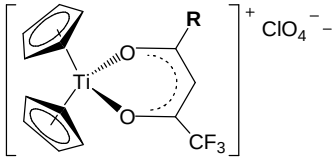

R = tfaa

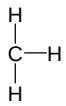

[3]

tfth

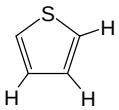

[4]

tffu

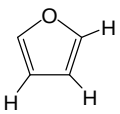

[5]

tfba

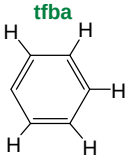

[6]

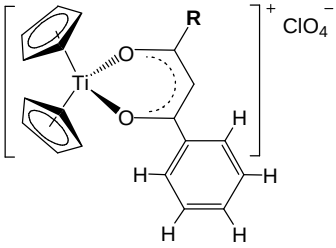

R = ba

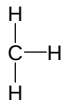

[7]

tfba

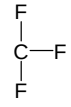

[6]

thba

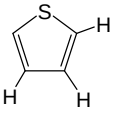

[8]

dbm

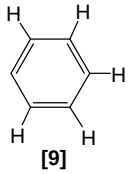

[9]

acac

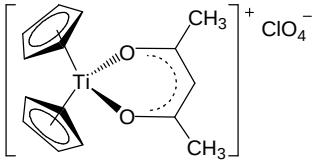

[10]

maa

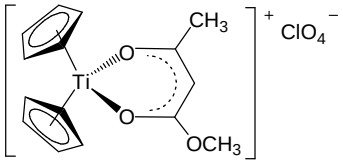

[11]

Mono(aryl-diolato) Ti(IV) Complexes: $Cp_2Ti(biphen)$

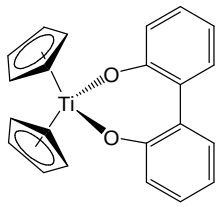

[12]

Bis(β-diketonato)-dichloro Ti(IV) Complexes: $Ti(\beta)_2Cl_2$

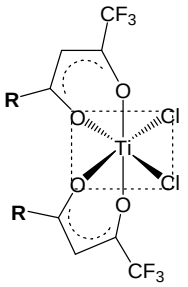

tfaa **hfaa** **tfth** **tffu** **tfba**

R =

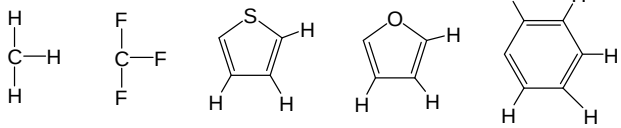

[13] **[14]** **[15]** **[16]** **[17]**

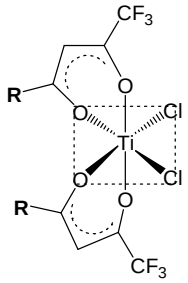

tfaa **tfma** **tfdma** **tftma**

R =

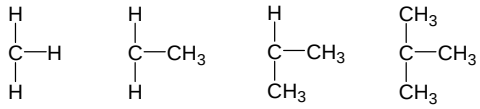

[13] **[18]** **[19]** **[20]**

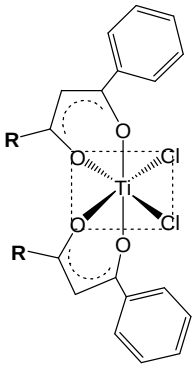

ba **tfba** **dbm** **acac**

R =

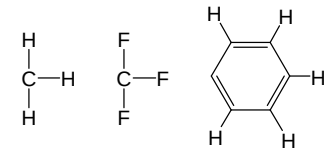

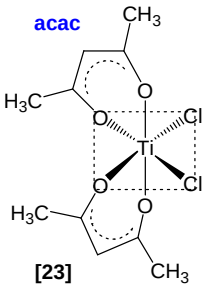

[21] **[17]** **[22]** **[23]**

Bis(β-diketonato)-(biphenolato) Ti(IV) Complexes: $Ti(\beta)_2$biphen

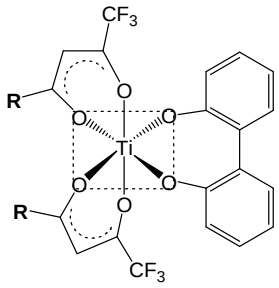

R = tfaa hfaa tfth tffu tfba

[24] [25] [26] [27] [28]

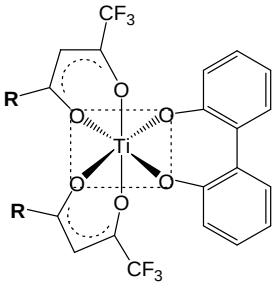

R = tfaa tfma tfdma tftma

[24] [29] [30] [31]

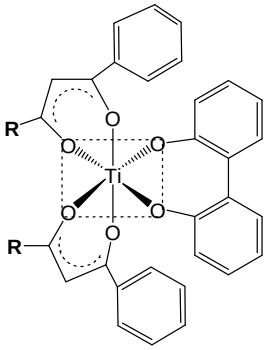

R = ba tfba dbm

[32] [28] [33]

Bis(β-diketonato)-(methylene-dinaphtholato) Ti(IV) Complexes: $Ti(\beta)_2$(mbinaph)

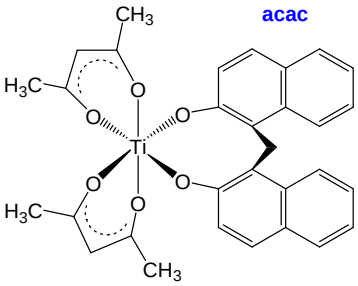

acac

[39]

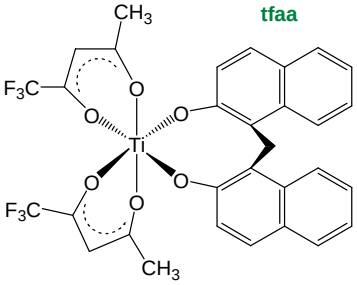

tfaa

[40]

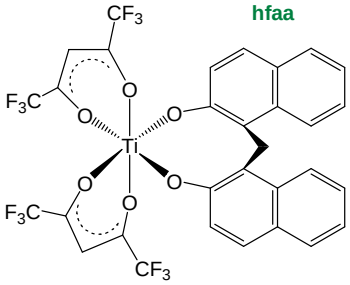

hfaa

[41]

Bis(acetylacetone)-(aryl-diolato) Ti(IV) Complexes: $Ti(acac)_2L$

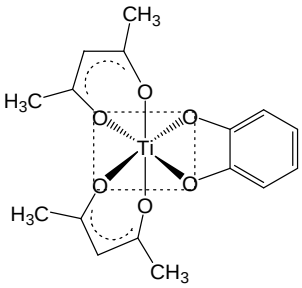

[34]

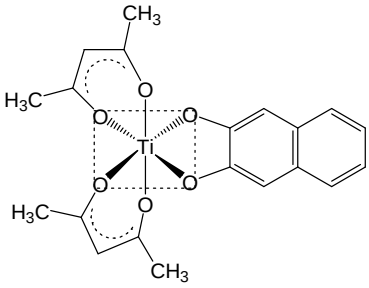

[35]

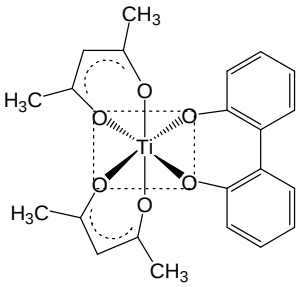

[36]

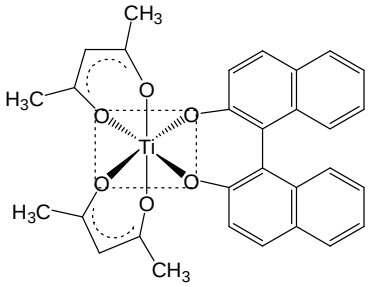

[37]

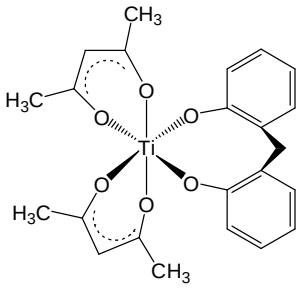

[38]

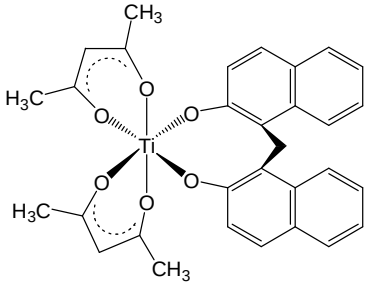

[39]

Dimeric Structures: $\{Ti(\beta)_2Cl\}_2(\mu\text{-}O)$

tfaa

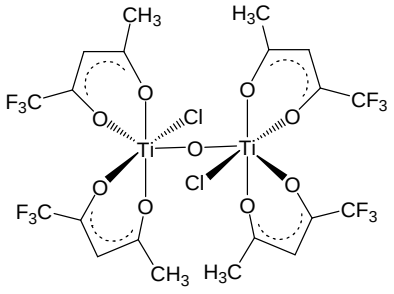

[42]

hfaa

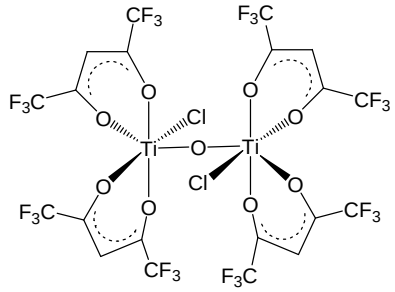

[43]

Dimeric Structure: $\{Ti(\beta)_2\}_2(\mu\text{-}O)(\mu\text{-biphen})$

hfaa

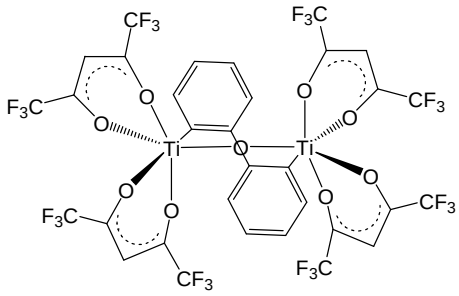

[44]

Tetrameric Structure: $[\,Ti(\beta)_2(\mu\text{-}O)\,]_4$

hfaa

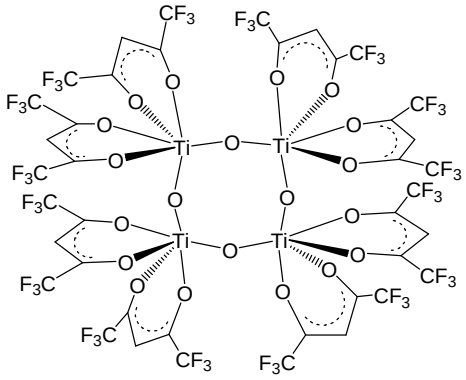

[45]

LIST OF MOLECULAR MASSES

LIGAND		Tetrahedral Complexes	Octahedral Complexes	
(β)	Hβ	$[Cp_2Ti\beta]^+ClO_4^-$	$Ti(\beta)_2Cl_2$	$Ti(\beta)_2$biphen
tfaa	154.10	430.62	424.95	538.24
hfaa	208.06	484.59	532.89	646.08
tfth	222.18	498.72	561.15	674.44
tffu	206.12	482.65	529.01	642.30
tfba	216.20	492.69	549.09	662.38
tfaa	154.10	--	424.95	538.24
tfma	168.13	--	453.01	566.30
tfdma	182.16	--	481.07	594.36
tftma	196.19	--	510.13	623.42
ba	162.19	438.72	441.16	555.25
tfba	216.20	492.69	549.09	662.38
thba	230.30	506.82	--	--
dbm	224.27	500.79	565.30	671.29
nba	253.07	--	--	--
acac	100.13	376.65	317.02	431.11
maa	116.13	392.65	--	--
(L)	H_2L	$Cp_2Ti(L)$	$Ti(acac)_2L$	
cat	110.11	--	354.21	
naph	160.18	--	404.28	
biphen	186.21	362.27	430.31	
binaph	286.33	--	530.43	
mbiphen	200.24	--	444.34	
mbinaph	300.36	--	acac:	544.46
			tfaa:	652.40
			hfaa:	760.34

LIST OF PUBLICATIONS

Methyl 4-{[(1Z)-1-benzoyl-3-oxo-3-phenyl-prop-1-en-1-yl]amino}benzoate.
M. Conradie, A. Kuhn, A. Muller and J. Conradie, *Acta Cryst*., E**62** (2006) o4717.

μ-2,2'-Biphenolato-κ_2*O*:*O*'-μ-oxido-κ_2*O*:*O*-bis[bis(hexafluoroacetylacetonato-κ_2*O*:*O*') titanium(IV)]. A. Kuhn, A. Muller and J. Conradie, *Acta Cryst*., E**63** (2007) m664.

Substitution kinetics of biphenol at dichlorobis(acetylacetonato-*O,O'*)titanium(IV): Isolation, Characterization, Crystal Structure and Enhanced Hydrolytic Stability of the Product bis(acetylacetonato-*O,O*')(biphenyldiolato-*O,O*')titanium(IV). T.A. Tsotetsi, A. Kuhn, A. Muller and J. Conradie, *Polyhedron*, **28** (2009) 209.

Isomer Distribution and Structure of (2,2'-biphenyldiolato)bis(β-diketonato)titanium(IV) Complexes: a Single Crystal X-ray, Solution NMR and Computational Study. A. Kuhn, T.A. Tsotetsi, A. Muller and J. Conradie, *Inorg. Chim. Acta*., **362** (2009) 3088.

Syntheses, crystal structure and theoretical modelling of tetrahedral mono-β-diketonato titanocenyl complexes. A. Kuhn, A. Muller and J. Conradie, *Polyhedron*, **28** (2009) 966.

1 Introduction

1.1 BACKGROUND

Complexes of titanium(IV) metal are widely studied for a variety of purposes, but mainly serving as catalysts in different organic reaction[1] and in medical applications in anti-cancer therapy.[2] One feature common to most titanium(IV) complexes is their hydrolytic instability, due to their d^0 configuration and thus highly oxophilic nature. Known ligands for titanium(IV) include numerous cyclopentadienyl (Cp) systems, as well as nitrogen- and oxygen-based compounds.

The use of titanium in the development of catalysts was born with the German chemist, Karl Ziegler's accidental discovery in 1953 that $TiCl_3$ and $AlEt_3$ combined together produced an extremely active heterogeneous catalyst for the polymerization of ethylene at atmospheric pressure. Karl Ziegler and Giulio Natta were both awarded the Nobel Prize in chemistry in 1963 for the discovery of this titanium based catalyst (now known as the Ziegler-Natta catalysts) and for its use to produce stereoregular polymers.

Recently, catalysts derived from high oxidation state titanium in combination with oxygen-containing ligands, have become a very important and diverse class of catalytic systems. The development of asymmetric catalysts involving chiral titanates is built upon the initial success of the Sharpless-Katsuki asymmetric epoxidation catalyst,[3] Ti_2(dialkyl tartrate)$_2$(O^iPr)$_4$ (**1**) followed by other chiral catalysts applied in asymmetric alkylation,[4] aldol condensation,[5] Diels-Alder,[6] and glyoxylate ene [7]and related electrocyclic reactions.[8]

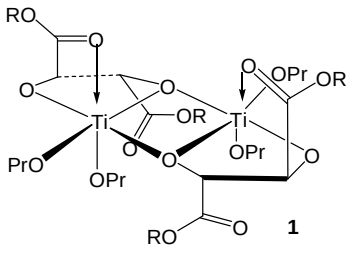

1

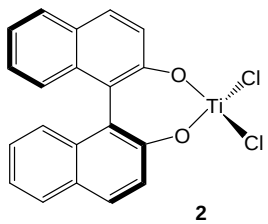

2

A very successful series of enantioselective catalysts, based on the bent metallocene template and C_2-symmetric binaphtholate ligands (BINOL), are widely employed (**2**).[9] Although BINOL was first synthesised in 1926,[10] its potential as a ligand for metal-mediated catalysis was first recognised in 1979 by Noyori in the reduction of aromatic ketones and aldehydes.[11] The key to the tremendous catalytic activity of titanium(IV) catalysts, is its high Lewis acidity or electron deficiency (which can be easily tuned by variations on the electronic properties of the ligands) coupled with designed coordinative unsaturation (which often obviates the need for ligand labialisation). Titanium is used extensively because the catalysts are easily generated in situ and the starting materials are commercially available and relatively inexpensive.

The second area of titanium research, focusing on the medical application to anti-cancer therapy, was initiated after the discovery of the tumour-inhibiting properties of cisplatin (**3**)[12] and its routine use as a leading cytostatic drug since 1979.[13] This was followed by the development of new antitumour metal agents including non-platinum metal complexes.[14] Among these, two monomeric titanium(IV) complexes have qualified for clinical trials: titanocene dichloride $[Cp_2Ti^{IV}Cl_2]$ (**4**)[15] and budotitane, $[Ti^{IV}(ba)_2(OEt)_2]$[16] (**5**), belonging to the bis(β-diketonato) metal complexes.

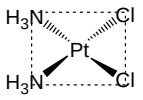

3

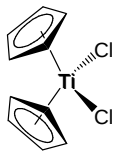

4

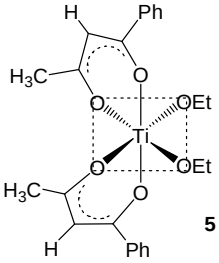

5

The mode of action of the Ti(IV) anticancer compounds is still poorly understood. A DNA interchelating mechanism has been proposed, in which the diaqua-complex, formed after elimination of the two X-ligands, binds to DNA.[17] Given the oxophilic nature of Ti(IV), it is possible that the hydrolysed species interact with the phosphate backbone of DNA. A specific Ti^{IV}-protein complex, formed by the binding of Ti^{IV} to the Fe^{III} binding sites of human serum transferrin, has been characterised, indicating a potential relevance to the anticancer activity of budotitane and titanocene.[18]

Many drawbacks are associated with current cancer therapies and many potentially useful antineoplastic materials suffer from negative side effects which limit or exclude their use in

clinical chemotherapy. Hydrolytic stability and toxicity are probably the most important of these factors. Current chemotherapeutic agents are unable to distinguish between cancer cell and healthy cells,[19] therefore, the development of antineoplastic materials with highly selective absorption by cancerous cells would be greatly advantageous. Also, by developing antineoplastic compounds with high aqueous solubility and stability, the body's own circulatory system (blood) can be used to distribute the drug within the patient.[20]

Since the exact parameters important for understanding anticancer activity are not yet clear, a group of compounds, modelled on the four-coordinate, tetrahedrally configurated titanocene and six-coordinate, octahedrally configurated budotitane have been prepared for this study. The systematic modification of these compounds was performed according to broad guidelines. Metals are known to possess a range of activities that can be influenced by ligand properties, for example, ligands regulate reactions occurring in the coordination sphere of a metal ion. Studies on sol-gel systems involving metal alkoxides, have shown that the rate of hydrolysis can be significantly reduced by the presence of bulky or chelating ligands. Hence, two families of *O,O'*-bidentate ligands were selected; the one-electron donor β-diketones and the two-electron donor dihydroxy-aryls. Although the subsequent compounds have not yet undergone cytotoxicity studies, important chemical properties have been characterised. A better understanding of these attributes may provide insight into antineoplastic properties and mechanisms. The results of this study are reported, both for their intrinsic interest and for their possible relevance to drug design.

Synthesising a compound with anticancer activity, which is able to overcome the present problems, would indeed be a giant leap forward in the continued battle against cancer. I hope I have made a small step.

1.2 AIMS OF THE STUDY

With this background, the following goals were set for this study:

1. Syntheses and characterisation of novel (and known) complexes containing titanium(IV) centre coordinated to oxygen donor bidentate ligands, with single (β^-) and/or double charge

(L^{2-}). These complexes have a four-coordinate, tetrahedral sphere, of the form $[Cp_2Ti(\beta)]^+$ and $[Cp_2Ti(L)]$ and a six-coordinate, octahedral sphere, of the form $[Ti(\beta)_2Cl_2]$ and $[Ti(\beta)_2L]$. A series of fluorinated β-diketones was selected.

2. Evaluation of the solution phase properties and isomer distribution of the six-coordinate, octahedrally configurated bis(β-diketonato) complexes, using variable temperature ^1H, ^{19}F NMR and computational studies.

3. Determination of the molecular structure and spatial arrangement of complexes of both tetrahedral and octahedral geometry, using single crystal X-ray crystallography and computational studies. Monomers, dimers and tetramers were analysed.

4. Assessment of the hydrolytic stability of the synthesised titanium(IV) complexes.

5. Kinetic studies determining the rate and mechanism for the:
(a) substitution of monodentate chlorine with bidentate biphenol ligands in $[Ti(\beta)_2Cl_2]$ complexes.
(b) consecutive substitution of the two bidentate β-diketonato ligands with Hacac, another β-diketonato ligand, in $[Ti(\beta)_2biphen]$ complexes.
(c) substitution of the bidentate biphenolato ligand in $[Ti(acac)_2biphen]$ with other bidentate dihydroxy-aryl ligands of different ring sizes.
(d) exchange of β-diketonato ligands between $[Ti(\beta^1)_2biphen]$ and $[Ti(\beta^2)_2biphen]$ complexes.
The reaction kinetics is monitored by means of ^1H NMR and/or UV/vis spectrophotometric techniques.

6. Electrochemical characterisation of the ligands and synthesised complexes using cyclic voltammetry. The formal reduction potential ($E^{0'}$) as well as the electrochemical and chemical reversibility/irreversibility will be evaluated for the redox active titanium(IV) centre. The effects of the electron donation/withdrawal by the substituent groups of the β-diketones will be highlighted.

7. The holistic evaluation to determine if relationships exist between physical quantities such as rate constants, reduction potentials, pK_a-values, group electronegativities, IR stretching frequencies, NMR data and molecular structure.

[1] (a) Y. Qian, J Huang, M.D. Bala, B. Lian, H. Zhang and H.Zhang, *Chem. Rev*., **103** (2003) 2633. (b) R. Beckhause and C Santamaria, *J. Organomet. Chem*., **617** (2001) 81. (c) E. Manek, D. Hinz and G. Meyer, *Coord. Chem. Rev*., **164** (1997) 5. (d) J.C. Vites and M.M. Lynam, *Coord. Chem. Rev*., **146** (1995) 1. (e) J.C. Vites and M.M. Lynam, *Coord. Chem. Rev*., **138** (1995) 71. (f) R.O. Duthaler and A. Hafner, *Chem. Rev*., **92** (1992) 807.
[2] E. Meléndez, *Crit Rev. Oncol. Hematol*., **42** (2002) 309.
[3] K.B. Sharpless, S.S. Woodward and M.G. Finn, *Pure Appl. Chem*., **55** (1983) 1823.
[4] (a) A. Aoki, K. Mikami, M. Terada and T. Nakai, *Tetrahedron* **49** (1993) 1783. (b) D. Seebach, D.A. Plattner, A.K. Beck, Y.M. Wang, D. Hunziker and W. Petter, *Helv. Chim. Acta*, **75** (1992) 2171.
[5] K. Mikami and S. Matusukawa, *J. Am. Chem. Soc*., **115** (1993) 7039.
[6] (a) K. Mikami, M. Terada, Y. Motoyama and N. Nakai, *Tetrahedron Asymm*., **2** (1991) 643. (b) K. Narasaka, M. Saitou and N. Iwasawa, *Tetrahedron Asymm*., **2** (1991) 1305. (c) K. Narasaka, *Pure Appl. Chem*. **64** (1992) 889.
[7] K. Mikami, M. Kaneko and T. Yajima, *Tetrahedron Lett*., **34** (1993) 4841.
[8] T.A. Engler, J.P. Reddy, K.D. Combrink and D.V. Vander Velde, *J. Org. Chem*., **55** (1990) 1248.
[9] (a) J. Balsells, T.J. Davis, P. Carroll and P.J. Walsh, *J. Am. Chem. Soc*., **124** (2002) 10336. (b) A. van der Linden, C.J. Schaverien, N. Meijboom, C. Ganter and A.G. Orpen, *J.Am. Chem. Soc*., **117** (1995) 3008. (c) T.J. Boyle, N.W. Eilerts, J.A. Heppert and F. Takusagawa, *Organometal*., **13** (1994) 2218. (d) K. Narasaka, *Synthesis* **1** (1991) 1. (e) K. Mikami and M. Shimizu, *Chem Rev*., **92** (1992) 1021.
[10] R. Pummerer, E. Prell and A. Rieche, *Chem. Ber*., **59** (1926**)** 2159.
[11] R. Noyori, I. Tomino and Y. Tanimoto, *J. Am. Chem. Soc*., **101** (1979) 3129.
[12] B. Rosenberg, L. VanCamp, J.E. Trosko and V.H. Mansour, *Nature*, **222** (1969) 385.
[13] (a) B. Lippert (Ed.), *Cisplatin: Chemistry and Biochemistry of a Leading Anticancer Drug*, Wiley-VCH, Weinheim (1999). (b) S.E. Sherman and S.J. Lippard, *Chem Rev*., **87** (1987) 1153. (c) J. Reedijk, *Chem. Commun*. (1996) 801.
[14] B.K. Keppler and E.A. Vogel in: H.M. Pinedo, J.H. Schornagel (Eds.), *Platinum and Other Coordination Compounds in Cancer Chemotherapy 2*, Plenum Press, New York, (1996) pp 253-268. (b) B.K. Keppler (Ed.), *Metal Complexes in Cancer Therapy*, VCH, Weinheim (1993) pp 297-323.
[15] P. Köpf-Maier, *Eur. J. Clin. Pharmacol*., **47** (1994) 1.
[16] B.K. Keppler, C. Friesen, H.G. Moritz, H.Vongerichten and E. Vogel, *Struct. Bonding*, **78** (1991) 97.
[17] (a) B.K. Keppler and M Hartmann, *Metal Based Drugs*, **1** (1994) 145. (b) M. Guo, H. Sun, H.J. McArdle, L.Gambling and P.J. Sadler, *Biochemisty*, **39** (2000) 10023. (c) M.M. Harding and G. Mokdsi, *Curr. Med. Chem.*, **7** (2000) 1289.
[18] H. Sun, H. Li, R.A. Weir and P.J. Sadler, *Angew. Chem. Int. Ed.*, **37** (1998) 1577.
[19] R. Duncan and J. Kopecek, *Adv. Polym. Sci*., **57** (1984) 51.
[20] J.C. Swarts, *Macromol. Symp*., **186** (2002) 123.

2 Literature Review and Fundamental Aspects

As this research program describes the preparation, characterisation and properties of oxygen chelated titanium(IV) complexes of both tetrahedral and octahedral coordination, the literature of typical titanium(IV) chemistry and associated ligands is reviewed. Topics related to the kinetics, electrochemistry and crystallography (molecular structure) of the above compounds are also examined. This review starts with a brief introduction to titanium.

2.1 TITANIUM

Titanium is widely distributed in stars, meteorites and on earth; the average titanium content of the earth's crust is 0.63 % by weight, which makes it the ninth most abundant element in the earth's crust, 20 times more abundant than carbon and only outranked by oxygen, silicon, aluminium, iron, magnesium, calcium, sodium and potassium.[1] The principal ores are ilmenite ($FeTiO_3$) and rutile (TiO_2) while other minerals are titanomagnetite [$Fe_3O_4(Ti)$], titanite ($CaTiSiO_5$), benitoite [$BaTi(Si_3O_9)$], warwickite [$(Mg,Fe)_3TiB_2O_8$], osbornite (TiN) and perovskite ($CaTiO_3$). Crystallographic details for all these are known.

Titanium was discovered in 1791 by an English amateur chemist, William Gregor, who identified it in a black sand sample (now known to be ilmenite). Four year later, the famous German chemist, Klaproth, rediscovered the element in the ore rutile, one form of titanium dioxide. He gave it the name titanium after the Titans who in Greek mythology were the sons of Earth. The element was first obtained pure in 1910 by Hunter[2] *via* reduction of titanium tetrachloride with sodium. In 1925, van Arkel and de Boer[3] obtained a very pure form of the metal by dissociation of the tetraiodide. Nonetheless, the titanium metal industry really dates from the publication of the Kroll process[4] in 1940, which involves the reduction of the tetrachloride with magnesium. Titanium has important industrial uses because of its rare combination of properties; low density (less dense than iron), strength (much stronger than aluminium) and resistance to corrosion (almost as corrosion resistant as platinum).[1]

Titanium is a member of the 3*d* transition series, with four valence electrons and electronic configuration, $3d^2 4s^2$. The most stable and important oxidation state is Ti(IV), achieved with the loss of all four valence electrons. The energy required for the removal of the four valence electrons of is so high (91.10 eV) that the Ti^{IV} ion does not exist as such; titanium(IV) compounds are, in general, covalent. Compounds of titanium, in less stable oxidation states, Ti(III) and Ti(II), are also well documented, while examples of Ti(I), Ti(0), Ti(-I) and Ti(-II) are limited and unstable to oxidation.[5] Even though there is a wide range in coordination numbers and coordination geometries, as seen in the examples listed in **Table 2.1**, the most important and prevalent stereo-chemistries in titanium compounds are four and six coordinated, with ligands arranged in tetrahedral and octahedral geometries, respectively.

Table 2.1 The three most common oxidation states of titanium together with the corresponding coordination numbers and principal ligand arrangements (some of which are irregular or distorted) of the titanium complexes.[1] The most important geometries are shown in bold. The *d* electron configurations are also given. See list of abbreviations.

Oxidation State	Coordination number	Geometry*	Examples
Ti^{IV} d^0	**4**	**tetrahedral**	$TiCl_4$, Cp_2TiCl_2, $[Cp_2Ti(acac)]^+$
	5	trigonal bipyramidal	$TiCl_5^-$, $K_2Ti_2O_5$
	5	square pyramidal	TiO(porphyrin)
	6	**octahedral**	$Ti(acac)_2Cl_2$, $[TiF_6]^{2-}$
	7	ZrF_7^{3-} type	$[Ti(O_2)F_5]^{3-}$
	7	pentagonal bipyramidal	$Ti(Me_2dtc)_3Cl$
	8	dodecahedral	Ti $(diars)_2Cl_4$
Ti^{III} d^1	3	planar	$Ti\{N(SiMe_3)_2\}_3$
	4	tetrahedral	$Cp_2Ti(acac)$
	5	trigonal bipyramidal	$TiBr_3(NMe)_3$
	6	**octahedral**	$[Ti(H_2O)_6]^{3+}$, $[TiF_6]^{3-}$, $TiCl_3(THF)_3$
Ti^{II} d^2	4	tetrahedral	$Cp_2Ti(CO)_2$
	6	octahedral	$TiCl_2 \cdot (THF)_4$

2.2 *O,O'*-DONOR LIGANDS

2.2.1 Introduction

Ligands can be classified: **(a) electronically**, according to the number of electrons they contribute to the central metal, i.e., *one-electron donor, two-electron donor etc*., **(b) structurally**, according to the number of connections they make with the central metal, i.e., *unidentate, bidentate, tridentate etc*., **(c) by the type of atom(s) through which they bond**, for example, *O,O'-*, *O,N'-*, *ONO-donor* ligands, or **(d) by the family of compounds**, examples shown in **Figure 2.1**

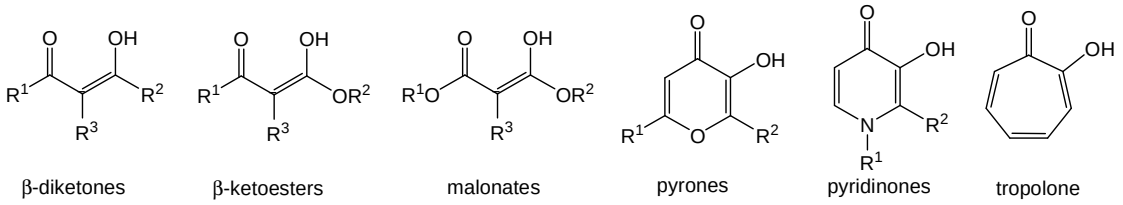

Figure 2.1 Different families of one electron, bidentate, oxygen donor ligands.

Bidentate ligands can further be classified according to the size of the chelate ring formed, for example, *five-membered, six-membered, etc*. If the bidentate ligand binds exclusively to one metal centre, it is termed chelating, as opposed to bridging, where the bidentate ligand binds to more than one metal centre.

The ligands selected for the current project are *bidentate O,O'*-ligands (**Figure 2.2**):

1. *one-electron donors*, forming six-membered chelate rings. The ligand (β^-) is derived from the neutral β-diketone, abbreviated, Hβ.
2. *two-electron donors*, forming five- to eight-membered chelate rings. The ligand (L^{2-}) is derived from the neutral dihydroxy-aryl, abbreviated, H_2L.

Note: β and L are abbreviations used for the ligands, i.e., β denotes the anion of Hβ and L, the dianion of H_2L. They are use instead of β^- and L^{2-} unless the charge on the ligand is being emphasised. An exception to this rule is "β-diketone" where β stands for beta.

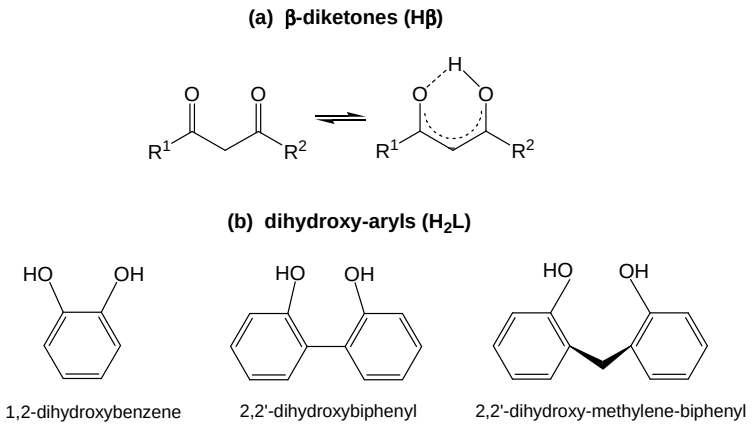

Figure 2.2 Structural formulae of bidentate *O,O'*-ligands, (a) β-diketones and (b) dihydroxy-aryls, in their neutral "free ligand" or "base" form**.**

2.2.2 β-diketones

β-diketones, which have been investigated with virtually every metal and metalloid in the periodic table, are amongst the most widely studied ligands.

2.2.2.1 Structural aspects

The basic structure of 1,3-diketones, commonly known as β-diketones, consists of the β-diketone backbone with various substituent groups attached at peripheral position R^1, R^2 as well as at the α-carbon, R^3 (see **Figure 2.1**). However, in this study, only the conventional β-diketones with a hydrogen in the α-position (i.e., no substitution at the α-carbon), are considered. The various combination of substituents, R^1 and R^2, leads to a large number of known β-diketones. Acronyms are used for selected ligands of principal interest (see list of abbreviations).

The electronic properties of the β-diketone can be modified by using side groups, R^1 and R^2, selected in terms of their electron donating and electron withdrawing properties expressed in terms of group electronegativity. Group electronegativities (χ_R) refer to the combined electronegativity of a specific side group, R, such as the CF_3 group, and not just one atom. Electronegativity is an empirical value and is expressed on four different scales: the Pauling (χ_P); Allerd & Rochow (χ_{A+R}); Allen (χ_{spec}) and Gordy (χ_G) scales.

Symmetry β-diketones, $R^1COCH_2COR^2$ can be classified in terms of symmetry of the R-groups. Identical substituent groups, $R^1 = R^2$ yield *symmetric* β-diketones (e.g., Hacac, Hdbm and Hhfaa where substituent groups are CH_3, Ph and CF_3 respectively) while unlike substituent groups, $R^1 \neq R^2$, yield *asymmetric* β-diketones, (e.g. Hba where substituent groups are CH_3 and Ph). This attribute plays an important role in terms of the number of possible isomers that can form in the chelated species, especially in octahedral geometry, see for example, **Figure 2.7** and **Figure 2.8**.

Keto-enol tautomerism β-diketones (I) enolise to *cis*-enols in a slow keto-enol tautomerism and in addition the latter exists as two fast interchanging enolic isomers (**II**) and (**III**).[6]

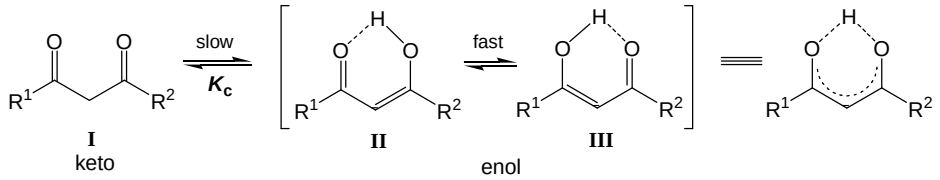

Figure 2.3 The keto-enol tautomeric process of β-diketones showing intramolecular hydrogen bonding and pseudo-aromatic character of the enol form.

Proton transfer and hydrogen bonding are two important behavioural aspects regarding structure and reactivity of simple and complex compounds.[7] 1,3-Diketones exhibit both features in the keto-enol tautomeric process, combining a slow proton transfer with intramolecular hydrogen bonding to form the stabilized enol forms[8] (**Figure 2.3**) The synergistic interplay of resonance and hydrogen bond formation, stabilising the enol form of the β-diketone, is called resonance assisted hydrogen bonding, (RAHB). Calculations show that the energy of the intramolecular bonding in the enol form is large, i.e., 50 - 100 kJ mol^{-1} (compared to the water-water hydrogen bond of ~20 kJ mol^{-1}).[9]

Many techniques (bromine titration,[10] HPLC,[11] polarographic measurements and IR,[12] UV[13] and NMR[14,15] spectroscopy) have been used to study the keto-enol tautomerism. An important feature is the ability to study the keto-enol equilibrium without affecting the position of the equilibrium itself.[14] The equilibrium constant for keto-enol equilibrium (K_c in **Figure 2.3**) is dependent on the nature of the solvent[16] and substituent groups (electronic and steric effects).[17] This is supported by theoretical calculations by Moon and Kwon.[18] In solution the enolic form is generally favoured by non-polar solvents[19] (it has a strong

tendency for intramolecular hydrogen bonding) and lower temperatures,[20,21] while protic solvents promote the keto-form *via* hydrogen bonding to the solvent. Both electron withdrawing and aromatic subtituents favour the enol tautomer in solution, i.e., the CF_3 group, attracts electron density from the enolic ring by induction and the aromatic subsituent donates electron density to the enolic ring by resonance.[17, 20]

The rate of the keto-enol conversion has been extensively studied.[22] NMR studies are very successful in evaluating the rate of keto-enol conversion, since separate NMR signals for the protons due to the enol and keto forms are observed and the relative ratio of the two forms can be determined by intensity measurements (integration of peak areas). The rate of the keto-enol interconversion is usually slow, with large amounts of enol tautomer at equilibrium. Conversion from one enol form to another, however, is very fast (rate constant $\approx 10^6$ s^{-1}) and cannot be observed directly by NMR.[23] The NMR spectrum of the enolic tautomer is a weighted average of the two forms, therefore the enolic forms of both symmetric and unsymmetric β-diketones, give only one resonance for each type of nuclei.

Two driving forces, electronic and resonance driving forces, controlling the conversion of the keto form into the preferred enol isomer, was postulated by du Plessis *et al*.[24] The electronic driving force is controlled by the electronegativity of the R^1 and R^2 substituents on the β-diketone:

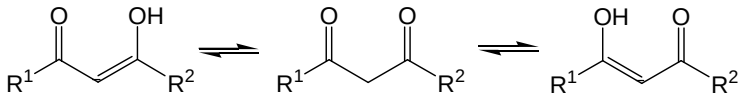

(I) **(a)** **(II)**

When the electronegativity of R^1 is greater than that of R^2, the carbon atom of the carbonyl group adjacent to R^2 on the β-diketone, **(a)**, will be less positive in character than the carbon atom of the other carbonyl, implying that the enol **(I)** will dominate. Alternatively, when the electronegativity of R^2 is greater than that of R^1, enol **(II)** dominates. However, it has been shown that the electronic driving force is not the only factor determining the dominant enol isomer. When either R^1 or R^2 is an aromatic group, such as phenyl or ferrocenyl, the resonance driving force leading to the formation of different canonical forms of the specific enol isomer lowers the energy of this isomer enough to allow it to dominate over the existence of other isomers, which may be favoured by electronic force.[24,20]

β-diketones are powerful chelating species and a key factor to the enhance reactivity, is the dominance of the more reactive enol form. The reactivity order generally appears to be keto < enol < enolate ion.[25] Consequently, in many β-diketones reactions, the reaction proceeds without the use of a base or hydrogen acceptor. This research project focuses primarily on CF_3 (and secondly on phenyl) containing β-diketones, which generally have an enolic content ≥ 0.99 and 0.92 respectively, compared to, for example, the enol content of Hdfcm ($FcCOCH_2COFc$) of 0.67.[26]

Solid state structure In solution and in the vapour phase, β-diketones exist as an equilibrium mixture of keto and enol tautomers, while in the solid state, the enol is the predominantly observed form. There are two extreme forms of intramolecular bonding, symmetric and asymmetric. In symmetric enolisation, the ring hydrogen is equally bound to the two oxygens, while in asymmetric enolisation, the hydrogen is bound much more tightly to one oxygen atom than to another. This is clearly observed in the crystal structures, since in symmetric enolisation, the CO and CC bonds in the enolic ring are similar, while in asymmetric enolisation, these bonds have more single and double bond character.

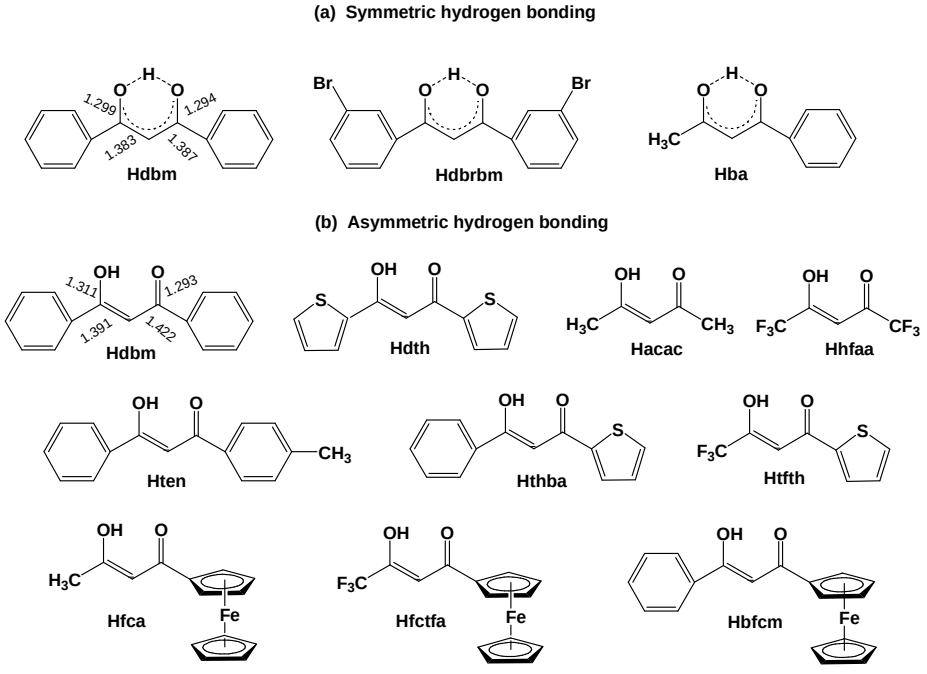

Figure 2.4 β-diketones with **(a) symmetric hydrogen bonds**; Hdbm,[37] Hdbrbm,[27] Hba[28] and **(b) asymmetric hydrogen bonds**; Hdbm,[38] Hdtm,[29] Hacac,[30] Hhfaa,[31] Hten,[32] Hthba,[33] Htfth,[34] Hfca,[35] Hfctfa,[36] Hbfcm,[20] determined from x-ray crystal structures. Selected bond lengths (Å) for Hdbm are shown to illustrate the difference between class (a) and class (b) β-diketones.

Both symmetric and asymmetric hydrogen bonds have been observed in symmetric (identical substituents) and in asymmetric (different substituent) β-diketones. Representative examples of these are shown in **Figure 2.4**. The fine balance between symmetric and asymmetric hydrogen bonding is indicated by the occurrence of both these forms in two polymorphs of the same compound Hdbm.[37,38]

Bonding modes [39] β-diketones can bond to a central metal through the oxygen, carbon or olefin group as shown below.

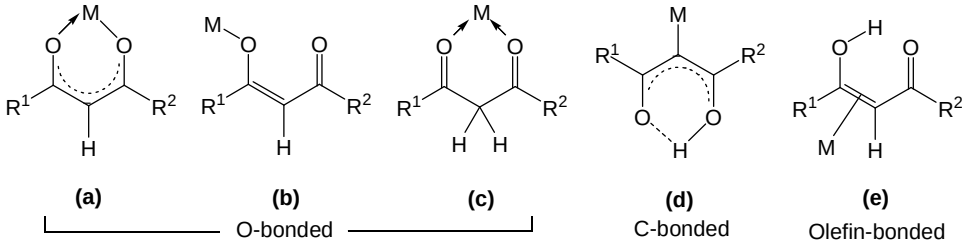

<u>O-Bonding:</u> The usual and most common mode of bonding of the β-diketone is as the enolate (or β-ketoenolate anion), $[R^1COCHCOR^2]^-$ forming a bidentate ligand. A metal cation replaces the enolic hydrogen of the ligand and a stable six-membered chelate ring **(a)** is produced. Since the enolate ion carries a single negative charge, metal atoms can react with one or more enolate ions to give either neutral or charged compounds, depending on the coordination number and valency of the central metal atom. It can also act as a monodentate ligand, where the β-diketone moeity binds to the central metal atom through only one carbonyl group **(b)**.[39] This bonding mode is very rare because of the alternative extraordinary stability of the six-membered chelate ring formed by these ligands with metals. The β-diketone in its neutral keto form, can serve as a ligand where both carbonyl groups act as donor atoms **(c)**, but again this is very rare.[39]

<u>C-Bonding</u>: The ligand moiety bonds to the metal through the C-atom and the carbonyl groups do not appear to participate in the bonding **(d)**. Carbon-bonded β-diketonate complexes are well known and the metal-carbon bond is quite stable in these complexes.[39]

<u>Olefin-bonding</u>: The neutral ligand moiety bonds to the metal through the C=C, double bond (**e)**. Although no X-ray crystallographic evidence has yet been established for the existence of metal-olefin bonds in metal β-diketonates, infrared and n.m.r spectra of these derivatives are consistent with this structure.[39]

2.2.2.2 Synthesis

Syntheses of β-diketones have been reviewed in detail[40] and the most common method is by the Claisen-condensation reaction. In this reaction, a ketone **[A]**, which possesses an α-hydrogen, reacts with a suitable acylation reagent (ester, acid anhydride, acid chloride) **[B]**, in the presence of an appropriate base, to enhance the relatively low reactivity of the ester carbonyl group.[41] The process involves a carbon-carbon bond formation through the replacement of the α-hydrogen atom of the ketone by an acyl group.

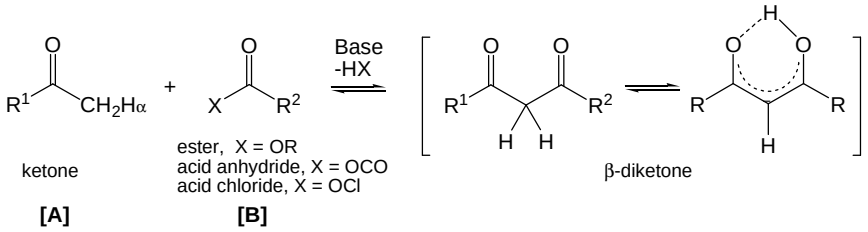

Mechanism The reversible, three-step ionic mechanism,[40] depicted in **Scheme 2.1**, shows the formation of the β-diketone anion, followed by acidification to yield the neutral β-diketone. For this illustration the base, lithium diisopropylamide (LDA), and an ester, R^2COOEt, are used.

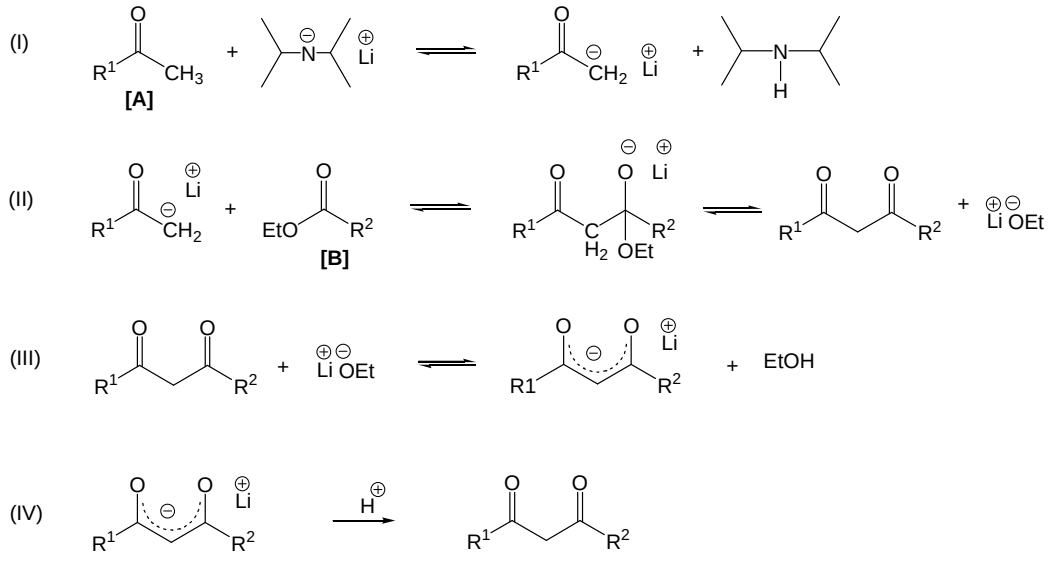

Scheme 2.1 The three-step ionic mechanism, (I) - (III), showing the formation of β-diketone anion by the acylation of a ketone R^1COCH_3 with an ester R^2COOEt using lithium diisopropylamide (LDA) as a base. The acidification (IV) of the anion yields the final β-diketone product.

The first step **(I)** involves the removal of an α-hydrogen on the ketone, to form a ketone anion, which is a hybrid of the resonance structures $R^1CO(C^-)H_2$ and $R^1C(O^-)=CH_2$. The addition of the ketone anion to the carbonyl carbon of the ester **(II)** is accompanied by the release of ethoxide ion to form the β-diketone. The final step **(III)** is the removal of a methine hydrogen on the β-diketone forming the β-diketone anion, which is a resonance hybrid of structures $R^1CO(C^-)HCOR^2$, $R^1C(O^-)=CHCOR^2$ and $R^1COCH=C(O^-)R^2$. The three steps are reversible, but in practice, the synthesis can be forced to completion by either removing the ethanol from the reaction mixture[42] or by precipitating the β-diketone salt (anionic form of the β-diketone). The neutral β-diketone is obtained after the acidification of the β-diketone anion **(IV)**.

Factors influencing the synthesis Properties of the starting ketone, acylation reagent and the base, influence the synthesis of the β-diketone. The pK_a of the starting ketone, determines the ease with which the α-hydrogen is removed by the base. In general the more electron donating the substituent R group, the stronger the base should be to remove the α-hydrogen. For example, the rate of acylation of a ketone with a specific ester and base is proportional to the substituent groups according to the following series

(fastest) $CH_3 > CH_2R' > CHR''$ (slowest)[43]

The strength of the acylation reagent is as follows:

(strongest) acid chloride > acid anhydride > ester (weakest)[43]

The most frequently used bases, arranged from the weakest to the strongest, are, NaOH, alkyloxides (R-OM, M = alkali-metal), hydrides, alkalimetals and simple amides (MNH_2, M = alkali-metals). Sterically hindered base, such as lithium-diisopropylamide (LDA), are also popular. Stoichiometric amounts of base should be used if sodium alkoxides are used, seeing that half of the alkoxide is generated in the second part of the reaction. For sodium, sodium amide or sodium hydride, however, a ratio of ketone**:** acylation reagent**:** base of 1**:**1**:**2 yields better results.[42]

Many by-products can form by competing reaction and consequently, reducing the yield of the β-diketone. Purification of the β-diketone by column chromatography or other methods is thus normally necessary. A few examples of side reactions are:

(a) Self condensation of the ketone (Aldol reaction),[44] to form an α,β-unsaturated ketone or more complex condensation products.

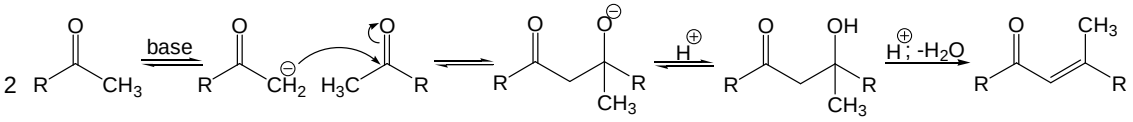

(b) β-keto-ester formation, especially if the ketone which has to acylate, is unreactive.[45]

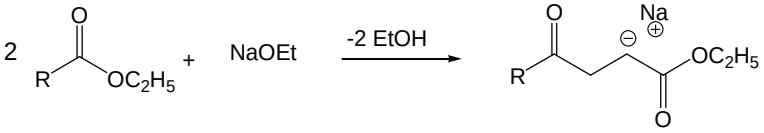

(c) When the alkyl group is exchanged with the alkyloxide group of the ester, the reactivity of the newly formed ester can be lowered to a point where no acylation of the ketone occurs.[46]

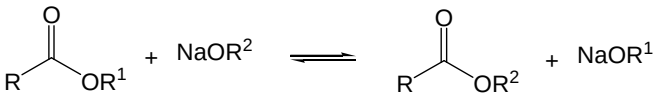

(d) Conversion of the ester to an amide, when using an amide as the base, terminates β-diketone formation.[47] However, use of the sterically hindered base, LDA, largely eliminates this side reaction.[48]

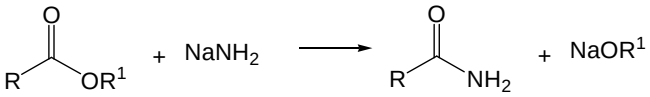

2.2.2.3 Fluorinated β-diketones

The introduction of fluorine substituents on a β-diketone produces large changes in the properties of the resulting β-diketone compared to the non-fluorinated analogues.[49] The presence of fluorine atoms is known to reduce intermolecular interactions (van der Waals forces and hydrogen bonding) and therefore fluorinated β-diketones are highly volatile. In particular the combination of bulky linear side chains and high fluorine content lead to high volatility.[49] As a consequence, special care has to be exercised during the synthesis and subsequent isolation of the fluorinated β-diketones which are easily lost by co-evaporation with the solvent. Fluorinated ligands have a smaller complexation power, however, once chelated, the presence of the fluorine substituents create a protective, repulsive shell around the metal centre.[50]

Substitution of fluorine for hydrogen in β-diketones results in a marked increase in the acidity of the methylene hydrogen, due to the strong electron-withdrawing effect of the fluorine. For example, the pK_a of Hacac, Htfaa and Hhfaa ($CH_3COCH_2COCH_3$, $CH_3COCH_2COCF_3$ and $CF_3COCH_2COCF_3$) with the consecutive replacement of CH_3 with a CF_3 group, are 8.9, 6.7 and 4.6 respectively.[49]

Fluorine substituents shift the enol-keto tautomeric equilibrium in favour of the enol isomer and ^1H NMR based evidence shows that β-diketones with more than four fluorine atoms exist exclusively as the enol isomer. However, two noticeable exceptions, 1,1,1,5,5,5-hexafluoro-3-(trifluoromethyl)pentane-2,4-dione[51] and 1,1,1,2,2,7,7,7-octafluoro-heptane-3,5-dione,[50] are reported to exist as a mixture of enol and keto forms. For the latter compound, the keto-enol equilibrium was displaced in favour of the enol form, with 70 % enol. The occurance of the keto form for these two diketones is difficult to explain.[50]

Park *et al.*[52] investigated the enolic content of eight fluorinated β-diketones and found the percentage enol to be over 90% compared to ~80% for Hacac. An explanation for the very high enolic content was in terms of increased intramolecular hydrogen bonding in fluoro-β-diketones compared to the non-fluorinated analogues. The stability of the enol form depends, in part, on hydrogen bonding between the enolic hydroxyl group and a carbonyl group. The two possible stereoisomers of the enol tautomer, the *syn* and the *anti* form,[53] are shown in **Figure 2.5**. In the case of fluorinated β-diketones, in the *syn*-isomer, hydrogen bonding can occur not only with the carbonyl oxygen **(a)** but also with the fluorine atom of the CF_3 group **(b)**. In the *anti*-isomer, although hydrogen bonding between the enolic OH hydrogen and the carbonyl group is not possible, O-H···F bonding can occur and would tend to stabilize this isomer.

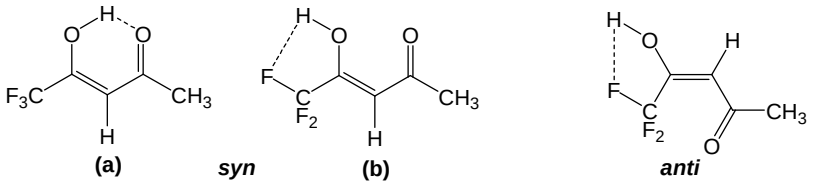

Figure 2.5 The two stereoisomers of the enol tautomer of a fluorinated β-diketone (Htfaa), the syn and anti conformations, showing the hydrogen bonding with the carbonyl oxygen, *syn* (a) and with a fluorine atom, *syn* (b) and *anti*.

Fluoro-β-diketones react with water and even with minor amounts Hhfaa forms a *gem diol*[54] which has been isolated in the solid state.[55]

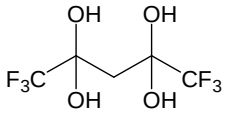

Htfth and Htfaa also form hydrated species. **Scheme 2.2** shows the equilibrium for Htfth, in which the principal species in aqueous solution is the hydrated form (**II**) while in dry organic solvents, it is the enol (**III**). The equilibrium is shifted to 94.5% enol in dry benzene and only 1.6% enol in aqueous solution.[56] Stabilization of the hydrate is due both to the strong inductive effect of the fluorine atoms (producing a positive carbon which is capable of adding a hydroxyl ion) and to possible formation of a strong hydrogen bond between the oxygen and the fluorine on adjacent carbon atoms. Since hydration is not possible in dry benzene, the principal species present is the enol (**III**), stabilized by intramolecular hydrogen bonding either of the O-H-O or O-H-F type (also see **Figure 2.5**).

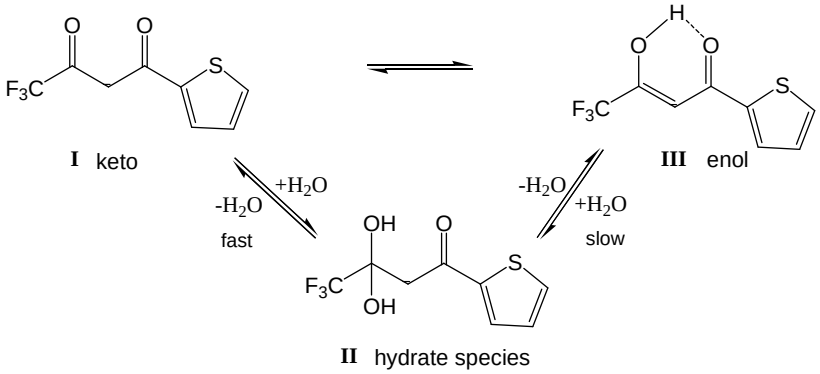

Scheme 2.2 The keto-enol-hydrate equilibrium of Htfth.

The synthetic procedures for the fluorine-containing β-diketones essentially parallel those employed for the nonfluorinated compounds with some experimental variation. The most common synthetic route consists of methoxide-promoted acylation of the appropriate ketone with fluorinated esters. The yields are generally good because fluorinated esters have electrophilic carbonyl moieties that are highly reactive in Claisen condensations. Alternatively, due to lack of reactivity or even decomposition of the reactants, the condensation of alkyl perfluoroalkyl ketones with nonfluorinated esters is used. Yields of the β-diketones using the Claisen condensation reaction are optimal when the ketonic reactant possesses a methyl group (since increasing substitution at the alpha position in the starting ketone results in reduced yields due to the incursion of cleavage reactions).[57] Fluoro-β-

diketones were synthesised extensively in the 1950's and 1960's, however, reported experimental detail pertaining to the synthesis of these β-diketones is often inaccurate or irreproducable.[50]

2.2.3 Dihydroxy-aryls

The second class of ligands for the current project, is composed of dihydroxy-aryls, i.e., compounds containing aromatic ring structures ((di)phenols and (di)naphthols), with two hydroxyl groups attached at fixed ring positions generating a series of bidentate diolato ligands. The exact arrangement of the hydroxy groups (e.g., 1,2-arrangement in catechol) in the ligands is essential for the chelation of the ligand to a metal.

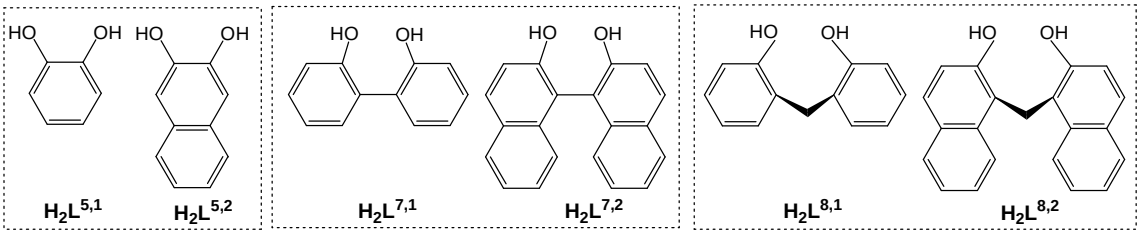

There are many variations in this broad "class" of molecules, but the ligands of interest have been selected in terms of (a) size of the chelating ring, i.e., L^5, L^7 and L^8 , forming five-, seven- and eight-membered rings, respectively and (b) degree of aromaticity, defined by the number of rings, either one ($L^{X,1}$) or two-fused rings ($L^{X,2}$). The stability of the chelated ligand (due angular strain of formation of the 5-, 7- and 8-membered rings) can be evaluated in the series. The ligands are: 1,2-dihydroxybenzene (H_2cat, $H_2L^{5,1}$), 2,3-dihydroxy-naphthalene (H_2naph, $H_2L^{5,2}$), 2,2'-dihydroxybiphenyl (H_2biphen, $H_2L^{7,1}$), 2,2'-dihydroxy-binaphthyl (H_2binaph, $H_2L^{7,2}$), 2,2'-dihydroxy-methylene-biphenyl (H_2mbiphen, $H_2L^{8,1}$) and 2,2'-dihydroxy-methylene-binaphthyl (H_2mbinaph, $H_2L^{8,2}$).

The H_2L ligands can be deprotonated by treatment with a base, such as NR_3, KOH or $NaNH_2$. In the anodic form the most observed coordination mode is the *O,O*'-chelating bidendate form. The driving force of the reaction of these donor ligands with titanium(IV), is based on the electrophilic character of titanium(IV) and the nucleophilicity of oxygen in these ligands. Several of these dihydroxy-aryls have been used independently in various studies with titanium(IV).[58]

2.3 *O,O'*- CHELATED TITANIUM COMPLEXES

2.3.1 Tetrahedral Complexes

2.3.1.1 Introduction

The type of tetrahedral Ti(IV) complexes discussed in this study, falls into the metallocene class of compounds, which in organometallic chemistry, is a compound consisting of a metal covalently bonded to a cyclopentadienyl (Cp) ring by electrons moving in orbitals extending above and below the plane of the ring, η^5-C_5H_5 − M. The hapto (η) nomenclature system is used to describe this π type structure, where pentahapto, η^5, indicates that all five carbon atoms are involved in the π bonding. (The η^5 is often excluded from the notation). Metallocenes exist in different structural formations: (a) parallel sandwich complexes, i.e., dicyclopentadienyl-metals with the general formula $(C_5H_5)_2M$, (**I**) (b) bent sandwich complexes, i.e., dicyclopentadienyl-metal halides, $(C_5H_5)_2MX_{1\text{-}3}$, (**II**) and (c) half-sandwich complexes, i.e., monocyclopentadienyl-metal compounds, $(C_5H_5)MR_{1\text{-}3}$, (**III**) where R = CO, NO, halide group, alkyl group, etc.

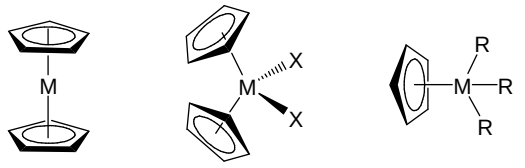

I **II** **III**

The first two types are known as molecular sandwiches because the two cyclopentadiene rings lie above and below the plane on which the metal atom is situated. Group 4 metallocenes, e.g., titanocene dichloride, form bent-sandwich structures, binding to two single donating ligands. When the central metal atom is in a stable oxidation state, the metallocene does not decompose by high temperature, air, water, dilute acids or bases.

Bonding models for $(\eta^5\text{-}C_5H_5)_2Ti(IV)$ compounds according to Ballhausen and Dahl[59] and Allcock[60] are shown in **Figure 2.6**. The bond between the $(\eta^5\text{-}C_5H_5)$ group and a metal, involves six electrons and it occupies three coordination sites on the metal. Of the nine hybrid metal orbitals, six are directed towards the two Cp ligands, and the remaining three orbitals, directed away from the Cp ligands, are used to house nonbonding electrons or to bond to other

ligands **(a)**. This leaves an unpaired central orbital, which can act as a Lewis acid. However, it was found that in some Cp_2MX_2 compounds, the X-M-X angle was two small to accommodate the lone pair of electrons, and thus it was proposed by Alcock that the one orbital lay along the Y-axis, symmetrically arranged on either side of the metal **(b)**. In Cp_2MX_2 compounds, the X-M-X angle is known as the bite angle and the X-X distance, the bite distance **Figure 2.6(c)**. For titanocene dichloride, Cp_2TiCl_2, the bite angle (α) and bite distance are 94.60° and 3.475 Å respectively.[61] The cyclopentadienyl ligands can rotate freely; two conformations often encountered are the staggered and eclipsed conformation.

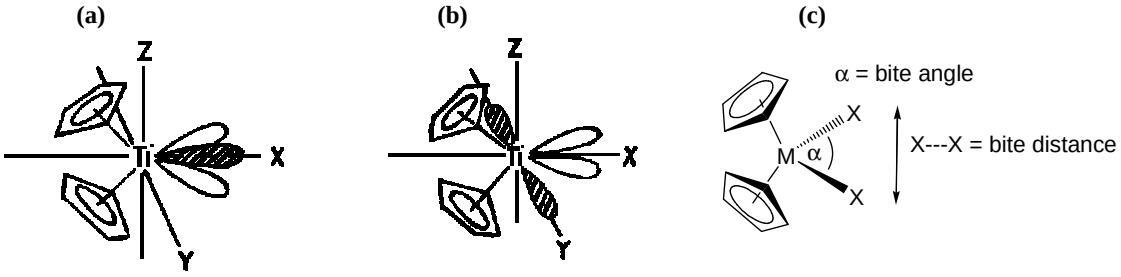

Figure 2.6 Bonding models for Cp_2Ti compounds according to **(a)** Ballhausen and Dahl[59] and **(b)** Alcock.[60] **(c)** The bite angle and bite distance are shown for Cp_2MX_2 complexes.

2.3.1.2 The chemistry of titanocene dichloride

Titanocene dichloride, a tetrahedral bent metallocene, possesses a unique chemical structure where substituents or replacements at three different sites can be used to tailor diverse physical, chemical and biological properties.

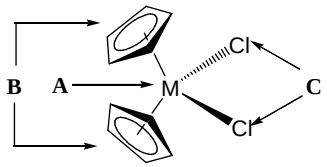

While still maintaining a tetrahedral structure, the central metal atom (**A**) can be varied using the metal ions Ti, Zr, Hf, V, Nb, Ta, Mo and W. Various substituents can be introduced into the cyclopentadienyl ring (**B**) prior to forming the metallocene dihalide and different ligands can replace the two Cl^- ions coordinated to the central metal atom (**C**). It is an ideal starting material for ligand exchange and redox reactions because the chloride ligands on the central metal atom can be exchanged for a wide range of ligands. Many well-documented reviews[62] on the chemistry of titanocenes are available.

Aqueous chemistry In aqueous media titanocene dichloride hydrolyses[63] according to **Scheme 2.3**. Marks[64] investigated the ease with which the η^5-clopentadienyl and chloride ligands undergo hydrolytic displacement. It was found that the stability of the Ti-(η^5-C_5H_5) bond is pH dependant; it is stable over a period of days in low-pH solutions, while near neutral pH, cyclopentadienyl protonolysis occurs. The kinetics for the chloride hydrolysis in pure water (or 0.32 M KNO_3), revealed that the half-life for the displacement of the first Cl^- by water was too fast to measure and that for the second chloride displacement, $t_{½}$ = ~50 min.[64]

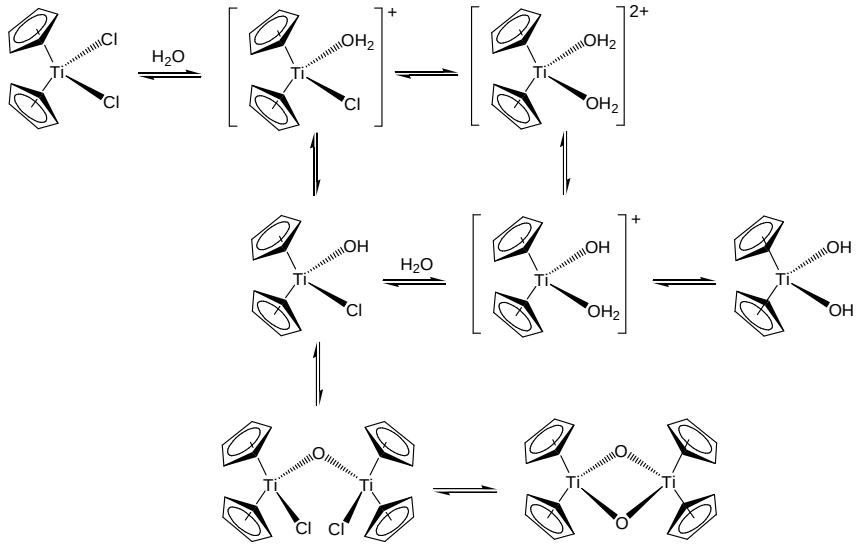

Scheme 2.3 Hydrolysis of titanocene dichloride.

2.3.1.3 Bis(cyclopentadienyl) titanium(IV) cationic complexes

The synthesis of Cp_2Ti(O,O'-ligand) cationic complexes, is usually based on an anion metathesis reaction, which is driven by precipitation of one of the products. Doyle and Tobias[65] prepared Cp_2Ti(β-diketonato) and Cp_2Ti(tropolonato) cationic complexes *via* this procedure, shown in **Scheme 2.4**. Titanocene dichloride, dissolved in anhydrous THF, was converted to the perchlorate complex, $Cp_2Ti(ClO_4)_2$, with the addition of $AgClO_4$. The precipitated AgCl was removed and from the solute, orange crystalline $Cp_2Ti(ClO_4)_2$ was isolated at -80°. $Cp_2Ti(ClO_4)_2$ was aquated generating Cp_2Ti^{2+}(aq), ionic and some polynuclear species. The addition of the β-diketone or tropolone, yielded the final product, the cationic $[Cp_2Ti$(O,O-ligand)$]^+$ complexes with ClO_4^- as the counter-ion.

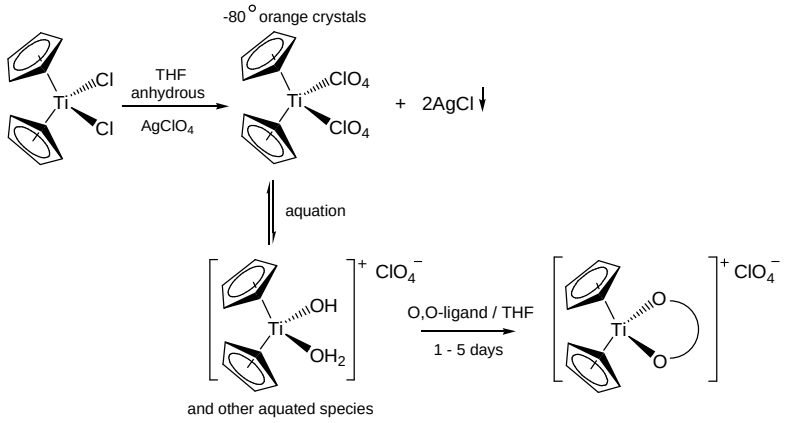

Scheme 2.4 Synthesis of the dicyclopentadienyl titanium(IV)-perchlorate salts. The bidentate O,O'-ligands used were β-diketones (Hacac, Hba, Hdpm) and tropolone.

This synthetic method was adjusted depending on the solubility of the incoming bidentate O,O-ligand, which were water soluble Hacac and water-insoluble β-diketones (Hba, Hdbm and Hbpm) and tropolone. In the case of the water soluble ligand, the whole reaction was performed in water and the perchlorate complex was not isolated prior to the addition of the β-diketone.

Infrared and NMR spectra indicated that the ligand is chelating and the $[Cp_2Ti(O,O\text{-ligand})]^+$ complex undoubtedly possesses a wedge-like sandwich structure with tetrahedral coordination about the titanium centre, similar to that found for titanocene dichloride.[66] Doyle and Tobias[65] were unsuccessful in their attempt to force the bis(cyclopentadienyl)-titanium(IV) moiety into a six-coordinate titanium sandwich structure with parallel rings, by using very high concentrations of the chelating ligand.

Bond *et al.* [67] prepared cationic $[Cp_2Ti(O,O'\text{-ligand})]^+$ complexes *via* the chemical oxidation of $Cp_2Ti^{III}(O,O'\text{-ligand})$, as shown in **Scheme 2.5**.

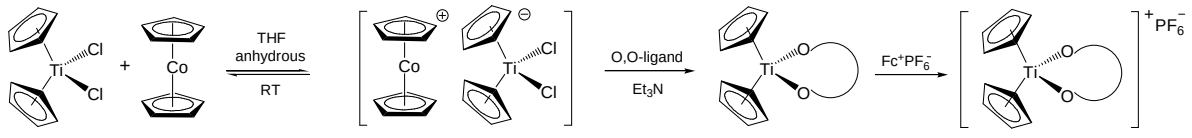

Scheme 2.5 Synthesis of $[Cp_2Ti^{IV}\beta]^+$ complexes via the chemical oxidation of $Cp_2Ti^{III}\beta$. The bidentate O,O'-ligands were β-diketones (Hacac, Hba), 2-acetylphenole and 3-acetyl-1-benzyl-2-hydroxy-5-methoxy-indole.[67]

First the reduction of $Cp_2Ti^{IV}Cl_2$ by coboltocene, Cp_2Co, in THF yields $[Cp_2Co]^+[Cp_2Ti^{III}Cl_2]^-$. The anion, $[Cp_2Ti^{III}Cl_2]^-$, reacts immediately at ambient temperatures with oxygen donor bidentate ligands and Et_3N to form the paramagnetic titanocene(III) species, Cp_2Ti^{III}(*O,O*'-ligand). It is readily extracted from hexane after the removal of THF. Finally the oxidation with ferricinium hexafluorophosphate, $Fc^+PF_6^-$, generates the cationic titanium(IV) species, $[Cp_2Ti^{IV}$(*O,O*'-ligand)$]^+PF_6^-$ with *O,O*'-ligand = β-diketones (Hacac, Hba), 2-acetylphenole and 3-acetyl-1-benzyl-2-hydroxy-5-methoxy-indole.

The β-keto ester analogue, $[Cp_2Ti(CH_3COCHCO(OCH_3))]ClO_4$, has also been prepared.[68, 69] The complex possesses the same wedge-like sandwich structure with tetrahedral coordination, but Doyle and Tobias[68] suggested, based on infrared spectra, that the β-keto ester chelated through one keto oxygen and one "ether" type oxygen atom as in (**I**).

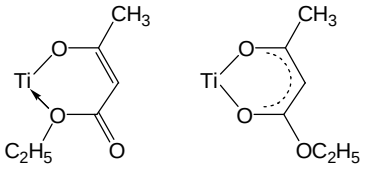

I **II**

Later studies done by White[69] (also based on IR data), however, showed that the ligand is bonded in the classical coordination mode (**II**), chelating through two keto oxygens. The IR spectra of the compound revealed only bands characteristic of coordination mode (**II**) with no bands in the 1600-1700 cm^{-1} region, characteristic of C=O bonding. It was suggested that the materials prepared previously by Doyle and Tobias may have been a mixture containing some partially hydrolysed compound.

2.3.1.4 Bis(cyclopentadienyl) titanium(IV) neutral complexes

This class of complexes is produced by replacement of the labile halides of Cp_2TiCl_2 with one dianionic (or two monoanionic) oxygen-donor ligands.

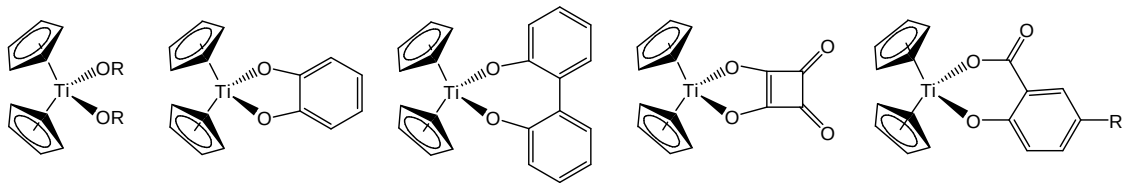

I **II** **III** **IV** **V**

There are many known derivatives of type **I**. A series of bis(phenoxy) and bis(alkoxy) complexes were prepared by Andrä[70] and Jones *et al.*[71] by treating Cp_2TiCl_2 with monodentate phenols and alcohols respectively, in the presence of a base (tertiary amine or sodamide, $NaNH_2$). Bidentate phenols, 1,2-dihydroxybenzene and 2,2'-dihydroxybiphenyl, reacted similarly forming cyclic compounds **II**[70] and **III**[70], with 5- and 7-membered chelate rings respectively. 1,8-Dihydroxynaphthalene did not form the analogous 6-membered ring. When the reaction conditions were changed, using Et_3N instead of the stronger base, sodamide ($NaNH_2$), the bidentate, 1,8-dihydroxynaphthalene, coordinated in a monodentate manner[70], i.e.,

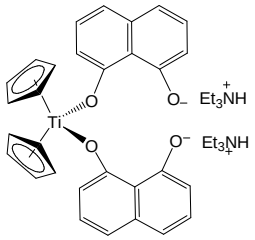

Doyle and Tobias[68] synthesised **IV** *via* the metathesis reaction used for the preparation of the cationic $[Cp_2Ti\beta]^+ClO_4^-$ analogues; first converting squaric acid (1,2-dihydroxy-cyclobutenedione) to the dipotassium salt with KOH and then reacting it with $Cp_2Ti(ClO_4)_2$. The aqueous-phase synthesis of **V**[72] and other similar complexes were successfully prepared by briefly treating an aqueous solution of Cp_2TiCl_2 with a series of acids (as ligands), in the presence of an alkali carbonate as base.

The reaction of Cp_2TiCl_2 in acetonitrile, CH_3CN, with oxygen donor ligands, *i.e.*, linear alcohols (ROH), glycols (H_2G), β-diketones (Hβ), and a base, was found to be distinctly different relative to the reaction in other organic solvents, i.e., a Cp group and then a chlorine atom were substituted instead of the usual halide replacement. Bharara,[73] Nesmeyanov et al[74] and Newton and Frazer,[75] using Et_3N/CH_3CN, found the following,

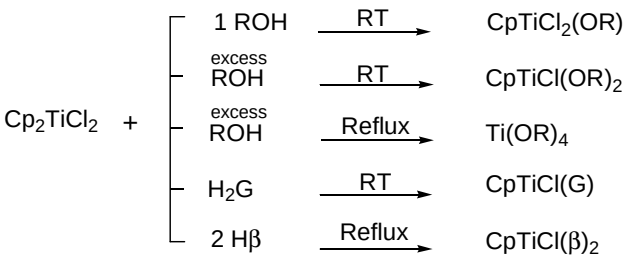

2.3.2 Octahedral Complexes

2.3.2.1 Bis-β-diketonato Ti(IV) complexes

The bis(β-diketonato) metal complexes, $Ti(\beta)_2X_2$, where the monodentate X ligand is a halide,[76] pseudohalide[77] or alkoxide,[78] are synthesised from the corresponding metal tetrahalides, $TiCl_4$, or tetraalkoxides, $Ti(OR)_4$, and the diketonates in an anhydrous organic solvent, according to **Scheme 2.6**

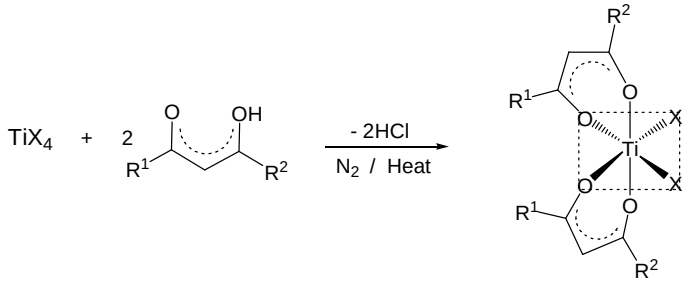

Scheme 2.6 General synthesis of $Ti(\beta)_2X_2$ complexes where X = halide or OR.

The compounds synthesised this way are six-coordinated with quasi-octahedral configuration existing in different isomeric forms. The number of possible isomers depends on the symmetry of the β-diketone. For a symmetrical β-diketone ligand (identical substituents), there are two possible isomers, one *cis* and one *trans* isomer.

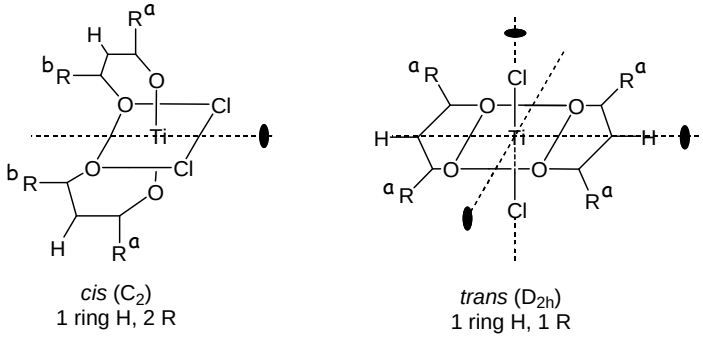

Figure 2.7 The two isomeric forms of octahedral $Ti(\beta)_2Cl_2$ with a symmetric β–diketonato ligand. The two R environments are non-equivalent (^{a}R and ^{b}R) in the *cis*-isomer and equivalent (^{a}R) in the *trans*-isomer. The point group and the number of ^{1}H NMR signals are shown below each isomer**.**

For an asymmetric β-diketone ligand (different substituents, $R^1 \neq R^2$) there are five possible isomers, three *cis* and two *trans* isomers. To distinguish between the isomers, the isomers are named with reference to three prefixes which specify first the relative position of the labile Cl,

followed by the relative orientation of the R^1 and R^2 groups of the β-diketone ligand respectively.

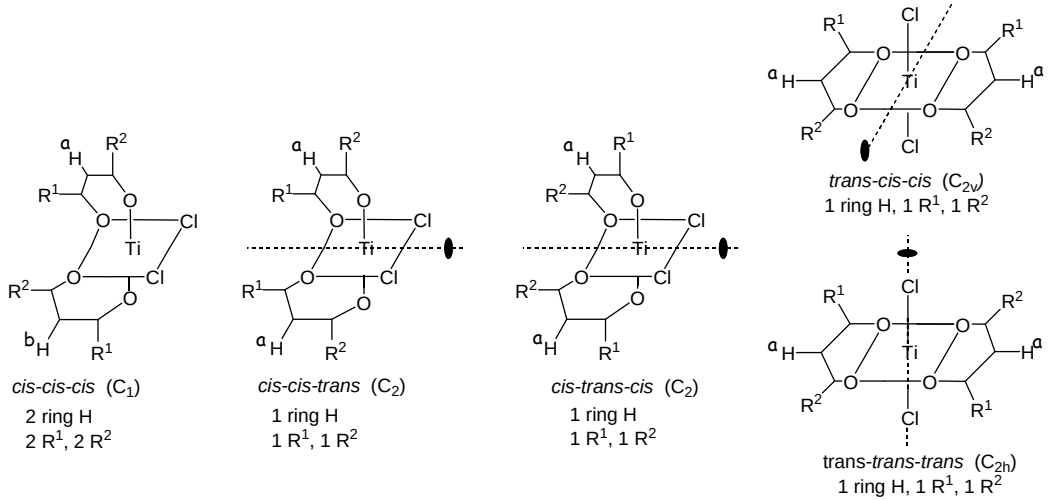

Figure 2.8 The five isomeric forms of octahedral $Ti(\beta)_2Cl_2$ with asymmetric β–diketonato ligands, ($R^1 \neq R^2$). The two ring H are equivalent in all isomers except in *cic-cis-cis* (^{a}H and ^{b}H). The point group and the number of ^{1}H NMR signals are shown below each isomer.

From the symmetry of these isomeric configurations, the NMR signals can be predicted.

(a) If no symmetry element is present, as in the case of the *cis-cis-cis* isomer (point group C_1): all the β-diketonato positions (R^1, R^2 and ring H) are nonequivalent and the NMR gives rise to two ring H, two R^1 and two R^2 resonances.

(b) If one twofold axis of symmetry is present, as in the case of the *cis-cis-trans*- (C_2), *cis-trans-cis*- (C_2), *trans-cis-cis*- (C_{2v}) and *trans-trans-trans*- (C_{2h}) isomers: a single resonance for each of the three (H, R^1 and R^2) groups on the β-diketone ligand, is given. The *cis* isomer (with a symmetrical β-diketonate ligand), yields a single ring H and two non-equivalent R resonances.

(c) If three twofold rotation axes are present, as in the case of the *trans* isomer (with symmetrical β-diketonate ligand, point group D_{2h}: a single resonance for both of the ring H and the equivalent R groups is given.

Solution phase properties Octahedral bis(β-diketonato) titanium(IV) complex have been studied extensively and based on variable-temperature NMR data, it has been shown that all the dihalo- and dialkoxy-bis(β-diketonato)-titanium compounds, $Ti(\beta)_2X_2$ with X = F, Cl, Br, OR, exist in solution exclusively as the *cis* geometrical configuration.[76, 78] The diiodo complex, $Ti(acac)_2I_2$ is the only titanium complex which shows evidence of the *trans*

configuration, being present in DCM as an equilibrium mixture of rapidly isomerising *cis* and *trans* isomers.[79] In fact, all group (IV) metal dichlorobis(β-diketonato) complexes, $M^{IV}(\beta)_2Cl_2$, with the exception of germanium(IV), have been assigned *cis* configurations. For $Ge(\beta)_2Cl_2$,[80] a slow *trans*-*cis* equilibrium was observed; where initially, the trans isomer in a fresh solution converted (over a few hours), to a *cis*-*trans* isomeric mixture in the aged sample.

$Ti(\beta)_2X_2$ compounds are stereochemically nonrigid, undergoing rapid rearrangement processes interchanging the substituent side groups of the β-diketonato ligands *via* intramolecular twist mechanisms. Substantial evidence[81] has been cited in support of a twist mechanism (*i.e.*, twisting of an octahedral face to give a trigonal-prismatic transition state) as opposed to a bond-rupture process (i.e., rapture of one metal-diketonate bond to give a five-coordinate intermediate). The identification of the *cis*-isomers and the stereochemical non-rigidity of the $Ti(\beta)_2X_2$ complex in solution have been established by variable-temperature NMR (see **Figure 2.9**). At ambient temperature, NMR spectra show only one set of relatively sharp resonances. With decreasing temperature, the peaks first broaden and then fine structure appears. The line broadening is due to the slowing down of the rapid isomerisation process which exchanges R groups of the β-diketonato ligand between the nonequivalent environments. Below a certain temperature, known as the coalescence temperature, the exchange process slows down sufficiently so that separate signals for the three *cis*-isomers (for complexes with asymmetric β-diketones) are detected. Raising the temperature above RT, results in the peaks becoming even sharper (relative to the peaks at RT) due to increasing the rate of intramolecular rearrangement.

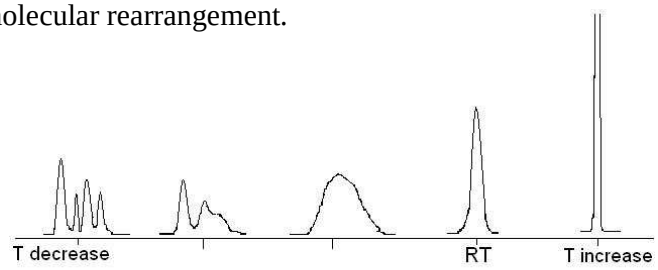

Figure 2.9 Simulated ^1H NMR spectra of the methine (ring proton) for $Ti(\beta)_2Cl_2$ complexes, showing the expected spectral lineshape changes with temperature. The low-temperature spectra, resolved into four separate peaks, indicate that the complex exists as the three *cis* geometrical isomers.

Stabilisation of the *cis*-configuration Geometry is determined by a combination of steric and electronic factors. In the case of $Ti(\beta)_2X_2$ complexes, steric factors favour the *trans*-configuration but experimentally the *cis*-configuration is found to be more stable. The

effect of increasing steric hinderence in the $Ti(\beta)(OR)_2$ series, with R = Me, Et, ^{i}Pr, ^{t}Bu, is simply to raise the coalescence temperature, *i.e.*, to *slow down* the rate of intramolecular rearrangement. The higher stability of the *cis*-configuration is attributed to electronic factors. Octahedrally coordinated titanium(IV) has a 12-electron valency shell on the basis of σ-bonds, and to attain the 18-electron group, which confer enhanced stability on transition metal complexes, π-electron donation involving the metal *d*-orbitals occurs. Since titanium(IV) is a d^0 system, only ligand→metal π-bonding exists. A considerable body of experimental evidence[82] supports the existence of π-electron interactions in β-diketonato-metal complexes and it is this factor which stabilises the *cis*-configuration in $Ti(\beta)_2X_2$ compounds. In the *cis*-configuration, three of the empty *d*-orbitals (t_{2g} or d_{xy}, d_{yz}, and d_{xz}) interact with the β-diketonato π-electrons in the pπ-dπ back donation, compared to only two *d*-orbitals (d_{xy}, d_{xz}) in the *trans*-configuration. The *cis*-configuration is thus stabilised relative to the *trans* configuration.

NMR Characterisation In the six-coordinated $Ti(\beta)_2X_2$ complexes, 1,3-diketones form a six-membered, planar chelate with the metal, where the transition metal atom participate in the aromatic system by forming π bonds.[83,84] The planarity or "near" planarity of the ring has been shown by X-ray analyses. ^{1}H NMR measurements supports the "aromaticity" of the system; the ring proton (methine proton) of the metal chelate ring, shows downfield shifts relative to the free β-diketone, which is caused by the anisotropic effects of the chelate ring.

Hydrolysis The bis-β-diketonato metal complexes are highly susceptible to hydrolysis and hydrolyse according to **Scheme 2.7**.[85] The order of stability against hydrolysis, which depends on the hydrolysed group X, is OEt > F > Cl > Br > I.

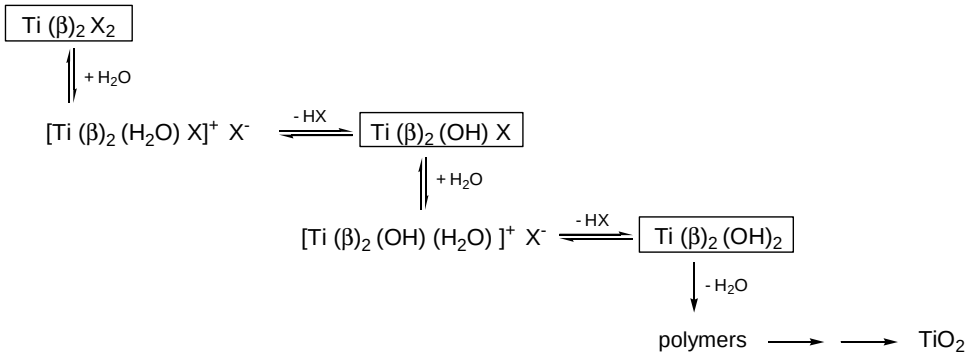

Scheme 2.7 Hydrolysis of bis-β-diketonato titanuim(IV) complexes.

When $Ti(acac)_2X_2$ complexes with X = F, Cl, Br, were exposed to the atmosphere, the crystalline solids showed pitting of the crystal faces, loss of sharp extinction and loss of colour.[86] The dibromo and dichloro-bis(acetylacetonato)titanium complexes converted to an opaque white powder, which was presumed to be TiO_2. Different degrees of hydrolysis occurred; the dibromide was almost completely hydrolysed in 2h; the dichloride in *ca.* 5 days and the difluoride was only partially hydrolysed after 10 days. When these complexes were dissolved in acetonitrile and treated with water, the hydrolysed products precipitated out immediately. However, it was found that when budotitane, $Ti(ba)_2(OEt)_2$ was first treated with cremophor and propylene glycol, micelles formed.[85] When dissolved in water, these micelles surrounded the substance, protecting it from hydrolysis and making it water-soluble and stable over several hours.

2.3.2.2 Bis-β-diketonato-(cyclopentadienyl) Ti(IV) complexes

Another type of 6-coordinate bis-β-diketonato titanium(IV) complex, $CpTi(\beta)_2Cl$, is readily synthesised from Cp_2TiCl_2 and β-diketones in the presence of a hydrogen halide acceptor such as Et_3N, in acetonitrile and under anhydrous conditions[75] (**Scheme 2.8**).

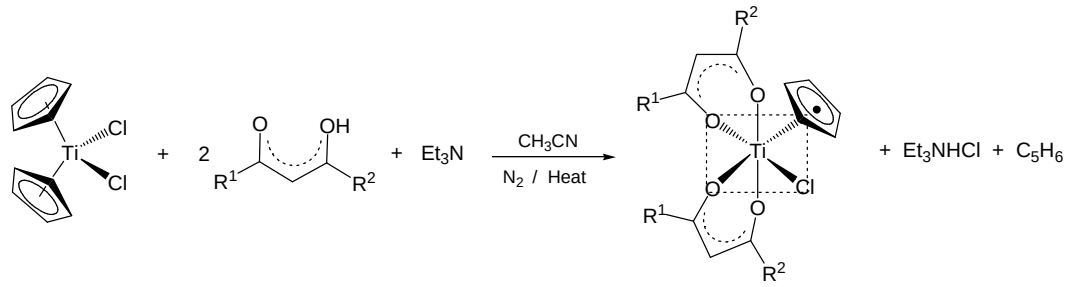

Scheme 2.8 General synthesis of $Ti(\beta)_2CpCl$ complexes.

The compounds exist as monomers with an "approximate" coordination number of six (considering the cyclopentadienyl ring as occupying one coordination position only and undergoing rapid rotation). Based on the octahedron, two geometrical isomers, are possible for symmetric β-diketones, *i.e.*, the *cis* and *trans*-isomers and six isomers for asymmetric β-diketones, i.e., four *cis* and two *trans* (see **Figure 2.7** and **Figure 2.8** for analogous geometric isomers of $Ti(\beta)_2Cl_2$ complexes). The Variable-temperature NMR studies indicate that these

compounds generally exist as the *cis*-isomers in solution.[75] However, titanium compounds incorporating symmetric chelates (*e.g.*, acac[75] and hfaa[87]) appear to give two solution isomers with similar spectra, indicating that both the *cis* and *trans*-isomers are present in solution. An alternative description was rationalised on the basis of the compound having dodecahedral coordination in solution (increasing the number of possible geometric isomers) with the presence of two isomers being an isomerisation between two "dodecahedral" isomer.[75, 87]

Doyle and Tobias[65] wanted to determine if the bis(cyclopentadienyl)-titanium(IV) moiety could be forced into a sandwich structure with parallel rings and six-coordinate titanium [**A]** similar to the known octahedral structure of [**B].**[75]

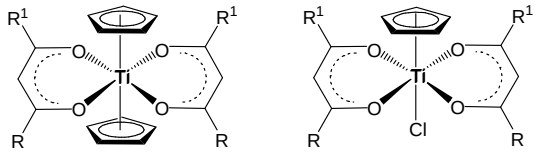

However, it was impossible to produce this octahedral coordination even when very high concentrations of the chelating ligand were used with the aqueous reaction conditions described for the synthesis of $[Cp_2Ti(\beta)]^+$. The structure of [**A]** appears reasonable on steric grounds, but coordination of four oxygen atoms in the xy plane by strong covalent bonds would lead to weakening of the metal ring bonds and would be energetically unfavourable. The six-coordinated $CpTi(\beta)_2Cl$ [**B]**[75] and the five-coordinated, $Cp_2Ti(\beta)Cl$[88] complexes, are energetically favourable as the nine hybrid orbitals are utilised optimally.

2.3.2.3 Bis-β-diketonato-(aryl-diolato) Ti(IV) complexes

Structural aspects of $[Ti(\beta)_2(binaph)]$ complexes with symmetric β-diketones, *i.e.*, β = RCOCHCOR, R = CH_3 (acac), Ph (dbm), ^{t}Bu (dpm), **Figure 2.10 (a),** were investigated by Brown *et al.*[89] At room temperature, the complexes are fluxional exchanging axial and equatorial substituents on the β-diketonate ligands. Titanium bis(β-diketonato)-complexes undergo facile trigonal twists, which not only interconvert equatorial and axial substituents, but also epimerises the titanium centre allowing the diastereometric binaphtholate complexes to equilibrate. When CD_2Cl_2 solutions of the $Ti(\beta)_2(binaph)$ complexes are cooled sufficiently to freeze out the fluxional process, in each case only a single diastereomer was

observed by NMR (within the limits of detection). The identity of the diastereomer formed, determined in the solid state by X-ray crystallography for the dbm and dpm complexes, was the Λ-S/Δ-R isomer. This was in agreement with the electronic predictions based on overlap of the binaph lone pairs with the titanium LUMO. Thus it was showed that a chiral electronic structure can exist even in the symmetrical bis(β-diketonato) titanium(IV) fragment, and that the electronic dissymmetry in these complexes can have sufficient energetic consequence to give rise to useful levels of chiral recognition. It was also reported that $Ti(acac)_2$binaph dimerises in the solid state and both monomer and dimer were detected in solution. No indication of the structure of the dimer was given.

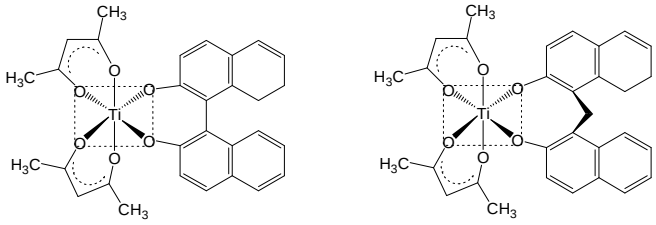

Figure 2.10 The formation of a 7-membered chelate ring in $[Ti(\beta)_2(binaph)]$[89] for β = acac, dbm, dpm and the 8-membered analogue in $[Ti(acac)_2(mbinaph)]$.**Error! Bookmark not defined.**

In the study into the coordination behaviour and reactivity of hydroxy rich ligands (containing varying numbers of OH groups) towards *cis*-$[Ti(acac)_2Cl_2]$, the 8-membered chelated ring complex, $[Ti(acac)_2(mbinaph)]$ **Figure 2.10 (b)**, was isolated and characterised by single crystal X-ray diffraction methods.[90]

2.4 SOLID STATE STRUCTURAL ASPECTS

Certain structural aspects of the various compounds related to this study have been discussed in previous sections. This section concentrates mainly on crystallographic details which have been obtained from the Cambridge Structural Database (CSD)**.**[91]

2.4.1 Tetrahedral Structures

The solid state structures reviewed in this class, are the bent metallocene complexes with a $(\eta^5\text{-}C_5H_5)_2Ti^{IV}$ fragment, in which the Ti atom is attached to one bidentate ligand, $[Cp_2Ti^{IV}(\beta)]^+$ or $[Cp_2Ti^{IV}(O,O'\text{-ligand})]$ and two monodentate ligands, $[Cp_2Ti^{IV}(O\text{-ligand})_2]$. Single crystal structures of the form $[Cp_2Ti^{IV}(\beta)]^+$ will be reported and discussed in chapter 3. Since only one structure of this form has been reported, the analogous Ti^{III}, $[Cp_2Ti^{III}(\beta)]$, structures have also been reviewed for comparison.

Cp_2Ti^{IV} structures Selected crystal data are summarised in **Table 2.2** and the structures are drawn in **Figure 2.12**. The angles and distances discussed are shown alongside **Table 2.2**. The Ti atom is located inside a distorted tetrahedron whose apices are formed by the centres of the Cp ligands and the coordinated oxygen atoms (**Figure 2.11**). The (centroid C_5H_5)-Ti-(centroid C_5H_5) angle (θ_2) is in the range of 128°-136° for the series of structures examined, which is larger than the standard tetrahedral angle of 109.5°; the higher value is attributed to steric hinderance between the cyclopentadienyl ligands. Consequently, the O-Ti-O angle (θ_1) is reduced to an angle which is smaller than the standard 109.5°, depending on whether the coordinated oxygen atoms are part of (a) a restrained ring formed by one bidentate ligand (70° - 103°) or (b) two unrestrained monodentate ligands (90° - 98°). The other valence angles at the Ti atom are close to the standard tetrahedral angle.

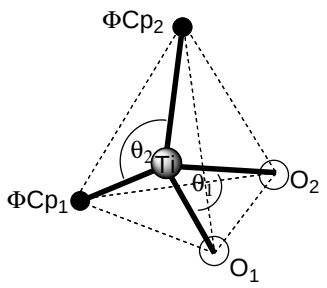

Figure 2.11 Distorted tetrahedral Cp_2Ti structure (Φ =centroid of Cp ring).

Table 2.2 Selected crystallographic data for (a) $[Cp_2Ti^{IV}(\beta)]^+$, (b) Cp_2Ti^{IV}(O,O'-ligand) and (c) Cp_2Ti^{IV}(O-ligand)$_2$ complexes. The **average** Ti-O and Ti- **Φ**Cp distances are listed (**Φ** = centroid). Data for Cp_2TiCl_2 is included for comparison. The data marked in red ($\theta_1$and the non-bonded O-O distance) for structures with a *O,O'*-ligand, are the variables that show the greatest variation.

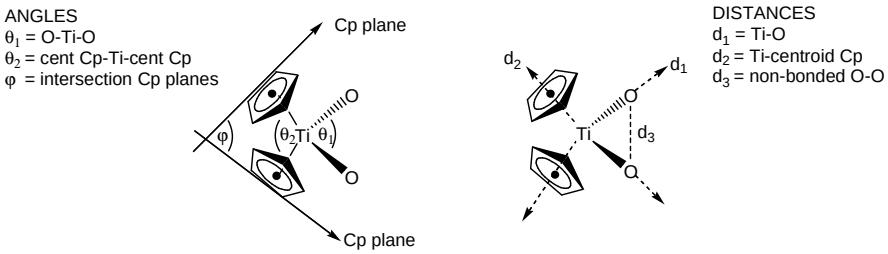

Complex	Ti-Ligand ring size	Angles (Deg)			Distances (Å)			Cp Conformation
		θ_1	θ_2	φ	Ti-O ave	Ti-ΦCp ave	O-O non-bond	
(a) $[Cp_2Ti(\beta)]^+$								
A[92]	6	86.6	133.8	47.5	1.975	2.035	2.710	staggered
(b) $[Cp_2Ti$(O,O'-ligand)$]$								
B[93]	5	81.8	131.6	49.4	1.963	2.082	2.571	staggered
C[94]	5	79.5	133.3	49.0	1.999	2.054	2.555	staggered
D[95]	6	88.3	133.6	50.4	1.932	2.066	2.692	staggered
E[96]	6	70.5	132.0	50.3	1.945	2.042	2.686	staggered
F[97]	7	91.0	131.0	50.5	1.927	2.105	2.753	staggered
G[98]	7	95.2	130.6	52.4	1.942	2.146	2.868	staggered
H[99]	8	103.0	130.4	52.1	1.941	2.130	3.039	staggered
Average values →		87.0	131.8	50.6	1.950	2.089	2.738	
(c) $[Cp_2Ti$(O-ligand)$_2]$								
I[100]	mono	98.1	131.4	49.5	1.907	2.089	2.880	eclipsed
J[101]	mono	97.6	128.3	53.6	1.934	2.117	2.900	staggered
K[102]	mono	97.0	129.9	50.7	1.946	2.073	2.914	staggered
L[103]	mono	90.5	132.1	51.2	1.952	2.054	2.771	staggered
M[104]	mono	90.2	132.0	49.7	1.983	2.038	2.808	staggered
N[105]	mono	89.9	131.5	49.7	1.965	2.057	2.762	staggered
P[106]	mono	91.5	132.5	49.7	1.945	2.047	2.786	staggered
Q[107]	mono	91.8	132.2	48.5	1.995	2.051	2.866	staggered
R[108]	mono	91.4	131.9	50.8	1.928	2.052	2.761	staggered
S[109]	mono	91.7	134.9	50.1	1.916	2.061	2.750	eclipsed
Average values →		92.9	131.7	50.4	1.947	2.064	2.820	
Cp_2TiCl_2[110]	mono	94.6	130.9	51.3	2.364	2.058	3.475	staggered

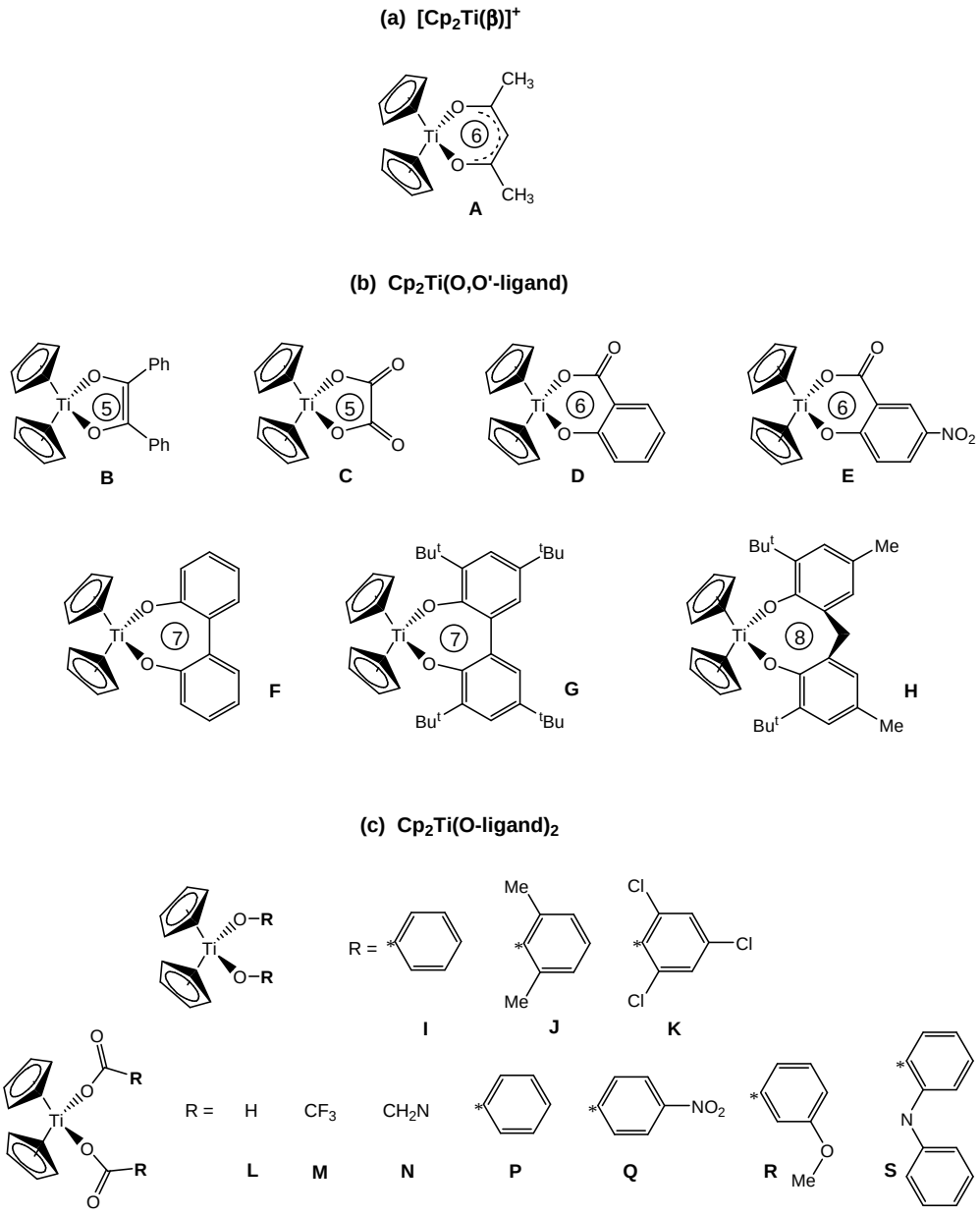

Figure 2.12 Structures of tetrahedral bent metallocene complexes reviewed in **Table 2.2.**
The * indicates the position of R group connection.

The two Cp rings are planar in all cases, with a dihedral angle (φ) between the planes of the rings, varying between 49° - 53°. The Cp rings can tip slightly to increase non-bonded contacts between the cyclopentadienyl C atoms and the coordinated O atoms. This tipping is reflected in the Ti-C distances (of the Ti-Cp ring) which vary slightly. The favoured conformation of the sandwich is staggered, although in many cases the energy barrier to cyclopentadienyl rotation is very small.[111]

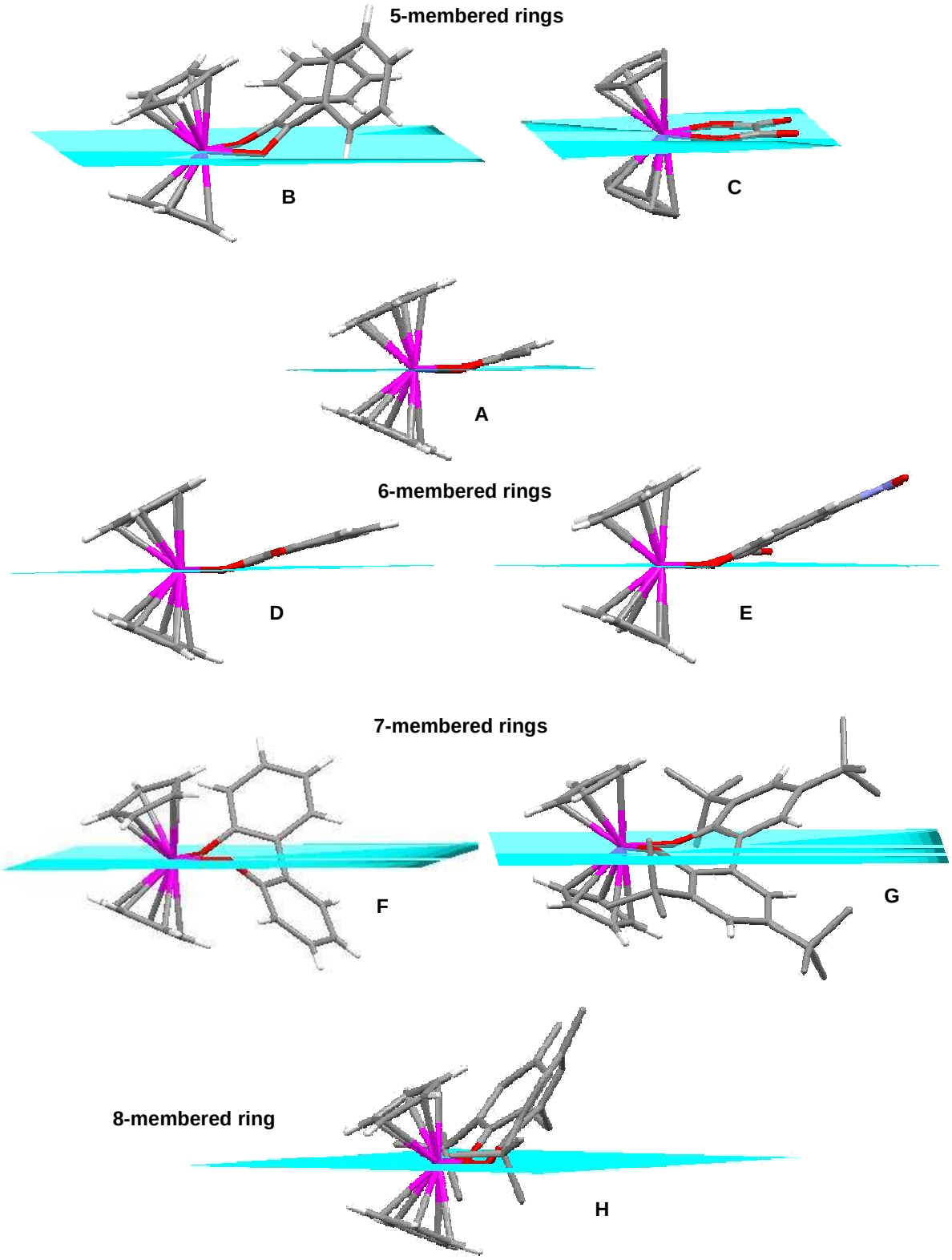

Figure 2.13 The Cp_2Ti(O,O'-ligand) complexes (drawn in **Figure 2.12** and tabulated in **Table 2.2**) showing the position of the chelated ligand relative to the O-Ti-O plane (Some H atoms have been omitted).

The average distance from the Ti atom to the centroids of the C_5H_5 rings (Ti−ΦCp) shows little variation over the different Cp_2Ti complexes, *i.e.*, 2.04 Å for $[Cp_2Ti(\beta)]^+$, 2.09 Å for Cp_2Ti(O,O'-ligand) and 2.06 Å for Cp_2Ti(O-ligand)$_2$. Similarly, the average Ti−O bond length is relatively constant. In contrast, especially regarding the chelated structures, the bite (O-Ti-O) angle and bite (non bonded O-O) distance, have the widest variation (shown in red in **Table 2.1**).

The chelated $[Cp_2Ti(\beta)]^+$ and $[Cp_2Ti$(O,O'-ligand)] complexes (**A**, **B**, **C**, **D**, **E**, **F**, **G** and **H**), in which the bidentate ligand forms a 5, 6, 7 or 8 membered ring, have to accommodate ring strain while maximising Ti-O orbital overlap in the tetrahedral environment. **Figure 2.13** shows the position of the chelated ligand relative to the O-Ti-O plane. The position of the 5-membered ring depends on the ligand type; in **C** it lies directly in the plane, while in **B** it is bent above the plane with a dihedral angle, ω = 34.9°. In **A**, **D** and **E**, the β-diketonato and salicylato ligands, forming 6-membered rings, are similarly bent out of the O-Ti-O plane with a dihedral angle of 16.8°, 18.4° and 21.6º respectively. The biphenolato ligands in the 7-membered ring complexes, **F** and **G** are twisted, with one phenol ring lying above, and the other, below the plane. The methylene-bis(phenolato) ligand, is more flexible than the related biphenolato ligand, since the CH_2 group joining the two phenols acts as a hinge, allowing the ring more freedom to rotate. This 8-membered ring, lies above the O-Ti-O plane in an open-book conformation, **H**. A trend, relating ring size and O-Ti-O angle size is observed; as the size of the ring increase the O-Ti-O angle increases, ranging from 79.5° to 103.0° for 5, 6, 7 to 8-membered rings.

Cp_2Ti^{III} structures Selected crystal data of the three known crystal structures of $Cp_2Ti^{III}(\beta)$ with β = acac, ba, dbm, are summarised in **Table 2.3**. The chelating β-diketone forms a six-membered ring in $Cp_2Ti^{III}(\beta)$ similar to the six-membered ring form by the β-diketonato and salicylato ligand in structures **A**, **D** and **E**, shown in **Figure 2.12**. A comparison of these structures *i.e.*, $Cp_2Ti^{III}(\beta)$ compared to $[Cp_2Ti^{IV}(\beta)]^+$ and Cp_2Ti^{IV}(salicylato), in terms of angles (θ_1, θ_2, θ_3) and the average distances (Ti-O, Ti-ΦCp and non-bonded O-O), indicates that they are structurally very similar. The most significant variation, the difference in the average Ti-O bond distance, suggests that the *O,O*'-ligand is bound more strongly in the titanium(IV) complexes, than in the titanium(III), $Cp_2Ti^{III}(\beta)$ complexes.

Table 2.3 Selected crystallographic data for (a) $Cp_2Ti^{III}(\beta)$ with β = acac, ba, dbm. The **average** Ti-O and Ti-(centroid Cp) distances are listed. (**Φ** = centroid).

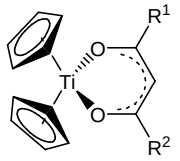

$R^1 = CH_3$ or Ph, $R^2 = CH_3$ or Ph

Complex	β-diketone R groups R^1, R^2	Angles (Deg)			Distances (Å)			Cp Conformation
		θ_1	θ_2	φ	Ti-O ave	Ti-ΦCp ave	O-O non-bond	
$Cp_2Ti(acac)$[112]	CH_3, CH_3	84.3	134.4	45.9	2.068	2.054	2.775	staggered
$Cp_2Ti(ba)$[113]	CH_3, Ph	83.0	135.2	46.6	2.082	2.069	2.758	staggered
$Cp_2Ti(dbm)$[114]	Ph, Ph	82.5	134.3	44.9	2.077	2.062	2.740	staggered
Average values →		83.3	134.6	45.8	2.076	2.062	2.758	

Also the titanium atom lies slightly above of the plane defined by the β-diketonato ligand, i.e., the dihedral angle between the ligand and O-Ti-O plane, is ω = 4.4°, 1.0° and 13.3° for the acac, ba and dbm ligands respectively. But this angle is much smaller than in the Ti(IV) 6-membered-ring complexes **A**, **D** and **E** (shown in **Figure 2.12**), with ω = 16.8°, 18.4° and 21.6°, respectively.

2.4.2 Octahedral Structures

The solid state bis(β-diketonato)titanium(IV) structures, $Ti^{IV}\beta_2X_2$, where X = Cl, OR and $Ti^{IV}\beta_2$(*O*,*O*'-ligand), are reviewed. The Ti atom in the $Ti^{IV}\beta_2$ fragment is attached to two monodentate ligands or one bidentate ligand. This class of compounds is very susceptible to hydrolysis, which is thought to occur in two stages; first the formation of Ti-OH bonds and secondly, Ti-O-Ti bonds (through a condensation polymerisation reaction), forming dimeric and tetrameric structures.[115] These di- and tetratitanium oxygen-bridged structures are also examined.

Monomeric structures Selected crystal data are summarised in **Table 2.4** and the structures are drawn in **Figure 2.14**. The Ti atom is located inside a distorted octahedron whose apices are formed by the six coordinated oxygen atoms (or four oxygen and two

chlorine atoms). The molecules all adopt *cis* configurations in the solid state, *i.e.*, the labile X groups or the two oxygens in the (*O,O*'-ligand) group are *cis* to each other, which agrees with solution studies. The isomeric configuration, using *cis* and *trans* prefixes according to the definition applied in **Figure 2.7** and **Figure 2.8** for symmetric and asymmetric β-diketones, respectively, is shown below and in **Table 2.4**.

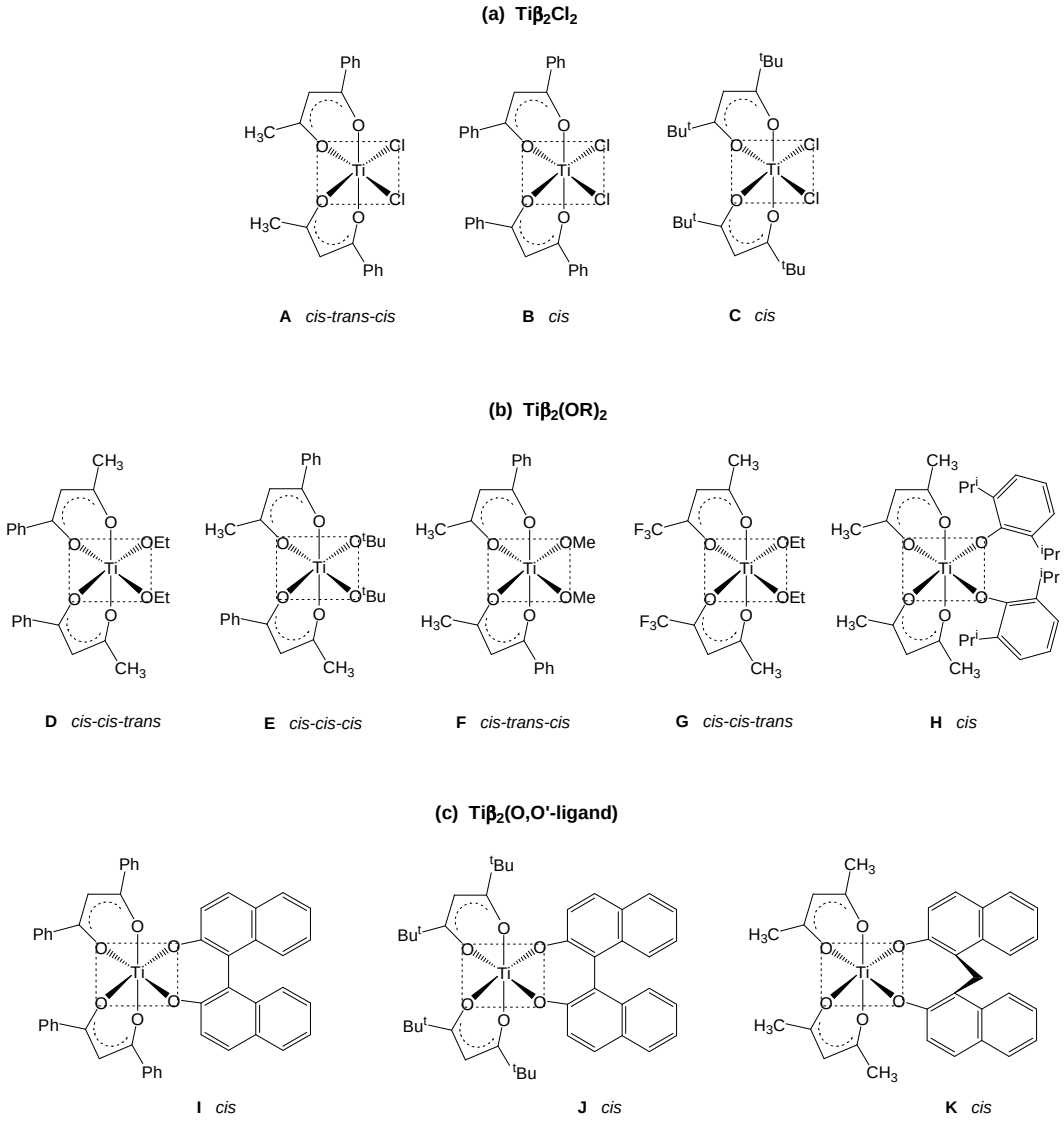

Figure 2.14 Structures of monomeric bis(β-diketonato) titanium(IV) complexes reviewed in Table 2.4, i.e., $Ti\beta_2X_2$, where X = Cl, OR and $Ti\beta_2$(*O,O*'-ligand), where (*O,O*'-ligand) = bidentate oxygen-donor ligand.

Table 2.4 Selected crystallographic data for (a) $Ti^{IV}\beta_2Cl_2$, (b) $Ti^{IV}\beta_2(OR)_2$ and (c) $Ti^{IV}\beta_2(O,O'\text{-ligand})$ complexes. The structures are shown in **Figure 2.14**.

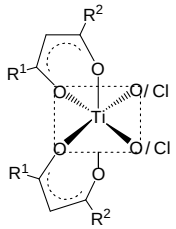

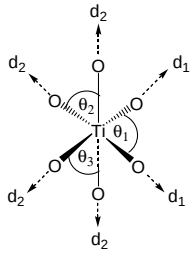

Complexes	Configuration[a]	O-Ti-O Angles / Deg			Distances[c] / Å	
		θ_1[b]	θ_2	θ_3	d_1[b]	d_2
(a) $Ti\beta_2Cl_2$						
A $Ti(ba)_2Cl_2$[116]	*cis-trans-cis*	93.8	83.9	84.0	2.293	1.953
B $Ti(dbm)_2Cl_2$[117]	*cis*	90.2	76.5	81.6	2.245	1.987
C $Ti(dpm)_2Cl_2$[118]	*cis*	95.5	83.0	82.8	2.267	1.958
Average value →		93	82		2.268	1.966
(b) $Ti\beta_2(OR)_2$						
D $Ti(ba)_2(OEt)_2$[119]	*cis-cis-trans*	98.3	81.4	82.7	1.796	2.016
E $Ti(ba)_2(O^tBu)_2$[120]	*cis-cis-cis*	101.8	83.7	83.3	1.761	2.045
F $Ti(ba)_2(OMe)_2$[121]	*cis-trans-cis*	99.7	--	--	1.788	2.020
G $Ti(tfba)_2(OEt)_2$[122]	*cis-cis-trans*	100.8	81.3	81.3	1.785	2.050
H $Ti(acac)_2(OPh)_2$[123]	*cis*	97.4	82.6	82.6	1.837	2.016
Average value →		100	82		1.793	2.029
(c) $Ti\beta_2$(O,O'-ligand)						
I $Ti(dbm)_2$binaph[124]	*cis*	90.8	83.3	83.2	1.870	2.181
J $Ti(dpm)_2$binaph[125]	*cis*	92.5	82.1	83.1	1.855	1.996
K $Ti(acac)_2$mbinaph[126]	*cis*	94.0	83.9	83.4	1.834	2.019
Average value →		92	83		1.853	2.065

[a]The isomeric configuration, using *cis* or *trans* prefixes according to the definition given in **Figure 2.7** and **Figure 2.8** for symmetric and asymmetric β-diketones, respectively. [b]For $Ti\beta_2Cl_2$ α = Cl-Ti-Cl angle and d_1 = Ti-Cl distance. [c]An average of the two Ti-X (d_1) and four Ti-O (d_2) distances are shown.

A distorted octahedral coordination is observed, with bond angle distortions *ca* 10° from a regular octahedron. The O-Ti-O(β-diketonato) angles, ranging between 77° and 84°, are about ~10° less than the O-Ti-O(alkoxy) angles (ranging between 90° - 102°). There are two types of Ti-O bonds, *i.e.*, the titanium atom coordinated to the oxygen atoms of the β-diketonato group (d^2 = Ti-O(β-diketonato)) and the bond between Ti and the other ligand, either monodentate or bidentate, (d^1 = Ti-O(alkoxy)/(O,O'-ligand)). There is a *ca.* 0.2 – 0.3 Å difference between the two types of Ti-O bonds.

All the β-diketonato groups excluding the titanium atom are fairly planar. In the chelating ring the endocyclic C-O and C-C bond distances have values which indicate almost complete π-electron delocalisation over the β-diketonato group. This is evidence of a certain aromaticity of the system.

Dimeric structures The monomeric structures, $Ti\beta_2X_2$, X = Cl or OR, hydrolyses to form dimeric, $\{Ti\beta_2(\mu\text{-}O)\}_2$ if X = OR[127] and $\{Ti\beta_2Cl\}_2(\mu\text{-}O)$ if X = Cl, [128] see **Figure 2.15**.

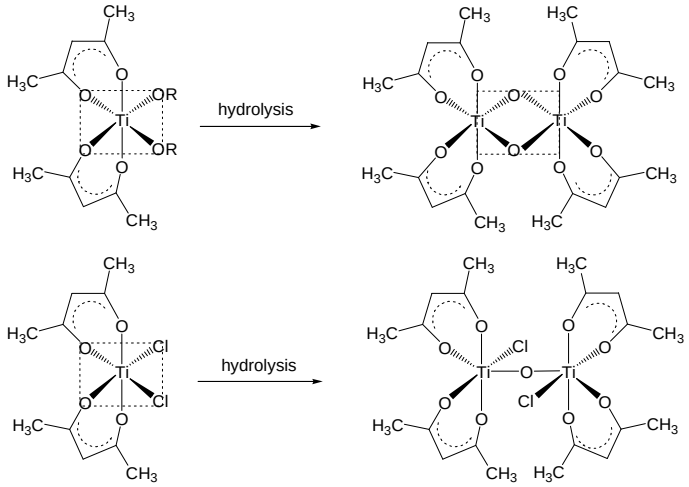

Figure 2.15 Formation of the dimeric structures, $\{Ti(acac)_2(\mu\text{-}O)\}_2$[129] and $\{Ti(acac)_2Cl\}_2(\mu\text{-}O)$[130] by hydrolysis of the monomer, $Ti(acac)_2X_2$, X = Cl or OR.

$\{Ti(acac)_2(\mu\text{-}O)\}_2$[129] The structure consists of a cyclic dimer placed around a centre of symmetry, with the titanium atoms linked through two oxygen atoms. The di-μ-oxo-dititanium ring is planar and slightly distorted from a square, the angle at oxygen being 96.6° and at titanium 83.4°. The Ti-Ti distance is 2.729 Å while the O-O distance is 2.430 Å. Each titanium atom is near the centre of the octahedron and nearly coplanar with the six coordinated oxygens. The acetylacetonate rings are very nearly planar. There are three different Ti-O bond distances, i.e., those in the di-μ-oxo-dititanium ring that average 1.83 Å and those bonding to the axial and equatorial positions of the β-diketonato ligand, which average 1.97 and 2.06 Å respectively. The longer Ti-O bond to each acac is found to be *trans* to the bridging oxygen as a result of the trans effect across the titanium atom.

$\{Ti(acac)_2Cl\}_2(\mu\text{-}O)$[130] The structure consists of two octahedrally coordinated titanium atoms linked through one oxygen atom. The two portions of the molecule are approximately related to each other by a centre of symmetry at the joining oxygen. In each portion, one acetylacetonate group is considerably more planar than the other. Once again there are three different Ti-O bond distances, averaging from the shortest, 1.80 Å (Ti-O-Ti bridge), 1.94 Å (Ti-acac axial position) and 2.17 Å (Ti-acac equitorial position). The longer Ti-O bond to each acac is found to be *trans* to the bridging oxygen.

Tetrameric structures Tetratitanium oxygen-bridged complexes adopt eight different configurations, as observed in a search of the Cambridge Structural Database (CSD)[131] by Allen:[132] square, cube, capped parallelogram, butterfly, planar linear, planar, bowed linear or plate and zigzag.[133] An analysis of multititanium oxygen-bridged compounds was given by Boyle et al.[134] The tetrameric molecule, $[TiO(dpm)_2]_4$,[135] forms a square configuration with a planar, eight-membered cycle (see **Figure 2.16**). The four titanium atoms each have a distorted octahedral coordination. Three pairs of Ti-O bonds are present: the short Ti-O bonds in nearly linear Ti-O-Ti bridges (*ca* 1.81 Å), the long Ti-O bonds with oxygen, *trans* to μ-O (*ca* 2.12 Å) and the Ti-O bonds of intermediate length with O, *cis* to μ-O (*ca* 1.96 Å). Thus, the strong trans influence is clearly observed in the plane of the $(Ti\text{-}O)_4$ ring.

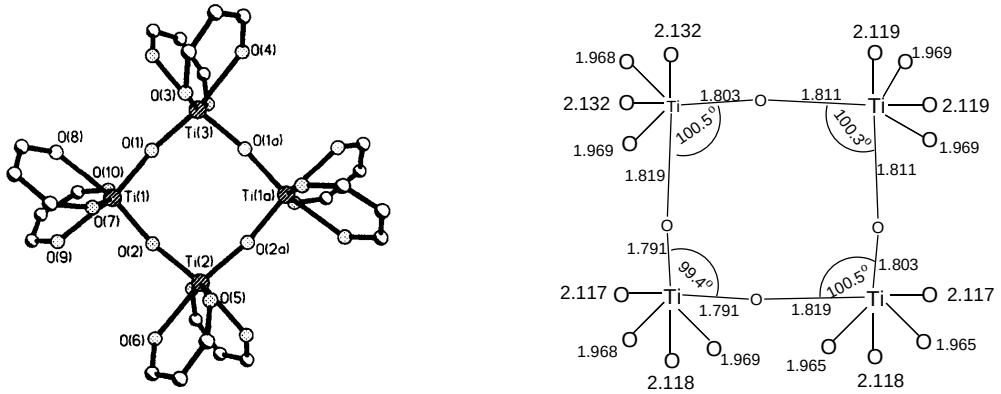

Figure 2.16 **Left**: The structure of cyclo-$[TiO(dpm)_2]_4$ and **Right**: diagram showing coordination, angles and distances around titanium.[135]

The structures of two related tetranuclear oxo-bridged compounds, $[Ti(\mu\text{-}O)(3\text{-oxy-}2\text{-methyl-pyran-}4\text{-onato})_2]_4$ **(A)**[136] and $[Ti(\mu\text{-}O)(4\text{-benzoyl-}3\text{-methyl-}1\text{-phenylpyrazol-}5\text{-onato})_2]_4$ **(B)**[137] adopt the same square configuration as for $[TiO(dpm)_2]_4$.

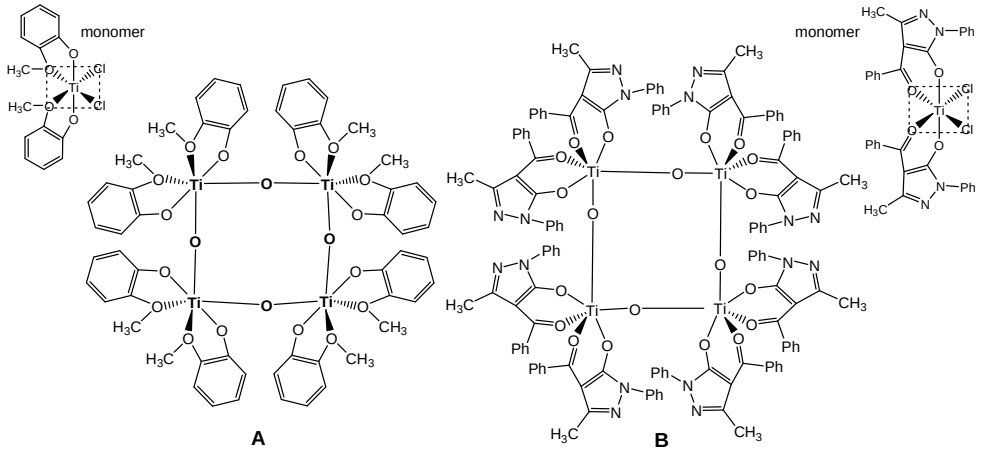

2.4.3 Non-bonded Interactions

Hydrogen bonding and π-stacking (interactions between aromatic rings) are important non-covalent intermolecular forces. The enthalpies of nonbonded interactions are relatively small: *ca*. 2 kJ mol^{-1} for π-stacking interactions and weak hydrogen bonds and *ca*. 20 kJ mol^{-1} for conventional H-bonds as compared with covalent bond enthalpies of *ca*. 200 kJ mol^{-1} and up.[138,139] Nevertheless, these bonds can have a profound effect on the properties, structure and reactivity of substances in which they occur.

2.4.3.1 Hydrogen bonding

The conventional hydrogen bond (written D−H···A) is formed when H, bonded to a highly electronegative atom, D = F, O, N and Cl, interacts with another electron-rich atom, A. The D−H bond is a normal 2 e^-covalent bond but it is polarised with H bearing a partial positive charge such that the H···A interaction is an electrostatic attraction. Structural evidence for hydrogen bonds is provided by the D···A distances (the distance between donor and acceptor atoms should be less than the sum of their van der Waals radii) and the D−H···A angle (should be greater than 100°).[140] The weak and non-conventional hydrogen bonds (C−H···A, D−H···C and C−H···C) are also described.[141] For example, a longer C−H···O contact (d > 3.6 Å) may be acceptable as a hydrogen bond if the angle tends towards linearity (θ > 150°). Very short C−H···O contacts (d < 3.2 Å) with very bent angles (90°-100°) should be viewed with some scepticism. In cases of doubt, angular considerations should take precedence over length considerations.

2.4.3.1 Aromatic−aromatic Interactions

π-stacking interactions are important non-covalent intermolecular forces similar to hydrogen bonding. In the arrangement of aromatic rings one can distinguish generally between an edge-to-face, T-shaped conformation (C–H··π interaction[142]) and a stacked arrangement (π-π interaction), shown in **Figure 2.17**. Facial stacking, termed "π-π stacking", can be perfectly aligned in the face-to-face, parallel conformation or it can be offset in the slipped conformation with the aromatic rings either parallel or at an angle to each other. These π-stacking interactions are not very well defined; they are commonly used for stacks of aromatic groups arranged with molecular planes ranging from parallel to some degree of deviation

from coplanarity and separated by interplanar distances of about 3.3−3.8 Å.[143] The enthalpically favoured orientation is the edge-to-face, T-shaped (C–H··π) interaction but ab initio electronic theory suggests that the off-centered parallel displaced and T-shaped structures are nearly isoenergetic.[144]

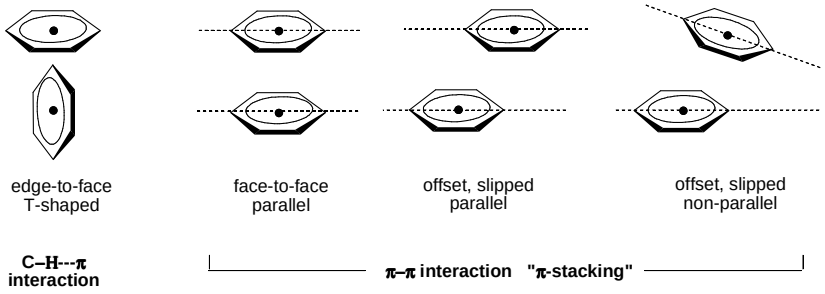

Figure 2.17 Principal orientations of aromatic-aromatic interactions.

The aromatic ring can be represented in terms of the ring centroid, (centre of gravity of the ring) and the surface normal vector (the unique axis perpendicular to the ring plane), see **Figure 2.18 (a)**. The intermolecular orientational information of one aromatic ring with respect to another is typically described by the centroid-centroid separation (R_{cen}), a centre-normal angle (θ), the horizontal displacement of the centroids (d_2) and the interplanar distance (d_1) if the ring planes are parallel. In addition the closest contact distance between the two rings (R_{cd}) and the angle between the π-π stacked planes (φ), are often given, **Figure 2.18 (b)**.

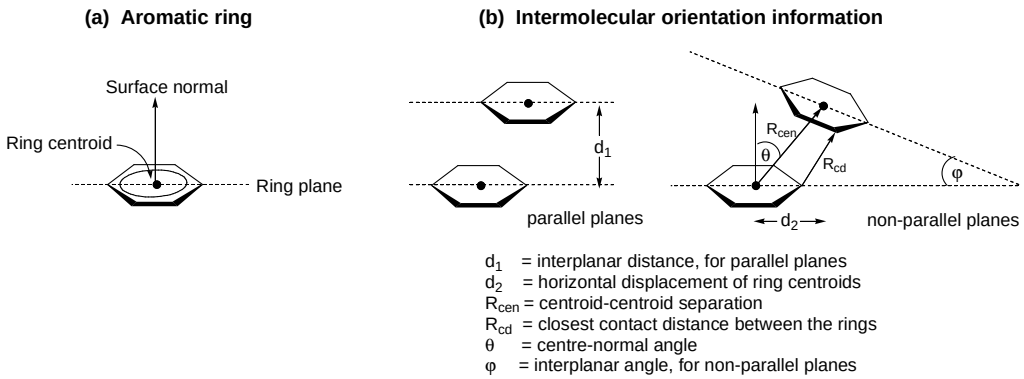

Figure 2.18 **(a)** Aromatic ring representation and **(b)** intermolecular ring orientation information.

2.5 REACTION KINETICS

2.5.1 Introduction

Chemical reactions are often grouped for convenience into the following types; substitution, exchange (both intra-and intermolecular), addition or elimination, solvolysis, and redox.[145]

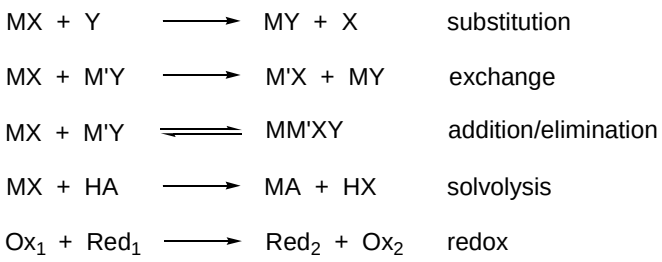

In this study, substitution and exchange reactions of **octahedral** complexes have been examined; therefore a brief overview is given. These reactions involve the replacement of one ligand (the leaving group, X) by another (the entering group, Y), with no change in oxidation state or coordination number of the central metal, although, a *temporary* change in the coordination number of the reaction centre can occur. In exchange reactions, the movement of ligands, takes place between two complexes, while in substitution reactions it is between the complex and a free ligand.

The rate of reaction is given by the rate of decomposition of the activated complex to form products[146] (the activated complex is in equilibrium with the reactants before the reaction takes place), *i.e*.

where K_c^* = equilibrium constant and k = rate constant. In general, many steps may be required to complete the transformation from reactants to products. Most often, a single step, known as the rate determining step, is much slower than all the other steps and the speed of this step effectively determines the form of the rate law expression. Hence, kinetic studies lead to an *empirical rate law* that relates the reaction rate to the concentration of reactants, products and intermediates. The mechanism for the chemical reaction (which consists of a series of elementary steps by which products are formed from reactants), is derived by

postulating steps that are consistent with the empirical rate law and other kinetic data. The transformation from reactants to products proceeds *via* four basic pathways, *i.e.*, dissociative (***D***), associative (***A***) or interchange (***I_d*** or ***I_a***) mechanisms.

Dissociative mechanism (*D*) Bond breaking is the rate-determining step. The leaving ligand (X), dissociates from the coordination metal sphere, forming an intermediate of reduced coordination (*i.e.*, five-coordinate in the case of octahedral reactions). This is followed by a fast reaction, in which the incoming ligand (Y) reacts with the coordinatively unsaturated and very reactive intermediate [ML_5], forming the final product.

$$[\,ML_5X\,] \xrightarrow[\text{slow}]{k} [\,ML_5\,] + X$$

$$[\,ML_5\,] + Y \xrightarrow[\text{fast}]{} [\,ML_5Y\,]$$

Associative mechanism (*A*) Bond formation is the rate-determining step. The incoming ligand (X) binds to the metal centre, producing an intermediate of increased coordination number (*i.e.*, seven-coordinate in the case of octahedral reactions). Subsequently, the leaving group (Y) detaches to form the final substituted product.

$$[\,ML_5X\,] + Y \xrightarrow[\text{slow}]{k} [\,ML_5XY\,]$$

$$[\,ML_5XY\,] \xrightarrow[\text{fast}]{} [\,ML_5Y\,] + X$$

The associative mechanism is associated often with solvolysis (**Scheme 2.9**), especially if the solvent is polar or has a tendency to solvate (coordinating solvent).

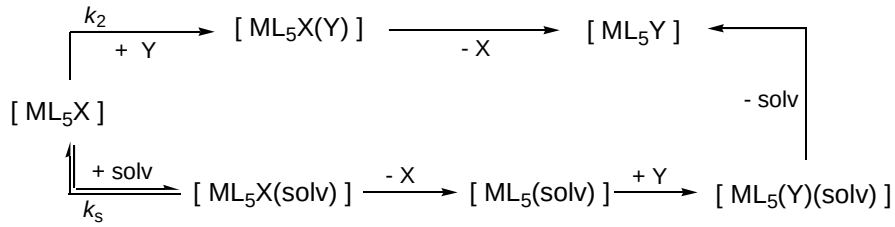

Scheme 2.9 Schematic representation of the direct and solvent pathway for the associative mechanism.

The kinetic rate law including both pathways is given by

$$\text{rate} = (\,k_s + k_2\,[Y]\,)\,[\,ML_5X\,] = k_{obs}\,[\,ML_5X\,]$$

where , k_s = rate constant of solvent pathway and k_2 = rate constant of the direct pathway. $k_{obs} = k_s + k_2[Y]$, is a pseudo first order rate constant when [Y] » [ML_5X].

Interchange mechanism (I_d or I_a) A rapid equilibrium between the incoming ligand (Y) and the reactant [ML_5X] forms a loosely bonded molecular combination. Bond formation and bond breaking happen simultaneously during the formation of this activated complex, but the mechanism may be dominated by bond breaking ($\boldsymbol{I_d}$, dissociative interchange) or bond formation ($\boldsymbol{I_a}$, associative interchange) The intermediate species, which is not directly detectable, does not change in coordination number; it reacts to form the product and releases the leaving ligand X. The distinction between the two is very subtle and careful experimental design is required to determine which description fits a given reaction.

Important information concerning the reaction mechanism is gained by observing the influence of specific factors on the reaction rate. These factors are the nature of the ligands involved (entering-, leaving- and non-labile remaining ligands), the central metal and the solvent. Activation parameters, *i.e.*, entropy of activation (ΔS^*) and volume of activation (ΔV^*) also give an indication of the mechanism, *i.e.*,

(a) dissociative mechanism: ΔS^* = small negative or positive value and ΔV^* = positive value.

(b) associative mechanism: ΔS^* = large negative value and ΔV^* = large negative value.

The activation volume is the most reliable activation parameter in determining the reaction mechanism. Octahedral complexes of metal ions with d^0, d^1, d^2 electron configuration are coordinatively unsaturated and therefore prefer an associatively activated pathway for substitution.[147] The associative mechanism implies an increase in coordination number for the transition state. This is conceivable since stable complexes of Ti(IV) exist with coordination spheres of seven and eight, for example, 7-coordinate [$Ti(Me_2dtc)_3Cl$] and 8-coordinate [$Ti(diars)_2Cl_4$].

2.5.2 Substitution Reactions of Octahedral Ti(IV) Complexes

Substitution reactions of octahedral bis(O,O'-ligand) titanium(IV) complexes, of the form $Ti(L)_2X_2$, were investigated by Burgess *et al.*[148] Reaction involving the nature of the leaving group, the entering group and the non-leaving ligand revealed two kinetically distinct steps:

$$Ti(L)_2X_2 \xrightarrow[\text{fast}]{Y^-} Ti(L)_2XY + X^- \xrightarrow[\text{slow}]{Y^-} Ti(L)_2Y_2 + 2\,X^-$$

where L = O,O'-bidentate ligand, X = labile leaving group (halide or alkoxide), Y = incoming nucleophile. By reducing the concentrations of the incoming ligand, it was possible to detect the relatively fast first stage for some reactions. However, often either the first or the second step proved to be impracticably fast or slow and kinetic data for both steps were established in only a few cases. The rate constant for the first step, is at least 10 times (generally more than 30 times) faster than the second step, resulting in negligible coupling between two stages, and rate constants being determined independently. Pseudo first-order conditions were applied, where the nucleophile is present in large excess.

The rate law for both the first and second stage of substitution is given by:

$$\frac{d[A]}{dt} = \{k_s + k_2 [Y]\} [A]$$

where [A] = [reactant], k_s is the rate constant of the solvent pathway, and k_2 the second order rate constant for the bimolecular substitution reaction (the k_2 pathway corresponds to the simple second-order rate law that is observed in reactions in non-interfering solvents). The k_s and k_2 values are obtained from the graph of k_{obs} *vs.* concentration of incoming nucleophile; $k_{obs} = k_s + k_2[Y]$, and k_s is the y-intercept and k_2 the gradient of the line. In all cases, $k_s \ll k_2$ concluding that the k_2 pathway is the dominant pathway.

An associative mechanism postulated for the k_2 pathway, was supported by (a) the negative volume of activation, e.g., $\Delta V^* = -12.6$ cm^3 mol^{-1} for the nucleophilic attack of NCS^- at $Ti(pyrone)_2Cl_2$ [**A**] and (b) the sensitivity of k_2 to the nature of the entering nucleophile (Y).

Results for different incoming ligands The substitution reaction of $Ti(pyrone)_2Cl_2$ [**A**], with incoming nucleophiles Y = CN^-, NCS^-, MeOH, EtOH, ^{i}PrOH, pyrazine, 2,2'-dipyridyl and malonoic acid (H_2mal), was evaluated. The rate constant, k_2 showed sensitivity to the nature of the entering group, as is expected for an associative substitution, while k_s values were almost equal, consistent with a common rate-limiting solvolysis pathway. In the substitution of the bidendate ligand, *e.g.*, malonoic acid (H_2mal), the second kinetic step was rate-limiting ring closure and not the substitution of a second molecule of entering group (H_2mal). Hence the final product was $Ti(pyrone)_2(mal)$ and not $Ti(pyrone)_2(Hmal)_2$ with two molecules of entering group coordinated in a monodentate manner (see **Scheme 2.10**).

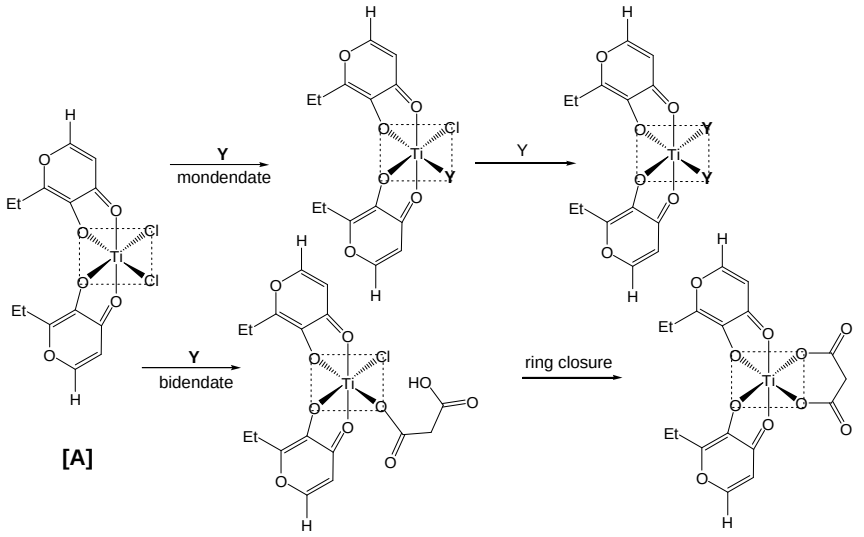

Scheme 2.10 The substitution reaction of $Ti(pyrone)_2Cl_2$ [**A**] with monodentate and bidentate ligands forming $Ti(pyrone)_2Y_2$, Y = CN^-, NCS^-, MeOH, EtOH, ^{i}PrOH, pyrazine, 2,2'-dipyridyl and $Ti(pyrone)_2(mal)$, respectively.

This was firmly supported by product identification and kinetic evidence, *i.e.*, for the second step, k_{obs} is independent of the concentration of the incoming ligand. In Chapter 3 (Section 3.5), the substitution reaction of $Ti(\beta)_2Cl_2$, where the labile Cl^- ligands are substituted by the bidentate ligand, 2,2'-dihydroxybiphenyl (H_2biphen), will be reported.

Results for different leaving Groups The relative reactivities of different leaving ligands in nucleophilic attack of NCS^- at $Ti(pyrone)_2X_2$, X = Cl, F, OMe, OEt, O^{i}Pr, OPh and mal, was evaluated. The rate constant for the dominant bimolecular pathway, k_2, is very sensitive to the different leaving groups (*i.e.*, covers a range of over 20-fold for the complexes studied), while there is a small range of rate constants for the k_s pathway.

Results for different non-leaving Groups The effect of changing non-leaving chelating ligands, L, in $Ti(L)_2Cl_2$ complexes on substitution reactivity of NCS^{-1}, was evaluated for the following family of ligands.

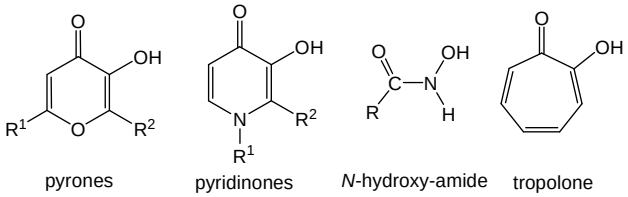

The rate constants k_2, and k_s, are only slightly influenced by the non-leaving ligands. This is due to electron withdrawal or release by the chelating ligand assisting or discouraging entry of the incoming thiocyanate nucleophile. The net electron density at titanium increases when a high degree of σ-electron donation is associated with strong ligand-metal bonding, *i.e.* the effective positive charge decreases on the central metal and discourages nucleophilic attack. The most stable complexes are expected to be formed by ligands with the smallest k_2 values.

2.5.3 Exchange Reactions of Octahedral Ti(IV) Complexes

Dialkoxy- and dihalobis(β-diketonato)titanium(IV) complexes, $Ti(\beta)_2X_2$, undergo rapid intramolecular ligand-exchange (described in section 2.3.2) as well as intermolecular ligand-exchange (redistribution reactions) which scramble both the monodentate (**I**) and the bidentate ligands (**II**).

$$Ti(\beta)_2X_2 + Ti(\beta)_2Y_2 \overset{K_c}{\rightleftharpoons} 2\ Ti(\beta)_2XY \qquad \text{I}$$

$$Ti(\beta^1)_2X_2 + Ti(\beta^2)_2X_2 \overset{K_c}{\rightleftharpoons} 2\ Ti(\beta^1)(\beta^2)X_2 \qquad \text{II}$$

Fay and Lowry[149] studied factors which determine the position of ligand-exchange **equilibria** (but no kinetics), using ^{1}H NMR techniques. The spectra below identify the equimolar mixtures of parent complexes, as well as the mixed-ligand complex for both monodendate and bidendate ligand-exchange, at equilibrium. Generally, the ring proton resonances of the parent complexes are found at the highest and lowest field, with the signal for the mixed-ligand complex at intermediate field.

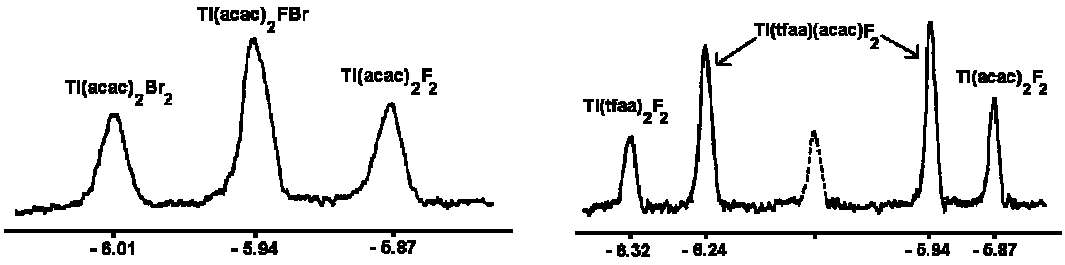

Figure 2.19 ^{1}H NMR spectra in the region of the ring proton showing (**Left**) monodendate ligand-exchange of an equilibrium mixture of $Ti(acac)_2F_2$ + $Ti(acac)_2Br_2$ and (**Right**) bidendate ligand-excange of $Ti(acac)_2F_2$ + $Ti(tfaa)_2F_2$ at 31° in DCM. The dashed peak is a solvent spinning side band.[149]

Exchange of monodendate ligands When both of the monodendate ligands in reaction (**I**) are halogen atoms (X = F, Cl, Br) and β = acac, the equilibrium constant, *K*, is close to the statistical value of 4 expected for random scrambling of ligands. However, when X = F and Y = OEt, the equilibrium constant exceeds the statistical value by a factor of ~10^2, i.e., the mixed-ligand complex is favoured at the expense of the parent complexes. Nonstatistical behaviour for halogen-alkoxide exchange (explained in terms of the difference in ligand electronic structure) has also been observed by Van Wazer and coworkers[150] for the $TiCl_4$−$Ti(OR)_4$ and $SiCl_4$−$Si(OR)_4$ systems.

Exchange of bidendate ligands The equilibrium constant, for the exchange reactions in (**II**) with $\beta^1 \neq \beta^2$ = acac, ba, dbm, dpm, tfaa, tfba, tfth, hfaa and X = F, OEt, is dependent on the relative number of CF_3 substituents on the β-diketonate ligands. (a) K = ~4 (expected for random scrambling) if the exchange ligands contained the same number of CF_3 groups (or no CF_3 groups), *e.g.*, exchange between tfaa-tfba or acac-ba, (b) K = ~2-6 times the statistical value, if the exchange ligands differ by one CF_3 group, *e.g.*, acac-tfaa. (c) K = ~10^2 -10^3 times the statistical value, if the exchange ligands differ by two CF_3 group, *e.g.*, acac-hfaa. These results are in full accord with previous studies of β-diketonate exchange on Zr(IV) Hf(IV), Al(III), Ga(III) and Y(III).[151]

In this research project the kinetics of the exchange reaction $Ti(\beta^1)_2Cl_2$ + $Ti(\beta^2)_2Cl_2$ were studied and rate constants, a reaction mechanism, as well as the equilibrium constants (K_c) will be reported.

2.6 ELECTROCHEMISTRY

2.6.1 Introduction to fundamental concepts

Voltammetry comprises a group of electroanalytical methods in which information about an analyte is derived from the measurement of current as a function of applied potential obtained under conditions that encourage polarization of a working electrode. It is widely used by inorganic, physical and biological chemists for characterisational purposes, including fundamental studies of oxidation and reduction processes in various media, adsorption processes on surfaces and electron transfer mechanisms at chemically modified electrode surfaces.

Cyclic voltammetry This is possibly the simplest and most versatile electroanalytical technique for the study of electroactive species. The effectiveness of CV is its ability to probe the redox behaviour of an electroactive species rapidly, over a wide potential range.[152] Cyclic voltammetry is a simple and direct method for the measurement of the formal reduction potential of a reaction when both oxidized and reduced forms are stable during the time when the voltammogram is taken.[153] Both thermodynamic and kinetic information are available in one experiment. Therefore, both reduction potential and heterogeneous electron transfer rates can be measured. The rate and nature of a chemical reaction coupled to the electron transfer step can also be studied. Knowledge of the electrochemistry of a metal complex can be useful in the selection of the proper oxidizing agent to oxidize the metal complex to an intermediate oxidation state.

Basic CV experiment[152,154] **Figure 2.20** depicts a typical cyclic voltammogram (CV). Important parameters of a CV are the magnitude of the peak currents (i_{pa} = anodic peak current and i_{pc} = cathodic peak current) and the potentials at which the peaks occurs (E_{pa} = anodic peak potential and E_{pc} = cathodic peak potential). CV studies typically monitor two current-related parameters, namely,

Current function: $i_p = {}^{a}c\nu^{1/2}$ where $\nu^{1/2}$ = scan rate (V s^{-1})

[a] $c = 2.69 \times 10^5\ n^{3/2}\ A\ D^{1/2}\ C^{o}$ from the Randles Sevcik equation where n = number of electrons, A = electrode surface area (cm^2), D = diffusion coefficient ($cm^2\ s^{-1}$) and C° = concentration of substrate (mol cm^{-3}).

Current ratio: i_{rev} / i_{fwd}

and three potential-related parameters, namely

Peak potential: E_{pa} and E_{pc}

Peak (potential) separation: $\Delta E_p = E_{pa} - E_{pc}$

Formal reduction potential: $E^{0'} = (E_{pa} + E_{pc})/2$

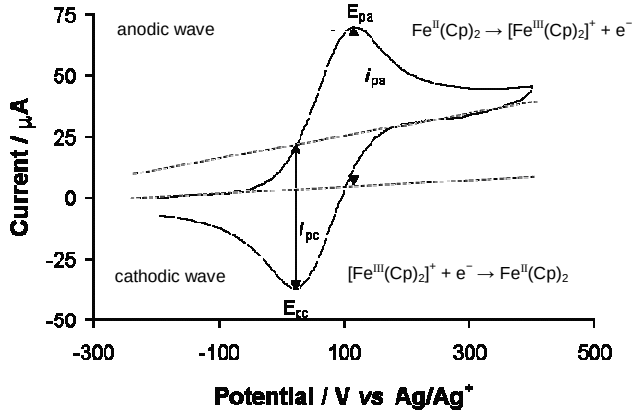

Figure 2.20 Cyclic voltammogram of a 3.0 mmol dm^{-3} solution of ferrocene measured in 0.1 mol dm^{-3} $[NBu_4][PF_6]/CH_3CN$ on a glassy carbon electrode at 25˚C, scan rate 100 mV s^{-1}. Cp = $(C_5H_5)^-$.

Two important processes considered in electrochemistry are, **electrochemical** processes (defined in terms of peak separation, i.e., $\Delta E_p = E_{pa} - E_{pc}$) and **chemical** processes (measured in terms of current ratios, i.e., i_{rev}/i_{fwd}). For a redox couple to be **electrochemically reversible**, the difference in peak potentials (ΔE_p) should be theoretically 59 mV at 25˚C for a one electron transfer process and ΔE_p should be independent of the scan rate (and slightly dependent on the switching potential of the scan and cycle number).[155] Peak separation increases above 59 mV due to slow electron transfer kinetics at the electrode surface as well as high solvent resistance and over potentials. Therefore, in practice, and within the context of this research program, a redox couple with $\Delta E_p \leq 90$ mV is considered reversible. For the redox couple to be **chemically reversible**, the i_{rev} and i_{fwd} values should be identical, i.e., $i_{rev}/i_{fwd} = 1$, showing that the electron transfer process is not followed by a chemical reaction.

The redox couple is electrochemically quasi-reversible or irreversible, when both the oxidation and reduction processes take place, but there is slow electron exchange between the electrode and the molecule (redox species) in solution. Peak separations of 90 mV $\leq \Delta E_p \leq$ 150 mV indicates quasi-reversible behaviour while $\Delta E_p >$ 150 mV, is treated as obeying

irreversible charge-transfer kinetics. A complete chemical irreversible system is one where only oxidation or reduction occurs.[156]

Mechanisms[157] The electron-transfer process occurring at the electrode-solution interface can be accompanied by chemical reactions. Common mechanisms are characterised below. Complete diagnosis of the mechanism includes knowledge of the electrode reaction products and the sequential steps by which they are formed. For example, if a chemical reaction follows rapidly upon electron transfer, the new (secondary) products may be produced close to the electrode, and may be subject to further electrochemistry. If the secondary products are formed slowly, after the primary electrolysis product has diffused away from the electrode, their formation will not influence the electrode mechanism, except in bulk electrolysis. In practice, mechanistic studies make use of a variety of electrochemical, spectroelectrochemical and other physical and chemical methods. Digital simulation techniques allow the entire trace for a particular mechanism to be calculated and compared to the experimental curve for consistency and agreement. Many texts describe how cyclic voltammetry can be employed to study the mechanisms and rates of electrode processes.[155, 156, 157] E = electron-transfer process (electrode reaction) and C = other chemical reactions (chemical reaction).

E mechanism $O + ne^- \rightleftharpoons^{E^{0'}} R$

Represents the couple redox reaction, where the reduction of electroactive species O is followed by the oxidation of R in the reverse scan. The system can be reversible, quasi-reversible or irreversible depending on the electron transfer kinetics as explained above.

EE mechanism $O + e^- \rightleftharpoons^{E_1^{0'}} R + e^- \rightleftharpoons^{E_2^{0'}} Z$

The first electron transfer is followed by a second electron transfer. If the peak separation of the two redox couples is large, i.e., $E_2^{0'} << E_1^{0'}$, then two separate peaks are observed but if the peak separation is sufficiently small, i.e., $E_2^{0'} \approx E_1^{0'}$, then the waves merge.

EC mechanism $O + e^- \rightleftharpoons^{E^{0'}} R \xrightarrow{k} Z$

The electron transfer is followed by an irreversible reaction where the electrogenerated species, R, rearranges or reacts with some other solution component to form electroinactive products, Z. The *catalytic regeneration mechanism* is a variation of the EC mechanism in which the initial electroactive species is regenerated by the following chemical reaction.

ECE mechanism $O + e^- \overset{E_1^{0'}}{\rightleftharpoons} R \xrightarrow{k} Z + e^- \overset{E_2^{0'}}{\rightleftharpoons} Z^-$

The electrochemically generated specie, R, reacts with some other component in solution to form another electroactive species, Z. This species electrolyses immediately if it is more easily oxidized/reduced than the starting material.

CE mechanism $Y \xrightarrow{k} O + e^- \overset{E^{0'}}{\rightleftharpoons} R$

The electroactive species is generated from an electroinactive species, Y, by a chemical reaction. (The preceeding chemical reaction can also be reversible).

Solvent system[158,159] A suitable medium is needed for electrochemical phenomena to occur. The term "solvent system" is used to describe the medium consisting of both solvent and supporting electrolyte. Important properties that an ideal solvent system should possess are:

(a) *electrochemical and chemical inertness* – the solvent system should not undergo any electrochemical reactions over a wide range of potentials and it should not react with the electroactive species nor with intermediates or products of the electrode reaction under investigation.

(b) *high electrical conductivity* – in order to support passage of an electrical current, the solvent system should contain a solvent with low electrical resistance, *i.e.*, large dielectric constant ($\varepsilon \geq 10$) and a recommendable supporting electrolyte, to increase the conductivity of the medium (*i.e.*, most of the current is carried by the ions of the supporting electrolyte).

(c) *good solvent power* – the electroactive substances under investigation must be soluble at least to the extent of 1×10^{-4} dm^{-3} and the electrolyte concentration must be 10 times but preferably 100 times that of the electrochemical species under investigation (~0.1 M).

There is not one good solvent system suitable for all experiments. However, a widely used system for both inorganic salts and organic compounds is acetonitrile (CH_3CN), $\varepsilon = 37$, with tetrabutylammonium hexafluorophosphate ($TBAPF_6$, $[NBu_4][PF_6]$) as supporting electrolyte. The $CH_3CN/[NBu_4][PF_6]$ system exhibits a wide potential range with positive and negative decomposition potentials of +3.4 V and -2.9 V respectively *vs* SCE.[158] A disadvantage is that CH_3CN is rather nucleophilic and can act as a coordinating solvent. DCM or THF can be used when a strictly non-coordinating solvent is required.

New supporting electrolytes and the use of non-traditional solvents have increased options in electrochemical studies. The use of the non-coordinating but very expensive supporting electrolyte tetrabutylammonium tetrakis(pentafluorophenyl)borate, $[NBu_4][B(C_6F_5)_4]$, improves electrochemistry results compared to results obtained when using the weak coordinating electrolyte $[NBu_4][PF_6]$.[160] It was shown that with the use of this new electrolyte, electrochemistry could be conducted in solvents of low dielectric strength and reversible electrochemistry could be obtained for compounds that are normally irreversible.[161] It was also shown that the peak separation between two very close oxidation peaks could be better analysed with the use of this electrolyte.[162]

Reference electrode Prior to the 1980's, nearly all experimental papers specified potentials of a reference electrode *vs* normal hydrogen electrode (NHE) or saturated calomel electrode (SCE). However, IUPAC has since recommend that all electrochemical data be reported *vs* an internal standard.[163,164] In organic media the Fc/Fc^+ couple (Fc = ferrocene) is a convenient internal standard (Fc/Fc^+ couple exhibits $E^{0'}$ = 400 mV *vs* NHE).[165] NHE and SCE are used for measurements in aqueous solutions. However, in many instances electrochemical measurements in water are impossible due to insolubility or instability. With non-aqueous solvents, an experimental reference electrode such as Ag/Ag^+ (0.01 mol dm^{-3} $AgNO_3$ in CH_3CN) or Ag/AgCl may be used.

2.6.2 Redox behaviour of *O,O'*-ligands

The electrochemical behaviour of many β-diketones were investigated during the period 1930 – 1970's under a wide range of conditions. Many studies result in complex electrochemical behaviour due to the chemistry of the β-diketones under those particular conditions. In order to assign the redox behaviour and mechanisms for the electrode reactions, it is necessary to recognize the various redox active species present in the solvent system. For example, polarographic characteristics have been reported for protic solvents, usually ethanol-water and in varying pH. Fluorinated- β-diketones react readily with water to form hydrated species (see **Scheme 2.2**) or in the presence of strong acidic systems, undergo monoprotonation, converting to the allylic carbonium ion.[166, 167]

This result in complex electrochemical behaviour involving the formation of species or radicals produced from the starting material through chemical reactions prior or subsequent to the initial charge transfer. Consequently, the electrochemical reduction of the neutral enol form of the β-diketone can be missed.

Buchta and Evans investigated the electrochemical behaviour of several β-diketones containing aromatic side groups (aromatic β-diketone) in aprotic solvents by polargraphy[168] and cyclic voltammetry.[169] It was found that the electrochemical reduction of Hdbm in DMSO/[NBu_4][ClO^{4-}], was followed by a chemical reaction (EC mechanism). Three reduction peaks were observed at -1420, -1720 and -2280 mV (*vs* SCE). The first wave corresponds to a one-electron reversible reduction of the β-diketone **I** (-1420 mV), while the latter two are those observed for the products of the subsequent chemical reaction, pinacol **III** (-1730 mV) and the enolate **II** (-2280 mV). A proposed reaction sequence consistent with the CV and electrolysis results is presented in **Scheme 2.11**.

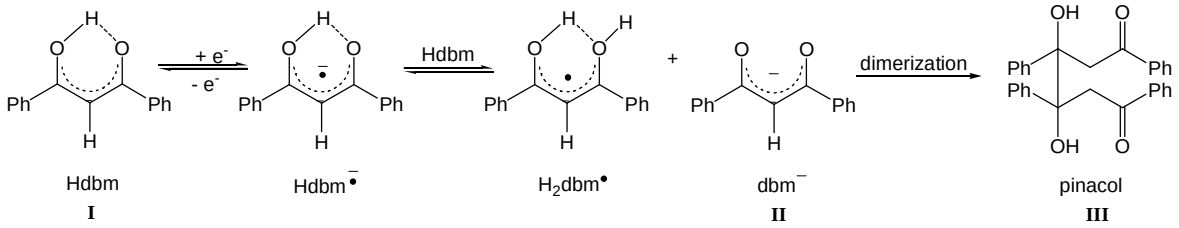

Scheme 2.11 Proposed reaction sequence consistent with the redox behaviour of Hdbm.

The central elements of this scheme are the reversible one electron reduction of (**Hdbm**) **I** to its radical anion (**Hdbm**$^{\bullet-}$) and the subsequent rapid equilibrium reaction in which the unreacted Hdbm transfers a proton to the radical anion producing a neutral radical (**H_2dbm**$^{\bullet}$) and the enolate **(dbm**$^{-}$**) II**. Dimerization, which can occur in different ways, results in the formation of **pinacol III**. The pinacol undergoes an electrolytic autocatalyzed decomposition on a relatively slow time scale, giving benzil and acetophenone. Other β-diketones containing aromatic side groups showed similar behaviour.[169]

The waves show the expected dependence on scan rate, i.e., as the scan rate increases, the values of i_{pa}/i_{pc} for the first wave, increase and approach the limiting value of 1.00, indicating that the scan rate is fast enough to prevent appreciable following reaction. However, the two following waves decrease (with increasing scan rate) relative to the main wave, indicating that

given less time for the following chemical reaction to occur, less products, pinacol and enolate, are available for the subsequent electrochemical reductions. The overall stoichiometry for the reaction is shown in **Scheme 2.12**.

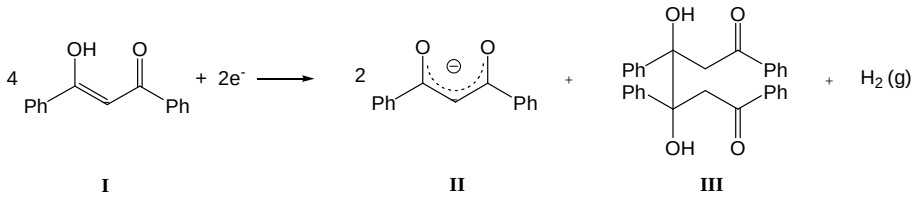

I **II** **III**

Scheme 2.12 The three cathodic peaks, E_{pc} = -1420, -1720 and -2280, correspond to the reduction of the β-diketone, Hdbm (**I**) and products of the subsequent chemical reaction, pinacol (**III**) and enolate (**II**).

The electrochemical behaviour of the 1,3-diketones in the keto form differ from enolised compounds. (By substituting an alkyl groups at the α-carbon position, compounds can be prepared which cannot exist in the enol form, for example, 2,2-dimethyl-1,3-diphenyl-1,3-propanedione). Two important differences have been identified. (a) The relative stability of the primary product of the electrode reaction, the radical anion, is more stable in the keto compounds[170] than in the enol compounds. (b) The radical anions of both the keto and the enol compounds are subject to decomposition but the nature of the reactions differs. Predominantly cleavage reactions occur in keto compounds,[170] while protonation-dimerisation reactions[169] and decomposition to the enolate and hydrogen gas[171] occur in enol compounds (see **Scheme 2.12**). The keto compounds do not possess the relatively acidic enol proton and the rapid protonation by the starting material is not possible. No evidence has been found indicating cleavage reactions during the electrolysis of enolized compounds but such reaction may become important under conditions in which the dimerisation reactions are slow.

Reduction waves for aliphatic Hacac have been reported in aqueous media,[172] but other reports[173] note an inability to observe reduction in a variety of electrolytes. Neal and Murray, in their study on the electrochemical behaviour of Hacac in CH_3CN, observed a well formed but completely irreversible wave at E_{pc} = -2200 mV (*vs* SCE).[171] They found that the reduction of Hacac was not diffusion-controlled; it was kinetically controlled by a preceding chemical reaction, postulated to be the keto-enol conversion of Hacac that exits as a 56:44 enol-keto mixture in CH_3CN.[174] The reduction process, indicated by the spectral results, occurs through the enol form with a keto-enol tautomeric shift permitting exhaustive conversion. This type of kinetic behaviour was termed autocatalysis of a prekinetic equilibrium.

The electrochemical behaviour of Htfth was investigated to determine which electroreducible structure(s) of the β-diketone (i.e., the carbonyl group, the conjugated double bond system or the β-diketone structure) was involved in the electrochemical reduction of Htfth.[175] Typically two polargraphic reduction waves are observed in a buffered (pH 5.2 – 8.2) 1% ethanol/water solution, at $E_{½}$ = -980 and -1500 mV, shifting slightly to more negative values with increase in pH. By correlating the half-wave potentials and behaviour of Htfth with compounds having related functional groups (*i.e.*, thiophene, acetylthiophene, thenoylacetone (Htha), trifluoroacetylacetone (Htfaa), acetylacetone (Hacac), acetone and methyl ethyl ketone), it was concluded that the carbonyl group is associated with the reduction of the β-diketone. In aqueous Htfth solution, an equilibrium forms in which the hydrated form is the principal species (see **Scheme 2.2**, p19). The first wave results from the reduction of the carbonyl group in the hydrated form **II**, while the second wave, the reduction of the carbonyl group in the small amount of enol species **III** that remains unhydrated.

Comprehensive studies on the electrochemical behaviour of other *O,O'*-ligands were not found. However, cyclic voltammograms and peak potentials of ligands are reported with reference to the titanium complexes incorporating the ligands. In this way a comparison between the cyclic voltammograms of the free ligand and the chelated complex is drawn. For example, Basso *et al.*,[191] in their investigation into the electrochemical behaviour of $Ti(pyrone)_2X_2$, X = Cl_2, OEt, displayed the CV of the organic ligand, 3-hydroxy-2-methyl-4-pyrone (**Figure 2.21 Left**), showing reduction and oxidation peaks, E_{pc} = -2050 mV and E_{pa} = 790 and 1420 mV (*vs* Ag/AgCl). Similarly, Bond *et al.*,[67] used an indole derivative in their electrochemical study of a Cp_2Ti(O,O'-ligand) series and reported the CV of the ligand, 3-acetyl-1-benzyl-2-hydroxy-5-methoxyindole (**Figure 2.21 Right)**.

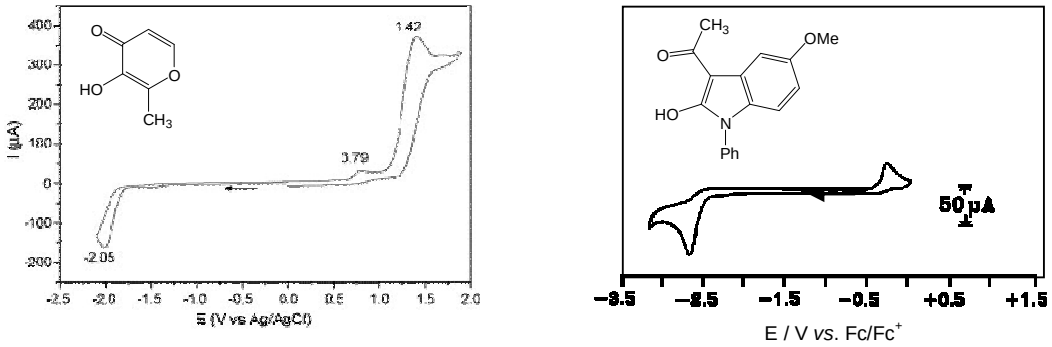

Figure 2.21 Cyclic voltamograms of organic ligands **Left**: 3-hydroxy-2-methyl-4-pyrone (pyrone) in $CH_3CN/[NBu_4][PF_6]$[191] and **Right**: 3-acetyl-1-benzyl-2-hydroxy-5-methoxyindole in butyronitrile/$[NBu_4][PF_6]$.[67]

2.6.3 Redox behaviour of Tetrahedral Ti(IV) Complexes

2.7.3.1 d^0 Ti^{IV} neutral complexes

Cp_2TCl_2 The electrochemical behaviour of titanocene dichloride and derivatives have been the subject of numerous studies revealing important features. Titanocene dichloride in THF, is reduced electrochemically in three successive one-electrontransfer steps (**Figure 2.22**). Three reduction peaks are observed at -1325, -2533 and -2932 mV (vs Fc/Fc^+),[176] in accordance with electrochemical data obtained at the dropping mercury,[177,178] platinum[177,179] and glassy carbon[177,180] electrodes. It was found that the first electron reduction was highly reversible and formed a stable anion $[Cp_2Ti^{III}Cl_2]^-$, while the other two reductions were only slightly reversible at high scan rates becoming completely irreversible at low scan rates.

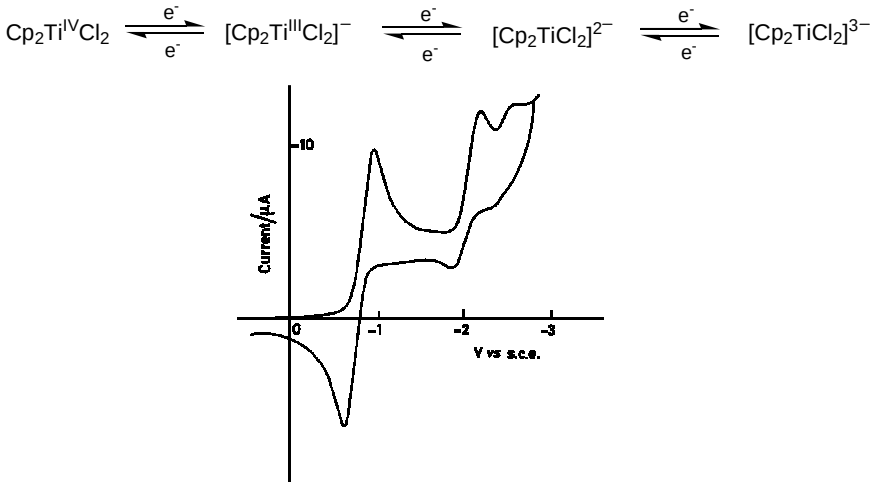

Figure 2.22 **Top**: Reaction scheme for the reduction of Cp_2TiCl_2 corresponding to **Bottom**: the cyclic voltammogram in THF/$[NBu_4][PF_6]$ at glassy carbon electrode; scan rate = 100 mV s^{-1}.[177]

The simple reaction scheme first proposed by Murr *et al.*,[177] involving three successive one-electron transfer steps (**Figure 2.22** (**Top**)) was later modified.[176] At each transfer step, a chemical oxidation of the electrochemically reduced species (catalytic regeneration reaction) and a chemical reaction yielding decomposition products were included. Although the exact nature of the species involved in these chemical steps was not solved, no evidence could be obtained for the formation of a Ti^{II} species or for Cp cleavage. Products connected with halogen cleavage, $[Cp_2TiCl(THF)]$[181] and $[Cp_2TiCl]^-$,[177] have been identified.

The mechanism for the first electrochemical reduction, $Ti^{IV} \rightarrow Ti^{III}$, of titanocene dihalides, Cp_2TiX_2 (X = Cl, Br, I), in THF has been fully described (**Scheme 2.13**),[182] resolving the dispute concerning whether the Ti^{III} anion, $[Cp_2Ti^{III}Cl_2]^-$, generated from the reduction of $Cp_2Ti^{IV}Cl_2$, is stable[176,177,183] or dissociates to give $[Cp_2Ti^{III}Cl]$ and Cl^-.[184,185] From extracted data pertaining to electrochemically reduced solutions of Cp_2TiX_2, it became evident that while $[Cp_2TiX_2]^-$ is the major constituent for X = Cl, Cp_2TiX and $(Cp_2TiX)_2$ are the main species in the case of X = Br, I. The presence of $(Cp_2TiX)_2$ was surprising, as the solvent THF was believed to be capable of breaking the weak dimeric structure.

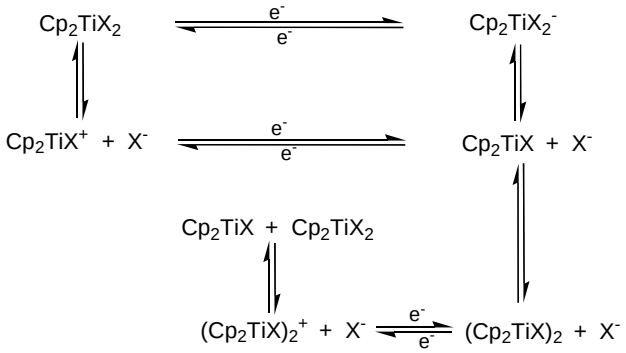

Scheme 2.13 Mesh scheme describing the mechanism for the electrochemical reduction of Cp_2TiX_2.

Solvent studies[186] revealed that T^{IV}/Ti^{III} redox behaviour of Cp_2TiCl_2 is strongly solvent dependent. The following was observed; reversible (*i.e.*, ΔE_p = 90 mV, $i_{pa}/i_{pc} > 0.9$) in THF, quasi-reversible (*i.e.*, ΔE_p = 100 mV, i_{pa}/i_{pc} = ~0.7) in DCM, while irreversible in CH_3CN *i.e.*, ΔE_p = 400 mV, with a small reoxidation peak, strongly shifted to the positive direction, (see **Figure 2.23** and **Table 2.5**).

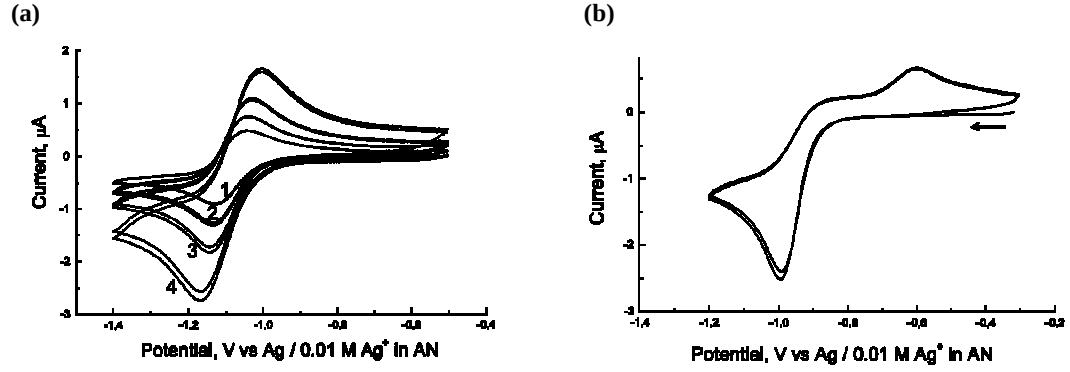

Figure 2.23 Cyclic voltammograms of Cp_2TiCl_2 with supporting electrolyte $[NBu_4][PF_6]$ in: (**a**) THF solution, ν = 50, 100, 200 or 500 mV s^{-1} (curves 1–4) (**b**) CH_3CN solution, scan rate ν = 100 mV s^{-1}.[186]

Table 2.5 Redox potentials in different solvents *vs* Ag/Ag^+ and SCE (Pt electrode and supporting electrolyte 0.2 M $[NBu_4][PF_6]$ of Cp_2TiCl_2, $CpC_5H_4PyTiCl_2$ where $Py=(CH_2)_3NC_4H_4$ and Fc.[186]

Compound	Solvent	$E^{0'}$ *vs* Ag/Ag^+ / mV	$E^{0'}$ *vs* SCE / mV	$E^{0'}$ *vs* Fc/Fc^+ / mV	i_{pa}/i_{pc}	ΔE_p / mV
Cp_2TiCl_2	THF	-1080	-760	-1280	>0.9	90
	DCM	-950	-730	-1160	~0.7	100
	CH_3CN	-800	-470	-900	-	400
$CpC_5H_4PyTiCl_2$	THF	-1120	-790	-1320	~0.8	95
	DCM	-980	-760	-1190	~0.7	115
	CH_3CN	-845	-250	-945	-	425
Fc	THF	200	530	0.00	1.0	100
	DCM	210	430	0.00	1.0	100
	CH_3CN	100	430	0.00	1.0	80

These features can be explained within the framework of the 'square scheme,[187] where the electrochemical reduction step is accompanied by the rapid substitution of one chloride ligand by the solvent molecule (**Scheme 2.14**). In the course of the reverse scan the product (depending on the solvent used) is reoxidised; this process takes place in a quasi-reversible manner in a weakly coordinating media (DCM) while the stronger coordinating solvent (CH_3CN) gives the reduction products which have much more positive oxidation potentials. Several electrochemical studies on Cp_2TiCl_2 in THF, report a reversible system with relatively consistent formal reduction potentials, E^{01} = -1313 mV, -1325 mV,[176] -1280 mV,[186] and -1270 mV[182] *vs* Fc/Fc^+).

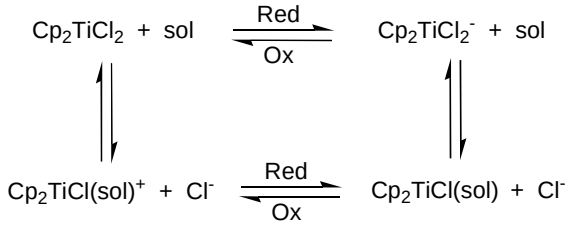

Scheme 2.14 The 'square scheme' illustrating the role of the solvent in the oxidation and reduction of titanocene dichloride.

Cp_2TiQ_2 The electrochemical behaviour of a series of Cp_2TiQ_2 complexes, where Q = R, OAr, $OSiR_3$ and $Cp_2Ti(O,O'Ar)$ were studied in THF with $[NBu_4][PF_6]$ as supporting electrolyte.[188] The reduction potentials, E_{pc}, of the compounds are shown in **Table 2.6**. At high scan rates, i.e., 1000 mV s^{-1}, the reduction is reversible. The reversibility decreases with decreasing scan rate and is only slightly reversible at 25 mV s^{-1}.

Table 2.6 Reduction potentials of Cp_2TiQ_2 complexes, where Q = R, OAr, $OSiR_3$ and Cp_2Ti (O,O'Ar) in THF, potentials were relative to the standard calomel electrode, SCE.[188]

Compound		E_{pc} *vs* SCE / mV
$Cp_2Ti(R)_2$	$Cp_2Ti(Me)_2$	-2007
	$Cp_2Ti(CH_2Ph)_2$	-1860
$Cp_2Ti(OAr)_2$	$Cp_2Ti(OC_6H_3\text{-}3\text{-}Me\text{-}6\text{-}Pr^i)_2$	-1680
	$Cp_2Ti(OC_6H_4\text{-}4\text{-}Me)_2$	-1700
$Cp_2Ti(OSiR_3)_2$	$Cp_2Ti(OSiMePh_2)_2$	-1400
$Cp_2Ti(O,O'Ar)$	Cp_2Ti(biphen)	-1520

It was proposed that the electron reduction transfer, leading to the d^1 Ti^{III} anion was followed by a rapid chemical rearrangement, leading to a neutral monocyclopentadienyl Ti^{III} species, as shown in **Scheme 2.15**. After bulk electrolysis, the CV of the solution did not exhibit the anodic peak corresponding to the $[Cp_2Ti^{III}Q_2]^-$ anion and an anodic peak at about -200 mV (vs SCE) was detected, characteristic of the oxidation of the free cyclopentadienyl anion. This result was consistent with the chemical rearrangement proposed in **Scheme 2.15** and showed that the reduced $[Cp_2Ti^{III}Q_2]^-$ anion species is not chemically stable. In the case of, $[Cp_2Ti(biphen)]$, bearing a bidentate ligand, the reduced anion was found to be more stable, compared to the other $[Cp_2TiQ_2]$ complexes, where Q = monodentate ligands.

$$[Cp_2Ti^{IV}Q_2] \underset{e^-}{\overset{e^-}{\rightleftharpoons}} [Cp_2Ti^{III}Q_2]^- \longrightarrow [CpTi^{III}Q_2] + Cp^-$$

Scheme 2.15 The redox behaviour of Cp_2TiQ_2 complexes, where Q = R, OAr, $OSiR_3$ and Cp_2Ti (O,O'Ar) in THF, showing the Ti^{IV}/Ti^{III} reduction followed by a rapid chemical rearrangement eliminating Cp^-.

$CpTiQ_3$ An analogous series, $CpTiQ_3$, where Q = R, OAr, $OSiR_3$, was studied under the same conditions as above.[188] The reduction of Ti^{IV}/Ti^{III} was followed by a rapid rearrangement leading to the same neutral monocyclopentadienyl Ti^{III} species. In this case the Q ligand was eliminated instead of the Cp ligand (see **Scheme 2.16**). Bulk electrolysis of Cp_2TiQ_2 and $CpTiQ_3$, yielded the same compound (confirmed by e.s.r. studies) and the CV in the case of $CpTiQ_3$, showed no peak for the free cyclopentadienyl anion at *ca* -200 mV.

$$[CpTi^{IV}Q_3] \underset{e^-}{\overset{e^-}{\rightleftharpoons}} [CpTi^{III}Q_3]^- \longrightarrow [CpTi^{III}Q_2] + Q^-$$

Scheme 2.16 The redox behaviour of $CpTiQ_3$ complexes, where Q = R, OAr, $OSiR_3$ in THF, showing the Ti^{IV}/Ti^{III} reduction followed by a rapid chemical rearrangement eliminating Q^-.

2.7.3.2. *d^0* Ti^{IV} cationic complexes

$[Cp_2Ti(\beta)]^+$ Electrochemical studies[189] of a series of cationic dicyclopentadienyl titanium(IV)-β-diketonato complexes, $[Cp_2Ti^{IV}\beta]^+ClO_4^-$ in CH_3CN, established that the reduction $Ti^{IV} \rightarrow Ti^{III}$ process is a chemically and electrochemically reversible one-electron reduction, forming stable reduced species, $[Cp_2Ti^{III}\beta]$. The investigation by Bond *et al.*[67] on the oxidation of titanium(III) compounds, $[Cp_2Ti^{III}(O,O\text{-ligands})]$, in butyronitrile, led to the same redox behaviour; the expected reversible oxidation process at the same formal potentials, $E^{0'}$ = -850 and -870 mV *vs* Fc/Fc^+ for $[Cp_2Ti^{III}\beta]$ where β=acac and ba respectively. A probable reason for this reversible titanium system is that $[Cp_2Ti^{IV}(\beta)]^+$ and $[Cp_2Ti^{III}(\beta)]$ are both stable and structurally isomorphous and hence no structural changes occur during the reduction of Ti^{IV} or oxidation of Ti^{III}.

It was found that the titanium centre was sensitive to the electronic properties of the substituent R-groups of the β-diketonato moiety $(CH_3COCHCOR)^-$, where R = CF_3, OCH_3 C_6H_5 CH_3 and Fc (see **Table 2.7** and **Figure 2.24**). The formal reduction potential of the titanium centre shifted to more cathodic potentials as the R group of the β-diketonato ligand became more electron donating. The difference in $E^{0'}$ was -635 – (-903) = 268 mV. A correlation of $E^{0'}$ *vs* the group electronegativity of the R-group (χ_R), demonstrated that a good communication between the titanium centre and the R-groups of the β-diketonato ligand exits.

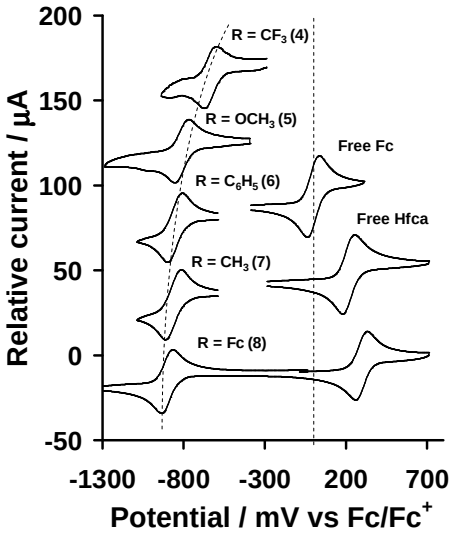

Figure 2.24 Cyclic votammograms of $[Cp_2Ti(CH_3COCHCOR)]^+ClO4^-$, free Fc and free CH_3COCH_2COFc obtained in CH_3CN (0.2 M $[NBu_4][PF_6]$) at a scan rate of 100 mV.[189]

Table 2.7 Cyclic voltammetry data *vs* Fc/Fc^+ for $[Cp_2Ti(CH_3COCHCOR)]^+ClO_4^-$ where R = CF_3, OCH_3, C_6H_5, CH_3, Fc.[189]

Complex	χ_R	$E^{0'}$ / mV	ΔE_p / mV	i_{pa}/i_{pc}
R = CF_3	3.01	-635	78	0.94
R = OCH_3	2.64	-805	78	0.84
R = C_6H_5	2.21	-859	78	0.81
R = CH_3	2.34	-864	84	0.96
R = Fc	1.87	-903	78	0.88

Bond *et al.*,[67] in their study of $[Cp_2Ti^{III}(O,O\text{-ligands})]$ complexes, showed that both the metal and the β-diketonato ligand were electrochemically active. The metal coordinated ligand was irreversibly reduced at potentials between -2930 to -2240 mV *vs* Fc/Fc^+, depending on the ligand, to an extremely unstable radical species, which decomposed to form unidentified species. However, the decomposition of these unstable reduced species could be slowed down at very low temperatures, allowing the ligand reduction of $Cp_2Ti(ba)$ to become chemically reversible at -50 °C in butyronitrile ($E^{0'}$ = -2320 mV). It is interesting to note that the Ti^{III}/Ti^{IV} couple appears to be insensitive to the electronic structure of the selected ligand series (see series below) or the ligands possess similar electron-donor ability, even though the reduction of the coordinated ligand differs by -2930 – (-2240) = 690 mV.

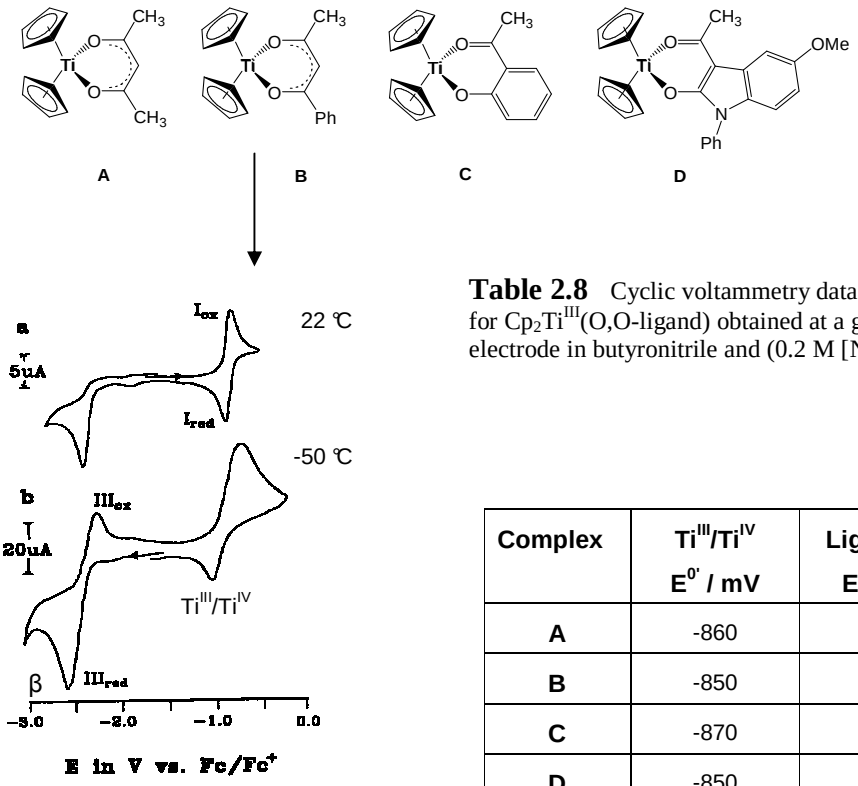

Figure 2.25 **Above**: Cp_2Ti^{III}(O,O-ligand) complexes. **Below**: CV of [Cp_2Ti(ba)] obtained in butyronitrile/ [NBu_4][PF_6]), scan rate of 200 mV s^{-1} at (a) 22˚C and (b) -50˚C. For Ti^{III}/Ti^{IV} couple, $E^{0'}$ = -850 mV while the reduction of the β-diketonato ligand, E_{pc} = -2330 mV.[67]

Table 2.8 Cyclic voltammetry data (vs Fc/Fc^+) for Cp_2Ti^{III}(O,O-ligand) obtained at a glassy carbon electrode in butyronitrile and (0.2 M [NBu_4][PF_6]).[67]

Complex	Ti^{III}/Ti^{IV} $E^{0'}$ / mV	Ligand red E_{pc} / mV
A	-860	-2850
B	-850	-2330
C	-870	-2240
D	-850	-2930

2.7.4 Redox behaviour of Octahedral Ti(IV) Complexes

Ti(O,O-ligand)R_2 Electrochemical studies of oxygen bound octahedral titanium(IV) complexes are often hampered by the instability of complexes in the solvent/electrolyte medium and resulting rapid chemical reactions. Thus reported $Ti^{IV}\rightarrow Ti^{III}$ reduction potentials for these complexes are very limited and inconsistent.[190,191,192]

The electrochemical behaviour of dichlorobis(3-hydroxy-2-methyl-4-pyrone)titanium(IV), $Ti(pyrone)_2Cl_2$, and the alkoxy analogue, $Ti(pyrone)_2OEt_2$, in CH_2Cl_2/[NBu_4][PF_6] were investigated,[190]reversible peaks at cathodic potentials, E_{pc} = -990 and -1000 mV (*vs* SCE) respectively were detected and assigned to the $Ti^{IV}\rightarrow Ti^{III}$ process. For the chloro derivative, other reduction processes were also observed at potentials E_{pc} = -760 and -520 mV on

subsequent scans (voltammograms not shown in article). A dimerisation process, where $Ti(pyrone)_2OEt_2$ was spontaneously converted to the dinuclear, $Ti(pyrone)_2(\mu\text{-}OEt)_2(OEt)_4$, with ligand liberation (**Scheme 2.17**) was observed and monitored electrochemically. The reduction potentials of the monomer (reversible) and dimer (irreversible) were -1000 m V and -1550 mV (*vs* SCE) respectively. The former wave was progressively replaced by the latter one with the addition of a cathodic peak at E_{pc} = -2060 mV *vs* SCE (due to the reduction of the liberated pyrone ligand). The crystal structures of $Ti(pyrone)_2Cl_2$, $Ti(pyrone)_2OEt_2$ and $Ti(pyrone)_2(\mu\text{-}OEt)_2(OEt)_4$ were solved.

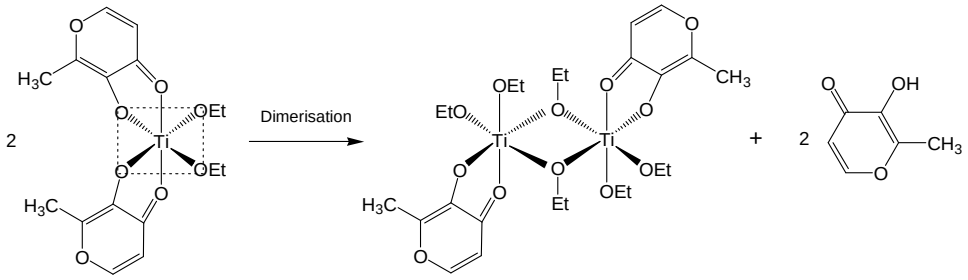

Scheme 2.17 Dimerisation of $Ti(pyrone)_2OEt_2$ to $Ti(pyrone)_2(\mu\text{-}OEt)_2(OEt)_4$.[190]

The electrochemical behaviour of $Ti(pyrone)_2Cl_2$, and the pyrone organic ligand were re-evaluated by Basso *et al.*[191] in $CH_3CN/[NBu_4][PF_4]$, with a very different outcome. The assignment of the detected waves as the reduction of the ligand or of the metal ion was supported by cyclic voltammetry, differential pulse voltammetry and controlled potential electrolysis. The reduction processes, represented through a proposed set of equations, and corresponding cyclic voltammogram are shown in **Figure 2.26**. The reduction processes at -480, -720, -1520, -1900 and -2200 mV (*vs* AgCl) were observed. The reduction wave at -2200 mV is related to the ligand reduction, (the free ligand has a reduction process at -2000 mV), while the redox process at E_{pc} = -480, -720, -1520 and -1900 mV are centred on the metal ion; -480 mV corresponds to the $Ti^{IV/III}$ reduction and -1900 mV is a result of the spontaneous conversion of the initial complex into another species through pyrone ligand release. After electrolysis, the CV illustrated that peaks which were attributed to the reduction process of the metal ions disappeared while a cathodic peak at -2000 mV for the free pyrone ligand appeared. No chlorine ligand substitution was detected.

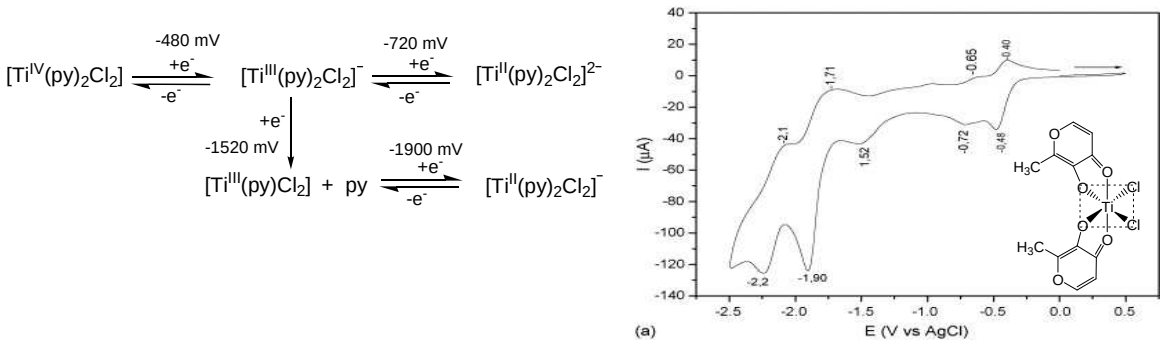

Figure 2.26 **Left**: Proposed set of equations representing the redox process of $Ti(pyrone)_2Cl_2$ and **Right**: the corresponding cyclic voltammogram.[191]

Another titanium(IV) complex with pyrazolonato ligands, i.e., $TiQ_2(OCH_2CH_2CH_3)_2$, Q = (3-methyl-4-neopentylcarbonyl-1-phenylpyrazol-5-onato) was reported to have E_{pc} = -1710 mV (*vs* Fc/Fc^+)[192] for the $Ti^{IV/III}$ reduction.

Studies examining the redox behaviour of Ti^{IV} in tetranuclear oxo-bridged compounds of the form $[Ti(\mu\text{-}O)(O,O\text{-ligand})_2]_4$ (see **Figure 2.27**), indicate irreversible behaviour with E_{pc} = -1940 mV (*vs* SCE) for **A**[190] and reversible behaviour with E_{pc} = -1460 mV (*vs* Fc/Fc^+) for **B**.[192] In both cases all four Ti atoms undergo the same process and are indistinguishable.

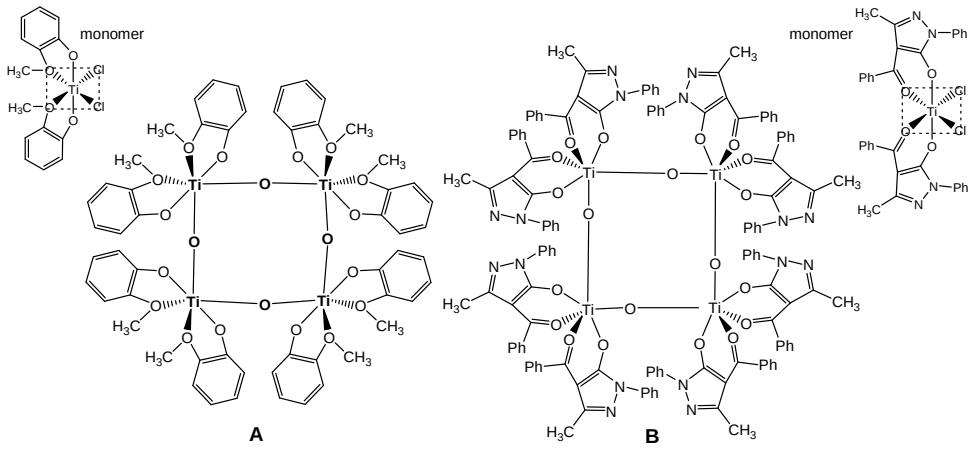

Figure 2.27 Tetranuclear titanium(IV) species of the form $[Ti(\mu\text{-}O)(O,O\text{-ligand})_2]_4$. **A** = $[Ti(\mu\text{-}O)_4$(3-oxy-2-methyl-pyran-4-onato)$_2]_4$ and **B** = $[Ti_2(\mu\text{-}O)_4$(4-benzoyl-3-methyl-1-phenylpyrazol-5-onato)$_2]_4$. The spacial arrangement of the ligands are not accurately represented.

[1] C.A. McAuliffe and D.S. Barratt in *Comprehensive Coordination Chemistry*, G Wilkinson, R.D. Gillard and J.A. McCleverty, Eds., Pergamon, Oxford, **vol 3** (1987) pp 323–360.
[2] M.A. Hunter, *J. Am. Chem. Soc*., **32** (1910) 330.
[3] A.E. van Arkel and J.H. de Boer, *Z. Anorg. Allg. Chem*., **148** (1925) 345.
[4] W. Kroll, *Trans. Electrochem. Soc*., **78** (1940) 35. (b) W. Kroll, *J. Less-Commom Met*. **8** (1965) 361.
[5] R.J.H. Clark, *The chemistry of Titanium and Vanadium*, Elsevier, Amsterdam, (1968).
[6] J. Bordner, P.D. Hammen and E.B. Whipple, J. Am. Chem. Soc., **111** (1989) 6572.
[7] (a) M. Calvin and K.W. Wilson, *J. Am. Chem. Soc.,* **67** (1945) 2003. (b) R.H. Holm and F.A. Cotton, *J. Am. Chem. Soc.,* **80** (1958) 5658.
[8] (a) S. Kawaguchi, *Coord. Chem. Rev.*, **70** (1986) 51. (b) S. Kawaguchi, *Variety in Coordination of Ligands in Metal Complexes: Inorganic Concepts*, S. Kawaguchi, Ed., Springer Verlag, Berlin, **vol. 11** (1988) pp 79–119.
[9] G. Gilli and V. Bertolasi in *The chemistry of enols*, Z. Rappoport, Ed., John Wiley & Sons Ltd., England, (1990) pp 714-764.
[10] (a) A. Gero, *J. Org. Chem.,* **19** (1954) 469. (b) A. Gero, *J. Org. Chem.,* **20**, (1955) 960. (c) R.P. Bell and G.G. Davis., *J. Chem. Soc.,* (1965) 353.
[11] M. Moriyasu, A. Kato and Y. Hashimoto, *J. Chem. Soc., Perkin Trans.* **2** (1986) 515.
[12] (a) R.D. Campbell and H.M. Gilow, *J. Am. Chem. Soc.,* **84** (1962) 1440. (b) A.S.N. Murthy, A. Balasubramanian, C.N.R. Rao and T.R. Kasturi, *Can. J. Chem.,* **40** (1962) 2267. (c) J.U. Lowe and L.N. Ferguson, *J. Org. Chem.,* **30** (1965) 3000.
[13] (a) A. Yogev and Y. Mazur, *J. Org. Chem.*, **32**, (1967) 2162. (b) S.G. Mills and P. Beak, *J. Org. Chem.,* **50** (1985) 1216.
[14] J.L. Burdett and M.T. Rogers, *J. Am. Chem. Soc*., **86** (1964) 2105.
[15] (a) J.U. Lowe and L.N. Ferguson, *J. Org. Chem.*, **30** (1965) 3000. (b) A. Yogev and Y. Mazur, *J. Org. Chem.*, **32** (1967) 2162. (c) S.G. Mills and P.J. Beak, *J. Org. Chem.*, **50** (1985) 1216. (d) D.J. Sarella, D.H. Heinert and B.L. Shapiro, *J. Org. Chem.,* **34** (1969) 2817. (e) J.N. Spencer, E.S. Holmboe, M.R. Kirshenbaum, D.W. Firth and P.B. Pinto, *Can. J. Chem.*, **60** (1982) 1178. (f) P. Battesti, O. Battesti and M. Selim, *Bull. Soc. Chim. Fr.,* (1974) 2214. (g) G. Klose, P. Thomas, E. Uhlemann and J. Mark, *Tetrahedron*, **22**, (1966) 2695. (h) N.N. Shapet'ko, S.S. Berestova, G.M. Lukovkin and Y.S. Bogachev, *Org. Mag. Res.*, **7** (1975) 237. (i) G. Gorodetshy, Z. Luz and Y. Mazur, *J. Am. Chem. Soc.*, **89** (1967) 1183. (j) D.C. Nonhebel, *Tetrahedron*, **24** (1968) 1869. (k) D. Isaazson and K.J. Morokuma, *J. Am. Chem. Soc.*, **102 (**1975) 4453.
[16] (a) H. Jarret, M. Sadler and J. Shoolery, *J. Chem. Phys.,* **21** (1953) 2092. (b) L. Reeves, *Can. J. Chem.,* **35** (1957) 1351.
[17] R.L. Lindtvedt and H.F. Holtzclaw Jr, *J. Am. Chem. Soc.*, **88** (1966) 2713.
[18] S. Moon and Y. Kwon, *Magn. Reson. Chem*., **39** (2001) 89.
[19] M. Moriyasu, A. Kato and Y. Hashimoto, *J. Chem. Soc., Perkin Trans*., **2** (1986) 515.
[20] W.C. du Plessis, W.L. Davis, S.J. Cronje and J.C. Swarts, *Inorg. Chim. Acta*, **314** (2001) 97.
[21] A. Yogev and Y. Mazur, *J. Org. Chem*., **32** (1967) 2162.
[22] J. Toullec in *The chemistry of enols*, Z. Rappoport, (Ed.), John Wiley & Sons Ltd., England, (1990) pp 323-398.
[23] C.F.G.C. Geraldes, M.T. Barros, C.D.Maycock and M.I. Silva, *J. Mol. Struct.*, **238** (1990) 335.
[24] W.C. du Plessis, T.G. Vosloo and J.C. Swarts, *J. Chem. Soc., Dalton Trans.*, (1998) 2507.
[25] M.R. Jaffe, D.P. Fay, M. Scefola and N. Sutin, *J. Am. Chem. Soc*., **93** (1971) 2878.
[26] W.C. (Ina) du Plessis, W.L. Davis, S.J. Cronje and J.C. Swarts, *Inorg. Chim. Acta*, **314** (2001) 97.
[27] D.E. Williams, W.L. Dumke and R.E. Rundle, *Acta Cryst*., **15** (1962) 267.
[28] R.D.G. Jones, *Acta Cryst*., **B32** (1976) 2133.
[29] L.A.M. Baxter, A.J. Blake, G.A. Heath and T.A.Stephenson, *Acta Cryst*., **C46** (1990) 508.
[30] A. Camerman, D. Mastropaolo and N. Camerman, *J. Am Chem Soc*., **105** (1983) 1584.
[31] S. Wang, Z. Pang, K.D.L. Smith, Y. Hua, C. Deslippe and M.J. Wanger, *Inorg. Chem*., **34** (1995) 908.
[32] K.Kato, *Acta Cryst*., **B27** (1971) 2028.
[33] M.M. Conradie, A.J. Muller and J. Conradie, *S. Afr. J. Chem*., **61** (2008) 13.
[34] R.D.G. Jones, *Acta Cryst*., **B32** (1976) 1224.
[35] W. Bell, J.A. Crayston, C. Glidewell, M.A. Mazid and B. Hursthouse, *J. Organomet. Chem*., **434** (1992) 115.
[36] W.C. du Plessis, J.J.C. Erasmus, G.J. Lamprecht, J. Conradie, T.S. Cameron, M.A.S. Aquino and J.C. Swarts, *Can. J. Chem*., **77** (1999) 378.
[37] M.C. Etter, D.A. Jahn and Z. Urbañczyk-Lipkowska, *Acta Cryst*., **C43** (1987) 260.
[38] (a) R.D.G. Jones, *Acta Cryst*., **B32** (1976) 1807. (b) D.E. Williams, *Acta Cryst*., **21** (1966) 340. (c) F.J. Hollander, D.H. Templeton and A. Zalkin, *Acta Cryst*., **B29** (1973) 1552.
[39] R.C. Mehrotra, R. Bohra and D.P. Gaur, *Metal β-betadiketonates and Allied Derivatives*, Academic Press, New York, (1978) pp 10-16.

[40] C.R. Hauser, F.W. Swamer and J.T. Adams, in *Organic reactions*, (R. Adams *et al*., eds.) John Wiley & Sons, **vol 8** (1954) p 59.
[41] (a) R. Levine, J.A. Conroy, J.T. Adams and C.R. House, *J. Am. Chem. Soc*., **67** (1945) 1510. (b) D.F. Martin, M. Shamma and W.E. Ferrielius, *J. Am. Chem. Soc*., **80** (1958) 4891. (c) D.F. Martin, M. Shamma and W.E.Ferrielius, *J. Am. Chem. Soc*., **80**, (1958) 5851. (d) J.J. Bloomfield, *J. Org. Chem*., **27** (1962) 2742. (e) A.I. Vogel, *Practical Organic Chemistry*, 5th Ed., Longman Scientific & Technical, London (1989) p. 632.
[42] C.R. Hauser, F.W. Swamer and J.T. Adams, in *Organic reactions*, (R. Adams *et al*., eds.) John Wiley & Sons, **vol 8** (1954) pp. 111-114.
[43] C.R. Hauser, F.W. Swamer and J.T. Adams, in *Organic reactions*, (R. Adams *et al*., eds.) John Wiley & Sons, **vol. 8** (1954), pp. 65.
[44] A.T. Nielson and W.J. Houlihan, *Organic reactions*, Robert E. Krieger Publishing Company, Huntington, New York, **vol 16** (1975) pp 20.
[45] R.T. Morrison and R.N. Boyd, *Organic Chemistry*, Allyn and Bacon Inc. 1987, 5th edition, pp. 922.
[46] B.V. Bhide and J. Suchborough, *Indian Inst. Science*, **8A** (1925) 89.
[47] C.R. Hause, R. Levine and R.F. Kibler, *J. Am. Chem. Soc.*, **68** (1946) 26.
[48] W.R. Cullen and E.B. Wickenheiser, *J. Organomet. Chem.*, **370** (1989) 141.
[49] P. Mushak, M.T. Glenn and J. Savory, *Fluorine Chem. Rev.*, **6** (1973) 43.
[50] A. Chauvin, F. Gumy, I. Matsubayashi, Y. Hasegawa and J.G. Bünzli, *Eur. J. Inorg. Chem.*, (2006) 473.
[51] K.I. Pashkevich, V.I. Saloutin, I.Y.A. Postovskii, *Russ. Chem. Rev*. **50** (1981) 325.
[52] J.D. Park, H.A. Brown and J.R. Lacher, *J. Am. Chem. Soc.*, **75** (1953) 4753.
[53] H. Henecka, *Chem. Ber*., **81** (1948) 189.
[54] M. Ellinger, H. Duschner and K. Starke, *J. Inorg. Nucl. Chem*., **40** (1978) 1063.
[55] B.G. Schultz and E.M. Larsen, *J. Am. Chem. Soc.*, **71** (1949) 3250.
[56] J.C. Reid and M. Calvin, *J. Am. Chem. Soc*. **72** (1950) 2948.
[57] L.B. Barkley and R. Levine, *J. Am. Chem. Soc*., **73** (1953) 2059.
[58] (a) Yu Chen, Y. Yekta and A.K. Yudin, *Chem. Rev*., **103** (2003) 3155. (b) P. Kočovský, Š. Vyskočil and M. Smrčina, *Chem. Rev*., **103** (2003) 3213. (c) J. Balsells, T.J. Davis, P. Carroll and P.J. Walsh, *J. Am. Chem. Soc*., **124** (2002) 10336. (d) A. van der Linden, C.J. Schaverien, N. Meijboom, C. Ganter and A.G. Orpen, *J. Am. Chem. Soc*., **117** (1995) 3008. (e) D. Kitamoto, H. Imma and T. Nakai, *Tetrahedron Letters*, **36** (1995) 1861. (f) T.J. Boyle, D.L. Barnes, J.A. Heppert, L. Morales, F. Takusagawa and J.W. Connolly, *Organometallics* **11** (1992) 1113. (g) M. Barthel, D. Dini, S. Vagin and M. Hanack, *Eur. J. Org. Chem.*, (2002) 3756. (h) N. Kobayashi, A. Muranaka and K. Ishii, *Inorg. Chem*., **39** (2000) 2256. (i) S.N. Brown, E.T. Chu, M.W. Hull and B.C. Noll, *J. Am. Chem. Soc*., **127** (2005) 16010. (j) P.V. Rao, C.P. Rao, E.K. Wegelius, E. Kolehmainen and K. Rissanen, *J. Chem. Soc., Dalton Trans*., (1999) 4469. (k) K. Andrä, *J. Organomet. Chem*., **11** (1968) 567.
[59] C.J. Ballhausen and J.P. Dahl, *Acta Chem. Scand*., **15** (1961) 1333.
[60] N.W. Allcock, *J. Chem. Soc*., *A* (1967) 2001.
[61] (a) A. Clearfield, D.K. Warner, C.H. Saldarriaga-Molina, R. Ropal and I. Bernal, *Can. J. Chem*., **53** (1975) 1622. (b) H. Köpf and P. Köpf-Maier, *Aangew. Chem. Int. Ed. Engl*., **18** (1979) 477.
[62] (a) E. Manek, D. Hinz and G. Meyer, *Coord. Chem. Rev.*, **16**4 (1997) 5. (b) J.C. Vites and M. Lynam, *Coord. Chem. Rev.*, **138** (1995) 71. (c) J.R. Uffod and N. Serpone, *Coord. Chem. Rev*., **57** (1984) 301. (d) N. Serpone, M.A. Jamieson, F. iSalvio, P.A. Takats, L. Yeretsian and J.R. Ufford, *Coord. Chem. Rev*., **58** (1984) 87. (e) R.C. Fay, *Coordination Chemistry Reviews*, **45** (1982) 9.
[63] (a) K. Döppert, *J. Organomet. Chem.*, **178** (1979), C3. (b) Y.L. Page, *J. Organomet. Chem.*, **193** (1980) 201. (c) U. Thewalt and G. Schleussner, *Aangew. Chem.*, **90** (1978) 559. (d) H. Köpf, S. Grabowski and R. Voigtlander, *J. Organomet. Chem*., **216** (1981) 185.
[64] J.H. Toney and T.J. Marks, *J. Am. Chem. Soc.*, **107** (1985) 947.
[65] G. Doyle and R.S. Tobias, *Inorg. Chem.*, **6** (1967) 1111.
[66] (a) N.V. Alekseev and I.A. Ronova, *Zh. Strukt. Khim.*, **7** (1966) 103. (b) S.A. Giddings and R.J. Best, *J. Amer. Chem. Soc*., **83** (1961) 2393. (c) I.A. Ronova and N.V. Alekseev, *Dokl. Akad. Nauk. SSSR*, **174** (1967) 614. (d) V.V. Tkachev and L.O. Atovmyan, *Zh. Strukt. Khim*., **13** (1972) 287. (e) A. Clearfield, D.K. Warner, C.H. Saldarriaga-Molina, R. Ropal and I. Bernal, *Can. J. Chem*. **53** (1975) 1622.
[67] A.M. Bond, R. Colton, U. Englert, H. Hűgel and F. Merken, *Inorg. Chim. Acta*, **235** (1995) 117.
[68] G. Doyle and R.S. Tobias, *Inorg. Chem.*, **7** (1968) 2484.
[69] D.A. White, *J. Inorg. Nucl. Chem*., **33** (1971) 691.
[70] K. Andrä, *J. Organomet. Chem*., **11** (1968) 567.
[71] B.S. Kalirai, J-D. Foulon, T.A. Hamor, C.J. Jones, P.D. Beer and S.P. Fricker, *Polyhedron*, **10** (1991) 1847.
[72] M.G. Meirim, E.W. Neuse, M. Rhemtula and S. Schmitt, *Trans. Met. Chem.*, **13** (1988) 272.
[73] P.C. Bharara, *J. Organomet. Chem*., **121** (1976) 199.

[74] A.N. Nesmeyanov, O.V. Nogina, A.M. Berlin, A.S. Gershovich and G.V. Shatalov, *Izv. Akad. Nauk. SSSR*, (1961) 2146.
[75] M.J. Frazer and W.E. Newton, *Inorg. Chem*., **10** (1971) 2137.
[76] (a) R.C. Fay and R.N. Lowry, *Inorg. Chem*. ***6*** (1967) 1512. (b) N. Serpone and R.C. Fay, *Inorg. Chem*. ***6*** (1967) 1835. (c) D.W. Thompson, W.A.Somers and M.O. Workman, *Inorg. Chem*. **9** (1970) 1252. (d) R.C. Fay and R.N. Lowry, *Inorg. Chem*. **9** (1970) 2048. (e) R.C. Fay and R.N. Lowry, *Inorg. Chem*. **13** (1974) 1309. (f) A.F. Linmark and R.C. Fay, *Inorg. Chem*. **14** (1975) 282. (g) D.G. Bickley and N. Serpone, *Inorg. Chim. Acta*, **25** (1977) L139. (h) C.A. Wilkie, G.-Y. Lin and D.T. Haworth, *J.Inorg. Nucl. Chem*., **40** (1978) 1009. (i) D.G. Bickley and N. Serpone, *Inorg. Chim. Acta*, **28** (1978) 169. (j) D.G. Bickley and N. Serpone, *Inorg. Chim. Acta*, **38** (1980) 177. (k)) D.G. Bickley and N. Serpone, *Inorg. Chim. Acta*, **40** (1980) 213. (l)) D.G. Bickley and N. Serpone, *Inorg. Chim. Acta*, **43** (1980) 185.
[77] A.F. Linmark and R.C. Fay, *Inorg. Chem*. **14** (1975) 282.
[78] (a) D.C. Bradley and C.E. Holloway, *Chem. Commun*., (1965) 284. (b) D.C. Bradley and C.E. Holloway, *J. Chem. Soc. A*, (1969) 282. (c) J.F. Harrod and K. Taylor, *J. Chem. Soc*., *Chem Commun*. (1971) 696. (d) N. Baggett, D.S.P. Poolton and W.B. Jennings, *J. Chem. Soc*., *Chem Commun*. (1975) 239. (e) N. Baggett, D.S.P. Poolton and W.B. Jennings, *J. Chem. Soc*., *Dalton Trans*. (1979) 1128. (f) R.C. Fay and A.F. Linmark, *J. Am. Chem. Soc*., **97** (1975) 5928. (g) P. Finocchiaro, *J. Am. Chem. Soc*., **97** (1975) 4443. (h) N. Serpone and D.G. Bickley, *Inorg. Chim. Acta*, **32** (1979) 217. (h) D.G. Bickley and N. Serpone, *Inorg. Chem.*, **18** (1979) 2200. (i) N. Serpone and D.G. Bickley, *Inorg. Chim. Acta*, **57** (1982) 211.
[79] R.C. Fay and R.N. Lowry, *Inorg. Chem*., **9** (1970) 2048).
[80] T.J. Pinnavaia, L.J. Matienzo and Y.A. Peters, *Inorg. Chem*., **9** (1970) 994.
[81] R.C. Fay and A.F. Lindmark, *J. Am. Chem. Soc*., **105** (1983) 2118.
[82] (a) F.A. Cotton and R.H. Holm, *J. Amer. Chem. Soc*., **80** (1958) 5658. (b) D.W. Barnum, *J. Inorg. Nuclear Chem*., **21** (1961) 221. (c) D.W. Barnum, *J. Inorg. Nuclear Chem*., **22** (1961) 183. (d) A. Forman, J.N. Murrel and L.E. Orgel, *J. Chem. Phys*., **31** (1959) 1129. (e) R.E. Hester, *Chem. anal. Ind*. (1963) 1397.
[83] M. Calvin and K.W. Wilson, *J. Amer. Chem. Soc*., **67** (1945) 2003.
[84] (a) J.P. Collman, *Angew. Chem*., **77** (1966) 154. (b) R.F. Martell and M. Calvin, *Die Chemie der Metallverbindungen Verlag Chemie Weinheim* (1958). (c) E Bayer, *Angew. Chem*., **3** (1964) 325. (d) E. Bayer, *Angew. Chem*., **76** (1964) 76.
[85] B.K. Keppler and M.E. Heim, *Drugs of the Future*, **3** (1998) 638.
[86] R.C. Fay and R.N. Lowry, *Inorg. Chem*., **6** (1967) 1512.
[87] (a) M. Elder, J.G. Evans and W.A.G. Graham, *J. Am. Chem. Soc*., **91** (1969) 1245. (b) J.J. Howe and T.J. Pinnavaia, *J. Am. Chem. Soc*., **92** (1970) 7342.
[88] D.N. Sen and U.N. Kantak, *J. Indian Chem. Soc*., **46** (1969) 358.
[89] S.N. Brown, E.T. Chu, M.W. Hull and B.C. Noll, *J. Am. Chem. Soc*., **127** (2005) 16010.
[90] P.V. Rao, C.P. Rao, E.K. Wegelius, E. Kolehmainen and K. Rissanen, *J. Chem. Soc., Dalton Trans*., (1999) 4469.
[91] Cambridge Structural Database (CSD), January 2007 update.
[92] M. Casado, J.J. Perez-Torrente, M.A. Ciriano, A.J. Edwards, F.J. Lahoz and L.A. Oro, *Organometallics*, **18** (1999) 5299. CSD Ref.: LIHDUB.
[93] L-C. Song, P-C. Liu, C Han and Q-M. Hu, *J. Organomet. Chem.*, **648** (2002) 119. CSD Ref.: MUQLAL.
[94] K. Doppert, R. Sanchez-Delgado, H-P. Klein and U. Thewalt, *J. Organomet. Chem*., **233** (1982) 205. CSD Ref.: BIMPOC.
[95] D.A. Edwards, M.F. Mahon, T.J. Paget and N.W. Summerhill, *Transition Met. Chem*., **26** (2001) 116. CSD Ref.: HUFKO1.
[96] Z. Gao, C. Zhang, M. Dong, L.Gao, G. Zhang, Z. Liu, G.Wang and D. Wu, *Appl. Organomet. Chem*., **20** (2006) 117. CSD Ref.: MEDTOF
[97] H. Gritzo, F. Schaper and H-H. Brintzinger, Private Communication (2004) CSD Ref.: ISAQAU.
[98] H. Gritzo, U. Wieser and H-H. Brintzinger, Private Communication (2004) CSD Ref.: ISANEV.
[99] H. Gritzo, F. Schaper and H-H. Brintzinger, Private Communication (2004) CSD Ref.: ISAPUN.
[100] B.S. Kalirai, J-D. Foulon, T.A. Hamor, C.J. Jones, P.D. Beer and S.P. Fricker, *Polyhedron*, **10** (1991) 1847. CSD Ref.: JOBCIM.
[101] H. Gritzo, F. Schaper and H-H. Brintzinger, Private communication (2004). CSD Ref.: ISANUL.
[102] Yang Qingchuan, Jin Xianglin, Xu Xiaojie, Li Genpei, Tang Youqi and Chen Shoushan, *Sci Sin. Ser. B (Engl. Ed.)* **25** (1982) 356. CSD Ref.: BIWMID.
[103] D.H. Gibson, Yan Ding, J.F. Richardson and M.S. Mashuta, *Acta Crystallogr. Sect. C. Cryst. Struct. Commun*. **52** (1996) 1614. CSD Ref.: WIRFIM.

[104] L.I. Strunkina, M.K. Minacheva, K.A. Lyssenko, Z.S. Klemenkova, A.Yu. Volkonsky, P.V. Petrovskii, V.V. Burlakov and V.B. Shur, *Izv. Akad. Nauk. SSSR Ser. Khim. (Russ.)(Russ. Chem. Bull.*) (2003) 1299. CSD Ref.: KIDLOY01.
[105] D.A. Edwards, M.F. Mahon and T.J. Paget, *Polyhedron* **16** (1997) 25. CSD Ref.: REXBIF.
[106] K. Doppert, H-P. Klein and U. Thewalt, *J. Organomet. Chem.*, **303** (1986) 205. CSD Ref.: BUSNAEO1.
[107] T.S. Kuntsevich, E.A. Gladkikh, V.A. Lebedev, A.N. Lineva and N.V. Belov, *Kristallografiya (Russ.) (Crystallogr. Rep.)*, **21** (1976) 80. CSD Ref.: CPNBTI10.
[108] B. Bracke, Y. Dong, A.T. Lenstra and H.J. Geise, *Acta Crystallogr. Sect. C. Cryst. Struct. Commun.*, **47** (1991) 2043. CSD Ref.: TAZYIC.
[109] Zhi-Qiang Wang, Shi-Wei Lu, He-Fu Guo, Qiang-Jin Wu and Jian-Qiu Shi, *Jiegou Huaxue (Chin.) (Chineses J. Struct. Chem.*), **11** (1992) 130. CSD Ref.: VOYPOO.
[110] A. Clearfield, D.K. Warner, C.H. Saldarriaga-Molina. R. Ropal and I. Bernal, *Can. J. Chem.*, **53** (1975) 1622. CSD Ref.: CDCPTI01.
[111] A. Haaland and J. Nilsson, J. Chem. Soc. Chem. Commun., 88 (1968)
[112] A.M. Bond, R. Colton, U. Englert, H. Hűgel and F. Merken, *Inorg. Chim. Acta*, **235** (1995) 117. CSD Ref.: HIDPOZ.
[113] S.S. Yun, I-H. Suh, E.H. Kim and S.K. Lee, *J. Coord. Chem.*, **51** (2000) 219. CSD Ref.: MOYJEP
[114] S.S. Yun, I-H. Suh, E.H. Kim and S.K. Lee, *J. Coord. Chem.*, **51** (2000) 219. CSD Ref.: MOYJIT
[115] J.K. Park, J.J. Myoung, J.B. Kyong and H.K. Kim, *Bull. Korean Chem. Soc.*, **24** (2003) 671.
[116] E. Dubler, R. Buschmann and H.W. Schmalle, *J. Inorg. Biochem.*, **95** (2003) 97. CSD Ref.: JABYAN.
[117] K. Matilainen, I. Mutikainen and M. Leskela, *Acta Chem. Scand.*, **50** (1996) 755. CSD Ref.: TOPZUT.
[118] C. Glidewell, G.M. Turner and G. Ferguson, *Acta Crystallogr. Sect. C. Cryst. Struct. Commum.*, 52 (1996) 11. CSD Ref.: ZITROJ.
[119] E. Dubler, R. Buschmann and H.W. Schmalle, *J. Inorg. Biochem.*, **95** (2003) 97. CSD Ref.: JABXUG.
[120] U. Schubert, H. Buhler and B. Hirle, *Chem. Ber.*, **125** (1992) 999. CSD Ref.: VUGPES.
[121] W. Oehlschläger, PhD. Thesis, University of Utrecht, Utrecht, 1997. Referenced by E. Dubler, R. Buschmann and H.W. Schmalle, *J. Inorg. Biochem.*, **95** (2003) 97.
[122] J.L. Wang, F.M. Miao, X. J. Fan, X. Feng and J.T. Wang, *Acta Crystallogr. Sect. C. Cryst. Struct. Commun.*, **46** (1990) 1633. CSD Ref.: SICROL.
[123] P.H. Bird, A.R. Fraser and C.F. Lau, *Inorg. Chem.*, **12** (1973) 1322. CSD Ref.: ACIPTI.
[124] S.N. Brown, E.J. Chu, M.W. Hull and B.C. Noll, *J. Am. Chem. Soc.*, **127** (2005) 16010. CSD Ref.: RAWWES.
[125] S.N. Brown, E.J. Chu, M.W. Hull and B.C. Noll, *J. Am. Chem. Soc.*, **127** (2005) 16010. CSD Ref.: RAWWIW.
[126] P.V. Rao, C.P. Rao, E.K. Wegelius, E. Kolemainen and K. Rissanen, *J. Chem. Soc. Dalton Trans.*, (1999) 4469. CSD Ref.: HOXTIX.
[127] (a) G.D. Smith, C.N. Caughlan and J.A. Campbell, *Inorg. Chem.*, **11** (1972) 2989. (b) M. Pathak, R. Bohra, R.C. Mehrotra, I-P. Lorenz and H. Piotrowski, *Transition Met. Chem.*, **28** (2003) 187.
[128] (a) K. Watenpaugh and C.N. Caughlan, *Inorg. Chem.*, **6** (1967) 963. (b) Z. Quan-Fa, M. Fang-Ming and L. Xiao-Lao, *Jiegou Huaxue (Chin.) (Chinese J. Struct. Chem.)*,**11** (1992) 453.
[129] G.D. Smith, C.N. Caughlan and J.A. Campbell, *Inorg. Chem.*, **11** (1972) 2989. CSD Ref. OXACTI.
[130] K. Watenpaugh and C.N. Caughlan, *Inorg. Chem.*, **6** (1967) 963. CSD Ref. .
[131] Cambridge Structural Database (CSD), July 2003 update.
[132] F.H. Allen, *Acta Cryst.*, B**58**, (2002) 380.
[133] T. Kemmitt, G.J. Gainsford and N.I. Al-Salim, *Crystal Struct. Commun.*, **60** (2004) 42.
[134] T.J. Boyle, T.M. Alam, E.R. Mechenbier, B.L. Scott and J.W. Ziller, *Inorg. Chem.*, **36** (1997) 3293.
[135] S.I. Troyanov and O. Yu Gorbenko, *Polyhedron*, **16** (1997) 777. CSD Ref. RONBUR.
[136] P. Sobota, K. Przybylak, J. Utko, L.B. Jerzykiewicz, A.J.L. Pombeiro, M.F.C. Guedes da Silva and K. Szczegot, *Chem. Eur. J.*, **7** (2001) 951. CSD Ref.
[137] F. Caruso, L. Massa, A. Gindulyte, C. Pettinari, F. Marchetti, R. Pettinari, M. Ricciutelli, J. Costamagna, J.C. Canales, J. Tanski and M. Rossi, *Eur. J. Inorg. Chem.*, (2003) 3221. CDS Ref. VIMQIR.
[138] W.L. Jorgensen and D.L. Severance, *J. Am. Chem. Soc.*, **112** (1990) 4768.
[139] F.A. Cotton, G. Wilkinson and P.L. Gaus, *Basic Inorganic Chemistry*, 2nd Ed., John Wiley& Sons, New York (1987) pp 260.
[140] F.A. Cotton, G. Wilkinson and P.L. Gaus, *Basic Inorganic Chemistry*, 2nd Ed., John Wiley& Sons, New York (1987) pp 258.
[141] G.R. Desiraju, *Acc. Chem. Res.*, **29** (1996) 441; T. Steiner, *Crystallogr. Rev.*, **6** (1996) 1; T. Steiner, *Chem. Commun.*, (1997) 727; G.R. Desiraju and T. Steiner, *The weak Hydrogen Bond in Structural Chemistry and Biology*, Oxford University Press (1999).

[142] Review on C−H···π interactions: (a) M. Nishio, M. Hirota and Y. Umezawa, *The CH/π Interactions (Evidence, Nature and Consequences)*, Wiley-VCH, New York, 1998. (b) Y. Umezawa, S. Tsuboyama, K. Honda, J. Uzawa and M.Nishio, *Bull. Chem. Soc. Jpn*., **71** (1998) 1207. (c) M.J. Calhorda, *Chem. Commun*., (2000) 801. (d) G.R. Desiraju and T. Steiner, *The Weak Hydrogen Bond*, (IUCr Monograph on Crystallography 9), Oxford Science Publ., 1999.
[143] (a) C. Janiak, *J. Chem. Soc., Dalton Trans*., (2000) 3885. (b) G.B. McGaughey, M. Gagné and A.K. Rappé, *J. Bio. Chem*., **273** (1998) 15458.
[144] (a) P. Hobza, H.L. Selzle and E.W. Schlag, *J. Am. Chem. Soc*., **116** (1994) 3500. (b) S. Tsuzuki, T. Uchimaru, M. Mikami and K. Tanabe, *Chem. Phys. Lett*., **252** (1996) 206. (c) R.L. Jaffe and G.D. *Smith, J. Chem. Phys*., **105** (1996) 2780. (d) C. Chipot, R. Jaffe, B. Maigret, D.A. Pearlman and P.A. Kollman, *J. Am. Chem. Soc*., **118** (1996) 11217. (e) P. Hobza, H.L. Selzle and E.W. Schlag, *J. Phys. Chem*., **100** (1996) 18790.
[145] K.F. Purcell and J.C. Kotz, *Inorganic Chemistry*, Holt-Sanders International Ed., Japan (1977) pp 359.
[146] B. Stevens, *Chemical Kinetics*, London, Chapman & Hall (1965) pp 48.
[147] M.L.Tobe and J. Burgess, *Inorganic Reaction Mechanisms*, Addison Wesley Longman, New York (1999) pp 130.
[148] J. Burgess, and S.A. Parsons, *Applied Organomet. Chem.,* **7**(1993) 345.
[149] R. Fay and R.N. Lowry, *Inorg. Chem*., **13** (1974) 1309.
[150] (a) H. Weingarten and J.R. Van Wazer, *J. Amer. Chem. Soc.*, **87** (1965) 724, (b) K. Moedritzer and J.R. van Wazer, *Inorg. Chem*., **3** (1964) 268.
[151] (a) A.C. Adams and E.M. Larsen, *Inorg. Chem*., **5** (1966) 228. (b) T.J. Pinnavaia and R.C. Fay, *Inorg. Chem*., **5** (1966) 233. (c) T.J. Pinnavaia, M.T. Mocella, B.A. Averill and J.T. Woodward, *Inorg. Chem*., **12** (1973) 763. (d) J.J. Fortman and R.E. Sievers, *Inorg. Chem*., **6** (1967) 2022. (e) T.J. Pinnavaia and S.O. Nweke, *Inorg. Chem*., **8** (1969) 639. (f) F.A. Cotton, P. Legzdins and S.J. Lippard, *J. Chem. Phys.*, **45** (1966) 3461. (g) N. Serpone and R. Ishayek, *Inorg. Chem*., **10** (1971) 2650.
[152] P.T. Kissinger and W.R. Heineman, *J. Chem. Educ.*, **60** (1983) 702.
[153] D.H. Evans, K.M. O'Connell, R.A. Peterson and M.J. Kelly, *J. Chem. Educ.*, **60** (1983) 290.
[154] G.A. Mobbot, *J. Chem. Educ.*, **60** (1983) 697.
[155] A.J. Bard and L.R. Faulknaer, *Electrochemical Methods: Fundamentals and Applications*, Wiley, New York, (1980), chapter 6.
[156] P.A. Christensen and A. Hamnett, *Techniques and Mechanisms in Electrochemistry*, Blackie Academic & Professional, London, (1994) pp. 55-67, 170-175.
[157] P.T. Kissinger and W.R. Heineman, *Laboratory Techniques in Electroanalytical Chemistry*, Dekker, New York, (1984) pp 39-43.
[158] P.T. Kissinger and W.R. Heineman, *Laboratory Techniques in Electroanalytical Chemistry*, Dekker, New York, (1984) pp 469-485.
[159] J.J. Van Benschoten, J.Y. Lewis, W.R. Heineman, D.A. Roston and P.T. Kissinger, *J. Chem. Educ.*, **60** (1983), 772.
[160] L. Pospisil, B.T. King and J. Michl, *Electrochim. Acta,* **44** (1998) 103.
[161] R.J. Le Suer and W.E. Geiger, *Aangew. Chem., Int. Ed. Engl.,* **39** (2000) 248.
[162] W.J. Moore, *Physical Chemistry*, 4th Ed, Longman Group Limited, (1972) pp 333-334.
[163] R.R. Gagné, C.A. Koval and G.C. Lisensky, *Inorg. Chem.,* **19** (1980) 2855.
[164] G. Gritzener and J. Kuta, *Pure and Appl. Chem*., **56** (1984) 461.
[165] H.M. Koepp, H. Wendt and H. Stehlow, *Z. Electrochem.,* **64** (1960) 483.
[166] D.M. Brower, *Chem Commun*., (1967) 515.
[167] G.A. Olah and C.U. Pittman, Jr., *J. Am. Chem. Soc*., **88** (1966) 3310.
[168] R.C. Buchta and D.H.Evans, *Anal. Chem*., **40** (1968) 2181.
[169] R.C. Buchta and D.H.Evans, *J. Electrochem. Soc.: Electrochemical Science*, **117** (1970) 1494.
[170] R.C. Buchta and D.H.Evans, *J. Org. Chem*., **35** (1970) 2844.
[171] T.E. Neal and R.W. Murray, *Anal. Chem*., **42** (1970) 1654.
[172] (a) G. Semerano and A. Chisini, *Gazz. Chim. Ital*., **66** (1963) 504. (b) A. Winkel and G. Proske, *Ber*. **69** (1936) 1917. (c) I. Tachi, *Mem. Coll. Agr., Kyoto Imp. Univ*. **42** (1938) 1.
[173] (a) H. Adkins and F.W. Cox, *J. Amer. Chem. Soc*., **60** (1938) 1151. (b) S. Harrison, *Collect. Czech. Chem. Commun*., **15** (1950) 818.
[174] (a) G.S. Hammond, W.G. Borduin and G.A. Guter, *J. Am. Chem. Soc*., **81** (1959) 4682. (b) A.S.N. Murthy, A. Balasubranian and C.N.R. Rao, *Can. J. Chem*., **40** (1962) 2267.
[175] P.J. Elving and C.M. Callahan, *J. Am. Chem. Soc*., **77** (1955) 2077.
[176] J. Langmaier, Z. Samec, V. Varga, M. Horáček and K. Mach, *J. Organomet. Chem.,* **579** (1999) 348.
[177] N. El Murr, A. Chaloyard and J. Tirouflet, *J. Chem. Soc. Chem. Commun*., (1980) 446.
[178] G.L. Soloveichik, A.B. Gavrilov and V.V. Strelets, *Metalloorg. Khimia.,* **2** (1989) 431.

[179] H. Schwemlein, W. Tritschler, H. Kiesele and H.H. Brintzinger, *J. Organomet. Chem*., **293** (1985) 353.
[180] N. El Murr and A. Chaloyard, *J. Organomet. Chem*., **231** (1982) 1.
[181] E. Samuel and D. Vedel, *Organometallics*, **8** (1989) 237.
[182] R.J. Enemærke, J. Larsen, T. Skrydstrup and K. Daasbjerg, *Organometallics*, **23** (2004) 1866.
[183] R.F. Johnston, R.F. Borjas and J.L. Furilla . *Electrochim. Acta*, **40** (1995) 473.
[184] Y. Mugnier, C. Moise and E. Laviron, *J. Organomet. Chem*., **210** (1981) 69.
[185] R. Meunier-Prest, G. Lamblin, A. Mailfert and M.S. Raveau, *J. Electroanal. Chem.*, **541** (2003) 175.
[186] M.A Vorotyntsev, M. Casalta, E. Pousson, L. Roullier, G. Boni and C. Moise, *Electrochim. Acta*, **46** (2001) 4017.
[187] Y. Mugnier, C. Moise, E. Laviron, *J. Organomet. Chem*., **204** (1981) 61.
[188] A. Chaloyard, A. Dormond, J. Tirouflet and N. El Murr, *J. Chem. Soc. Chem. Commun*., (1980) 214.
[189] E. Erasmus, J. Conradie, A. Muller and J.C. Swarts, *Inorg. Chim. Acta*, **360** (2006) 2277.
[190] P. Sobota, K. Przybylak, J. Utko, L.B. Jerzykiewicz, A.J.L. Pombeiro, M.F.C. Guedes da Silva and K. Szczegot, *Chem. Eur. J*., **7** (2001) 951.
[191] N.R. de S. Basso, P.P. Greco, C.L.P. Carone, P.R. Livotto, L.M.T. Simplício, Z.N. da Rocha, G.B. Galland and J.H.S. dos Santos, *Journal of Molecular Catalysis A: Chemical*., **267** (2007) 129.
[192] F. Caruso, L. Massa, A. Gindulyte, C. Pettinari, F. Marchetti, R. Pettinari, M. Ricciutelli, J. Costamagna, J.C. Canales, J. Tanski and M. Rossi, *Eur. J. Inorg. Chem*., (2003) 3221.

3 Results and Discussion

3.1 INTRODUCTION

Two distinct types of O,O'-bidendate ligands, *i.e.*, mono-ionic β-diketonato (β) and bi-ionic aryl-diolato (L) ligands, have been chelated to titanium(IV), forming tetrahedral, $[Cp_2Ti(\beta)]^+$, $Cp_2Ti(L)$, and octahedral, $Ti(\beta)_2Cl_2$ and $Ti(\beta)_2(L)$, complexes. A schematic representation of the ligands and classes of complexes synthesised, are shown in **Figure 3.1**.

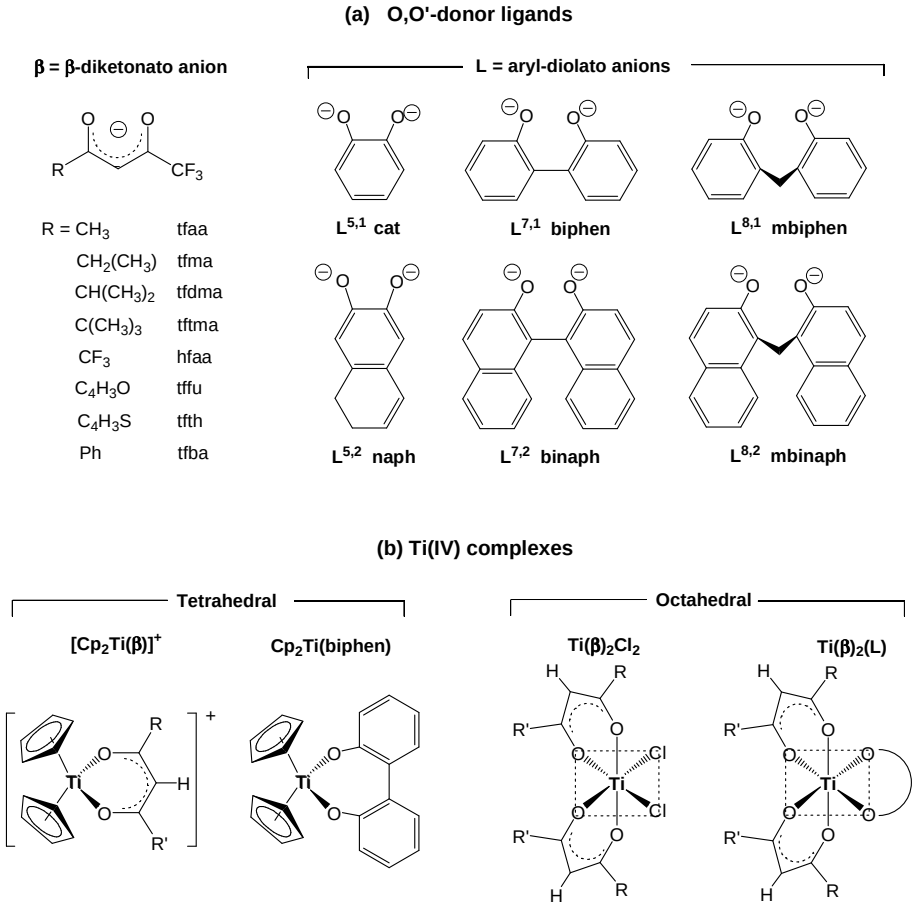

Figure 3.1 (a) *O,O'*-donor ligands used in the synthesis of (b) Ti(IV) complexes of the form $[Cp_2Ti(\beta)]^+$, $Cp_2Ti(L)$, $Ti(\beta)_2Cl_2$ and $Ti(\beta)_2(L)$.

Titanium(IV) containing fluorinated β-diketonato ligands are the focus compounds, with selected other β-diketones being used for a comparative study. It is important to note that there are significant differences when dealing with fluorinated β-diketonato titanium(IV) compounds compared to the non-fluorinated anologues. For example, the strong electron withdrawing power of the CF_3 group makes the β-diketone a poorer electrophile, which in turn makes chelation more difficult. Secondly, the Ti-F bond (E_{Ti-F} = 581 kJ mol^{-1}) is the only bond stronger than the Ti-O bond (E_{Ti-O} = 478 kJ mol^{-1});[1] this can result in favouring the Ti-F bond formation as apposed to the Ti-O bond, leading to large scale side products (lower yields) or no product formation. Fluorinated titanium (IV) compounds are also much more sensitive to hydrolysis, which results again in lower yields and dramatic decomposition effects. This series of compounds has proved to be of considerable interest because its behaviour is in a number of respects strikingly different from that of the non-CF_3-β-diketonato analogues.

The synthesis, characterization and properties of these organometalic complexes are discussed in **Section 3.2**. Characterisation of the complexes is performed by spectroscopic (^{1}H NMR and ^{19}F NMR), spectrophotometric (IR and UV), microanalytical, electrochemical and crystallographic methods. The three dimentional structure of some of the products, determined by single crystal X-ray diffraction, is described in **Section 3.3** and electrochemistry in **Section 3.5.** Reaction kinetics is reported in **Section 3.4**. A computational study has been done on selected compounds to further the understanding of the structural, kinetic and electronic properties of these complexes.

The electronic structure of the complexes in an isostructural series is varied by manipulating the electron density around the metal centre. This is achieved by changing the R group on the β-diketones, for example, **CF_3**$COCH_2CO$**R** with **R** = CH_3, $CH_2(CH_3)$, $CH(CH_3)_2$, $C(CH_3)_3$, C_4H_3O, C_4H_3S, Ph and CF_3, chelated to the titanium complex. The group electronegativities of these R groups range from 2.10 to 3.01 on the Gordy scale (see **Table 3.1**). The variation in electron density on the central coordinating metal can be correlated to parameters such as ^{1}H NMR chemical shifts (δ), formal reduction potential ($E^{0'}$), kinetic rate constants (k_{obs}), carbonyl stretching frequencies (ν_{CO}) and calculated ionisation potentials (IP).

3.2 SYNTHESIS AND CHARACTERISATION OF COMPOUNDS

3.2.1 O,O'-Donor Ligands

3.2.1.1 β-Diketones

Two phenyl-containing β-diketones, **Ph**$COCH_2CO$**R**, R = C_4H_3S (Hthba) **[1]** and $C_6H_4NO_2$ (Hnba) **[2]**, were prepared by the Claisen condensation of acetophenone and the appropriate ester, under the influence of the hindered base, lithium diisopropylamide (LDA) (**Scheme 3.1**). Acetophenone and LDA were stirred under an inert atmosphere at 0 °C for 30 minutes to abstract a methyl proton of acetophenone. After the addition of the ester (ethyl 2-thiophene carboxylate or methyl 4-nitrobenzoate), the reaction mixture was stirred at room temperature for 16 hours yielding the condensation product by precipitation of the β-diketone lithium salt. The synthesis is completed by the acidification of the β-diketone anion, generating Hthba (thenoylbenzoylacetone) [**1**] and Hnba (nitrophenoylbenzoylacetone) [**2**] respectively.

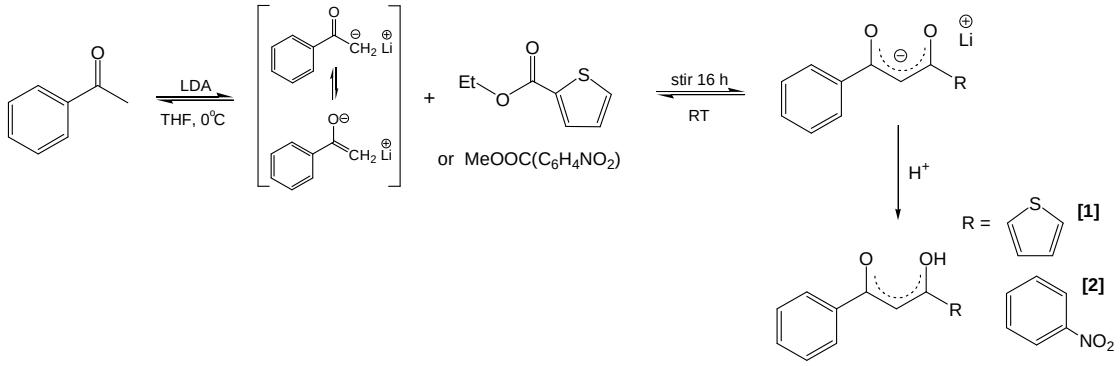

Scheme 3.1 Synthetic route for the synthesis of phenyl-containing β-diketones, Hthba **[1]** and Hnba **[2]**.

The cleaning procedure of Hnba was extensive and even after purification by column chromatography, a mixture of Hnba and a by-product, methyl 4-{[(1Z)-1-benzoyl-3-oxo-3-phenyl-prop-1-en-1-yl]amino}benzoate,[2] was eluted. The pure β-diketone was obtained in *ca.* 5 % yield by fractional recrystallisation from DMF. The by-product, present in high concentration, was isolated and shown to have the structure indicated in **Figure 3.2**.

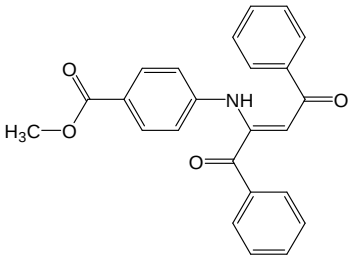

Figure 3.2 The structure of by-product in the synthesis of Hnba: methyl 4-{[(1Z)-1-benzoyl-3-oxo-3-phenyl-prop-1-en-1-yl]amino} benzoate.

The crystal structures of both Hthba[3] and Hnba[4] have been determined and the published ^{1}H NMR characterisation is the same as is found in this study. The ^{1}H NMR spectra of the synthesized β-diketones are shown relative to the CF_3 analogues in **Figure 3.3**. The spectra are very similar except for the addition of the phenyl resonances and downfield shifting of the methine proton (relative to the CF_3 analogues). Physical properties of all the β-diketones utilised in this study are listed in **Table 3.1**.

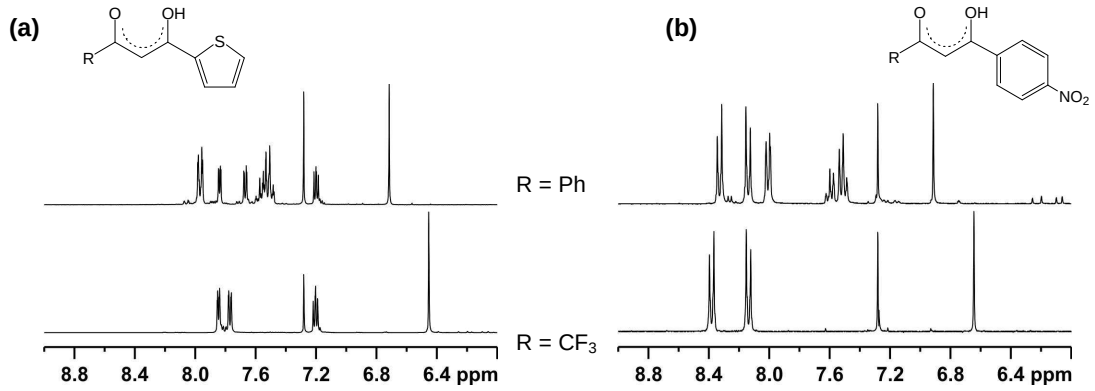

Figure 3.3 ^{1}H NMR spectra of **(a)** the thenoyl- (Hthba and Htfth) and **(b)** the nitrophenoyl- (Hnba and Htfnb) containing β-diketones.

NMR Characterisation NMR is a powerful diagnostic tool as it provides information about the chemical environment of a nucleus. The most important single parameter to be derived from the NMR spectrum is the chemical shift (δ) of a magnetic nucleus. It is influenced by two major factors; (a) *inductive effect*, where a strongly electronegative atom or group attached to or near a magnetic nucleus *deshields* the nucleus resulting in downfield shifts (inductive shift) and (b) *anisotropic effect*, where conjugated systems supporting induced electron currents, *deshield* the magnetic nucleus close to the plane of the ring, resulting in downfield shifts (ring current shift). These trends are observed in the listed β-diketone series (^{1}H chemical shift of the methine proton are listed in **Table 3.1**).

Table 3.1 Physical properties of β-diketones; ^{1}H and ^{19}F NMR chemical shifts (δ), of the CH and CF_3 respectively, group electronegativity (χ_R) of the R groups and pK_a.

β-diketone	R	χ_R [(a)]	pK_a [(b)]	^{1}H : CH δ / ppm $CDCl_3$	^{1}H : CH δ / ppm Acetone-d_6	^{19}F : CF_3 δ / ppm $CDCl_3$
CF_3 $COCH_2CO$**R**						
Series 1:						
Htfaa	CH_3	2.34[5]	6.30[6]	6.00	6.20	-76.82
Hhfaa	CF_3	3.01[7]	4.71[8]	6.40	6.62	-76.55
Htfth	C_4H_3S	2.10	6.50[3]	6.45	6.89	-75.74
Htffu	C_4H_3O	--	--	6.49	6.67	-76.12
Htfba	Ph	2.21[7]	6.3[6]	6.59	6.95	-76.49
Htfnb	$PhNO_2$	2.11[9]	--	6.64	7.10	--
Series 2						
Htfaa	CH_3	2.34[5]	6.3[6]	6.00	--	-76.82
Htfma	$CH_2(CH_3)$	2.31[10]	6.64[11]	5.95	--	-76.60
Htfdma	$CH(CH_3)_2$	2.29[12]	6.80[13]	5.95	--	-76.65
Htftma	$C(CH_3)_3$	2.27[12]	7.13[11]	6.05	--	-76.50
Ph$COCH_2CO$**R**						
Hba	CH_3	2.34[5]	8.70[6]	6.19	6.50	--
Htfba	CF_3	3.01[7]	6.3[6]	6.59	6.95	--
Hthba **[1]**	C_4H_3S	2.10[3]	9.01[3]	6.71	7.16	--
Hdbm	Ph	2.21[7]	9.35[6]	6.85	7.30	--
Hnba **[2]**	$PhNO_2$	2.11[9]	8.02[9]	6.92	--	--
CH_3 $COCH_2CO$**R**						
Hacac	CH_3	2.34[5]	8.95[6]	5.50	--	--
Hmaa	OCH_3	2.64[14]	--	--	--	--

(a) χ_R (Gordy scale) group electronegativity values from references indicated
(b) pK_a values from references indicated

The relative downfield shift, Δ, of the methine proton, when the electronegativity of the R group is increased from χ_{CH_3} = 2.34 to χ_{CF_3} = 3.01, is

For **CF_3**$COCH_2CO$**R** with **R** = CH_3 (δ = 6.00) to CF_3 (δ = 6.40) Δ = 0.4

For **Ph**$COCH_2CO$**R** with **R** = CH_3 (δ = 6.19) to CF_3 (δ = 6.59) Δ = 0.4

Thus one observes a relative downfield shift of 0.4 in both cases.

Similarly, if the aromaticity is increased (with minor changes to the electronegativity of the R group, i.e., χ_{CH_3} = 2.34 to χ_{Ph} = 2.21),

For **CF_3**$COCH_2CO$**R** with **R** = CH_3 (δ = 6.00) to Ph (δ = 6.59) Δ = 0.59

For **Ph**$COCH_2CO$**R** with **R** = CH_3 (δ = 6.19) to Ph(δ = 6.85) Δ = 0.66,

the realive downfield shift is approximately 0.6.

In general, chemical shifts can be roughly correlated to the electronegativity of the substituents (known as the group electronegativity) but in the case of the above β-diketones series, no correlation exists because two factors contribute to the deshielding of the CH signal. This leads to, for example, the methine proton of **CF_3**$COCH_2CO$**Ph** (δ = 6.59) being futher downfield shifted relative to **CF_3**$COCH_2CO$**CF_3** (δ = 6.40), even though the electronegativity of the substituent groups, i.e., χ_{Ph} = 2.21 and χ_{CF_3} = 3.01, shows the opposite trend. In conclusion, chemical shifts are correlated to the *deshielding* of the magnetic nucleus and thus the only observable trend is the downfield shifting of the methine proton resonances with the combined effect of increasing electronegativity **and** increasing aromaticity of substituent groups.

^{19}F NMR spectra were taken of the fluorinated β-diketones (δ listed in **Table 3.1**). Fluorine chemical shifts span a very wide range (500 ppm) compared to that of proton (10 ppm) and in general are significantly more sensitive to changes in electron density. The position of the CF_3 resonances (~76 ppm) referenced against $CFCl_3$ is correct for a C-CF_3 functional group. However, it is evident that the CF_3 environment is not affected significantly by the electronegativity or aromaticity of the substituent R groups. The bond distance of the R group to the CF_3 fluorine nucleus (5 bonds) is much larger than the R group to the CH proton (3 bonds), i.e., a difference of two bond lengths. This difference is reflected in the relative chemical shifts of the β-diketones series, i.e., the relative C**H** chemical shifts, spanning a range of 0.6 ppm (out of 10 ppm for ^1H NMR), see **Figure 3.4**, is more significant than the C**F**$_3$ chemical shifts of 0.6 ppm (out of 500 ppm for ^{19}F NMR).

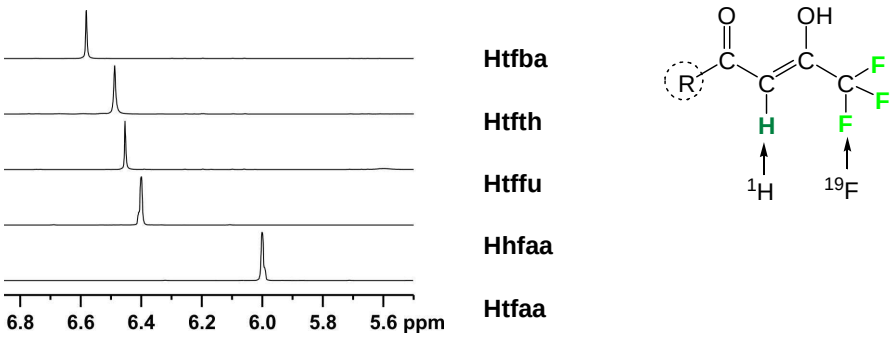

Figure 3.4 Comparative ^1H NMR spectra ($CDCl_3$) of the methine proton (CH) of the fluorinated β-diketones: Htfaa, Hhfaa, Htffu, Htfth and Htfba.

3.2.1.2 Dihydroxy-aryls

These dihydroxy-aryl ligands all have irritant/toxic properties. Comparative ^{1}H NMR spectra are shown in **Figure 3.5**. The OH (oxygens) in this series, feed electron density into the π system making it more electron-rich relative to benzene. Hence the replacement of two H atoms by OH groups in benzene yielding 1,2-dihydroxybenzene (catechol), results in an upfield resonance shift of the ring protons, from δ = 7.27 to δ = 6.8 – 6.9 (ring protons shielded relative to those of benzene). The addition of the second fused ring forming naphthol results in a downfield shift relative to catechol due to enhance aromaticity. The same trend (with the addition of the second fused ring) is observed for the other dihydroxy ligands used in this study.

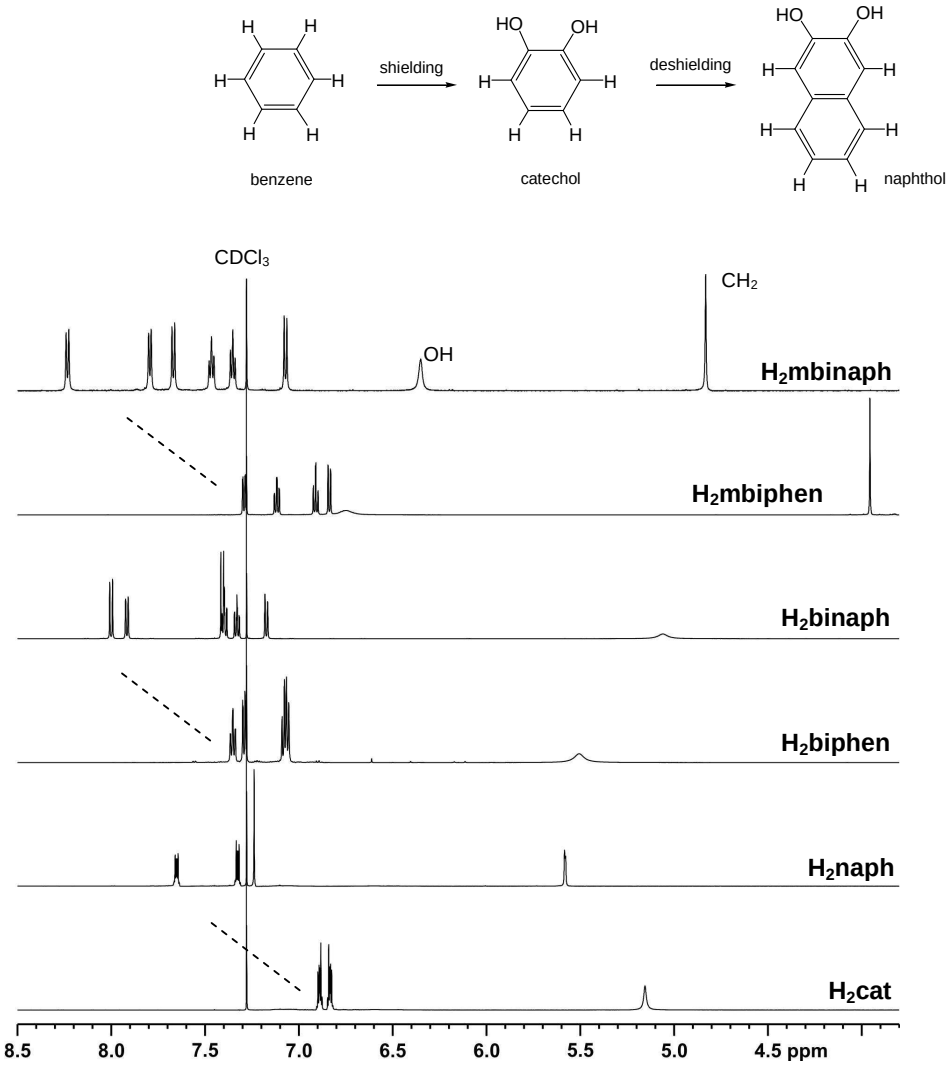

Figure 3.5 Comparison of ^{1}H NMR spectra of dihydroxy-aryls. (Structures shown in **Figure 3.1 (a)**).

3.2.2 Tetrahedral Complexes

3.2.2.1 Mono-β-diketonato-Ti(IV) complexes: $[Cp_2Ti(\beta)]^+$

The series of new bis(η^5-cyclopentadienyl)-mono(β-diketonato)titanium(IV) salts of the form $[Cp_2Ti(\beta)]^+ClO_4^-$ with β = **CF_3**COCHCO**R,** R = CH_3 (tfaa) **[3]**, C_4H_3S (tfth) **[4]**, C_4H_3O (tffu) **[5]** and Ph (tfba) **[6]** was synthesised according to the reaction described in **Scheme 3.2**. The synthesis of $[Cp_2Ti(hfaa)]^+$ failed with side reactions dominating. The second series, with β = **Ph**COCHCO**R**, R = CH_3 (ba) **[7]**, CF_3 (tfba) **[6]**, C_4H_3S (thba) **[8],** Ph (dbm) **[9]** was prepared to incorporate a wider range of group electronegativities. The synthesis of $[Cp_2Ti(nba)]^+$ with R = Ph-NO_2 also failed. Previously synthesised, $[Cp_2Ti(acac)]^+$ **[10]** and $[Cp_2Ti(maa)]^+$ **[11]** were included.

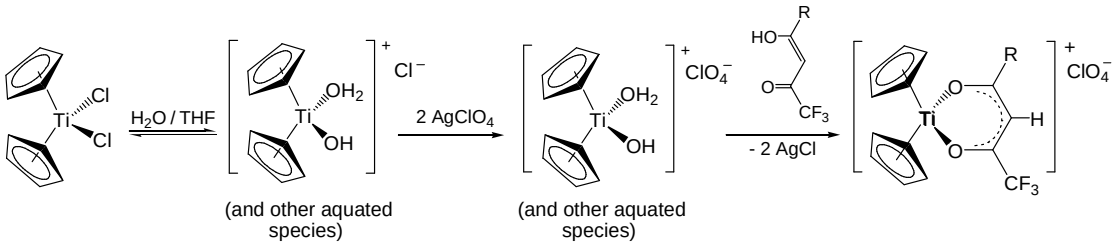

Scheme 3.2 Synthesis of the mono-β-diketonato titanium(IV) salts of the form $[Cp_2Ti(\beta)]^+ClO_4^-$, **[3] - [11]**. The aquated species depicted above is one of several possible species which exist in solution (see **Scheme 2.3,** Hydrolysis of titanocene dichloride).

The synthesis of these mono-β-diketonato titanium(IV) salts is based on an anion metathesis reaction (which is driven by precipitation of one of the products), followed by a β-diketone substitution reaction. An important step is the aquation of titanocene dichloride (Cp_2TiCl_2). In pure water Cp_2TiCl_2 hydrolyses completely with the displacement of the two Cl^-, forming a wide range of cationic species, that include $[Cp_2Ti(H_2O)(OH)]^+$, $[Cp_2Ti(H_2O)(H_2O)]^{2+}$, $[Cp_2Ti(OH)_2]$ (see **Scheme 2.3** Hydrolysis of titanocene dichloride). Addition of silver perchlorate ($AgClO_4$) removes the Cl^- ions by precipitating silver chloride (AgCl) while the aquated perchlorate titanium salt, *e.g.*, $[Cp_2Ti(H_2O)(OH)]^+ClO_4^-$ remains in solution. Finally, the β-diketone replaces the hydrolysed leaving group, forming an ionic species, $[Cp_2Ti(\beta)]^+ClO_4^-$, with ClO_4^- as the counter ion. Only one bidentate β-ligand could be coordinated to the Cp_2Ti^{IV} moiety, even with the addition of high concentration of β-diketone in the final step, it was impossible to produce the bis chelate.

No base or hydrogen acceptor was required for this reaction because the chelation of the β-diketonato to the titanium(IV) centre was facilitated by two factors. Firstly, the better leaving group (OH^- or H_2O) replaced the Cl^- groups of the parent, Cp_2TiCl_2 and secondly, the β-diketone exists chiefly as the more reactive enol tautomer.

The syntheses of these mono-β-diketonato complexes were complicated by the insolubility of the β-diketones in water. This problem was overcome by means of a mixed solvent system, using 1:2 ratio of H_2O/THF. Initially it was thought that the aquation of titanocene dichloride was essential for a successful reaction, but it was found that these salts could also be synthesised in anhydrous THF. Other solvent, e.g., DCM, acetonitrile and chloroform, were tried without success. Both H_2O and THF have similar coordinating sites, see **Figure 3.6 (a)**, a property playing an important role in this solvation process. For example, instead of hydrolysis in water, a similar solvated species could be formed as illustrated in **Figure 3.6 (b)**

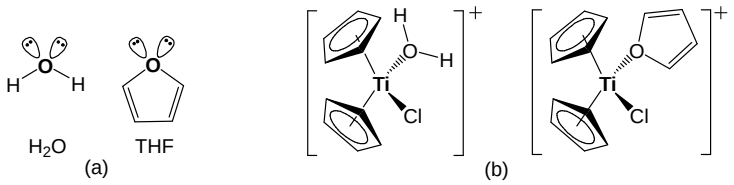

Figure 3.6 **(a)** The coordination sites of H_2O and THF and **(b)** possible solvated species with Cp_2TiCl_2.

Slightly better yields were obtained when solvents were degassed and the reaction was performed under N_2 (to remove any free O_2), but the most critical factor was the amount of $AgClO_4$ used; an excess of $AgClO_4$ completely destroyed the reaction, possibly due to the catalytic or redox properties of Ag ion. A second factor affecting the yield was the type of β-diketone; on average the yield was at least 20 % less for β-diketones containing a CF_3 group compared to non-CF_3-containing β-diketones. When the β-diketones containing two CF_3 group, *i.e*., Hhfaa, was used, no product was obtained.

An alternative synthetic route, a substitution reaction in which the β-diketonato ligand in $[CpTi(\beta)]^+$ is exchanged for another β-diketone (see **Scheme 3.3**) could only be performed for complexes where the incoming β-diketone contained R groups which were less electronegative than those of the leaving β-diketonato ligand. For example, producing

$Cp_2Ti(acac)]^+$ from $[Cp_2Ti(tfba)]^+$ was possible. The reaction was followed by NMR and UV (**Figure 3.7**). However the attempt to synthesise the highly electronegative hexafluoroacetyl-acetone salt, $[Cp_2Ti(hfaa)]^+$, from any other salt, was again unsuccessful.

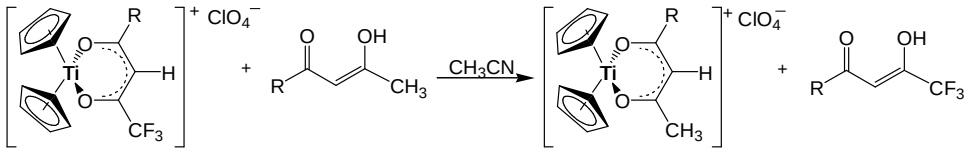

Scheme 3.3 Alternative synthetic route of $[Cp_2Ti(\beta)]^+$ complexes, the β-diketone substitution reaction; $[Cp_2Ti(\beta^1)]^+ClO_4^- + H\beta^2 \rightarrow [Cp_2Ti(\beta^2)]^+ClO_4^- + H\beta^1$

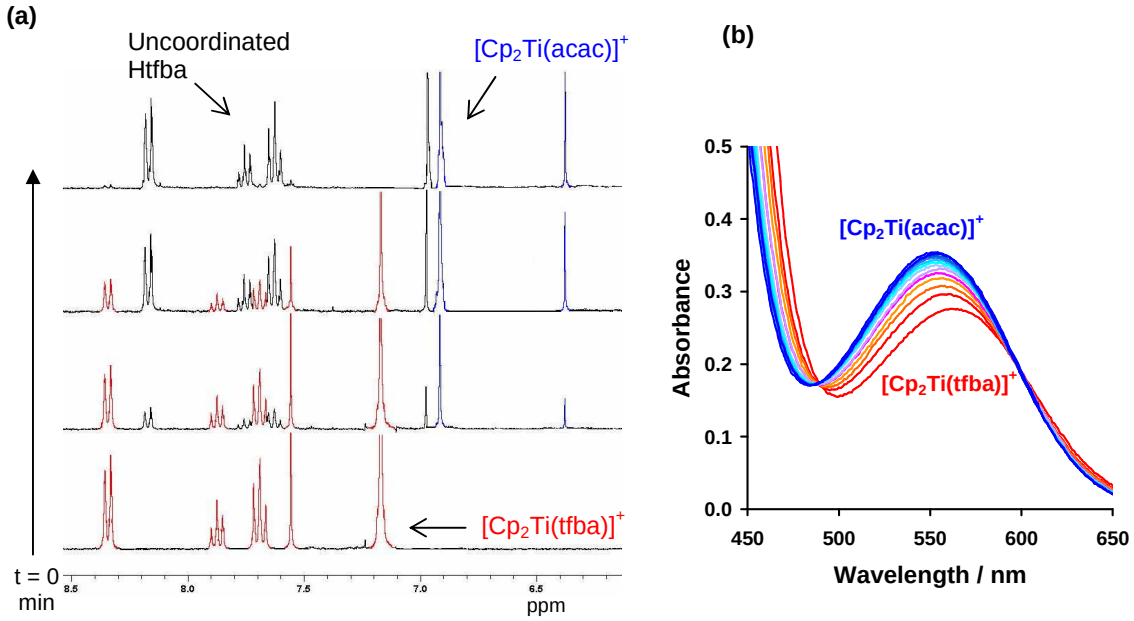

Figure 3.7 The substitution reaction, $[Cp_2Ti(tfba)]^+ClO_4^- + Hacac \rightarrow [Cp_2Ti(acac)]^+ClO_4^- + Htfba$ observed by **(a)** ^1H NMR (acetone-d_6) and **(b)** UV (time between scans = 10 min)

All the synthesised salts were insoluble in water, hexane and diethyl ether, slightly soluble in organic solvents such as chloroform and DCM, and soluble in acetone, THF and ethanol. However, dissolving the product in ethanol caused decomposition of the product by the

splitting off of one of the cyclopentadienyl rings. The $[Cp_2Ti(\beta)]^+$ cation is sensitive to moisture in solution, but has been found to be stable in the solid state for more than two years.

NMR Characterisation Since the chelated complexes were salts, a solvent of relatively high dielectric constant was required; $CDCl_3$ (ε = 4.8) gave very poor spectra due to poor solubility, while acetone-d_6 (ε = 20.7) was found to be more than adequate. ^{1}H NMR spectral data of the synthesised perchlorate salts and the uncoordinated β-diketones are compared in **Table 3.2** and the ^{1}H NMR spectra of the CF_3-β-diketones series are shown in **Figure 3.8**.

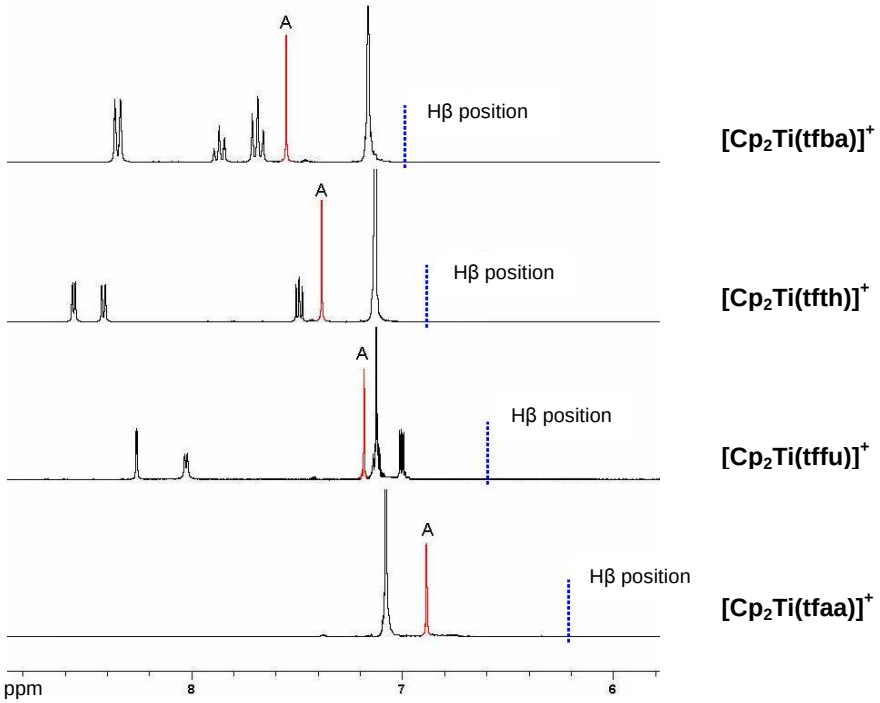

Figure 3.8 ^{1}H NMR spectra (acetone-d_6) of CF_3-β-diketone containing $[Cp_2Ti(\beta)]^+$ perchlorate salts with β = tfaa **[3]**, tffu **[5]**, tfth **[4]** and tfba **[6]**. The pseudo-aromatic system generated when the β-diketonato ligand coordinates to the Ti(IV) centre results in the methine proton (marked **A**, red) shifting downfield relative to the uncoordinated β-diketone (marked in blue). The presence of a formal charge also leads to substantial deshielding.

The ^{1}H NMR spectra consist of three groups of signals: the cyclopentadienyl (Cp) protons (singlet, δ ~7.1 ppm), the methine proton of the β-diketonato ligand (singlet, between δ 6.99 – 7.89 ppm) and the R group protons (CH_3, OCH_3, Ph, C_4H_3O, C_4H_3S). The intensity ratio of the first two signals is 10:1; the third is varied according to R groups. The following general trends were observed:

• The electronic properties of the R groups of the β-diketonato ligand don't significantly influence the cyclopentadienyl ring (Cp resonance varies from δ 6.99 to 7.16 ppm, Δ = 0.17

ppm) but has a large effect on the methine proton which varies from δ 6.90 to 7.86 ppm (Δ = 0.96) for the series. The change in R groups causes shifts in the position of the methine ring proton due to electronic communication through the C-C bonds in the β-diketonato backbone *via* conjugation.

• The Cp chemical shift of $[Cp_2Ti(\beta)]^+$ (δ ~7.1 ppm) is significantly downfield shifted compared to neutral parent compound Cp_2TiCl_2 (δ 6.66 ppm) and related Cp_2Ti(biphen) complex (δ = 6.34 ppm, see spectrum **Section 3.2.2.2**) The large downfield shift can be supported in terms of the presence of a formal positive charge which leads to substantial deshielding.

• The methine proton of the chelated ring is downfield shifted by ~0.6 ppm relative to the uncoordinated β-diketone (see **Table 3.2** and **Figure 3.8**). This is due to the *pseudo*-aromatic system which is generated when the β–diketone coordinates to the Ti(IV) metal. The study of the electrochemical behaviour of $[Cp_2Ti(\beta)]^+$ and Hβ supports this view (**Section 3.5.3.1)**; a comparison of the CVs (see **Figure 3.70**) shows that the coordinated β–diketonato ligand is more electron-rich relative to its uncoordinated counterpart.

Table 3.2 ^{1}H NMR chemical shifts (acetone-d_6) of the Cp and methine protons of the synthesised $[Cp_2Ti(\beta)]^+$ complexes. The spectra of the fluorinated $[Cp_2Ti(\beta)]^+$ complexes are shown in **Figure 3.8**, where the methine proton of the chelated β-diketonato ligand are shown in red and the uncoordinated β-diketone is shown in blue.

$Cp_2Ti(\beta)^+ClO_4^-$					Free β-diketone
Compound $[Cp_2Ti(\beta)]^+ClO_4^-$	**R**	**^{1}H / ppm Cp** Acetone-d_6	**^{1}H / ppm CH (A)** Acetone-d_6	**Δ (A-Hβ) / ppm**	**^{1}H / ppm CH (Hβ)** Acetone-d_6
CF_3-β-diketones **(CF_3COCH_2COR)**					
$[Cp_2Ti(tfaa)]^+$ **[3]**	CH_3	7.08	6.90	0.70	6.20
$[Cp_2Ti(tffu)]^+$ **[5]**	C_4H_3O	7.13	7.18	0.51	6.67
$[Cp_2Ti(tfth)]^+$ **[4]**	C_4H_3S	7.13	7.38	0.50	6.89
$[Cp_2Ti(tfba)]^+$ **[6]**	Ph	7.16	7.55	0.60	6.95
Ph- β-diketones **($PhCOCH_2COR$)**					
$[Cp_2Ti(ba)]^+$ **[7]**	CH_3	6.99	7.20	0.70	6.50
$[Cp_2Ti(tfba)]^+$ **[6]**	CF_3	7.16	7.55	0.60	6.95
$[Cp_2Ti(thba)]^+$ **[8]**	C_4H_3S	7.06	7.74	0.58	7.16
$[Cp_2Ti(dbm)]^+$ **[9]**	Ph	7.06	7.86	0.56	7.30
(CH_3COCH_2COR)					
$[Cp_2Ti(acac)]^+$ **[10]**	CH_3	6.90	6.35	--	--
$[Cp_2Ti(maa)]^+$ **[11]**	OCH_3	7.00	5.66	--	--

Infrared Characterisation Characteristic vibrational frequencies for the $[Cp_2Ti(\beta)]^+ClO_4^-$ salts and the parent compound, Cp_2TiCl_2 are listed in **Table 3.3**. The bands expected for the various bonding modes of cyclopentadienyl groups have been compiled by Huggins and Kaesz[15] and Fritz.[16] Cyclopentadienyltitanium compounds show strong bands in their infrared spectra at ~3100 cm^{-1} (C-H stretch), ~1320 cm^{-1} (C-C stretch), 1020 cm^{-1} (C-H deformation in-plane) and ~820 cm^{-1} (C-H deformation out-of-plane). The vibrational frequencies assigned to the ClO_4^- group as a "free" anion, are ~1095 cm^{-1} (ν_3) and ~620 cm^{-1} (ν_4).[17] This is in contrast to the bands expected for the bonding modes of the perchlorate group bound to titanium, for example, in $Cp_2Ti(ClO_4)_2$ the vibrational frequencies assigned to the ClO_4^- group are: 1130 vs, 1072 vs, 1009 vs, 920 w, 624 s and 460 w.[18] Identification of the vibrations arising from the chelate β-diketonato ligand is quite complex and in this study, only the β-diketonato C-O stretch (ν_{CO}), has been identified. A complete evaluation and assignment of the vibrations for β = acac was done by Doyle and Tobias.[19]

The infrared spectra of $[Cp_2Ti(\beta)]^+ClO_4^-$ for β=acac and tfaa are illustrated in **Figure 3.9**, highlighting the typical bands for the bonding modes of the Cp and ClO_4 groups and the β-diketonato C-O stretch (ν_{CO}). Infrared spectra can be used to indicate successful coordination of the β-diketone to the Cp_2Ti^{2+} moiety by the absence of the single carbonyl (C=O) vibration band of the uncoordinated β-diketone, in the finger print region of 1800 – 1650 cm^{-1}. The IR data (see **Table 3.3**) is consistent with the β-diketonatato ligand chelating through the oxygen atoms and the perchlorate group, ClO_4^-, existing as a counter ion and not directly bonded to the titanium.

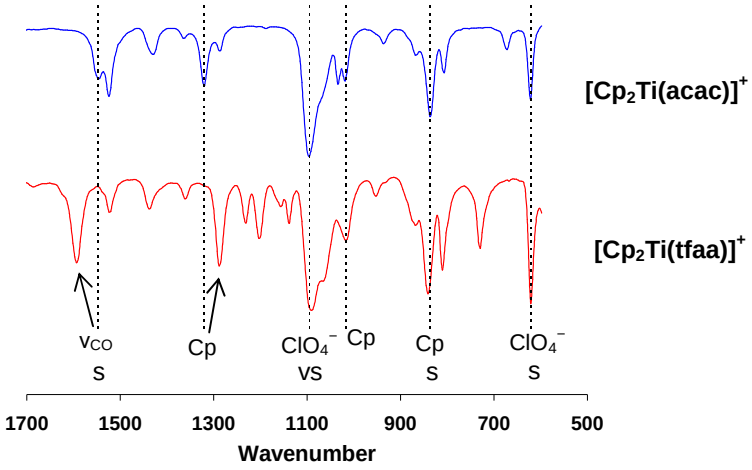

Figure 3.9 Infrared spectra of $[(\eta^5\text{-}C_5H_5)Ti(\beta)]^+ClO_4^-$ for β=acac **[10]** (assignments according to Doyle and Tobias[19]) and tfaa **[3]** (this study).

Table 3.3 Infrared data for several bis(cyclopentadienyl)titanium (IV) compounds.

$[Cp_2Ti(\beta)]^+ClO_4^-$	β-ligand	Cyclopentadienyl ring				Perchlorate	
	ν_{CO} cm^{-1}	ν_a cm^{-1}	ν_b cm^{-1}	ν_c cm^{-1}	ν_d cm^{-1}	ν_3 cm^{-1}	ν_4 cm^{-1}
tfaa **[3]**	1592 s	3103 w	1289	1019	841 s	1091 vs	620 s
tffu **[5]**	1578 s	3103 w	1309	1015	835 s	1094 vs	620 s
tfth **[4]**	1566 s	3106 w	1288	1015	840 s	1093 vs	620 s
tfba **[6]**	1554 s	3101 w	1290	1015	833 s	1091 vs	620 s
acac **[10]**[a]	1547 s	3108 w	1320	1019	836 s	1094 vs	620 s
maa **[11]**	1562 s	3105 w	1295	1015	831 s	1090 vs	620 s
ba **[7]**	1542 s	3108 w	1328	1015	836 s	1090 vs	620 s
thba **[8]**	1519	3107 w	1305	1016	850 s	1090 vs	620 s
dbm **[9]**	1511 s	3113 w	1329	1013	826 s	1093 vs	620 s
$CpTiCl_2$	--	3114 w	1363	1014	852 s	--	--

vs-very strongh, s-strong, m-medium, w-weak

ν_{CO} = C-O stretch, ν_a = C-H stretch, ν_b = C-C stretch, ν_c= C-H in-plane deformation, ν_d= C-H out-of-plane deformationa and ν_3 ,ν_4 = degenerate frequencies.

[a] similar values obtained for $[Cp_2Ti(acac)]^+ClO_4^-$ in reference 19.

3.2.2.2 Mono(aryl-diolato) Ti(IV) complex: Cp_2Ti(biphen)

The neutral bis(η^5-cyclopentadienyl)-mono(aryl-diolato)titanium(IV) complex of the form $Cp_2Ti(L)$ with L = H_2biphen **[12]**, was synthesised in relatively low yields (25 %), according to the method described for $[Cp_2Ti(\beta)]^+ClO_4^-$ (see **Scheme 3.4**). The alternative method of treating Cp_2TiCl_2 with the ligand in the presence of a base, Et_3NH, and refluxing for 3 hours produced the product in even lower yields.

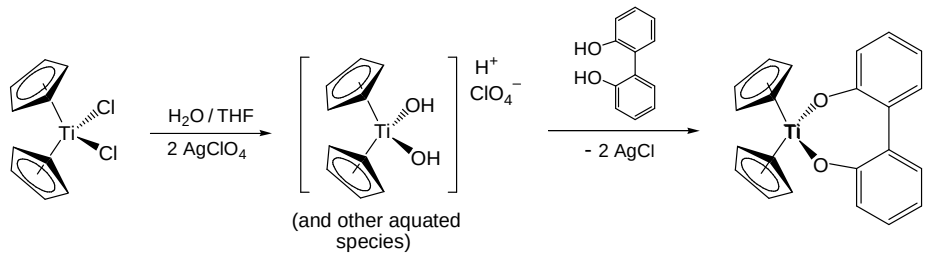

Scheme 3.4 Synthesis of Cp_2Ti(biphen). The aquated species depicted above is one of several possible species which exist in solution (see **Scheme 2.3,** Hydrolysis of titanocene dichloride).

Cp_2Ti(biphen) is insoluble in water and hexane and soluble in chloroform, DCM, acetone and THF. It doesn't decompose in MeOH and EtOH by splitting off one of the Cp rings, like in its $[Cp_2Ti(\beta)]^+$ counterpart. It was found to be stable in the solid state for more than three years.

NMR Characterisation The ^{1}H NMR spectrum of Cp_2Ti(biphen) **[12]** is shown relative to that of the uncoordinated H_2biphen in **Figure 3.10**. The product spectrum consist of two groups of signals: the cyclopentadienyl (Cp) protons (singlet, δ 6.26 ppm, 10H), and the aromatic protons of the aryl-diolato ligand with intensity ratio of 4:2:2 (m, t, d), at δ 7.26, 6.93 and 6.68, compared to the 2:2:4 (t, d, m) pattern at δ 7.36, 7.33 and 7.07 in the uncoordinated ligand. The disappearance of the phenolic-OH protons in the spectrum of **[12]**, compared to the uncoordinated ligand, suggests that the bidentate ligand is chelated through the two oxygen to the Ti(IV) centre.

The following general trends were observed:

• The Cp chemical shift of Cp_2Ti(biphen) (δ 6.26 ppm) is upfield shifted compared to parent compound, Cp_2TiCl_2 (δ 6.66 ppm). This indicates that the biphenolato ligand is more electron-donating than the chlorine ligands.

• The aromatic protons of the chelated biphenolato rings (δ 7.26, 6.93 and 6.68 ppm) are upfield shifted relative to the uncoordinated ligand (δ 7.36, 733. and 7.07 ppm). This indicates that electron density is pumped into the biphenolato aromatic system *via* the Cp system in the coordinated Cp_2Ti(biphen) complex.

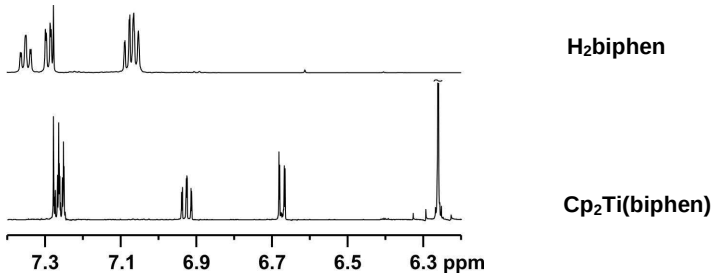

Figure 3.10 ^{1}H NMR spectra of Cp_2Ti(biphen) and the uncoordinated H_2biphen ligand.

3.2.3 Octahedral complexes

3.2.3.1 Bis(β-diketonato)-dichloro Ti(IV) complexes: $Ti(\beta)_2Cl_2$

The series of new bis(β-diketonato)dichloro titanium(IV) complexes of the form $[Ti(\beta)_2Cl_2]$ with β = **CF_3**COCHCO**R**, (*Series 1*): R = CH_3 (tfaa) **[13]**, CF_3 (hfaa) **[14],** C_4H_3S (tfth) **[15]**, C_4H_3O (tffu) **[16]** and Ph (tfba) **[17]** and (*Series 2)*: R = CH_3 (tfaa) **[13]**, $CH_2(CH_3)$ (tfma) **[18]**, $CH(CH_3)_2$ (tfdma) **[19]**, $C(CH_3)_3$ (tftma) **[20]**, were synthesised according to **Scheme 3.5**. $Ti(ba)_2Cl_2$ **[21],**[20] $Ti(dbm)_2Cl_2$ **[22]**[20] and $Ti(acac)_2Cl_2$ **[23]**[21], originally synthesized by Fay *et al*., were reproduced for comparative reasons.

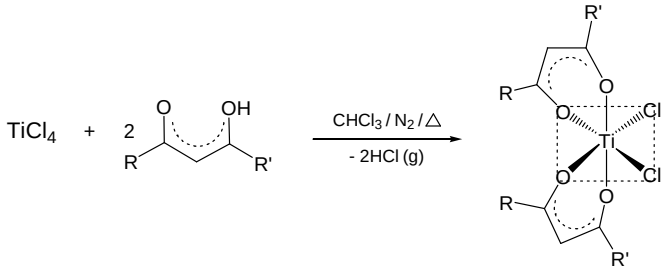

Scheme 3.5 Synthesis of $Ti(\beta)_2Cl_2$ complexes with β = tfaa, hfaa, tfth, thfu, thba, tfma. tfdma, and tftma.

$TiCl_4$ (1 eq) was added slowly to a stirred solution of the appropriate β-diketone (2 eq) in DCM or chloroform under an inert atmosphere. There was an instant colour change from the clear β-diketone solutions to yellow (for complexes with R = CF_3 and CH_3), orange (R = $CH_2(CH_3)$, $CH(CH_3)_2$, $C(CH_3)_3$ and Ph) or reddish (R = C_4H_3S and C_4H_3O). Stir for 20 min with a slow stream of dry nitrogen passing through the solution to aid the evolution of hydrogen chloride gas. Then reflux for 2 h for the solid β-diketones (R = Ph, C_4H_3S and C_4H_3O) and ½ h for the liquid β-diketones (R = CH_3 $CH_2(CH_3)$, $CH(CH_3)_2$, $C(CH_3)_3$ and CF_3). Hexane was added until the reaction mixture turned milky and then it was allowed to precipitate slowly overnight in the freezer. The product was obtained from the filtrate in the case of (hfaa, tfaa, tfma and tfth) and from the precipitate in the case of (tfba, tffu and tftma). $Ti(hfaa)_2Cl_2$ was a mixture of products and only after the crude mixture was allowed to stand in the freezer for 10 days, was it possible to separate out the pure product.

Lower yields were obtained for the CF_3-containing β-diketones compared to others. It may be ascribed to any of the factors described earlier, i.e., the CF_3-β-diketones are poorer electrophiles (due to the strong electron withdrawing CF_3 group), which in turn makes chelation more difficult or the interference of Ti-F bond formation as opposed to the Ti-O bond formation or the increased sensitivity to hydrolysis. Although different reaction conditions all led to some free β-diketone, it is advisable to use shorter reaction times so as to reduce the exposure time for hydrolysis and oxidation. For example, in the synthesis of $Ti(acac)_2I_2$ increasing the reaction time from 10 minutes to 12 hours resulted in severe oxidation and hydrolysis.[22] Cleaning the products of uncoordinated β-diketone proved to be very difficult. Removal of free β-diketones of lower boiling points, *e.g.*, Hhfaa (70-71 °C) and Htfaa (105-107 °C) however, was done by reduced pressure evaporation. The complexes are soluble in dichloromethane, chloroform, acetonitrile, slightly soluble in acetone and nearly insoluble in diethyl ether and saturated hydrocarbons.

The complexes are pleochroic, displaying different colours when viewed from different directions. These colour changes are due to the plane of polarisation being either parallel or perpendicular to the crystal plate.[20] The colour variations observed were red-orange-yellow.

Stereochemistry Octahedral $Ti(\beta)Cl_2$ complexes exist in different isomeric forms depending on the symmetry of the β-diketonato ligand. Symmetrical β-diketones, *e.g.*, β = hfaa (R = CF_3), could yield two possible isomers, one *cis* and one *trans* isomer (see **Figure 3.11**)

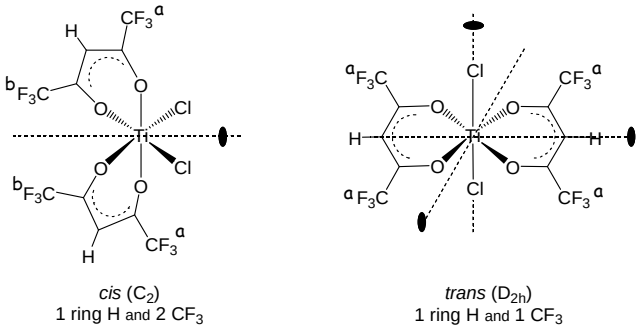

cis (C_2)
1 ring H and 2 CF_3

trans (D_{2h})
1 ring H and 1 CF_3

Figure 3.11 The stereochemistry of octahedral $Ti(hfaa)_2Cl_2$ with symmetric β-diketones, showing the two possible isomers and the number of ^1H and ^{19}F NMR signals.

Asymmetric β-diketones, *e.g.*, β = tfaa, tfma, tfdma, tftma, tfba, tfth, tffu (R = CH_3, $CH_2(CH_3)$, $CH(CH_3)_2$, $C(CH_3)_3$, Ph, C_4H_3S and C_4H_3O respectively), could yield five possible isomers, three *cis* and two *trans* isomers (see **Figure 3.12**). The isomers are referred to by three prefixes which specify the relative position firstly of the Cl, followed by the relative orientation of the CF_3 and R groups of the β-diketone ligand respectively. The symmetry elements and the expected NMR signals are shown in **Figure 3.12**.

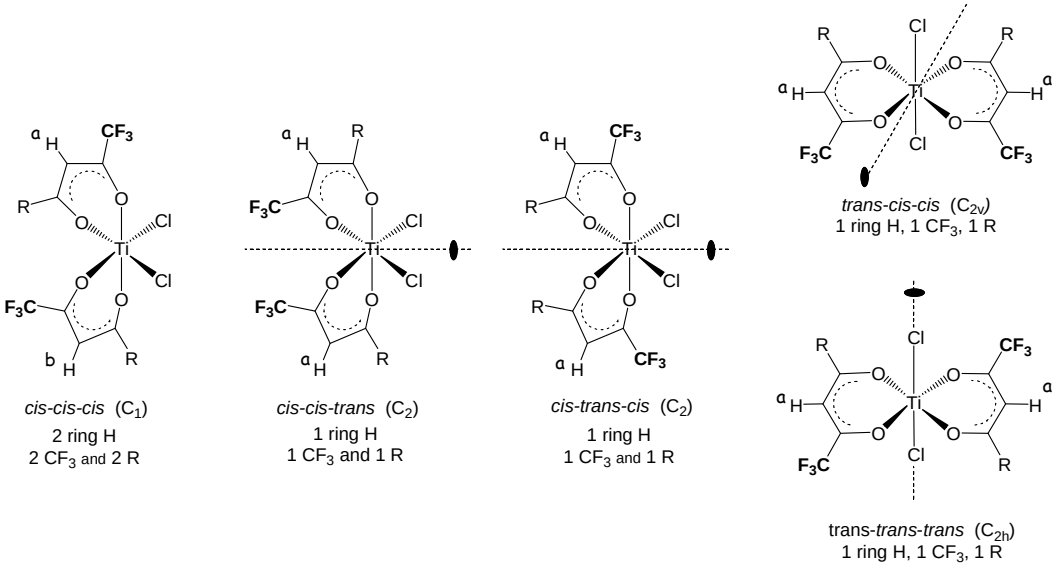

Figure 3.12 The stereochemistry of octahedral $Ti(\beta)_2Cl_2$ with asymmetric β–diketones, showing the five possible isomers and the number of expected ^1H and ^{19}F NMR signals.

NMR Characterisation Selected room temperature ^1H NMR spectra are shown in **Figure 3.13** and the chemical shift data for the methine protons of the chelated and uncoordinated β-diketone in $Ti(\beta)_2Cl_2$ and Hβ respectively, are listed in **Table 3.4**. The proton spectra of $Ti(acac)_2Cl_2$, $Ti(ba)_2Cl_2$ and $Ti(dbm)_2Cl_2$ reveal a single methine resonance, while all the CF_3-β-diketonato analogues show two resonances in the methine region (and two sets of corresponding peaks for the R groups) indicating that two NMR distinguishable complexes (marked **A** and **B**) are present. All documented $Ti(\beta)Cl_2$ complexes exist in solution as nonrigid *cis* geometrical isomers showing a single methine proton resonance at room temperature. The new fluorinated $Ti(\beta)_2Cl_2$ complexes of this study, appear to behave in a strikingly different manner.

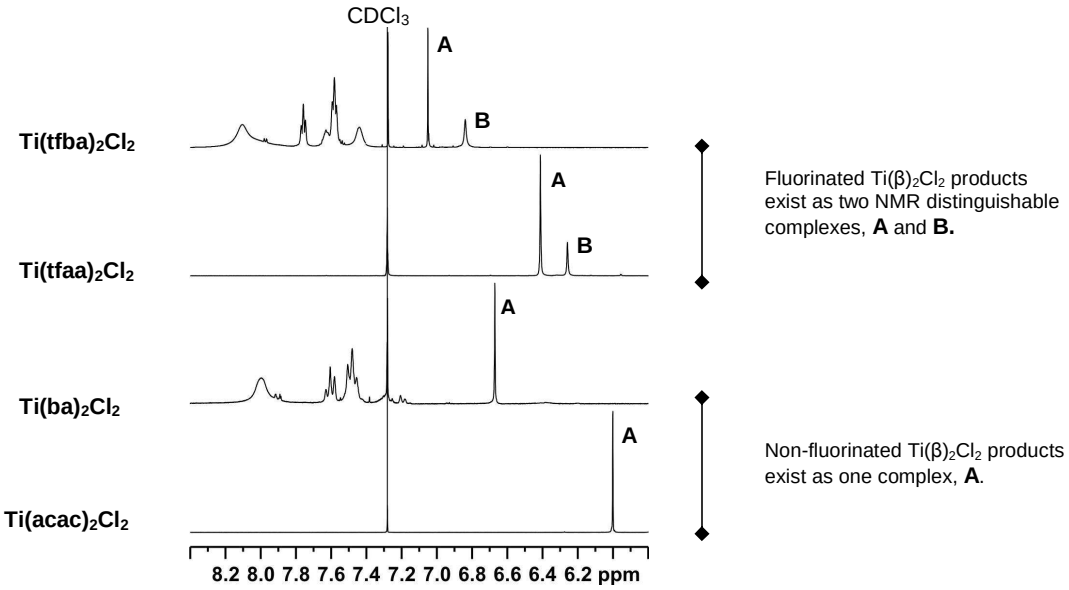

Figure 3.13 Selected room temperature ^{1}H NMR spectra ($CDCl_3$) of $Ti(\beta)_2Cl_2$ complexes in the methine region showing the existance of two complexes, **A** and **B**, in the CF_3-β-diketonato complexes with β = tfaa and tfba and only one complex, **A**, in the non-CF_3-β-diketonato complexes with β = acac and ba.

^{1}H NMR measurement of complex **A** and **B** show the expected downfield shifts (*ca*. 0.4 and 0.25 ppm for **A** and **B**, respectively) for the methine proton of the metal chelate ring, relative to the uncoordinated β-diketone. The β-diketonato ligand forms a six-membered, planar chelate ring with the metal, where the transition metal participates in the aromatic system by forming π-bonds. Thus the downfield shift is due to the anisotropic effect of the *pseudo*-aromatic system generated when the β-diketonato ligand coordinates to the Ti centre. The downfield shifts of ~0.4 ppm for resonance **A** is comparable to the downfield shifts of *cis*-$Ti(acac)_2Cl_2$, $Ti(ba)_2Cl_2$ and $Ti(dbm)_2Cl_2$ relative to the uncoordinated β-diketone. Since it has been shown that the complexes, $Ti(\beta)_2Cl_2$ with β = acac, ba and dbm, are in the *cis*-conformation,[21,20] peak **A** is assigned to the signal for the *cis*-geometric isomers. Complex **B** is ~0.25 ppm up-field shifted relative to **A.** Two possible structures for complex **B** are the *trans*-isomer or a dimeric structure. These room temperature spectra are time averaged spectra and do not reveal the true nature of complexes **A** and **B** or the stereochemistry of this octahedral complex.

Table 3.4 ^{1}H NMR chemical shift data of the methine protons (CH) for the chelated and uncoordinated β-diketones in $Ti(\beta)_2Cl_2$ and Hβ respectively.

$Ti(\beta)_2Cl_2$					Free β-diketone
Compound	**Colour**	**^{1}H / ppm CH**	**Δ (A-B)**	**Δ (A-Hβ) Δ (B-Hβ)**	**^{1}H / ppm CH (Hβ)**
(a) CF_3-β-diketones: Series 1					
$Ti(tfaa)_2Cl_2$ [**13**]	Yellow	**A** = 6.40 **B** = 6.24	0.16	0.40 0.24	6.00
$Ti(hfaa)_2Cl_2$ [**14**]	Yellow	**A** = 6.80 **B** = 6.70	0.10	0.40 0.30	6.40
$Ti(tfth)_2Cl_2$ [**15**]	Red	**A** = 6.82 **B** = 6.63	0.19	0.37 0.18	6.45
$Ti(tffu)_2Cl_2$ [**16**]	Red	**A** = 6.93 **B** = 6.74	0.19	0.44 0.25	6.49
$Ti(tfba)_2Cl_2$ [**17**]	Orange	**A** = 7.05 **B** = 6.84	0.21	0.46 0.25	6.59
Series 2					
$Ti(tfaa)_2Cl_2$ [**13**]	Yellow	**A** = 6.40 **B** = 6.24	0.16	0.40 0.24	6.00
$Ti(tfma)_2Cl_2$ [**18**]	Orange	**A** = 6.38 **B** = 6.22	0.16	0.43 0.27	5.95
$Ti(tfdma)_2Cl_2$ [**19**]	Orange	**A** = 6.37 **B** = 6.22	0.15	0.42 0.27	5.95
$Ti(tftma)_2Cl_2$ [**20**]	Orange	**A** = 6.48 **B** = 6.34	0.14	0.43 0.29	6.05
b) Non-CF_3-β-diketones					
$Ti(acac)_2Cl_2$ [**23**]	Orange	*cis* 6.00	-	0.50	5.50
$Ti(ba)_2Cl_2$ [**21**]	Red	*cis* 6.67	-	0.48	6.19
$Ti(dbm)_2Cl_2$ [**22**]	Red	*cis* 7.35	-	0.50	6.85

Variable temperature NMR Room temperature NMR spectra are time-averaged spectra of a rapidly isomerising $Ti(\beta)_2Cl_2$ mixture and it is only by lowering the temperature that one can observe the individual isomers on the NMR time scale. The results obtained for variable temperature ^{1}H and ^{19}F NMR spectroscopy are discussed together, because they provide information about the same β-diketonato fragment of the complex. Peak positions and ratios, related to the methine protons (CH) and CF_3 groups, are presented in **Table 3.5**.

Symmetric β-diketone Ti(hfaa)$_2$Cl$_2$: ^{1}H and ^{19}F NMR spectra of Ti(hfaa)$_2$Cl$_2$ in the temperature range of RT to -50 ºC, are shown in **Figure 3.14**, where the two observed structures are marked **A** and **B**. At room temperature there are two methine peaks ($\mathbf{A}_H$ and $\mathbf{B}_H$) and two corresponding (overlapping) CF_3 peaks ($\mathbf{A}_{CF3}$ and $\mathbf{B}_{CF3}$). As the temperature is lowered, the effect on complex **A** and **B** is strikingly different. For complex **A**, the methine resonance, $\mathbf{A}_H$, remains a singlet and the CF_3 resonance, $\mathbf{A}_{CF3}$, splits into two equally intense lines. This low-temperature one-line methine and two-line CF_3 spectra of structure **A** is consistent with complex **A** having the *cis* configuration in solution (see **Figure 3.14** and **Figure 3.11**). Coalescence of the CF_3 resonances is due to a rapid exchange process which interchanges CF_3 groups between the two nonequivalent sites of the *cis* isomers. Two separate peaks were visible only after the temperature was lowered below -10 °C (known as the coalesence temperature). Raising the temperature above room temperature only results in sharper peaks. For complex **B**, both $\mathbf{B}_H$ and $\mathbf{B}_{CF3}$ transform from a single peak, through a broad, structureless peak into multiple peaks. This is not consistent with complex **B** being the *trans* isomer, because one expects the methine- and the CF_3-resonances, ($\mathbf{B}_H$ and $\mathbf{B}_{CF3}$ respectively) to remain single peaks with temperature lowering. The temperature lowered NMR spectra is, however, consistent with complex **B** being a dimeric structure.

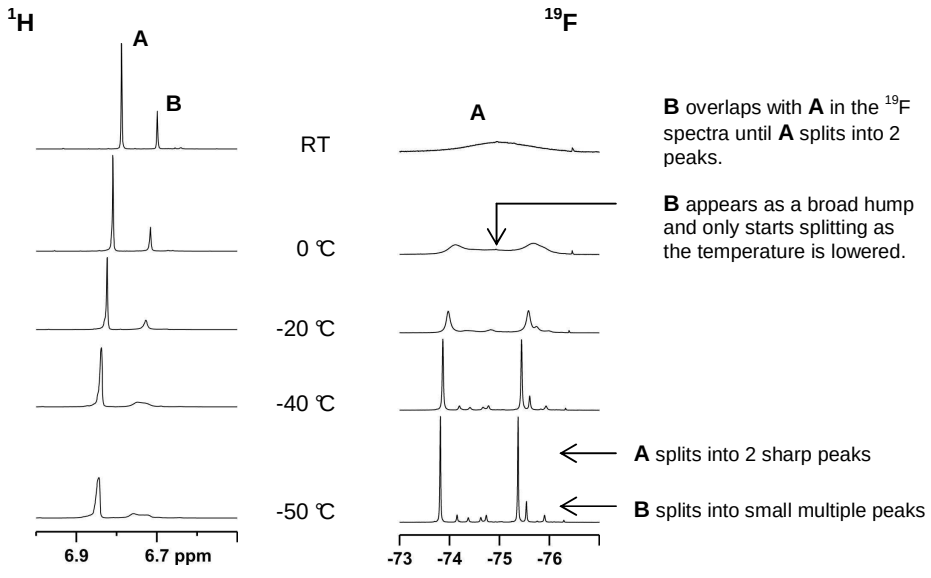

Figure 3.14 Variable temperature NMR spectra ($CDCl_3$) of Ti(hfaa)$_2$Cl$_2$ in the methine region for ^{1}H NMR spectra and the CF_3 region for ^{19}F NMR spectra. Temperature range: RT to -50 °C.

Asymmetric β-diketone Ti(tfaa)$_2$Cl$_2$: ^{1}H and ^{19}F NMR spectra of Ti(tfaa)$_2$Cl$_2$ in the temperature range of 40 ºC to -50 ºC, are shown in **Figure 3.15**, where the two complexes are marked **A** and **B**. At room temperature, the ^{1}H NMR spectrum shows two methine peaks (**A**$_H$ and **B**$_H$) and corresponding methyl resonances (**A**$_{CH3}$ and **B**$_{CH3}$, not shown in **Figure 3.15**) in the correct ratio of 2:6 and the ^{19}F NMR spectrum shows two overlapping CF_3 peaks (**A**$_{CF3}$ and **B**$_{CF3}$). As the temperature is lowered, resonances of complex **A** (**A**$_H$, and **A**$_{CF3}$), first broaden, then form shoulders and finally split into the four expected peaks for the three *cis* isomers (**Figure 3.15** and **Figure 3.12**). For complex **B**, both **B**$_H$ and **B**$_{CF3}$ transform into multiple peaks, consistent with complex **B** having a dimeric structure.

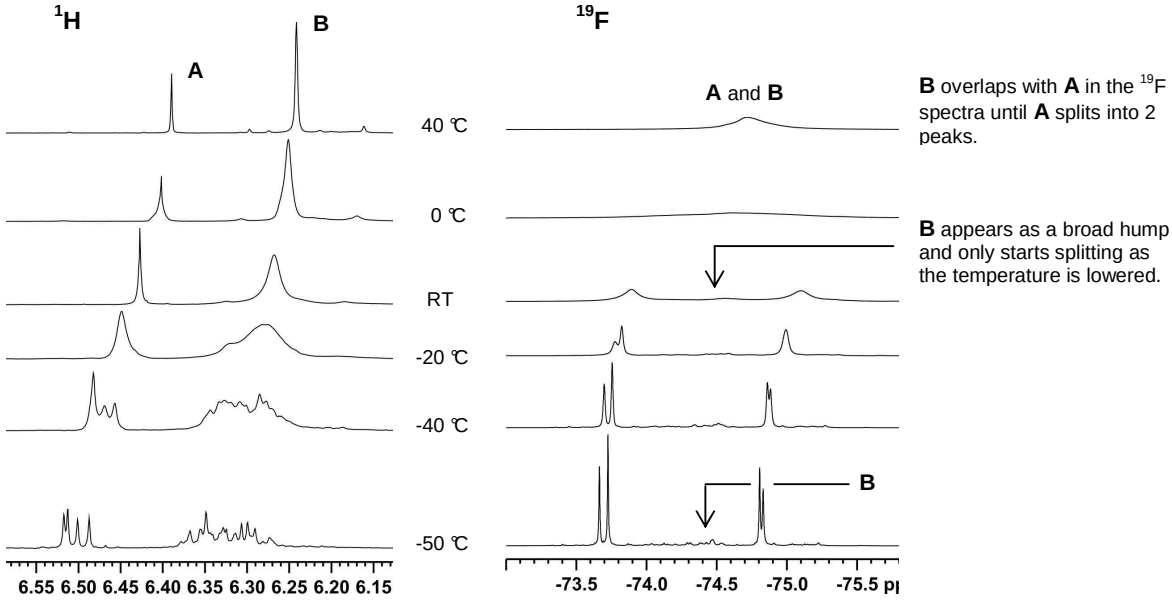

Figure 3.15 Variable temperature NMR spectra ($CDCl_3$) of Ti(tfaa)$_2$Cl$_2$ in the methine region for ^{1}H NMR spectra and the CF_3 region for ^{19}F NMR spectra. Temperature range: 40 °C to -50 °C

All the fluorinated Ti(β)$_2$Cl$_2$ complexes with asymmetric β-diketonato ligands, show the same pattern in the low temperature spectra, (see **Figure 3.16**), *i.e.*, peak **A**$_H$, and **A**$_{CF3}$ split into two to four peaks (temperature lowering below -60 °C, needed for complete peak slitting, is limited by the freezing point of $CDCl_3$, -63.5 °C) and **B**$_H$, and **B**$_{CF3}$ spilt into multiple peaks. This is consistent with complex **A** having the *cis* configuration and complex **B** having a

dimeric structure in solution. DFT calculations on the isomer distribution of these $Ti(\beta)_2Cl_2$ complexes with β = tfba, ba and dbm (see **Section 3.2.3.2,** pp 111) also indicate that complex **B** is not *trans* isomer(s). The relative equilibrium concentrations (%) of the *cis*-isomers, determined from peak integrals, are shown in **Table 3.9**.

Table 3.5 ^{1}H and ^{19}F NMR chemical shifts of the methine proton (CH) and CF_3 of *cis*-$Ti(\beta)_2Cl_2$ complexes, at T = -60 °C. Values shown in blue are the relative contributions of the indicated signals (%) of the three *cis*-isomers.

Compound	^{1}H / CH ppm	№ of Peaks	^{19}F / CF_3 ppm	№ of Peaks
(a) Symmetric-β-diketones				
$Ti(hfaa)_2Cl_2$ **[14]**	6.85 (100)	1	-73.39, -73.49 (50.0), (50.0)	2
(b) Ansymmetric-β-diketones				
$Ti(tfba)_2Cl_2$ **[17]**	7.16, 7.13, 7.12, 7.10 (18.5), (24.6), (38.4), (18.5)	4	-73.39, -73.49, -74.52, -74.55 (16.1), (25.8), (16.1), (41.9)	4
$Ti(tffu)_2Cl_2$ **[16]**	--	--	-73.48, -73.57, -73.62, -74.55 (15.3), (11.5), (22.7), (50.5)	4
$Ti(tfth)_2Cl_2$ **[15]**	--	--	-73.31, -73.52, -74.39, -74.43 (14.3), (57.1), (14.3), (14.3)	4
$Ti(tftma)_2Cl_2$ **[20]**	6.54, 6.53, 6.51, 6.47 (40.0), (24.0), (24.0), (12.0)	4	-73.47, -73.76, -74.71, -74.88 (24.4), (39.0), (24.4), (12.2)	4
$Ti(tfdma)_2Cl_2$ **[19]**	6.45, 6.44, 6.43, 6.40 (41.1), (23.2), (23.2), (12.5)	4	-73.60, -73.86, -74.83, -74.98 (21.3), (36.2), (21.3), (21.2)	4
$Ti(tfma)_2Cl_2$ **[18]**	6.48, 6.47, 6.46 (24.3), (53.7), (22.0)	3*	-73.56, -73.80, -74.74, -74.77 (21.5), (40.9), (21.5), (16.5)	4
$Ti(tfaa)_2Cl_2$ **[13]**	6.52, 6.51, 6.50, 6.49 (26.3), (26.3), (23.7), (23.7)	4	-73.66, -73.72, -74.80, -74.83 (24.3), (30.8), (24.3), (20.6)	4
$Ti(ba)_2Cl_2$ **[21]**	6.77, 6.76 (27.9), (72.1)	2*	**^{1}H / CH_3**: 2.48, 2.47, 2.37 (17.4), (27.9), (54.7)	3*

* Temperature lowering below -60 °C, needed for complete peak slitting, is limited by the freezing point of $CDCl_3$ (-63.5 °C).

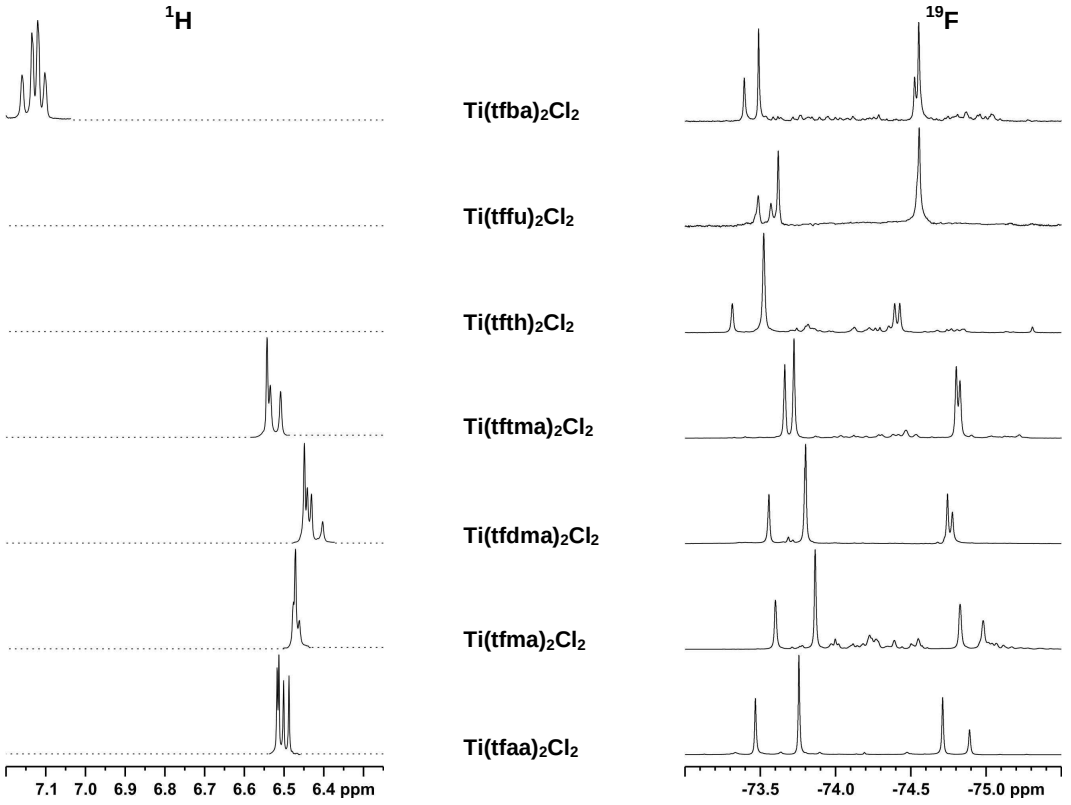

Figure 3.16 Partial ^{1}H and ^{19}F NMR spectra ($CDCl_3$) of Ti(β)$_2$Cl$_2$ complexes with β = tfba, tffu,, tfth, tftma, tfdma and tfaa, at T = -60 °C.

Equilibrium It was found that equilibrium **A** $\rightleftharpoons^{K_c}$ **B** exists. The equilibrium constant, defined by K_c = [**B**]/[**A**], may be determined by calculating the ratio of peak integrals of the non-overlapping corresponding methine signals (of the β-diketonato ligand in Ti(β)$_2$Cl$_2$) of **A** and **B**. The variation of the K_c with temperature for the equilibrium may be mathematically quantified by the van't Hoff equation

$$\ln K_{c2} = \ln K_{c1} - \frac{\Delta_r H}{R}\left(\frac{1}{T_2} - \frac{1}{T_1}\right)$$

where K_{c1} and K_{c2} are the equilibrium constants at temperatures T_1 and T_2, R is the universal gas constant and $\Delta_r H$ the reaction enthalpy[23]. The graph of lnK_c *vs.* 1/T should be linear[23] with slope = $-\Delta_r H/R$. **Figure 3.17** illustrates this linearity for [Ti(tfba)$_2$Cl$_2$] and [Ti(tfaa)$_2$Cl$_2$]. The thermodynamic quantities "Gibbs free energy", $\Delta_r G$, and reaction entropy, $\Delta_r S$, may be calculated from the equations $\Delta_r G = -RT\ln K_c$ and $\Delta_r G = -\Delta_r H - T\Delta_r S$.[24] Results at 298K are summarized in **Table 3.6**.

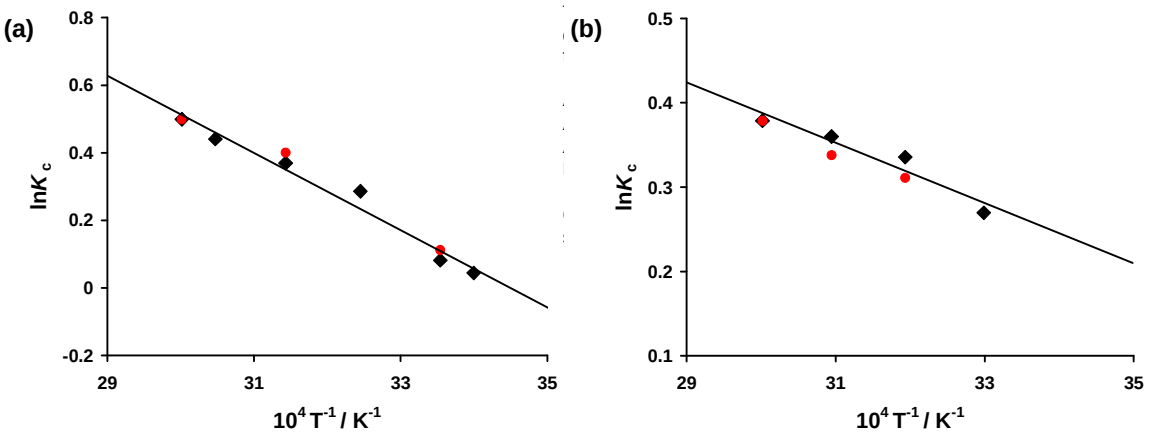

Figure 3.17 Van't Hoff plot: temperature dependence of K_c for the equilibrium position between the **A** and **B** of the **(a)** $[Ti(tfba)_2Cl_2]$ and **(b)** $[Ti(tfaa)_2Cl_2]$ complexes. The black markers represent ln K_c at different temperatures when heating the solution and the red markers ln K_c when cooling the solution**.**

Table 3.6 Thermodynamic values at T= 298 K for **A** $\overset{K_c}{\rightleftharpoons}$ **B** observed in the ^{1}H NMR spectrum of CF_3-containing $Ti(\beta)_2Cl_2$ complexes.

Complex	K_c	$\Delta_r H$ kJ mol^{-1}	$\Delta_r G$ kJ mol^{-1}	$\Delta_r S$ J mol^{-1} K^{-1}
$Ti(tfba)_2Cl_2$ **[17]**	1.12	10	-0.3	33
$Ti(tfaa)_2Cl_2$ **[13]**	0.79	3	-0.7	12

The ^{1}H NMR spectrum of a very concentrated, fresh sample of $Ti(tfaa)_2Cl_2$, contains only peak **A** and with dilution, peak **B** immediately appears (see **Figure 3.18** (a)).

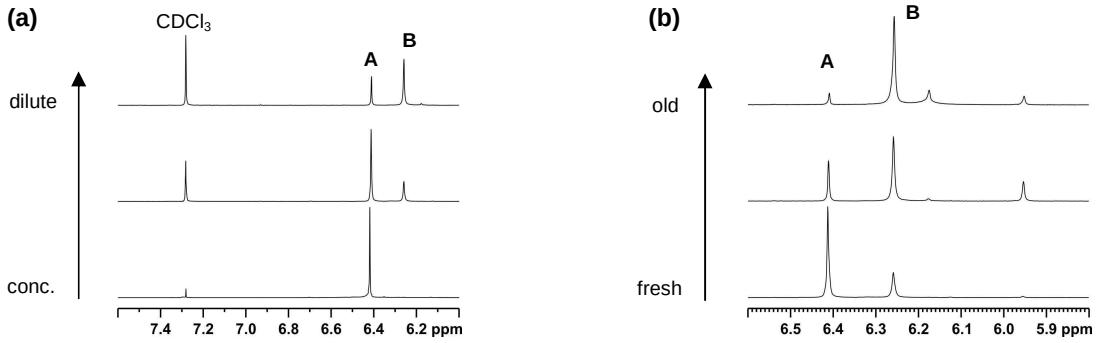

Figure 3.18 ^{1}H NMR spectra of $Ti(tfaa)_2Cl_2$ in $CDCl_3$ showing **(a)** concentrated equilibrium effects and **(b)** the slow equilibrium (and decomposition) over time.

The **A:B** ratio on the dilution cycle is concentration dependent. However, the reverse process could not be followed successfully because while concentrating the sample by evaporating the solvent under a stream of Ar, the sample decomposed. In addition to the fast (concentration dependent) equilibrium, a slow (time dependent) equilibrium exists in which **A** (in a fresh sample) slowly converts to **B** reaching equilibrium, **A** $\rightleftharpoons$ **B** , after a few days at constant temperature and concentration. (**Figure 3.18 (b)**)

If the fluorinated $Ti(\beta)_2Cl_2$ complexes (which exist as an equilibrium mixture of the monomeric *cis*-$Ti(\beta)_2Cl_2$ (**A**) and proposed dimeric complex **B**, are converted to $Ti(acac)_2Cl_2$ *via* β-diketonato substitution, then complex **B**, disappears (observed on ^1H NMR).

$$\textit{cis}\text{-Ti}(\beta)_2\,Cl_2\ \mathbf{A}\ +\ \text{dimer}\ \mathbf{B}\ \xrightarrow[\text{excess}]{\text{Hacac}}\ \textit{cis}\text{-Ti}(acac)_2\,Cl_2\ +\ H\beta$$

This is consistent with the existence of an equilibrium between **A** and **B**; as the monomeric *cis*-$Ti(\beta)_2Cl_2$ transforms to *cis*-$Ti(acac)_2Cl_2$, the dimeric complex **B** converts back to monomeric *cis*-$Ti(\beta)_2Cl_2$, followed by the completion of the substitution reaction in which *cis*-$Ti(acac)_2Cl_2$ is the final and only Ti product.

Hydrolysis The fluorinated $Ti(\beta)_2Cl_2$ complexes are extremely moisture and oxygen sensitive but are stable if sealed and stored under Argon, at room temperature. They appear to be more stable in the solid phase, than in solution, probably because solutions are more susceptible to atmospheric oxygen and water vapour. However, in either case, if exposed to atmosphere, the complex converts to a fine, white powder, titanium dioxide (TiO_2), consistent with the complete hydrolysis and decomposition, proposed by Keppler and Heim.[25] Hydrolysis occurs in different stages; the easily hydrolysable Cl^- groups, substitute rapidly, followed by the relatively slower substitution of the β-diketonato ligand. The replacement of the β-diketonato ligand is observed by the development of turbidity caused by the precipitation of TiO_2.

Scheme 3.6, adapted from the hydrolysis reaction proposed by Keppler and Heim,[25] shows the hydrolysis of $Ti(\beta)_2Cl_2$ under different conditions. When $Ti(\beta)_2Cl_2$ complexes are exposed to minor quantities of water, dimeric or tetrameric structures form. The replacement of one Cl^- group with H_2O (developing a Ti-OH bond with the removal of HCl), is followed by the formation of a Ti-O-Ti bridge in the dimeric structure. The replacement of both Cl^- groups results in the oxo-bridged tetramer (see **Scheme 3.7**).

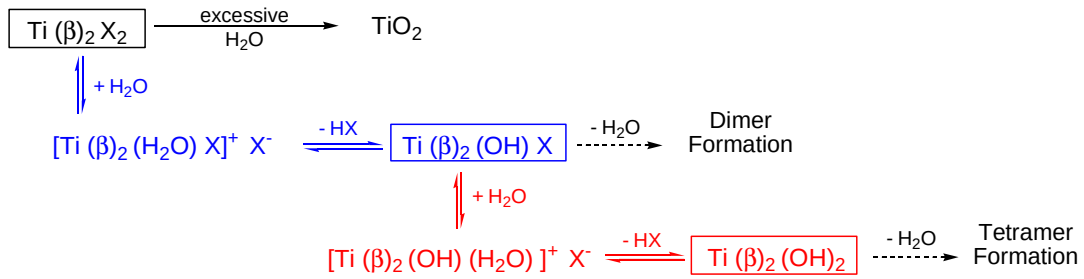

Scheme 3.6 Hydrolysis of $Ti(\beta)_2Cl_2$ under different conditions.

The balance equations for the dimerisation and tetramerisation are

$$4\ Ti(\beta)_2Cl_2 + 2\ H_2O - 4\ HCl \longrightarrow 2\ \{Ti(\beta)_2Cl\}_2\ (\mu\text{-}O)$$

$$4\ Ti(\beta)_2Cl_2 + 4\ H2O - 8\ HCl \longrightarrow [Ti(\beta)_2\ (\mu\text{-}O)]_4$$

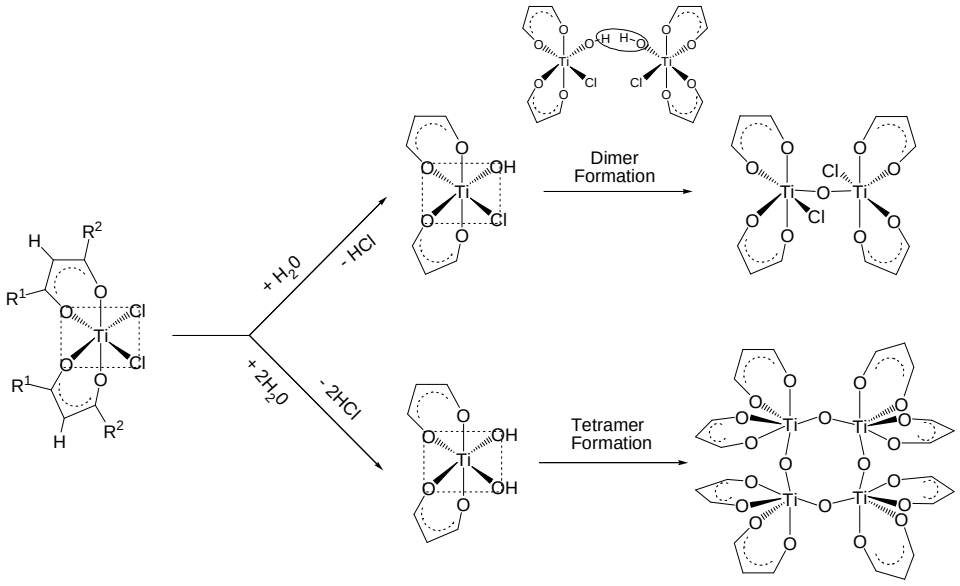

Scheme 3.7 The hydrolysis reaction of $Ti(\beta)_2Cl_2$ with minor quantities of water, showing the formation of dimeric $\{Ti(\beta)_2Cl\}_2$ (μ-O) and tetrameric $[Ti(\beta)_2(\mu\text{-}O)]_4$ structures.

The formation of the dimeric, $\{Ti(hfaa)_2Cl\}(\mu\text{-}O)$ and $\{Ti(tfaa)_2Cl\}(\mu\text{-}O)$ and tetrameric, $[Ti(hfaa)_2(\mu\text{-}O)]_4$, crystals is rapid and can be observed visually (crystal structures shown in **Section 3.3.2.2** and **Section 3.3.2.4**). The oxo-bridged complexes appeared to be considerably more stable to atmospheric moisture, than the monomeric $Ti(\beta)_2Cl_2$ complexes. They are insoluble in $CHCl_3$ as opposed to the monomers which dissolve readily, and only after the crystalline compounds were crushed and heated to 60 °C, could ^1H NMR spectra of the dimeric and tetrameric complexes be taken (see **Figure 3.19**).

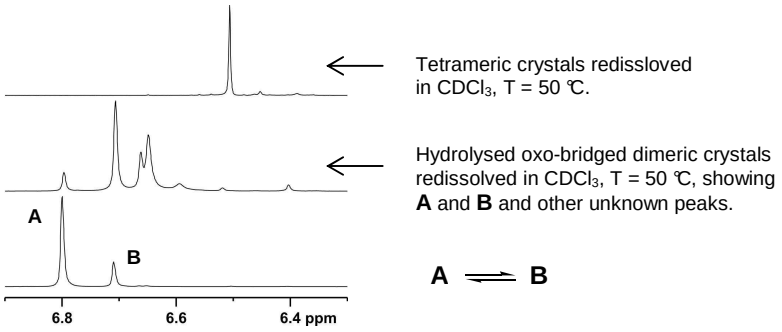

Figure 3.19 ^{1}H NMR spectra of $Ti(hfaa)_2Cl_2$ as a monomer, dimer and tetramer.

Proposed Dimeric structure The proposed structure for **B**, shown in **Figure 3.20**, is of the same form as the hydrolysed oxo-bridged dimeric structure, $\{Ti(hfaa)_2Cl\}_2(\mu\text{-}O)$ (crystal structure shown in **Section 3.3.2.2)**. The high temperature ^{1}H NMR spectrum of the hydrolysed dimer (see **Figure 3.19**), shows two peaks that correspond to monomeric *cis*-$Ti(hfaa)_2Cl_2$ (**A**) and proposed dimer (**B**) and other unknown peaks. Although this ^{1}H NMR spectrum does not conclusively indicate whether the structure of complex **B** is the same as the hydrolysed dimer, it does however, agree with them being the same structure. If the hydrolysed dimer, $\{Ti(\beta)_2Cl\}_2(\mu\text{-}O)$, and equilibrium dimer **B** are identical, one would expect to observe the monomeric *cis*-$Ti(hfaa)_2Cl_2$ (**A**) in the spectrum, since **A** is in equilibrium with **B**. However, if the hydrolysed dimer and equilibrium dimer **B** are not identical, it would be difficult to explain why **A** and **B** are present in the ^{1}H NMR spectrum of the crystalline hydrolysed dimer. The unknown peaks are likely to be decomposition products, which are expected, since the crystals were crushed in the open atmosphere.

The equilibrium between monomer **A** and dimer **B** would imply the breaking and forming of Ti-O and Ti-Cl bonds. This is conceivable since the strength of the Ti-O and Ti-Cl bonds are very similar, i.e., 478 and 494 kJ mol^{-1}, respectively.[1,26]

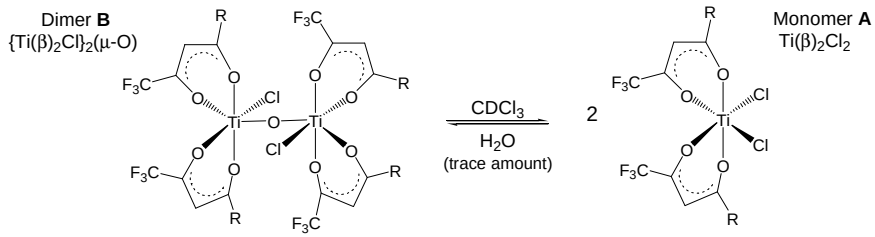

Figure 3.20 Possible structure for complex **B** $\{Ti(\beta)_2Cl\}_2(\mu\text{-}O)$ in equilibrium with *cis*-$Ti(\beta)_2Cl_2$ when β = fluorinated β-diketonato ligand.

3.2.3.2 Bis(β-diketonato)$_2$-(biphenyldiolato) Ti(IV) complexes: Ti(β)$_2$biphen

The series of new bis(β-diketonato)biphendiolatotitanium(IV) complexes of the form Ti(β)$_2$biphen with β = **CF$_3$**COCHCO**R**, (*Series 1*): R = CH_3 (tfaa) **[24]**, CF_3 (hfaa) **[25]**, C_4H_3S (tfth) **[26]**, C_4H_3O (tffu) **[27]**, Ph (tfba) **[28]** and (*Series 2*): R = CH_3 (tfaa) **[24]**, $C(CH_3)H_2$ (tfma) **[29]**, $C(CH_3)_2H$ (tfdma) **[30]** and $C(CH_3)_3$ (tftma) **[31]**, was synthesised in high yields according to **Scheme 3.8**. Non-CF_3-containing complexes, i.e., Ti(ba)$_2$biphen **[32]**, Ti(dbm)$_2$biphen **[33]** and Ti(acac)$_2$biphen **[36]**, were also synthesised to extend the ligand-exchange equilibria studies, including the exchange of non-CF_3-β-diketonato ligands and also to confirm the products in the substitution kinetics of Ti(β)$_2$Cl$_2$ + H$_2$biphen → Ti(β)$_2$biphen + 2HCl, where β = ba, dbm, tfba.

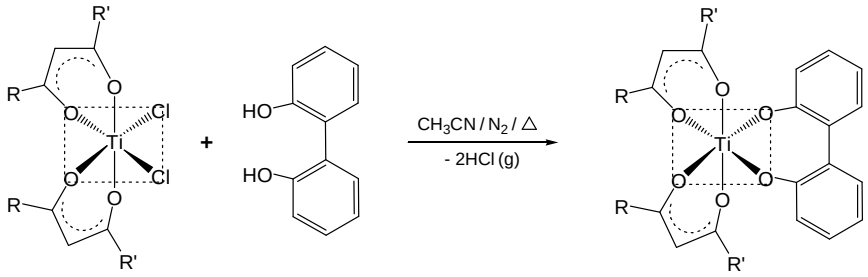

Scheme 3.8 Synthesis of Ti(β)$_2$(biphen) complexes, with β = tfaa, hfaa, tfth, tffu, tfba, tfma, tfdma, tftma, acac, ba and dbm.

The starting material Ti(β)$_2$Cl$_2$ was prepared by treating $TiCl_4$ with two equivalents of the appropriate β-diketone and isolated and purified by recrystallisation before use (see **Section 3.2.3.1**). The reaction of Ti(β)$_2$Cl$_2$ with 2,2'-biphenol in 1:1 ratio in CH_3CN yielded the mixed ligand complex, Ti(β)$_2$(biphen). Even with the use of higher ligand ratios, 1:2 or 1:3, the reaction yielded Ti(β)$_2$(biphen) rather than a product possessing more than one biphenolato ligand in the coordination sphere of Ti. This is similar to what was found for the reaction between Ti(acac)$_2$Cl$_2$ and 1,1'-methylene-di-2-naphthol.[27] The fluorinated biphenolato complexes are soluble in DCM, chloroform, acetonitrile, acetone, slightly soluble in methanol, diethyl ether and nearly insoluble in hexane and H_2O. The solubility of the fluorinated biphenolato complexes differs from the solubility of the non-CF_3 analogues, for example, Ti(tfaa)$_2$biphen and Ti(tfba)$_2$biphen are soluble in acetonitrile while Ti(acac)$_2$biphen and Ti(ba)$_2$biphen are poorly soluble.

NMR Characterisation Selected ^{1}H NMR spectra at room temperature are shown in **Figure 3.21** and the chemical shifts of the methine protons are listed in **Table 3.7**, where values for the uncoordinated β-diketone (enol) are included for comparison. The spectra consist esssentially of the biphenol ring protons, arranged in the ratio of 2:2:2:2, in a (d, t, t, d) pattern, compared to the 2:2:4, (d, t, m) pattern in the uncoordinated ligand (**Figure 3.5**); the methine protons, a singlet, integrating for two and the corresponding resonances for the R-groups of the β-diketone ligands. The disappearance of the phenolic–OH protons, suggests that the bidentate biphenolato ligand is chelated through the two oxygens to the Ti(IV) centre. The ^{1}H NMR spectra, are consistent with a mononuclear structure of Ti(β)$_2$biphen.

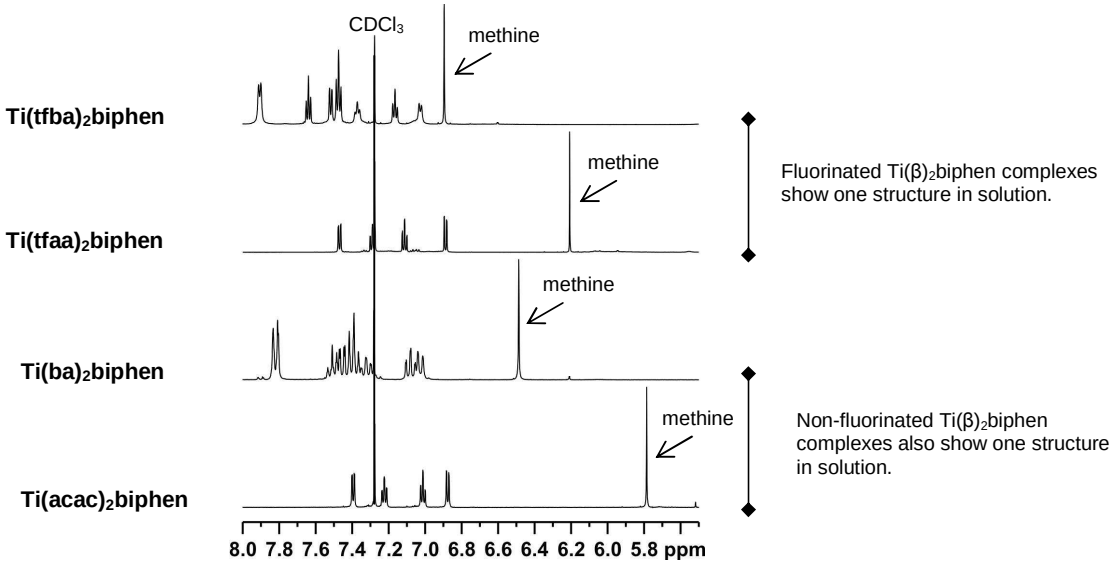

Figure 3.21 Selected room temperature ^{1}H NMR spectra ($CDCl_3$) of Ti(β)$_2$biphen complexes in the methine region, with β = acac, ba, tfaa and tfba, showing that both the fluorinated and non-fluorinated complexes exist as monomers in solution.

The chemical shifts of the chelated, biphenol protons remain relatively constant for the entire series of complexes**,** indicating that the electronic environment of these ring protons is not influenced significantly by the R groups of the β-diketones. This is in contrast to the methine proton which varies from δ 5.78 ppm (acac) to 7.18 ppm (dbm), reflecting the direct influence of the R-groups of the β-diketones. The chemical shifts of the methine proton of Ti(β)$_2$biphen and the parent compound, Ti(β)$_2$Cl$_2$, are downfield shifted by *ca.* 0.2 to 0.3 ppm (see **Table 3.7**) and *ca* 0.4 to 0.5 ppm (see **Table 3.4**), respectively, relative to the corresponding uncoordinated β-diketone. In both Ti(β)$_2$biphen and Ti(β)$_2$Cl$_2$, a *pseudo*-aromatic system is generated when the β-diketonato ligand coordinates to the Ti(IV) centre and thus, a downfield

shift (relative to the uncoordintaed ligand) is expected. However, one can conclude that the chlorine ligands affords more deshielding than the biphenol ligand in these bis(β-diketonato)Ti(IV) complexes, since the methine proton of $Ti(\beta)_2Cl_2$ is shifted futher downfield than $Ti(\beta)_2$biphen.

Table 3.7 ^{1}H NMR chemical shifts for the methine protons (CH) in the chelated $Ti(\beta)_2$(biphen) complexes and the uncoordinated β-diketone.

$Ti(\beta)_2$biphen				**Free β-diketone**
Compound	**Colour**	**^{1}H / ppm CH (A)**	**Δ (A-Hβ)**	**^{1}H / ppm CH (Hβ)**
CF_3-β-diketones:				
Series 1				
$Ti(tfaa)_2$biphen **[24]**	Deep red	6.21	0.21	6.00
$Ti(hfaa)_2$biphen **[25]**	Deep red	6.61	0.21	6.40
$Ti(tfth)_2$biphen **[26]**	Deep red	6.67	0.22	6.45
$Ti(tffu)_2$biphen **[27]**	Deep red	6.78	0.29	6.49
$Ti(tfba)_2$biphen **[28]**	Deep red	6.89	0.29	6.60
Series 2				
$Ti(tfaa)_2$biphen **[24]**	Deep red	6.21	0.21	6.00
$Ti(tfma)_2$biphen **[29]**	Deep red	6.20	0.25	5.95
$Ti(tfdma)_2$biphen **[30]**	Deep red	6.21	0.28	5.95
$Ti(tftma)_2$biphen **[31]**	Deep red	6.33	0.27	6.05
Non-CF_3-β-diketones				
$Ti(acac)_2$biphen **[36]**	Orange	5.79	0.29	5.50
$Ti(ba)_2$biphen **[32]**	Red	6.49	0.30	6.19
$Ti(dbm)_2$biphen **[33]**	Red	7.18	0.33	6.85

Hydrolysis The biphenolato complexes exhibit high hydrolic stability and are "air stable" for more than 3 years. The solution stability was tested under the same conditions as Keppler and Heim,[25] i.e., 0.01 % water/CH_3CN, and it was found that the biphenolato complexes do not precipitate within 4 weeks compared to the dichloro complexes which precipitate within seconds.

A batch of single crystals grown from $Ti(hfaa)_2$biphen, yielded the oxo- and biphenolato-bridged dinuclear, $\{Ti(hfaa)_2\}_2(\mu\text{-}O)(\mu\text{-biphen})$ complex, shown in **Figure 3.22**. Ti(IV) has a

d^0 configuration and thus a highly oxophilic nature. Ti(hfaa)$_2$biphen is more susceptible to oxygen-bridging and dimer formation (than the other biphenolato complex in the series), since the strong electron withdrawing influence of the hexafluoroacetylacetonato ligand further depletes the electron density around the Ti(IV) centre.

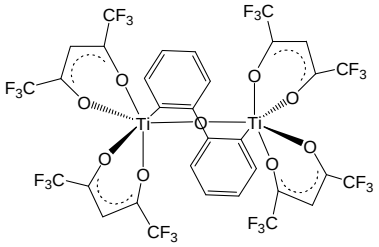

Figure 3.22 Hydrolysed dimeric structure, {Ti(hfaa)$_2$}$_2$(μ-O)(μ-biphen) with a bridging biphenolato ligand (see **Section 3.3.2.3** for crystal structure).

When selected dinuclear crystals were redissolved in $CDCl_3$, a mixture of monomer and dimer was identified by ^{1}H NMR spectroscopy. After 2 days the solution still revealed a mixture of both monomer and dimer. Since the batch of crystals appeared to be uniform, (i.e., all the crystals had the same deep purple/red colour and a similar shape) and the six crystals selected for a single crystal study all gave the cell dimensions of the dimer, it was assumed that the entire batch was of the dinuclear form in the solid state.

Stereochemisty Ti(β)$_2$X$_2$ complexes can theoretically adopt a *cis* and *trans* orientation, but once the two monodentate ligands are replaced by the bichelating 2,2'-biphenol, only the *cis* geometry is possible. For symmetrically substituted Ti(β)$_2$biphen complexes (*e.g.*, β = hfaa, R = CF_3), there is only one *cis* isomer, while for asymmetrically substituted complexes (*e.g.*, β = tfaa, tfma, tfdma, tftma, tfth, tffu and tfba with R = CH_3, $CH_2(CH_3)$, $CH(CH_3)_2$, $C(CH_3)_3$, C_4H_3S, C_4H_3O and Ph respectively), there are three possible *cis* isomers (see **Figure 3.23**). In order to keep the naming of the isomers consistent with the Ti(β)$_2$Cl$_2$ nomenclature, three prefixes, specifying relative positions, are used; first the relative position of the chelated oxygen atoms of biphenol, followed by the relative orientation of the CF_3 and R groups of the β-diketone ligand respectively. The symmetry elements and the expected NMR signals are shown in **Figure 3.23**.

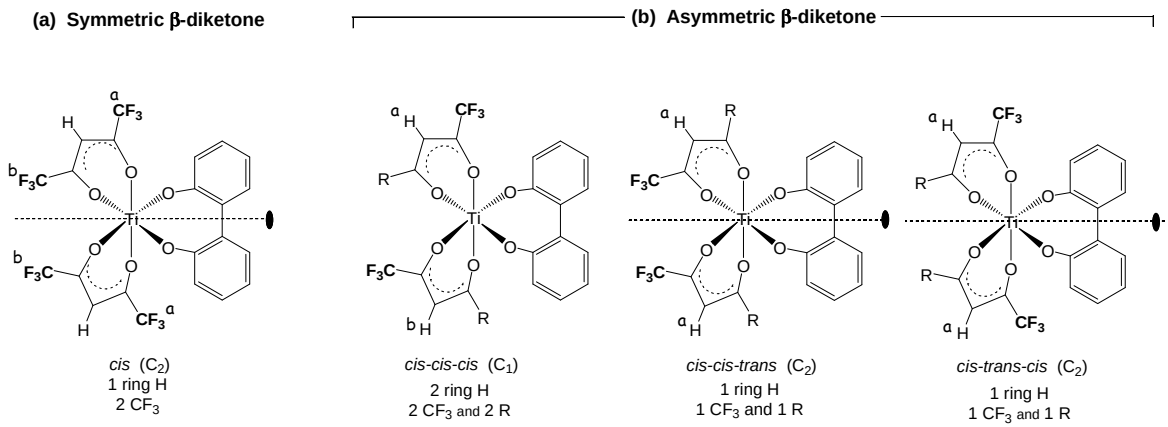

Figure 3.23 The stereochemistry of octahedral Ti(β)$_2$biphen complexes with **(a)** symmetric β–diketonato ligands and **(b)** asymmetric β–diketonato ligands, showing the possible isomers and the expected number of ^{1}H and ^{19}F NMR signals.

Variable temperature study In order to observe the individual isomers on the NMR time scale the temperature was lowered to the solvent limit of -60 °C. The results obtained by variable temperature ^{1}H and ^{19}F NMR spectroscopy are discussed together, because they provide information about the same β-diketonato fragment. Peak positions and ratios, related to the methine protons (CH) and CF_3 groups, are presented in **Table 3.8**.

Asymmetric β-diketone Ti(tfba)$_2$biphen: ^{1}H NMR spectra of Ti(tfba)$_2$biphen in the methine region and temperature range of 25 ºC to -60 ºC, are shown in **Figure 3.24**. At RT, the ^{1}H NMR spectrum shows one time averaged methine (CH) peak. As the temperature is lowered, the resonance first broadens, then form shoulders and finally split into the four expected peaks for the three *cis* isomers.

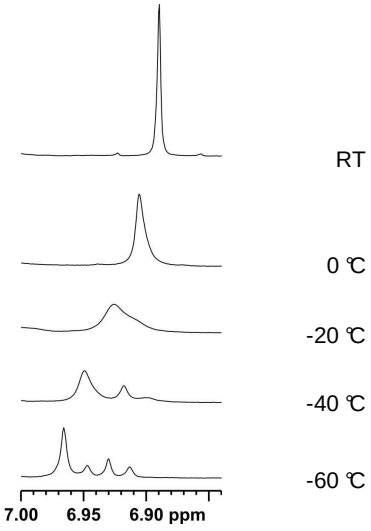

Figure 3.24 The ^{1}H NMR spectra ($CDCl_3$) of Ti(tfba)$_2$biphen in the methine region and temperature range of RT to -60 °C.

All the Ti(β)$_2$biphen complexes with asymmetric β-diketonato ligands, show the same pattern in the low temperature spectra, (see **Figure 3.25** for fluorinated complexes), *i.e.*, the CH peaks split each into two to four peaks (temperature lowering below -60 °C, needed for complete peak slitting, is limited by the freezing point of $CDCl_3$,-63.5 °C) and the CF_3 peaks split into four peaks. This is consistent with the Ti(β)$_2$biphen complexes being monomeric and having the *cis* configuration. The relative equilibrium concentrations (%) of the three *cis*-isomers of Ti(β)$_2$biphen complexes with β = tfba, ba and dbm, calculated from the peak integrals, are shown in **Table 3.9**.

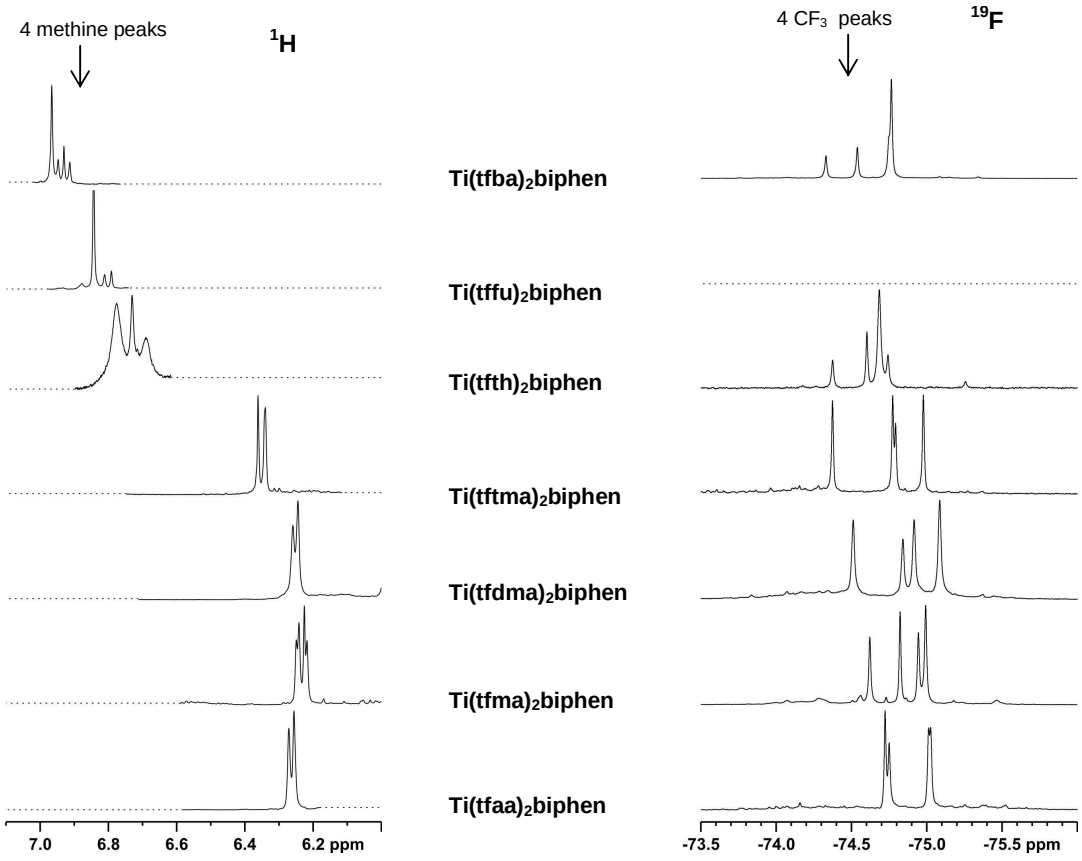

Figure 3.25 Partial ^{1}H and ^{19}F NMR spectra ($CDCl_3$) of Ti(β)$_2$biphen complexes with β = tfba, tffu, tfth, tftaa, tfdma, tfma and tfaa, at T = -60 °C.

Isomer Distribution of Ti(β)$_2$Cl$_2$ and Ti(β)$_2$biphen complexes

If a statistical distribution of three *cis*-isomers exists, the relative equilibrium concentrations will be 50 % *cis-cis-cis*, 25 % cis-*cis-trans* and 25 % *cis-trans-cis* and four equally intense resonances are expected.

Table 3.8 ^{1}H and ^{19}F NMR chemical shifts of the methine proton (CH) and CF_3 of Ti(β)$_2$biphen complexes, at T = -60 °C. Values shown in blue are the relative contributions to the indicated signals (%) of the three *cis*-isomers.

Compound	^{1}H / CH ppm	№ of Peaks	^{19}F / CF_3 ppm	№ of Peaks
Unsymmetric-β-diketones				
Ti(tfba)$_2$biphen **[28]**	6.97 6.95, 6.93, 6.91 (62.4), (8.5), (20.6), (8.6)	4	-74.33, -74.54, -74.75, -74.76 (10.7), (17.2), (10.5), (61.6)	4
Ti(tffu)$_2$biphen **[27]**	6.88, 6.84, 6.81, 6.79 (9.5), (68.1), (11.2), (11.2)	4	--	--
Ti(tfth)$_2$biphen **[26]**	6.78, 6.73, 6.69 (47.6), (23.8), (28.6)	3*	-74.37, -74.60, -74.68, -74.74 (12.8), (20.9), (53.5), (12.8)	4
Ti(tftma)$_2$biphen **[31]**	6.36, 6.34 (46.7), (53.3)	2*	-74.37, -74.77, -74.79, -74.98 (28.5), (25.1), (17.9), (28.5)	4
Ti(tfdma)$_2$biphen **[30]**	6.26, 6.24 (46.5), (53.5)	2*	-74.51, -74.84, -74.92, -75.08 (25.2), (16.5), (25.2), (33.0)	4
Ti(tfma)$_2$biphen **[29]**	6.25, 6.24, 6.23, 6.22 (20.4), (30.6), (28.6), (20.4)	4	-74.62, -74.82, -74.94, -74.99 (21.6), (28.8), (21.6), (28.0)	4
Ti(tfaa)$_2$biphen **[24]**	6.27, 6.26 (45.5), (54.5)	2*	-74.72 -74.75, -75.01, -75.02 (28.0), (23.2), (24.4), (24.4)	4
Ti(ba)$_2$biphen **[32]**	6.53, 6.51, 6.50 (25.6), (49.2), (25.2)	3*	**^{1}H / CH_3** 2.21, 2.18, 2.13 (25.2), (51.6), (23.2)	3*

* Temperature lowering below -60 °C, needed for complete peak slitting, is limited by the freezing point of $CDCl_3$ (-62.5 °C).

Density functional theory (DFT) calculations were carried out on the different isomers of the dichloro- and biphenolato- bis(β-diketonato)Ti(IV) complexes, Ti(β)$_2$Cl$_2$ and Ti(β)$_2$(biphen) with β = tfba, ba and dbm (Ph series). The validity of the density functional method was obtained by comparing the calculated data with known single crystal X-ray diffraction structural data of Ti(ba)$_2$Cl$_2$ **[21]**[28] and Ti(ba)$_2$(biphen) **[32]**. The root-mean-square distances (RMSD) calculated for non-hydrogen atoms for the best three-dimensional superposition of calculated structures on experimental structures give a qualitative measurement of the accuracy of the ground state geometry of the calculated structures. Excellent agreement between experimental and theoretical structures is obtained as reflected by the RMSD values of 0.061 and 0.041 Å for **[21]** and **[32]** respectively. Overlay of the calculated and solid state structures are presented in **Figure 3.26**. The bonds were reproduced by DFT calculations within 0.01-0.07 Å for Ti-O bonds, within 0.00 – 0.01 for O-C bonds and within 0.01-0.02 Å for C-C bonds from the experimental values. Since comparisons of experimental metal-ligand

bond lengths with calculated bond lengths below a threshold of 0.02 Å are considered as meaningless,[29] the computational method used thus gives a good account of experimental bond lengths. The O1-Ti-O2 angles were calculated accurately within 1.2°. Structural data computed with this computational method for related compounds may therefore be presented with an extrapolative equally high degree of accuracy.

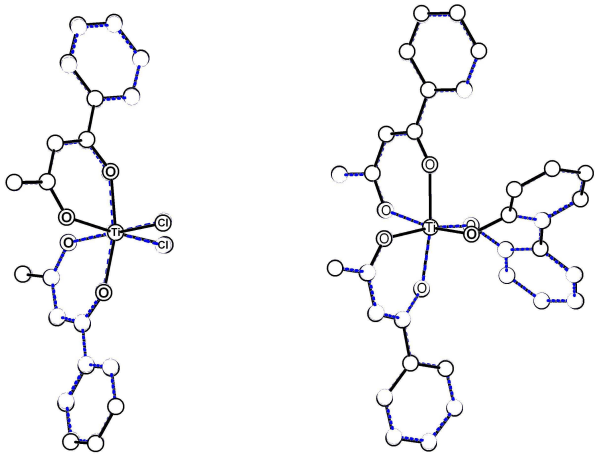

Figure 3.26 An overlay view of the calculated (solid) and the experimental (dashed) X-ray determined structure of $Ti(ba)_2Cl_2$ **[21]** and $Ti(ba)_2$biphen **[32]**. All the unmarked molecules are C. H are omitted for clarity.

The relative energies of the three *cis* isomers of each complex clearly highlight the geometry preferences and by applying the Boltzmann equation a population analysis of the isomers distribution was done. The calculated isomer distributions together with the experimentally observed populations (which are assigned according to the calculated isomer distribution) are given in **Table 3.9**. It was found that the geometry of the lowest energy isomer of both **[21]** and **[32]** was the same as the isomer that crystallised from solution. A generally good agreement is obtained between the experimentally observed isomer distribution and the calculated values. (*Note*: The isomers of complexes with asymmetric β-diketonato ligands are referred to by three prefixes which specify the relative position firstly of the Cl (or chelated O atoms of the biphenol), followed by the relative orientation of the CF_3 (or Ph if no CF_3 present in complex) and lastly, R groups of the β-diketone ligand respectively).

Table 3.9 Calculated and experimentally observed isomer distribution of $Ti(\beta)_2Cl_2$ and $Ti(\beta)_2$biphen complexes.

Compound	Isomer	% Observed ^{1}H NMR	% Observed ^{19}F NMR	% Calculated
$Ti(tfba)_2Cl_2$ **[17]**	*cis-cis-cis*	37.0	32.2	39.5
	cis-trans-cis	24.6	25.8	18.4
	cis-cis-trans	38.4	41.9	41.9
	trans-trans-trans	0.0	0.0	0.2
	trans-cis-cis	0.0	0.0	0.0
$Ti(ba)_2Cl_2$ **[21]**	*cis-cis-cis*	27.9	--	31.0
	cis-trans-cis	54.7	--	61.7
	cis-cis-trans	17.4	-	6.7
	trans-trans-trans	0.0	--	0.5
	trans-cis-cis	0.0	--	0.1
$Ti(dbm)_2Cl_2$ **[22]**	*cis*	100.0	--	97.1
	trans	0.0	--	2.9
$Ti(tfba)_2$biphen **[28]**	*cis-cis-cis*	17.1	21.2	19.5
	cis-cis-trans	62.4	61.6	62.2
	cis-trans-cis	20.6	17.2	18.3
$Ti(ba)_2$biphen **[32]**	*cis-cis-cis*	25.6	--	26.5
	cis-cis-trans	25.2	--	29.8
	cis-trans-cis	49.2	--	43.7
$Ti(dbm)_2$biphen **[33]**	*cis*	100.0	--	100.0

3.2.3.3 Bis(β-diketonato)$_2$-(aryl diolato) Ti(IV) complexes:Ti(β)$_2$L

The new series of bis(acetylacetonato)-aryl-diolato-titanium(IV) complexes of the form $Ti(acac)_2L$ with L = cat ($L^{5,1}$) **[34]**, naph ($L^{5,2}$) **[35]**, biphen ($L^{7,1}$) **[36]**, binaph ($L^{7,2}$) **[37]**, mbiphen ($L^{8,1}$) **[38]**, mbinaph ($L^{8,2}$) **[39]**, was synthesised according to **Scheme 3.9**. The synthetic route was adapted from the "one-pot" method published by Brown *et al.*[30] for the reaction of $TiCl_4$ + Hacac + binaphthol yielding $Ti(acac)_2$binaph. Complexes in this series form 5-, 7- and 8-membered chelated rings while keeping the acac ligands constant.

The reaction, initiated by adding $Ti(acac)_2Cl_2$ to the poorly dissolved ligand in DCM, changes colour immediately to dark red in all cases. These aryl-diolato ligands which are slightly soluble in DCM at room temperature dissolve rapidly (as the reaction proceeds) on shaking. After standing 4.5 h at room temperature, the mixture is layered with hexane and allowed to stand for 2 days, after which the red crystaline product is isolated by filtration and washed with hexane.

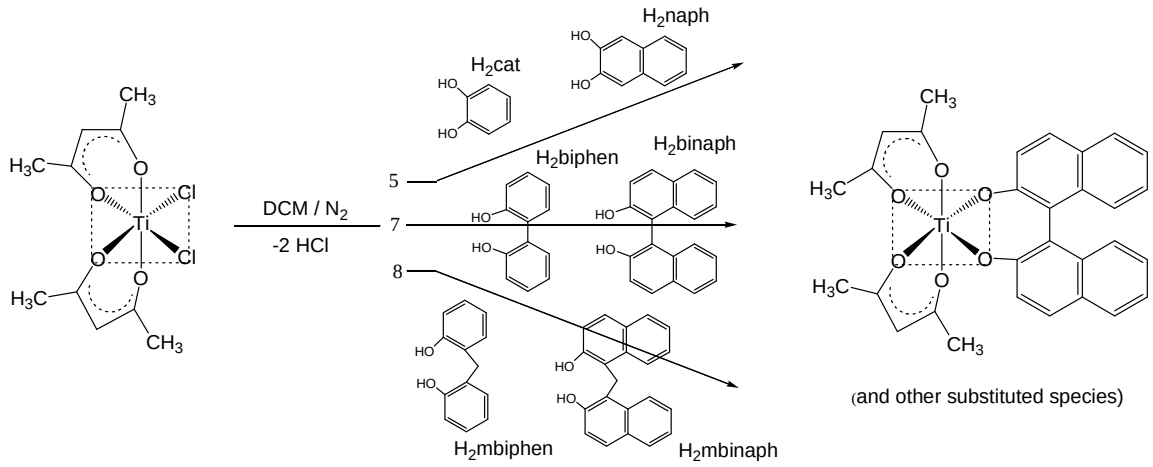

Scheme 3.9 Synthesis of $Ti(acac)_2(L)$ complexes, L = H_2cat **[34]**, H_2naph **[35]**, H_2biphen **[36]**, H_2binaph **[37]**, H_2mbiphen **[38]**, H_2mbinaph **[39]**

NMR Characterisation Selected ^{1}H NMR spectra (in aromatic region) of the $Ti(acac)_2L$ series are shown in **Figure 3.27**. The chemical shifts of the methine proton of acac in the coordinate complex and for the uncoordinated acac (included for comparison) are listed in **Table 3.10**. The spectra consist of three groups of signals: the aromatic aryl-diolato ring protons, the methine protons (singlet, 2x CH) and the corresponding CH_3 resonances for the R-groups of the acac ligands (4x CH_3). For $Ti(acac)_2$mbiphen and $Ti(acac)_2$mbinaph, an additional signal is observed for the methylene protons (singlet CH_2). The disappearance of the phenolic–OH protons, suggests that the bidentate ligand is chelated through the two oxygens to the Ti(IV) centre.The following trends were observed for the $Ti(acac)_2L$:

• The acac methine proton of $Ti(acac)_2L$ (δ = 5.90 - 5.77 ppm) is on average upfield shifted by, δ = 0.17 ppm relative to the parent, $Ti(acac)_2Cl_2$ (δ = 6.00 ppm). This is expected since the aryl-diolato ligands are more electron-donating than Cl.

• The size of the aryl-diolato ring in the $Ti(acac)_2L$ series does have an effect on the shift of the acac methine proton, although it does not increase with increasing ring size. For example, $Ti(acac)_2$cat, $Ti(acac)_2$biphen and $Ti(acac)_2$mbiphen, with ring size 5, 7 and 8 respectively, have δ = 5.90, 5.79 and 5.82 ppm respectively (see **Table 3.10**).

• The addition of an extra phenyl ring on the aryl-diolato ligand has an insignificant effect on the shift of the acac methine proton. For example, $Ti(acac)_2$cat and $Ti(acac)_2$naph (with ring

size-5), have δ = 5.90 and 5.89 ppm respectively. The other couple with L = biphen and binaph (ring size-7) and mbiphen and mbinaph (ring size-8), show the same trend (see **Table 3.10** and **Figure 3.27**).

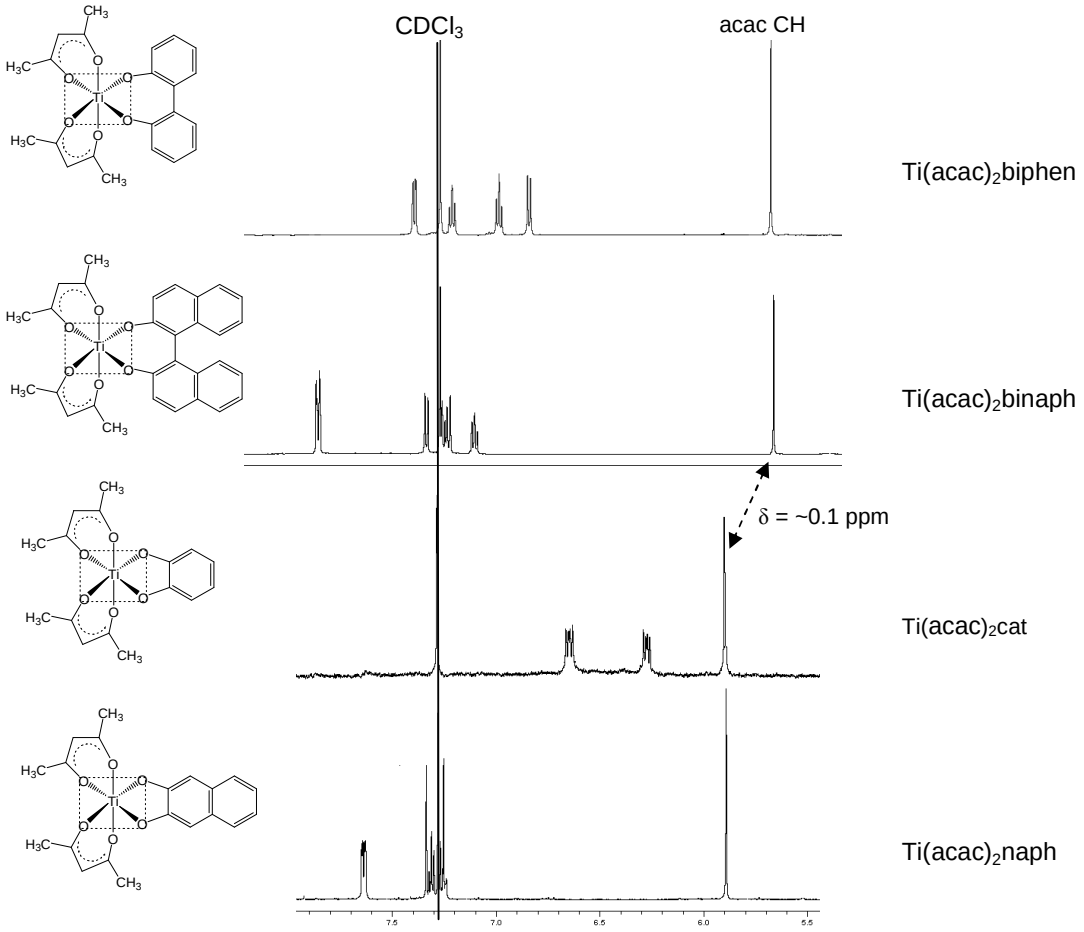

Figure 3.27 Partial ^{1}H NMR spectra ($CDCl_3$) in the aromatic and methine region of **(a)** $Ti(acac)_2$cat and $Ti(acac)_2$naph and **(b)** $Ti(acac)_2$biphen and $Ti(acac)_2$binaph**.**

• The aryl-diolato ring protons of the chelated complex are shifted slightly upfield relative to the uncoordinated ligand. In **Figure 3.28** the ^{1}H NMR spectra in the aromatic region for $Ti(acac)_2$biphen and $Ti(acac)_2$binaph, show the shift relative to the uncoordinated ligands. This same trend was observed for the tetrahedral CpTi(biphen) complex (see **Figure 3.10**). In contrast, the resonance for the chelated β-diketonato ligand is always shifted downfield relative to the uncoordinated β-diketone (in the studied complexes), due to the formation of a *pseudo*-aromatic system when the β-diketone coordinates to the Ti(IV) metal.

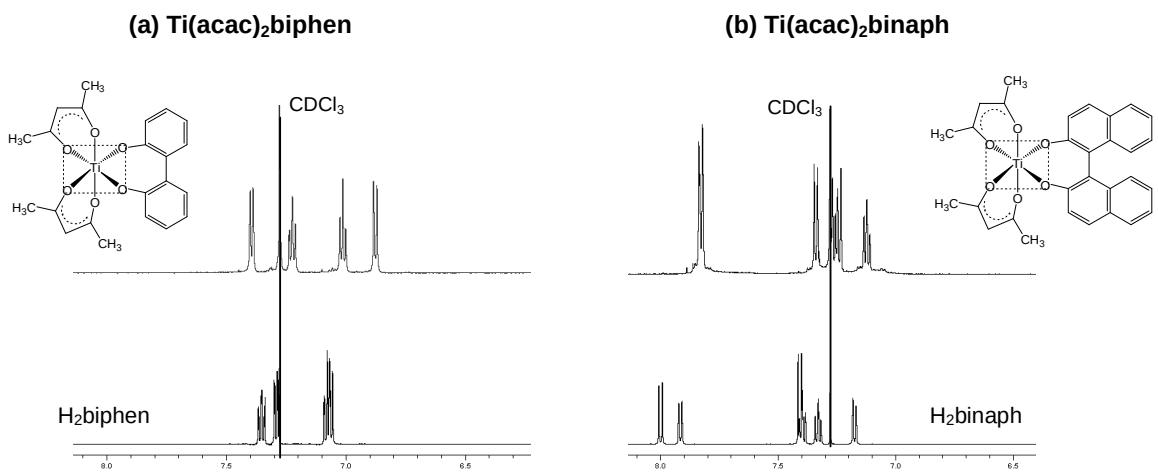

Figure 3.28 Partial ^{1}H NMR spectra ($CDCl_3$) in the aromatic region of **(a)** Ti(acac)$_2$biphen and **(b)** Ti(acac)$_2$binaph**.**

A second series, Ti(β)$_2$(mbinaph) with β = acac **[39]**, tfaa **[40]** and hfaa **[41]** was synthesised according to the method used for the synthesis of the biphenolato analogues (shown in **Scheme 3.8**, Ti(β)$_2$Cl$_2$ + L refluxed in CH_3CN). The effect of changing the electron density on the Ti(IV) centre, by changing the β-diketonato ligand from acac (R, R' = CH_3, relatively e^--donating), tfaa (R, R' = CH_3, CF_3) to hfaa (R, R' = CF_3, relatively e^--withdrawing), on the chelated 8-membered mbinaph ligand, is determined.

Partial ^{1}H NMR spectra are shown relative to the uncordinated H$_2$mbinaph ligand in **Figure 3.29** for comparison. The chemical shifts of the methine proton of the chelated β-diketonato ligand of Ti(β)$_2$mbinaph and parent compound, Ti(β)$_2$Cl$_2$, and of the uncoordinated β-diketone are listed in **Table 3.10**.

The protons of the uncoordinated H$_2$mbinaph ligand resonante as a d,d,d,t,t,d (12 ring protons) and singlet (CH_2) pattern expected for the symmetrical molecule. However once the ligand is chelated in Ti(β)$_2$mbinaph, the symmetry of the ligand is lost and the resonaces are replace by broad peaks for the ring protons (except for 2 doublets) and two separate signals for the two methylene hydrogens (CH_2). The crystal stucture of Ti(acac)$_2$mbinaph compared to Ti(acac)$_2$biphen in **Figure 3.30** clearly shows the loss of H$_2$mbinaph symmetry through coordination to the Ti(β)$_2$ moiety. The CH_2 group, acting as a hinge in the bridge between the two naphthyl rings, lies above the horizontal Ti-ligand plane, with one H directed towards the Ti(β) moiety and the other, towards the naphthyl rings.

The methine protons (2x CH) of Ti(β)$_2$mbinaph with β = acac, tfaa and hfaa display an interesting trend. The resonance, a singlet for acac splits progessively into two separate signals for tfaa and hfaa (see **Figure 3.29**), according to increasing electronegativity of the R groups. The downfield shift of the CH in the series is expected and follows the same trend as the uncoordinated β-diketones (see **Table 3.10**).

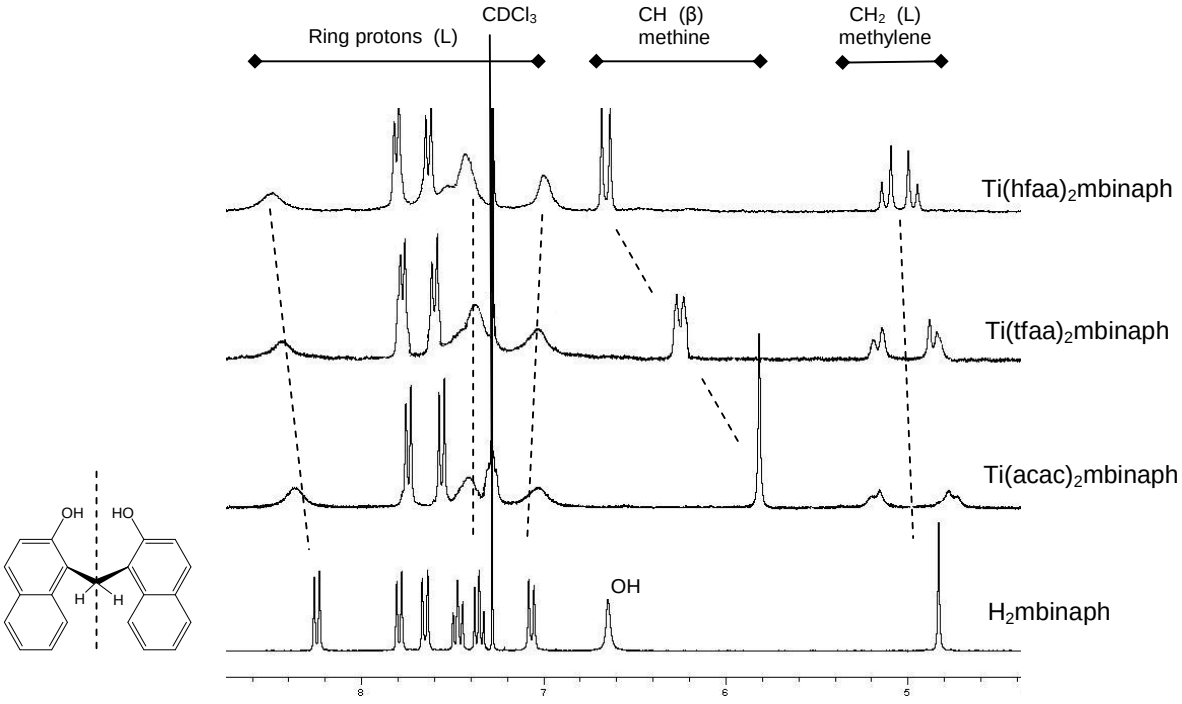

Figure 3.29 Partial ^{1}H NMR spectra ($CDCl_3$) of Ti(acac)$_2$mbinaph, Ti(tfaa)$_2$mbinaph and Ti(hfaa)$_2$mbinaph relative to the uncoordinated H_2mbinaph ligand. (L) = mbinaph and (β) = acac, tfaa and hfaa.

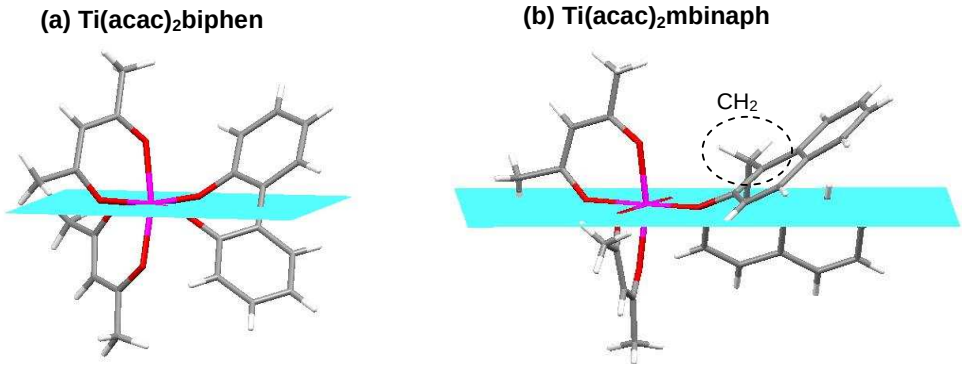

Figure 3.30 **(a)** Ti(acac)$_2$biphen and **(b)** Ti(acac)$_2$mbinaph[27] showing the symmetrically coordinated biphenolato ligand and unsymmetrically coordinated mbinaphtholato ligand.

Table 3.10 ^{1}H NMR chemical shifts for the methine protons of the chelated and uncoordinated β-diketone.

Ti(β)$_2$L					Free β-diketone
Compound		**Ring Size**	**^{1}H / ppm methine (A)**	**Δ (A-β)**	**^{1}H / ppm methine (Hβ)**
Series 1					
Ti(acac)$_2$cat	**[34]**	5	5.90	0.40	5.50
Ti(acac)$_2$naph	**[35]**	5	5.89	0.39	5.50
Ti(acac)$_2$biphen	**[36]**	7	5.79	0.29	5.50
Ti(acac)$_2$binaph	**[37]** [a]	7	5.77	0.27	5.50
Ti(acac)$_2$mbiphen	**[38]**	8	5.83	0.33	5.50
Ti(acac)$_2$mbinaph	**[39]** [b]	8	5.82	0.32	5.50
Parent Compound					
Ti(acac)$_2$Cl$_2$	**[23]**	none	6.00	0.50	5.50
Series 2					
Ti(acac)$_2$mbinaph	**[39]** [b]	8	5.82	0.32	5.50
Ti(tfaa)$_2$mbinaph	**[40]**	8	6.25	0.25	6.00
Ti(hfaa)$_2$mbinaph	**[41]**	8	6.66	0.26	6.40
Parent Compound					
Ti(acac)$_2$Cl$_2$	**[23]**	none	6.00	0.50	5.50
Ti(tfaa)$_2$Cl$_2$	**[13]**	none	6.40	0.40	6.00
Ti(hfaa)$_2$Cl$_2$	**[14]**	none	6.80	0.40	6.40

[a] Synthesised previously[30]

[b] Synthesised previously and crysral structure known[27]

3.3 CRYSTAL STRUCTURES

To further the characterisation of the synthesised titanium (IV) complexes, the results of the single crystal structure determination for **tetrahedral** (a) monomeric $[Cp_2Ti(\beta)]^+ClO_4^-$ complexes with β = tfba, tfth, tffu, ba, dbm and the β-ketoester, maa, and **octahedral** (b) monomeric $Ti(\beta)_2$(bipben) with β = acac, ba, (c) dimeric $\{Ti\beta_2Cl\}_2O$ with β = tfaa, hfaa and $\{Ti(hfaa)_2\}(\mu\text{-}O)(\mu\text{-biphen})$ and (d) tetrameric $[Ti(hfaa)_2(\mu\text{-}O)]_4$ structures are presented. The author acknowledges Dr. A. J. (Fanie) Muller of the Deparment of Chemistry, University of the Free State, for the data collection and refinement of the crystal structures and helpful discussions.

3.3.1 Tetrahedral Structures

3.3.1.1 Monomeric Structures: $[Cp_2Ti(\beta)]^+ ClO_4^-$

Geometrical Aspects The molecular diagram showing atom labelling, accompanied by a schematic diagram showing bond lengths and coordination environment around the titanium of $[Cp_2Ti(tfba)]^+ClO_4^-$ **[6]**, $[Cp_2Ti(tfth)]^+ClO_4^-$ **[4]**, $[Cp_2Ti(tffu)]^+ClO_4^-$ **[5]**, $[Cp_2Ti(ba)]^+ ClO_4^-$ **[7]**, $[Cp_2Ti(dbm)]^+ClO_4^-$ **[9]** and $[Cp_2Ti(maa)]^+ClO_4^-$ **[11]**[14] respectively, are presented in **Figure 3.31**. Crystal data and details of data collection and refinement are summarised in **Table 3.11**. Complete tables of bond lengths and angles are available in digital format.

The following features are of interest:

• The $[Cp_2Ti\beta]^+$ cation consist of a tetrahedrally coordinated titanium atom. It is evident, from examination of the bond angles (see **Table 3.12**), that the coordination tetrahedron is distorted. The (centroid Cp_1)-Ti-(centroid Cp_2) angle (θ_2) is on average *ca.* 134° for the series of structures, which is a significant deviation from the ideal tetrahedral bond angle of 109.5°.

Table 3.11 Crystal and structure refinement data for $[Cp_2Ti(\beta)]^+ClO_4$ complexes with β = tfba, tfth, tffu, ba, dbm and maa.

	$[Cp_2Ti(tfba)]^+ ClO_4^-$	**$[Cp_2Ti(tfth)]^+ ClO_4^-$**
Formula	$TiO_2C_{20}H_{16}F_3$ (ClO_4)	$TiO_2C_{18}H_{14}F_3S$ (ClO_4)
Formula weight	492.68	498.70
Crystal colour/habit	red, cubic	red, plate
Crystal system	Monoclinic	Monoclinic
Space group	$P2_1/n$	$P2_1/n$
Unit cell dimension /Å / °	a = 10.088(2) b = 16.613(3) c = 12.443(3) α = 90 β = 96.86(3) γ = 90	a = 9.872(2) b = 15.346(3) c = 13.134(3) α = 90 β = 97.46(3) γ = 90
Volume / Å^3	2060.4(7)	1973.1(7)
Z	4	4
Density$_{calc}$ / Mg m^{-3}	1.588	1.679
Temperature / ℃	20	20
Wavelength / Å	0.71073	0.71073
Absorption coefficiet / mm^{-1}	0.607	0.737
F(000)	1000	1008
Crystal size / mm^3	0.12 x 0.12 x 0.12	0.20 x 0.14 x 0.06
Theta range for data collection / °	2.06 to 25.00	2.05 to 28.30
Index ranges	-11 ≤ h ≤ 11, -11 ≤ k ≤ 19, -14 ≤ l ≤ 14	-13 ≤ h ≤ 9, -20 ≤ k ≤ 18, -17 ≤ l ≤ 13
Reflections collected	11 213	13 654
Independent reflections	3622[R(int) = 0.1037]	4871[R(int) = 0.0727]
Completeness to theta = 28.35 / %	100.0	99.3
Absorption correction	Semi-empirical from equivalents	Semi-empirical from equivalents
Max. and min. transmission	0.9307 and 0.9307	0.9571 and 0.8666
Refinement method	Full-matrix least-squares on F^2	Full-matrix least-squares on F^2
Data/restraints/parameters	3622 / 367 / 391	4871 / 319 / 383
Goodness-of-fit on F^2	1.010	0.969
Final R indices [I>2sigma(I)]	R_1 = 0.0601, wR_2 = 0.1294	R_1 = 0.0517, wR_2 = 0.1166
R indices (all data)	R_1 = 0.1852 wR_2 = 0.1812	R_1 = 0.1628 wR_2 = 0.1555
Largest diff. peak and hole / e.Å^{-3}	0.355 and -0.385	0.300 and -0.427

$[Cp_2Ti(tffu)]^+ ClO_4^-$	$[Cp_2Ti(ba)]^+ ClO_4^-$	$[Cp_2Ti(dbm)]^+ ClO_4^-$	$[Cp_2Ti(maa)]^+ ClO_4^-$
$TiO_3C_{18}H_{14}F_3 (ClO_4)$	$TiO_2C_{20}H_{19} (ClO_4)$	$TiO_2C_{25}H_{21} (ClO_4)$	$TiO_2C_{15}H_{17} (ClO_4)$
482.64	438.70	500.77	392.64
red, plate	red, cuboid	red, cuboid	red, cuboid
Monoclinic	Orthorhombic	Orthorhombic	Monoclinic
$P2_1/n$	*Pnma*	$P2_12_12_1$	$P2_1/c$
a = 10.0303(5) b = 16.0338(9) c = 11.6124(6) α = 90 β = 97.046(2) γ = 90	a = 16.2588(6) b = 8.0470(3) c = 14.7451(5) α = 90 β = 90 γ = 90	a = 11.5010(14) b = 13.6450(17) c = 14.2540(18) α = 90 β = 90 γ = 90	a = 7.5326(2) b = 20.8283(5) c = 10.7927(3) α = 90 β = 103.839(2) γ = 90
1853.45(17)	1929.17(12)	2236.9(5)	1644.13(7)
4	4	4	4
1.730	1.510	1.487	1.586
-123	20	20	-100
0.71073	0.71073	0.71073	0.71073
0.677	0.617	0.542	0.717
976	904	1032	808
0.27 x 0.11 x 0.07	0.29 x 0.25 x 0.16	0.40 x 0.24 x 0.14	0.33 x 0 22 x 0.19
2.41 to 28.32	1.86 to 28.30°.	2.07 to 28.26	2.18 to 28.35
-13 ≤ h ≤ 13, -21 ≤ k ≤ 20, -15 ≤ l ≤ 15	-21 ≤ h ≤ 19, -10 ≤ k ≤ 5, -15 ≤ l ≤ 19	-15 ≤ h ≤ 13, -18 ≤ k ≤ 16, -18 ≤ l ≤ 18	-10 ≤ h ≤ 10, -27 ≤ k ≤ 25, -14 ≤ l ≤ 14
17 806	9 773	15 725	30 323
4606[R(int) = 0.0316]	2567[R(int) = 0.0300]	5468[R(int) = 0.0459]	4091[R(int) = 0.0295]
99.4	100	99.5	99.8
Semi-empirical from equivalents	Semi-empirical from equivalents	Semi-empirical from equivalents	Semi-empirical from equivalents
0.9542 and 0.8384	0.9078 and 0.8414	0.9279 and 0.8122	0.8757 and 0.7977
Full-matrix least-squares on F^2	Full-matrix least-squares on F^2	Full-matrix least-squares on F^2	Full-matrix least-squares on F^2
4606 / 0 / 271	2567 / 118 / 218	5468 / 0 / 298	4091 / 0 / 219
1.046	1.041	0.989	1.050
R_1 = 0.0339, wR_2 = 0.0787	R_1 = 0.0444, wR_2 = 0.1192	R_1 = 0.0473, wR_2 = 0.1164	R_1 = 0.0379, wR_2 = 0.0966
R_1 = 0.0465 wR_2 = 0.0858	R_1 = 0.0609 wR_2 = 0.1319	R_1 = 0.0932 wR_2 = 0.1330	R_1 = 0.0441, wR_2 = 0.1017
0.586 and -0.364	0.469 and -0.466	0.503 and -0.404	0.763 and -0.404

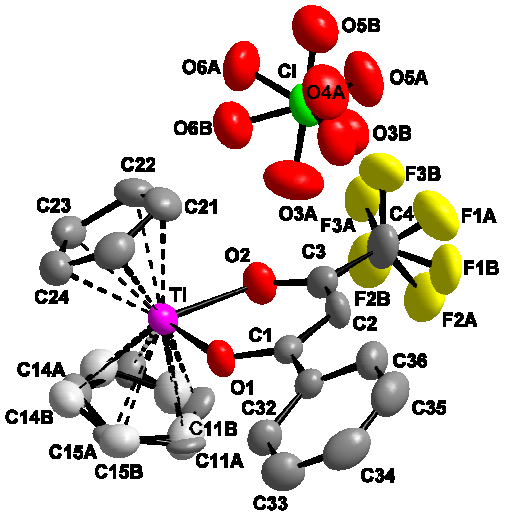

(a) $[Cp_2Ti(tfba)]^+ ClO_4^-$

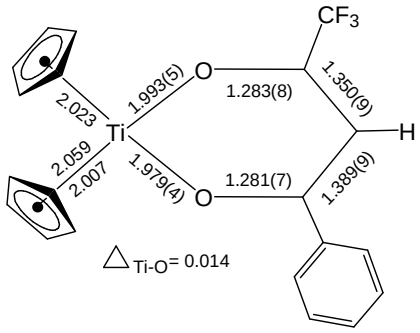

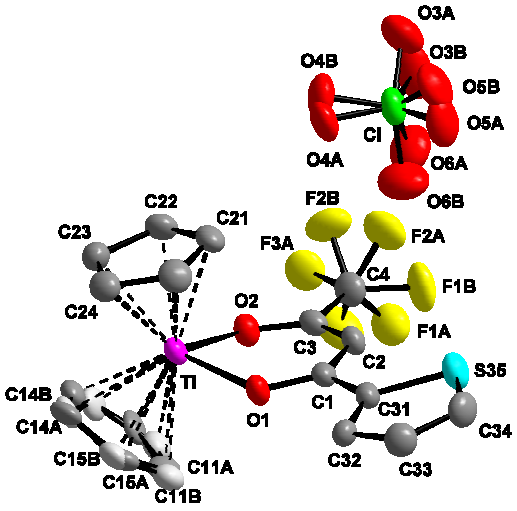

(b) $[Cp_2Ti(tfth)]^+ ClO_4^-$

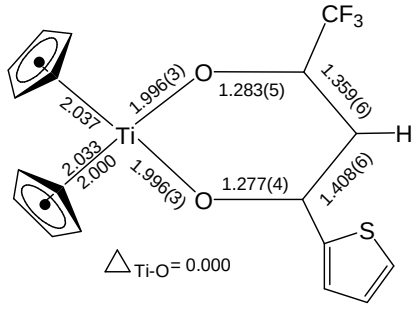

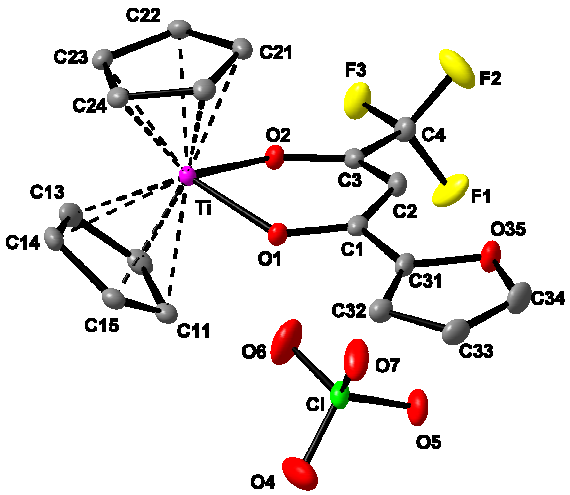

(c) $[Cp_2Ti(tffu)]^+ ClO_4^-$

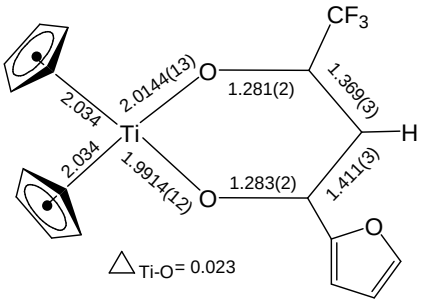

Figure 3.31 continued on next page

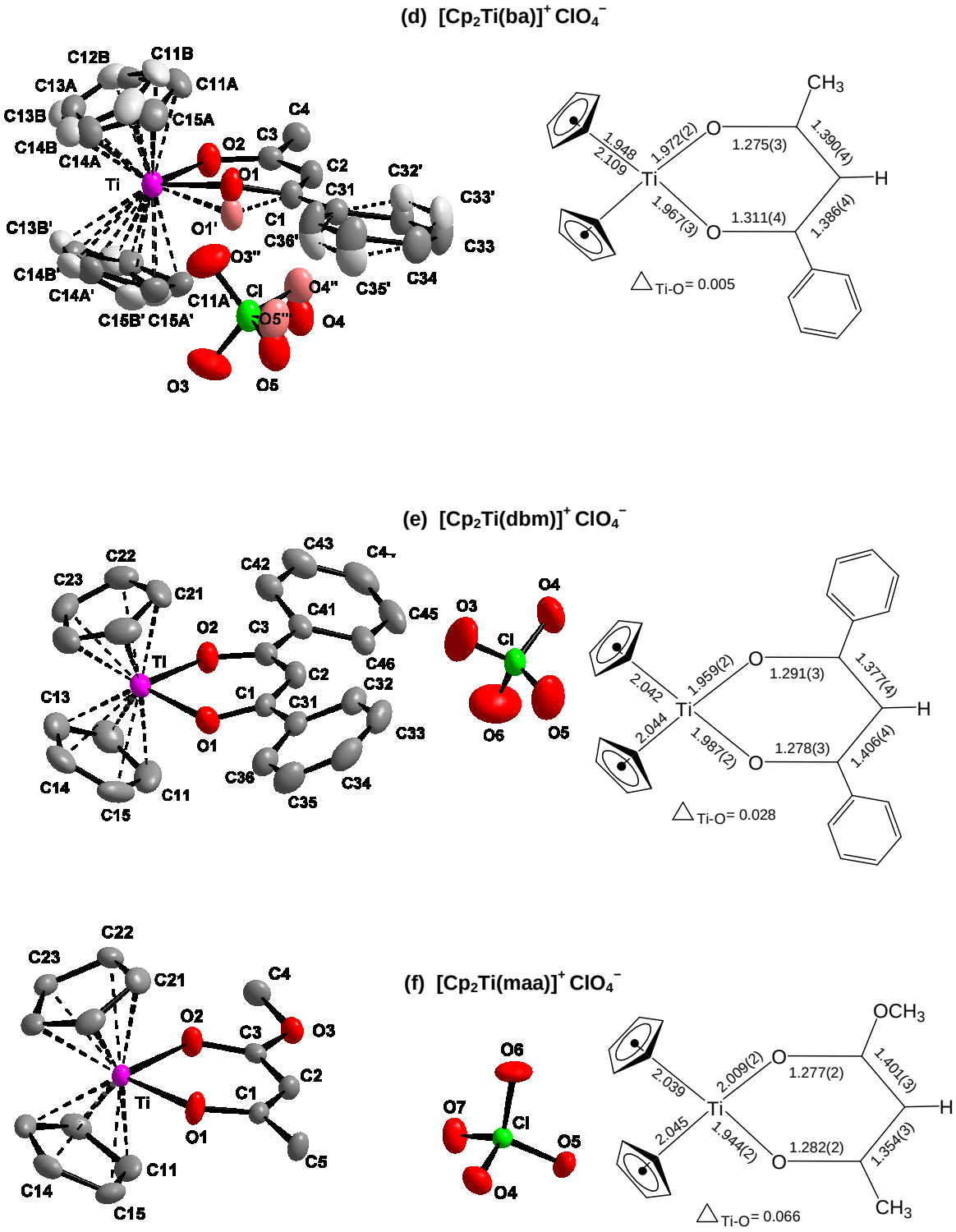

Figure 3.31 **Left**: The molecular structure of $[Cp_2Ti(\beta)]^+ClO_4^-$ complexes with β = (a) tfba, (b) tfth, (c) tffu, (d) ba, (e) dbm and (f) maa , with 30 % probability displacement ellipsoids, indicating the numbering scheme.

Right: Diagram showing selected bond lengths (Å). (● indicates centroid of Cp ring). $\Delta_{Ti\text{-}O}$ = difference in the Ti-O bond lengths of the chelate ring / Å.

Continued from page 117

The large θ_2 angle is attributed to steric hinderence between the Cp ligands. In contrast, the O_1-Ti-O_2 angle (θ_1) is on average *ca.* 86° which is considerably smaller than the standard tetrahedral 109.5°. The small θ_1 angle is attributed to constraints in accommodating the chelated β-diketonato ligand. The other angles around the Ti atom (θ_3, θ_4, θ_5, and θ_6), ranging from *ca.* 103 to 108°, are close to the ideal tetrahedral angle.

Table 3.12 Tetrahedral bond angles (°) around titanium. (Φ = centroid of Cp ring).

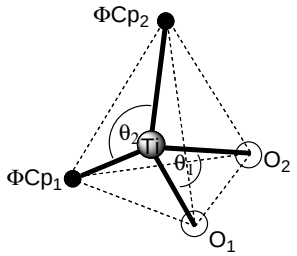

$\theta_1 = O_1\text{-Ti-}O_2$
$\theta_2 = \Phi Cp_1\text{ -Ti -}\Phi Cp_2$
$\theta_3 = O_1\text{-Ti-}\Phi Cp_1$
$\theta_4 = O_1\text{-Ti-}\Phi Cp_2$
$\theta_5 = O_2\text{ -Ti -}\Phi Cp_1$
$\theta_6 = O_2\text{-Ti-}\Phi Cp_2$

Complex	β-diketone R groups R^1, R^2	Angles (°)					
		θ_1	θ_2	θ_3	θ_4	θ_5	θ_6
$[Cp_2Ti(tfba)]^+$ **[6]**	CF_3, Ph	85.9	136.9	106.7	103.4	107.0	105.2
$[Cp_2Ti(tfth)]^+$ **[4]**	CF_3, C_4H_3S	85.9	132.1	106.6	107.0	107.1	108.4
$[Cp_2Ti(tffu)]^+$ **[5]**	CF_3, C_4H_3O	85.9	133.3	106.9	106.2	106.9	107.4
$[Cp_2Ti(ba)]^+$ **[7]**	CH_3, Ph	86.3	134.0	106.5	106.5	106.7	106.7
$[Cp_2Ti(dbm)]^+$ **[9]**	Ph, Ph	85.3	132.8	107.2	106.7	108.1	106.7
$[Cp_2Ti(maa)]^+$ **[11]**	CH_3, OCH_3	86.3	133.7	106.0	107.6	106.6	106.4
AVERAGE →		85.9	133.8	106.7	106.2	107.1	106.8

• Typical C-C and C-O single and double bond lengths are: C-C (1.54 Å), C=C (1.34 Å), C-O (1.43 Å), C=O (1.23 Å).[31] The large double bond character of the C-C and C-O bonds in the chelate ring of the β-diketonato ligand (see **Figure 3.31**) emphasises effective electron delocalisation in the *pseudo*-aromatic core of the β-diketonato ligand. This electron delocalisation enhances electronic communication between the R-groups of the β-diketonato ligand and the Ti centre. This is supported by the electrochemical investigation.

• The backbone of the β-diketonato ligand is near planar but the angles in the β-diketonato backbone, O-C_1-C_2 ($\hat{C}_1$), C_1-C_2-C_3 ($\hat{C}_2$) and C_2-C_3-O ($\hat{C}_3$) vary significantly from the theoretical value of 120°, expected for carbon sp^2 hybridisation. This is in contrast to the corresponding angles in the uncoordinated β-diketone, which are much closer to the ideal value (see **Table 3.13**). The distortion of the *pseudo*-aromatic β-diketonato ring in the $[Cp_2Ti\beta]^+$ complexes, is also reflected in the elongation of the non-bonded O-O distance of *ca.* 0.2 Å (see **Table 3.13**) relative to the uncoordinated β-diketone.

Table 3.13 Angles ($\hat{C}_1$, $\hat{C}_2$ and $\hat{C}_3$) and non-bonded O-O distance of the β-diketone backbone for the $[Cp_2Ti^{IV}(\beta)]^+$ and $[Cp_2Ti^{III}(\beta)]$ omplexes and for the uncoordinated β-diketone; Htfth,[32] Hdbm,[33] Hacac[34] and Hba.[35]

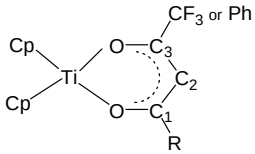

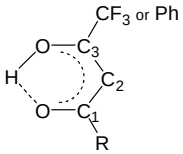

β-diketone	$[Cp_2Ti^{IV}\beta]^+$				Hβ			
	$\hat{C}_1$ /°	$\hat{C}_2$ /°	$\hat{C}_3$ /°	O-O / Å	$\hat{C}_1$ /°	$\hat{C}_2$ /°	$\hat{C}_3$ /°	O-O / Å
tfba **[6]**	121.1	124.6	126.8	2.705	--	--		--
tfth **[4]**	121.8	123.2	127.8	2.720	120.6	120.9	124.7	2.551
tffu **[5]**	123.1	121.8	128.2	2.729	--	--		--
ba **[7]**	120.5	124.9	123.3	2.694	121.76	120.48	120.71	2.493
dbm **[9]**	122.5	123.8	123.1	2.674	120.3	120.3	120.2	2.459
acac[37]	123.4	126.1	123.4	2.710	121.82	121.04	121.82	2.548
	$Cp_2Ti^{III}\beta$				Hβ			
acac[38]	126.8	123.4	125.7	2.775	121.82	121.04	121.82	2.548
ba[39]	123.8	124.9	125.0	2.758	121.76	120.48	120.71	2.493
dbm[40]	124.8	122.8	125.4	2.740	120.3	120.3	120.2	2.459

• The titanium atom lies slightly out of the plane defined by the β-diketonato ligand. This can be quantified by constructing two planes, one through the backbone of the β-diketonato ligand (O_1-C_1-C_2-C_3-O_2) and the other through Ti and the chelated O-atoms (O_1-Ti-O_2) as shown in **Figure 3.32 (a)**. The displacement of the Ti atom from the ligand plane (d) is related to the angle between the two intersecting planes (ω), shown in **Figure 3.32 (b)**.

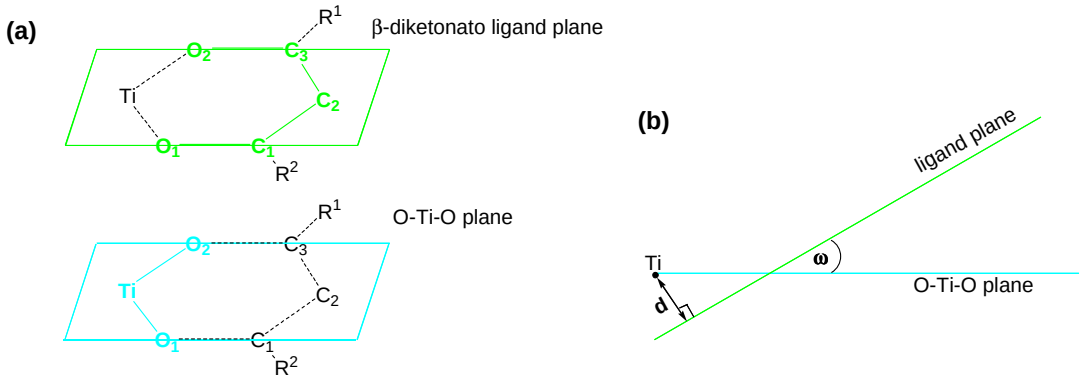

Figure 3.32 **(a)** A sketch of the β-diketonato ligand plane (through atoms O_1-C_1-C_2-C_3-O_2) and the O-Ti-O plane. **(b)** The intersection of the β-diketonato ligand and O-Ti-O plane showing ω = dihedral angle between the two planes and d = displacement of the Ti atom from the ligand plane.

The out-of-plane bending of the ligand varies considerably from ω = 7.9°, 12.2°, 14.5°, 19.4° to 19.9° (with d = 0.19, 0.29, 0.36, 0.49 and 0.51 Å) for β = tfba, ba, dbm, tfth and tffu, respectively. **Figure 3.33** shows a side on view of the smallest and largest out-of-plane bending of the β-diketonato ligand. The dihedral angle is larger for the d^0 Ti^{IV} complexes compared to d^1 Ti^{III} complexes, *e.g.* for β = acac, ba and dbm, ω = 16.8°,[37] 12.2°, 14.5° for Ti^{IV} and 4.4°,[38] 1.0°,[39] 13.3°[40] for Ti^{III} respectively.

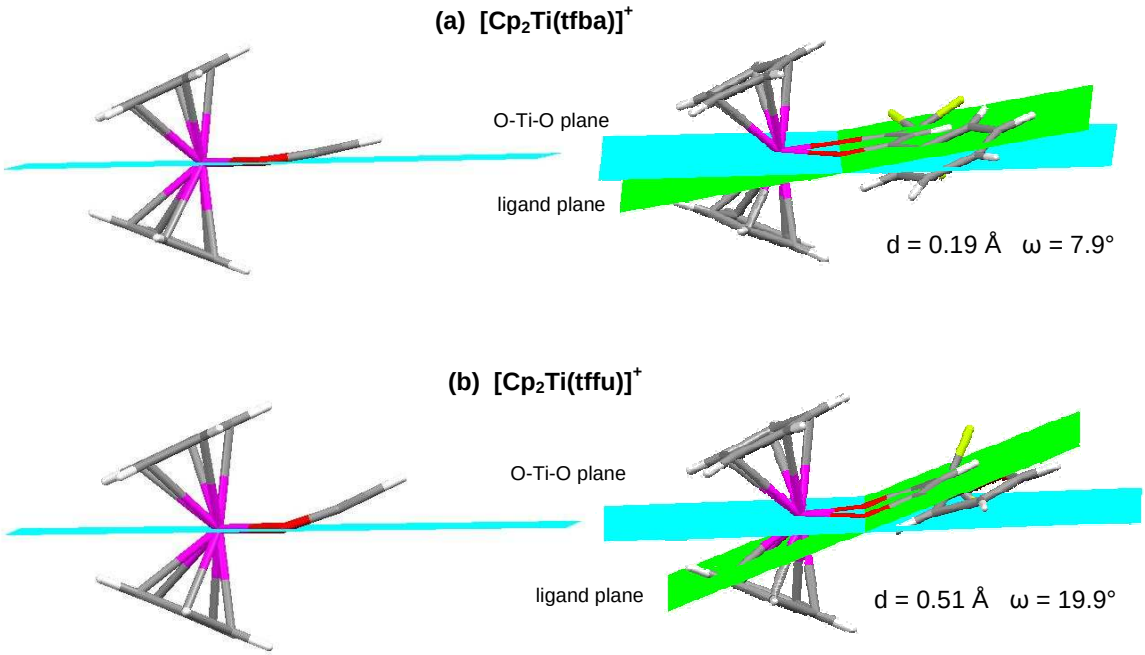

Figure 3.33 (a) $[Cp_2Ti^{IV}(tfba)]^+$ and (b) $[Cp_2Ti^{IV}(tffu)]^+$ showing the position of Ti atom and the chelated β-diketonato ligand relative to **Left**: the O-Ti-O plane and **Right**: both the O-Ti-O and ligand planes. The values of ω and d are given according to the definition of **Figure 3.32**.

• The β-diketonato ligand in $[Cp_2Ti(\beta)]^+$ binds, within experimental error (taken as three times the bond e.s.d.), symmetrically to the titanium core for β = tfth, ba and tfba and asymmetrically for β = tffu, dbm and maa. The difference in the two Ti-O bond lengths, (shown as Δ_{Ti-O} in **Figure 3.31**), are 0.000, 0.005, 0.014, 0.023, 0.028 and 0.066 Å, respectively. This implies that the electron donating properties of the substituted R groups of the β-diketonato ligand do not show an effect on the Ti-O bond length in the solid state. The stronger electron withdrawing properties of the CF_3 group (χ_{CF3} = 3.01[7]), compared to the relatively electron donating non-CF_3 groups, R = Ph, CH_3, C_4H_3S, C_4H_3O, OCH_3, (χ_R = 2.21,[7] 2.34,[5] 2.10,[3] unknown, 2.39[14]) are thus not directly correlated to the Ti-O bond length.

• The Ti-O bond length is shorter in the Ti^{IV} complexes (ave. 1.986 Å) compared to the Ti^{III} analogues (ave. 2.076 Å), see **Table 3.14** and this indicates that the more electron deficient Ti^{IV} centre binds oxygen more strongly than Ti^{III}. The same trend is observed in the Ti-Cp bonding; the Ti-(centroid Cp) bonds (ave. 2.036 Å) for the Ti^{IV} complexes are shorter than the Ti^{III} complexes (ave. 2.062 Å).

• The Cp rings are in a staggered conformation, except for in $[Cp_2Ti(ba)]^+$ and $[Cp_2Ti(dbm)]^+$, where they are eclipsed (examples illustrated in **Figure 3.34**). The complexes with eclipsed conformation, i.e., ba and dbm, have Ph rings. According to the CSD[36], the favoured conformation for the sandwich in bent metallocene $Cp_2Ti^{IV}(O\text{-ligand})_2$ and $Cp_2Ti^{IV}(O,O'\text{-ligand})$ complexes, is staggered and the less common eclipsed conformation have Ph rings (see **Table 2.2, Chapter 2**).

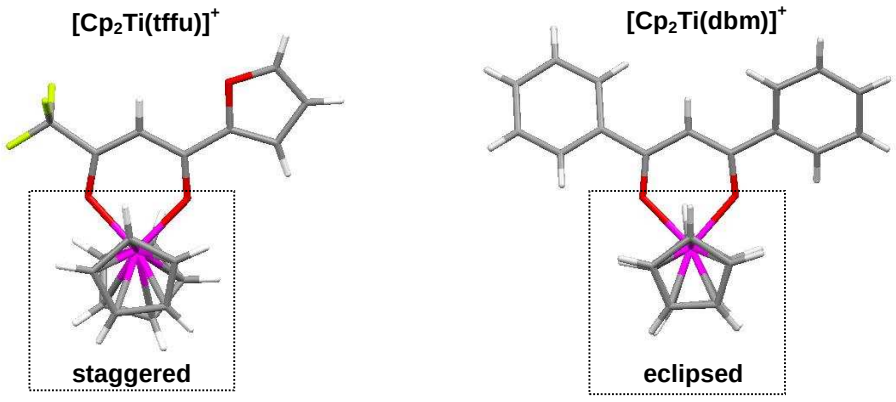

Figure 3.34 **Left**: The common staggered conformation of the Cp rings and **Right**: the eclipsed conformation for $[Cp_2Ti(dbm)]^+$

Table 3.14 Selected geometrical parameters (°, Å) for monomeric structures type $[Cp_2Ti^{IV}\beta]^+$ for β = tfba, tfth, tffu, ba, dbm, acac and $[Cp_2Ti^{IV}(\beta\text{-ketoester})]^+$ for β-ketoester = maa, compared to type (d) $[Cp_2Ti^{III}\beta]$ structures for β = acac, ba, dbm. The average Ti-O and Ti-centroid Cp distances are listed. The angles, distances and numbering system, used in the table, are shown below (**Φ** = centroid).

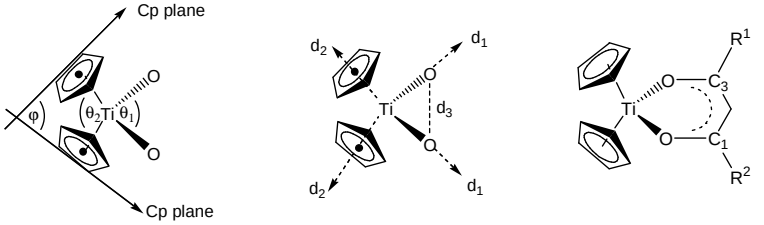

θ_1 = O-Ti-O
θ_2 = Φ Cp -Ti -Φ Cp
φ = intersection Cp planes

d_1 = Ti -O
d_2 = Ti - Φ Cp
d_3 = non-bonded O-O

Complex	β-diketone R groups R^1, R^2	Angles (°)			Distances (Å)			
		θ_1	θ_2	φ	d_1 Ti-O	d_2 Ti-ΦCp	d_3 O-O	$C_1 - C(R^2)$ $C_3 - C(R^1)$
(a) $[Cp_2Ti^{IV}(\beta)]^+ ClO_4^-$								
$[Cp_2Ti(tfba)]^+$ **[6]**	CF_3, Ph	85.9	136.3	46.6	1.988	2.040	2.705	1.516, 1.467
$[Cp_2Ti(tfth)]^+$ **[4]**	CF_3, C_4H_3S	85.9	133.4	48.4	1.996	2.035	2.720	1.534, 1.449
$[Cp_2Ti(tffu)]^+$ **[5]**	CF_3, C_4H_3O	85.9	133.3	47.4	2.003	2.034	2.729	1.531, 1.445
$[Cp_2Ti(ba)]^+$ **[7]**	CH_3, Ph	86.3	134.0	46.3	1.970	2.026	2.694	1.481, 1.492
$[Cp_2Ti(dbm)]^+$ **[9]**	Ph, Ph	85.3	132.8	47.0	1.972	2.043	2.674	1.490, 1.480
	AVERAGE →	86	134	47	1.986	2.036	2.704	
(b) $[Cp_2Ti^{IV}(\beta\text{-ketoester})]^+ ClO_4^-$								
$[Cp_2Ti(maa)]^+$ **[11]**	CH_3, OCH_3	86.3	133.7	48.9	1.976	2.042	2.704	1.495, 1.315*
(c) $[Cp_2Ti^{IV}(\beta)]^+ [Ir_3S_2(CO)_6]^-$								
$[Cp_2Ti(acac)]^+$ [37]	CH_3, CH_3	86.6	133.8	47.5	1.975	2.035	2.710	1.481, 1.511
(d) $Cp_2Ti^{III}(\beta)$								
$Cp_2Ti(acac)$ [38]	CH_3, CH_3	84.3	134.4	45.9	2.068	2.054	2.775	1.540, 1.531
$Cp_2Ti(ba)$ [39]	CH_3, Ph	83.0	135.2	46.6	2.082	2.069	2.758	1.513, 1.501
$Cp_2Ti(dbm)$ [40]	Ph, Ph	82.5	134.3	44.9	2.077	2.062	2.740	1.500, 1.515
	AVERAGE →	83	135	46	2.076	2.062	2.758	

*C – O bond distance since $R^2 = OCH_3$

Crystallographic aspects The structures in this series crystallise on general positions (except for $[Cp_2Ti(ba)]^+$ which lies on a mirror plane) within the unit cells with one molecule only in the asymmetric unit. The structures containing a CF_3-β-diketonato ligand, *i.e.*, β = tfba, tfth and tffu are isomorphous; they crystallise in the same monoclinic centrosymmetric space group, $P2_1/n$, with unit cell parameters varying slightly to accommodate the differences

in the substituted R-groups and on fairly similar coordinates within the unit cell. The large thermal vibrations observed may be attributed to the fact that these collections were unfortunately done at room temperature (see **Table 3.11**). Recollection at low temperature was not deemed necessary for the purpose of this study. The refinements of $[Cp_2Ti(tfba)]^+$, $[Cp_2Ti(tfth)]^+$ and $[Cp_2Ti(ba)]^+$showed large thermal vibrations on parts of the periphery of the molecules, such as the CF_3, Cp ring and ClO_4^- groups These were treated by disordered refinement techniques, such as geometric and anisotropic restraints, to obtain more satisfactory refinement parameters. Where sub-zero temperatures were utilised these disorders became less pronounced and considered negligible in the final refinements (as in the case of tffu and maa). Site occupancies for both disordered parts (indicated by A and B numbering) were refined freely but restricted to add up to one. These refined to ratios which are shown in **Table 3.15**.

Table 3.15 Site occupancies (%) for disordered parts (marked A and B in **Figure 3.31**) of the CF_3, ClO_4^- and Cp_1-ring groups in $[Cp_2Ti(\beta)]^+ClO_4^-$, with β = tfba, tfth and ba. Crystal data collected at T = 20°.

Complex	R-groups	Disordered Group		
		CF_3 $F_A : F_B$	**ClO_4^-** $O_A : O_B$	**Cp_1** $C_A : C_B$
$[Cp_2Ti(tfba)]^+$ **[6]**	CF_3, Ph	56.9 : 43.1	80.0 : 20.0	42.0 : 58.0
$[Cp_2Ti(tfth)]^+$ **[4]**	CF_3, C_4H_3S	83.7 : 16.3	58.9 : 41.1	80.0 : 20.0
$Cp_2Ti(ba)]^+$ **[7]**	CH_3, Ph	--	--	43.5: 56.5

Hydrogen-interactions, although relatively weak, plays a part in the site occupation ratios. There are H-interactions between the atoms in the higher occupied site, *e.g*., the interactions C_2–H_2---F_{1A} have higher occupation rates of 56.9 % and 83.7 % (position A) for the disordered F atoms in $[Cp_2Ti(tfba)]^+$ and $[Cp_2Ti(tfth)]^+$ respectively. Similarly, H-interactions to the perchlorate exist, which lead to the higher occupation rate of 80.0 % and 58.9 % (position A) for the disordered O atoms in the perchlorate ion.

In addition to the thermal disorder of the Cp rings as seen above, a positional disorder (governed by a symmetry element), is observed in $[Cp_2Ti(ba)]^+ ClO_4^-$, where the ba moiety alternates between two positions in a 50 % ratio. The two conformations of the ba ligand, are shown in **Figure 3.35 (b)**, with O1 and the Ph side chain bent above or below the horizontal

mirror plane. The averaged position, with the ligand situated on the mirror plane is also shown, **Figure 3.35** (a).

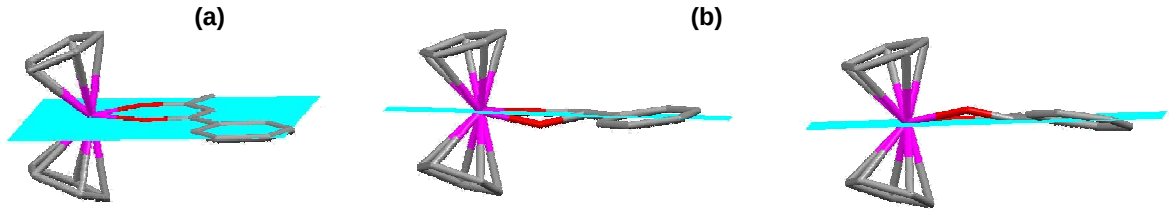

Figure 3.35 Positional disorder of $[Cp_2Ti(ba)]^+$. (a) Ligand in averaged position on the horizontal mirror plane. (b) Ligand bent above and below the horizontal plane showing the two positions of $[Cp_2Ti(ba)]^+$ in the mattrix.

Packing features: (I) $[Cp_2Ti(tfba)]^+$, $[Cp_2Ti(tfth)]^+$ and $[Cp_2Ti(tffu)]^+$ The three complexes are isomorphous and they also have very similar packing arrangements with π-π stacking between one Cp ring and the R-group ring, *i.e.*, C_6H_5, C_4H_3S and C_4H_3O fragments for tfba, tfth and tffu respectively. The π-π stacking interactions are between pairs of Ti complexes, forming dimeric units, see **Figure 3. 36**. The closest contact distance between the rings and the geometric parameters for the π-π stacking (the distance between the ring centroids, R_{cen}, the horizontal displacemen of the centroids, d, the angle between the ring normal and the centroid vector, θ and the dihedral angle between the planes of the π-stacked rings) are given in **Table 3.16**.

The planes of the π-stacked rings are near parallel in $[Cp_2Ti(tfth)]^+$, with only a small deviation of 0.9° between the planes, compared to 7.4 and 11.0° for the corresponding tffu and tfba complexes respectively. In all three cases, the rings are displaced from each other, in a slipped or offset alignment, with the horizontal displacement of the ring centroids, ranging from 0.65 to 0.93 Å (a shift of less than one C-C bond length from the face-to-face alignment). This translates to a π-π stacking interaction which is quite often observed: the ring planes are offset such that a ring atom lies almost over the centre of the other ring and its hydrogen atom almost on top of a carbon atom. The shortest C-H separation, R_{cd}, between the rings range between 3.22 - 3.49 Å compared to the distance between the ring centroids, R_{cen}, ranges between 3.59 - 3.72. These parameters fall well within those required for effective π-π stacking.

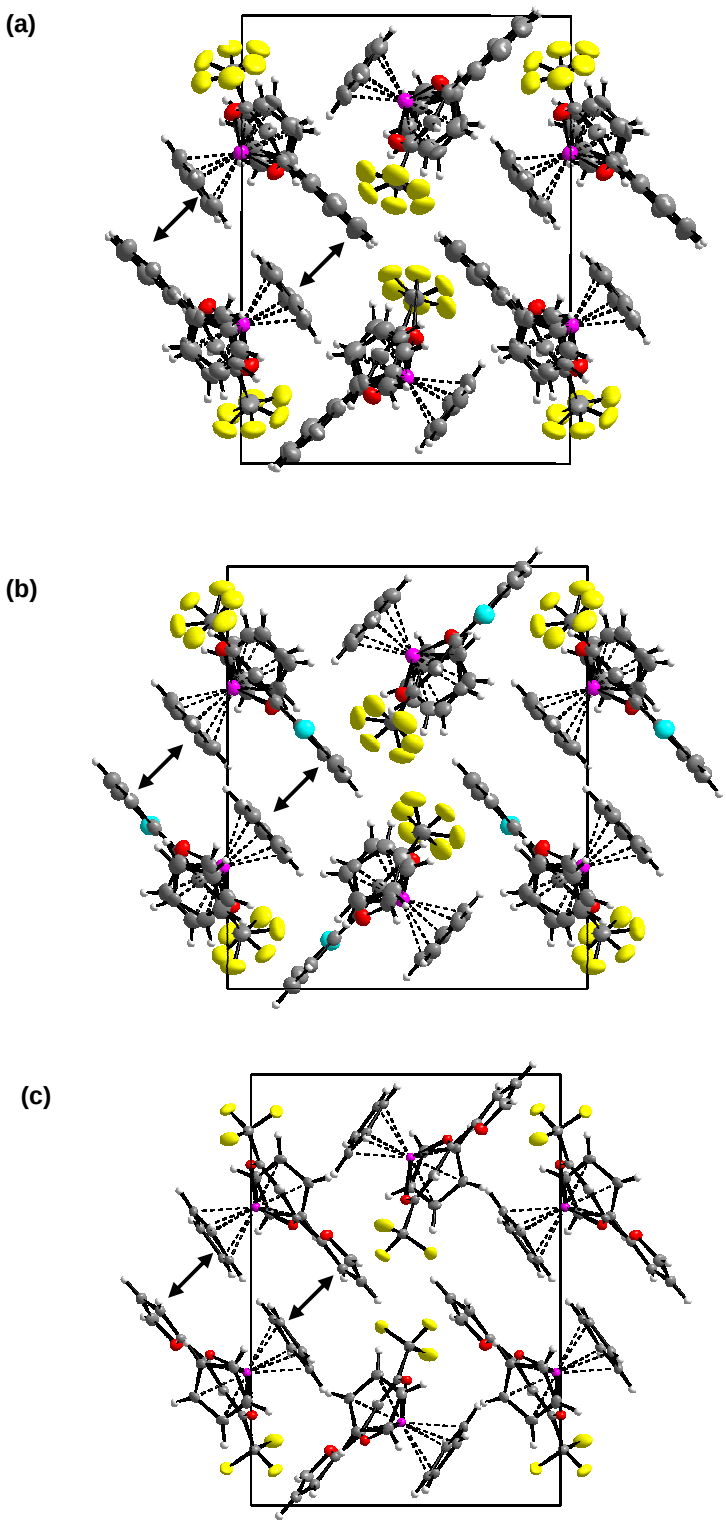

Figure 3. 36 The packing of **(a)** $[Cp_2Ti(tfba)]^+ClO_4^-$, **(b)** $[Cp_2Ti(tfth)]^+ClO_4^-$ (at T = 20°) and **(c)** $[Cp_2Ti(tffu)]^+ClO_4^-$ (at T = -123°) viewed along the a-axis. Monomeric cationic entities in the crystal are linked by π-π stacking interactions (indicated by double headed arrows) forming dimeric units. The perchlorate anions have been removed for clarity. Displacement ellipsoids are drawn at the 30% probability level.

Table 3.16 π-stacking geometrical parameters in $[Cp_2Ti(\beta)]^+ClO_4^-$ complexes with β = tfba, tfth, tffu, ba and dbm. The π-π stacked planes are coplanar for β= ba.

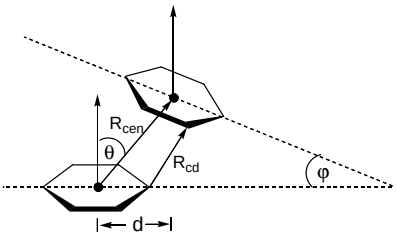

R_{cd} = closest contact distance between the rings
R_{cen} = centroid-centroid separation
d = horizontal displacement of ring centroids
θ = displacement (centre-normal) angle
φ =angle between π-stacked planes (non-parallel)

π-π interaction parameters	$[Cp_2Ti(\beta)]^+ClO_4^-$ complexes					
	tfba [6]	tfth [4]	tffu [5]	ba [7]	dbm [9]	
π-π stacked groups* →	$(Cp)_2$ - $(Ph)_3$	$(Cp)_2$ - (C_4H_3S)	$(Cp)_2$ - (C_4H_3O)	$(Ph)_3$ - $(Ph)_3$	$(Cp)_1$ - $(Ph)_4$	$(Cp)_2$ -$(Ph)_3$
R_{cd} / Å	3.264	3.486	3.217	3.916	3.370	3.421
R_{cen} / Å	3.724	3.590	3.667	4.116	3.600	3.510
d / Å	0.926	0.648	0.800	2.037	1.073	0.123
θ / °	14.4	10.4	12.6	9.0	17.3	2.0
φ / °	11.0	0.9	7.4	parallel	2.6	4.1

* The subscripts after the brackets refer to the ring numbering as indicated in **Figure 3.31**.

(II) $[Cp_2Ti(ba)]^+$ The π-π stacking interactions are between the Ph groups of two adjacent Ti cations forming dimeric units, shown in **Figure 3.37**. The Ph rings are coplanar with slipped packing; rings are displaced by *ca.* 2.0 Å from each other resulting in R_{cen} = ca. 4.1 Å (Geometric parameters for the π-stacking are listed in **Table 3.16**). Futher stabilisation is due to head-to tail C−H···π interactions (with interaction distance of 3.2 Å), involving the Cp rings and methyl H of the β-diketonato ligand of adjacent molecules.

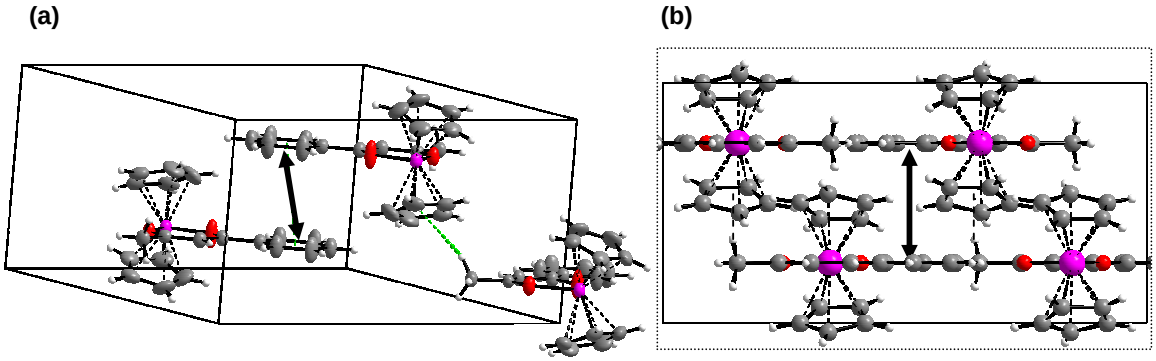

Figure 3.37 The packing of $[Cp_2Ti(ba)]^+ClO_4^-$, with displacement ellipsoids drawn at the 30% probability level. (a) Monomeric cationic entities in the crystal are linked by π-π stacking interactions (indicated by double headed arrows) forming dimeric units and intermolecular C−H···π interaction (dotted green line) futher stabilise the formation of linear chains. (b) Packing viewed along the c-axis.

(III) $[Cp_2Ti(dbm)]^+$ Both Cp rings and both Ph rings are involved in the π-stacking forming infinite arrays (chained networks), as shown in **Figure 3.38**. The geometric parameters for the π-stacking are shown in **Table 3.16** indicating effective π-stacking The planes of the π-stacked rings are close to parallel with only small deviations of 2.6 and 4.1° between the planes.

Channels form along the c-axis in which the ClO_4^- ions are located. A rigid framework is formed by this π-stacking which could be a factor in there being no disordered groups in $[Cp_2Ti(dbm)]^+$, even at high (room) temperature, compared to the disorder on the Cp, ClO_4^- and CF_3 groups in $[Cp_2Ti(tfba)]^+$ and $[Cp_2Ti(tfth)]^+$. H-interactions from the Cp's and Ph's to the neighbouring ClO_4 further stabilise the structure.

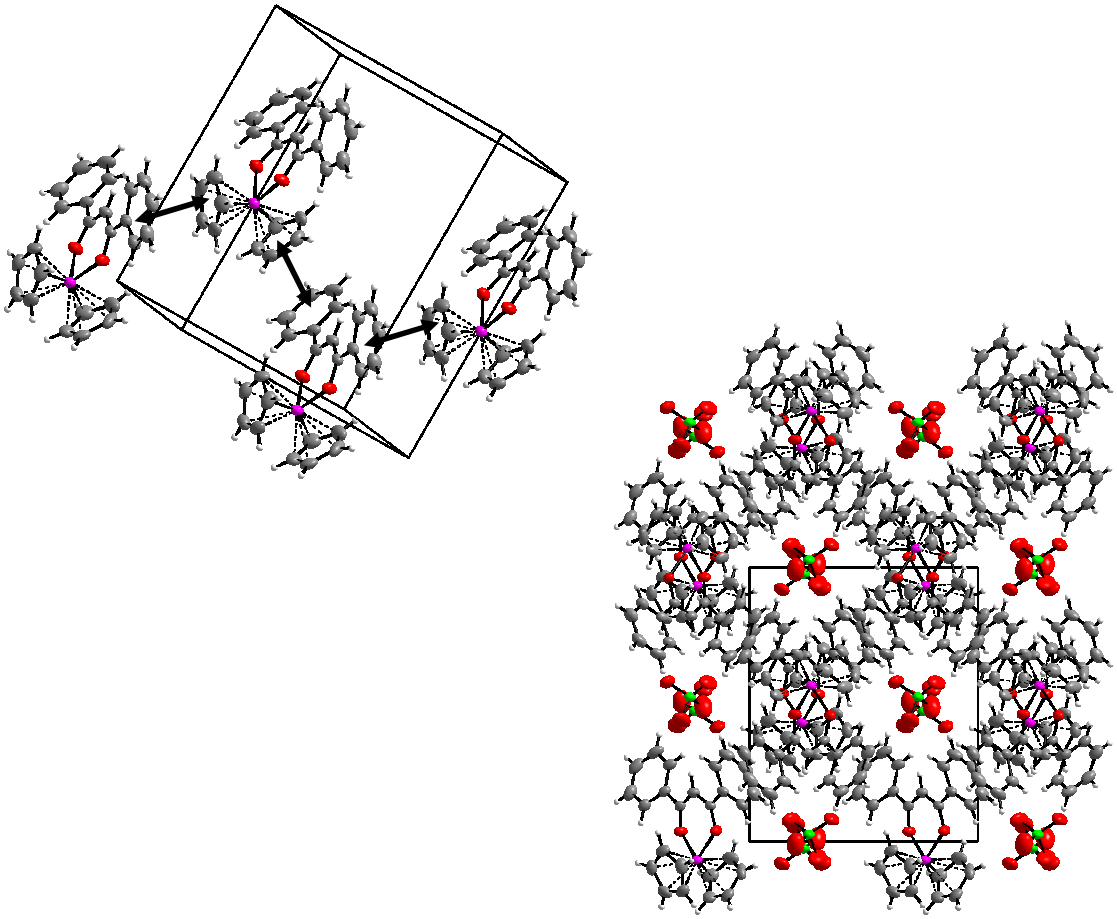

Figure 3.38 Packing diagrams of $[Cp_2Ti(dbm)]^+ClO_4^-$ showing **Top:** π-π stacking interactions between the Ph and Cp ring (indicated by double headed arrows). The ClO_4^- units have been removed for clarity. **Bottom:** the formation of channels along the c-axis, occupied by the ClO_4^- ions.

(IV) $[Cp_2Ti(maa)]^+$ Two inversion-related complex cations are linked to form a head-to-head centrosymmetric dimer, shown in **Figure 3.39**. The Ti cation and the uncoordinate ClO_4^- anion, are linked by intermolecular C–H···O hydrogen interactions. In the centrosymmetric dimer, the *pseudo*-aromatic β-diketonato maa ligands are parallel to each other and appear to be involved in π-π stacking. However, the two ligands are horizontally shifted, with d = 3.911 Å, resulting in negligible overlap of the rings. The distance between the parallel planes is small, *i.e.*, 3.199 Å, but the centroid-centroid separation, R_{cen} = 5.053 Å, is large.

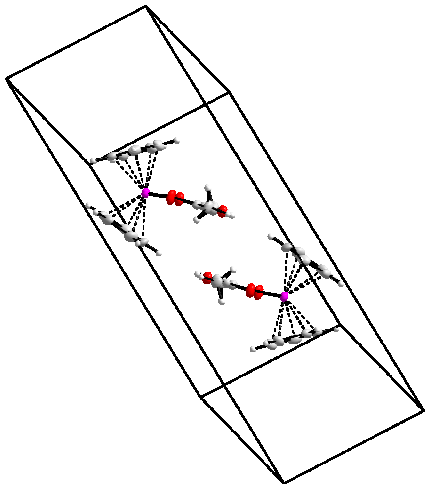

Figure 3.39 View of the packing of $[Cp_2Ti(maa)]^+ClO_4^-$.

Comparison of crystal packing in the series with β = tfba, ba and dbm

In all three structures, $[Cp_2Ti(PhCOCH_2COR)]^+$ with R = CF_3, CH_3 and Ph, the molecular packing is stabilised by ligand π-stacking but the π-π interactions are between different groups of atoms. Dimeric units are formed in the case of tfba and ba while a chained network is formed in dbm (see **Figure 3.40**). In tfba there are two π-π interaction in the dimeric unit, between the Ph and Cp rings, i.e., Ph^1–Cp^2 and Ph^2–Cp^1, while for ba, the stabilisation is due to π-π interactions between the Ph rings, i.e., between Ph^1–Ph^2 and a C–H···π interaction involving the Cp rings, i.e., Cp^2–H^3 (superscript numbering refers to adjacent molecules, molecules 1, 2 and 3). In dbm, the π-interaction is between Ph^1–Cp^2 and Cp^2–Ph^3, forming the chain. The results show that, small changes to the ligands have great effect on the molecular structure, significantly influencing the weak interactions as well as the specific framework structure that forms.

The packing pattern of these Ti^{IV} $[Cp_2Ti(β)]^+$ complexes reported here, appears to be unique. As long as the structure posseses an aromatic ring structure in the β-diketonato ligand, then π-π interactions are possible. However, the only other example currently known, $[Cp_2Ti(fca)]^+ClO_4^-$,[41] does not show these π-π interactions.

The oxidation state of the Ti centre also appears to play a part in the packing interactions, as no π-stacking is observed in the Ti^{III} analogues with the dbm[40] and ba[39] ligands. The $Cp_2Ti^{III}(\beta)$ complexes do not have a counter-ion such as ClO_4^- in the case of Ti^{IV}. The function of the ClO_4^- counter ion should not be disregarded as it might play a vital role in the π-π-stacking and in the case of dbm, keeping the observed channels intact. However, in order to draw conclusions the investigation needs to be expanded to include many more similar cystal structures.

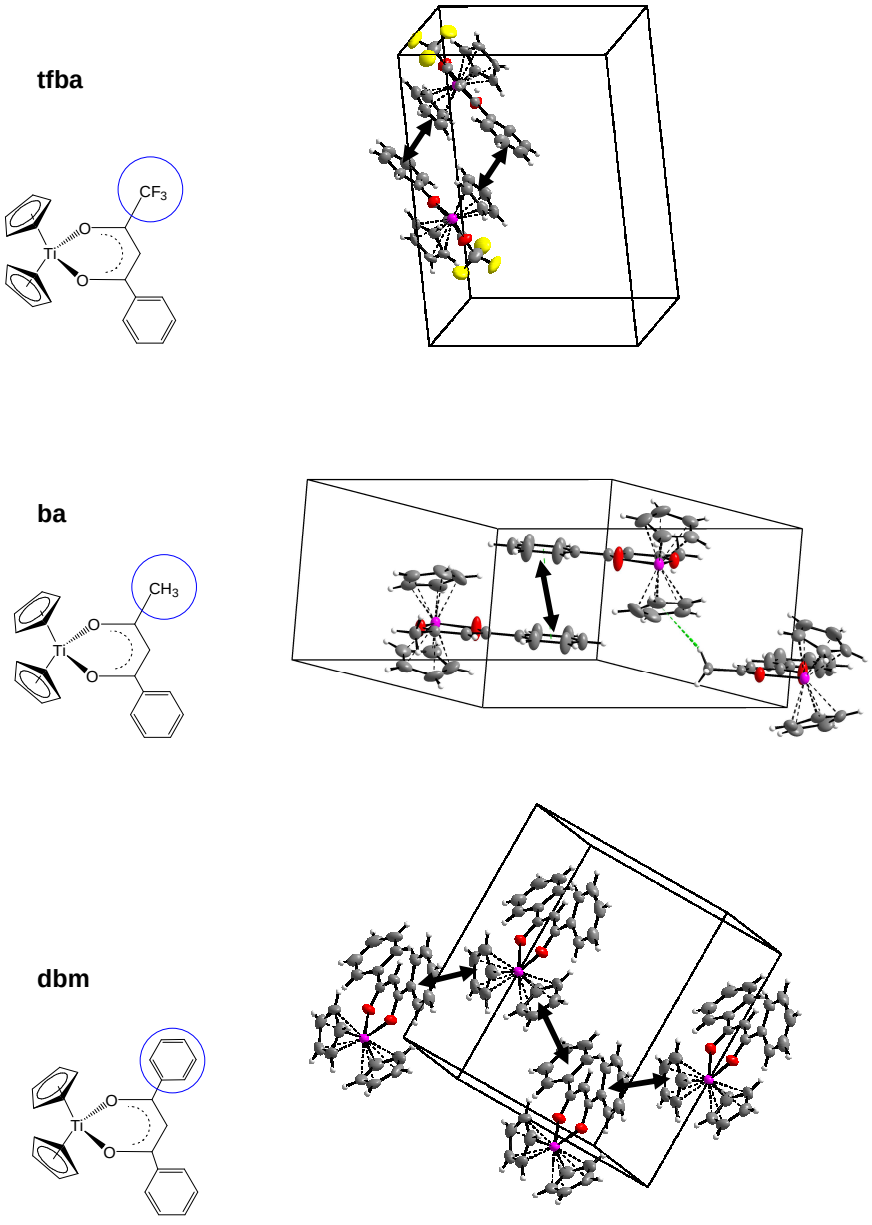

Figure 3.40 The varied π-π stacking in the three related $[Cp_2Ti(\beta)]^+$ structures, with β = tfba, ba and dbm. All perchlorate ions and disorders are removed for clarity.

3.3.2 Octahedral Structures.

3.3.2.1 Monomeric Structure: Ti(β)$_2$ biphen

Geometrical Aspects The molecular diagram indicating atom labelling accompanied by a schematic diagram indicating bond lengths and coordination around the titanium centre, of Ti(acac)$_2$biphen **[36]** and Ti(ba)$_2$biphen **[32]** are presented in **Figure 3.41**. Crystal data and details for data collections and refinements are summarised in **Table 3.17.** Complete tables of bond lengths and angles are available in digital format.

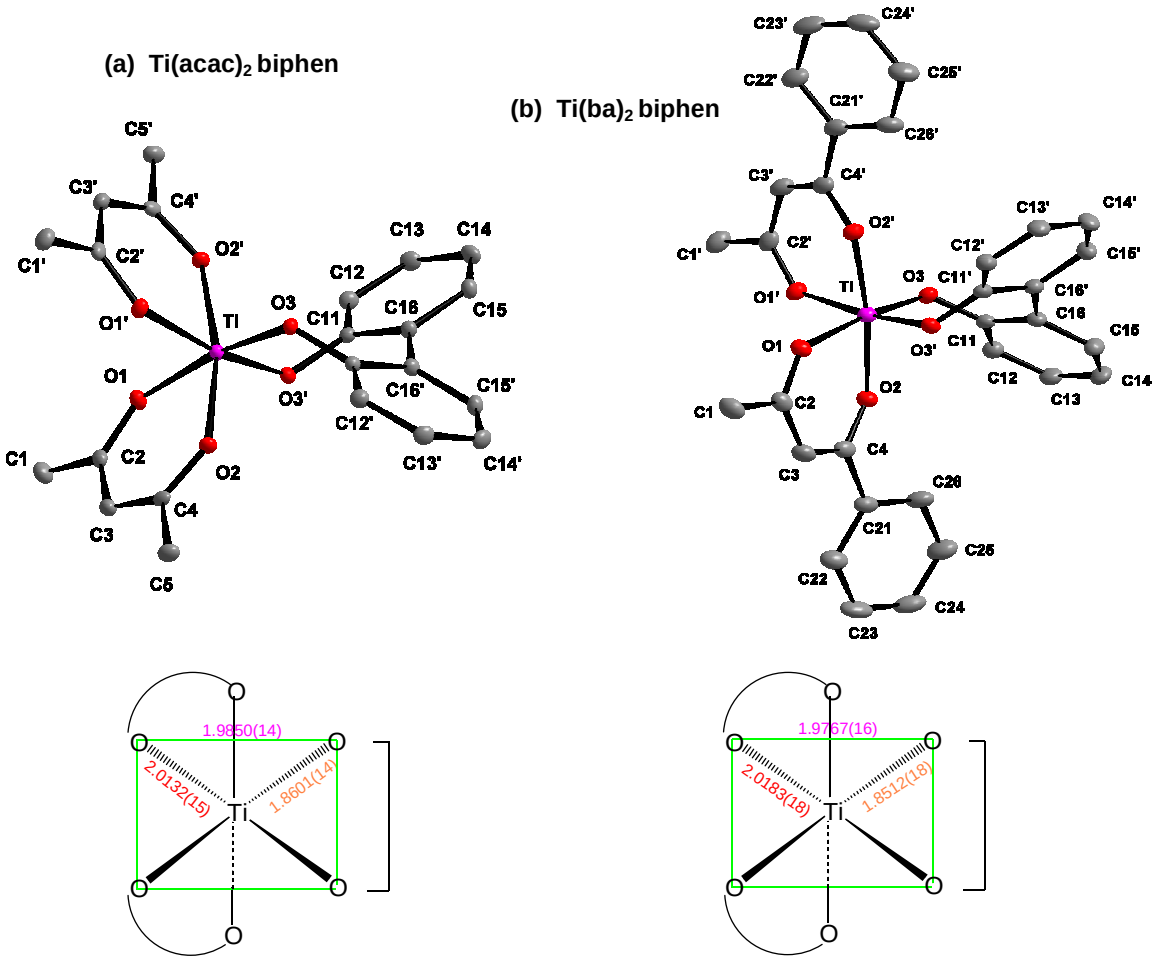

Figure 3.41 **Top**: The molecular structure (30 % probability displacement ellipsoids) of Ti(acac)$_2$biphen and Ti(ba)$_2$biphen, showing the numbering scheme (primed labels indicate atoms generated by symmetry operations). **Bottom**: Diagram indicating coordination and distances around the titanium centre

Table 3.17 Crystal and structure refinement data for Ti(acac)$_2$biphen and Ti(ba)$_2$biphen

	Ti (acac)$_2$ biphen	**Ti (ba)$_2$ biphen**
Formula	$TiO_6C_{22}H_{22}$	$TiO_6C_{32}H_{26}$
Formula weight	430.30	554.43
Crystal colour/habit	orange, cuboid	orange, cuboid
Crystal system	Monoclinic	Trigonal
Space group	*C*2/*c*	$P\,3_2\,2\,1$
Unit cell dimension **/Å** **/ °**	a = 15.8796(13) b = 9.7062(6) c = 13.2038(11) α = 90 β = 93.097(2) γ = 90	a = 8.91750(10) b = 8.91750(10) c = 29.2648(7) α = 90 β = 90 γ = 120
Volume / Å^3	2032.1(3)	2015.40(6)
Z	4	3
Density$_{calc}$ / Mg m^{-3}	1.406	1.370
Temperature / ℃	-173	-173
Wavelength / Å	0.71073	0.71073
Absorption coefficiet / mm^{-1}	0.457	0.363
F(000)	896	864
Crystal size / mm^3	0.46 x 0.34 x 0.21	0.40 x 0.22 x 0.20
Theta range for data collection / °	2.46 to 28.00	2.09 to 28.30
Index ranges	-20 ≤ h ≤ 20, -7 ≤ k ≤ 12, -17 ≤ l ≤ 16	-11 ≤ h ≤ 10, -11 ≤ k ≤ 11, -39 ≤ l ≤ 39
Reflections collected	6844	25 594
Independent reflections	2358[R(int) = 0.0307]	3326[R(int) = 0.0468]
Completeness to theta = 28.35 / %	96.1	99.9
Absorption correction	Semi-empirical from equivalents	Semi-empirical from equivalents
Max. and min. transmission	0.9101 and 0.8173	0.9309 and 0.8684
Refinement method	Full-matrix least-squares on F^2	Full-matrix least-squares on F^2
Data/restraints/parameters	2358 / 0 / 134	3326 / 0 / 178
Goodness-of-fit on F^2	1.188	1.242
Final R indices [I>2sigma(I)]	R_1 = 0.0395, wR_2 = 0.1213	R_1 = 0.0370, wR_2 = 0.1001
R indices (all data)	R_1 = 0.0538 wR_2 = 0.1544	R_1 = 0.0552 wR_2 = 0.1410
Largest diff. peak and hole / e.Å^{-3}	0.567 and -0.752	0.500 and -1.054

The following features are of interest:

• The structures Ti(acac)$_2$biphen and Ti(ba)$_2$biphen consist of an octahedrally coordinated titanium atom. The octahedral coordination around titanium is distorted to accomodate the three chelated ligands, i.e., the six-membered β-diketonato and seven-membered biphenolato rings. The twelve O-Ti-O bond angles vary from 83° to 103° compared to 90° in the perfect octahedron. This maximum angle deviation of *ca.* 13° is the same as the deviation found in the octahedron of the dimeric bridging biphen structure, {Ti(hfaa)$_2$}(μ-O)(μ-biphen), where angles vary from 77° to 100° (structural details in **Section 3.3.2.3**).

• The Ti-O bond distances in the TiO_6 octahedron vary considerably; the shortest are the Ti-O bonds in the chelated biphenolato ligand (*ca*. 1.86 Å), the intermediate are the axial (*ca.* 1.98 Å) and the longest, equatorial (*ca.* 2.02 Å) bonds of the chelated β-diketonato ligand in Ti(acac)$_2$biphen and Ti(ba)$_2$biphen.

• Selected geometrical parameters, i.e., Ti-O distances (d_{ax}, d_{eq} and d_L / Å) and O-Ti-O angles (θ_1 and θ_2 / °) for monomeric bis(β-diketonato) titanium(IV) complexes, (TiO_6) (**Figure 3.42**), are shown in **Table 3.18**. Certain trends can be seen. The Ti-O bond lengths in the TiO_6 octahedron all vary systematically, the shortest are the Ti-O bonds in the chelated ligand, L, (*ca*. 1.85 Å), the intermediate are the axial (*ca.* 1.98 Å) and the longest, equatorial (*ca.* 2.02 Å) bonds of the chelated β-diketonato ligand, β. The formal Ti-O single bond is 1.94 -1.99 Å (Ti-O distances found in rutile, TiO_2[42]) and Ti=O double bond is 1.61-1.68 Å.[43] Therefore the shortest Ti-O distance is clearly shorter than one expected for a single bond, suggesting that this Ti-O bond possesses partial double bond character arising from donation of the electrons from the p_y and p_z filled oxygen orbitals to the empty titanium *d* orbitals.[56] The β-Ti bonds *trans* to another β-diketonate oxygen, are shorter (*ca.* 1.98 Å) than those *trans* to the oxygen of the chelated dianion ligand, L, (*ca.* 2.02 Å).

• The O-Ti-O angle of the chelated 7-membered ring (*ca*.91°) is the closest to the perfect octahedron angle of 90°. The angle is smaller in the chelated 6-membered β-diketonato ring (*ca*. 83°) and increases from *ca*. 94° (8-membered ring) to 97° for monodentate ligands (see **Table 3.18**)

• The backbone of each β-diketonato ligand is very close to planar. The titanium atom lies slightly out of the plane defined by the β-diketonato ligand with a Ti atom displacement (d) of *ca.* 0.18 Å (ω = 7.1°) and 0.24 Å (ω = 9.2°) (see **Figure 3.32** for definition of d and ω) for acac and ba complexes respectively.

Table 3.18 Selected geometrical parameters (°, Å) for octahedral monomeric bis(β-diketonato) titanium(IV) complexes (sketched above). The average of the two θ_1 angles are tabulated.

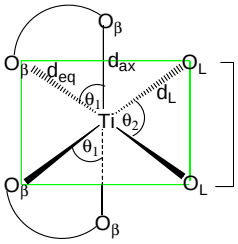

Complex	Ring size of L	Ti-O Distances (Å)			O-Ti-O Angles (°)		
		d_{ax}	d_{eq}	d_L	θ_1	θ_2	range
A $Ti(acac)_2$biphen **[36]**	7	1.984	2.012	1.859	82.8	89.9	83 - 103
B $Ti(ba)_2$biphen **[32]**	7	1.977	2.018	1.851	82.9	91.3	83 - 97
C $Ti(dbm)_2$binaph [44]	7	1.954	2.008	1.870	83.3	90.8	83 - 97
D $Ti(dpm)_2$binaph [45]	7	1.970	2.022	1.855	82.6	92.4	82 - 96
E $Ti(acac)_2$mbinaph [46]	8	1.998	2.039	1.834	83.7	94.0	83 - 96
F $Ti(acac)_2(OPh)_2$ [47]	mono-dentate	1.984	2.048	1.837	82.6	97.4	83 - 99

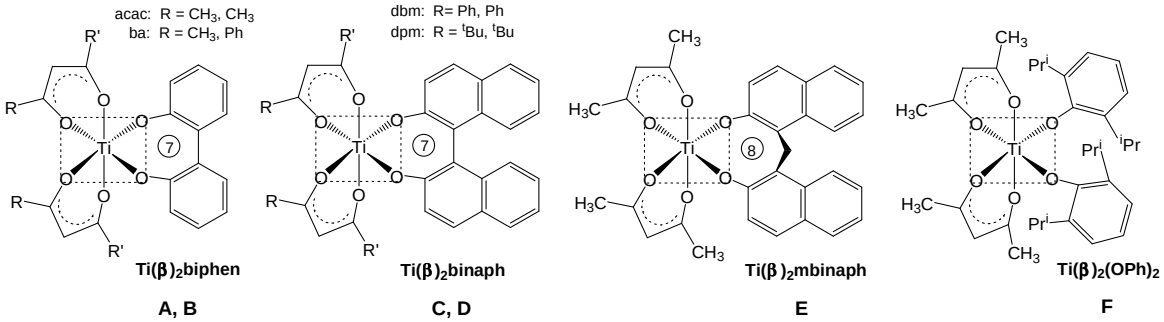

Figure 3.42 Schematic structure of bis(β-diketonato) titanium(IV) complexes reviewed in **Table 3.18**.

Comparison of β-diketonato ligand coordination in tetrahedral and octahedral complexes Ring strain on the chelated β-diketonato ligand increases when going from octahedral to tetrahedral coordination. **Figure 3.43** shows the ideal O-Ti-O angle and non-bonded O-O distance for an uncoordinated β-diketone, i.e., 78° (calculated) and 2,51 Å (measured) respectively. These values increase when the β-diketone chelates to titatium (IV), and tries to attain the standard octahedral (90°) and tetrahedral (109.5°) angles. The O-Ti-O angle increases from the stable *ca* 78° (uncoordinated) to *ca*. 83° (octahedral) and *ca*. 86° (tetrahedral).

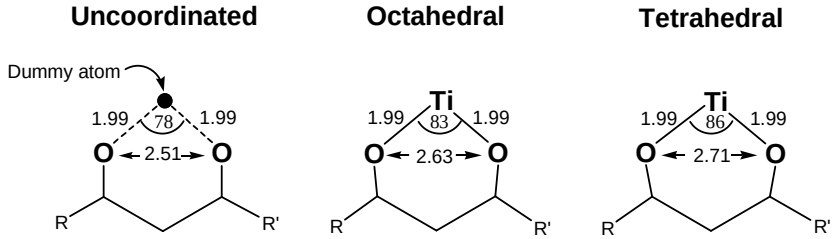

	Uncoordinated	Octahedral	Tetrahedral
Ti-O / Å	--	1.99	1.99
O-O / Å	2.51	2.63	2.71
O-Ti-O / °	--	83	86

Figure 3.43 Diagrams showing the increase in non-bonded O-O distance (Å) and O−Ti−O angle (°) for β-diketones as **Left**: uncoordinated ligand (using dummy atom and Ti−O = 1.99 Å) and as a ligand in **Middle**: octahedral and **Right**: tetrahedral Ti(IV) coordination. The tabulated values are average values obtained from known crystals.

Crystallographic aspects The two structures are not isomorphous; Ti(acac)$_2$biphen crystallises in the monoclinic, centrosymmetric space group, C_2/c while Ti(ba)$_2$biphen, in the non-centrosymmetric trigonal space group, $P\bar{3}_2$ 2 1. Both structures crystallise on special positions, with only half the molecule in the asymmetric unit. The molecular packing arrangement of the two complexes differs greatly; intermolecular π-π stacking of the chelated β-diketonato acac moieties are clearly observed in Ti(acac)$_2$biphen (see **Figure 3.44 (a)** and **Table 3.19**). In contrast, the ba-derivative does not exhibit π-π stacking interactions of the chelated β-diketonato backbone or of neighboured phenyl rings (of the ba or biphen moieties), but the aromatic rings are arranged in an edge- or point-to-face, T-shaped conformation allowing for C-H···π interactions (see **Figure 3.44 (b)**). Ti(ba)$_2$biphen has four Ph residues and each Ph has a C-H···π interaction with another neighbouring Ph, resulting in a stabilised interlocking 3D network.

(a) Ti(acac)$_2$ biphen

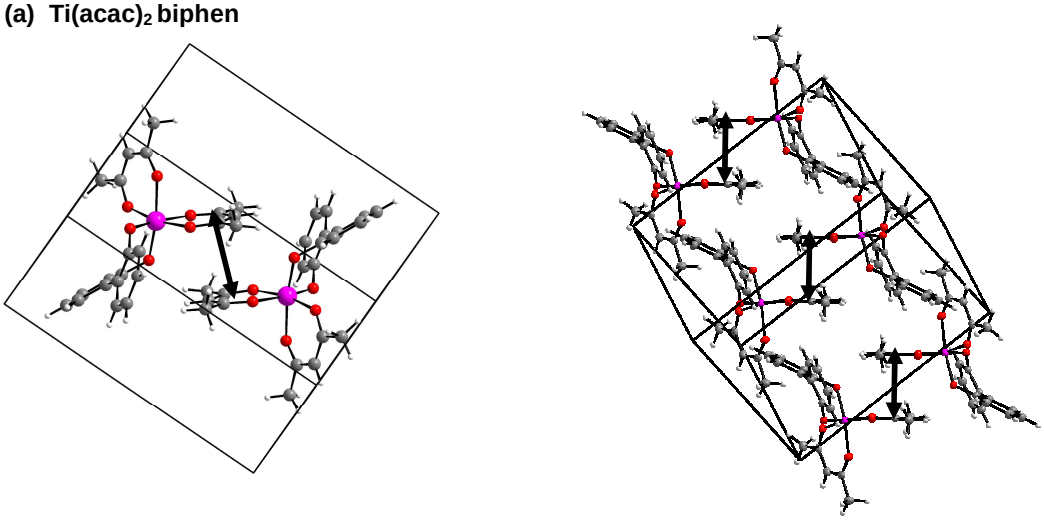

(b) Ti(ba)$_2$ biphen

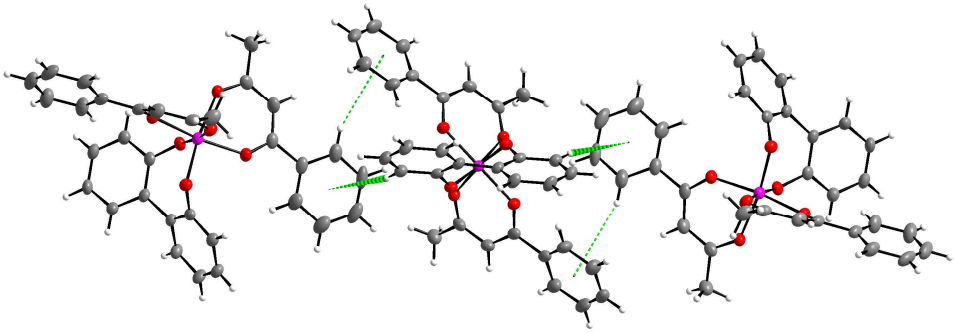

Figure 3.44 Packing diagrams of Ti(β)$_2$ biphen with β = acac and ba showing intermolecular **(a)** π-π stacking interactions between chelated *pseudo*-aromatic acac rings (indicated by double headed arrows) for Ti(acac)$_2$ biphen and **(b)** intermolecular C−H···π interactions between the Ph ring of the ba ligand and C-H of adjacent β-diketonate and biphen (indicated by dotted lines) for Ti(ba)$_2$ biphen.

Table 3.19 Geometrical parameters for the coplanar π-π stacking in Ti(acac)$_2$ biphen.

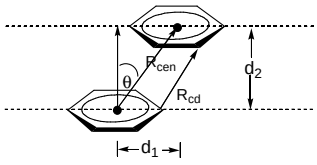

R_{cd} = closest contact distance between the rings
R_{cen} = centroid-centroid separation
d_1 = horizontal displacement of ring centroids
d_2 = interplanar distance
θ = displacement (centre-normal) angle

π-π Interaction Parameters		
π-stacked groups		**acac-acac**
R_{cd} / Å	H5-O1	3.168
	H5-C2	3.134
R_{cen} / Å		3.619
d_1 / Å		0.958
d_2 / Å		3.490
θ / °		8.6

3.3.2.2 Dimeric Structures: $\{Ti(\beta)_2Cl\}_2$ (μ-O)

Geometrical Aspects The molecular diagram indicating atom labelling accompanied by a schematic diagram indicating bond lengths and coordination around the titanium centre, of $\{Ti(tfaa)_2Cl\}_2O$ **[42]** and $\{Ti(hfaa)_2Cl\}_2O$ **[43]** respectively, are presented in **Figure 3.45**. Crystal data and details for data collections and refinements are summarised in **Table 3.20.** Complete tables of bond lengths and angles are available in digital format.

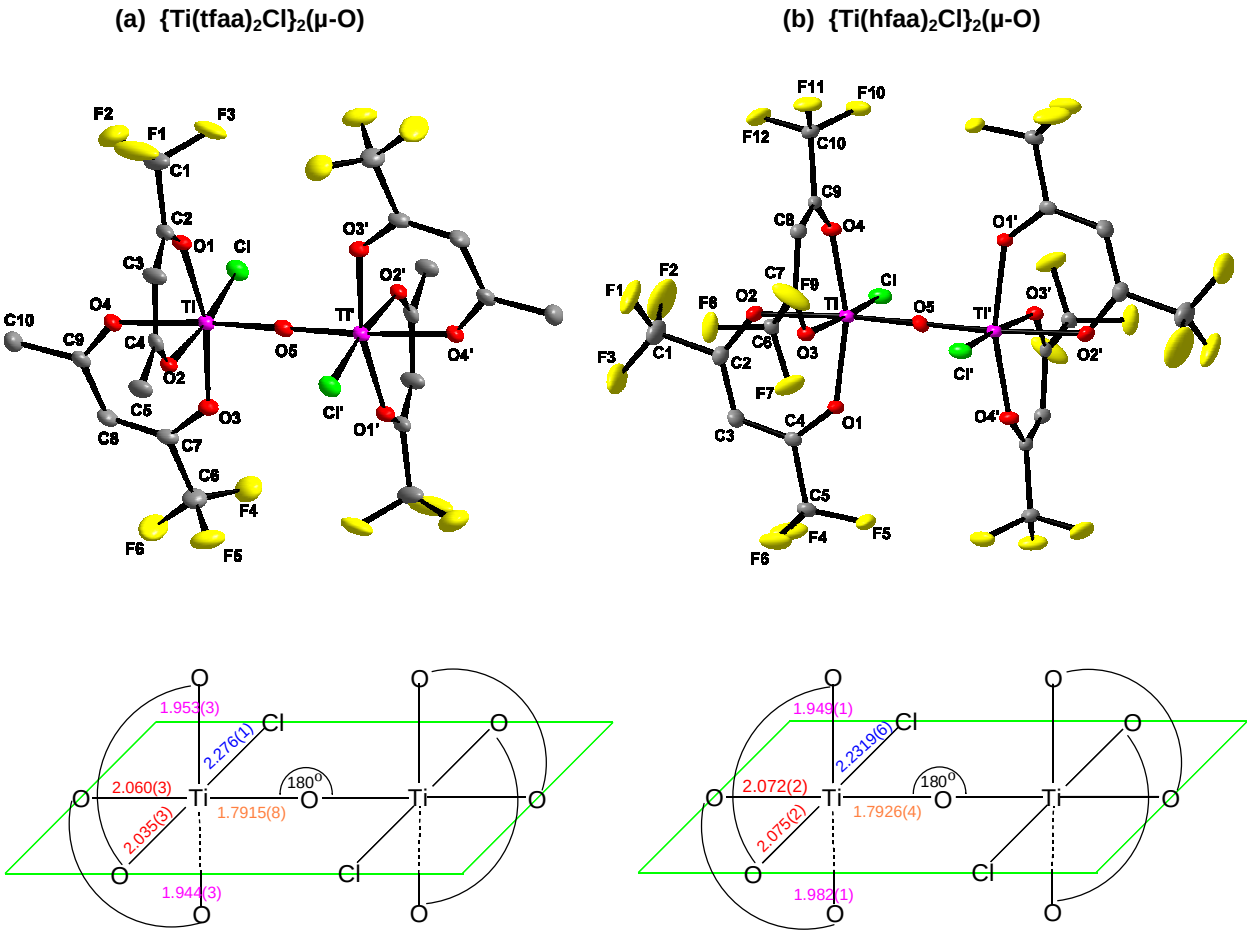

Figure 3.45 **Top**: Molecular structures (30 % probability displacement ellipsoids) of (a) $\{Ti(tfaa)_2Cl\}_2(\mu$-O) and (b) $\{Ti(hfaa)_2Cl\}_2(\mu$-O), showing the numbering scheme (primed labels indicate atoms generated by symmetry operations). **Bottom**: Diagrams indicating coordination and distances around the titanium centres.

Table 3.20 Crystal data and structure refinement data for dimeric $\{Ti(tfaa)_2Cl\}_2(\mu\text{-O})$, $\{Ti(hfaa)_2Cl\}_2(\mu\text{-O})$ and $\{Ti(hfaa)_2\}_2(\mu\text{-O})(\mu\text{-biphen})$ structures.

	$\{Ti(tfaa)_2Cl\}_2(\mu$-O)	**$\{Ti(hfaa)_2Cl\}_2(\mu$-O)**	**$\{Ti(hfaa)_2\}_2(\mu$-O) (μ-biphen)**
Formula	$Ti_2O_9C_{20}H_{16}Cl_2F_{12}$	$Ti_2O_9C_{20}H_4Cl_2F_{24}$	$Ti_2O_{11}C_{32}H_{12}F_{24}$
Formula weight	795.03	1010.93	1124.22
Crystal colour/habit	Yellow, needle	Yellow, cuboid	Red-purple, needle
Crystal system	Monoclinic	Tetragonal	Monoclinic
Space group	$P2_1/n$	$I4_1/a$	C_2/c
Unit cell dimension /Å / °	a = 10.4051(15) b = 12.3279(13) c = 11.5145(15) α = 90 β = 96.815(5) γ = 90	a = 23.1255(4) b = 23.1255(4) c = 12.3948(5) α = 90 β = 90 γ = 90	a = 20.742(2) b = 8.5997(12) c = 23.463(3) α = 90 β = 108.969(4) γ = 90
Volume / Å^3	1466.6(3)	6628.6(3)	3957.9(9)
Z	2	8	4
Density$_{calc}$ / Mg m^{-3}	1.800	2.026	1.887
Temperature / ℃	-173(2)	-173(2)	-173(2)
Wavelength / Å	0.71073	0.71073	0.71073
Absorption coefficiet / mm^{-1}	0.849	0.825	0.575
F(000)	788	3920	2208
Crystal size / mm^3	0.14 x 0.08 x 0.03	0.29 x 0.20 x 0.18	0.46 x 0.16 x 0.14
Theta range for data collection / °	2.43 to 28.41	2.49 to 28.27	2.08 to 28.31
Index ranges	-13 ≤ h ≤ 13, -16 ≤ k ≤ 15, -15 ≤ l ≤ 15	-30 ≤ h ≤ 29, -29 ≤ k ≤ 30, -16 ≤ l ≤ 15	-27 ≤ h ≤ 23, -11 ≤ k ≤ 11, -28 ≤ l ≤ 31
Reflections collected	11 345	34 701	18 134
Independent reflections	3670[R(int) = 0.0624]	4105[R(int) = 0.0399]	4902[R(int) = 0.0347]
Completeness to theta = 28.35 / %	99.5	100.0	99.5
Absorption correction	Semi-empirical from equivalents	Semi-empirical from equivalents	Semi-empirical from equivalents
Max. and min. transmission	0.9750 and 0.8904	0.8657 and 0.7958	0.9238 and 0.7779
Refinement method	Full-matrix least-squares on F^2	Full-matrix least-squares on F^2	Full-matrix least-squares on F^2
Data/restraints/parameters	3670 / 0 / 207	4105 / 0 / 259	4902 / 78 / 340
Goodness-of-fit on F^2	1.030	1.017	1.026
Final R indices [I>2sigma(I)]	R_1 = 0.0692, wR_2 = 0.1694	R_1 = 0.0357, wR_2 = 0.0812	R_1 = 0.0381, wR_2 = 0.0894
R indices (all data)	R_1 = 0.1148 wR_2 = 0.1959	R_1 = 0.0454 wR_2 = 0.0871	R_1 = 0.0547 wR_2 = 0.0986
Largest diff. peak and hole / e.Å^{-3}	1.168 and -0.777	0.524 and -0.377	0.565 and -0.349

The following features are of interest:

• The structure consists of two octahedrally coordinated titanium atoms linked through an oxygen atom at 180 °. The two TiO_5Cl octahedra of the dimeric structure are related to each other by a centre of inversion at the joining oxygen. The octahedral coordination around titanium is slightly distorted, *i.e.*, the bond angles vary from 83° to 99° compared to 90° in a perfect octahedron.

• The Ti-Cl distances, 2.276 Å (tfaa) and 2.232 Å (hfaa), are comparable to the values found in monomeric $Ti\beta_2Cl_2$ structures (2.245, 2.269, 2.293 Å for β = dbm[48], dpm[49], ba[50] respectively) and other dimeric $\{Ti\beta_2Cl\}_2O$ structures (2.313, 2.319 Å for β = acac[51], dbm[52] respectively) but longer than the average 2.185 Å distance for $TiCl_4$.[53] The Ti-Cl bonds both lie in the equatorial plane for tfaa and hfaa (and acac[51]) compared to dbm,[52] where one Ti-Cl bond lies in the equatorial position and the other in an axial position, see **Figure 3.46**.

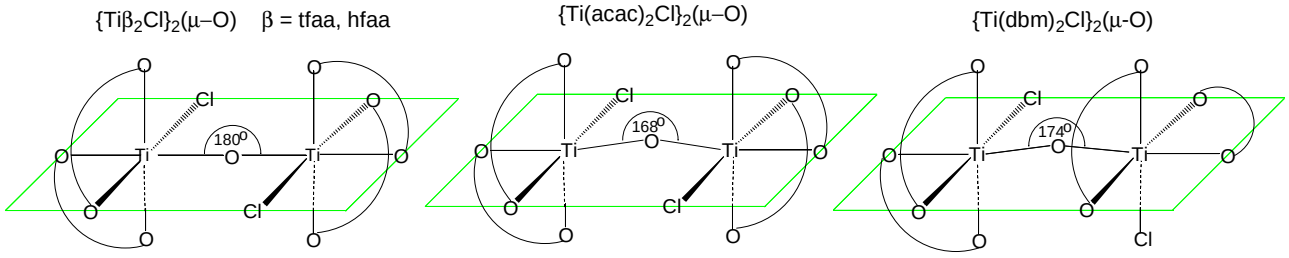

Figure 3.46 Diagrams indicating relative positions of the Ti-Cl bonds and bridging angle in $\{Ti\beta_2Cl\}_2(\mu\text{-}O)$ complexes for β = tfaa, hfaa, acac and dbm.

• The backbone of each β-diketonato ligand, *i.e.*, tfaa and hfaa, is very close to planar. The titanium atom lies slightly out of the plane defined by the β-diketonato ligand with a Ti atom displacement of *ca.* 0.17, 0.30 Å and *ca.* 0.17, 0.24 Å (for β = tfaa and hfaa) from the ligand plane.

• There are three different classes of Ti-O bond distances in the TiO_5Cl octahedron which vary considerably, *i.e.*, the short Ti-O bonds in the linear Ti-O-Ti bridge (*ca.* 1.79, 1.79 Å), and the intermediate, axial (mean *ca.* 1.95, 1.97 Å) and longer, equatorial (mean *ca.* 2.05, 2.07 Å) bonds of the chelated β-diketonato ligands, for tfaa and hfaa respectively (see **Figure**

3.45 and **Table 3.21**) The shortest Ti-(μ-O) distance is clearly shorter than one expected for a single bond (1.92 Å); suggesting that the bridging Ti-O bond possesses partial double bond character arising from donation of the electrons from the p_y and p_z filled oxygen orbitals to the unfilled titanium *d* orbitals.[56] This double bond character may in turn stabilise the unusual *sp* hybridisation of the oxygen atom.

Table 3.21 Selected bond lengths (Å) and angles (°) for dimeric structures type (a) $\{Ti\beta_2Cl\}_2(\mu\text{-O})$, (b) $\{Ti\beta_2\}_2(\mu\text{-O})(\mu\text{-biphen})$, tetrameric structure type (c) $[Ti\beta_2(\mu\text{-O})]_4$ and monomeric structures type (d) $Ti\beta_2Cl_2$ for the β-diketones indicated. Average bond lengths are used where necessary. Bond lengths, equatorial (red), μ−O (orange) and axial (pink) are depicted in **Figure 3.45** for $\{Ti\beta_2Cl\}_2(\mu\text{-O})$ structures with β = tfaa and hfaa, **Figure 3.47** for $\{Ti(hfaa)_2\}_2(\mu\text{-O})(\mu\text{-biphen})$ and **Figure 3.48** for $[Ti(hfaa)_2(\mu\text{-O})]_4$.

β	Ti-O / Å			Ti-Cl / Å	Bridging Angle / °
	Equatorial	μ-O	Axial		
(a) Dimer: $\{Ti\beta_2Cl\}_2(\mu\text{-O})$					
tfaa **[42]**	2.048	1.792	1.948	2.276	180.0
hfaa **[43]**	2.074	1.793	1.966	2.232	180.0
acac[51]	2.045	1.797	1.939	2.313	167.6
dbm[52]	2.025	1.786	1.947	2.319	173.9
(b) Dimer: $\{Ti\beta_2\}_2(\mu\text{-O})(\mu\text{-biphen})$					
hfaa **[44]**	2.105	1.814	1.992	--	135.7
(c) Tetramer: $[Ti\beta_2(\mu\text{-O})]_4$					
hfaa **[45]**	2.102	1.797	1.983	--	158.5, 157.2 171.0, 174.4
dpm[54]	2.122	1.806	1.968	--	169.3, 169.3 170.3, 170.3
(d) Monomer: $Ti\beta_2Cl_2$					
dbm[48]	1.968	--	2.007	2.245	--
dpm[49]	2.006	--	1.912	2.269	--
ba[50]	1.990	--	1.916	2.293	--

• The β-diketonate Ti-O bonds *trans* to another β-diketonate oxygen, are shorter (*ca.* 1.96 Å) than those *trans* to a μ-O or Cl atom(*ca.* 2.06 Å). The higher *p*-donor capacity of the *trans* ligands chloride and oxide compared with β-diketonate oxygen may account for these differences.[55]

• The angle at the bridging oxygen joining the two titanium atoms is 180°. This, although unusual, is expected for *sp* hybridised atoms. Large oxygen bond angles have been observed in other titanium dimeric compounds, *i.e.*, in $\{Ti\beta_2Cl\}_2(\mu\text{-O})$, where the Ti-O-Ti angles are 167.5° and 173.9° for β = acac[51], dbm[52] and in $\{CpTiCl_2\}_2(\mu\text{-O})$[56] where the angle is 180°. In the case of $\{TiCl_2(OPh)(\mu\text{-OPh})\}_2$,[57] a non-bridging angle, Ti-O-C(Ph), is 165.9°, which is somewhat different in that the two atoms attached to oxygen are different.

• The metal coordination is influenced by the nature of the β-diketonato ligand, which can be rationalised by considering the enhanced electron-withdrawing power of the hexafluorinated **hfaa** ligand *vs.* the trifluorinated **tfaa** ligand. The coordination ability of the O atom in the former is weaker (longer Ti-O bond lengths) due to the presence of an additional electron-withdrawing CF_3 group in hfaa. Consequently, the Ti-Cl bond is stronger in $\{Ti(hfaa)_2Cl\}_2(\mu\text{-O})$ than in $\{Ti(tfaa)_2Cl\}_2(\mu\text{-O})$, *i.e.*, 2.232 *vs.* 2.276 Å. This trend is also observed for the less electron withdrawing (non-fluorinated) ligands, acac and dbm, where the Ti-Cl bond is even weaker, *i.e.*, 2.313 and 2.319 Å respectively (see **Table 3.21**).

• Although Ti^{IV} has the electronic configuration $3d^0$, complexes of the type $[Ti\beta_2Cl_2]$ are generally coloured. It was initially proposed by Fay, *et al.*,[58] that the orange colour in $Ti(acac)_2Cl_2$ was due to charge transfer from the chlorine atom to the titanium atom. However, after the crystal structure determination of $\{Ti(acac)_2Cl\}_2(\mu\text{-O})$ (orange) in 1967, no evidence for such a charge transfer was obtained from the Ti-Cl bond lengths. Similarly, there is no indication in $\{Ti(tfaa)_2Cl\}_2(\mu\text{-O})$ (yellow) and $\{Ti(hfaa)_2Cl\}_2(\mu\text{-O})$ (yellow) as evidenced by the Ti-Cl bond lengths of such a transfer. There is however, involvement of oxygen *p* electrons in the μ-O (and also from oxygens on the β-diketonato groups) with the *d* orbitals of titanium, suggesting that the colour in these compounds is probably due to these electrons. Such a ligand-metal charge transfer mechanism is consistent with the colour variation in the series: yellow, yellow-orange, orange, orange-red and red.[49] The monomeric structures all fall within this colour range: $[Ti\beta_2Cl_2]$ for β = tfaa, hfaa (yellow), tfma, tfba (orange), tfdma, tftma, (deep orange) and tffu, tfth (red).

Crystallographic aspects Large displacement ellipsoids are observed at the periphery (on the fluorine atoms) of the molecule, indicating a less restricted packing environment. No obvious or significant packing effects or interactions are noted.

3.3.2.3 Dimeric Structure $\{Ti(\beta)_2\}_2(\mu\text{-}O)(\mu\text{-biphen})$

Geometrical Aspects A molecular diagram indicating atom labelling accompanied by a schematic diagram indicating bond lengths and coordination around the titanium centre of $\{Ti(hfaa)_2\}(\mu\text{-}O)(\mu\text{-biphen})$ **[44]**[59], are presented in **Figure 3.47**. Crystal data and details for data collection and refinement are summarised in **Table 3.20.** Complete tables of bond lengths and angles are available on digital format.

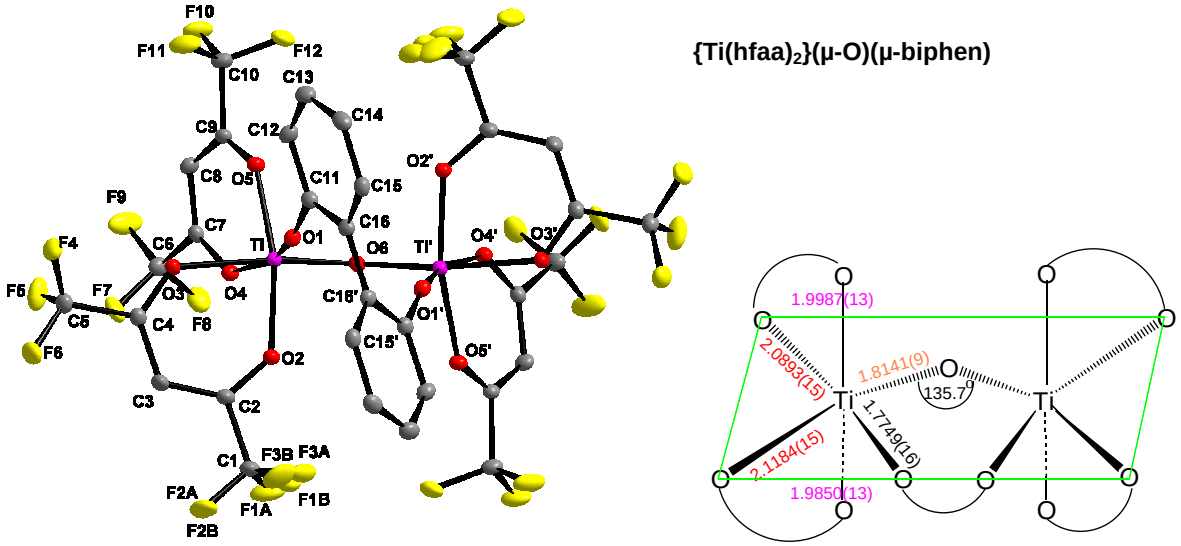

Figure 3.47 **Left**: The molecular structure (30 % probability displacement ellipsoids) of $\{Ti(hfaa)_2\}_2(\mu\text{-}O)(\mu\text{-biphen})$, showing the numbering scheme (primed labels indicate atoms generated by symmetry operations). **Right**: Diagram indicating coordination and distances around the titanium centre.

The following features are of interest:

• The structure consists of two octahedrally coordinated titanium atoms linked through an oxygen atom, forming an angle of 135.7° and a biphenolato-O,O' group. The two portions of the molecule are related to each other by a twofold rotation axis which passes through the joining oxygen and the mid-point of the central C-C bond of the bridging biphenolate ligand. The octahedral coordination around the titanium is slightly more distorted than in the $\{Ti\beta_2Cl\}_2O$ structures due to the bridging biphenolato group; the titanium atom is near the centre of the octahedron and bond angles vary from between 77° to 100°. This maximum angle deviation of *ca.* 13° compares to 9° in the $\{Ti\beta_2Cl\}_2O$ dimers.

• The biphenolato ligand acts as a unidentate bridging ligand. It also has the ability to act as a bidentate chelating ligand as in the case of the monomeric $Ti(\beta)_2$biphen structures, see section 3.3.2.1.

• The Ti-O bond distances in the TiO_6 octahedron vary considerably; the shortest being part of the bridging atoms, *i.e.*, the Ti-O bonds in the biphenolato bridge (ca 1.78 Å) and the Ti-O-Ti bridge (*ca* 1.81 Å) and the intermediate, axial (*ca* 1.99 Å) and longer, equatorial (*ca* 2.10 Å) bonds of the chelated β-diketonato ligand (see **Figure 3.47**). There is evidence of a *trans influence* of the bridging oxygen across the titanium atom; the longer Ti-O bond to each hfaa is found to be *trans* to the bridging oxygen. The length of the bridging bonds, Ti-(μ-O) and Ti-(biphelato-O,O'), once again, suggests partial double bond character, arising from donation of the electrons from filled oxygen *p* orbitals to the unfilled titanium *d* orbitals. This ligand-metal charge transfer from the oxygen atom (*p* electrons) to the titanium atom (empty *d* orbitals) could justify the fact that $\{Ti(hfaa)_2\}(\mu\text{-O})(\mu\text{-biphen})\}$ complex, with $3d^0$ electronic configuration, is strongly coloured (deep red-purple).

• The angle at the bridging oxygen, joining the two titanium atoms, is 135.7°, which according to *sp* hybridised geometry, should be 180°. The corresponding bridging oxygen angle is much larger in dimeric structures, $\{Ti\beta_2Cl\}_2(\mu\text{-O})$, where the Ti-O-Ti angles are 167.5°, 173.9°, 180°, 180° for β = acac[51], dbm[52], tfaa and hfaa respectively. This large distortion (deviation from ideal, 44°) can be attributed to the strain in accommodating the bridging biphenolato ligand.

• The β-diketonato rings (hfaa), are very nearly planar. The titanium atom lies slightly outside on the plane defined by the β-diketonato ligand with a Ti atom displacement of *ca.* 0.01 Å and 0.25 Å from the ligand plane.

Crystallographic aspects Large displacement ellipsoids are observed at the periphery of the molecule, indicating a less restricted packing environment. No obvious or significant packing effects or interactions are noted. The one CF_3 group, showing extensive thermal vibrations, was treated by disordered refinement techniques, to obtain more satisfactory refinement parameters. Site occupancies for disordered parts refined to a ratio of 72.2 : 27.8 for disordered parts A and B respectively.

3.3.2.4 Tetrameric Structure [Ti(β)$_2$ (μ-O)]$_4$

Geometrical Aspects A molecular diagram indicating atom labelling accompanied by a schematic diagram indicating bond lengths and coordination around the titanium centre of [Ti(hfaa)$_2$(μ-O)]$_4$ **[45]**, are presented in **Figure 3.48**.. Crystal data and details for data collection and refinement are summarised in **Table 3.22** Complete tables of bond lengths and angles are available on digital format.

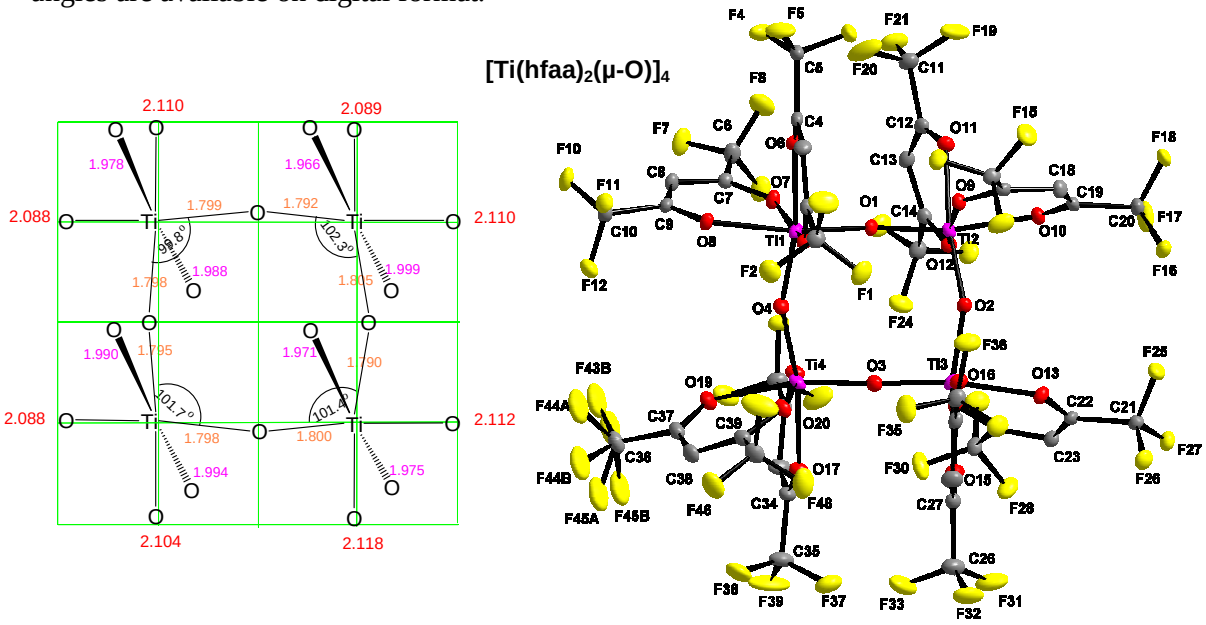

Figure 3.48 **Right**: The molecular structure (30 % probability displacement ellipsoids) of [Ti(hfaa)$_2$(μ-O)]$_4$ indicating the numbering scheme. **Left**: Diagram indicating coordination and distances (Å) around the titanium centre (values are given without esd.).

The following features are of interest:

• The four titanium atoms lie in a plane forming a square (**Figure 3.49**). This is one of eight different configurations that tetratitanium oxygen-bridged complexes can adopt: square, cube, capped parallelogram, butterfly, planar linear, planar, bowed linear/plate and zigzag.[60]

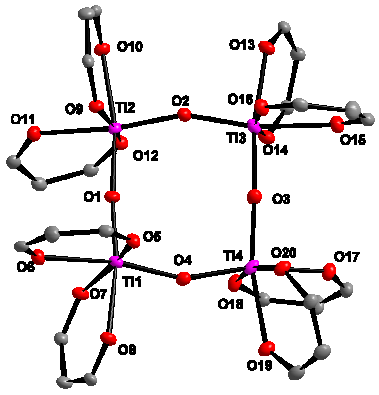

Figure 3.49 The backbone of [Ti(hfaa)$_2$(μ-O)]$_4$ showing the square formation by the four Ti atoms.

Table 3.22 Crystal data and structure refinement data for tetrameric, $[Ti(hfaa)_2(\mu\text{-}O)]_4$.

Formula	$Ti_4O_{20}C_{40}H_8F_{48}$	**Crystal size / mm^3**	0.40 x 0.35 x 0.29
Formula weight	1912.06	**Theta range for data collection / Deg**	1.44 to 28.35
Crystal colour/habit	Yellow, cuboid	**Reflections collected**	55 209
Crystal system	Monoclinic	**Independent reflections**	15 535[R(int) = 0.0301]
Space group	$P2_1/n$	**Completeness to theta = 28.35 / %**	98.7
Unit cell dimension /Å / Deg	a = 13.7394(4) b = 16.4156(4) c = 28.3400(7) α = 90 β = 99.7990(10) γ = 90	**Index ranges**	-17 ≤ h ≤ 18, -21 ≤ k ≤ 15, -35 ≤ l ≤ 37
		Absorption correction	Semi-empirical from equivalents
Volume / Å^3	6298.6(3)	**Max. and min. transmiss.**	0.8227 and 0.7670
Z	4	**Refinement method**	Full-matrix least-squares on F^2
Density$_{calc}$ / Mg m^{-3}	2.016	**Data/restraints/param.**	15 535 / 0 / 1007
Temperature / ℃	-173(2)	**Goodness-of-fit on F^2**	1.030
Wavelength / Å	0.71073	**Final R indices [I>2sigma(I)]**	R_1 = 0.0465, wR_2 = 0.1189
Absorption coefficiet / mm^{-1}	0.700	**R indices (all data)**	R_1 = 0.0608 wR_2 = 0.1333
F(000)	3712	**Largest diff. peak and hole / e.Å^{-3}**	1.953 and -1.241

Each titanium atom has a distorted TiO_6 octahedral coordination. The μ-oxo atoms are nearly in the same plane, but they are shifted out from the square sides, with O-Ti-O angles of 99.8°, 101.4°, 101.7° and 102.3° (see **Figure 3.48**). This is comparable to $[Ti(dpm)_2(\mu\text{-}O)]_4$, [54] with O-Ti-O angles of 100.5°, 100.3°, 100.5° and 99.4. Similar tetranuclear $(Ti\text{-}O)_4$ rings have also been found in $[Cp'TiCl(\mu\text{-}O)]_4$ derivatives where $Cp' = C_5H_{5-n}Me_n$; n = 0, 1, 4, 5[61] with O-Ti-O angles in the range 103 - 105°.

• The angles of the two opposite bridging oxygen are 158.5°, 157.3° and 174.4°, 171.0° respectively, which is smaller than the expected 180° according to *sp* hybridisation geometry. However, these angles are consistent with the oxygen-bridging angles found in the dimeric structures, $\{Ti\beta_2Cl\}_2(\mu\text{-}O)$, 167.5° and 173.9° for β = acac[51], dbm[52] and larger than 135.7° for $\{Ti(hfaa)_2\}(\mu\text{-}O)(\mu\text{-biphen})$.

• Three different Ti-O bonds are present: the short Ti-O bonds in the near linear Ti-O-Ti bridge (*ca*. 1.80 Å), the long Ti-O bonds with oxygen *trans* to μ-O (*ca* 2.10 Å) and the Ti-O bonds of intermediate length with oxygen *cis* to μ-O (*ca.* 1.98 Å), see **Figure 3.49**. Similar pairs of bonds were found in the preceding dimeric structures. A strong *trans influence* of the bridging oxygen, in the plane of the $[Ti\text{-}(\mu\text{-}O)]_4$ ring is observed, where the β-diketonate Ti-O bonds *trans* to the μ–O are elongated.

Crystallographic aspects Slightly larger displacement ellipsoids are observed at the periphery of the molecule, indicating a less restricted packing environment. No obvious or significant packing effects or interactions are noted. The one CF_3 group, showing extensive thermal vibrations, was treated by disordered refinement techniques, to obtain more satisfactory refinement parameters. Site occupancies for disordered parts refined to a ratio of 49.0 : 51.0 for disordered parts A and B respectively.

3.4 REACTION KINETICS

3.4.1 Substitution Kinetics

Three types of substitution reactions of octahedral Ti(IV) complexes were investigated. The first involves the substitution of two monodentate chlorine ligands of $Ti(\beta)_2Cl_2$ with the chelating biphenolato ligand. The second involves the successive substitution of the two chelating β-diketonato ligands of $Ti(\beta)_2$biphen with another β-diketonato ligand, Hacac and the third, the substitution of the bidentate biphenolato ligand (L^7) of $Ti(acac)_2$biphen with ligands of different ring sizes, i.e., 5-membered (L^5), 7-membered (L^7) and 8-membered (L^8).

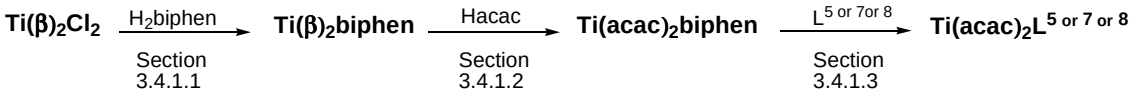

3.4.1.1 Substitution of $Ti(\beta)_2Cl_2$ complexes with biphenol

The results for the substitution of monodentate Cl^- ligands in complexes of the form $Ti(\beta)_2Cl_2$ with bidentate biphenol is reported. Initially the substitution of $Ti(acac)_2Cl_2$ **[23]** was monitored and then the behaviour pattern of the series with β = ba, dbm, tfba, closely related by only varying the R-group in the β-diketonato ligand, i.e., β= PhCOCHCOR with R = CH_3 (ba) **[21]**, Ph (dbm) **[22]** and CF_3 (tfba) **[17]**, was assessed.

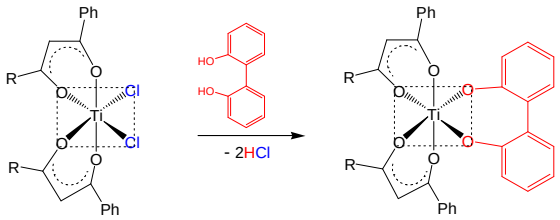

The reaction was studied by means of UV/vis techniques under pseudo first order conditions with incoming [H_2biphen] at least ten times higher than the concentration of the titanium complex.

UV/Vis Spectroscopic properties The UV spectra of the reactant, $[Ti(\beta)_2Cl_2]$, and the product of substitution $[Ti(\beta)_2$biphen] were recorded in acetonitrile at 25°C, see **Figure 3.50** for β = acac. The experimental wavelengths, λ_{exp}, are listed in **Table 3.23**. The complexes obey the Beer Lambert law, $A = \varepsilon C l$, with ε = extinction coefficient and *l* = path length (1 cm), in the concentration range utilised for the kinetic studies. This is confirmed by the linear relationship of absorbance (A) *vs.* concentration (C) measurements, **Figure 3.51**

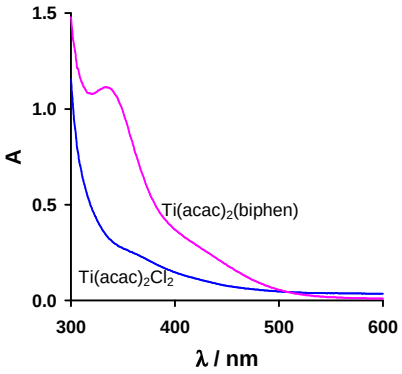

Figure 3.50 UV spectra of 0.2 mmol dm^{-3} solutions of reactant, $[Ti(acac_2Cl_2]$ and product, $[Ti(acac)_2$biphen] at 20 °C in CH_3CN.

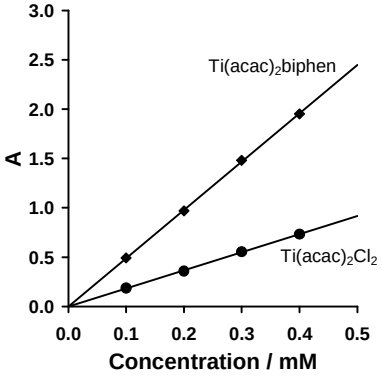

Figure 3.51 The graph of absorbance *vs.* concentration, measured at λ_{exp} as indicated in **Table 3.23**.

Product identification The products, $Ti(\beta)_2$biphen with β = acac, ba, dbm, tfba, of the substitution reaction, $Ti(\beta)_2Cl_2 + H_2$biphen, were synthesised as described in the experimental section; by refluxing stoichiometric amounts of $[Ti(\beta)_2Cl_2]$ and H_2biphen in CH_3CN (bp 82 °C), under an inert atmosphere for *ca.* 6 hours. To confirm product formation at the experimental temperatures at which the substitution kinetics was followed, i.e., 10 °C - 40 °C, the synthesis was repeated at room temperature. Stoichiometric amounts (representing second-order conditions), stirred at room temperature for 24 hours under an inert atmosphere, generated the product in low yields (<10%). It would appear that heat or an excess of biphenol is needed to drive the reaction to completion:

$$[Ti(\beta)_2Cl_2] + H_2\text{biphen} \rightleftharpoons [Ti(\beta)_2\text{biphen}] + 2\,HCl$$

The ^1H NMR spectra obtained in each case was consistent with the correct product as described in **Section 3.2.3.2**. The products, $Ti(acac)_2$biphen and $Ti(ba)_2$biphen, were also characterised by single crystal Xray crystallography, see **Section 3.3.2.1.**

Substitution kinetics Two kinetically distinct steps were observed when following the reaction on a UV/vis spectrophotometer; a fast first step followed by the second slower step (see **Figure 3.52**). The rate of the second reaction is *ca*.10 times slower than the first reaction, thus there is negligible coupling between the two stages and the rate constants can be determined independently.

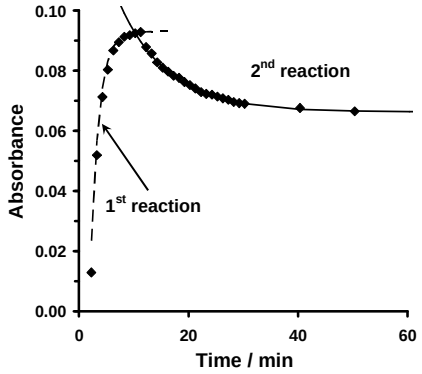

Figure 3.52 Absorbance *vs.* time data of the UV/vis monitored reaction of $Ti(acac)_2Cl_2$ at λ = 336 nm, illustrating the two reaction steps observed. [Ti] = 0.2 mmol dm^{-3} and [H_2biphen] = 0.04 mol dm^{-3}.

From the absorbance-time data of the first reaction, the pseudo-first-order rate constant, k_{obs}, was determined by fitting[62] the absorbance data to the first-order equation,[63]

$$\ln \frac{(A_0 - A_\infty)}{(A_t - A_\infty)} = k_{obs}\, t$$

where A_0 indicates initial absorbance, A_t absorbance at time t and A_∞ absorbance at infinity.

The graph of k_{obs} plotted as a function of the incoming H_2biphen concentration is a straight line with a non-zero intercept (see **Figure 3.54**), which implies a first-order dependence on [H_2biphen]. The general rate law applicable to this substitution reaction, is a two-term expression,

$$\text{rate} = \{k_s + k_2\,[H_2\text{biphen}]\}\,[Ti(\beta)_2Cl_2]$$
$$= k_{obs}\,[Ti(\beta)_2Cl_2]$$

For [H_2biphen] >> [$Ti(\beta)_2Cl_2$], the pseudo-first-order rate constant, $k_{obs} = k_s + k_2[H_2\text{biphen}]$ with k_2 the second-order rate constant for the substitution process and k_s the rate constant for the solvent pathway. (k_s = y-intercept and k_2 = gradient of k_{obs} *vs.* [H_2biphen] graph).

The non-zero intercept of these graphs (see **Figure 3.54**), implies that the solvent, CH_3CN, contributes to the reaction mechanism, although in only a relatively minor way. **Scheme 3.10** shows the two pathways followed in the substitution reaction. The coordinating ability of CH_3CN is confirmed by the ^1H NMR spectra of $Ti(acac)_2Cl_2$ (see **Figure 3.53**). In $CDCl_3$ the uncoordinated $Ti(acac)_2Cl_2$ species, shows one set of proton signals corresponding to the methyl protons of acac as a singlet at δ 2.19 and methine protons of acac as a singlet at δ 5.99. In CH_3CN, both the uncoordinated and solvent-coordinated $Ti(acac)_2Cl_2$ species are observed in the ration of 10:1. Split resonances are observed because the methyl and methine groups are not chemically equivalent in the seven-coordinated $Ti(acac)_2(CH_3CN)Cl_2$ species.

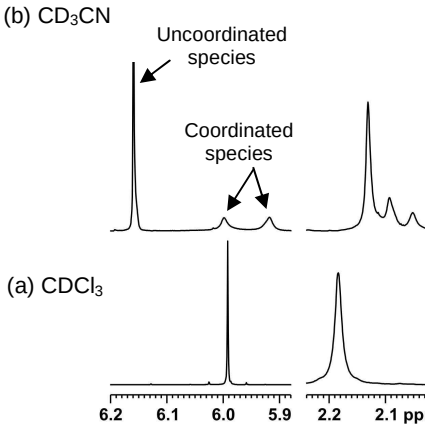

Figure 3.53 Partial ^1H NMR spectra of $Ti(acac)_2Cl_2$ in uncoordinating solvent (a) $CDCl_3$ and coordinating solvent (b) CD_3CN.

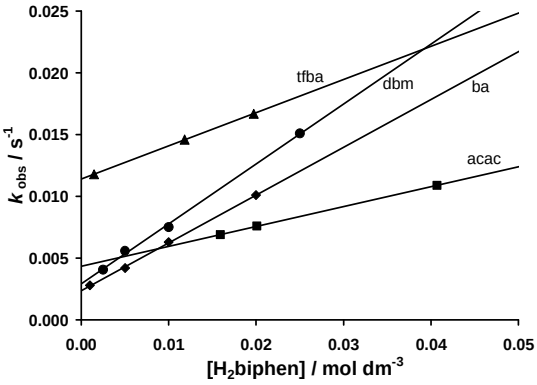

Figure 3.54 Graphs of pseudo-first-order rate constants, k_{obs}, *vs.* [Hbiphen] at 25 °C for $Ti(\beta)_2Cl_2$ with β = ba, dbm and tfba, showing non-zero intercept. [Ti complex] = 0.1 mmol dm^{-3}.

The solvent contribution is more noticeable in the substitution reaction of $Ti(tfba)_2Cl_2$, containing the highly electron-withdrawing group, CF_3. The β-diketonates are non-labile ligands; and the influence on the reactivity is by indirectly affecting the electron density around the titanium centre. In the series studied; $Ti(dbm)_2Cl_2$ and $Ti(ba)_2Cl_2$ with R = Ph and CH_3 respectively have similar electron-withdrawing tendencies (*i.e.*, χ_{Ph} = 2.21 and χ_{CH_3} = 2.34) and identical k_s values while $Ti(tfba)_2Cl_2$ with R = CF_3 has an increased electron withdrawing ability (i.e., χ_{CF3} = 3.01) and a larger k_s value.

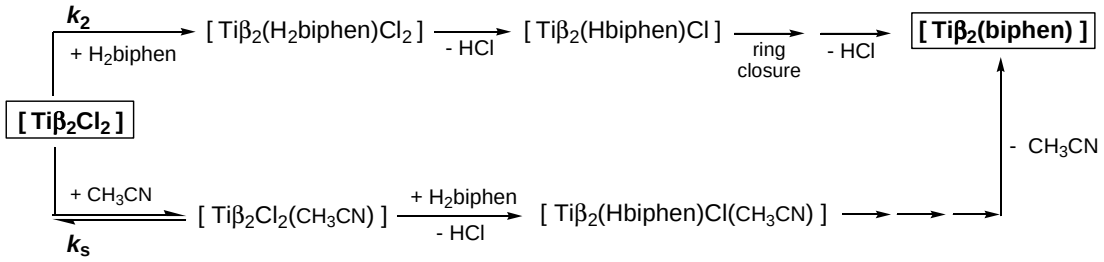

Scheme 3.10 Diagram showing both the direct and solvent pathways

The second order rate constant, k_2, was large relative to k_s and of similar order for the series with β = dbm, ba and tfba (ranges from 0.2 - 0.5 mol^{-1} dm^3 s^{-1}, T = 25 °C). This implies that the β-diketonato ligands, which are non-labile ligands, do not significantly influence the rate of substitution in $Ti(\beta)_2Cl_2$ The second substitution reaction was [H_2biphen] independent and more than10 times slower than the first step. The rate constants are summarised in **Table 3.23**.

Table 3.23 Kinetic data and activation parameters for the substitution reaction of $Ti(PhCOCHCOR)_2Cl_2$, R = CH_3 (ba), Ph (dbm), CF_3 (tfba) with H_2biphen. Data for $Ti(acac)_2Cl_2$, acac = $CH_3COCHCOCH_3$ is also included.

Complex	R	χ_R[a]	λ_{exp}	T	Rate constants		Activation parameters		
$Ti(\beta)_2Cl_2$			nm	℃	k_2 mol^{-1} dm^3 s^{-1}	k_s s^{-1}	$\Delta H^{\#}$ kJ mol^{-1}	$\Delta S^{\#}$ J mol^{-1} K^{-1}	$\Delta G^{\#}$ kJ mol^{-1}
dbm	Ph	2.21	450	9.5	0.1429	0.0006	52.6	-79	76
				25.5	0.4853	0.0029			
				40.0	1.3458	0.0097			
ba	CH_3	2.34	380	10.0	0.1409	0.0004	36.0	-133	76
				25.0	0.3314	0.0028			
				40.0	0.6905	0.0082			
tfba	CF_3	3.01	450	10.0	0.0947	0.0034	39.1	-126	77
				25.0	0.2275	0.0117			
				40.0	0.5036	0.0263			
acac	CH_3 CH_3	--	340	15.0	0.062	0.0001	59.6	-62	78
				25.0	0.153	0.0046			
				36.2	0.365	0,0133			

[a] χ = group electronegativity (Gordy scale).
For the second kinetically observable step of $Ti(\beta)_2Cl_2$ at T = 25 °C, the rate constant, k_1 = 0.0003 s^{-1} (dbm), 0.0009 s^{-1} (ba) and 0.0015 (acac).

Activation Parameters The enthalpy, $\Delta H^{\#}$, and entropy, $\Delta S^{\#}$, of activation for the reaction were determined from the temperature dependence study, where the dependence of k_2 in the temperature range of T = 10 - 40 °C was evaluated, see **Figure 3.55**. The rate constants, *vs.* temperature data were least-squares fitted according to the linear form of the Eyring relationship,[64]

$$\ln \frac{k}{T} = \frac{-\Delta H^{\#}}{RT} + \frac{\Delta S^{\#}}{R} + \ln \frac{k_B}{h}$$

where R is the universal gas constant, k_B the Boltzmann's constant and h Planck's constant. The Eyring curve of $\ln(k_2/T)$ *vs.* T^{-1}, is linear (see **Figure 3.55** insets), with a slope of $-\Delta H^{\#}/R$, and an intercept of $\{\ln(k_B/h) + \Delta S^{\#}/R\}$. The free energy of activation, $\Delta G^{\#}$, is calculated from the equation, $\Delta G^{\#} = \Delta H^{\#} - T\Delta S^{\#}$.[65] The activation parameters are summarized in **Table 3.23**.

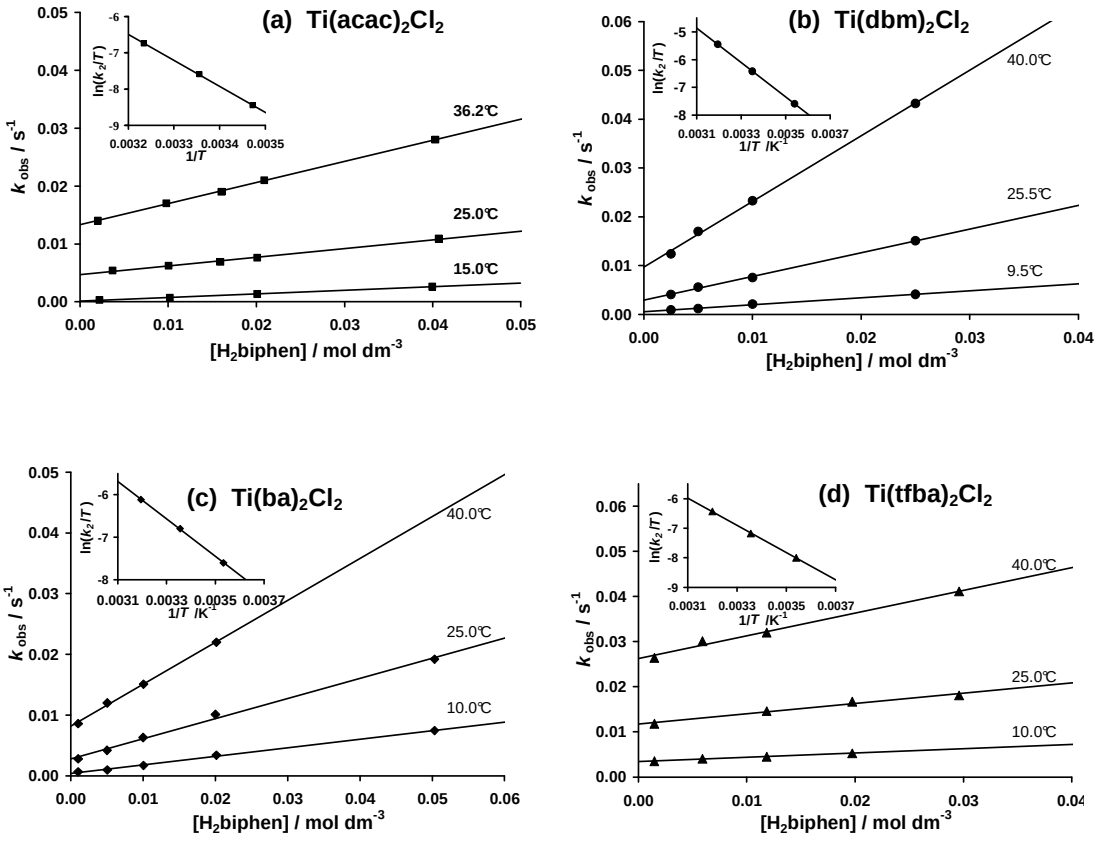

Figure 3.55 Graphs of $\ln(k_2/T)$ *vs.* T^{-1} for the substitution reactions of $Ti(\beta)_2Cl_2$ with H_2biphen, β = acac, ba, dbm and tfba. [Ti complex] = 0.1 mmol dm^{-3}.

Proposed Mechanism The proposed reaction pathway from reactant to product is illustrated in **Scheme 3.11**. The substitution takes place in two kinetically distinct steps, a relatively fast, concentration dependent first reaction, followed by a slower concentration independent step. The order of the reaction kinetics suggests that the first reaction is the binding of the incoming ligand, H_2biphen, and the second reaction, rate-limiting ring closure.

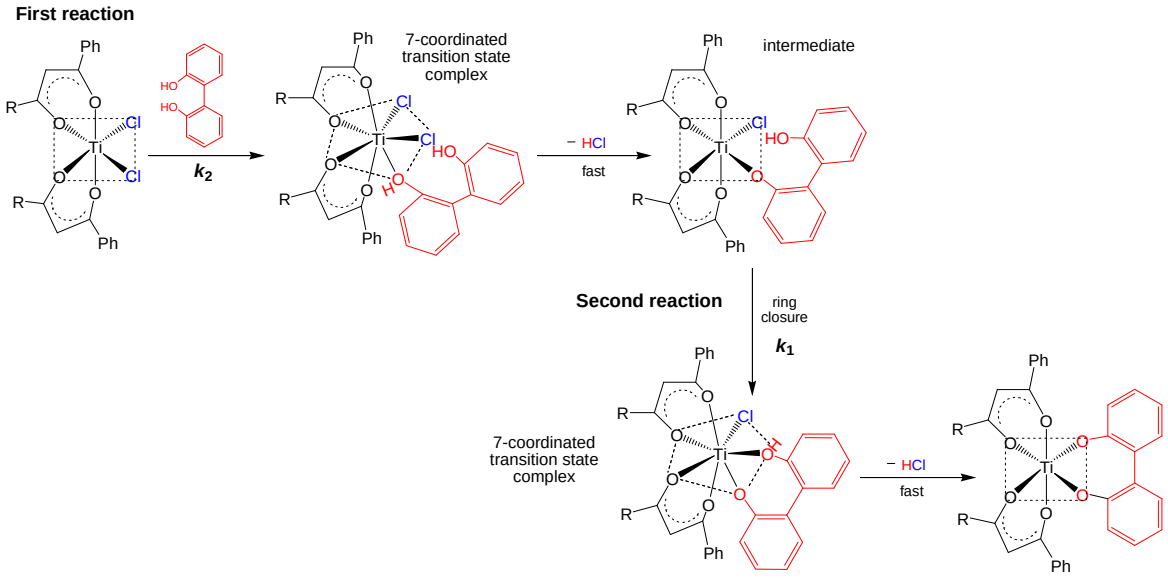

Scheme 3.11 Proposed reaction pathway illustrating the associative mechanism for the direct substitution of $[Ti(\beta)_2Cl_2]$ with biphenol.

The large negative activation entropy of the first step is consistent with the substitution proceeding *via* an associative mechanism. This is expected, since octahedral complexes of Ti^{IV} (d^0) are coordinatively unsaturated (i.e., $Ti(\beta)_2Cl_2$ is a 12-electron species) and therefore an associatively activated pathway would be preferred. The existence of the solvent pathway (i.e., $k_s \neq 0$) is mutually consistent with an associative mechanism since it demonstrates that the reacting species, $Ti(\beta)_2Cl_2$, easily coordinates to the solvent or binds associatively to the incoming ligand, H_2biphen, forming a seven-coordinate transition state complex.

When considering the nature of the transition state, $[Ti(\beta)_2Cl_2(H_2biphen)]$, in which the biphenolato binds to the Ti nucleus through only one of the O-atoms, is expected to form first. This transition state may then convert to another transition state in which the biphenol ligand becomes bidentate. A seven-coordinate transition state complex is viable, as stable

complexes with coordination numbers greater than six are known for Ti(IV), for example, 7- and 8-coordination are shown in **Table 2.1.** The common geometry for 7-coordinated Ti(IV) complexes is pentagonal bipyramidal, as in the case of $Ti(Me_2dtc)_3Cl$.[66] In a dissociative mechanism, the 5-coordinated cationic species, $[Ti(\beta)_2Cl]^+$, formed by breaking the first Ti-Cl bond, is considerably less likely.

Computational Study A DFT computational study was carried out to identify the transition states and calculate activation parameters of the two step substitution reaction of bidentate biphenol for the two monodentate Cl^- ligands in $Ti(acac)_2Cl_2$. It was found that the 6-coordinated reactant proceeds through a 7-coordinated transition state, which collapses to give a 6-coordinated intermediate structure. The calculated optimized geometries are shown on the right. Distances are in Angstrom (Å) and bonds that are breaking or forming are shown in dashed representation.

The optimised reactant structure, comprising $Ti(acac)_2Cl_2$ and biphenol, indicates the formation of an O-H---Cl interaction.

Reactant structure

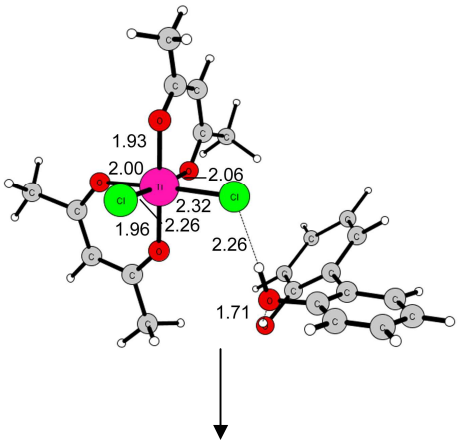

At the transition state, the attacking oxygen atom is positioned 2.14 Å from the Ti ion, while the Ti-Cl distance is 3.17 Å, which is 0.89 Å longer than in the reactant complex. The OH proton is located 2.02 Å from the chloride atom. The O-H bond of the hydroxyl moiety is only slightly elongated compared to the reactant structure (from 0.98 Å to 1.0 Å at the transition state). Analysis of the transition state eigenvector shows dominating contributions from the four bonds, O-Ti, Ti-Cl, Cl-H and O-H, indicating that formation and dissociation of these bonds (i.e., attack of the OH oxygen on the Ti atom, dissociation of Cl^- and proton transfer from the attacking OH to the Cl) occur almost simultaneously suggesting an interchange (associative) mechanism.

Transition state (1) structure

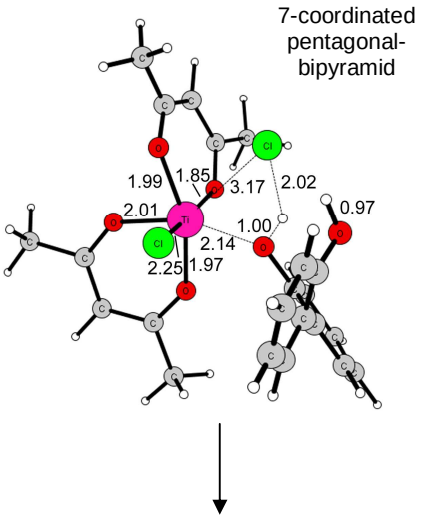

The intermediate geometry exhibits coordination of the biphenol molecule to the Ti through one oxygen atom. The released HCl molecule is hydrogen-bonded to the second OH of biphenol.

Intermediate structure

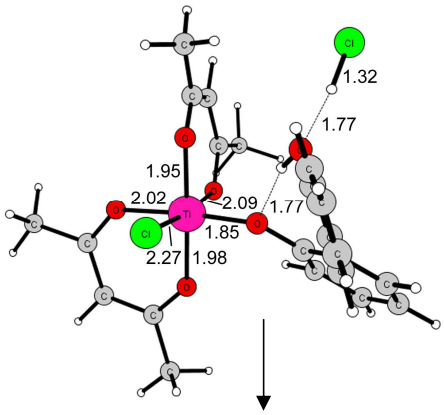

The second transition state, for attack of the second OH oxygen on Ti is similar to the first transition state, exhibiting a 7-coordinated structure and involving concerted oxygen attack, chloride release and proton transfer. At the second transition state, the attacking oxygen atom is found 2.24 Å from the Ti ion. The Cl^- ion is partially displaced and is located 3.13 Å from Ti. The O-H bond is elongated to 1.03 Å, while the H-Cl distance is 1.83 Å.

Transiton state (2) structure

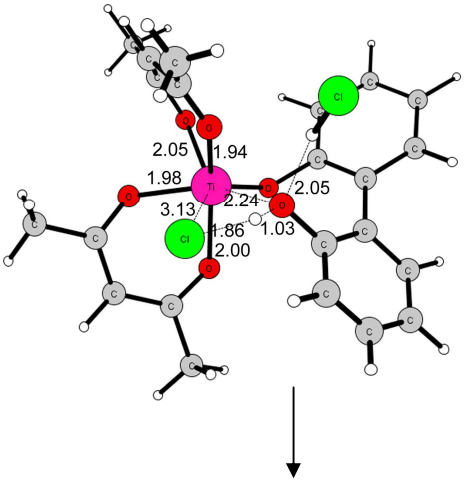

The optimized product structure is six-coordinated. The two released HCl molecules are found hydrogen bonded to the complex. Removal of the HCl, either by evaporization (during synthesis) of by diffusing away into solution (during reaction kinetics) drives the reaction to completion.

Product structure

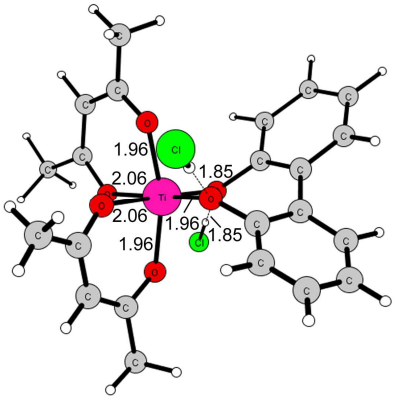

The computed thermodynamic parameters for the first transition state (TS1), intermediate, second transition state (TS2) and final product are shown in **Table 3.24**. The experimentally obtained activation energies are comparable to the values computed for TS1. The computed

activation enthalpy, $\Delta H^{\#}$, (including thermal corrections, 298.15 K) for the first transition state of 66.1 kJ mol^{-1}, is only a slight overestimation of the experimentally determined reaction enthalpy of 59.6 kJ mol^{-1}. Entropy calculations are very sensitive to low frequency modes, and thus should be considered an estimate value. Nonetheless, the calculated entropy, $\Delta S^{\#} = -46.5$ J mol^{-1} K^{-1}, compares well with the experimentally obtained activation entropy of −62 J mol^{-1} K^{-1}. Employing both computed enthalpy and entropy, the final activation, $\Delta G^{\#}$, is 80.0 kJ mol^{-1}, which is practically the same than the experimentally determined value of 78 kJ mol^{-1}.

Table 3.24 Computed energies for biphenol substitution at $Ti(\beta)_2Cl_2$ (298.15 K). All values are given compared to the reactant.

$Ti(\beta)_2Cl_2$	Computed			Experimental		
	ΔH kJ mol^{-1}	ΔS J mol^{-1} K^{-1}	ΔG kJ mol^{-1}	ΔH^* kJ mol^{-1}	ΔS^* J mol^{-1} K^{-1}	ΔG^* kJ mol^{-1}
Reactant	0.0	0.0	0.0			
TS1	66.1	-46.5	80.0	59.6	-62	78
Intermediate	-11.5	4.0	12.7			
TS2	65.5	-47.8	79.7			
Product	13.9	13.2	10.0			

The computed activation enthalpy for the second step is 76.9 kJ mol^{-1} compared to the intermediate (and 51.6 kJ mol^{-1} compared to the reactant). The higher activation enthalpy for the second step, agrees with experimental results, which indicate that the second step of the reaction is about 10 times slower than the first step. The removal of HCl bring the final calculated ΔG for the overall reaction

$$[Ti(acac)_2Cl_2] + H_2biphen \rightleftharpoons [Ti(acac)_2biphen] + 2\,HCl \qquad \Delta G^{\#} = -15.1 \text{ kJ mol}^{-1}$$

The computed mechanism for biphenol substitution at $Ti(acac)_2Cl_2$ is in agreement with the experimental data and proposed reaction pathway as shown in **Scheme 3.11**.

3.4.1.2 Substitution of Ti(β)$_2$biphen complexes with β-diketone

The results for the substitution of two bi-chelating β-diketonato ligands in complexes of the form Ti(β)$_2$biphen, with another bi-chelating β-diketone, Hacac, is reported. The behaviour pattern of this series, closely related by only varying the R-group in the β-diketonato ligand, i.e., β= PhCOCHCOR with R = CH_3 (ba) **[32]**, Ph (dbm) **[33]**, and CF_3 (tfba) **[28]**, is assessed.

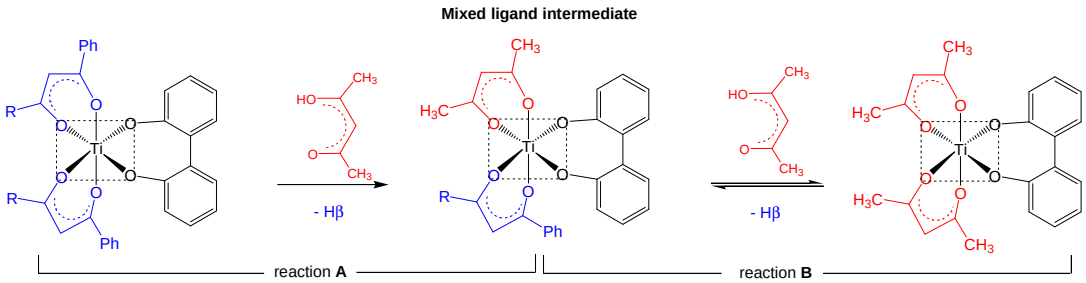

The substitution takes place *via* two consecutive reactions, **A** and **B**, with each reaction involving two steps. The observed reactions are the substitution of one β-diketonato ligand at a time, i.e., the product of one reaction becomes the reactant in the next and the intermediate, the mixed-ligand complex, is directly detectable on ^{1}H NMR. The reaction was studied by means of ^{1}H NMR and UV/vis techniques.

^{1}H NMR Spectroscopy The reaction, Ti(tfba)$_2$biphen + Hacac, and the reverse reaction, Ti(acac)$_2$biphen + Htfba, were monitored at 25 °C under both *pseudo*-first order and second order (equimolar) conditions. Equilibrium exists between the intermediate and the final product of substitution under both excess and equimolar conditions since the mixed-ligand complex is more stable than either of the parent or product complex.[67] In addition, under second order conditions, equilibrium exists between the parent and intermediate, i.e., reaction **A** is only driven to completion with a large excess of the incoming ligand.

$$\text{Ti(tfba)}_2\text{biphen} \underset{k_{-A}}{\overset{k_A}{\underset{\text{- Htfba}}{\overset{\text{Hacac}}{\rightleftharpoons}}}} \text{Ti(tfba)(acac)biphen} \underset{k_{-B}}{\overset{k_B}{\underset{\text{- Htfba}}{\overset{\text{Hacac}}{\rightleftharpoons}}}} \text{Ti(acac)}_2\text{biphen}$$

If Hacac >>Ti(β)$_2$biphen, then $k_{-A} = 0$

The substitution reaction was followed by monitoring the methine resonances of the complexes involved; the disappearance of reactant, [Ti(tfba)$_2$biphen], at lowest field, and the

appearance of two signals of the mixed-ligand complex at intermediate field and the final product of substitution, [Ti(acac)$_2$biphen], at highest field. The β-diketone can also be monitored, i.e., the appearance of Htfba and the disappearance of Hacac (under second order conditions). The partial ^{1}H NMR spectra for the substitution of [Ti(tfba)$_2$biphen] + Hacac under *pseudo*-first order (40x excess) and second order (equimolar mixture) conditions are shown in **Figure 3.56 (a)** and **(b).** For reaction **A**, the decrease of Ti(tfba)$_2$biphen and increase of Ti(tfba)(acac)biphen is monitored while for reaction **B**, the increase of Ti(acac)$_2$biphen is monitored. The resonances at lowest and highest field are due to Ti(tfba)$_2$biphen and Ti(acac)$_2$biphen, respectively, while the two lines at intermediate field are assigned, in order of increasing field, to the tfba and acac resonances, respectively, of the mixed-ligand complex, Ti(tfba)(acac)biphen.

Similarly, the partial ^{1}H NMR spectra for the reverse substitution reaction, [Ti(acac)$_2$biphen] + Htfba are shown in **Figure 3.57 (a)** and **(b).** The decrease of Ti(acac)$_2$biphen and increase of Ti(tfba)(acac)biphen is monitored for reaction **A**, while the increase of Ti(tfba)$_2$biphen is monitored for reaction **B**. The time trace of the results is shown in **Figure 3.56** and **Figure 3.57** on the right hand side. Both the *pseudo*-first and second order data fitted to first order kinetics indicating that the the rate determining step is independent of the concentration of the incoming ligand.

The time-based data was processed *via* normal single stage treatment (i.e., by utilising the first part of concentration-time data for reaction **A** and the last part of concentration-time data for reaction **B**) and the consecutive reaction model.[68] Similar rate constants were obtained when using either treatment. Kinetic data is summarised in **Table 3.25**.

Table 3.25 ^{1}H NMR kinetic data for the substitution reaction of Ti(tfba)$_2$biphen + Hacac and the reverse reaction Ti(acac)$_2$biphen + Htfba at T = 25 °C. For *pseudo*-first order, [Ti complex] = 5 mmol dm^{-3}, [Hacac] = 200 mmol dm^{-3} and [Htfba] = 50 mmol dm^{-3} and for second order conditions, [Ti complex] = 10 mmol dm^{-3}, [Hacac] = 10 mmol dm^{-3} and [Htfba] = 10 mmol dm^{-3}.

Reaction	*Pseudo*-first order		Second order	
	$k_{(A)\ obs}$ / s^{-1}	$k_{(B)\ obs}$ / s^{-1}	$k_{(A)\ obs}$ / s^{-1}	$k_{(B)\ obs}$ / s^{-1}
Ti(tfba)$_2$biphen + Hacac	0.0026*	0.0022*	0.0020	0.0024
Ti(acac)$_2$biphen + Htfba	0.0027	0.0010	0.0019	0.0025

*Rate constants for reaction **A** and **B** are the same. Comparison of k_{obs} - ^{1}H NMR results (**Table 3.25**, highlighted yellow, reaction **A** and **B**) to UV/vis results (**Table 3.26**, highlighted yellow, either reaction **A** or **B**), shows identical values.

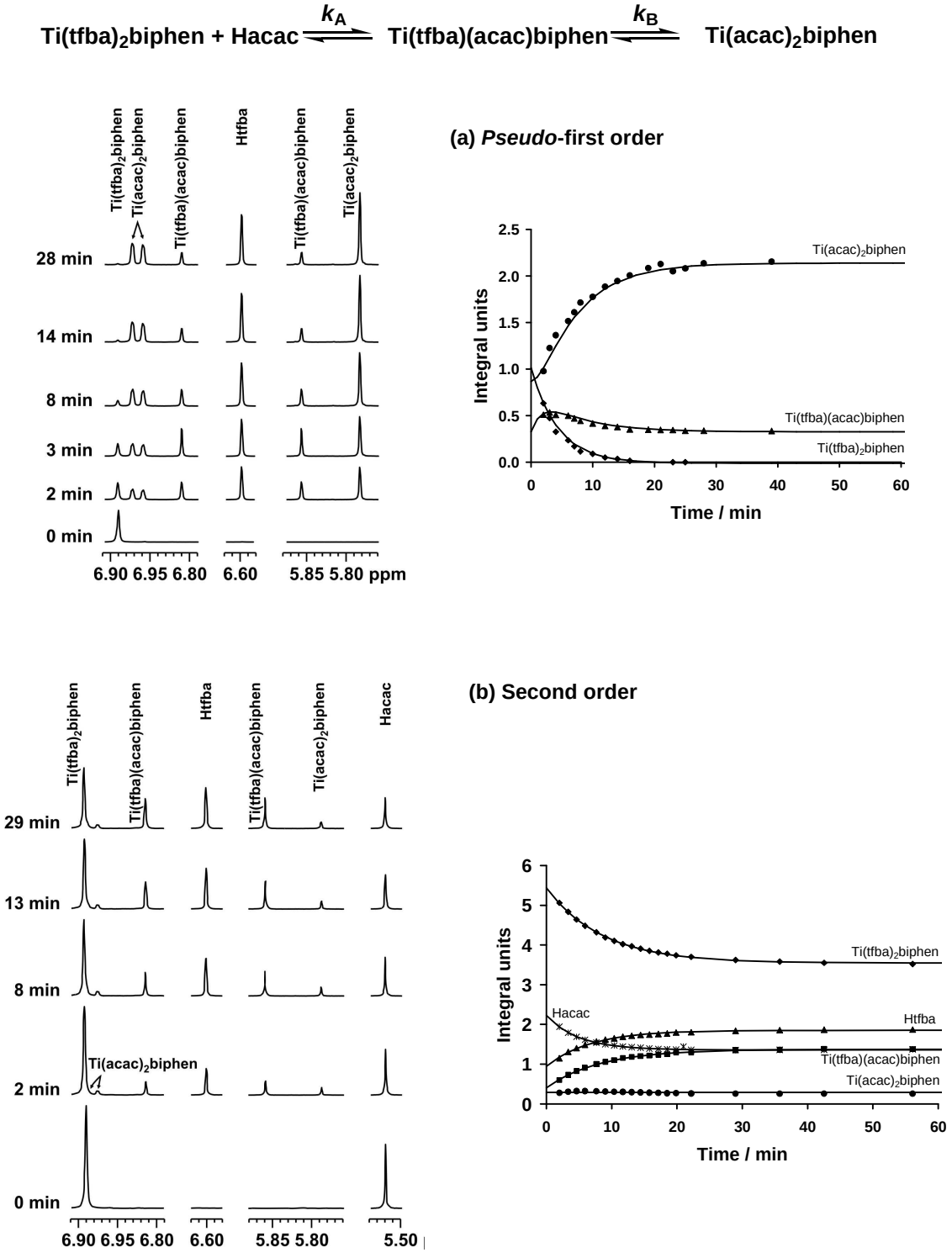

Figure 3.56 **Left:** Partial dynamic ^{1}H NMR spectra of the substitution reaction in $CDCl_3$ taken immediately before dissolution of Ti(tfba)$_2$biphen + Hacac, under **(a)** *pseudo*-first order (40x excess Hacac: [Ti] = 5 mmol dm^{-3} and [Hacac] = 200 mmol dm^{-3}) and **(b)** second order (equimolar: [Ti] = 10 mmol dm^{-3} and [Hacac] = 10 mmol dm^{-3}) conditions. **Right:** Integration units *vs*. time data obtained for the ^{1}H NMR monitored substitution reaction, Ti(tfba)$_2$biphen + Hacac, in $CDCl_3$ at 25 °C

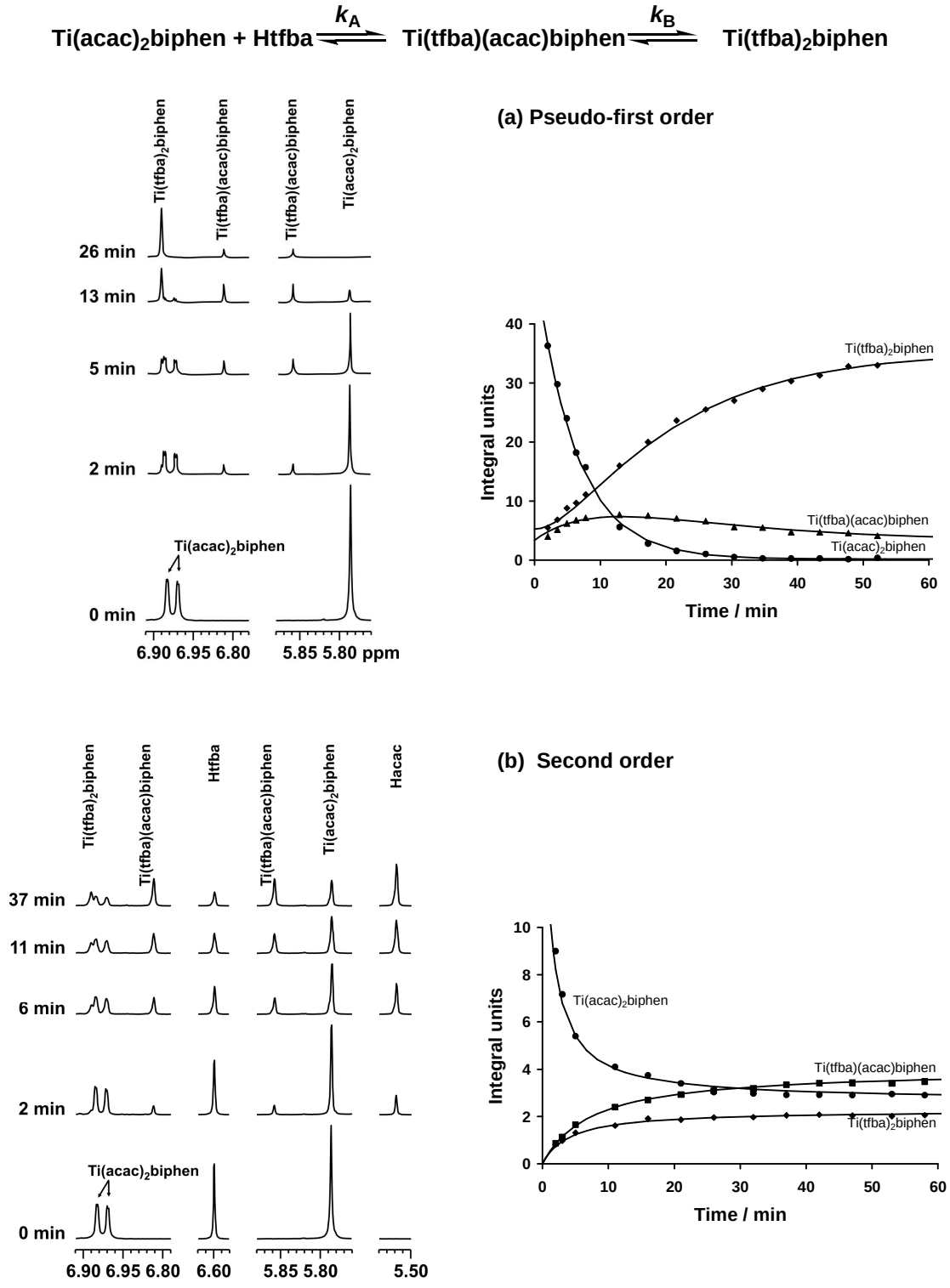

Figure 3.57 **Left:** Partial dynamic ^{1}H NMR spectra of the substitution reaction in $CDCl_3$ taken immediately before dissolution of Ti(acac)$_2$biphen + Htfba, under **(a)** *pseudo*-first order (10x excess Htfba: [Ti] = 5 mmol dm^{-3} and [Hacac] = 50 mmol dm^{-3}) and **(b)** second order (equimolar: [Ti] = 10 mmol dm^{-3} and [Hacac] = 10 mmol dm^{-3}) conditions. **Right:** Integration units *vs*. time data obtained for the ^{1}H NMR monitored substitution reaction, Ti(acac)$_2$biphen + Htfba, in $CDCl_3$ at 25 °C

UV/vis Spectroscopy The UV spectra of the reactant, [Ti(β)$_2$biphen], and the product of substitution [Ti(acac)$_2$biphen] were recorded in acetonitrile at 25°C. The titanium complexes obey the Beer Lambert law in the concentration range of kinetic study, confirmed by the linear relationship of absorbance *vs.* concentration measurements (see **Figure 3.51** for β = acac). The experimental wavelengths, λ_{exp}, at which the substitution reactions were monitored (listed in **Table 3.26**), allow one to observe only reaction **A** or reaction **B**. Since both consecutive β-diketonato substitution reactions proceed at similar rates (according to ^{1}H NMR data in previous section), one cannot distinguish between reaction **A** and reaction **B** in terms of rate constants, i.e., $k_{obs(A)} \approx k_{obs(B)}$. However monitoring the reaction *via* UV/vis spectroscopy provided additional information. The individual steps, i.e., addition of Hacac (**step 1**) and ring closure (**step 2**) are observed as two kinetically distinct steps. The proposed mechanism in **Scheme 3.12** shows the two steps in both reaction **A** (first β-substitution) and reaction **B** (second β-substitution).

No kinetic data was obtained for the first step as it proved to be impracticably fast, but it was detected from the UV/vis spectra of [Ti(β)$_2$biphen] + Hacac measured immediately after mixing at constant time intervals; the large difference between the first and second scan relative to the following scans, is indicative of a very fast initial reaction.

The rate of the second reaction was independent of concentration of the incoming Hacac (as observed on ^{1}H NMR). This is confirmed by the graph of k_{obs} *vs.* concentration of incoming ligand (see **Figure 3.59**), which yields a horizontal straight line (zero gradient). A solvent pathway is not expected since CH_3CN does not readily coordinate to Ti(β)$_2$biphen as demonstrated by the ^{1}H NMR spectra of Ti(acac)$_2$biphen in both $CDCl_3$ and CD_3CN (see **Figure 3.58**). In $CDCl_3$ the uncoordinated Ti(acac)$_2$biphen species, shows methine protons of acac as a singlet at δ 5.78 and the biphenolato ring protons arranged in the ratio, 2:2:2:2 (d,t,t,d) at δ 6.83; 6.96; 7.18; 7.36. In CH_3CN, only one species is observed, in the same pattern and slightly shifted as expected. The kinetic data for the second reaction is reported in **Table 3.26**. The substitution reaction, Ti(tfba)$_2$biphen + Hacac, at T = 25 °C and under pseudo-first order conditionon was monitored *via* both ^{1}H NMR and UV/vis, allowing one to compare the k_{obs} values (see **Table 3.25** and **Table 3.26**, values highlighted in yellow). These values are mutually consistent.

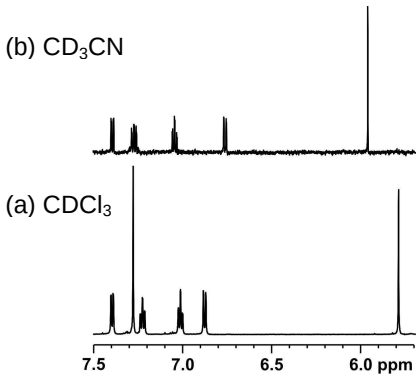

Figure 3.58 Partial ^{1}H NMR spectra of Ti(acac)$_2$biphen in uncoordinating solvent (a) $CDCl_3$ and coordinating solvent (b) CD_3CN.

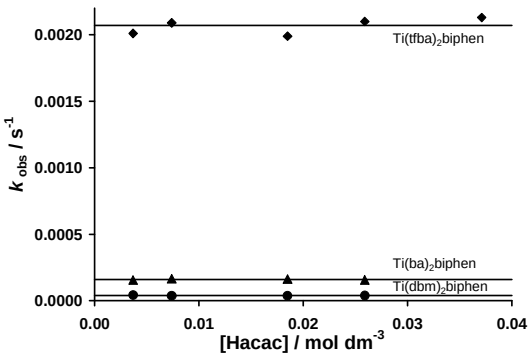

Figure 3.59 Graphs of pseudo-first-order rate constants, $k_{obs,}$ *vs.* [Hacac] at 25 °C for Ti(β)$_2$biphen with β = ba, dbm and tfba, showing horizontal straight lines (zero gradient). [Ti complex] = 0.1 mmol dm^{-3}.

Table 3.26 Kinetic data and activation parameters at 25 °C for the substitution reaction (**A** or **B**) of Ti(β)$_2$biphen + Hacac with β = dbm, ba and tfba.

Complex	R	χ_R	λ_{exp}	T	Rate values		Activation parameters		
Ti(β)$_2$biphen			nm	℃	$t_{½}$ min	k_{obs} s^{-1}	$\Delta H^{\#}$ kJ mol^{-1}	$\Delta S^{\#}$ J mol^{-1} K^{-1}	$\Delta G^{\#}$ kJ mol^{-1}
dbm	Ph	2.21	420	25	289	0.00004	58.4	-134.7	98.5
				40		0.00010			
				60		0.00050			
ba	CH_3	2.34	390	25	72	0.00016	37.3	-192.5	94.6
				40		0.00037			
				60		0.00088			
tfba	CF_3	3.01	410	10		0.00055	55.8	-109.6	88.5
				25	6	0.00208*			
				40		0.00590			

Comparison of k_{obs} - UV/vis results (**Table 3.26**, highlighted yellow, either reaction **A** or **B**) to ^{1}H NMR results (**Table 3.25**, highlighted yellow, reaction **A** and **B**), shows identical values.

The effect of the substituents R on the behaviour of $(PhCOCHCOR)^-$ as a leaving ligand was observed; the reactivity towards substitution in Ti(β)$_2$biphen increases with an increase in the electronegativity of the substituents R of the β-diketonato ligand. There is more than a 10x

increase in the rate of substitution for tfba compare to ba or dbm. It can be seen that k_{obs} is larger (substitution is faster) if the leaving β-diketonato ligand is less e^- rich (more electronegative) than the incoming β-diketonato ligand. Replacement of strongly electron-withdrawing ligands from the Ti^{IV} core with relatively electron-donating ligands will lessen the electrophilic nature of the electron starved Ti^{IV} core, thereby stabilising it.

Activation Parameters The dependence of k_{obs} on temperature (see **Figure 3.61**), allows for the determination of the activation parameters, $\Delta H^{\#}$, $T\Delta S^{\#}$ and $\Delta G^{\#}$, which are listed in **Table 3.26**. The large negative activation entropy is consistent with the substitution process proceeding *via* an associative mechanism.

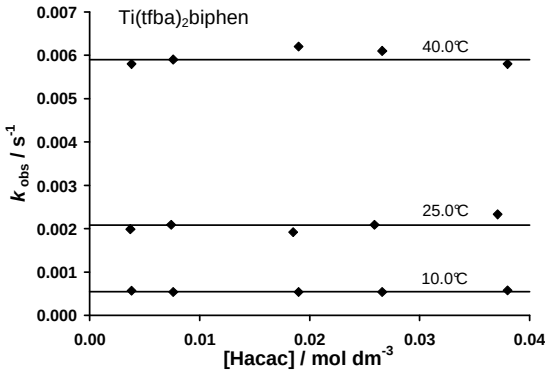

Figure 3.60 Graphs of pseudo-first-order rate constants, $k_{obs,}$ *vs.* [Hacac] for the substitution reaction of $Ti(tfba)_2biphen$ with Hacac in the temperature range 10 - 40°C. [Ti] = 0.1 mmol dm^{-3}

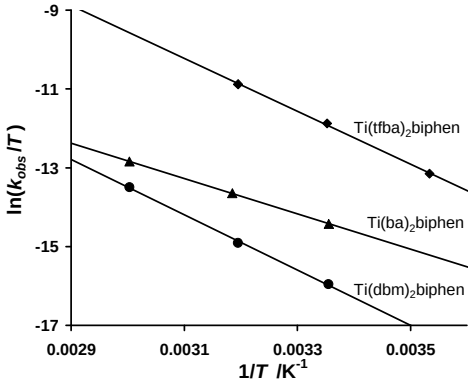

Figure 3.61 Graph of $\ln(k_{obs}/T)$ *vs.* T^{-1} for the substitution reaction of $Ti(\beta)_2biphen$ with Hacac.

Proposed Mechanism The proposed reaction pathway from reactant to product consistent with ^1H NMR and UV/vis data is illustrated in **Scheme 3.11**. The rapid formation of the mixed ligand complex, Ti(β)(acac)biphen, followed by the final substitution product, $Ti(acac)_2biphen$, were clearly observed on the dynamic ^1H NMR spectra. The UV/vis data shows two kinetic steps, **step 1** (observed but not calculated; expected to be dependent on the concentation of the incoming Hacac) and **step 2** (rate constant k_{obs} calculated and is independent on the concentration oif the incoming Hacac). The substitution process proceeds *via* an associatively activated pathway, consistent with the large negative activation entropy.

The rate of the consecutive first and second Hacac substitution reactions **A** and **B** was found to be the same, i.e., $k_{obsA} \approx k_{obsB}$. This is not expected since the parent, Ti(β)$_2$biphen, of the first substitution **A** is different to the mixed-ligand parent, Ti(β)(acac)biphen, of the second substitution **B.** And since it was shown that the substitutents R in Ti(β)$_2$biphen affect the rate of reactivity towards substitution (i.e., rate of substitution increases with an increase in the electronegativity of the substituents R of the β-diketonato ligand), it is not clear why the rate the first and second substitution are the same.

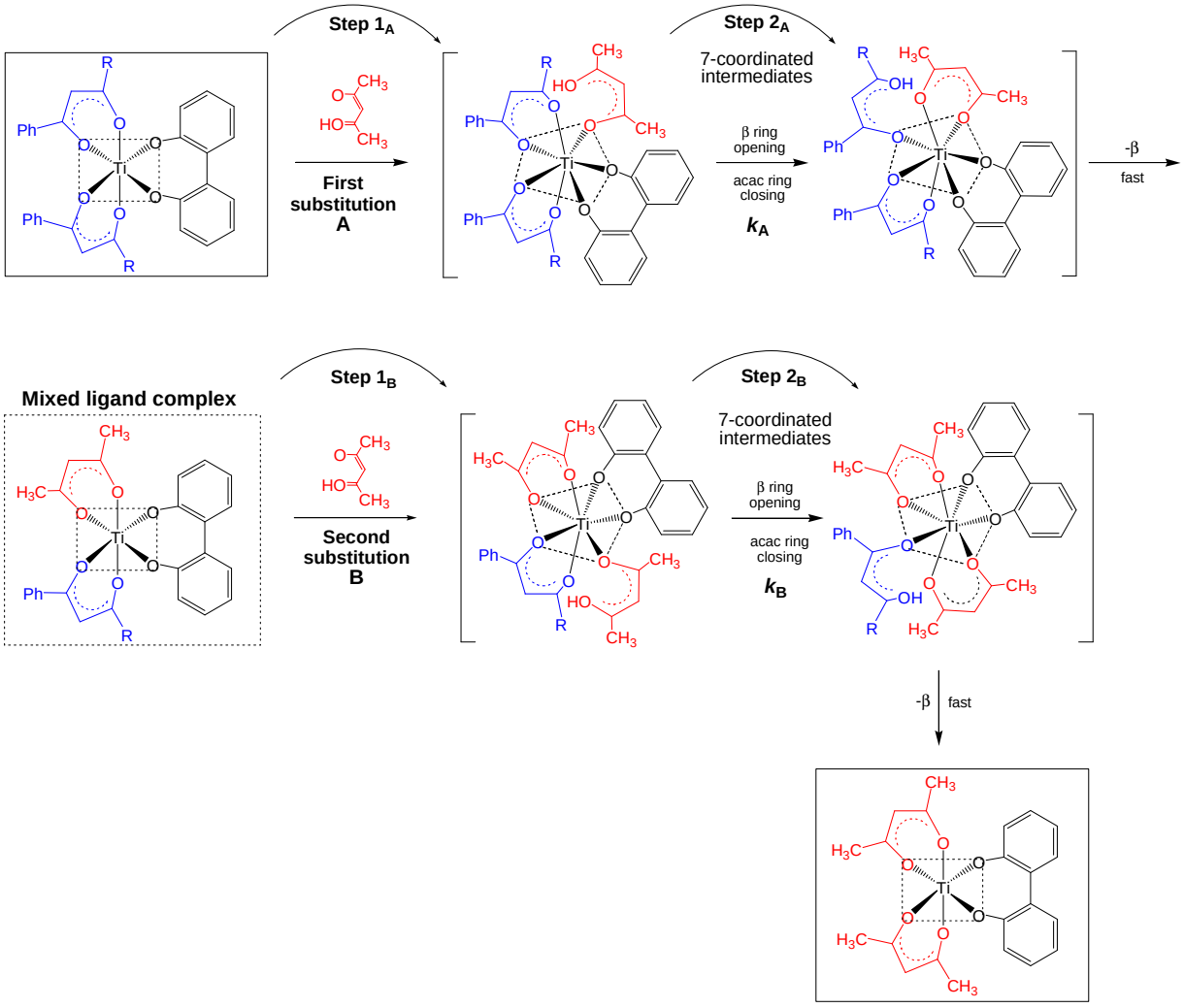

Scheme 3.12 Proposed reaction pathway illustrating the associative mechanism for the successive substitution of [Ti(β)$_2$biphen with Hacac.

3.4.1.3 Substitution of $Ti(acac)_2$ biphen with dihydroxy-aryls

The results for the substitution of the bidentate biphenolato ligand in $Ti(acac)_2$ biphen with bidentate ligands of different ring sizes, i.e., H_2cat (5), H_2naph (5), H_2binaph (7), H_2mbiphen (8) and H_2mbinaph (8), is presented.

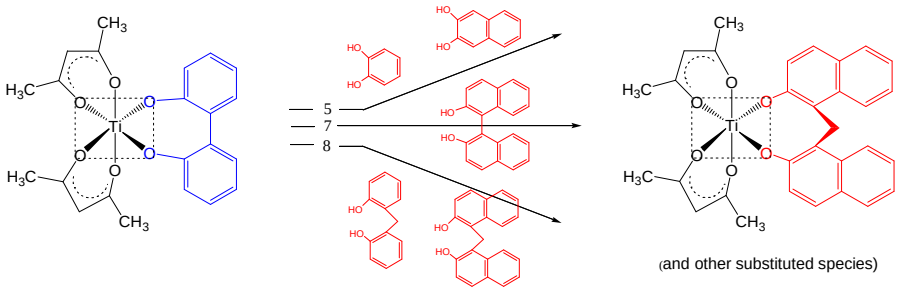

The reactions were studied by means of ^{1}H NMR spectroscopy under *pseudo*-first order conditions with the incoming [ligand] 6x greater than the concentration of the titanium complex.

The substitution of [$Ti(acac)_2$biphen] with the 5-membered ring ligands run to completion while an equilibrium in favour of the substituted product exist for the substitution of the 7-membered biphen ring for another 7-membered ring (binaph) or for the 8-membered rings. However with a larger excess (30x) these reactions are all driven to completion.
The reactions are very rapid (completed/almost completed by the time the first scan was taken) and only the substitution reaction with largest and bulkiest ligand, i.e., [$Ti(acac)_2$biphen] + H_2mbinaph, could be followed by ^{1}H NMR. The reverse reaction, $Ti(acac)_2$mbinaph + H_2biphen was also investigated.

The reactions were monitored by following the disappearance of the methine peak of the reactant and the appearance of the methine peak of the product. The partial dynamic ^{1}H NMR spectra and the time trace of the forward and reverse reactions are shown in **Figure 3.62**. The first order rate constants, k_{obs}, obtained for the ligand exchange reactions are, k_{obs} = 0.0035 and 0.0017 s^{-1} respectively.

This investigation into the effects of different ring sizes on the substitution of a stable 7-membered ring, shows that with excess in-coming ligand, the 7-membered biphen ring can successfully be replaced by a 8-membered ring. Also the 8-membered mbinaph ring can be replaced by a 7-membered ring in the reverse reaction.

(a) $Ti(acac)_2$ biphen + H_2mbinaph (excess) → $Ti(acac)_2$ mbinaph + H_2biphen

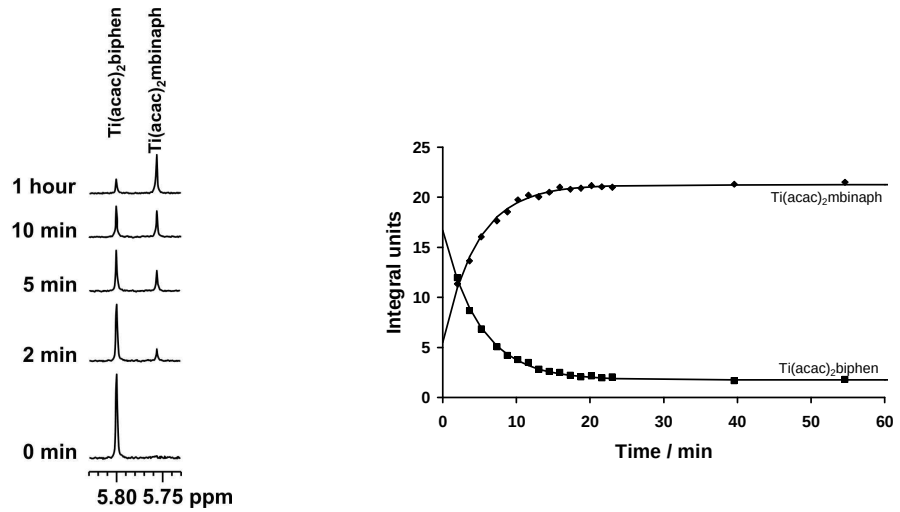

(b) $Ti(acac)_2$ mbinaph + H_2biphen (excess) → $Ti(acac)_2$ biphen + H_2mbinaph

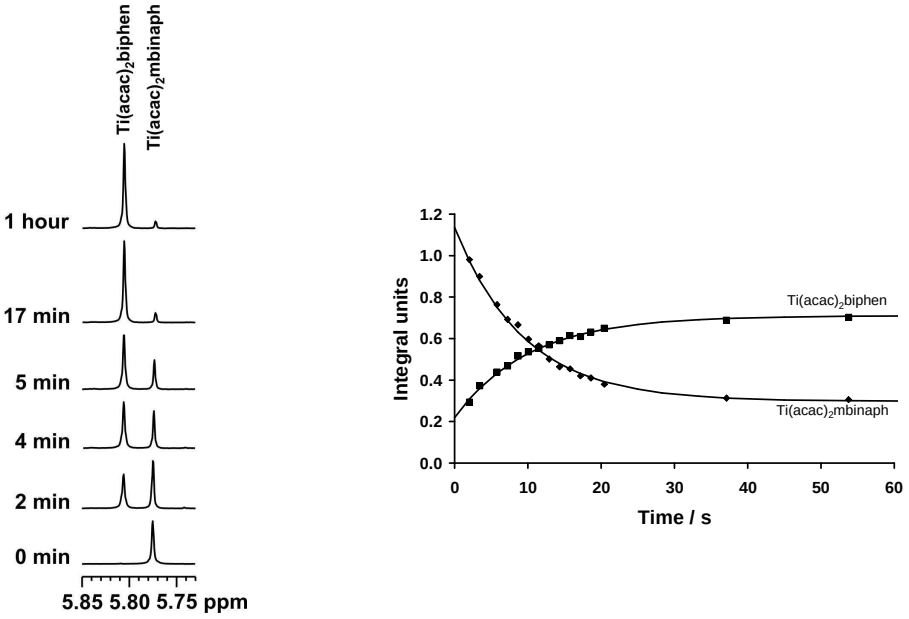

Figure 3.62 Substitution reactions (a) $Ti(acac)_2$biphen + H_2mbinaph and (b) $Ti(acac)_2$mbinaph + H_2biphen. **Left**: Partial dynamic ^{1}H NMR spectra in $CDCl_3$ at 25 °C, taken immediately before dissolution of reactants. **Right**: Concentration (integration units) *vs*.time data obtained for the ^{1}H NMR monitored substitution reactions in $CDCl_3$ at 25 °C.

3.4.2 Ligand Exchange Kinetics

Bis(β-diketonato)titanium(IV) complexes undergo rapid intramolecular ligand exchange (described in **Section 3.2.3.1**) as well as slower intermolecular ligand exchange reactions. Both the intra- and intermolecular ligand exchange are equilibrium processes. In the following section, the ligand-exchange equilibria and kinetics of the intermolecular process are investigated.

3.4.2.1 Exchange of β-diketonates in Ti(β)$_2$biphen

The results for the bi-chelating ligand exchange reactions in octahedral Ti(IV) complexes of the form Ti(β)$_2$biphen, are reported. The reaction was studied spectroscopically by means of ^{1}H NMR techniques under second order conditions.

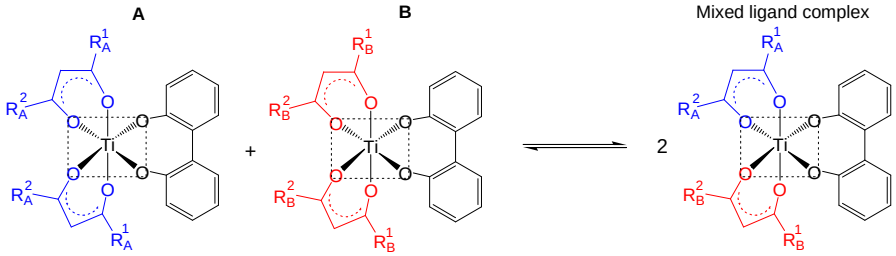

^{1}H NMR Spectroscopy The reaction solution was made up of a solution containing equimolar amounts of **A** and **B** in $CDCl_3$ and the ^{1}H NMR was recorded at regular time intervals. It was found that the ligand exchange reaction yielding the mixed ligand complex is an equilibrium process.

$$\text{Ti}(\beta)_2\text{biphen} + \text{Ti}(\beta')_2\text{biphen} \underset{}{\overset{K_c}{\rightleftharpoons}} 2\ \text{Ti}(\beta)(\beta')\text{biphen}$$

$$K_c = \frac{[\text{Ti}(\beta)(\beta')\text{biphen}]^2}{[\text{Ti}(\beta)_2\text{biphen}]\,[\text{Ti}(\beta')\text{biphen}]}$$

Chemical shift data of the methine (ring) proton for the parent and mixed-ligand complexes in the Ti(β)$_2$biphen + Ti(β')$_2$biphen mixtures studied are presented in **Table 3.27**. The assignments are straight forward because chemical shifts of the parent complexes are, in general, unaltered, ±0.02 ppm, (by reference to spectra of solutions of the pure parent complexes) on going to the equilibrium mixtures. Hence the methine resonance of the parent

complexes are found at lowest and highest field with the two signals of the mixed-ligand complex at intermediate field. For example, the partial ^{1}H NMR spectra for a typical equimolar mixture of two different β-diketonate complexes, Ti(tfba)$_2$biphen and Ti(ba)$_2$biphen, are shown in **Figure 3.63**. The resonances at lowest and highest field are due to Ti(tfba)$_2$biphen and Ti(ba)$_2$biphen, respectively, while the two lines at intermediate field are assigned, in order of increasing field, to the tfba and ba resonances, respectively, of the mixed-ligand complex, Ti(tfba)(ba)biphen. The inter-molecular ligand exchange, although slow on the NMR time scale, is relatively fast on the laboratory time scale; a spectrum taken immediately after dissolution of the parent complexes and at equal time intervals thereafter, indicates that equilibrium is attained, on average, within 35 min at room temperature.

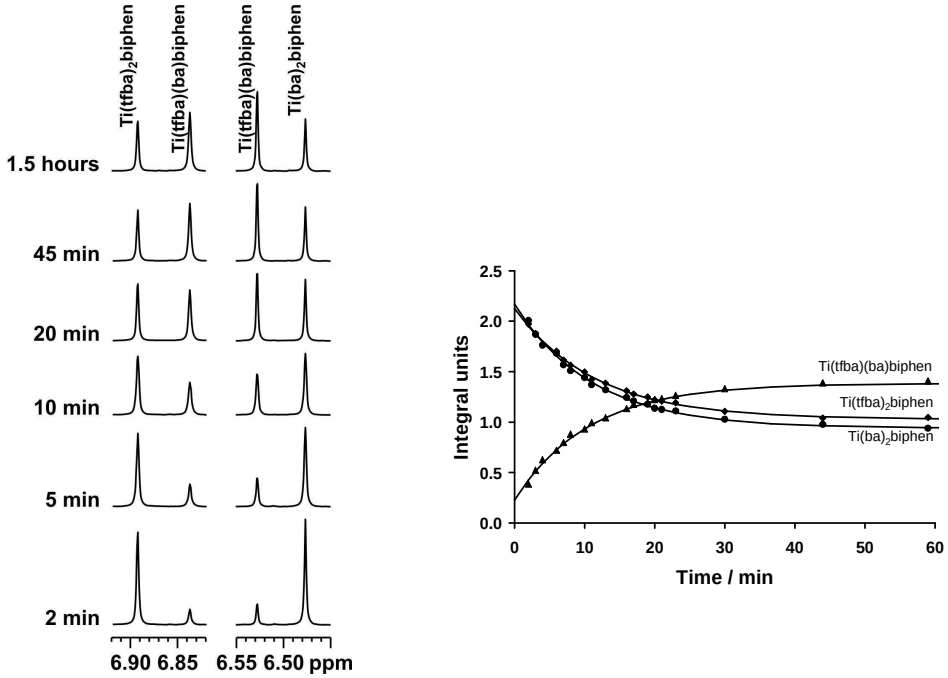

Figure 3.63 **Left**: Partial dynamic ^{1}H NMR spectra of the ligand exchange reaction, Ti(tfba)$_2$biphen + Ti(ba)$_2$biphen (with K_c = 8), in $CDCl_3$ taken immediately after dissolution of the parent complexes until equilibrium was reached (equimolar conditions: [Ti complex] = 10 mmol dm^{-3} each). **Right**: Concentration (interation units) *vs*.time data obtained for the ^{1}H NMR monitored exchange reaction at 25 °C.

The equilibrium constants, K_c, for exchange reactions in $CDCl_3$ are presented in **Table 3.28**. An equilibrium constant, K_c = ~4 (the statistical value expected for random scrambling) is obtained when the exchange ligands contain the same number of CF_3 groups (e.g., tfaa-tfba) or no CF_3 groups (e.g., acac-ba). K_c = ~8, double the statistical value, is obtained when the exchange ligands differ by one CF_3 group (e.g., acac-tfaa, acac-tfba and ba-tfba). These

results are in full accord with previous studies,[69] showing that the equilibrium constants depend primarily on the relative number of CF_3 substituents on the exchangeing ligands.

Table 3.27 Chemical shift (ppm) data of the methine (ring) proton for parent, Ti(β)$_2$biphen and Ti(β')$_2$biphen, and mixed-ligand, Ti(β)(β')biphen complexes in $CDCl_3$ solution.

(a) Parent and Mixed-ligand compounds in equilibrium mixture				
β-diketonato ligands β	β'	Parent (β)	Mixed-ligand (β)(β')	Parent (β')
ba	acac	6.48	6.45 5.80	5.79
tfba	tfaa	6.89	6.87 6.23	6.21
tfba	tfma	6.89	6.87 6.36	6.33
tfaa	acac	6.21	6.15 5.83	5.78
tfba	acac	6.89	6.81 5.86	5.79
tfba	ba	6.89	6.84 6.53	6.48
(b) Parent Compound, Ti(β)$_2$biphen in pure solution				
Ti(acac)$_2$biphen 5.79				
Ti(ba)$_2$biphen 6.49				
Ti(tfaa)$_2$biphen 6.21				
Ti(tfma)$_2$biphen 6.20				
Ti(tfba)$_2$biphen 6.89				

Table 3.28 Equilibrium Constants, K_c, and % product measured at 25 °C for the reaction:

$$Ti(\beta)_2biphen + Ti(\beta')_2biphen \rightleftharpoons_{K_c} 2\ Ti(\beta)(\beta')biphen$$

Ti(β)$_2$biphen β	Ti(β')$_2$biphen β'	Terminal groups β	β'	K_c	% Product	$\Delta G^{o\ a}$ kJ mol^{-1}
Group 1						
ba	acac	CH_3 Ph	CH_3 CH_3	4.1	50.4	-3.4
tfba	tfaa	CF_3 Ph	CF_3 CH_3	4.3	51.0	-3.5
tfba	tfma	CF_3 Ph	CF_3 $CH_2(CH_3)$	3.9	49.6	-3.3
Group 2						
tfaa	acac	CF_3 CH_3	CH_3 CH_3	8.6	59.0	-5.2
tfba	acac	CH_3 Ph	CF_3 CH_3	8.1	58.6	-5.1
tfba	ba	CF_3 Ph	CH_3 Ph	8.1	58.6	-5.1

[a] $\Delta G^o = -RT\ln K_c$ (Standard free energy)

[b] Theoretical values: $K_c = 4$ then % product = 50; $K_c = 8$ then % product = 58.5

The observed deviation from random scrambling, (K_c = 8) is due to the mixed-ligand complex being stabilised relative to the parent complexes, resulting in parent**:**mixed-ligand complex ratios of 41:59 compared to 50:50 for random scrambling, (K_c = 4). In terms of the electrostatic model, it has been shown that electrostatic effects always stabilise mixed-ligand complexes relative to the parent complexes whenever the effective charge on the two exchanging ligands are unequal.[67] The effective charges on the donor oxygen atoms of β-diketonato ligands, which carry either zero or one CF groups, will differ because of the inductive effect of the fluorine atoms (χ_{CF3} = 3.01 while χ_{Ph} = 2.21 and χ_{CH3} = 2.34). Consequently, the mixed complex, Ti(β)(β')biphen and the corresponding parent complexes will have comparable stability when β and β' contain the same number of CF_3 groups, but the mixed-ligand complex will be more stable (K_c larger) when β and β' have different number of CF_3 groups.

Exchange Kinetics The exchange reaction was followed with time by monitoring the disappearance of the parent methine peaks and the appearance of the mixed-ligand complex methine peaks. Although the reaction was followed under second order conditions, the data obtained was found to fit the first order kinetic model. A typical time trace of the results is shown in **Figure 3.63**.

$$\text{Ti}(\beta)_2\text{biphen} + \text{Ti}(\beta')_2\text{biphen} \underset{k_{-1}}{\overset{k_1}{\rightleftharpoons}} 2\ \text{Ti}(\beta)(\beta')\text{biphen} \qquad \text{with} \begin{cases} k_{obs} = k_1 + k_{-1} \\ K_c = \dfrac{k_1}{k_{-1}} \end{cases}$$

The first order rate constants, $k_{obs} = k_1 + k_{-1}$ where k_1 is the rate constant for the forward reaction and k_{-1}, the rate constant for the reverse reaction. By simultaneously solving equations, $k_{obs} = k_1 + k_{-1}$ and $K_c = k_1/k_{-1}$, rate constants k_1 and k_{-1} can be calculated in terms of k_{obs} and K_c, i.e.,

$$k_1 = k_{obs}\left(\frac{K_c}{K_c + 1}\right) \qquad \text{and} \qquad k_{-1} = k_{obs} - k_1$$

The kinetic data obtained for the ligand exchange reactions are summarised in **Table 3.29**. The rate constants are all of the same order and very similar, showing that the rate of ligand exchange is independent of the nature of the exchanging β-diketonato ligands. The

dependence of k_{obs} on temperature allowed for the determination of the activation parameters, $\Delta H^{\#}$, $\Delta S^{\#}$ and $\Delta G^{\#}$, which are also listed in **Table 3.29**.

Table 3.29 Kinetic data and activation parameters for the ligand exchange reaction, using ^{1}H NMR Spectroscopy. Equimolar conditions used: for the temperatue variation, [Ti complex] = 5 mmol dm^{-3} and for the ligand variation, [Ti complex] = 10 mmol dm^{-3} for each parent complex. The reactions highlighted in red show that the rate of exchange is the same under varying equimolar concentration conditions.

	Parent Complexes		T	Rate values			Activation parameters		
	β	β'	℃	k_{obs} s^{-1}	k_1 s^{-1}	k_{-1} s^{-1}	$\Delta H^{\#}$ kJ mol^{-1}	$\Delta S^{\#}$ J mol^{-1} K^{-1}	$\Delta G^{\#}$ kJ mol^{-1}
Temp	tfba	ba	5	0.00026			65.7	-77.1	88.7
			10	0.00040					
			15	0.00071					
			25	0.00181					
			35	0.00431					
Ligand	ba	acac	25	0.0015	0.0012	0.0003			
	tfba	tfaa		0.0044	0.0036	0.0008			
	tfba	tfma		0.0036	0.0029	0.0007			
	tfaa	acac		0.0040	0.0036	0.0004			
	tfba	acac		0.0022	0.0020	0.0002			
	tfba	ba		0.0018	0.0016	0.0002			

K_c values are shown in **Table 3.28**

Both the ligand exchange and substitution reactions form the mixed-ligand complex,

Ligand Exchange: $Ti(\beta)_2biphen + Ti(\beta')_2biphen \rightleftharpoons 2\ Ti(\beta)(\beta')biphen$

Ligand Substitution: $Ti(\beta)_2biphen + H\beta' \underset{-H\beta}{\rightleftharpoons} Ti(\beta)(\beta')biphen$

In both cases the rates of reaction are independent of the incoming Hacac ligand. However, the influence of the nature of the β-diketonato ligand on the rate of reaction is dissimilar; i.e., the rate of substitution is significantly influenced by the labile β-diketonato ligands (depending on the electronegativity of the substituent groups, R, see **Table 3.26**) while the rate of exchange appears to be independent of the nature of the β-diketonato ligand (see **Table 3.29**). For example, when comparing the rates of the following,

		β = ba	β = tfba
Exchange:	$Ti(\beta)_2$biphen + $Ti(acac)_2$biphen	k_{obs} = 0.0015 s^{-1}	0.0022 s^{-1}
Substitution:	$Ti(\beta)_2$biphen + Hacac → Ti(β)(acac)biphen	k_{obs} = 0.00016 s^{-1}	0.0021 s^{-1}

with β = ba and tfba, the rates of exchange are of the same order while the rates of substitution increase by an order of 10, respectively.

Proposed Mechanism A proposed mechanism consistent with an associative process (large negative entropy value) is shown in **Scheme 3.13**.

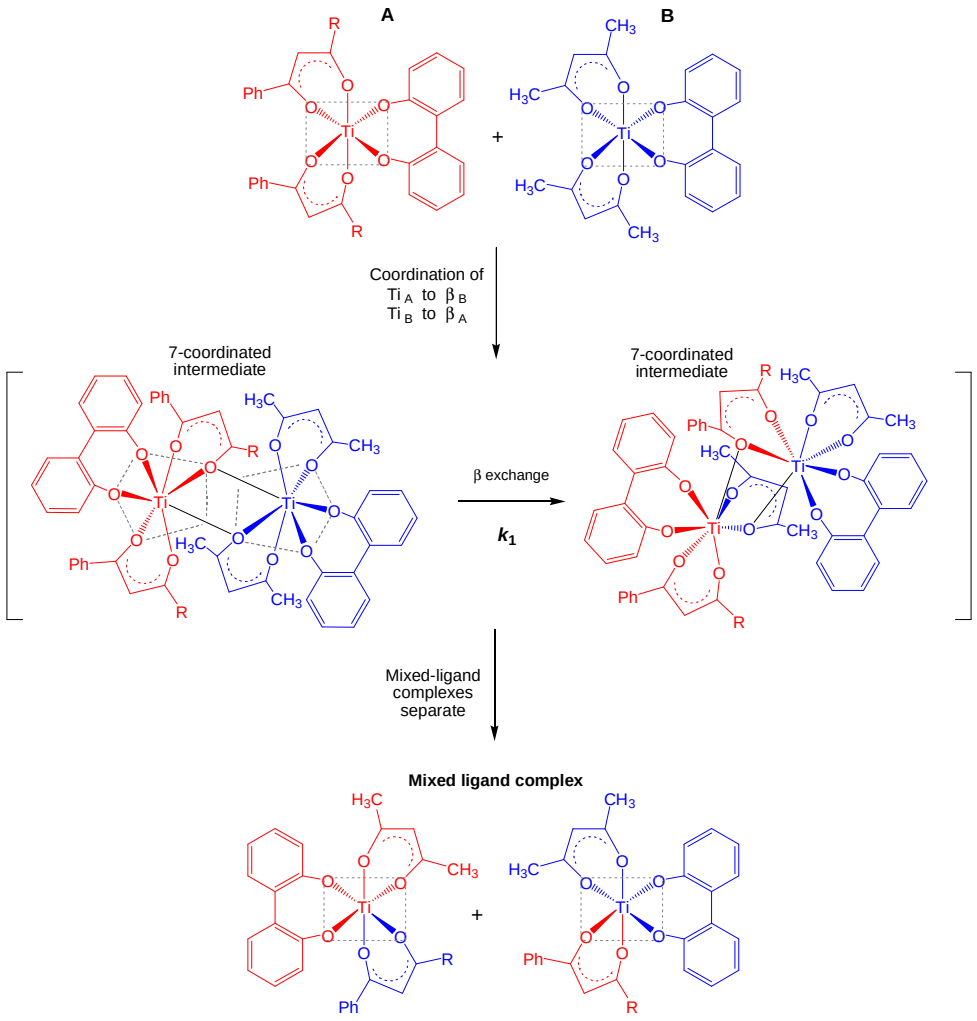

Scheme 3.13 Schematic representation of the proposed reaction pathway illustrating the associative mechanism for the ligand exchange reaction between [$Ti(\beta)_2$biphen] with [$Ti(acac)_2$biphen].

3.5 ELECTROCHEMISTRY

3.5.1 Introduction

Cyclic voltammetry (CV) was conducted on most of the synthesised titanium complexes as well as on the uncoordinated ligands. The formal reduction potentials, $E^{0'}$, of the redox active metal Ti^{IV}/Ti^{III} centre of the synthesised complexes were determined. Analysis of the formal reduction potential was performed in an attempt to quantify the electronic influence, if any, of the different R substituents (group electronegativity, χ_R) of the coordinated β-diketonato ligand on the redox active metal centre of each of these compounds. The redox active couples vary from being electrochemically reversible (theoretically this implies $\Delta E = 59$ mV although experimentally $\Delta E < 90$ mV was taken to imply electrochemical reversibility in this study), quasi-reversible (defined as 90 mV $< \Delta E <$ 150 mV for this study) to irreversible (defined as $\Delta E >$ 150 mV for this study). Formal redox potentials ($E^{0'}$), peak cathodic potentials (E_{pc}) and peak anodic potentials (E_{pa}) were measured against the Ag/Ag^+ reference electrode but are reported *vs.* Fc/Fc^+ as an internal standard. $E^{0'}(Fc/Fc^+) = 77$mV *vs.* Ag/Ag^+, $\Delta E_p = 62$ mV and $i_{pc}/i_{pa} = 1.00$.[70] Under the experimental conditions of this study, ferrocene (Fe^{III}/Fe^{II}) showed electrochemical and chemical reversible redox behaviour (except in DCE as reported[71]) with $i_{pc}/i_{pa} = \sim 1.00$ but $E^{0'}$ and ΔE deviated from the published values as shown in **Table 3.30** for each compound series. The potential range for the electrolyte/solvent ($[NBu_4][PF_6]$ /CH_3CN) system is between-2300 and 1800 mV *vs.* Ag/Ag^+ (and between -2400 and 1700 mV *vs.* Fc/Fc^+).

Table 3.30 Elecrochemical data, $E^{0'}$and ΔE, for ferrocene (*vs.* Ag/Ag^+) as an internal standard in the indicated compound series. Measured in 0.1 mol dm^{-3} $[NBu_4][PF_6]$ on a glassy carbon working electrode at $v = 100$ mV s^{-1} and T = 25 °C.

Compound Series	Solvent	Ferrocene (Fe^{III}/Fe^{II}) *vs.* Ag/Ag^+	
		$E^{0'}$ / mV	ΔE_p / mV
Ligands			
β-diketones	CH_3CN	63 - 80	61 - 84
H_2biphen	CH_3CN	74	68
Ti(IV) Complexes			
$[Cp_2Ti(\beta)]^+$	CH_3CN	82 - 89	59 - 70
Cp_2Ti(biphen)	CH_3CN	85	65
$Ti(\beta)_2Cl_2$	DCE	179 - 232	119 - 200
$Ti(\beta)_2$(biphen)	CH_3CN	63 - 91	65 - 78

3.5.2 *O,O*'- Donor Ligands

3.5.2.1 β-Diketones

The electrochemical behaviour of several β-diketones has been investigated under varying condition; often conflicting and complex electrochemical behaviour was observed due to the chemistry of the β-diketones under those particular conditions. In this comparative study, the cyclic voltammograms of the CF_3-containing β-diketones (Hβ), CF_3COCH_2COR, with R = CH_3 (Htfaa), $CH_2(CH_3)$ (Htfma), $CH(CH_3)_2$ (Htfdma), $C(CH_3)_3$ (Htftma), Ph (Htfba), C_4H_3O (Htffu), C_4H_3S (Htfth) and CF_3 (Hhfaa) and Ph-containing β-diketones, $PhCOCH_2COR$, with R = CH_3 (Hba), Ph (Hdbm) and C_4H_3S (Hthba) **[1]** are recorded in $[NBu_4][PF_6]$ / CH_3CN. **Figure 3.64** shows cyclic voltammograms at varying scan rates for Hhfaa and Hthba.

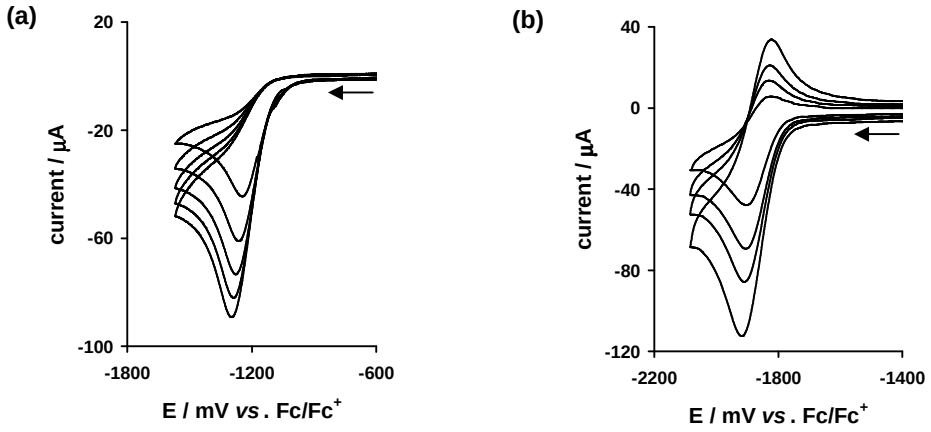

Figure 3.64 Cyclic voltammograms (*vs.* Fc/Fc^+) for **(a)** Hhfaa and **(b)** Hthba at scan rates of 100, 200, 300, (400) and 500 mV s^{-1}. Scans initiated in the direction of the arrow. Measured in 0.1 mol dm^{-3} $[NBu_4][PF_6]$ / CH_3CN on a glassy carbon working electrode at 25 °C. [Hβ] = 3 mmol dm^{-3}.

A one-electron reduction was observed according to:

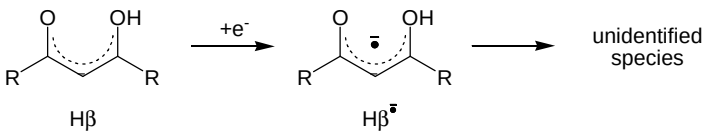

forming a chemically unstable radical anion. The formation of other unidentified species (by rearrangement or decomposition) follows according to an EC mechanism. For aromatic β-diketones (*i.e.*, $RCOCH_2COR'$ with R, R' = aromatic groups), the radical anion is stabilised

long enough such that the electrochemical reduction becomes reversible/quasi-reversible and chemically reversible at high scan rates. The waves show the expected dependence on scan rate (shown in **Table 3.31**), i.e., as the scan rate increases the i_{pa}/i_{pc} values of the first wave, increases approaching a value of 0.40 and 0.54 at ν = 2000 mV s^{-1}, for Hdbm and Hthba respectively. The electrochemical reduction behaviour of Hdbm in $[NBu_4][PF_6]/CH_3CN$ is similar to behaviour in $[NBu_4][ClO_4]$/DMSO reported by Buchta and Evans.[72] These results indicate that when the scan rate is fast enough to prevent appreciable following reaction the corresponding oxidation of the reduced species occurs.

In contrast, the aliphatic β-diketones (*i.e.*, $RCOCH_2COR'$ with R, R' both aliphatic groups or one aliphatic and one aromatic groups), show no reversible behaviour; no oxidation wave is observed even at scan rates up to ν = 5000 mV s^{-1}. This implies that the radical anion (reduced species) is less stable in aliphatic β-diketones and that the electron is stabilised in the delocalised aromatic system. Hence we see that the stability of the radical anion does not depend on the electronic (e^--withdrawing or e^--donating) properties of the R groups but on the aromaticity of the β-diketone. A comparison of the cyclic voltammograms, showing the reversibility of the β-diketone reduction at scan rates 100 and 1000 mV s^{-1}, of an aliphatic (example, Hhfaa) and aromatic (example, Hthba) β-diketone, are shown in **Figure 3.65**.

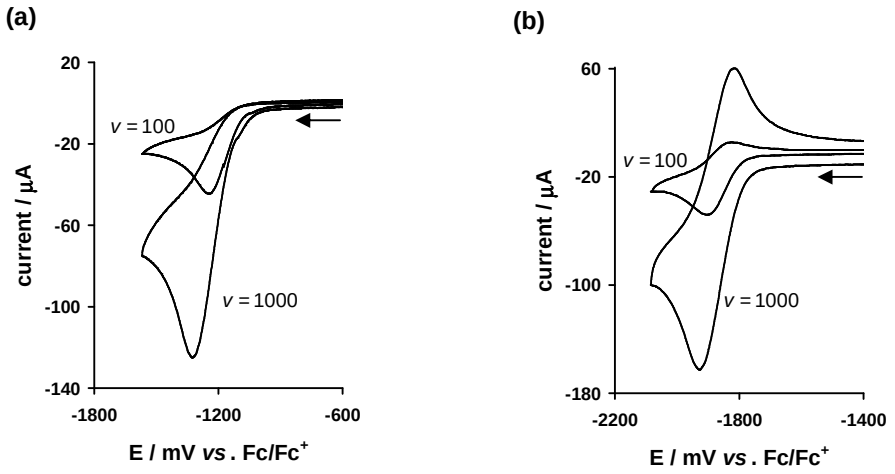

Figure 3.65 Cyclic voltammograms (*vs.* Fc/Fc^+) for **(a)** Hhfaa and **(b)** Hthba at scan rates of 100 and 1000 mV s^{-1}. Scans initiated in the direction of the arrow. Measured in 0.1 mol dm^{-3} $[NBu_4][PF_6]$ / CH_3CN on a glassy carbon working electrode at 25 °C. [Hβ] = 3 mmol dm^{-3}.

Table 3.31 Cyclic voltammetric data (*vs.* Fc/Fc^{+}) for Hdbm and Hthba at indicated scan rates. Measured in 0.1 mol dm^{-3} $[NBu_4][PF_6]$ / CH_3CN on a glassy carbon working electrode at 25 °C.

ν mV s^{-1}	**E_{pc}** mV	**ΔE_p** mV	**$E^{0'}$** mV	**i_{pc}** µA	**i_{pa}/i_{pc}**
Hdbm: **Ph**$COCH_2CO$**Ph**[a]					
100	-1934	71	-1899	51	0.21
200	-1942	82	-1901	75	0.28
300	-1952	98	-1903	94	0.32
500	-1967	123	-1906	124	0.35
1000	-1992	155	-1915	176	0.38
2000	-2027	222	-1916	244	0.40
Hthba: **Ph**$COCH_2CO$**C_4H_3S**					
100	-1884	61	-1854	43	0.27
200	-1891	71	-1856	63	0.34
300	-1896	81	-1856	79	0.38
500	-1903	93	-1857	103	0.43
1000	-1914	110	-1859	147	0.51
2000	-1932	139	-1863	209	0.54

[a]Compare to Buchta and Evans[72] Hdbm: Epc = -1420 mV *vs* SCE in $[NBu_4][ClO_4]$/DMSO.

Table 3.32 Reduction potentials, E_{pc}, (*vs.* Fc/Fc^{+}) and cathodic peak currents, i_{pc}, for β-diketones at a scan rate of 100 mV s^{-1}. Measured in 0.1 mol dm^{-3} $[NBu_4][PF_6]$ / CH_3CN on a glassy carbon working electrode at 25 °C. [Hβ] = 3.0 mmol dm^{-3}.

Hβ	**$RCOCH_2COR'$ R, R'**	**$\chi_R + \chi_{R'}$**	**pKa**	**E_{pc} mV**	**i_{pc} µA**
(a) Aromatic β-diketones[a]					
Hdbm	Ph, Ph	4.42	9.35	-1934	51
Hthba **[1]**	Ph, C_4H_3S	4.31	9.01	-1884	43
(b) Aliphatic β-diketones[b]					
Hhfaa	CF_3, CF_3	6.02	4.35	-1243	41
Htfth	CF_3, C_4H_3S	5.11	6.5	-1541	53
Htffu	CF_3, C_4H_3O	--	--	-1544	44
Htfba	CF_3, Ph	5.22	6.3	-1564	60
Htfaa	CF_3, CH_3	5.35	6.3	-1851	41
Htfma	CF_3, $CH_2(CH_3)$	5.32	6.64	-1860	55
Htfdma	CF_3, $CH(CH_3)_2$	5.30	6.80	-1872	42
Htftma	CF_3, $C(CH_3)_3$	5.28	7.13	-1889	42
Hba	CH_3, Ph	4.55	8.70	-2138	56

[a]Aromatic: R, R' = aromatic
[b]Aliphatic: (pure aliphatic); R, R' = aliphatic and (mixed aliphatic); R = aliphatic, R' = aromatic.

The reduction potentials of all the β-diketones are summarised in **Table 3.32** and the comparative cyclic voltammograms are shown in **Figure 3.66**. In general, the reduction potentials, E_{pc}, increase (becoming more anodic) as the group electronegativity of the R groups increase. This is expected, because the more electron-withdrawing the R group

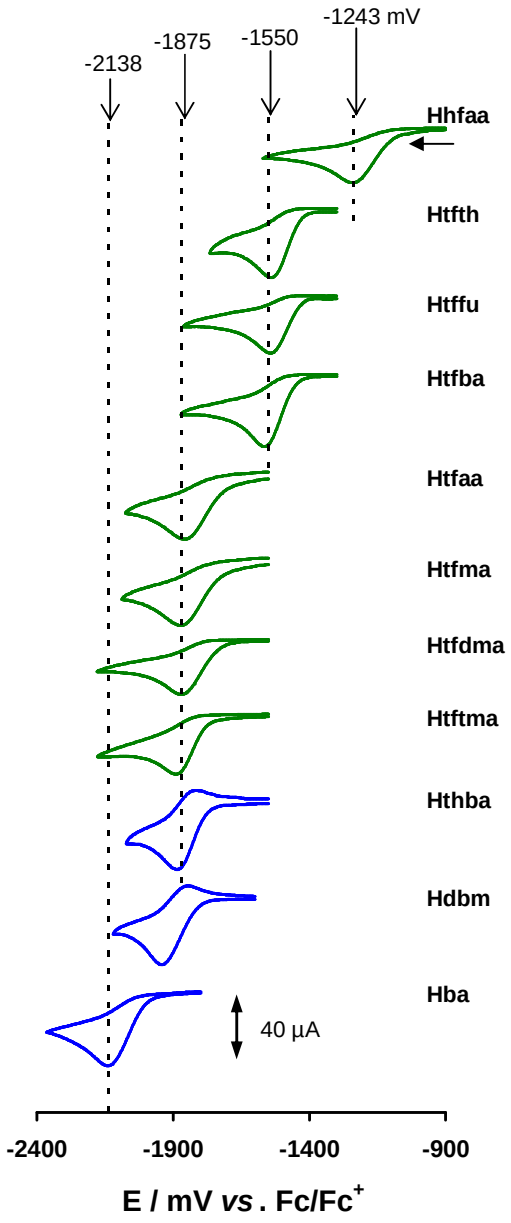

Figure 3.66 Comparative cyclic voltammograms (*vs.* Fc/Fc^{+}) for the indicated β-diketones at a scan rate of 100 mV s^{-1}. The CVs shown in green represent CF_3-β-diketones while those in blue are Ph-β-diketones. Vertical dotted lines indicate the reduction potential of a single complex or an average of a group. Scans initiated in the direction of the arrow. Measured in 0.1 mol dm^{-3} $[NBu_4][PF_6]$ / CH_3CN on a glassy carbon working electrode at 25 °C. [Hβ] = 3.0 mmol dm^{-3}.

becomes, the more electron density is removed from the β-diketone backbone, making it relatively more positive and more difficult to reduce. There is ~900 mV difference between the reduction potentials of the β-diketones investigate; from the most anodic reduction potential, Hfaa (E_{pc} = -1243 mV) with two electron-withdrawing CF_3 groups to the most cathodic, Hba (E_{pc} = -2138 mV) with relative electron-donating CH_3 and Ph groups.

The functional groups of the β-diketone are: the carbonyl group (C=O), the conjugated double bond system (C=C) and an alcohol group (C-OH), see **Figure 3.67 (a)**. The electrochemical behaviour of complexes containing the different functional groups of the β-diketone was investigated to determine which electroreducible structure of the β-diketone, is involved in the electrochemical reduction.

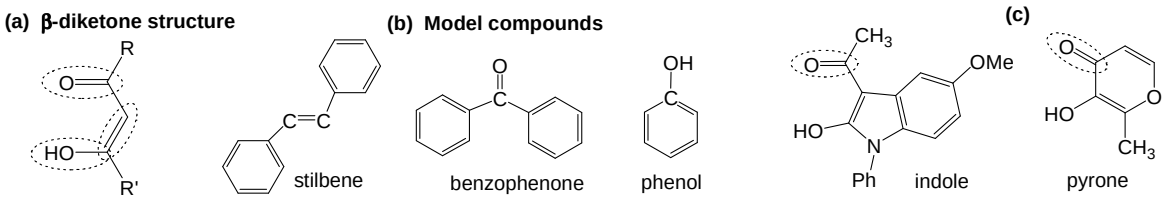

Figure 3.67 Schematic diagram showing **(a)** the C=O, C=C and C-OH functional groups of β-diketones, **(b)** model compounds and **(c)** Indole: 3-acetyl-1-benzyl-2-hydroxy-5-methoxyindole and Pyrone: 3-hydroxy-2-methyl-4-pyrone.

The half-wave potential of model compounds having only one of the related functional groups, i.e., stilbene (C=C), phenol (C-OH), and benzophenone (C=O) (see **Figure 3.67 (b)**) was investigated. Benzophenone was the only compound to have a reduction wave in the region from -1000 mV up to the onset of the solvent/electrolyte discharge. Hence it was concluded that the most probably functional group associated with the reduction of the β-diketone is the carbonyl group. This result is supported by findings of Erving and Callahan,[73] who came to the same conclusion by investigating the reduction potential of a wider range of model compounds. Other ligands which possess a carbonyl group and are electrochemically active are pyrone[74] and indole[38] shown in **Figure 3.67 (c)**. These lignds have irreversible reduction potentials (E_{pc} = -2100 and -2540 mV *vs*. Fc/Fc^+ respectively, CVs shown in Chapter 2, **Figure 2.21**) similar to the reduction potential of β-diketones. However, since chelated β-diketones (which no longer possess C=O) are also electrochemically active (see

Section 3.5.3.1), it would be more correct to assume that the reduction of the β-diketone is related to the C−O in a conjugated double bond system.

3.5.2.2 Biphenol

The cyclic voltammograms of biphenol, recorded in $[NBu_4][PF_6]/CH_3CN$, are shown at varying scan rates in **Figure 3.64 (a)**. The observed reduction is irreversible; no oxidation wave is observed even at scan rates up to $\nu = 5000$ mV s^{-1}. The electrochemical behaviour is similar to the aliphatic β-diketones. A comparison of the cyclic voltammograms in **Figure 3.68 (b)**, shows that the reduction wave of biphenol is much broader than that of the β-diketones and the E_{pc} position lies closer to that of the non-fluorinated β-diketones.

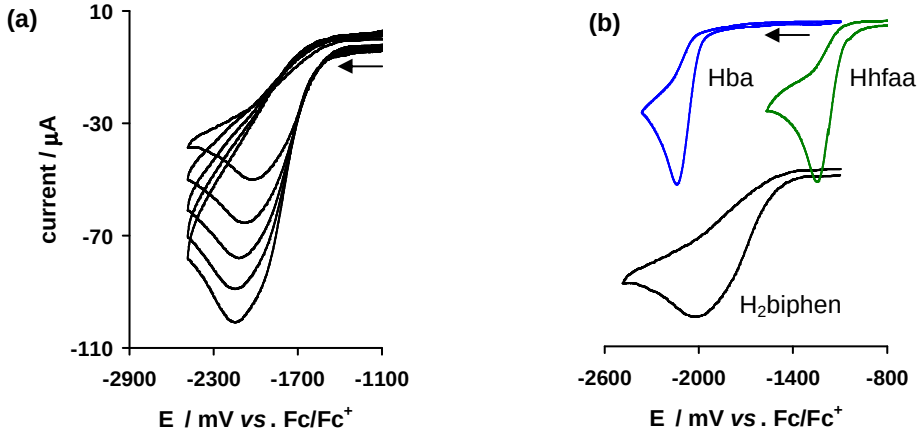

Figure 3.68...Cyclic voltammograms (*vs.* Fc/Fc^+) of **(a)** biphenol at scan rates 100, 200, 300, 400 and 500 mV s^{-1} and **(b)** Hba, Hhfaa and H_2biphen at a scan rate of 100 mV s^{-1}. Scans initiated in the direction of the arrow. Measured in 0.1 mol dm^{-3} $[NBu_4][PF_6]$ / CH_3CN on a glassy carbon working electrode at 25 °C. [β-diketone] = [H_2biphen] = 3 mmol dm^{-3}.

Table 3. 33 Cyclic voltammetric data (*vs.* Fc/Fc^+) for H_2biphen at indicated scan rates. Measured in 0.1 mol dm^{-3} $[NBu_4][PF_6]$ / CH_3CN on a glassy carbon working electrode at 25 °C. [H_2biphen] = 3 mmol dm^{-3}.

ν mV s^{-1}	E_{pc} mV	i_{pc} µA
100	-1934	51
200	-1942	75
300	-1952	94
500	-1967	124
1000	-1992	176
2000	-2027	244

3.5.3 Tetrahedral Complexes

3.5.3.1 Mono(β-diketonato) Ti(IV) complexes: $[Cp_2Ti(\beta)]^+$

The electrochemical behaviour of the new CF_3 series of the mono-β-diketonato titanocene complexes, $[Cp_2Ti(CF_3COCHCOR)]^+ClO_4^-$ with R = CH_3 (tfaa) **[3]**, C_4H_3S (tfth) **[4]**, C_4H_3O (tffu) **[5]** and Ph (tfba) **[6]** as well as the phenyl series, i.e. $[Cp_2Ti(PhCOCHCOR)]^+ClO_4^-$ with R = CH_3 (ba) **[7]**, C_4H_3S (thba) **[8]** and Ph (dbm) **[9]** were studied in 0.1 mol dm^{-3} $[NBu_4][PF_6]$ / CH_3CN The cyclic voltammograms exhibit two waves, revealing two reduction processes (see **Figure 3.70**), the first process at more positive potential is associated with the Ti^{IV}/Ti^{III} couple and the second, with the β-diketonato ligand reduction. The electrochemical data is summarised in **Table 3.34**.

Table 3.34 Cyclic voltammetric data (*vs.* Fc/Fc^+) for the $[Cp_2Ti(\beta)]^+ClO_4^-$ series at a scan rate of 100 mV s^{-1}. Measured in 0.1 mol dm^{-3} $[NBu_4][PF_6]$ / CH_3CN on a glassy carbon working electrode at 25 °C. [Ti complex] = 2 mmol dm^{-3}.

$[Cp_2Ti(\beta)]+$	Ti^{IV}/Ti^{III} couple					β-diketonanto reduction	
β	E_{pc} mV	ΔE_p mV	$E^{0'}$ mV	i_{pc} µA	i_{pa}/i_{pc}	E_{pc} mV	i_{pc} µA
CF_3COCH_2COR							
tfth **[4]**	-656	75	-619	39	0.86	-1890	32
tffu **[5]**	-659	70	-624	40	0.90	-1916	42
tfba **[6]**	-661	76	-623	41	0.97	-1915	43
tfaa **[3]**	-667	78	-628	41	0.95	-2162	33
$PhCOCH_2COR$ and R ≠ CF_3							
thba **[8]**	-869	66	-836	40	0.87	-2305	26
dbm **[9]**	-861	76	-823	41	0.90	-2110	41
ba **[7]** [a]	-882	84	-840	40	1.00	-2306	40
$FcCOCH_2COCH_3$							
fca[14]	-942	78	-903		0.88		

[a]Compare to Bond *et al.*[38] Cp_2Ti(ba): $E^{0'}$ = -850 mV (Ti^{III}/Ti^{IV}), E_{pc} = -2330 mV (ba reduction) at *v* = 200 mV s^{-1}

All the complexes exhibit a characteristic one electron, electrochemically and chemically reversible Ti^{IV}/Ti^{III} couple, according to:

$$[Cp_2Ti^{IV}(\beta)]^+ + e^- \rightleftharpoons Cp_2Ti^{III}(\beta)$$

with ΔE_p = ~75 mV and i_{pa}/i_{pc} = ~0.9 µA (ν = 100 mV s^{-1}). The ratio, $i_{pa}/i_{pc} \neq 1$ because the

reduced form of the analyte readily deposites on the electrode. A slow decrease of i_{pa}/i_{pc} and increase of ΔE with scan rate is consistent with electrode adsorption. Hence the electrode had to be well polished at all times. A graph of peak current *vs.* $v^{½}$ for the redox process was linear for all complexes, indicating that the electrochemistry is essentially diffusion controlled. This result is demonstated for $[Cp_2Ti(ba)]^+$ in **Figure 3.69**.

Reversible redox behaviour is expected because the reduced species, $Cp_2Ti^{III}(\beta)$, is stable as demostrated by Bond *et al.*,[38] who investigated the electrochemical behaviour of $Cp_2Ti^{III}(\beta)$, $Ti^{III} \rightarrow Ti^{IV}$. The coordination sphere of these complexes does not change when switching the redox state of the central coordinating metal from Ti^{IV} to Ti^{III} (see comparison of crystal structures in **Section 3.3.1.1**). Previously reported values, *i.e.*, $E^{0'}$ = -864[14] and -850 mV[38] for β = ba and $E^{0'}$ = -635 mV for β = tfaa, are in good agreement with the values reported in this study, *i.e.*, $E^{0'}$ = -840 and -629 mV for $[Cp_2Ti(\beta)]^+$with β = ba and tfaa respectively.

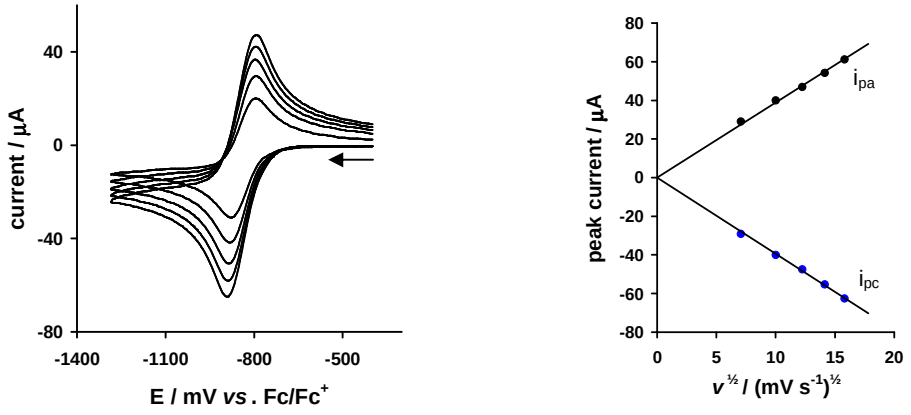

Figure 3.69 **Left:** Cyclic voltammograms (*vs.* Fc/Fc^+) for $[Cp_2Ti(ba)]^+ ClO_4^-$ showing the Ti^{IV}/Ti^{III} couple at scan rates of 50, 100, 150, 200 and 250 mV s^{-1}. Scans initiated in the direction of the arrow. Measured in 0.1 mol dm^{-3} $[NBu_4][PF_6]$ / CH_3CN on a glassy carbon working electrode at 25 °C. [Ti complex] = 2 mmol dm^{-3}. **Right**: The relationship between peak currents and $(scan\ rate)^{½}$ obeys the Randles-Sevcik equation.[75] Graph slope = +3.89 and -3.95 µA $(mV\ s^{-1})^{½}$

From the comparative voltammograms (see **Figure 3.70 Right**), it can be seen that the $E^{0'}$ of the Ti^{IV}/Ti^{III} couple falls into categories depending on the overall e^--withdrawing ability of the β-diketonato ligand; those containing a CF_3 group (χ_{CF3} = 3.01) $E^{0'}$ = ~ -623 mV , a Ph-group (χ_{Ph} = 2.21) $E^{0'}$ = ~ -833 mV and a ferrocene group (χ_{Fc} = 1.81) $E^{0'}$ = -903 mV.[14] The inclusion of an electron withdrawing CF_3 group gives a less negative (more cathodic) $E^{0'}$ than the relatively electron donating Ph group (more anodic). This is expected, because the more

electron withdrawing the R groups becomes, the more positive the titanium(IV) centre becomes and accordingly the more difficult it will be reduced.

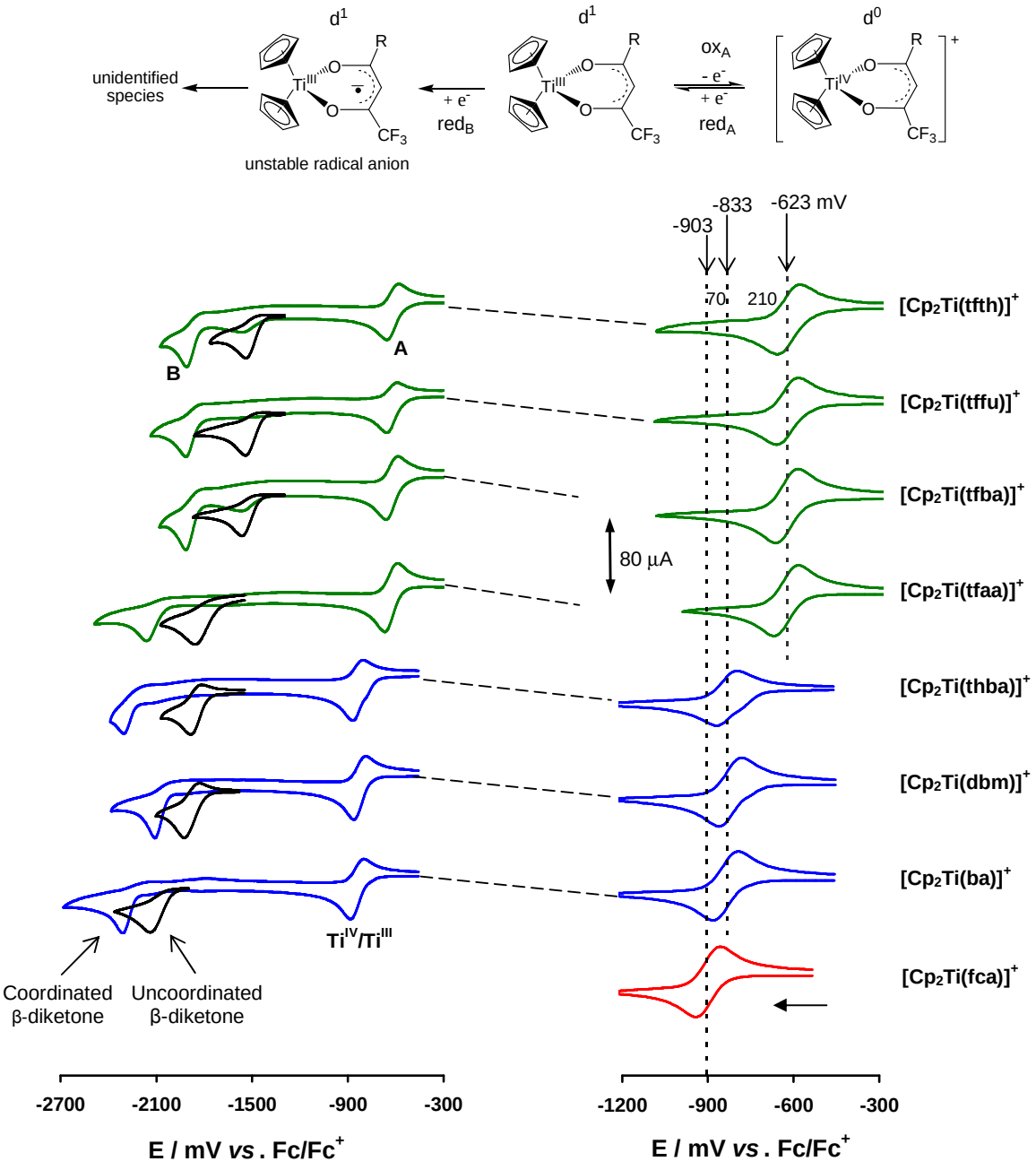

Figure 3.70 Comparative cyclic voltammograms (*vs.* Fc/Fc^+) at a scan rate of 100 mV s^{-1} for the $[Cp_2Ti(\beta)]^+$ series showing **Left**: the reduction of the titanium metal centre and the β-diketonato ligand (The uncoordinated β-diketones are inserted into the individual voltammograms as black waves) and **Right**: the Ti^{IV}/Ti^{III} couple. The CVs shown in green represent complexes containing CF_3-β-diketones, blue contain Ph-β-diketones and red Fc-β-diketone. Vertical dotted lines indicate the formal reduction potential of a single complex or an average of a group. Scans initiated in the direction of the arrow. Measured in 0.1 mol dm^{-3} $[NBu_4][PF_6]$ / CH_3CN on a glassy carbon working electrode at 25 °C. [Ti complex] = 2 mmol dm^{-3}.

The formal reduction potential of the Ti^{IV}/Ti^{III} couple varies by 10 mV and 17 mV within the CF_3 and Ph series respectively with a jump of -623 - (-833) = 210 mV from the CF_3 to the Ph series. There is a further decrease of 70 mV from the Ph series to the ferrocene complex, $[Cp_2Ti(FcCOCHCOCH_3)]^+ClO_4^-$. This result demonstates that there is good electronic communication between the titanium centre and the R-groups of the β-diketonato ligand.

The complexes are further reduced in a one electron irreversible process at very negative potentials (see **Figure 3.70 Left**), according to

$$Cp_2Ti^{III}(\beta) + e^- \longrightarrow [Cp_2Ti^{III}(\beta)]^{\bullet -}$$

This process, assigned to the reduction of the β-diketonato ligand, is supported by the observation of a similar reduction in uncoordinated β-diketones (see **Section 3.5.2.1**). The reduced species, $[Cp_2Ti^{III}(\beta)]^{\bullet -}$, is chemically unstable and decomposes rapidly to form other unidentified species, hence no corresponding oxidation peak is visible even at very high scan rates. The anionic species, $[Cp_2Ti^{III}(\beta)]^{\bullet -}$, is believed to have one unpaired electron on the metal as well as one unpaired electron on the ligand.[38] The oxidation of the metal centre, $Ti^{III} \rightarrow Ti^{IV}$ following the decomposition of $[Cp_2Ti^{III}(\beta)]^{\bullet -}$ (see **Figure 3.71**) is not expected. It could be due to the oxidation of freshly reduced $[Cp_2Ti^{IV}(\beta)]^+$ molecules moving in from the bulk solution. The decrease of the i_{pa}/i_{pc} ratio with increasing scan rate is consistent with this view, since as the scan rate increases there is less time for "fresh" molecules to move in from the bulk solution.

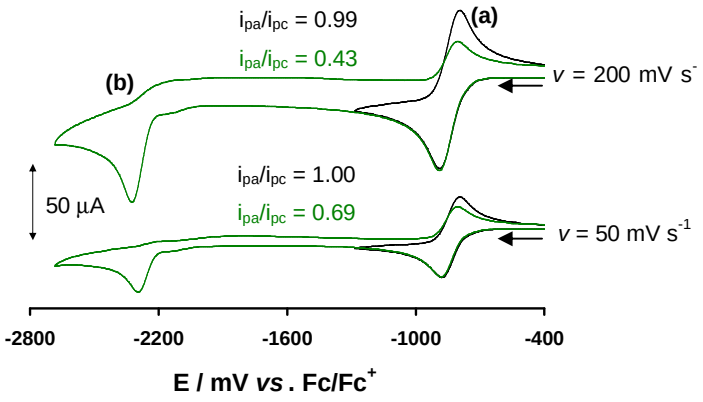

Figure 3.71 Cyclic voltammograms of $[Cp_2Ti(ba)]^+$ showing **(a)** the reversible T^{IV}/Ti^{III} couple in black and **(b)** the reduction of both the Ti centre and β-diketonato ligand followed by the oxidation of the Ti centre after the decomposition of the complex in green. Scans initiated in the direction of the arrow. Measured in 0.1 mol dm^{-3} $[NBu_4][PF_6]$ / CH_3CN on a glassy carbon working electrode at 25 °C. [Ti complex] = 2 mmol dm^{-3}.

The coordinated β-diketonato ligand in the titanium complex, $[Cp_2Ti^{IV}(\beta)]^+$, was found to be electroactive at more cathodic potentials relative to the uncoordinated β-diketone (see **Figure 3.70 Left**). The difference in the reduction potentials of the coordinated and uncooordinated β-diketone, ΔE_{pc}, is consistent for the CF_3-β-diketones, i.e., on average, ΔE_{pc} = ~ 346 mV (see **Table 3.35**). This result shows that the coordination of the β-diketone to the metal centre, forming the delocalised *pseudo*-aromatic system, results in the coordinated β-diketonato ligand possessing higher electron density (in the electroactive centre) relative to the uncoordinated β-diketone.

The unusual reversible redox behaviour of aromatic β-diketones (uncoordinated) at higher scan rates is not replicated in the coordinated β-diketones; even at a scan rate of 1000 mV the reduction of the coordinated β-diketone remains chemically and electrochemically irreversible. This implies that the reduced radical anion is more stable in the uncoordinated β-diketone ($Hthba^{\bullet}$) than in the chelated form ($Cp_2Ti^{III}(thba)^{\bullet}$).

Table 3.35 Reduction potential (*vs.* Fc/Fc^+) of uncoordinated β-diketone and the β-diketonato ligand in $[Cp_2Ti(\beta)]^+ClO_4^-$.

$[Cp_2Ti(\beta)]$+ β	Coordinated β E_{pc} / mV	Uncoordinated β E_{pc} / mV	ΔE_{pc}*
CF_3-β-diketones			
tfth **[4]**	-1890	-1541	349
tffu **[5]**	-1916	-1544	372
tfba **[6]**	-1915	-1564	351
tfaa **[3]**	-2162	-1851	311
Ph-β-diketones			ave → **346**
thba **[8]**	-2305	-1884	421
dbm **[9]**	-2110	-1934	176
ba **[7]**	-2306	-2138	167

*$\Delta E_{pc} = E_{pc}$ (coordinated β) - E_{pc} (uncoordinated β)

3.5.3.2 Mono(biphenyldiolato) Ti(IV) complex: Cp_2Ti(biphen)

The cyclic voltammetric behaviour of Cp_2Ti^{IV}(biphen) **[12]** was studied in 0.1 mol dm^{-3} $[NBu_4][PF_6]$ / CH_3CN. Cyclic voltammograms are shown in **Figure 3.72** and electrochemical data is summerised in **Table 3.36**. At a scan rate of 100 mV s^{-1} a one-electron irreversible

reduction was observed. As the scan rate increases the corresponding oxidation wave appears with the current ratio, i_{pa}/i_{pc} dependent on scan rate (see **Table 3.36**). This result is consistent with an EC mechanism in which the electron transfer is followed by an irreversible chemical reaction of the electroreduced species. Thus an increase of scan rate allows for the oxidation of the reduced species by preventing appreciable following reaction (see **Figure 3.72**). The previously reported value for the reduction of Cp_2Ti(biphen) in THF by El Murr *et al.* is in good agreement with the value reported in this study, *i.e.*, E_{pc} (*vs* Fc/Fc^+) = -1680[76] and -1701 mV (v = 100mV s^{-1}) respectively.

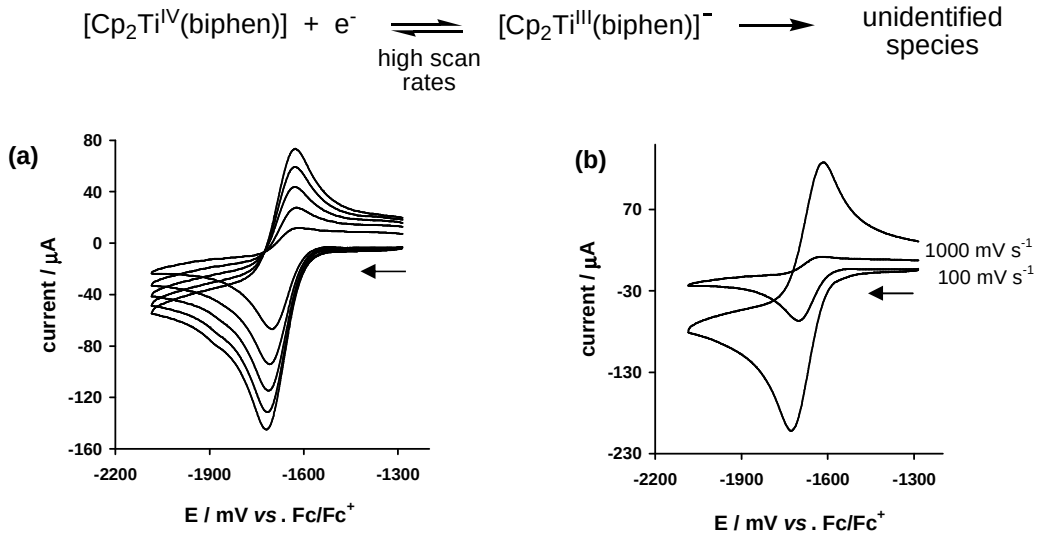

Figure 3.72 Cyclic voltammograms (*vs.* Fc/Fc^+) of Cp_2Ti^{IV}(biphen) at scan rates **(a)** 100, 200, 300, 400 and 500 mV s^{-1} and **(b)** 100 and 1000 mV s^{-1}, showing the dependence of reversibility on scan rate. Scans initiated in the direction of the arrow. Measured in 0.1 mol dm^{-3} $[NBu_4][PF_6]$ / CH_3CN on a glassy carbon working electrode at 25 °C. [Ti complex] = 2 mmol dm^{-3}.

Table 3.36 Cyclic voltammetric data (*vs.* Fc/Fc^+) for Cp_2Ti(biphen) **[12]** at indicated scan rates. Measured in 0.1 mol dm^{-3} $[NBu_4][PF_6]$ / CH_3CN on a glassy carbon working electrode at 25. [Ti complex] = 2.0 mmol dm^{-3}.

ν mV s^{-1}	**E_{pc}** mV	**ΔE_p** mV	**$E^{0'}$** mV	**i_{pc}** µA	**i_{pa}/i_{pc}**
100	-1701[a]	--	--	--	--
200	-1709	79	-1670	36	0.40
300	-1711	81	-1671	56	0.51
400	-1714	84	-1672	76	0.61
500	-1718	91	-1673	93	0.69
1000	-1727	110	-1673	160	0.86

[a]Compare to El Murr *et al.*[76]: E_{pc} = -1520 (*vs.* SCE) = -1680 mV (*vs.* Fc/Fc^+).
SCE relative NHE = 244 mV and Fc/Fc^+ relative NHE = 400 mV, therefore E_{pc} *vs* Fc/Fc^+ relative SCE = (400 - 244 = -156 mV).

3.5.4 Octahedral Complexes

3.5.4.1 Bis(β-diketonato)-dichloro Ti(IV) complexes: $Ti(\beta)_2Cl_2$

The electrochemical study of bis(β-diketonato)dichlorotitanium(IV) complexes in CH_3CN was hampered by their instability in the medium, adsoption at the electrode surface and electrode passivation. However in the solvent system, 0.1 mol dm^{-3} $[NBu_4][PF_6]$/DCE ($C_2H_5Cl_2$), the $Ti(\beta)_2Cl_2$ complexes with β = tfaa **[13]**, tfba **[17]**, ba **[21]** and dbm **[22]** were relatively stable and the Ti^{IV}/Ti^{III} reduction as well as ligand and other reductions were observed (marked **A**, **B**, **C** and **D** in **Figure 3.73 Right**) Wave D is in the correct position for the reduction of the β-diketonato ligand. The cathodic waves gradually change (position and size) hence a scan rate series for ν = 100, 200, 300, 400 and 500 mV s^{-1} had to be done promptly. The gradual changes could be a result of the conversion of starting complex into other species. Spontaneous dimerisation,[77] for example, has been observed during the electrochemical investigation of other octahedral dichloro Ti^{IV} complexes with *O,O*'-chelating ligands, (i.e., $Ti(mal)_2Cl_2$, mal = *O,O*'-3-oxy-2-methyl-pyran-4-onato). Electrochemical data for the Ti^{IV}/Ti^{III} couple is summarised in **Table 3.37** and comparative cyclic voltammograms are shown in **Figure 3.74**.

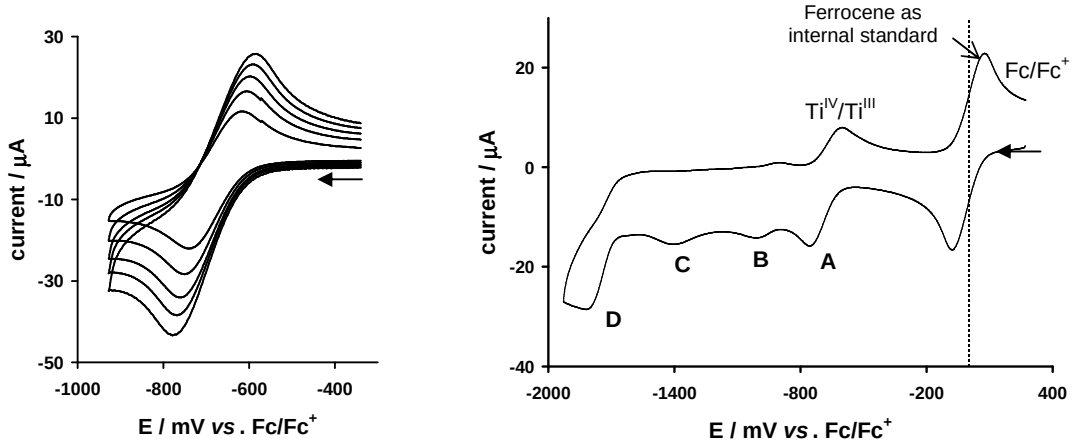

Figure 3.73 Cyclic voltammograms (*vs.* Fc/Fc^+) of $Ti(dbm)_2Cl_2$ showing, **Left**: the Ti^{IV}/Ti^{III} couple at scan rates 100, 200, 300, 400 and 500 mV s^{-1} and **Right**: a wide potential scan at 200 mV s^{-1} with ferrocene used as an internal standard (Fc/Fc^+, $E^{0'}$ = 0 mV). Scan initiated in the direction of the arrow. Measured in 0.1 mol dm^{-3} $[NBu_4][PF_6]$ / DCE on a glassy carbon working electrode at 25 °C. [Ti complex] = 2 mmol dm^{-3}.

The Ti^{IV}/Ti^{III} reduction according to:

$$Ti^{IV}(\beta)_2Cl_2 + e^- \rightleftharpoons [Ti^{III}(\beta)_2Cl_2]^- \longrightarrow \text{unidentified species}$$

is quasi-reversible at a scan rate of 100 mV s^{-1} (irreversible at higher scan rates) and chemically irreversible. The low i_{pa}/i_{pc} ratios of $Ti(tfaa)_2Cl_2$ and $Ti(tfba)_2Cl_2$ relative to $Ti(dbm)_2Cl_2$ and $Ti(ba)_2Cl_2$, suggest that the reduced species, $[Ti(\beta)_2Cl_2]^-$, is considerably less stable when containing CF_3-β-diketonato ligands (see **Table 3.37**). Since the reduction is followed by an irreversible chemical reaction, one would expect the i_{pa}/i_{pc} ratios to increase with increasing scan rate. However this event is obscured by the effects of excessive electrode deposition; a slow decrease of i_{pa}/i_{pc} and increase of ΔE with increasing scan rate is consistent with electrode adsorption (see **Table 3.38**). The shape of the CV is also typical of electrode adsorption.

Table 3.37 Cyclic voltammetric data (*vs.* Fc/Fc^+) for the $Ti(\beta)_2Cl_2$ series at a scan rate of 100 mV s^{-1}. Measured in 0.1 mol dm^{-3} $[NBu_4][PF_6]$ / DCE on a glassy carbon working electrode at 25 °C. [Ti complex] = 2 mmol dm^{-3}.

$Ti(\beta)_2Cl_2$ β	$RCOCH_2COR'$ R, R'	E_{pc} mV	ΔE_p mV	$E^{0'}$ mV	i_{pc} μA	i_{pa}/i_{pc}
tfba **[17]**	CF_3, Ph	-418	140	-348	14	0.28
tfaa **[13]**	CF_3, CH_3	-414	102	-363	16	0.29
dbm **[22]**	Ph, Ph	-740	117	-682	22	0.71
ba **[21]**	Ph, CH_3	-775	151	-700	21	0.85

Table 3.38 Cyclic voltammetric data (*vs.* Fc/Fc^+) for $Ti(dbm)Cl_2$ at indicated scan rates. Measured in 0.1 mol dm^{-3} $[NBu_4][PF_6]$ / DCE on a glassy carbon working electrode at 25 °C. [Ti complex] = 2 mmol dm^{-3}.

ν mV s^{-1}	E_{pc} mV	ΔE_p mV	$E^{0'}$ mV	i_{pc} μA	i_{pa}/i_{pc}
100	-740	117	-682	22	0.71
200	-750	138	-682	27	0.70
300	-758	150	-683	33	0.69
400	-768	166	-685	36	0.66
500	-779	179	-689	41	0.63
1000	-796	207	-692	55	0.53

The comparative cyclic voltammograms (see **Figure 3.74**) show the results of changing the β-diketonato ligand from an e^--withdrawing to a relatively e^-- donating group, on the Ti^{IV}/Ti^{III} reduction, namely, that the $Ti(\beta)_2Cl_2$ complexes containing more electron donating groups (CH_3 or Ph) have a greater tendency to be reduced (at more anodic/negative potentials) than the complexes containing electron withdrawing groups (CF_3).

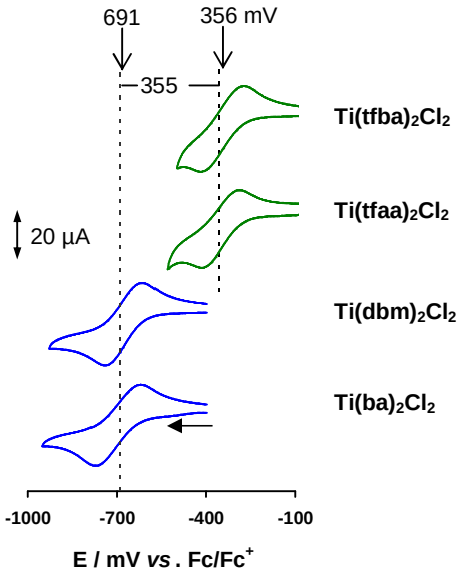

Figure 3.74 Comparative cyclic voltammograms (*vs.* Fc/Fc^+) at a scan rate of 100 mV s^{-1} for the $Ti(\beta)_2Cl_2$ series showing the Ti^{IV}/Ti^{III} couple. The CVs shown in green represents complexes containing a CF_3-β-diketone while the ones in blue contain non-CF_3-β-diketones. Vertical dotted lines indicate the average formal reduction potentials. Scans initiated in the direction of arrow. Measured in 0.1 mol dm^{-3} $[NBu_4][PF_6]$ / DCE on a glassy carbon working electrode at 25 °C.

3.5.4.2 Bis(β-diketonato)-(biphenyldiolato) Ti(IV) complexes: $Ti(\beta)_2$(biphen)

The electrochemical behaviour of the new CF_3 series of bis(β-diketonato)biphenolato-titanium(IV) complexes, $Ti(\beta)_2$biphen with β = tfaa **[24]**, tfth **[26]**, tffu **[27]**, tfba **[28]**, tfma **[29]**, tfdma **[30]** and tftma **[31]** were studied in 0.1 mol dm^{-3} $[NBu_4][PF_6]$ / CH_3CN. For comparison two non-CF_3 $Ti(\beta)_2$biphen complexes with β = ba **[32]** and acac **[36]** were included. A wide potential scan shows the reduction of both the Ti^{IV} metal centre and the β-diketonato ligand (see **Figure 3.75**). The electrochemical data for the Ti^{IV}/Ti^{III} couple is summarised in **Table 3.40** and the comparative cyclic voltammograms, shown in **Figure 3.76**.

All the complexes exhibit a characteristic one electron, electrochemically reversible Ti^{IV}/Ti^{III} couple, according to:

$$Ti^{IV}(\beta)_2biphen + e^- \rightleftharpoons [Ti^{III}(\beta)_2biphen]^- \longrightarrow \text{unidentified species}$$

with $62 \leq \Delta E_p \leq 91$ mV for the series of $Ti(\beta)_2$biphen complexes. The process is chemically irreversible, with $0.56 \leq i_{pa}/i_{pc} \leq 0.94$ µA, at $\nu = 100$ mV s^{-1} as shown in **Table 3.40**. The i_{pa}/i_{pc} ratios remain relatively constant with slight increases or decreases over the scanning rate of 100 - 500 mV s^{-1} (see **Table 3.39**).

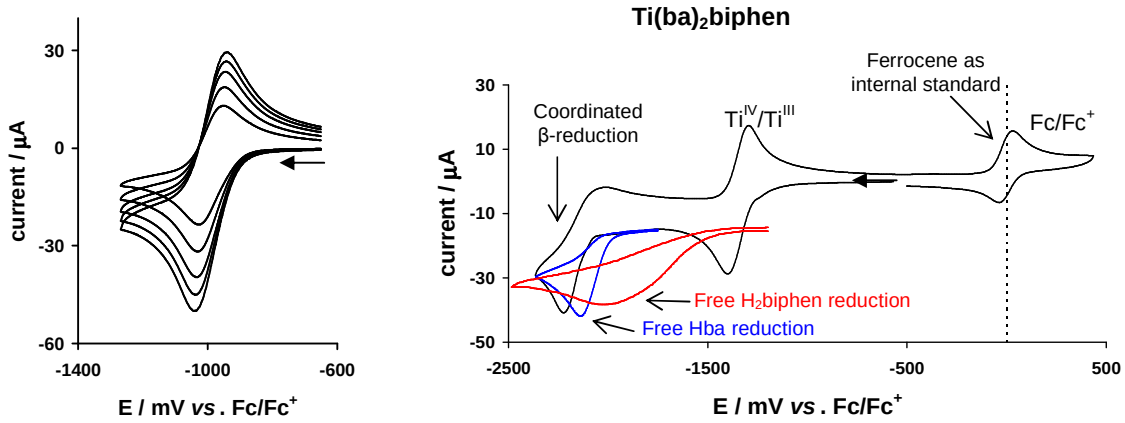

Figure 3.75 **Left**: Cyclic voltammograms (*vs.* Fc/Fc^+) of $Ti(tfth)_2$biphen at scan rates 100, 200, 300, 400 and 500 mV s^{-1}. **Right**: Wide potential scan (*vs.* Fc/Fc^+) of $Ti(ba)_2$biphen at 200 mV s^{-1} with ferrocene used as an internal standard (Fc/Fc^+, $E^{0'} = 0$ mV). Scans of uncoordinated ligand reductions, Hba (blue) and H_2biphen (red) at $\nu = 200$ mV s^{-1} are inserted for comparison. All scan initiated in the direction of the arrow. Measured in 0.1 mol dm^{-3} $[NBu_4][PF_6]$ / CH_3CN on a glassy carbon working electrode at 25 °C. {Ti complex] = 2 mmol dm^{-3}.

Table 3.39 Cyclic voltammetric data (*vs.* Fc/Fc^+) for Ti(tfth)biphen at indicated scan rates. Measured in 0.1 mol dm^{-3} $[NBu_4][PF_6]$ / CH_3CN on a glassy carbon working electrode at 25 °C. [Ti complex] = 2 mmol dm^{-3}.

ν mV s^{-1}	E_{pc} mV	ΔE_p mV	$E^{0'}$ mV	i_{pc} µA	i_{pa}/i_{pc}
100	-1028	76	-990	21	0.79
200	-1030	80	-990	28	0.79
300	-1032	83	-991	36	0.77
400	-1036	89	-992	40	0.77
500	-1039	93	-993	45	0.77

The comparative cyclic voltammograms of the Ti(β)$_2$biphen series (see **Figure 3.76**) show that the complexes containing electron withdrawing CF_3 groups, are reduced at *ca*. 340 mV more positive potentials relative to the non-fluorinated complexes, Ti(acac)$_2$biphen and Ti(ba)$_2$biphen, containing electron donating groups (CH_3 and Ph).

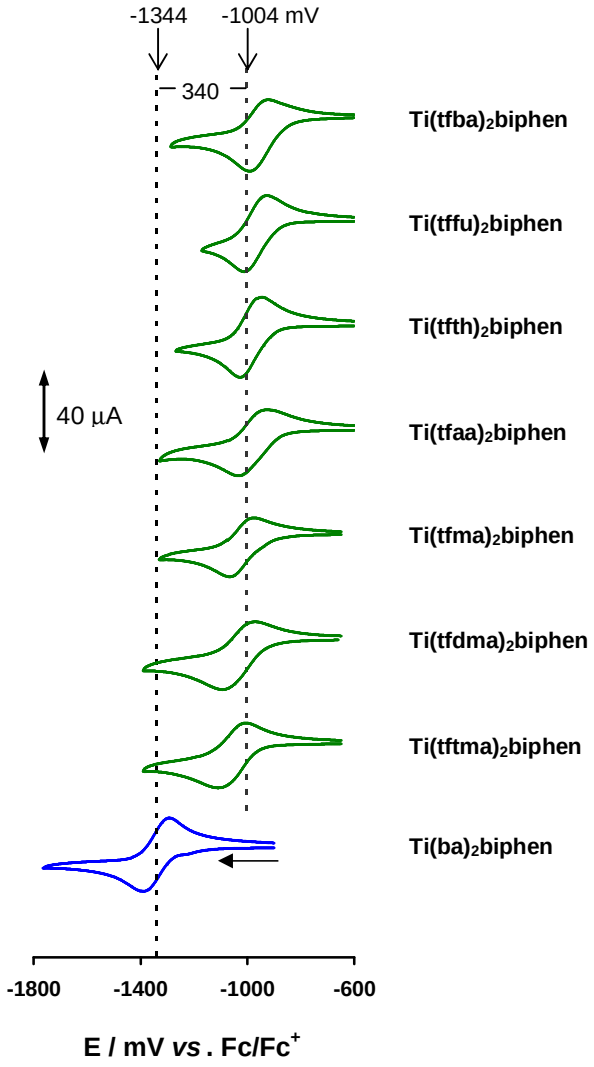

Figure 3.76 Comparative cyclic voltammograms (*vs*. Fc/Fc^+) at a scan rate of 100 mV s^{-1} for the Ti(β)$_2$(biphen) series showing the Ti^{IV}/Ti^{III} couple. The CVs shown in green represent complexes containing CF_3-β-diketones while the one in blue contains a non-CF_3-β-diketone. Vertical dotted lines indicate the formal reduction potential of a single complex or an average of a group. Scans initiated in the direction of the arrow. Measured in 0.1 mol dm^{-3} $[NBu_4][PF_6]$ / CH_3CN on a glassy carbon working electrode at 25 °C. Ti complex] = 2 mmol dm^{-3}.

Table 3.40 Cyclic voltammetric data (*vs.* Fc/Fc^+) for the $Ti(\beta)_2$biphen series at a scan rate of 100 mV s^{-1}. Measured in 0.1 mol dm^{-3} $[NBu_4][PF_6]$ / CH_3CN on a glassy carbon working electrode at 25 °C. [Ti complex] = 2 mmol dm^{-3}.

$Ti(\beta)_2$biphen β		R	E_{pc} mV	ΔE_p mV	$E^{0'}$ mV	i_{pc} μA	i_{pa}/i_{pc}
CF_3COCH_2COR							
tfba	**[28]**	Ph	-991	63	-960	22	0.56
tffu	**[27]**	C_4H_3O	-1012	83	-971	22	0.66
tfth	**[26]**	C_4H_3S	-1028	76	-990	21	0.79
tfaa	**[24]**	CH_3	-1030	91	-985	20	0.66
tfma	**[29]**	$CH_2(CH_3)$	-1075	90	-1030	21	0.78
tfdma	**[30]**	$CH(CH_3)_2$	-1076	91	-1031	19	0.60
tftma	**[31]**	$C(CH_3)_3$	-1108	91	-1063	19	0.65
		Average→	-1045	84	**-1004**		
CH_3COCH_2COR							
acac	**[36]**	CH_3	-1369	62	-1338	11*	0.78
ba	**[32]**	Ph	-1387	87	-1344	16*	0.94

*$Ti(acac)_2$biphen and $Ti(ba)_2$biphen dissolve poorly in CH_3CN

3.5.5 Reduction Potential Relationships

3.5.5.1 Comparison of reduction potentials with pK_a and χ_R

The reduction potential of a metal centre in a series of compounds gives an indication of the electron density of the metal centre. For example, if the reduction potential of Ti^{IV} in $Ti(\beta)_2Cl_2$ is higher (more anodic) than in $Ti(\beta')_2Cl_2$, then a lower electron density is expected on Ti in the first complex. Since both χ_R (of the R groups of β-diketones) and pK_a (of the uncoordinated β-diketones) are identities related indirectly to electron density, a correlation between reduction potentials and $\chi_R + \chi_{R'}$ and/or pK_a is expected. The relationships between the formal reduction potential of Ti^{IV}, $E^{0'}$, in $[Cp_2Ti(\beta)]^+$, $Ti(\beta)_2Cl_2$ and $Ti(\beta)_2$biphen (or the cathodic peak potential, E_{pc}, of the uncoordinated β-diketone) and the two variables, $\chi_R + \chi_{R'}$ and pK_a, are illustrated in **Figure 3.77** and the data is summarised in **Table 3.41.**

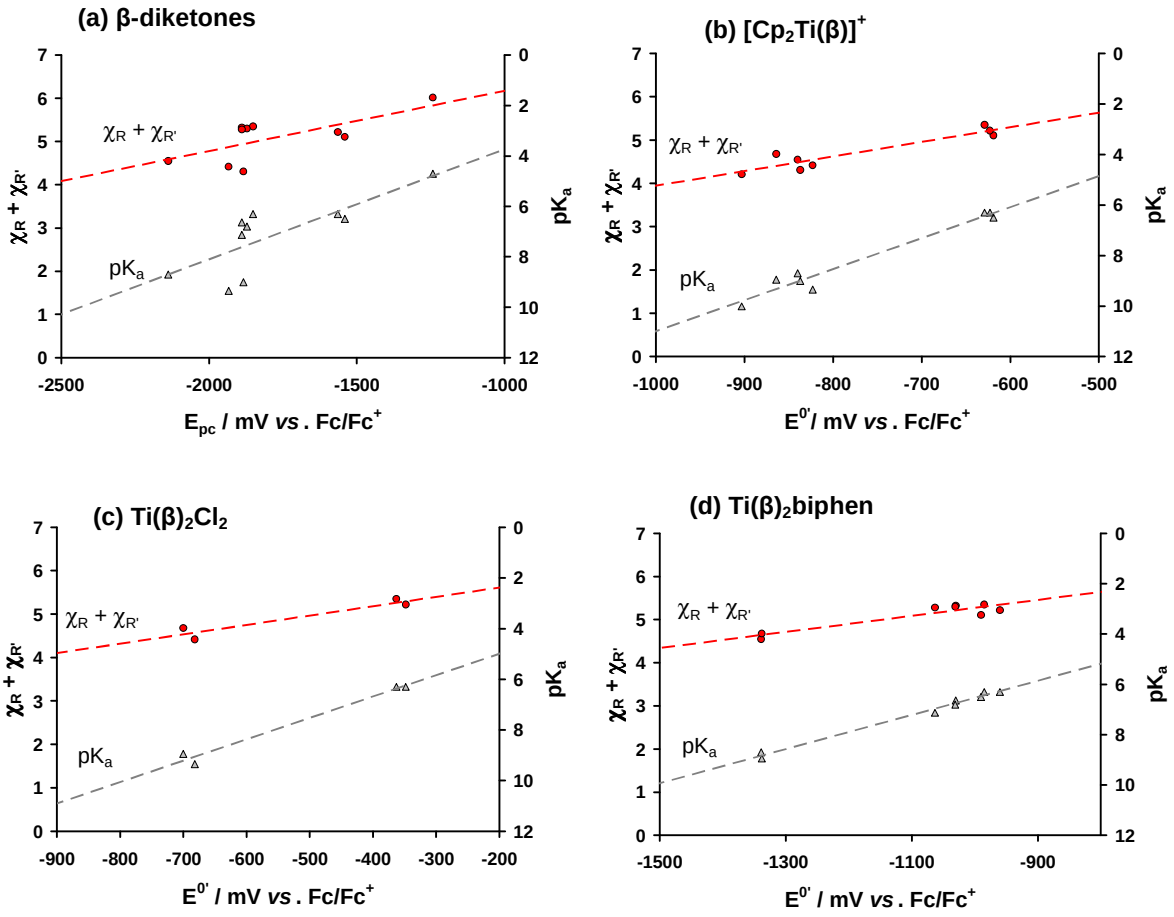

Figure 3.77 Relationship between the formal reduction potential, $E^{0'}$, (or E_{pc}) and (left y-axis): the sum of the group electronegativities of the β-diketone, $\chi_R + \chi_{R'}$ and (right y-axis): pK_a.

It can be seen from **Figure 3.77** that there is no direct linear relationship but the correct trends are observed. The trends for group electronegativity show that the larger the $\chi_R + \chi_{R'}$ (more e^--withdrawing) the larger (more anodic) the $E^{0'}$ for all the complexes investigated. The titanium metal centre is relatively more electron-deficient (with larger $\chi_R + \chi_{R'}$) and consequently a higher, less negative reduction potential is observed. The trends for pK_a show that the larger the pK_a (less acidic) the smaller (more cathodic) the $E^{0'}$. The titanium metal centre is relatively more electron-rich (with larger pK_a) and consequently a more negative reduction potential is observed. This is consistent with highly electron withdrawing groups on the β-diketone backbone resulting in a decrease in the pK_a of the β-diketone.

Table 3.41 Group electronegativities, pK_a and E_{pc} (*vs.* Fc/Fc^+) values for the indicated β-diketones and the $E^{0'}$ (*vs.* Fc/Fc^+) of the titanium complexes. References for χ_R and pKa are indicated in **Table 3.1**.

β-diketonato			$(\chi_R + \chi_{R'})$	pK_a	E_{pc} / mV	$E^{0'}$ / mV		
$RCOCH_2COR'$	R	R'	β	Hβ	Hβ	$[Cp_2Ti(\beta)]^+$	$Ti(\beta)_2Cl_2$	$Ti(\beta)_2$biphen
hfaa	CF_3	CF_3	6.02	4.71	-1243	--	--	--
tfth	CF_3	C_4H_3S	5.11	6.50	-1541	-619	--	-990
tffu	CF_3	C_4H_3O	--	--	-1544	-624	--	-971
tfba	C_6H_5	CF_3	5.22	6.3	-1564	-623	-348	-960
tfaa	CF_3	CH_3	5.35	6.3	-1851	-629	-363	-985
tfma	CF_3	CH_2CH_3	5.32	6.64	-1889	--	--	-1030
tfdma	CF_3	$CH(CH_3)_2$	5.30	6.80	-1872	--	--	-1031
tftma	CF_3	$C(CH_3)_3$	5.28	7.13	-1889	--	--	-1063
ba	C_6H_5	CH_3	4.55	8.70	-2138	-840	-700	-1344
thba	C_6H_5	C_4H_3S	4.31	9.01	-1884	-837	--	--
dbm	C_6H_5	C_6H_5	4.42	9.35	-1934	-823	-682	--
acac	CH_3	CH_3	4.68	8.95	--	-864	--	-1338
fca	Fc	CH_3	4.21	10.01	--	-903	--	--

3.5.5.2 Comparison of $Ti(\beta)_2Cl_2$ and $Ti(\beta)_2$biphen complexes

Wide potential cyclic voltammograms of $Ti(dbm)_2Cl_2$ and $Ti(ba)_2$biphen as examples of the dichloro- and biphenolato-bis(β-diketonato)titanium(IV) complexes, show the relative shape of the waves and positions of the Ti^{IV}/Ti^{III} couple and ligand reduction (see **Figure 3.78**). The uncoordinated β-diketone reduction, Hba, is inserted into the CV for comparison.

A comparison of the formal reduction potentials of the Ti^{IV} centre for the two classes of compounds, $Ti(\beta)_2Cl_2$ and $Ti(\beta)_2$biphen with β = tfba and ba, is shown in **Figure 3.79**. When changing from the dichloro- to the biphenolato- ligand, $E^{0'}$ decreases by ~620 mV This suggest that in $Ti(\beta)_2Cl_2$ and $Ti(\beta)_2$biphen, the biphenolato ligand behaves as a considerably stronger electron donor than the chloride ligands. The electronic effect of the β-diketone ligand on the formal reduction potentials of the Ti^{IV} centre is significantly smaller; $E^{0'}$

decreases by ~360 mV when changing from tfba to ba. The non-CF_3-β-diketonato ligand, ba, (with R, R' = CH_3, Ph) behaves as a stronger electron donor than the CF_3-β-diketonato ligand, tfba, (with R, R' = CF_3, Ph). The influence of the β-diketonato ligand on the Ti centre is independent of the dichloro- or biphenolato-ligands.

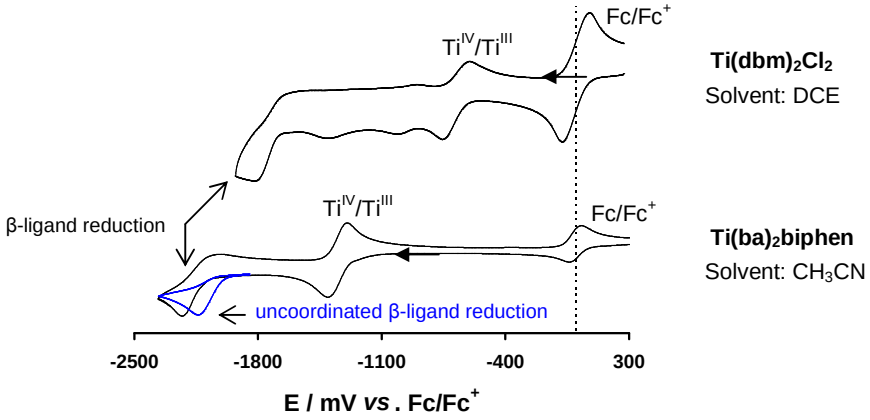

Figure 3.78 Comparative cyclic voltammograms (*vs.* Fc/Fc^+) of $Ti(dbm)_2Cl_2$ and $Ti(ba)_2$biphen at a scan rates 100 mV s^{-1} with ferrocene used as an internal standard (Fc/Fc^+, $E^{0'}$ = 0 mV). Scan initiated in the direction of the arrow.

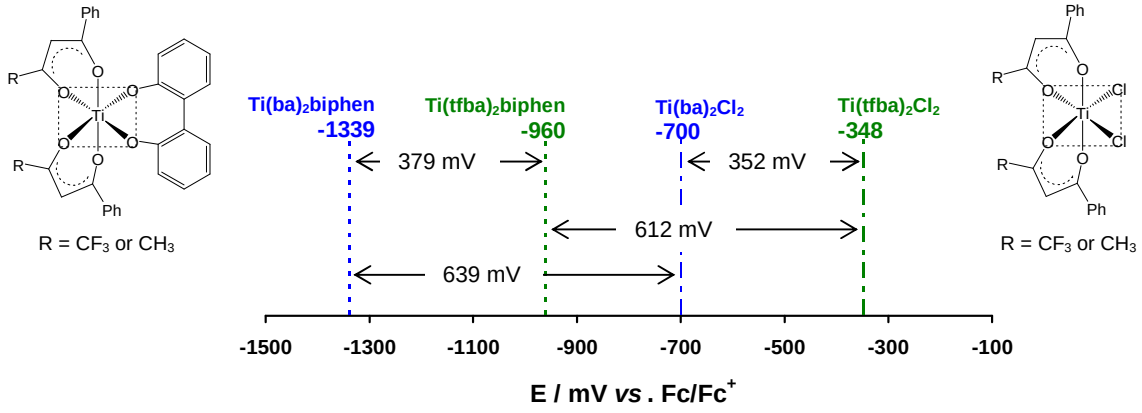

Figure 3.79 Formal reduction potentials, $E^{0'}$, (*vs.* Fc/Fc^+) of $Ti(\beta)_2Cl_2$ and $Ti(\beta)_2$biphen with β = ba and tfba at scan rate of 100 mV s^{-1}.

3.5.5.3 Calculated ionisation potential of $[Cp_2Ti(\beta)]^+$ correlated to pK_a, χ_R and $E^{0'}$

Density functional theory (DFT) calculations were carried out on the $[Cp_2Ti(\beta)]^+ClO_4^-$ series with β = tfaa **[3]**, tfth **[4]**, tffu **[5]** tfba **[6]**, ba **[7]**, thba **[8],** dbm **[9]** and acac **[10]** to study the ground state geometry of both $[Cp_2Ti^{IV}(\beta)]^+$ and $Cp_2Ti^{III}(\beta)$ and to determine the ionisation potential of $Cp_2Ti^{III}(\beta)$.

Since density functional methods are for the first time applied to β-diketonato titanocenyl complexes and reported here, some measure on the reliability of the approach was obtained by comparing the calculated data with known single crystal X-ray diffraction structural data of **[4]**, **[5]**, **[6]** and **[10]**,[37] as well as the $Cp_2Ti^{III}(\beta)$ complexes $Cp_2Ti^{III}(ba)$[39] **[7b],** $Cp_2Ti^{III}(dbm)$[40] **[9b]** and $Cp_2Ti^{III}(acac)$[38] **[10b]**. The root-mean-square distances (RMSD) calculated for non-hydrogen atoms for the best three-dimensional superposition of calculated structures on experimental structures give a qualitative measurement of the accuracy of the ground state geometry of the calculated structures. Excellent agreement between experimental and theoretical structures is obtained as reflected by the RMSD values of 0.07, 0.08, 0.20, 0.04, 0.12, 0.07 and 0.06 Å for **[4]**, **[5]**, **[6]**, **[10]**, **[7b]**, **[9b]** and **[10b]** respectively. For **[5]** and **[6],** containing disordered parts, the parts with the highest site occupancy, were used in the RMSD calculation. The largest deviation from experimental structure was found for **[6]**, containing a large % of disordered parts. All the bonds in the Ti-β-diketonato ring structure of **[4]**, **[5]**, **[6]** and **[10]** were reproduced by DFT calculations within 0.01-0.03 Å from the experimental values. Since comparisons of experimental metal-ligand bond lengths with calculated bond lengths below a threshold of 0.02 Å are considered as meaningless,[78] the computational method used thus gives a good account of experimental bond lengths. The O1-Ti-O2 angles were calculated accurately within 1°. Data computed with this computational method for related compounds may therefore be presented with an extrapolative equally high degree of accuracy.

The ionization potential (IP) of the $Cp_2Ti^{III}(\beta)$ complexes, calculated according to

$$[Cp_2Ti^{IV}(\beta)]^+ + e^- \underset{\text{oxidation}}{\overset{\text{reduction}}{\rightleftharpoons}} Cp_2Ti^{III}(\beta) + \text{energy}$$

as the amount of energy required to remove an electron from $Cp_2Ti^{III}(\beta)$ to form $[Cp_2Ti^{IV}(\beta)]^+$, is tabulated in **Table 3.42**. Parameters that are related to the electron density on the metal centre of $[Cp_2Ti^{IV}(\beta)]^+$, such as the pK_a of the β-diketone **R′**$COCH_2CO$**R**

coordinated to the titanium complex, the group electronegativities of the **R** and **R′** side groups on the β-diketonato ligand, the carbonyl stretching frequencies (ν_{CO}) in $[Cp_2Ti^{IV}(\beta)]^+$ and the formal reduction potentials, $E^{0'}$, of the redox active metal Ti^{IV}/Ti^{III} in $[Cp_2Ti^{IV}(\beta)]^+$ are also included in **Table 3.42**. The relationships between the calculated ionization potential (IP) and $\chi_R + \chi_{R'}$, $E^{0'}$, ν_{CO} and pK_a are shown graphically in **Figure 3.80**.

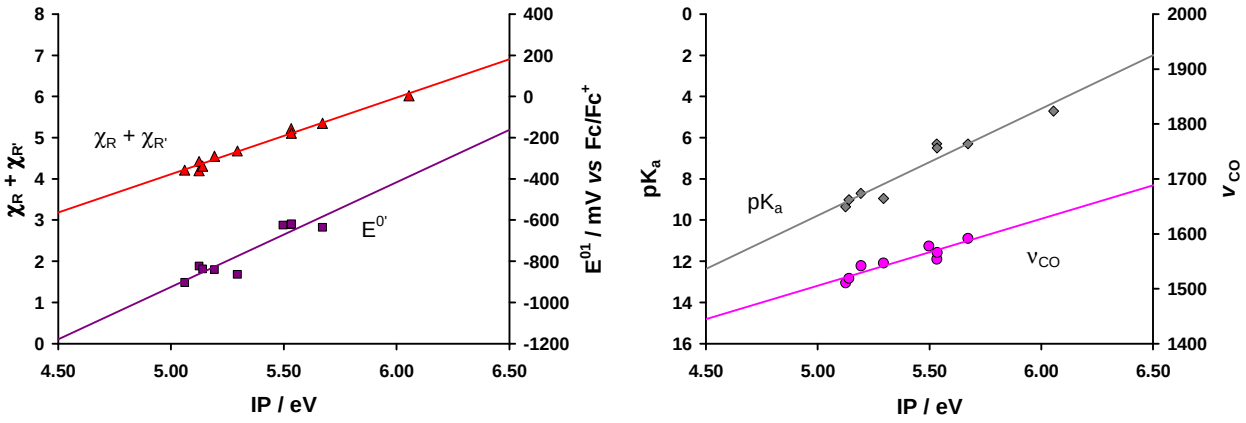

Figure 3.80 The correlation of the calculated ionization potential (IP) with $E^{0'}$ (*vs.* Fc/Fc^+) and ν_{CO} of the titanium complexes $[Cp_2Ti^{IV}(\beta)]^+$, pK_a values for the β-diketones $R'COCH_2COR$ and group electronegativities of the R and R′ groups.

The correlation of the calculated ionisation potentials shows the following trends:

IP *vs.* $\chi_R + \chi_{R'}$: shows that the IP increases linearly with the sum of the group electro-negativities $\chi_R + \chi_{R'}$. The titanium metal centre is relatively more electron-deficient with larger $\chi_R + \chi_{R'}$ and consequently more energy is needed to remove an electron from $Cp_2Ti^{III}(\beta)$, forming $[Cp_2Ti^{III}(\beta)]^+$.

IP *vs.* pK_a: shows that IP increases with decreasing pK_a. The titanium metal centre is relatively more electron-deficient (with smaller pK_a) and consequently more energy is needed to remove an electron from $Cp_2Ti^{III}(\beta)$.

IP *vs.* ν_{CO}: shows that IP increases with increasing ν_{CO}. Decreased electron density on a metal centre results in higher CO infrared frequencies and larger IP.

IP *vs.* $E^{0'}$: shows that IP increases with increasing (less negative) formal reduction potential. A larger $E^{0'}$ implies more energy is needed to oxidise $Cp_2Ti^{III}(\beta)$, i.e., more energy is needed to remove an electron from $Cp_2Ti^{III}(\beta)$, and thus a larger IP.

The linear equations (y = mx + c) defining the relationship between IP and parameters shown in **Figure 3.80** are:

$$\chi_R + \chi_{R'} = 1.859(IP) - 5.182$$

$$E^{0'} = 508.4(IP) - 3466$$

$$\nu_{CO} = 121.8(IP) + 896.9$$

$$pK_a = -5.191(IP) + 35.73$$

This allows one to predict electronegativities of the R and R′ side groups, pK_a-values of uncoordinated β-diketone, carbonyl stretching frequencies (ν_{CO}) and the formal reduction potentials, $E^{0'}$, of $[Cp_2Ti^{IV}(\beta)]^+$ if the calculated ionization potential is known.

Table 3.42 Calculated ionization potential (IP), formal reduction potential, $E^{0'}$, (*vs.* Fc/Fc^+) and ν_{CO} of the titanium complexes $[Cp_2Ti(\beta)]^+ClO_4^-$, pK_a values for the indicated β-diketones $RCOCH_2COR'$ and group electronegativities of the R and R′ groups.

$[Cp_2(\beta)]^+ClO_4^-$	β-diketone		Complex		
	$(\chi_R + \chi_{R'})$	pK_a	$E^{0'}$ / mV	ν_{CO}	IP / eV
$[Cp_2(hfaa)]^+$	6.02	4.71	--	--	6.05
$[Cp_2(tfth)]^+$ **[5]**	5.11	6.50	-619	1566	5.53
$[Cp_2(tffu)]^+$ **[4]**	--	--	-624	1578	5.50
$[Cp_2(tfba)]^+$ **[6]**	5.22	6.3	-623	1554	5.53
$[Cp_2(tfaa)]^+$ **[3]**	5.35	6.3	-629	1592	5.67
$[Cp_2(ba)]^+$ **[7]**	4.55	8.70	-840	1542	5.19
$[Cp_2(thba)]^+$ **[8]**	4.31	9.01	-837	1519	5.14
$[Cp_2(dbm)]^+$ **[9]**	4.42	9.35	-823	1511	5.12
$[Cp_2(acac)]^+$ **[10]**	4.68	8.95	-864	1547	5.29
$[Cp_2(fca)]^+$	4.21	10.01	-903	--	5.06

[1] O. Kubaschewski, E.L. Evans and C.B. Alcock *Metallurgical Thermochemistry*, 4th edition, Oxford, UK, 1967, Table A, p. 304.
[2] M. Conradie, A. Kuhn, A. Muller and J. Conradie, *Acta Cryst*. **E62** (2006) 4717.
[3] M.M. Conradie, A.J. Muller and J. Conradie, *S. Afr. J. Chem*., **61** (2008) 13.
[4] V. Bertolasi, P. Gilli, V. Ferretti and G. Gilli, *J. Am. Chem. Soc*., 113 (1991) 4917.
[5] R.E. Kagarise, *J. Am. Chem. Soc.*, **77** (1995) 1377.
[6] J. Starý, *The Solvent Extraction of Metal Chelates*, MacMillan Company, New York, 1964, Appendix.
[7] W.C. du Plessis, T.G. Vosloo and J.C. Swarts, *J. Chem. Soc. Dalton Trans.*, (1998) 2507.
[8] M. Ellinger, H. Duschner and K. Starke, *J. Inorg. Nucl. Chem*., **40** (1978) 1063.
[9] T. Tsotetsi, *Synthetic, kinetic and electrochemical aspects of betadiketonato titanium(IV) complexes*, MSc Thesis, University of the Free State, R.S.A., 2006.
[10] N.F. Stuurman and J. Conradie, *J. Organomet. Chem.*, **694** (2009) 259.
[11] J. Conradie, *Chemical kinetics, electrochemistry and structural aspects of ferrocene-containing β-diketonato complexes of rhodium(I) and iridium(I)*, PhD Thesis, University of the Free State, R.S.A., 1999.
[12] P Klaas, Synthesis, electrochemical, kinetic and thermodynamic properties of new ferrocene-containing betadiketonato rhodium(I) complexes with biomedical applications, MSc Thesis, University of the Free State, R.S.A., 2002.
[13] G.J.J. Steyn, A. Roodt and J.G. Leipoldt, *Inorg. Chem.*, **31** (1992) 3477.
[14] E. Erasmus, J. Conradie, A. Muller and J.C. Swarts, *Inorg. Chim. Acta*, **360** (2007) 2277.
[15] D.K. Huggins and H.D. Kaesz, *Progr. Solid State Chem*., **1** (1964) 471.
[16] H.P. Fritz, *Advan. Organometal. Chem*., **1** (1964) 280.
[17] H. Colm, *J. Chem. Soc*., (1952) 4282.
[18] (a) P.A. Giguère and R. Savoie, *Can. J. Chem*., **40** (1962) 495. (b) O. Redlich, E.K. Holt and J. Bigeleisen, *J. Am. Chem*., **55** (1944) 13. (c) S.D. Ross, *Spectrochim. Acta*, **18** (1962) 495.
[19] G. Doyle and R.S. Tobias, *Inorg. Chem*., **6** (1967) 1111.
[20] N. Serpone and R.C. Fay, *Inorg. Chem*., **6** (1967) 1836.
[21] R.C. Fay and R.N. Lowry, *Inorg. Chem*., **6** (1967) 1512.
[22] R.C. Fay and R.N. Lowry, *Inorg. Chem*., **9** (1970) 2048.
[23] (a) S.H. Maron and J.B. Lando, *Fundamentals of Physical Chemistry*, Macmillan Publishing Co. Inc., New York, 1974, pp 376-383. (b) P.W. Atkins, *Physical Chemistry*, 5th edition, Oxford University Press, Oxford, 1994, pp 141-154, 277-289.
[24] K.J. Laidler, J.H. Meiser and B.C. Sanctuary, *Physical Chemistry*, 4th edition., Houghton Mifflin Company, New York, 2003, pp. 124, 151, 169.
[25] B.K. Keppler and M.E. Heim, *Drugs of the Future*, **3** (1998) 638.
[26] V.N. Kondratiev, *Bond dissociation Energies, Ionization Potentials and Electron Affinities*, Mauka Publishing House, Moscow, 1974.
[27] P.V. Rao, C.P. Rao, E.K. Wegelius, E. Kolemainen and K. Rissanen, *J. Chem. Soc. Dalton Trans*., (1999) 4469.
[28] E. Dubler, R. Buschmann and H.W. Schmalle, *J. Inorg. Biochem*., **95** (2003) 97. CSD Ref.: JABYAN
[29] W.J. Hehre, *A Guide to Molecular Mechanisms and Quantum Chemical Calculations*, Wavefunction Inc., 2003, pp.153, 181.
[30] S.N. Brown, E.T. Chu, M.W. Hull and B.C. Noll, *J. Am. Chem. Soc.*, **127** (2005) 16010.
[31] R.C. Weast, Handbook of Chemistry and Physics, 63th edn., The Chemical Rubber Co., Ohio, pp F180-F181.
[32] R.D.G. Jones, *Acta Crystallogr., Sect. B: Struct. Crystallogr. Cryst. Chem*., **32** (1976) 1224. CSD Ref. THTFBD
[33] R.D.G. Jones, *Acta Crystallogr., Sect. B: Struct. Crystallogr. Cryst. Chem*., **32** (1976) 1807. CSD Ref. DBEZLM02
[34] R. Boese, M. Yu Antipin, D. Blaser and K.A. Lyssenko, *J. Phys. Chem.*, **102** (1998) 8654. CSD Ref.: LIWPIQ
[35] W. Winter, K-P. Zeller and S. Berger, *Z. Naturforsch, B: Chem. Sci*., **34** (1979) 1606. CSD Ref.: BZOYAC02
[36] Cambridge Structural Database (CSD), January 2007 updates.
[37] M. Casado, J.J. Perez-Torrente, M.A. Ciriano, A.J. Edwards, F.J. Lahoz and L.A. Oro, *Organometallics*, **18** (1999) 5299. CSD Ref.: LIHDUB
[38] A.M. Bond, R. Colton, U. Englert, H. Hűgel and F. Merken, *Inorg. Chim. Acta*, **235** (1995) 117. CSD Ref.: HIDPOZ
[39] S.S. Yun, I-H. Suh, E.H. Kim and S.K. Lee, *J. Coord. Chem.*, **51** (2000) 219. CSD Ref.: MOYJEP
[40] S.S. Yun, I-H. Suh, E.H. Kim and S.K. Lee, *J. Coord. Chem.*, **51** (2000) 219. CSD Ref.: MOYJIT
[41] N.I. Barnard, *Synthesis, structural aspects and electrochemistry of ferrocene-containing betadiketonato titanium(IV) complexes with biomedical applications*, MSc Thesis, University of the Free State, R.S.A., 2006.
[42] W.H. Baier, *Acta Cryst*., **9** (1956) 515.

[43] A. Bodner, P. Jeske, T. Weyhermuller, K. Wieghardt, E. Dubler, H. Schmalle and B. Nuber, *Inorg. Chem.*, **31** (1992) 3737.
[44] S.N. Brown, E.J. Chu, M.W. Hull and B.C. Noll, *J. Am. Chem. Soc*., **127** (2005) 16010. CSD Ref.: RAWWES
[45] S.N. Brown, E.J. Chu, M.W. Hull and B.C. Noll, *J. Am. Chem. Soc*., **127** (2005) 16010. CSD Ref.: RAWWIW
[46] P.V. Rao, C.P. Rao, E.K. Wegelius, E. Kolemainen and K. Rissanen, *J. Chem. Soc*. Dalton Trans., (1999) 4469. CSD Ref.: HOXTIX
[47] P.H. Bird, A.R. Fraser and C.F. Lau, *Inorg. Chem*., **12** (1973) 1322. CSD Ref.: ACIPTI
[48] K. Matilainen, I. Mutikainen and M. Leskela, *Acta Chem. Scand*., **50** (1996) 755. CSD Ref.: TOPZUT
[49] C. Glidewell, G.M. Turner and G. Ferguson, *Acta Crystallogr. Sect C. Cryst. Struct. Commum*., 52 (1996) 11. CSD Ref.: ZITROJ
[50] E. Dubler, R. Buschmann and H.W. Schmalle, *J. Inorg. Biochem*., **95** (2003) 97. CSD Ref.: JABYAN
[51] K. Watenpaugh and C.N. Caughlan, *Inorg. Chem*., **6** (1967) 963. CSD Ref.: OBPDTI
[52] Z. Quan-Fa, M. Fang-Ming and L. Xiao-Lao, *Jiegou Huaxue (Chin.) (Chinese J. Struct. Chem.)*, **11** (1992) 453. CSD Ref.: KUYHOB
[53] "Tables of Interatomic Distances and Configuration in Molecules and Ions" Supplement Special Publication No. 18, The Chemical Society, London, 1065, pp M20S.
[54] S.I. Troyanov and O.Y. Gorbenko, *Polyhedron* **16** (1997) 777.
[55] J.C. Huffman, K.G. Molay, J.A. Marsella and K.G. Caulton, *J. Am. Chem. Soc*., **102** (1980) 3009.
[56] P. Corradini and S. Allegra, *J. Am. Chem. Soc*., **81** (1959) 5510.
[57] K. Watenpaugh and C.N. Caughlan, *Inorg Chem* **5** (1966) 1782.
[58] R.C. Fay, T.J. Pinnavaia, N. Serpone and R.N. Lowry, *Proceedings of the 9th International Conference on Coordination Chemistry*, St Moritz-Bad, Switzerland, Sept 5-9, 1966, pp 486.
[59] A. Kuhn, A. Muller and J. Conradie, *Acta Cryst*., E**63** (2007).
[60] F.H. Allen, *Acta Cryst*., B**58**, (2002) 380.
[61] (a) S.I. Troyanov, V. Varga and K. Mach, *J. Organomet. Chem*., **201** (1991) 402. (b) J.L. Petersen, *Inorg. Chem*., **19** (1980) 181. (c) A.C. Skapsky and P.G.H. Troughton, *Acta Cryst*., **B26** (1970) 716.
[62] MINSQ, Non-Linear parameter estimation and model development, least squares parameter optimisation V3.12, MicroMath Scientific Software, Salt Lake City, UT, 1990.
[63] J.H. Espenson, *Chemical Kinetics and Reaction Mechanisms*, 2nd edition., McGraw-Hill, New York, 1995, pp. 46-49.
[64] J.H. Espenson, *Chemical Kinetics and Reaction Mechanisms*, 2nd edition., McGraw-Hill, New York, p. 156.
[65] P.W. Atkins, *Physical Chemistry*, 5th edition., Oxford University Press, Oxford, 1994, p. 939 – 950.
[66] L. Gastaldi and L. Scaramuzza, *Cryst. Struct. Commun*., **9** (1980) 469. CSD Ref.: CSACTI
[67] (a) S. Kida, *Bull. Chem. Soc. Jap*., **34** (1961) 962. (b) Y. Marcus and I. Eliezer, *J. Phys. Chem*., **66** (1962) 1661.
[68] J.H. Espenson, *Chemical Kinetics and Reaction Mechanisms*, 2nd edition., McGraw-Hill, New York, 1995, pp. 70-75.
[69] R.C. Fay and R.N. Lowey, *Inorg. Chem*., **13** (1974) 1309.
[70] W.C. du Plessis, J.C. Erasmus, G.J. Lamprecht, J. Conradie, T.S. Cameron, M.A.S. Aquino and J.C. Swarts, *Can. J. Chem*., **77** (1999) 378.
[71] N.G. Tsierkezos, *J. Solution Chem*., **36** (2007) 289.
[72] R.C. Buchta and D.H. Evans, *J. Electrochem. Soc.: Electrochemical Science*, **117** (1970) 1494.
[73] P.J. Erving and C.M. Callahan, *J. Am. Chem. Soc*., **77** (1955) 2077.
[74] N.R. de S. Basso, P.P. Greco, C.L.P. Carone, P.R. Livotto, L.M.T. Simplício, Z.N. da Rocha, G.B. Galland and J.H.S. dos Santos, *Journal of Molecular Catalysis A: Chemical*., **267** (2007) 129.
[75] A.J. Bard and L.R. Faulkner, *Electrochemical Methods: Fundamentals and Applications*, Wiley, New York, 1980 (Chapter 6).
[76] A. Chaloyard, A. Dormond, J. Tirouflet and N. El Murr, J. Chem. Soc. Chem. Commun., (1980) 214.
[77] P. Sobota, K. Przybylak, J.Utko, LB. Jerzykiewicz, A.J.L.Pombeiro, M.F.C.Guedes da Silva and K. Szczegot, *Chem. Eur. J*. **7** (2001) 951.
[78] W.J. Hehre, A Guide to Molecular Mechanisms and Quantum Chemical Calculations, Wavefunction Inc. 2003, pp.153, 181.

4 Experimental

In this chapter all materials, apparatus and experimental procedures (reaction conditions and techniques) are described.

4.1 MATERIALS

Solid reagents (Merck, Aldrich and Sigma) were used without further purification while liquid reactants were distilled prior to use. Solvents were dried and freshly distilled prior to use and water was double distilled. Special care was taken when drying solvents with high water absorbing capacity (MeOH, EtOH, THF and especially CH_3CN) compared to solvents with low water-absorbing capacity (*n*-Hexane, toluene, DCM, chloroform, diethyl ether). Drying methods included predrying solvents for at least 12 h, followed by refluxing for 6 - 8 hrs over Na wire for hexane, toluene and THF and over CaH_2 for CH_3CN, DCM, $CHCl_3$ and EtOH.

4.2 MEASUREMENTS

Listed below are the instruments used to make the corresponding measurements

NMR spectra (δ): ^1H and ^{19}F NMR spectra were recorded on either a Bruker Advance DPX 300 [^1H (300.130 MHz)] or a Bruker Advance II 600 [^1H (600.130 MHz) and ^{19}F (564,686 MHz)] spectrometer. Chemical shifts are reported as δ values, referenced to $SiMe_4$ (0.00 ppm) for the ^1H spectra and $CFCl_3$ (0.00 ppm) for the ^{19}F spectra. Abbreviations used when reporting chemical shift positions are: s = singlet, d = doublet, t = triplet, m = multiplet, br = broad hump (symmetrical or irregular), s_{br} = broad singlet, d_{br} = broad doublet, t_{br} = broad triplet and (abbreviations for selected ring systems), Cp = C_5H_5, Ph = C_6H_5, Ph_{NO2} = $C_6H_4NO_2$, Th = C_4H_3S and Fu = C_4H_3O.

IR spectra (cm^{-1}): Digilab FTS 2000 Fourier Transform spectrometer utilising a He-Ne laser at 632.6 nm. Abbreviations used when reporting intensity of IR peaks: vs = very strong, s = strong, m = medium and w = weak.

UV/vis spectra: Cary 50 Probe UV/Visible Spectrophotometer.

Melting points (M.p.): All melting points are uncorrected and were determined either with a Reichert Thermopan microscope fitted with a Koffler hot stage (up to 200 °C) or with an Olympus BX51 microscope fitted with a Linkam-THMS600 hot stage (up to 250 °C).

4.3 CRYSTALLOGRAPHIC MEASUREMENTS

General parameters

The crystals were mounted on glass fibres and used directly for the crystallographic analysis. The X-ray intensity data were measured on either a (a) Bruker SMART 1K CCD diffractometer area detector or (b) Bruker X8 Apex II 4K Kappa CCD diffractometer area detector. Both instruments were equipped with a graphite monochromator and Mo-Kα fine-focus sealed tube (λ = 0.71073 Å) operated at 1.5 KW power (50 KV, 30 mA).

All the structures were solved by the direct methods package SIR97[1] and refined using the WinGX software package[2] incorporating SHELXL.[3] The largest peaks on the final difference electron densities and the deepest holes were all within 1 Å from non-hydrogen atoms and presented no physical meaning in the final refinements. The protons were placed in geometrically idealized positions (C–H = 0.93–0.98 Å) and constrained to ride on their parent atoms with $U_{iso}(H)$ = x $U_{eq}(C)$ where x = 1.2 for aromatic and x = 1.5 for methyl H atoms. Disorders on the perchlorate ions (ClO_4^-) and CF_3 moieties and those on the Cp and chelate ba rings were treated with various geometrical and vibrational restraints. Atomic scattering factors were taken from the International Tables for Crystallography Volume C.[4] The molecular plot was drawn using the DIAMOND program[5] with a 30% thermal envelope probability for non-hydrogen atoms. Hydrogen atoms were drawn as fixed sized spheres with a radius of 0.135 Å.

Machine specific parameters

Bruker X8 Apex II 4K Kappa CCD diffractometer

Nine crystals were collected: $[Cp_2Ti(tffu)]^+ClO_4^-$, $[Cp_2Ti(ba)]^+ClO_4^-$, $[Cp_2Ti(maa)]^+ClO_4^-$, $Ti(acac)_2$biphen, $Ti(ba)_2$biphen, $\{Ti(tfaa)_2Cl\}_2(\mu\text{-}O)$, $\{Ti(hfaa)_2Cl\}_2(\mu\text{-}O)$, $\{Ti(hfaa)_2\}_2(\mu\text{-}O)$ (μ-biphen) and $[Ti(hfaa)_2(\mu\text{-}O)]_4$.

The initial unit cell and data collections were achieved by the Apex2 software[6] utilizing COSMO[7] for optimum collection of more than a hemisphere of reciprocal space. The frames were integrated using a narrow frame integration algorithm and reduced with the Bruker SAINT-Plus and XPREP software packages.[8] Analysis of all of the data collections showed no significant decay during the data collection. Data were corrected for absorption effects using the multi-scan technique SADABS.[11] Variable parameters are listed in the Table below.

Crystal	Scans	№ of frames	Exposure time / s	Detector distance / cm	Temp / ℃
$[Cp_2Ti(tffu)]^+ClO_4^-$ [5]	φ ω	948	20	3.75	-123
$[Cp_2Ti(ba)]^+ClO_4^-$ [7]	φ ω	473	180	3.75	20
$[Cp_2Ti(maa)]^+ClO_4^-$ [11]	φ ω	1688	10	3.75	-100
$Ti(acac)_2$biphen [36]	φ	632	20	3.75	-173
$Ti(ba)_2$biphen [32]	φ ω	1149	60	3.75	-173
$\{Ti(tfaa)_2Cl\}_2(\mu\text{-}O)$ [42]	φ ω	704	120	3.75	-173
$\{Ti(hfaa)_2Cl\}_2(\mu\text{-}O)$ [43]	φ ω	1143	35	3.75	-173
$\{Ti(hfaa)_2\}_2(\mu\text{-}O)(\mu\text{-biphen})$ [44]	φ ω	949	20	3.90	-173
$[Ti(hfaa)_2(\mu\text{-}O)]_4$ [45]	φ ω	1373	8	5.30	-173

Bruker SMART 1K CCD diffractometer

Three crystals were collected: $[Cp_2Ti(tfba)]^+ClO_4^-$, $[Cp_2Ti(tfth)]^+ClO_4^-$, $[Cp_2Ti(dbm)]^+ClO_4^-$. The initial unit cell and data collections were achieved by the SMART-NT software[9] with more than a hemisphere of reciprocal space collected. The frames were integrated using a narrow frame integration algorithm and reduced with the Bruker SAINT-Plus and XPREP software packages.[10] Analysis of all of the data collections showed no significant decay during the data collection. Data were corrected for absorption effects using the multi-scan technique SADABS.[11] Collection parametrs are listed in the Table below.

Crystal	Scans	№ of frames	Exposure time / s	Detector distance / cm	Temp / ℃
$[Cp_2Ti(tfba)]^+ClO_4^-$ [6]	ω	1350	10	4.00	20
$[Cp_2Ti(tfth)]^+ClO_4^-$ [4]	ω	1350	10	4.00	20
$[Cp_2Ti(dbm)]^+ClO_4^-$ [9]	ω	1350	10	4.00	20

Crystal growing conditions

Tetrahedral Structures:

$[Cp_2Ti(\beta)]^+ ClO_4^-$ Single crystals were obtained by slow diffusion of *n*-hexane into a concentrated solution of the complex in acetone for the fluorinated complexes, $[Cp_2Ti(tfba)]^+$, $[Cp_2Ti(tfth)]^+$ and $[Cp_2Ti(tffu)]^+$) and in DCM for the non-fluorinated complexes, $[Cp_2Ti(ba)]^+$, $[Cp_2Ti(dbm)]^+$ and $[Cp_2Ti(maa)]^+$) at room temperature.

Octahedral Structures

$Ti(\beta)_2$(biphen) Single crystals of $Ti(acac)_2$biphen and $Ti(ba)_2$biphen were obtained by slow evaporation of a solution of the complex in chloroform at room temperature.

$\{Ti(\beta)_2Cl\}_2(\mu\text{-}O)$ Single crystals of $\{Ti(tfaa)_2Cl\}_2(\mu\text{-}O)$ and $\{Ti(hfaa)_2Cl\}_2(\mu\text{-}O)$ formed from a sealed $CDCl_3$ solution of the monomeric $Ti(tfaa)_2Cl_2$ and $Ti(hfaa)_2Cl_2$ complexes respectively, at room temperature.

$\{Ti(hfaa)_2\}_2(\mu\text{-}O)$ (μ-biphen) Single crystals were obtained by slow diffusion of *n*-hexane into a concentrated solution of the monomeric $Ti(hfaa)_2$biphen complex in DCM at room temperature.

$[Ti(hfaa)_2(\mu\text{-}O)]_4$ Single crystals of $[Ti(hfaa)_2(\mu\text{-}O)]_4$ formed from a sealed $CDCl_3$ solution of the monomeric $Ti(hfaa)_2Cl_2$ complex at room temperature.

4.4 KINETIC MEASUREMENTS

UV/vis Kinetics Substitution reactions were monitored on the UV/vis (by monitoring the change in absorbance at the indicated wavelength) spectrophotometer. All kinetic measurements were monitored under pseudo-first-order conditions with [ligand] 10 to 200 times the concentration of the Ti(IV) complex in CH_3CN solution with [Ti complex] ≅ 0.1 mmol dm^{-3}. Kinetic measurements, under *pseudo*-first-order conditions for different concentrations of Ti complex at a constant [ligand], confirmed that the concentration of the Ti complex did not influence the value of the observed kinetic rate constant. A linear relationship between UV absorbance, A, and concentration, C, confirmed the validity of the Beer Lambert law ($A = \varepsilon C l$ with l = path length = 1 cm) for the complexes at experimental wave lengths, λ_{max}. The observed first-order rate constants were obtained from least-square fits of absorbance *vs* time data.[12] Stability of complexes in solution was confirmed by overlay spectra over 24 hours.

NMR Kinetics NMR kinetics was followed by monitoring the change in integration units of the specified signals with time. The observed first-order rate constants were obtained from least-squares fits of integration units (NMR) *vs.* time data.[12] Kinetics measurements were measured both under *pseudo* first order (10x and 40x excess) and second order conditions. ^1H NMR spectra of the title compounds after 48 hours in solution of $CDCl_3$ confirmed stability in solution.

Kinetic Calculations Pseudo-first-order rate constants, k_{obs}, were calculated by fitting kinetic data[12] to the first-order equation[13] $[A]_t = [A]_0\ e^{(-k_{obs}\ t)}$ with $[A]_t$ and $[A]_0$ the concentration of the indicated species at time t and at t = 0 (UV/vis). The experimentally determined pseudo first order rate constants were converted to second order rate constants, k_2, by determining the slope of the linear plots of k_{obs} against the concentration of the incoming biphenolato ligand. Non-zero intercepts implied that $k_{obs} = k_2[\text{ligand}] + k_s$ and that the first order rate constant for a solvent pathway, k_s, in the proposed reaction mechanism exists. All kinetic mathematical fits were done utilizing the fitting program MINSQ.[12] The error of all the data are presented according to crystallographic conventions, for example, k_{obs} = 0.0236(1) s^{-1} implies $k_{obs} = (0.0236 \pm 0.0001)\ s^{-1}$.

For two consecutive reactions A and B, the data was processed *via* the consecutive reaction model and the normal single stage treatement.[13]

$$A \xrightarrow{k_A} B \xrightarrow{k_B} C$$

Normal single treatement	Consecutive reaction treatement
$[A]_t = [A]_0\, e^{(-k_A t)}$	$[B]_t = \frac{k_A [A]_0}{k_B - k_A} [e^{(-k_A t)} - e^{(-k_B t)}]$
$[B]_t = [B]_0\, e^{(-k_B t)}$	$[C] = [A]_0 \left\{ 1 - \frac{1}{k_B - k_A} [k_B e^{(-k_A t)} - k_A e^{(-k_B t)}] \right\}$

The activation parameters were determined from the Eyring relationship,[13] $\ln\frac{k}{T} = -\frac{\Delta H^{\#}}{RT} + \frac{\Delta S^{\#}}{R} + \ln\frac{k_B}{h}$ with $\Delta H^{\#}$ = activation enthalpy, $\Delta S^{\#}$ = activation entropy, k = rate constant, k_B = Boltzmann's constant, T = temperature, h = Planck's constant, R = universal gas constant and the activation free energy $\Delta G^{\#} = \Delta H^{\#} - T\Delta S^{\#}$.[13]

4.5 ELECTROCHEMICAL MEASUREMENTS

Cyclic voltammetry measurements were performed on 2.0 mmol dm^{-3} solutions of the T(IV) complexes and 3.0 mmol dm^{-3} solutions of the β-diketones in dry CH_3CN (spectroscopic grade, HPCL) containing 0.1 mol dm^{-3} $[NBu_4][PF_6]$, (Fluka electrochemical grade) as supporting electrolyte (Cyclic voltammograms for $Ti(\beta)_2Cl_2$ complexes were performed in DCE, spectroscopic grade, HPCL). The measurements were conducted under a blanket of purified argon at 25.0˚C utilizing a BAS 100 B/W electrochemical workstation interfaced with a personal computer. A three-electrode cell, comprised of a Pt auxiliary electrode, a glassy carbon (surface area 0.0707 cm^2) working electrode and an Ag/Ag^+ (0.010 mol dm^{-3} $AgNO_3$ in CH_3CN) reference electrode[14] mounted on a Luggin capillary was used.[15,16] All temperatures were kept constant to within 0.5˚C. Successive experiments under similar experimental conditions showed that all formal reduction and oxidation potentials were reproducible to within 5 mV. In this work all cited potentials are referenced against Fc/Fc^+ couple as suggested by IUPAC.[17] Electrodes were cleaned by polishing with 3 μm followed by 1 μm Diapat diamond paste on an abrasive cloth (in a figure of 8 motions), rinsed with ethanol, water and CH_3CN and finally dried before each experiment. Scan rates were between 50 and 2000 mV s^{-1}.

4.6 COMPUTATIONAL MEASUREMENTS

Computational method for transition state kinetics (Section 3.4.1.1)

Calculations were performed with the B3LYP[18] (B3 Becke 3-parameter exchange and Lee-Yang-Parr correlation) functional for both exchange and correlation, as implemented in the Gaussian 03 package.[19] Geometries were optimized in gas phase with a triple-ζ basis set, 6-311G(d,p). Solvation effects were computed by performing single-point calculations on the optimized geometries with the IEFPCM model, using acetonitrile as solvent and a dielectric constant of 36.64. Thermochemical quantities were calculated from frequency calculations at the same level of theory as optimizations. The frequency calculations were also employed to confirm the nature of the obtained stationary points, which exhibited only positive eigenvalues for minima and one imaginary frequency for transition states.

Computational method for isomer distribution (Section 3.2.3.2) and ionisation potentials (Section 3.5.5.3)

Density Functional Theory (DFT) calculations were carried out using the Amsterdam Density Functional 2007 (ADF) program system[20] with the OLYP[21] (OPTX exchange functional[21] combined with the Lee-Yang-Parr correlation[22]) or PW91[23] (Perdew-Wang, 1991 exchange and correlation) functional. The TZP (Triple ζ polarized) basis set, a fine mesh for numerical integration (5.2 for geometry optimizations and 6.0 for frequency calculations), a spin-restricted (gas-phase) formalism and full geometry optimization with tight convergence criteria as implemented in the ADF 2007 program, were used. The accuracy of the computational method was evaluated by comparing the root-mean-square deviations (RMSD's) between the optimized molecular structure and the crystal structure, using the non-hydrogen atoms in the molecule. RMSD values were calculated using the "RMS Compare Structures" utility in ChemCraft Version 1.5.[24] Whether artificially generated atomic coordinates or coordinates obtained from X-ray crystal data were used in the input files, optimizations for each compound resulted in the same minimum energy optimized geometry. Optimized structures were verified as a minimum through frequency calculations.

4.7 SYNTHESIS

4.7.1 O,O'- Donor Ligands

4.7.1.1 β-Diketones: Hβ

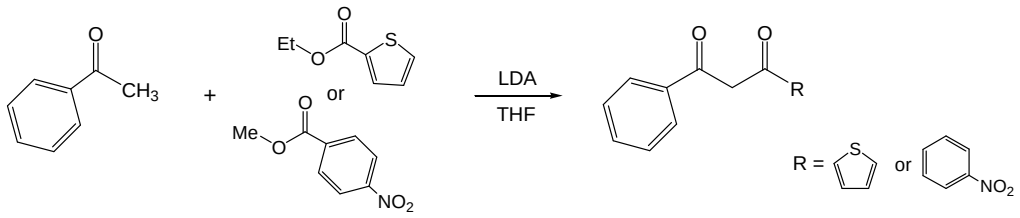

The reaction was performed under rigorous Schlenk conditions: the system was flame-dried and degassed with Ar for 30 min. An Ar atmosphere was maintained throughout the reaction. Acetophenone (1.2015 g, 10 mmol) was dissolved in THF (1.00 ml), transferred to a 3-neck flask and stirred for a few minutes. Lithium diisopropylamide, LDA, (5.60 ml of a 1.8 mol dm^{-3} solution in hexane, 10.0 mmol) was added slowly while stirring and kept cool on an ice-bath. The transparent yellow/brown solution was stirred for a further 15 min at 0 °C. The ester (ethyl 2-thiophenecarboxylate (1.562 g, 10 mmol) or methyl 4-nitro benzoate (1.8115 g, 10 mmol) was added and the reaction mixture was allowed to stir for 16 h at room temperature. Diethyl ether (20 ml) was added to the solution inducing precipitation. The precipitation was filtered, washed with diethyl ether (2 x 20 ml) and acidified with HCl (50 ml, 0.3 mol dm^{-3}) until 1 < pH < 4, stirring until solid dissolved. The product was extracted with diethyl ether (3 x 50 ml). The combined extracts were thoroughly washed with water, dried (anhydrous $MgSO_4$) and the solvent removed under reduced pressure. Recrystallisation from diethyl ether (for Hthba) and DMF (for Hnba) gave spectroscopically pure β-diketone product.

(a) **Hthba [1]**

1-phenyl-3-(2-thenoyl)-1,3-propanedione
(thenoylbenzoylacetone)

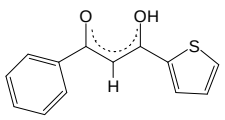

Yield 18 % (0.4192 g). M.p. = 76 ˚C. Colour: light orange. ^{1}H NMR: (600 MHz, δ/ppm, $CDCl_3$) enol isomer: 6.72 (s, 1H, CH), 7.20 (t, 1H, ThH), 7.47-7.58 (m, 3H, PhH), 7.67 (d, 1H, ThH), 7.84 (d, 1H, ThH), 7.97 (d, 2H, PhH) *Spectrum 11.*

***(b)* Hnba [2]**

1-phenyl-3-(4-nitrophenyl)-1,3-propanedione
(nitrophenylbenzoylacetone)

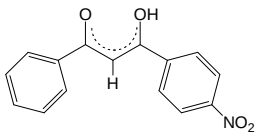

Yield 5 % (0.1261 g). M.p. = 141 ˚C. Colour: light yellow. ^{1}H NMR: (600 MHz, δ/ppm, $CDCl_3$) enol isomer: 6.91 (s, 1H, CH), 7.51 (t, 2H, PhH), 7.60 (t, 1H, PhH), 8.01 (d, 2H, PhH), 8.14 (d, 2H, $Ph_{NO2}H$), 8.33 (d, 2H, $Ph_{NO2}H$) *Spectrum 12.*

4.7.2 Tetrahedral Complexes

4.7.2.1 Mono(β-diketonato) Ti(IV) complexes: $[Cp_2Ti(\beta)]^+ClO_4^-$

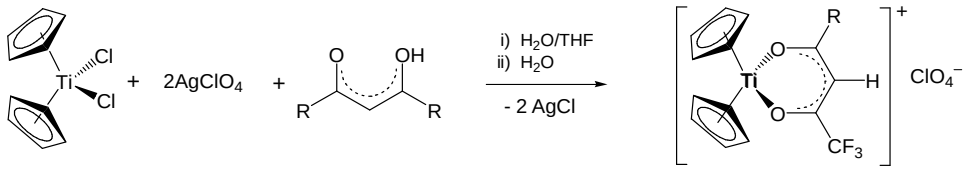

Different procedures were followed for the reactions with (i) water-insoluble β-diketones (Htfaa, Htfth, Htffu, Htfba, Hba, Hthba and Hdbm) and (ii) water-soluble β-diketones (Hacac and Hmaa). The general procedures are as follows:

(i) Titanocene dichloride, Cp_2TiCl_2, (0.249 g / 1.0 mmol) was dissolved in H_2O/THF, 2:1 mixture (9 ml) and stirred under nitrogen for ½ hr. The solution was cooled down on an ice-bath before silver perchlorate, $AgClO_4$, (0.406 g / 1.96 mmol) dissolved in water (2 ml) was added. The cooled mixture was stirred for a further ½ hr. $AgClO_4$ is light sensitive and the reaction must be light protected. A white precipitate, AgCl, was filtered off and washed with H_2O/THF (2 ml). The β-diketone (2.0 mmol) dissolved in cold THF (2 ml, *ca.* 4 ℃) was added dropwise to the orange filtrate while stirring causing a slight colour change. After ½ hr of stirring the solution was removed and left for 2 to 7 days to precipitate (turned brown/black); ba, dbm, thba (2 days) and CF_3-containing β-diketons, tfaa, tfth, tffu and tfba (7 days). The dark sticky precipitate was collected and washed with water (2x 100 ml) and diethyl ether (4x 50 ml). Recrystallisation from DCM/hexane afforded pure product. The product colour ranges from dark brown to reddish brown to purple brown.

(ii) Titanocene dichloride, Cp_2TiCl_2, (0.249 g / 1.0 mmol) was suspended in water (8 ml) and stirred under nitrogen for 1 hr. Silver perchlorate, $AgClO_4$, (0.406 g / 1.96 mmol) dissolved in water (2 ml) was added and the mixture stirred for a further ½ hr. $AgClO_4$ is light sensitive and the reaction must be light protected. A white precipitate, AgCl, was filtered off and washed with water (2 ml). The red filtrate was cooled on an ice-bath and cold β-diketone (Hacac or Hmaa) was added in large excess (4 ml, *ca.* 4 °C) dropwise while stirring. A grey-purple (acac) and purple (maa) precipitate formed immediately, which was filtered off and washed with water and diethyl ether.

(a) **$[Cp_2Ti(tfaa)]^+ClO_4^-$ [3]**

Bis(η^5-cyclopentadienyl) (trifluoroacetylacetonato-O,O') titanium(IV) perchlorate

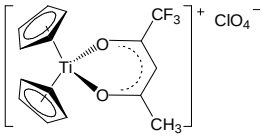

Yield 38 % (0.1642 g). M.p. = 194 ˚C. ν_{CO} = 1592 cm^{-1}. Colour: dark brown. ^1H NMR (300 MHz, δ/ppm, acetone-d_6): 2.63 (s, 3H, CH_3), 6.89 (s, 1H, CH), 7.08 (s, 10H, 2x CpH) *Spectrum 21*.

(b) **$[Cp_2Ti(tfth)]^+ClO_4^-$ [4]**

Bis(η^5-cyclopentadienyl) (trifluorothenoylacetonato-O,O') titanium(IV) perchlorate

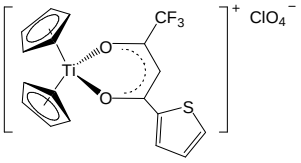

Yield 48 % (0.2398 g). M.p. = 191 ˚C. ν_{CO} = 1566 cm^{-1}. Colour: dark brown. ^1H NMR (300 MHz, δ/ppm, acetone-d_6): 7.13 (s, 10H, 2x CpH) , 7.38 (s, 1H, CH), 7.49 (t, 1H, ThH), 8.42 (d, 1H, ThH), 8.56 (d, 1H, ThH) *Spectrum 22*.

(c) **$[Cp_2Ti(tffu)]^+ClO_4^-$ [5]**

Bis(η^5-cyclopentadienyl) (trifluorofuroylacetonato-O,O') titanium(IV) perchlorate

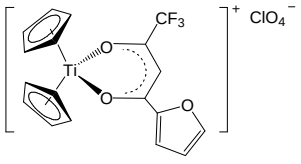

Yield 51 % (0.2501 g). M.p. = 195 ˚C. ν_{CO} = 1578 cm^{-1}. Colour: brown. ^1H NMR (300 MHz, δ/ppm, acetone-d_6): 7.00 (t, 1H, FuH), 7.12 (s, 10H, 2x CpH), 7.18 (s, 1H, CH), 8.03 (d, 1H, FuH), 8.26 (d, 1H, FuH) *Spectrum 23*.

(d) **$[Cp_2Ti(tfba)]^+ClO_4^-$ [6]**

Bis(η^5-cyclopentadienyl) (trifluorobenzoylacetonato-O,O') titanium(IV) perchlorate

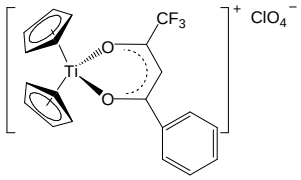

Yield 51 % (0.2525 g). M.p. = 200 ˚C. ν_{CO} = 1554 cm^{-1}. Colour: metallic brown. ^1H NMR (300 MHz, δ/ppm, acetone-d_6): 7.16 (s, 10H, 2x CpH), 7.55 (s, 1H, CH), 7.69 (t, 2H, PhH), 7.87 (t, 1H, PhH), 8.35 (d, 2H, PhH) *Spectrum 24*.

(e) **$[Cp_2Ti(ba)]^+ClO_4^-$ [7]**

Bis(η^5-cyclopentadienyl) (benzoylacetonato-O,O') titanium(IV) perchlorate

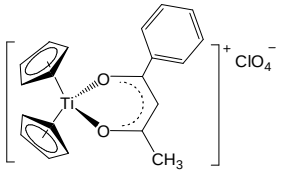

Yield 64 % (0.2810 g). M.p. = 204 ˚C. ν_{CO} = 1542 cm^{-1}. Colour: purple/ brown. ^1H NMR (300 MHz, δ/ppm, acetone-d_6): 2.48 (s, 3H, CH_3), 6.99 (s, 10H, 2x CpH), 7.20 (s, 1H, CH), 7.60 (t, 2H, PhH), 7.70 (t, 1H, PhH), 8.14 (d, 2H, PhH) *Spectrum 25*.

(f) **$[Cp_2Ti(thba)]^+ClO_4^-$ [8]**

Bis(η^5-cyclopentadienyl) (thenoylbenzoylacetonato-O,O') titanium(IV) perchlorate

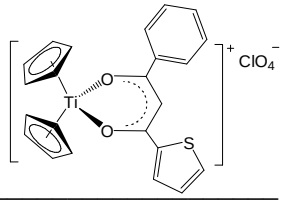

Yield 49 % (0.2483 g). M.p. > 200 ˚C. ν_{CO} = 1519 cm^{-1}. Colour: red/ brown. ^1H NMR (300 MHz, δ/ppm, acetone-d_6): 7.06 (s, 10H, 2x CpH), 7.42 (t, 2H, PhH) 7.63 (t, 3H, PhH), 7.74 (s, 1H, CH), 8.17 (d, 1H, $Ph_{NO2}H$), 8.23 (d, 2H, $Ph_{NO2}H$), 8.42 (d, 1H, $Ph_{NO2}H$) *Spectrum 26*.

(g) **$[Cp_2Ti(dbm)]^+ClO_4^-$ [9]**

Bis(η^5-cyclopentadienyl) (dibenzoylmethanato-O,O') titanium(IV) perchlorate

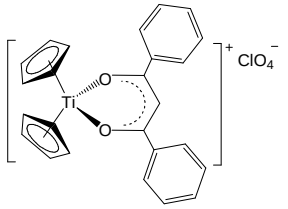

Yield 72 % (0.3621g). M.p. = 220 ˚C. ν_{CO} = 1511 cm^{-1}. Colour: red/ brown. ^1H NMR (300 MHz, δ/ppm, acetone-d_6): 7.06 (s, 10H, 2x CpH), 7.63 (t, 4H, 2x PhH), 7.75 (t, 2H, 2x PhH), 7.86 (s, 1H, CH), 8.29 (d, 4H, 2x PhH) *Spectrum 27*.

***(h)* $[Cp_2Ti(acac)]^+ClO_4^-$ [10]**

Bis(η^5-cyclopentadienyl) (acetylacetonato-O,O') titanium(IV) perchlorate

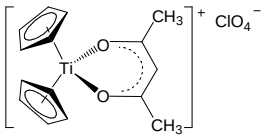

Yield 86 % (0.3229 g). M.p. > 200 °C. ν_{CO} = 1547 cm^{-1}. Colour: grey-purple. ^1H NMR (300 MHz, δ/ppm, acetone-d_6): 2.30 (s, 6H, 2x CH_3), 6.36 (s, 1H, CH), 6.90 (s, 10H, 2x CpH) *Spectrum 28*.

***(i)* $[Cp_2Ti(maa)]^+ClO_4^-$ [11]**

Bis(η^5-cyclopentadienyl) (methylacetylacetonato-O,O') titanium(IV) perchlorate

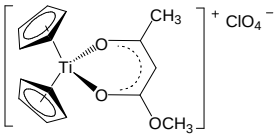

Yield 68 % (0.2688 g). M.p. > 200 ˚C. ν_{CO} = 1562 cm^{-1}. Colour: purple. ^1H NMR (300 MHz, δ/ppm, acetone-d_6): 2.33 (s, 3H, CH_3), 3.98 (s, 3H, OCH_3), 5.66 (s, 1H, CH), 7.00 (s, 10H, 2 x C_5H_5) *Spectrum 29.*

4.7.2.2 Mono(aryl-diolato) Ti(IV) complex: $[Cp_2Ti(L)]$

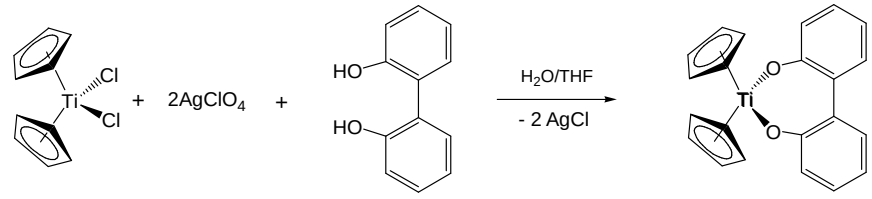

Titanocene dichloride, Cp_2TiCl_2, (0.249 g / 1.0 mmol) was dissolved in H_2O/THF, 2:1 mixture (9 ml) and stirred under nitrogen for ½ hr. The solution was cooled down on an ice-bath before silver perchlorate, $AgClO_4$, (0.406 g / 1.96 mmol) dissolved in water (2 ml) was added. The cooled mixture was stirred for a further ½ hr. $AgClO_4$ is light sensitive and the reaction must be light protected. A white precipitate, AgCl, was filtered off and washed with H_2O/THF (2 ml). 2,2'-biphenol (0,372 g, 2 mmol) dissolved in cold THF (2 ml, *ca*. 4 °C) was added dropwise to the clear orange filtrate while stirring with an immediate colour change (orange to dark red). After ½ hr of stirring the solution was removed and left for 4 days to precipitate at room temperature. The precipitate was washed with water, filtered and

dissolved in diethyl ether. The solvent was removed with reduced pressure,from filtrate and the product was washed with MeOH to remove unreacted biphenol.

$Cp_2Ti(biphen)$ [12]

Bis(η^5-cyclopentadienyl) (biphenyldiolato-O,O') titanium(IV) perchlorate

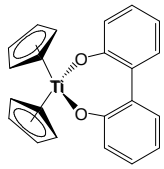

Yield 25 % (0.0820 g). M.p. > 200 ˚C. Colour: red. ^{1}H NMR (600 MHz, δ/ppm, acetone-d_6): 6.34 (s, 10H, 2x CpH), 6.71 (d, 2H; biphenH), 6.86 (t, 2H, biphenH), 7.18 (t, 2H, biphenH), 7.23 (t, 2H, biphenH) *Spectrum 30*. ^{1}H NMR (300 MHz, δ/ppm, $CDCl_3$): 6.26 (s, 10H, 2x CpH), 6.67 (d, 2H; biphenH), 6.93 (t, 2H, biphenH), 7.26 (m, 4H, biphenH) *Spectrum 30a*.

4.7.3 Octahedral Complexes

4.7.3.1 Bis(β-diketonato)-dichloro Ti(IV) complexes: $Ti(\beta)_2Cl_2$

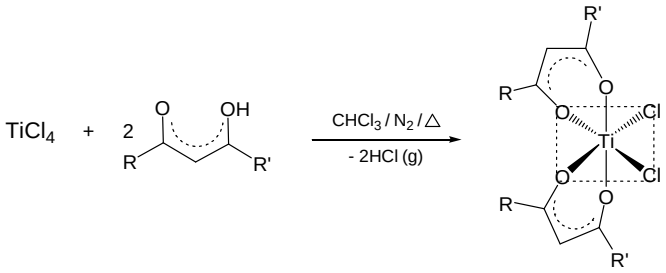

Since the $Ti(\beta)_2Cl_2$ complexes are readily hydrolysed, especially in solution, all syntheses and subsequent handling of the compounds were conducted under anhydrous conditions in a dry Ar atmosphere. All glassware was flame-dried and was allowed to cool in a stream of dry Ar. The Ar atmosphere was maintained throughout the reaction. Filtrations and recrystallisations were performed under a blanket of Ar. All solvents were dried and distilled under N_2 immediately before use. The product was stored under Ar atmosphere.

$Ti(acac)_2Cl_2$, $Ti(ba)_2Cl_2$ and $Ti(dbm)_2Cl_2$ were prepared according to the published procedures.[25,26] The general procedure used with CF_3-β-diketones: To a stirred solution of appropriate β-diketone (2.0 mmol) in chloroform (20 ml), titanium tetrachloride, $TiCl_4$, (0.2 ml / 1.0 mmol) in chloroform (0.8 ml) was syringed in dropwise with an immediate colour

change. The reaction mixture was stirred and purged with a slow stream of Ar (to evolve the hydrogen chloride gas) for 20 min. The solution was refluxed for ½ h (for liquid β-diketones: Hhfaa, Htfaa, Htfma, Htfdma and Htftma) and 2 h (for solid β-diketones: Htfth, Htffu and Htfba). Dry hexane (10 - 20 ml) was added until the reaction mixture turned milky and then the mixture was allowed to precipitate slowly for 12 h at 4 °C. The product was obtained from the filtrate (i) in the case of (hfaa*, tfaa and tfth) and from the precipitate (ii) in the case of the other β-diketones.

(i) The solvent was removed from the filtrate by reduced pressure and (ii) the precipitate was filtered off (with a pump) and washed with hexane. Recrystalisation from DCM/*n*-hexane afforded pure product as a mixture of three *cis*-isomers.

*Note: $Ti(hfaa)_2Cl_2$ did not precipitate after 12 h but the filtrate was a mixture of products. Only after the crude mixture was allowed to stand for 10 days at 4 °C, was the pure product isolated from the filtrate as above.

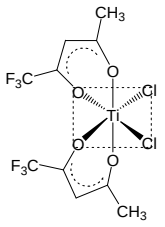

***(a)* Ti(tfaa)$_2$Cl$_2$ [13]**

Bis(trifluoroacetylacetonato-O,O') dichloro titanium(IV)

Yield 60 % (0.250 g). M.p. > 200 ˚C. Colour: yellow. ^{1}H NMR (600 MHz, δ/ppm, $CDCl_3$): Monomer: 2.44 (s, 6H, 2x CH_3), 6.40 (s, 2H, 2x CH). Dimer: 2.36 (s, 6H, 2x CH_3), 6.24 (s, 2H, 2x CH) *Spectrum 31.* ^{19}F NMR (600 MHz, δ/ppm, $CDCl_3$): Monomer and dimer: -72.73 − -76.16 (br, 6H, 2x CF_3) *Spectrum 68.*

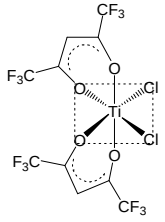

***(b)* Ti(hfaa)$_2$Cl$_2$ [14]**

Bis(hexafluoroacetylacetonato-O,O') dichloro titanium(IV)

Yield 40 % (0.200 g). M.p. > 200 ˚C. Colour: yellow. ^{1}H NMR (600 MHz, δ/ppm, $CDCl_3$): Monomer: 6.80 (s, 2H, 2x CH). Dimer: 6.70 (s, 2H, 2x CH) *Spectrum 32.* ^{19}F NMR (600 MHz, δ/ppm, $CDCl_3$): Monomer and dimer: -73.51 − -76.60 (br, 6H, 2x CF_3) *Spectrum 69.*

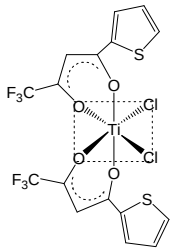

(c) **$Ti(tfth)_2Cl_2$ [15]**

Bis(trifluorothenoylacetonato-O,O') dichloro titanium(IV)

Yield 50 % (0.280 g). M.p. > 200 ˚C. Colour: red. ^{1}H NMR (300 MHz, δ/ppm, $CDCl_3$): Monomer: 6.82 (s, 2H, 2x CH), 7.29-7.35 (br, 2H, 2x 1H, ThH), 7.95-8.12 (br, 4H, 2x 2H, ThH). Dimer: 6.63 (s, 2H, 2x CH), 7.13-7.21 (br, 2H, 2x 1H, ThH), 7.75-8.05 (br, 4H, 2x 2H, ThH) *Spectrum 33*. ^{19}F NMR (600 MHz, δ/ppm, $CDCl_3$): Monomer and dimer: -72.78 − -75.72 (br, 6H, 2x CF_3) *Spectrum 70.*

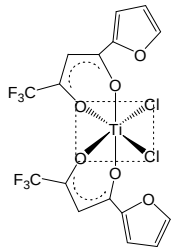

(d) **$Ti(tffu)_2Cl_2$ [16]**

Bis(trifluorofuroylacetonato-O,O') dichloro titanium(IV)

Yield 50 % (0.260 g). M.p. > 200 ˚C. Colour: red. ^{1}H NMR (300 MHz, δ/ppm, $CDCl_3$): Monomer: 6.71-6.82 (br, 2H, FuH), 6.93 (s, 2H, 2x CH), 7.70-7.78 (br, 2H, 2x 1H, FuH), 7.82-7.90 (br, 2H, 2x 1H, FuH). Dimer: 6.61-6.70 (br, 2H, 2x 1H, FuH), 6.75 (s, 2H, 2x CH), 7.59-7.78 (br, 4H, 2x 2H, FuH) *Spectrum 34.* ^{19}F NMR (600 MHz, δ/ppm, $CDCl_3$): Monomer and dimer: -73.54 − -75.50 (br, 6H, 2x CF_3) *Spectrum 71*.

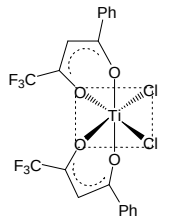

(e) **$Ti(tfba)_2Cl_2$ [17]**

Bis(trifluorobenzoylacetonato-O,O') dichloro titanium(IV)

Yield 60 % (0.330 g). M.p. > 200 ˚C. Colour: orange. ^{1}H NMR (300 MHz, δ/ppm, $CDCl_3$): Monomer: 7.05 (s, 2H, 2x CH), 7.58 (t_{br}, 4H, 2x 2H, PhH), 7.77 (t_{br}, 2H, 2x 1H, PhH), 8.11 (br, 4H, 2x 2H, PhH). Dimer: 6.85 (s, 2H, 2x CH), 7.44 (br, 4H, 2x 2H, PhH), 7.63 (t_{br}, 2H, 2x 1H, PhH), 8.02 (br, 4H, 2x 2H, PhH) *Spectrum 35.* ^{19}F NMR (600 MHz, δ/ppm, $CDCl_3$): Monomer and dimer: -73.44 − -75.43 (br, 6H, 2x CF_3) *Spectrum 72.*

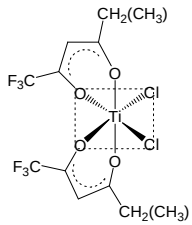

***(f)* Ti(tfma)$_2$Cl$_2$ [18]**

Bis(methyltrifluoroacetonato-O,O') dichloro titanium(IV)

Yield 50 % (0.230 g). M.p. > 200 ˚C. Colour: red. ^{1}H NMR (600 MHz, δ/ppm, $CDCl_3$): Monomer: 1.06-1.38 (br, 6H, 2x CH_3), 2.68 (br, 4H, 2x CH_2), 6.38 (s, 2H, 2x CH). Dimer: 1.06-1.38 (br, 6H, 2x CH_3), 2.60 (br, 4H, 2x CH_2), 6.23 (s, 2H, 2x CH) *Spectrum 36.* ^{19}F NMR (600 MHz, δ/ppm, $CDCl_3$): Monomer and dimer: -73.89 − -75.89 (br, 6H, 2x CF_3) *Spectrum 73.*

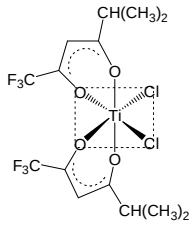

***(g)* Ti(tfdma)$_2$Cl$_2$ [19]**

Bis(dimethyltrifluoroacetonato-O,O') dichloro titanium(IV)

Yield 50 % (0.240 g). M.p. > 200 ˚C. Colour: red. ^{1}H NMR (600 MHz, δ/ppm, $CDCl_3$): Monomer: 0.95-1.44 (br, 12H, 4x CH_3), 2.83 (br, 2H, 2x CH), 6.38 (s, 2H, 2x CH). Dimer: 0.95-1.44 (br, 12H, 4x CH_3), 2.75 (br, 2H, 2x CH), 6.22 (s, 2H, 2x CH) *Spectrum 37.*
^{19}F NMR (600 MHz, δ/ppm, $CDCl_3$): Monomer and dimer: -73.40 − -75.68 (br, 6H, 2x CF_3) *Spectrum 74.*

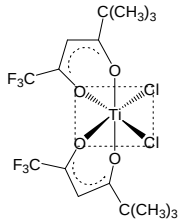

***(h)* Ti(tftma)$_2$Cl$_2$ [20]**

Bis(trimethyltrifluoroacetonato-O,O') dichloro titanium(IV)

Yield 50 % (0.260 g). M.p. > 200 ˚C. Colour: red. ^{1}H NMR (600 MHz, δ/ppm, $CDCl_3$): Monomer: 1.27 (s, 18H, 6x CH_3), 6.48 (s, 2H, 2x CH). Dimer: 0.90 (br, 18H, 6x CH_3), 6.34 (s, 2H, 2x CH) *Spectrum 38.* ^{19}F NMR (600 MHz, δ/ppm, $CDCl_3$): Monomer and dimer: -73.86 − -75.21 (br, 6H, 2x CF_3) *Spectrum 75.*

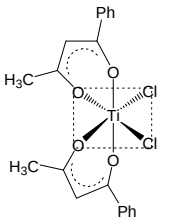

(i) **$Ti(ba)_2Cl_2$ [21]**

Bis(benzoylacetonato-O,O') dichloro titanium(IV)

Yield 71 % (0.3130 g). M.p. > 200 ˚C (literature[26] 209-210 °C). Colour: orange. ^{1}H NMR (600 MHz, δ/ppm, $CDCl_3$): 2.33 (s, 6H, 2x CH_3), 6.67 (s, 2H, 2x CH), 7.48 (t_{br}, 4H, 2x 2H, PhH), 7.61 (t_{br}, 2H, 2x 1H, PhH), 8.00 (br, 4H, 2x 2H, PhH) *Spectrum 39.*

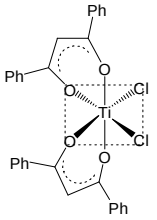

(j) **$Ti(dbm)_2Cl_2$ [22]**

Bis(dibenzoylmethanato-O,O') dichloro titanium(IV)

Yield 68 % (0.3838 g). M.p. > 200 ˚C (literature[26] 263-264 °C). Colour: orange/red. ^{1}H NMR (600 MHz, δ/ppm, $CDCl_3$): 7.35 (s, 2H, CH), 7.39-7.56 (br, 8H, 4x 2H, PhH), 7.56-7.69 (br, 4H, 4x 1H, PhH), 7.95-8.25 (br, 8H, 4x 2H, PhH) *Spectrum 40.*

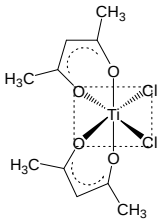

(k) **$Ti(acac)_2Cl_2$ [23]**

Bis(acetylacetonato-O,O') dichloro titanium(IV)

Yield 89 % (0.2816 g). M.p. = 192 ˚C (litrature, 191-192,[25] 190-193[27] °C). Colour: orange. ^{1}H NMR (600 MHz, δ/ppm, $CDCl_3$): 2.19 (s, 12H, 4x CH_3), 6.00 (s, 2H, 2x CH)
Spectrum 41.

4.7.3.2 Bis(β-diketonato)-(biphenyldiolato) Ti(IV) complexes: $Ti(\beta)_2$biphen

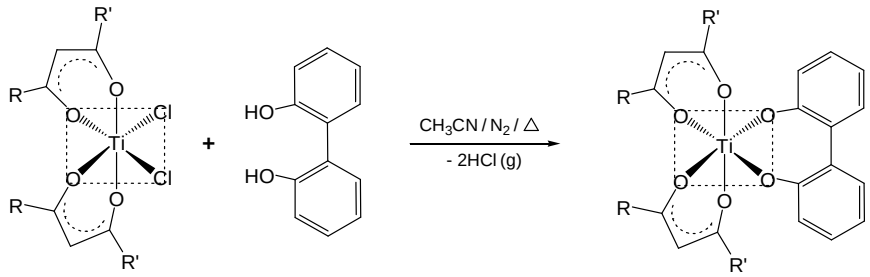

All operations were carried out under anhydrous conditions in a dry N_2 atmosphere. All glassware was flame-dried and was allowed to cool in a stream of dry N_2. The N_2 atmosphere

was maintained throughout the reaction. Filtrations and recrystallisations were performed under a blanket of N_2. All solvents were dried and distilled under N_2 immediately before use. The complex *cis*-Ti(β)$_2$Cl$_2$ was prepared as described in **Section 4.7.3.1** and purified by recrystallisation before use.

To a stirred solution of 2,2'-biphenol (0.186 g, 1 mmol) in CH_3CN (15 ml), the appropriate bis(β-diketonato)dichlorotitanium(IV), Ti(β)$_2$Cl$_2$, (1.0 mmol) in CH_3CN (5 ml) was syringed in dropwise at room temperature with an immediate colour change (clear/grey to orange/red). The reaction mixture was stirred and purged with a slow stream of N_2 (to evolve the hydrogen chloride gas) for 20 min and then refluxed for 4 h. The reaction mixture was cooled to room temperature and the solvent evaporated to dryness. Pure product as a mixture of three *cis*-isomers was obtained in two ways: (i) the residue was redissolved in CH_3CN and allowed to crystallise out or (ii) the residue was recrystallised from DCM/*n*-hexane.

*Note: The non-fluorinated Ti(β)$_2$biphen complex can be washed with MeOH to remove unreacted biphenol. The use of MeOH on the fluorinated analogues caused decomposition.

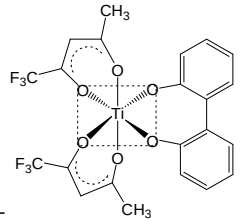

***(a)* Ti(tfaa)$_2$biphen [24]**

Bis(trifluoroacetylacetonato-O,O') (biphenyldiolato-O,O') titanium(IV)

Yield 40 % (0.218 mg). M.p. = 108 ˚C. Colour: red. ^{1}H NMR (600 MHz, δ/ppm, $CDCl_3$): 2.27 (s, 6H, 2x CH_3), 6.21 (s, 2H, 2x CH), 6.89 (d, 2H, biphenH), 7.11 (t, 2H, biphenH), 7.29 (t, 2H, biphenH), 7.47 (d, 2H, biphenH) *Spectrum 42.* ^{19}F NMR (600 MHz, δ/ppm, $CDCl_3$): -75.23 (s, 6H, 2x CF_3) *Spectrum 76.*

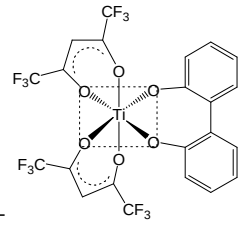

***(b)* Ti(hfaa)$_2$ biphen [25]**

Bis(hexafluoroacetylacetonato-O,O') (biphenyldiolato-O,O') titanium(IV)

Yield 15 % (0.091 mg). M.p. = xx ˚C. Colour: red. ^{1}H NMR (600 MHz, δ/ppm, $CDCl_3$): 6.61 (s, 2H, 2x CH), 6.90 (d, 2H, biphenH), 7.22 (t, 2H, biphenH), 7.35 (t, 2H, biphenH), 7.55 (d, 2H, biphenH) *Spectrum 43.*

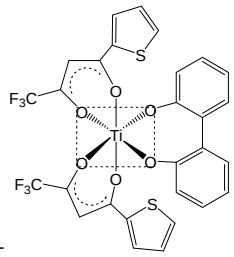

***(c)* Ti(tfth)$_2$ biphen [26]**

Bis(trifluorothenoylacetonato-O,O') (biphenyldiolato-O,O') titanium(IV)

Yield 52 % (0.3482 g). M.p. = 119 ˚C. Colour: red. ^{1}H NMR (600 MHz, δ/ppm, $CDCl_3$): 6.67 (s, 2H, 2x CH), 7.02 (d_{br}, 2H, biphenH), 7.14 (t, 2H, biphenH), 7.19 (t, 2H, 2x 1H, ThH), 7.36 (t_{br}, 2H, biphenH), 7.50 (d, 2H, biphenH), 7.80 (d, 2H, 2x 1H, ThH), 7.86 (d, 2H, 2x 1H, ThH) *Spectrum 44.* ^{19}F NMR (600 MHz, δ/ppm, $CDCl_3$): -74.98 (s, 6H, 2x CF_3) *Spectrum 77.*

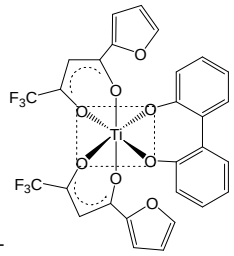

***(d)* Ti(tffu)$_2$ biphen [27]**

Bis(trifluorofuroylacetonato-O,O') (biphenyldiolato-O,O') titanium(IV)

Yield 46 % (0.2895 g). M.p. = 107 ˚C. Colour: red. ^{1}H NMR (600 MHz, δ/ppm, $CDCl_3$): 6.63 (d, 2H, 2x 1H, FuH), 6.79 (s, 2H, 2x CH), 6.99 (d_{br}, 2H, biphenH), 7.14 (t, 2H, biphenH), 7.27 (br, 2H, 2x 1H, FuH), 7.36 (t_{br}, 2H, biphenH), 7.49 (d, 2H, biphenH), 7.69 (s, 2H, 2x 1H, FuH) *Spectrum 45.* ^{19}F NMR (600 MHz, δ/ppm, $CDCl_3$): -75.13 (s, 6H, 2x CF_3) *Spectrum 78.*

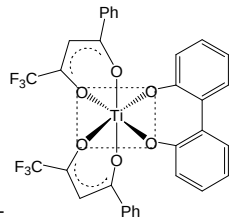

***(e)* Ti(tfba)$_2$ biphen [28]**

Bis(trifluorobenzoylacetonato-O,O') (biphenyldiolato-O,O') titanium(IV)

Yield 58 % (0.3824 g). M.p. = 86 ˚C. Colour: red. ^{1}H NMR (600 MHz, δ/ppm, $CDCl_3$): 6.89 (s, 2H, 2x CH), 7.02 (d_{br}, 2H, biphenH), 7.16 (t, 2H, biphenH), 7.37 (t_{br}, 2H, biphenH), 6.47 (t, 4H, 2x 2H, PhH), 7.52 (d, 2H, biphenH), 7.64 (t, 2H, 2x 2H, PhH), 7.91 (d, 4H, 2x 2H, PhH) *Spectrum 46.* ^{19}F NMR (600 MHz, δ/ppm, $CDCl_3$): -75.00 (s, 6H, 2x CF_3) *Spectrum 79.*

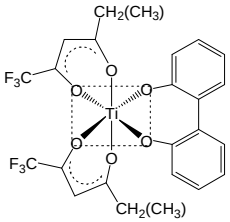

***(f)* Ti(tfma)$_2$ biphen [29]**

Bis(methyltrifluoroacetonato-O,O') (biphenyldiolato-O,O') titanium(IV)

Yield 22 % (0.1238 mg). M.p. = 109 ˚C. Colour: red. ^{1}H NMR (600 MHz, δ/ppm, $CDCl_3$): 1.08 (t, 6H, 2x CH_3), 2.54 (m, 4H, 2x CH_2), 6.20 (s, 2H, 2x CH), 6.90 (d, 2H, biphenH), 7.12 (t, 2H, biphenH), 7.29 (t, 2H, biphenH), 7.48 (d, 2H, biphenH) *Spectrum 47.* ^{19}F NMR (600 MHz, δ/ppm, $CDCl_3$): -75.21 (s, 6H, 2x CF_3) *Spectrum 80*

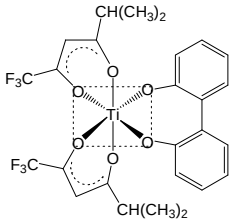

***(g)* Ti(tfdma)$_2$ biphen [30]**

Bis(dimethyltrifluoroacetonato-O,O') (biphenyldiolato-O,O') titanium(IV)

Yield 36 % (0.2128 g). M.p. = 95 ˚C. Colour: red. ^{1}H NMR (600 MHz, δ/ppm, $CDCl_3$): 1.11 (d, 12H, 4x CH_3), 2.69 (m, 2H, 2x CH), 6.21 (s, 2H, 2x CH), 6.89 (d, 2H, biphenH), 7.11 (t, 2H, biphenH), 7.29 (t, 2H, biphenH), 7.47 (d, 2H, biphenH) *Spectrum 48.* ^{19}F NMR (600 MHz, δ/ppm, $CDCl_3$): -75.23 (s, 6H, 2x CF_3) *Spectrum 81.*

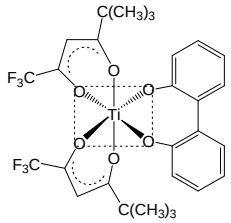

***(h)* Ti(tftma)$_2$ biphen [31]**

Bis(trimethyltrifluoroacetonato-O,O') (biphenyldiolato-O,O') titanium(IV)

Yield 36 % (0.2240 mg). M.p. = 105 ˚C. Colour: red. ^{1}H NMR (600 MHz, δ/ppm, $CDCl_3$): 1.16 (s, 18H, 6x CH_3), 6.33 (s, 2H, 2x CH), 6.89 (d, 2H, biphenH), 7.10 (t, 2H, biphenH), 7.29 (t, 2H, biphenH), 6.47 (d, 2H, biphenH) *Spectrum 49.* ^{19}F NMR (600 MHz, δ/ppm, $CDCl_3$): -75.18 (s, 6H, 2x CF_3) *Spectrum 82.*

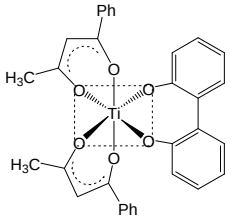

***(i)* Ti(ba)$_2$ biphen [32]**

Bis(benzoylacetonato-O,O') (biphenyldiolato-O,O') titanium(IV)

Yield 40 % (0.2212 g). M.p. > 200 ˚C. Colour: red. ^{1}H NMR (600 MHz, δ/ppm, $CDCl_3$): 2.21 (s, 6H, 2x CH_3), 6.49 (s, 2H, 2x CH), 6.98-7.14 (m, 4H, aromaticH), 7.29-7.55 (m, 10H, aromaticH), 7.00 (d, 4H, 2x 2H, PhH) *Spectrum 50.*

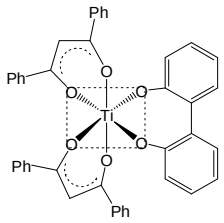

***(j)* Ti(dbm)$_2$ biphen [33]**

Bis(dibenzoylmethanato-O,O') (biphenyldiolato-O,O') titanium(IV)

Yield 36 % (0.2403 g). M.p. > 200 ˚C. Colour: red. ^{1}H NMR (600 MHz, δ/ppm, $CDCl_3$): 7.08-7.16 (m, 4H, aromaticH), 7.18 (s, 2H, 2x CH), 7.33-7.61 (m, 16H, aromaticH), 7.96 (d, 8H, 4x 2H, PhH) *Spectrum 51*.

4.7.3.3 Bis(β-diketonato)-(aryl-diolato) Ti(IV) complexes: Ti(β)$_2$L

(i) Ti(acac)$_2$L complexes

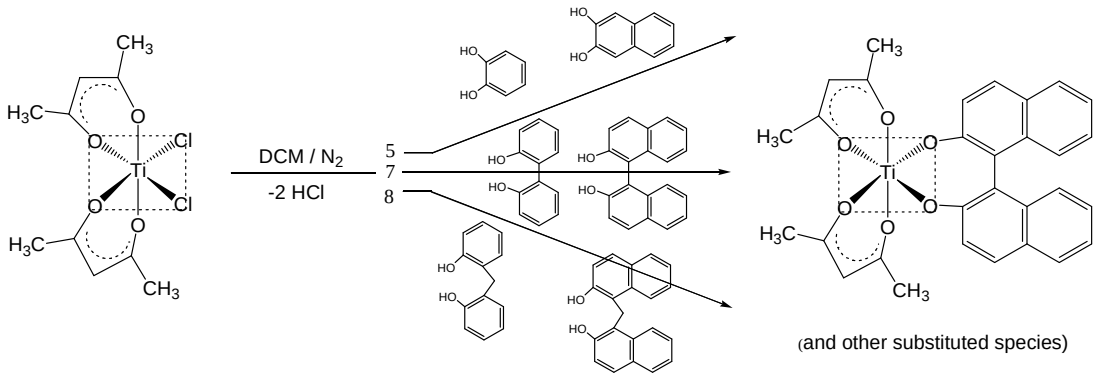

All operations were carried out under anhydrous conditions in a dry N_2 atmosphere. All glassware was flame-dried and was allowed to cool in a stream of dry N_2. The N_2 atmosphere was maintained throughout the reaction. Filtrations and recrystallisations were performed under a blanket of N_2. All solvents were dried and distilled under N_2 immediately before use. The complex *cis*-Ti(acac)$_2$Cl$_2$ **[23]** was prepared according to the published procedure[25] and purified by recrystallisation before use.

To a stirred solution of dihydroxy-aryl ligand (1 mmol) in DCM (3 ml), bis(acetylacetonato)-dichlorotitanium(IV), Ti(acac)$_2$Cl$_2$, (0.4311 g / 1 mmol) in DCM (2 ml) was syringed in dropwise at room temperature with an immediate colour change. The reaction mixture instantly turned dark red and the dihydroxy-aryl ligand dissolved on shaking. After standing 5 h at room temperature, the reaction mixture was layered with hexane (7 ml) and allowed to stand for 2 days. The precipitate was isolated by filtration and washed with hexane and recrystallised from DCM / *n*-hexane.

(k) **$Ti(acac)_2$ cat [34]**

Bis(acetylacetonato-O,O') (benzyldiolato-O,O') titanium(IV)

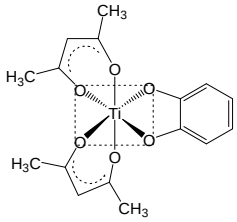

Yield 12 % (0.0428 g). M.p. > 200 ˚C. Colour: red/brown. ^{1}H NMR (300 MHz, δ/ppm, $CDCl_3$): 2.20 (s, 12H, 4x CH_3), 5.90 (s, 2H, 2x CH), 6.28 (m, 2H, catH), 6.65 (m, 2H, catH) *Spectrum 52.*

(l) **$Ti(acac)_2$ naph [35]**

Bis(acetylacetonato-O,O') (naphthyldiolato-O,O') titanium(IV)

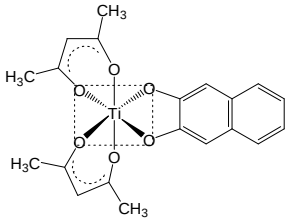

Yield 62 % (0.2488 g). M.p. > 200 ˚C. Colour: red/brown. ^{1}H NMR (300 MHz, δ/ppm, $CDCl_3$): 2.01-2.31 (br, 12H, 4x CH_3), 5.89 (s, 2H, 2x CH), 7.25 (s, 1H, naphH), 7.27 (t, 1H, naphH), 7.31 (t, 1H, naphH), 7.34 (s, 1H, naphH), 7.63 (d, 1H, naphH), 7.64 (d, 1H, naphH) *Spectrum 53.*

(m) **$Ti(acac)_2$ biphen [36]**

Bis(acetylacetonato-O,O') (biphenyldiolato-O,O') titanium(IV)

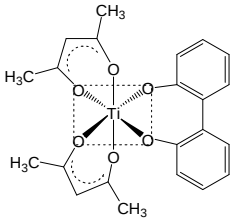

Yield 78 % (0.336 g). M.p. > 200 ˚C. Colour: red. ^{1}H NMR (600 MHz, δ/ppm, $CDCl_3$): 2.04 (s, 12H, 4x CH_3), 5.79 (s, 2H, 2 x CH), 6.88 (d, 2H, biphenH), 7.01 (t, 2H, biphenH), 7.22 (t, 2H, biphenH), 7.39 (d, 2H, biphenH) *Spectrum 54.*

(n) **$Ti(acac)_2$ binaph [37]**

Bis(acetylacetonato-O,O') (binaphthyldiolato-O,O') titanium(IV)

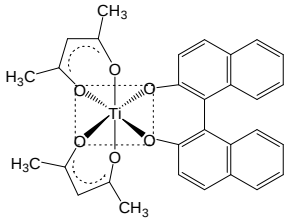

Yield 60 % (0.3112 g). M.p. > 200 ˚C. Colour: red/brown. ^{1}H NMR (600 MHz, δ/ppm, $CDCl_3$): 2.00 (s_{br}, 12H, 4x CH_3), 5.77 (s, 2H, 2x CH), 7.12 (t, 2H, binaphH), 7.25 (t, 2H, binaphH), 7.27 (d, 2H, binaphH), 7.34 (d, 2H, binaphH), 7.83 (d, 4H, binaphH) *Spectrum 55.*

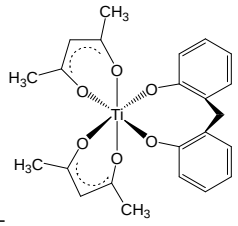

***(o)* Ti(acac)$_2$ mbiphen [38]**

Bis(acetylacetonato-O,O') (methylenebiphenyldiolato-O,O') titanium(IV)

Yield 62 % (0.2761 g). M.p. > 200 ˚C. Colour: red/brown. ^{1}H NMR (300 MHz, δ/ppm, $CDCl_3$): 2.00-2.46 (br, 12H, 4x CH_3), 3.94, 4.90 (br, br, 1H each, CH_2), 5.82 (s, 2H, 2x CH), 6.72 (br, 2H, mbiphenH), 6.90 (s_{br}, 2H, mbiphenH), 7.18 (s_{br}, 2H, mbiphenH), 7.36 (s_{br}, 2H, mbiphenH) *Spectrum 56.*

(ii) Ti(β)$_2$mbinaph complexes

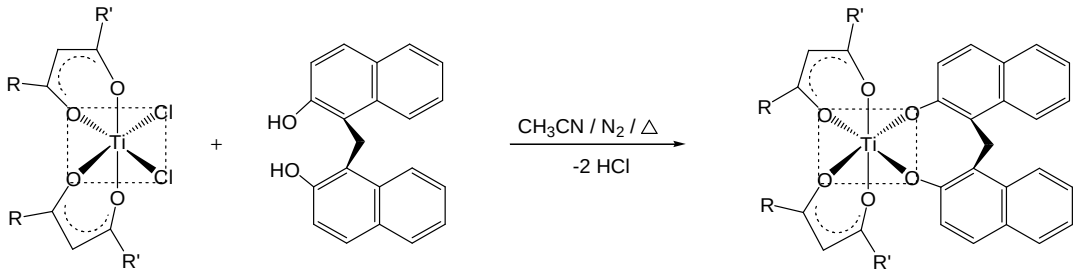

All operations were carried out under anhydrous conditions in a dry N_2 atmosphere. All glassware was flame-dried and was allowed to cool in a stream of dry N_2. The N_2 atmosphere was maintained throughout the reaction. Filtrations and recrystallisations were performed under a blanket of N_2. All solvents were dried and distilled under N_2 immediately before use. The complex *cis*-Ti(β)$_2$Cl$_2$ was prepared as described in **Section 4.7.3.1** and purified by recrystallisation before use.

To a stirred solution of 1,1'-methelene-bis(2-naphthol) (0.300 g, 1 mmol) in CH_3CN (15 ml), the appropriate bis(β-diketonato)dichlorotitanium(IV), Ti(β)$_2$Cl$_2$, (1.0 mmol) in CH_3CN (5 ml) was syringed in dropwise at room temperature with an immediate colour change (clear/grey to red). The reaction mixture was stirred and purged with a slow stream of N_2 (to evolve the hydrogen chloride gass) for 20 min and then refluxed for 4-6 h. The reaction mixture was cooled to room temperature and the solvent evaporated to dryness. The product was obtained in two ways (i) the residue was redissolved in CH_3CN and allowed to crystallise out or (ii) the residue was recrystallised from DCM/*n*-hexane.

***(p)* Ti(acac)$_2$ mbinaph [39]**

Bis(acetylacetonato-O,O')
(methylenebinaphthyldiolato-O,O') titanium(IV)

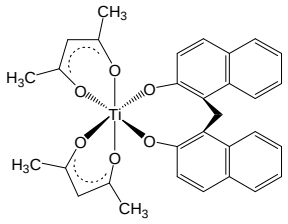

Yield 62 % (0.3368 g). M.p. > 200 ˚C. Colour: red. ^{1}H NMR (300 MHz, δ/ppm, $CDCl_3$): 2.07 (s, 12H, 4x CH_3), 4.79, 5.16 (br, br, 1H each, CH_2), 5.80 (s, 2H, 2x CH), 7.01 (br, 2H, mbinaphH), 7.27 (br, 2H, mbinaphH), 7.40 (br, 2H, mbinaphH), 7.54 (d, 2H, mbinaphH), 7.73 (d, H, mbinaphH), 8.36 (br, 2H, mbinaphH) *Spectrum 57.*

***(q)* Ti(tfaa)$_2$ mbinaph [40]**

Bis(trifluoroacetylacetonato-O,O')
(methylenebinaphthyldiolato-O,O') titanium(IV)

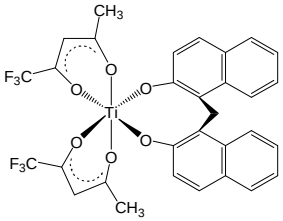

Yield 60 % (0.3900 g). M.p. > 200 ˚C. Colour: brick red. ^{1}H NMR (300 MHz, δ/ppm, $CDCl_3$): 2.33 (s, 6H, 2x CH_3), 4.86, 5.17 (dd, 1H each, CH_2), 6.23, 6.27 (s, s, 1H each, 2x CH), 7.03 (br, 2H, mbinaphH), 7.29-7.54 (br, 4H, mbinaphH), 7.60 (d, 2H, mbinaphH), 7.78 (d, 2H, mbinaphH), 8.43 (br, 2H, mbinaphH) *Spectrum 58.*

***(r)* Ti(hfaa)$_2$ mbinaph [41]**

Bis(hexafluoroacetylacetonato-O,O')
(methylenebinaphthyldiolato-O,O') titanium(IV)

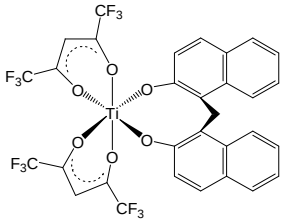

Yield 45 % (0.2055 g). M.p. > 200 ˚C. Colour: red. ^{1}H NMR (300 MHz, δ/ppm, $CDCl_3$): 4.98, 5.12 (dd, 1H each, CH_2), 6.64, 6.68 (s, s, 1H each, 2x CH), 7.00 (br, 2H, mbinaphH), 7.34-7.58 (br, 4H, mbinaphH), 7.64 (d, 2H, mbinaphH), 7.81 (d, 2H, mbinaphH), 8.49 (br, 2H, mbinaphH) *Spectrum 59.*

[1] A. Altomare, M.C. Burla, M. Camalli, G.L. Cascarano, C. Giacovazzo, A. Guagliardi, A.G.G. Moliterni, G. Polidori and R. Spagna, *J. Appl. Crystallogr*., **32** (1999) 115 SIR97.
[2] L.J. Farrugia, *J. Appl. Crystallogr*., **32** (1999) 837 WinGX (Version 1.70.01).
[3] G.M. Sheldrick, SHELXL97, Program for Crystal Structure Refinement, University of Göttingen, Germany, 1997.
[4] International Tables for Crystallography, Kluwer Academic Publishers, Dordecht, The Netherlands, 1002, vol. C.
[5] K. Brandenburg and H. Putz, DIAMOND Release 3.1a, Crystal Impact GbR, Bonn, Germany, 2005.
[6] Bruker (2005). Apex2 (Version 1.0–27), Bruker AXS Inc., Madison, Wisconsin, USA, 2005.
[7] Bruker (1993). COSMO (Version 1.48), Bruker AXS Inc., Madison, Wisconsin, USA, 2003.
[8] Bruker (2004). SAINT-Plus (Version 7.12 including XPREP), Bruker AXS Inc., Madison, Wisconsin, USA, 2004
[9] Bruker (1998). SMART-NT (Version 5.050), Bruker AXS Inc., Madison, Wisconsin, USA, 1998.
[10] Bruker (1999). SAINT-Plus (Version 6.02 including XPREP), Bruker AXS Inc., Madison, Wisconsin, USA, 1999.
[11] Bruker (2004). SADABS (Version, 2004/1), Bruker AXS Inc., Madison, Wisconsin, USA, 2004.
[12] L. Helm, MINSQ, Non-Linear parameter estimation and model development, least squares parameter optimization V3.12, MicroMath Scientific Software, Salt Lake City, UT, 1990.
[13] J[13] J.H. Espenson, *Chemical Kinetics and Reaction Mechanisms*, 2nd edition., McGraw-Hill, New York, 1995, pp. 15, 49, 70-75, 156.
[14] D.T. Sawyer and J.L. Roberts Jr, *Experimental electrochemistry for chemists*, Wiley, New York, 1974, p 54.
[15] D.H. Evans, K.M. O'Connell, R.A. Peterson and M.J. Kelly, *J. Chem. Educ.*, **60**, (1983) 291.
[16] G.A. Mabbott, *J. Chem. Educ.*, **60** (1983) 697.
[17] G. Gritzner and J. Kuta, *Pure Appl. Chem*., **56** (1984) 461.
[18] (a) P.J. Stephens, F.J. Devlin, C.F. Chabalowski and M.J. Frisch, *J. Phys. Chem*., **98** (1994**)** 11623. (b) A. Watson, N.C. Handy and A.J. Cohen, *J. Chem. Phys*., **119** (2003**)** 6475. (c) R.H. Hertwig, W. Koch, *Chem. Phys. Lett*., **268** (1997**)** 345.
[19] *Gaussian 03, Revision C.02*, M.J. Frisch, G.W. Trucks, H.B. Schlegel, G.E. Scuseria, M.A. Robb, J.R. Cheeseman, J.A. Jr. Montgomery, T. Vreven, K.N. Kudin, J.C. Burant, J.M. Millam, S.S. Iyengar, J. Tomasi, V. Barone, B. Mennucci, M. Cossi, G. Scalmani, N. Rega, G.A. Petersson, H. Nakatsuji, M. Hada, M. Ehara, K. Toyota, R. Fukuda, J. Hasegawa, M. Ishida, T. Nakajima, Y. Honda, O. Kitao, H. Nakai, M. Klene, X. Li, J.E. Knox, H.P. Hratchian, J.B. Cross, V. Bakken, C. Adamo, J. Jaramillo, R. Gomperts, R.E. Stratmann, O. Yazyev, A.J. Austin, R. Cammi, C. Pomelli, J.W. Ochterski, P.Y. Ayala, K. Morokuma, G.A. Voth, P. Salvador, J.J. Dannenberg, V.G. Zakrzewski, S. Dapprich, A.D. Daniels, M.C. Strain, O. Farkas, D.K. Malick, A.D. Rabuck, K. Raghavachari, J.B. Foresman, J.V. Ortiz, Q. Cui, A.G. Baboul, S. Clifford, J. Cioslowski, B.B. Stefanov, G. Liu, A. Liashenko, P. Piskorz, I. Komaromi, R.L. Martin, D.J. Fox, T. Keith, M.A. Al-Laham, C.Y. Peng, A. Nanayakkara, M. Challacombe, P.M.W. Gill, B. Johnson, W. Chen, M.W. Wong, C. Gonzalez and J.A. Pople, *Gaussian, Inc., Wallingford CT*, 2004.
[20] The ADF program system was obtained from Scientific Computing and Modeling, Amsterdam (http://www.scm.com/). For a description of the methods used in ADF, see: G.T. Velde, F.M. Bickelhaupt, E.J. Baerends, C.F. Guerra, S.J.A. van Gisbergen, J.G. Snijders and T.J. Ziegler, *J. Comp. Chem*. **22** (2001) 931.
[21] N.C. Handy and A. Cohen, *J. Mol. Phys*., **99** (2001) 403.
[22] (a) C. Lee, W. Yang and R.G. Parr, *Phys. Rev*., **B37** (1988) 785. (b) B. Miehlich, A. Savin, H. Stoll and H. Preuss, *Chem. Phys. Letters*, **157** (1989) 200.
[23] J.P. Perdew, J.A. Chevary, S.H. Vosko, K.A. Jackson, M.R. Perderson, D.J. Singh and C. Fioihais, *Phys. Rev.*, **B46** (1992) 6671.
[24] G.A. Zhurko and D.A. Zhurko, *CHEM CRAFT*, Version 1.5 (build 282), 2007.
[25] R.C. Fay and R.N. Lowry, *Inorg. Chem*., **6** (1967) 1512.
[26] N. Serpone and R.N. Lowry, *Inorg. Chem*., **6** (1967) 1835.
[27] M. Cox, J. Lewis and R.S. Nyholm, *J. Chem. Soc*., (1964) 6113.

5 Concluding Remarks

In this study, two β-diketones, four new (and six known) tetrahedral, mono-β-diketonato titanium(IV) complexes, 25 new (and five known) octahedral, bis-β-diketonato titanium(IV) complexes, three new dimeric and one new tetrameric titanium(IV) complexes were synthesised. Known synthetic protocols were optimised (to enhance synthetic yields) or new synthetic procedures had to be developed to achieve synthetic success. Key Ti(IV) compounds are shown below. These complexes were all characterised spectroscopically with UV/Vis, IR, ^{1}H and ^{19}F NMR spectroscopy. Crystal structures of selected mononuclear (tetrahedral and octahedral complexes) and oxo-bridged dinuclear and tetranuclear complexes are reported.

The physical properties of the complexes were investigated with electrochemical and kinetic techniques.

Ti(IV) complexes

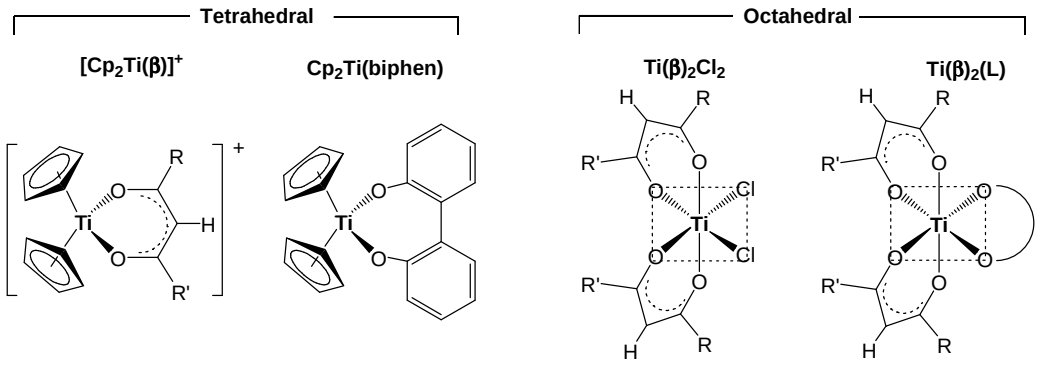

R = CF_3 and R' = CF_3 (hfaa), CH_3 (tfaa), $CH_2(CH_3)$ (tfma), $CH(CH_3)_2$ (tfdma), $C(CH_3)_3$ (tftma), C_4H_3S (tfth), C_4H_3O (tffu) and Ph (tfba)
R = Ph and R' = CH_3 (ba), Ph (dbm) and C_4H_3S (thba)
R = CH_3 and R' = CH_3 (acac)

L =  = cat ($L^{5,1}$), naph ($L^{5,2}$), biphen ($L^{7,1}$), binaph ($L^{7,2}$), mbiphen ($L^{8,1}$) and mbinaph ($L^{8,2}$)

^{1}H and ^{19}F NMR solution phase studies, supported by a computational (DFT) study, show that octahedral $Ti(\beta)_2Cl_2$ and $Ti(\beta)_2$biphen complexes exist as an equilibrium mixture of three cis isomers and that they engage in distinct intramolecular rearrangement (exchange) processes. The CF_3-containing $Ti(\beta)_2Cl_2$ complexes participate further in facile (monomer $\rightleftharpoons$ dimer) equilibrium, involving the interconversion of chemically distinct compounds in which the equilibrium favours higher nuclearity. Controlled hydrolysis of the $Ti(\beta)_2Cl_2$ complexes give dimeric and tetrameric products.

Three types of substitution reaction were investigated (shown below); involving the substitution of monodentate Cl^- ligands in $Ti(\beta)_2Cl_2$ for bidentate biphenol, the successive substitution of bidentate β-diketonato ligands and substitution of the biphenolato ligand in $Ti(acac)_2$biphen for bidentate ligands with varying ring sizes, $L^{5,7\text{ or }8}$ (L^n = *O,O'*-bidentate ligand of ring size n).

$$\mathbf{Ti(\beta)_2Cl_2} \xrightarrow{H_2\text{biphen}} \mathbf{Ti(\beta)_2biphen} \xrightarrow{\text{Hacac}} \mathbf{Ti(acac)_2biphen} \xrightarrow{L^{5,7\text{ or }8}} \mathbf{Ti(acac)_2L^{5,7\text{ or }8}}$$

The activation parameters are consistent with each consecutive substitution proceeding *via* a seven-coordinate transition state according to an associative mechanism. A DFT computational study for the biphenol substitution at $Ti(acac)_2Cl_2$ is in agreement with the experimental data and the proposed associative reaction pathway.

Bis(β-diketonato)titanium(IV) complexes undergo rapid intra- and slower intermolecular ligand exchange reactions. The ligand-exchange equilibria and kinetics of the intermolecular β-diketonato exchange process, forming a mixed ligand complex (shown below) was investigated.

$$Ti(\beta)_2\text{biphen} + Ti(\beta')_2\text{biphen} \underset{}{\overset{K_c}{\rightleftharpoons}} 2\ Ti(\beta)(\beta')\text{biphen}$$

The equilibrium constant, K_c, depends primarily on the relative number of CF_3 substituents on the exchanging β-diketonato ligands. When the exchanging ligands contain the same number of CF_3 groups, the equilibrium lies midway (~50% mixed-ligand complex) while when they differ by one CF_3 group, the equilibrium favours the mixed ligand complex (~60%). The exchange mechanism is consistent with an associative process.

Electrochemical (cyclic voltammetric) studies on the β-diketone ligands and the Ti(IV) complexes were performed in the weakly coordinating $CH_3CN/[NBu_4][PF_6]$ medium (or $DCE/[NBu_4][PF_6]$ for the $Ti(\beta)_2Cl_2$ series). The reduction of the Ti(IV) complexes which form negatively charged reduced species, i.e.,

$$Cp_2Ti^{IV}(biphen) \overset{e^-}{\rightleftharpoons} [Cp_2Ti^{III}(biphen)]^-$$

$$Ti^{IV}(\beta)_2Cl_2 \overset{e^-}{\rightleftharpoons} [Ti^{III}(\beta)_2Cl_2]^-$$

$$Ti^{IV}(\beta)_2biphen \overset{e^-}{\rightleftharpoons} [Ti^{III}(\beta)_2biphen]^-$$

are, to varying degrees, chemically unstable. The redox process at low scan rates shows anodic currents with $i_{pa}/i_{pc} < 1$ and are electrochemically reversible for $Cp_2Ti(biphen)$ and $Ti(\beta)_2biphen$ and irreversible for $Ti(\beta)_2Cl_2$. In contrast, the reduction of $[Cp_2Ti(\beta)]^+$, forming a neutral reduced species, is chemically and electrochemically reversible ($i_{pa}/i_{pc} = 1$ and $\Delta E_p <$ 90 mV).

$$[Cp_2Ti^{IV}(\beta)]^+ \overset{e^-}{\rightleftharpoons} Cp_2Ti^{III}(\beta)$$

The reduction of the β-diketone, which forms an unstable radical anion, reduced species, i.e.,

$$H\beta \xrightarrow{e^-} H\beta^{\bullet -}$$

is chemically irreversible and no reverse oxidation process is observed. However, when the β-diketone contains two aromatic side groups, then the radical anion is stabilised long enough such that the redox process becomes electrochemically reversible ($\Delta E_p <$ 90 mV) with an increased anodic current at higher scan rates.

The formal reduction potential, $E^{0'}$, of the Ti(IV) complexes (or the reduction potential, E_{pc}, of the β-diketones) was correlated to parameters related to electron density on the Ti centre, i.e., $\chi_R + \chi_{R'}$ (sum of the group electronegativities of R and R' of the coordinated β-diketonato ligand, **R**COCHCO**R'**$^-$) and pK_a of the β-diketones. Although there was no direct linear relationship between the reduction potential and the indicated parameters, the correct trends were observed; $E^{0'}$ (or E_{pc}) increased (became less negative/more anodic) with increasing $\chi_R + \chi_{R'}$ and decreasing pK_a. The titanium metal centre is relatively more electron deficient with larger $\chi_R + \chi_{R'}$ and lower pK_a and consequently a higher reduction potential is observed.

Ionisation potentials (IP), calculated (using DFT) as the amount of energy required to remove an electron from $Cp_2Ti^{III}(\beta)$ to form $[Cp_2Ti^{IV}(\beta)]^+$ according to

$$[Cp_2Ti^{IV}(\beta)]^+ + e^- \underset{\text{oxidation}}{\overset{\text{reduction}}{\rightleftharpoons}} Cp_2Ti^{III}(\beta) + \text{energy}$$

showed a linear correlation to $\chi_R + \chi_{R'}$, $E^{0'}$, ν_{CO} and pK_a, i.e.,

$$\chi_{R1} + \chi_{R'} = 1.859(IP) - 5.182$$
$$E^{0'} = 508.4(IP) - 3466$$
$$\nu_{CO} = 121.8(IP) + 896.9$$
$$pK_a = -5.191(IP) + 35.73$$

This allows one to predict electronegativities of the R and R′ side groups, pK_a-values of uncoordinated β-diketone, carbonyl stretching frequencies (ν_{CO}) and the formal reduction potentials, $E^{0'}$, of $[Cp_2Ti^{IV}(\beta)]^+$ if the calculated ionisation potential is known.

Perspectives for future studies are varied. In the present investigation, a series of mono-β-diketonato and bis-β-diketonato Ti(IV) complexes were synthesised and subjected to electrochemical and kinetic studies. Similar studies, extended towards $Ti(\beta)_2X_2$ complexes with X = F, Br and I, could lead to interesting solution phase studies. The *cis*-isomers are favoured by the tendency to maximise pπ-dπ bonding and symmetry effects while the *trans*-isomer only exists when these factors can be overcome by steric interactions. A bulky donor groups like I could force the $Ti(\beta)_2X_2$ complexes into the *trans*-configuration. Other metals series could be incorporated to quantify trends within a group (Ti, Zr and Hf) or period (Ti, V and Cr or Zr, Nb and Mo complexes) of the periodic table.

Ti(IV) complexes in the present study were modelled on two well known, anticancer compounds; four-coordinated tetrahedrally configured titanocene and six-coordinated, octahedrally configured budotitane. Hence application of the synthesised complexes in terms of anticancer activity should be addressed.

Future theoretical studies could involve the determination of transition states of other substitution reactions to support the proposed associative mechanisms and clearly understand why the associative substitution and exchange reactions are not dependent on the concentration of the incoming ligand. The isomer distribution of the $Ti(\beta)_2Cl_2$ and $Ti(\beta)_2$biphen complexes with phenyl containing β-diketones were modelled; the calculations could be extended to all relevant synthesised complexes.

ABSTRACT

Synthetic routes to prepare fluorinated tetrahedral mono-β-diketonato titanium(IV) complexes, $[Cp_2Ti(\beta)^+]$, octahedral bis-β-diketonato titanium(IV) complexes, $Ti(\beta)_2Cl_2$ and $Ti(\beta)_2$biphen, as well as dimeric and tetrameric titanium(IV) complexes, were developed and optimised. All complexes were fully characterised, *inter alia* with UV/vis, IR, ^1H and ^{19}F NMR and X-ray crystallography. Further characterisation of the complexes was done by means of electrochemical and kinetic techniques.

Solution phase studies using variable temperature ^1H and ^{19}F NMR show that all octahedral $Ti(\beta)_2Cl_2$ and $Ti(\beta)_2$biphen complexes exist in solution as an equilibrium mixture of three *cis* isomers which rearrange *via* fast (on NMR timescale) intramolecular exchange processes. The CF_3-containing $Ti(\beta)_2Cl_2$ complexes further participate in facile monomer $\rightleftharpoons$ dimer equilibrium, involving the interconversion of chemically distinct compounds.

Substitution and exchange reactions involving the ligand(s) in the octrahedrally coordinated bis(β-diketonato)Ti(IV) complexes were investigated by means of UV/Vis and NMR kinetics. Experimental and computational data were mutually consistent indicating that the substitution processes proceeded *via* a seven-coordinate transition state according to an associative mechanism. The ligand exchange equilibria studies of $Ti(\beta)_2$biphen complexes showed that the formation of mixed-ligand complexes is a random statistical process when the exchanging β-diketonato ligands contain the same number of CF_3 groups, while the equilibrium favours the mixed ligand complex when they differ by one CF_3 group,

Electrochemical (cyclic voltammetric) studies on the Ti(IV) complexes and the β-diketones were performed in the weakly coordinating CH_3CN or DCE/$[NBu_4][PF_6]$ medium. The reduction of the Ti(IV) complexes Cp_2Ti(biphen), $Ti(\beta)_2$biphen and $Ti(\beta)_2Cl_2$ which form negatively charged reduced species, are to varying degrees chemically unstable. However, the $[Cp_2Ti(\beta)]^+$ complexes, forming a neutral reduced species, are chemically stable. The redox process is electrochemically reversible for Cp_2Ti(biphen), $Ti(\beta)_2$biphen and $[Cp_2Ti(\beta)]^+$ and irreversible for $Ti(\beta)_2Cl_2$

The reduction of the uncoordinated β-diketone, forming an unstable radical anion, is not coupled with a reverse oxidation process. However, when the β-diketone contains two aromatic side groups, the radical anion is stabilised long enough that the redox process, becomes electrochemically reversible ($\Delta Ep < 90$ mV) with an increasing peak aniodic current at higher scan rates.

The electron density on the titanium(IV) metal centre was manipulated by changing the R groups on the coordinated β-diketonato ligand (RCOCHCOR′) from electron donating (R = CH_3, Ph) to strongly electron withdrawing (R = CF_3). The formal reduction potential, $E^{0'}$, of the Ti(IV) complexes (or the reduction potential, E_{pc}, of the ligands), correlated to parameters related to electron density on the Ti centre, i.e., $\chi_R + \chi_{R'}$ (sum of the group electronegativities of R and R' groups on the β-diketonato ligand R'COCHCOR$^-$) and pK_a of the β-diketones. Calculated (DFT) ionisation potentials of $[Cp_2Ti(\beta)]^+$ complexes showed a linear correlation to $\chi_R + \chi_{R'}$, allowing one to predict electronegativities of the R and R′ groups if the calculated ionization potential is known.

KEY WORDS

titanium, titanocene, β-diketone, aryl-diolato (L) ligands, DFT, crystallography, substitution, ligand exchange, kinetics, cyclic voltammetry, group electronegativity.

OPSOMMING

Sintese tegnieke om gefluoreerde tetraëdriese mono-β-diketonato titanium(IV) komplekse, [$Cp_2Ti(\beta)^+$], oktaëdriese bis-β-diketonato titanium(IV) komplekse, $Ti(\beta)_2Cl_2$ en $Ti(\beta)_2$biphen, asook dimeriese en tetraëdriese titanium(IV) komplekse, te berei is ontwikkel en geoptimeer. Alle komplekse is ten volle gekarakteriseer, onder andere met UV/sigbaar, IR, ^1H en ^{19}F KMR en kristallografiese X-straal tegnieke. Verdere karakterisering van die komplekse is met behulp van elektrochemiese en kinetiese tegnieke gedoen.

Oplossingsfase studies deur gebruik te maak van veranderlike temperatuur ^1H en ^{19}F KMR data, toon aan dat alle oktaëdriese $Ti(\beta)_2Cl_2$ en $Ti(\beta)_2$biphen komplekse in oplossing as 'n ewewigsmengsel van drie isomere, wat *via* 'n vinnige (op KMR tydskaal) intramolekulêre proses uitruil, bestaan. Die CF_3-bevattende $Ti(\beta)_2Cl_2$ komplekse toon 'n verdere monomeer $\rightleftharpoons$ dimeer ewewig, met chemies onderskeibare komplekse betrokke.

Substitusie en uitruilingsreaksies van die ligande in die oktaëdries gekoördineerde bis(β-diketonato)Ti(IV) komplekse is met UV/sigbaar en KMR kinetika ondersoek. Eksperimentele en berekeningschemie data stem ooreen dat die substitusie proses *via* 'n sewe gekoördineerde oorgangstoestand volgens 'n assosiatiewe meganisme, plaasvind. Die ligand uitruilings ewewigstudies van die $Ti(\beta)_2$biphen komplekse toon dat: (a) die vorming van die gemengde ligand kompleks is 'n willekeurige statistiese proses indien die uitruilings β-diketonato ligande dieselfde aantal CF_3 groepe bevat en (b) die ewewig die gemengde ligand kompleks word begunstig indien die aantal van die uitruilings β-diketonato ligande se CF_3 groepe met een verskil.

Elektrochemiese (sikliese voltammetriese) studies op die Ti(IV) komplekse en die β-diketone is uitgevoer in swak koördinerende CH_3CN of DCE/[NBu_4][PF_6] oplossings. Die reduksie van die Ti(IV) komplekse Cp_2Ti(biphen), $Ti(\beta)_2$biphen en $Ti(\beta)_2Cl_2$ wat negatief gelaaide gereduseerde spesies vorm, is chemiese onstabiel tot 'n verskillende graad. Die $[Cp_2Ti(\beta)]^+$ komplekse, egter, wat 'n neutrale gereduseerde spesie vorm, is chemies stabiel. Die redoks proses is elektrochemies omkeerbaar vir Cp_2Ti(biphen), $Ti(\beta)_2$biphen en $[Cp_2Ti(\beta)]^+$ en onomkeerbaar vir $Ti(\beta)_2Cl_2$.

Die reduksie van die ongekoördineerde β-diketoon vorm ŉ onstabiele anioon radikaal en toon geen gekoppelde oksidasie proses nie. Indien die β-diketoon egter twee aromatiese groepe bevat, word die anioon radikaal lank genoeg gestabiliseer dat die redoks proses elektrochemies omkeerbaar word met ŉ toenemende piek anodiese stroom met hoër skandeertempo's.

Die elektrondigtheid op die titanium(IV) metaalsentum is gemanipuleer deur die R groepe op die koördinerende β-diketonato ligand (RCOCHCOR′) te wissel van elektrondonerende (R = CH_3, Ph) na sterk elektrononttrekkende (R = CF_3). Die formele redokspotensiaal, $E^{0'}$, van die Ti(IV) komplekse (of die reduksie potensiaal, E_{pc}, van die β-diketone), korreleer met parameters wat met die elektrondigtheid op die Ti sentrum verband hou, i.e., $\chi_R + \chi_{R'}$ (som van die groep elektronegatiwiteite van die R en R' groepe op die β-diketonato ligand $R'COCHCOR^-$) en pK_a van die β-diketone. Berekende (DFT) ionisasie potensiale van die $[Cp_2Ti(\beta)]^+$ komplekse toon ŉ lineêre verband met $\chi_R + \chi_{R'}$, wat mens in staat stel om die elektronegatiwiteite van die R en R′ groepe te kan bepaal indien die berekende ionisasie potensiaal bekend is.

A ^{1}H NMR Spectra

A.1 LIGANDS

Spectrum 1: **Hhfaa** (*hexafluoroacetylacetone*) **$CDCl_3$**

6.40 (s, 1H, CH)

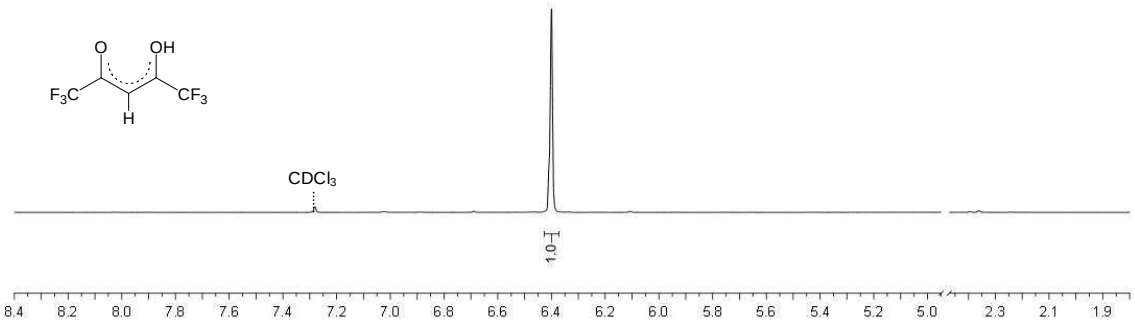

Spectrum 2: **Htfaa** (*trifluoroacetylacetone*) **$CDCl_3$**

6.00 (s, 1H, CH), 2.24 (s, 3H, CH_3)

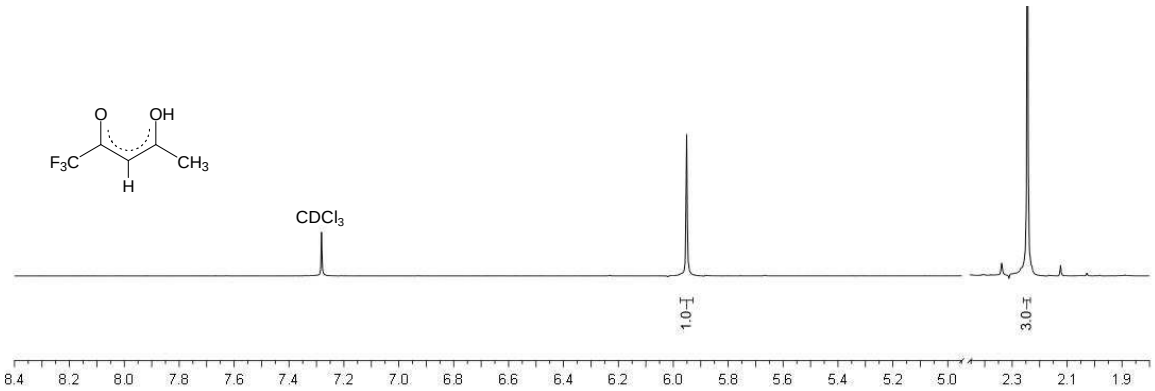

Spectrum 3: **Htfma** (*trifluoromethylacetylacetone*) **$CDCl_3$**

5.95 (s, 1H, CH), 2.51 (m, 2H, $C\underline{H}_2(CH_3)$), 1.22 (t, 3H, $CH_2(C\underline{H}_3)$)

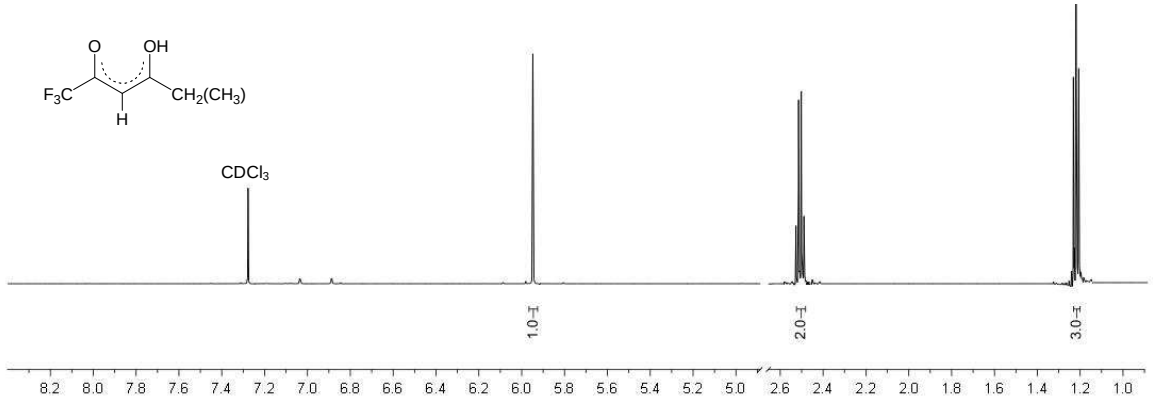

Spectrum 4: **Htfdma** (*trifluorodimethylacetylacetone*) **$CDCl_3$**

5.95 (s, 1H, CH), 2.64 (m, 1H, $C\underline{H}(CH_3)_2$), 1.23 (d, 6H, $CH(C\underline{H}_3)_2$)

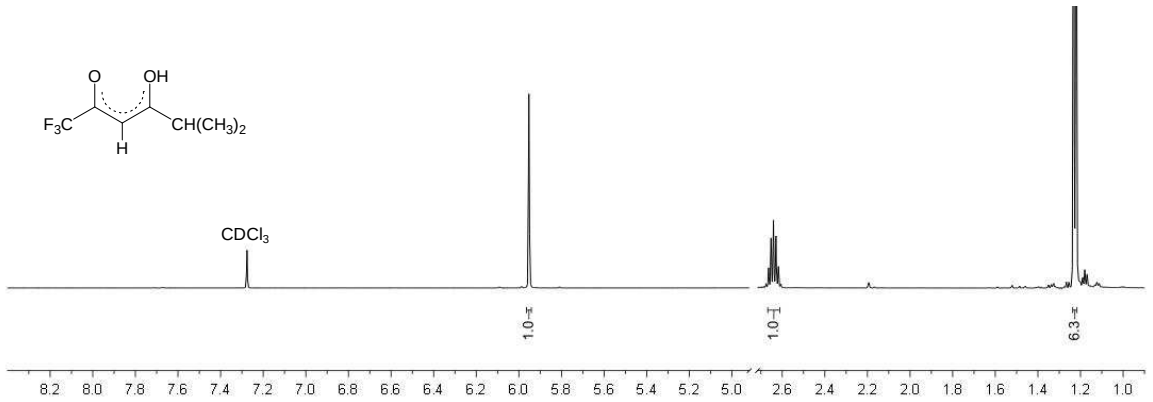

Spectrum 5: **Htftma** (*trifluorotrimethylacetylacetone*) **$CDCl_3$**

6.05 (s, 1H, CH), 1.25 (s, 9H, $C(C\underline{H}_3)_3$)

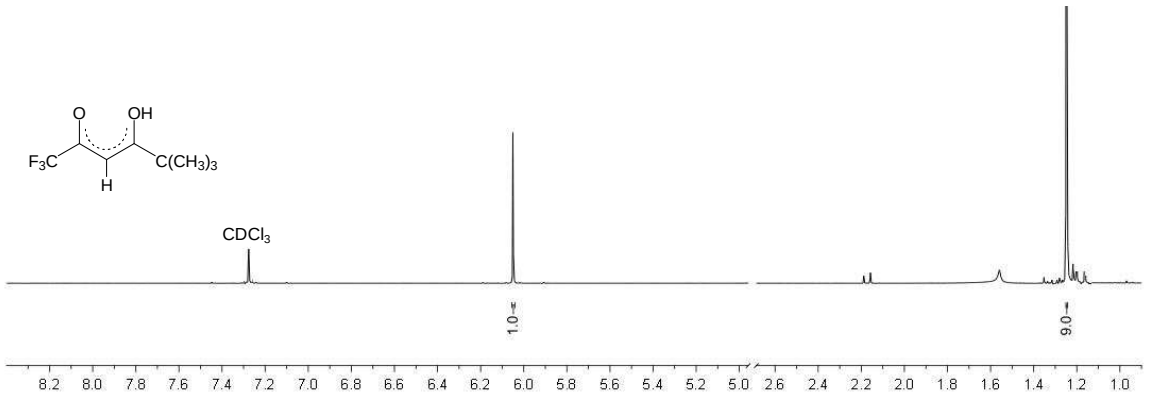

Spectrum 6: **Htfth** (*trifluorothenoylacetone*) **$CDCl_3$**

7.85 (d, 1H, ThH), 7.77 (d, 1H, ThH), 7.20 (t, 1H, ThH), 6.45 (s, 1H, CH)

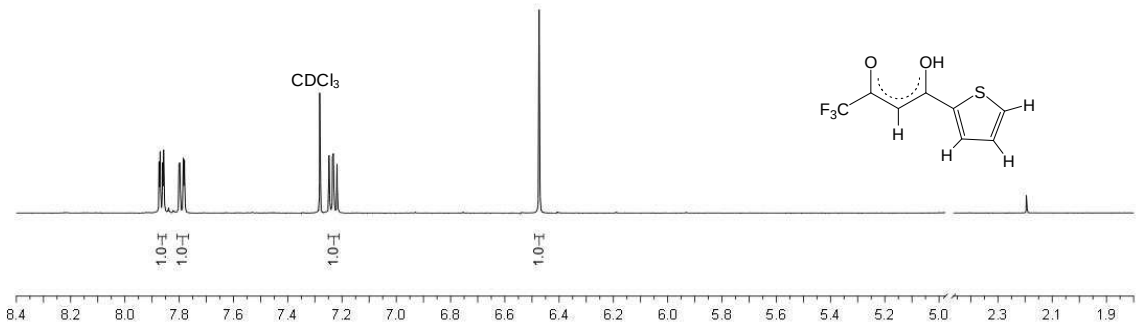

Spectrum 7: **Htffu** (*trifluorofuroylacetone*) **$CDCl_3$**

7.68 (d, 1H, FuH), 7.34 (d, 1H, FuH), 6.64 (m, 1H, FuH), 6.49 (s, 1H, CH)

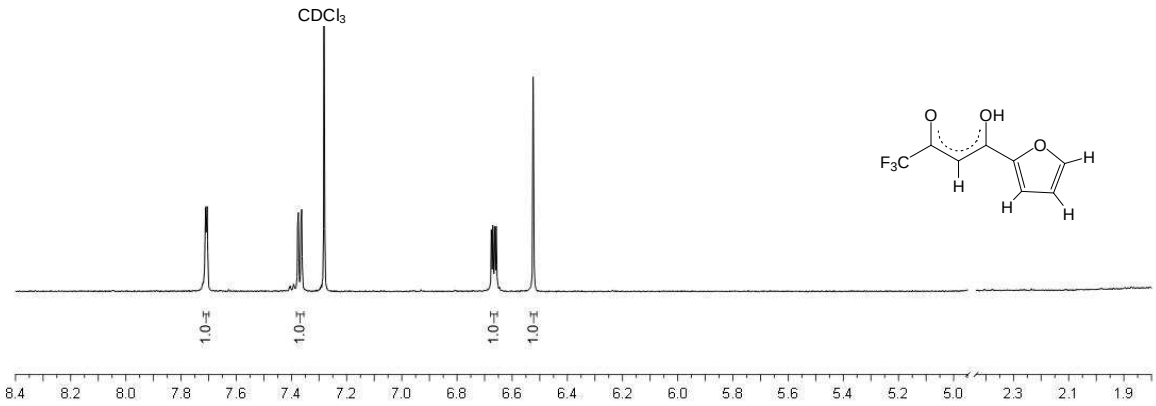

Spectrum 8: **Htfba** (*trifluorobenzoylacetone*) **$CDCl_3$**

7.95 (d, 2H, PhH), 7.63 (t, 1H, PhH), 7.51 (t, 2H, PhH), 6.58 (s, 1H, CH)

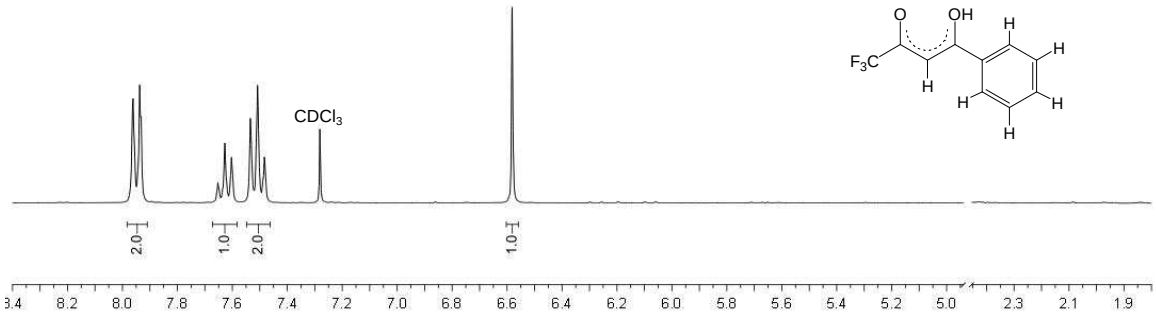

Spectrum 9: **Hba** (*benzoylacetone*) **$CDCl_3$**

7.91 (d, 2H, PhH), 7.56−7.44 (m, 3H, PhH), 6.19 (s, 1H, CH), 2.22 (s, 3H, CH_3)

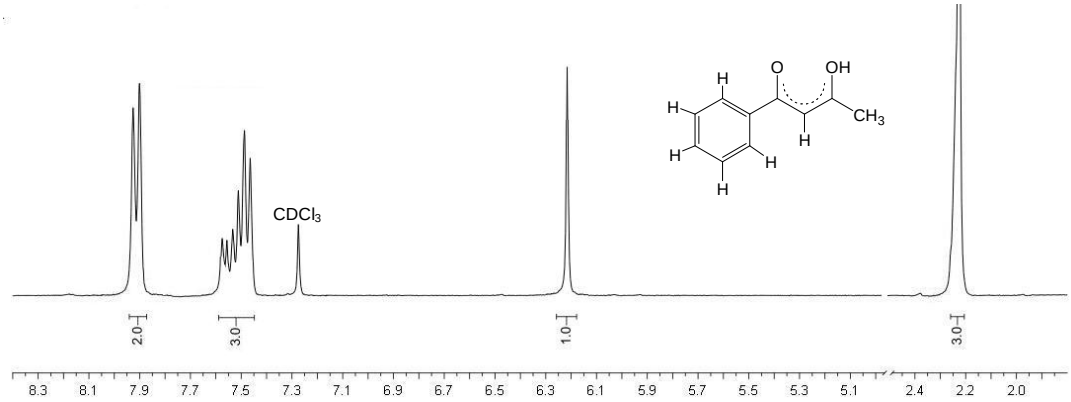

Spectrum 10: **Hdbm** (*dibenzoylmethane*) **$CDCl_3$**

8.02 (d, 4H, PhH), 7.62−7.46 (m, 6H, PhH), 6.85 (s, 1H, CH)

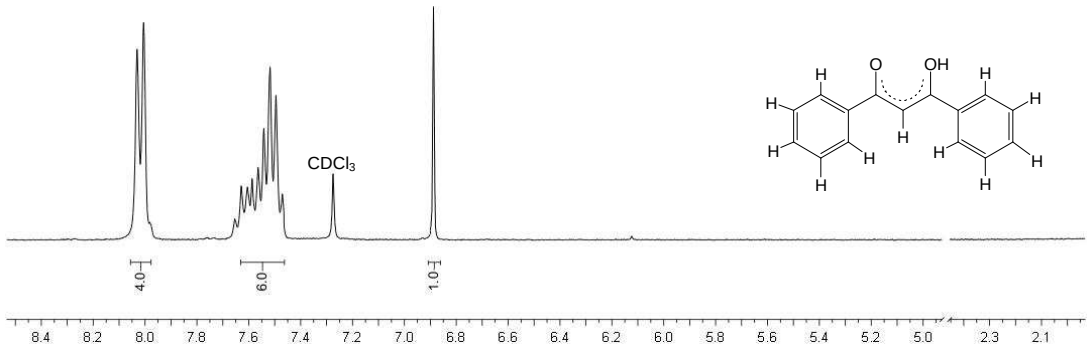

Spectrum 11: **Hthba [1]** (*thenoylbenzoylacetone*) **$CDCl_3$**

7.97 (d, 2H, PhH), 7.84 (d, 1H, ThH), 7.67 (d, 1H, ThH), 7.58−7.47 (m, 3H, PhH), 7.20 (t, 1H, ThH), 6.71 (s, 1H, CH)

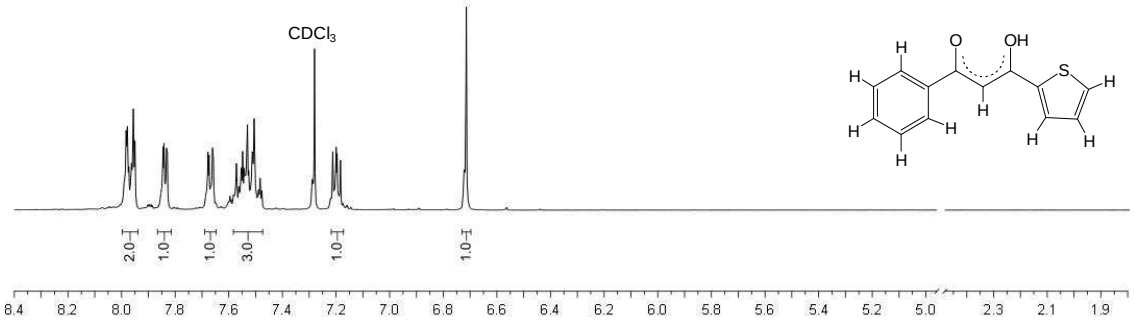

Spectrum 12: **Hnba [2]** (*nitrophenoylbenzoylacetone*) **$CDCl_3$**

8.33 (d, 2H, $Ph_{NO2}H$), 8.14 (d, 2H, $Ph_{NO2}H$), 8.01 (d, 2H, PhH), 7.60 (t, 1H, PhH), 7.51 (t, 2H, PhH), 6.92 (s, 1H, CH)

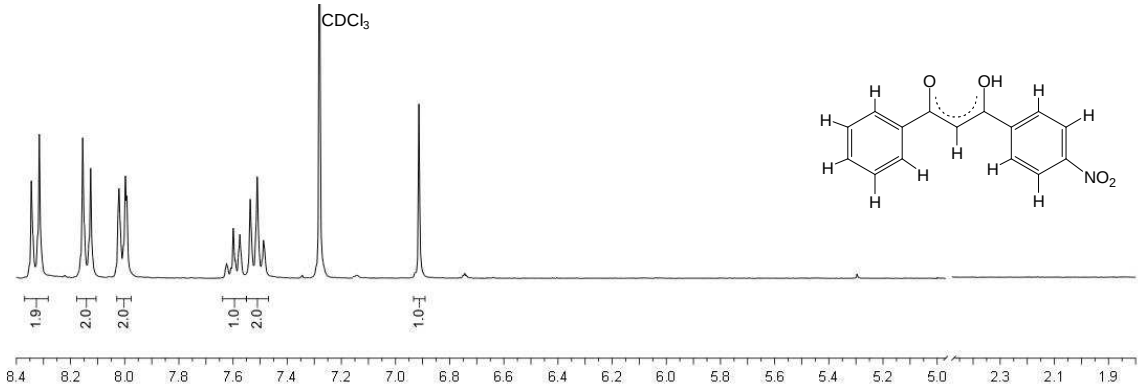

Spectrum 13: **Hacac** (*acetylacetone*) **$CDCl_3$**

Enol isomer: 5.50 (s, 1H, CH), 2.05 (s, 6H, 2x CH_3)

Keto isomer: 3.60 (s, 2H, CH_2), 2.25 (s, 6H, 2x CH_3)

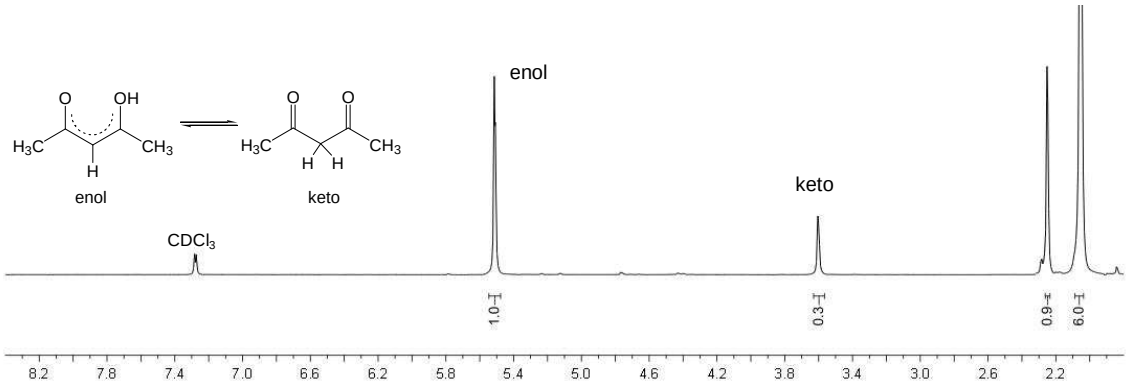

Spectrum 14: **Hmaa** (*methylacetylacetone*) **$CDCl_3$**

Keto isomer: 3.74 (s, 3H, OCH_3), 3.46 (s, 2H, CH_2), 2.27 (s, 3H, CH_3)

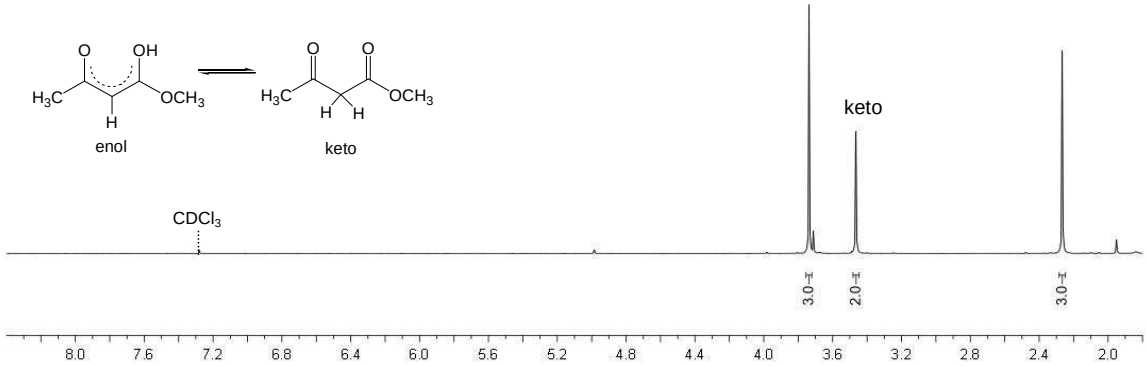

Spectrum 15: **H_2cat** (*catechol*) **$CDCl_3$**

6.91−6.87 (m, 2H, catH), 6.85−6.82 (m, 2H, catH), 5.16(s_{br}, 2H, OH)

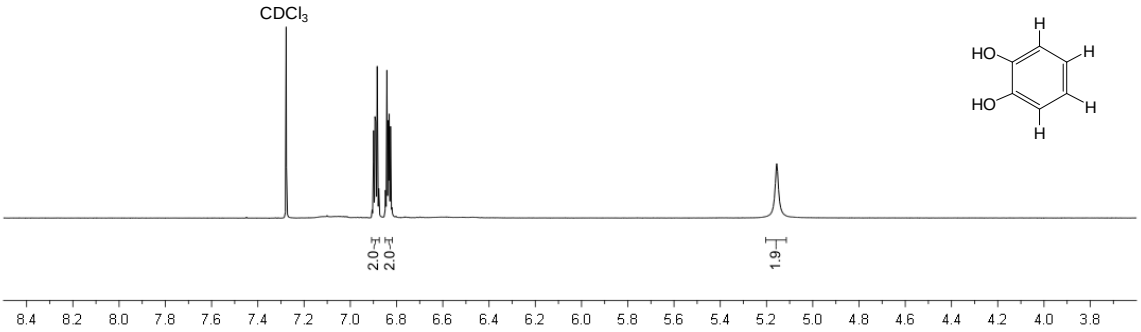

Spectrum 16: **H_2naph** (*naphthyldiol*) **$CDCl_3$**

7.67−7.63 (m, 2H, naphH), 7.34−7.31 (m, 2H, naphH), 7.24 (s, 2H, naphH), 5.16(s_{br}, 2H, OH)

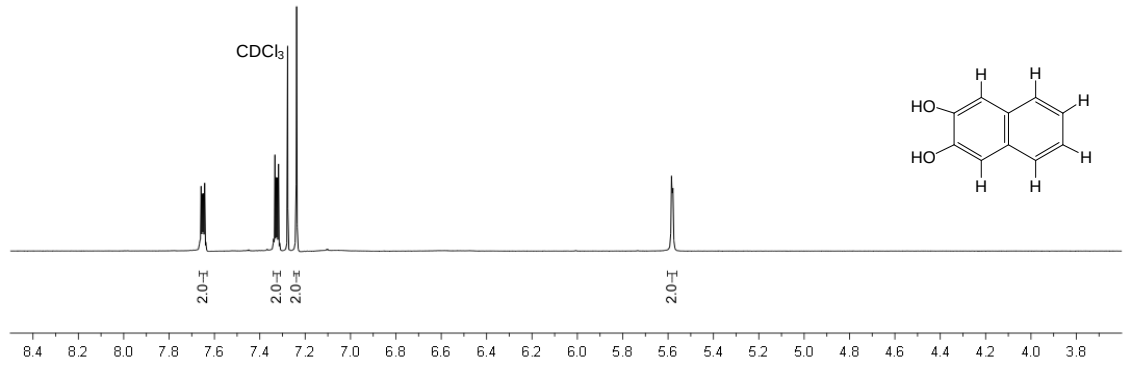

Spectrum 17: **H_2biphen** (*biphenol*) **$CDCl_3$**

7.35 (t, 2H, biphenH), 7.29 (d, 2H, biphenH), 7.11−7.03 (m, 4H, biphenH), 5.50 (s_{br}, 2H, OH)

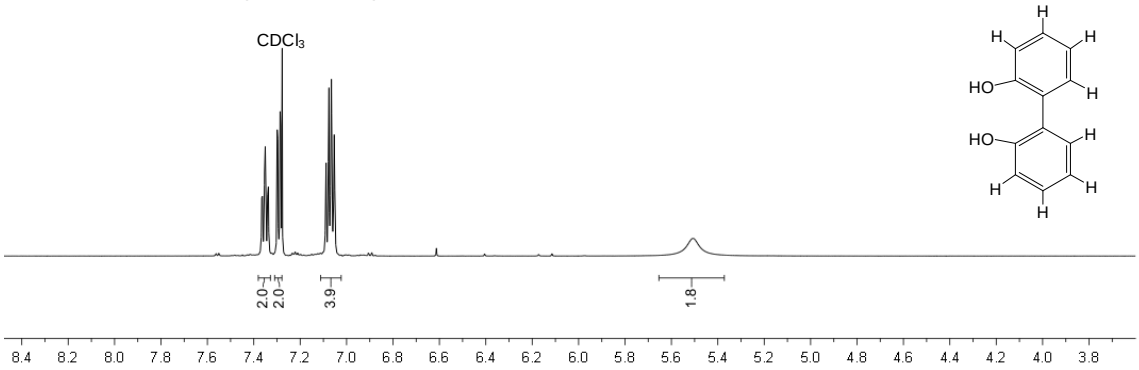

Spectrum 18: **H_2binaph** (bi*naphthol*) **$CDCl_3$**

8.00 (d, 2H, binaphH), 7.92 (d, 2H, binaphH), 7.41 (d, 2H, binaphH),
7.40 (t, 2H, binaphH), 7.33 (t, 2H, binaphH), 7.17 (d, 2H, binaphH), 5.06 (s_{br}, 2H, OH)

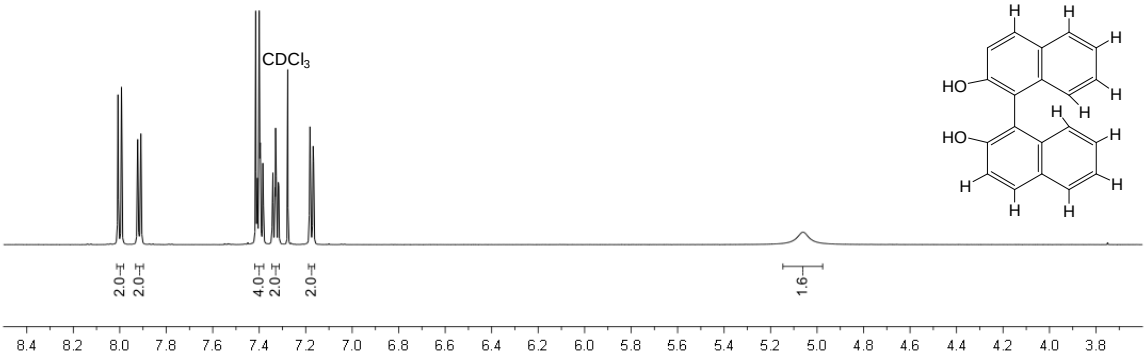

Spectrum 19: **H_2mbiphen** (*methylene-diphenol*) **$CDCl_3$**

7.29 (d, 2H, mbiphenH), 7.12 (t, 2H, mbiphenH), 6.91 (t, 2H, mbiphenH),
6.84 (d, 2H, mbiphenH), 6.75 (s_{br}, 2H, OH), 3.96 (s, 2H, CH_2)

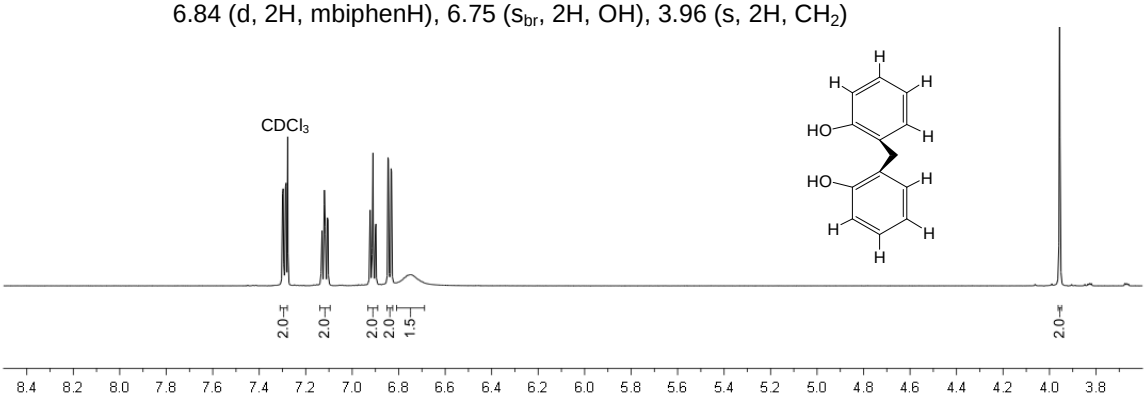

Spectrum 20: **H_2mbinaph** (*methylene-dinaphthol*) **$CDCl_3$**

8.23 (d, 2H, mbinaphH), 7.79 (d, 2H, mbinaphH), 7.67 (d, 2H, mbinaphH),
7.46 (t, 2H, mbinaphH), 7.35 (t, 2H, mbinaphH), 7.07 (d, 2H, mbinaphH),
6.35 (s_{br}, 2H, OH), 4.83 (s, 2H, CH_2)

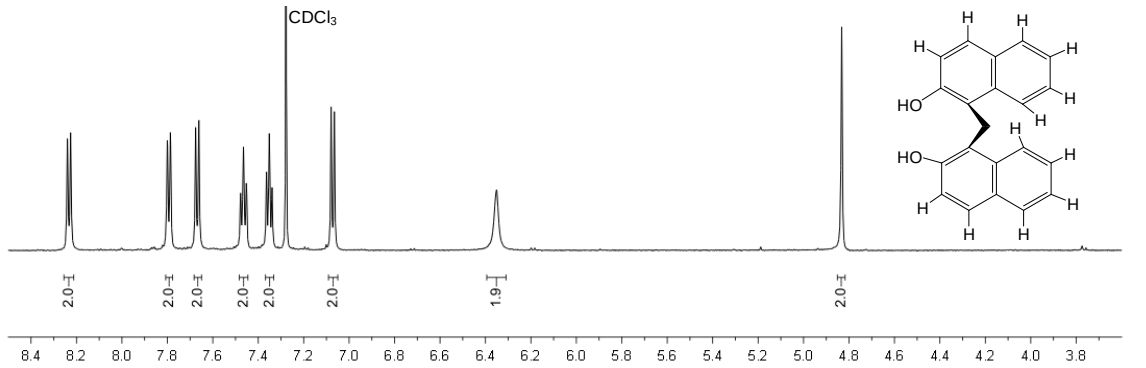

A.2 TETRAHEDRAL Ti(IV) COMPLEXES

Spectrum 21: **$[TiCp_2(tfaa)]^+ClO_4^-$ [3]** **Acetone-d_6**

Bis(η^5-cyclopentadienyl) (trifluoroacetylacetonato-O,O') titanium(IV) perchlorate

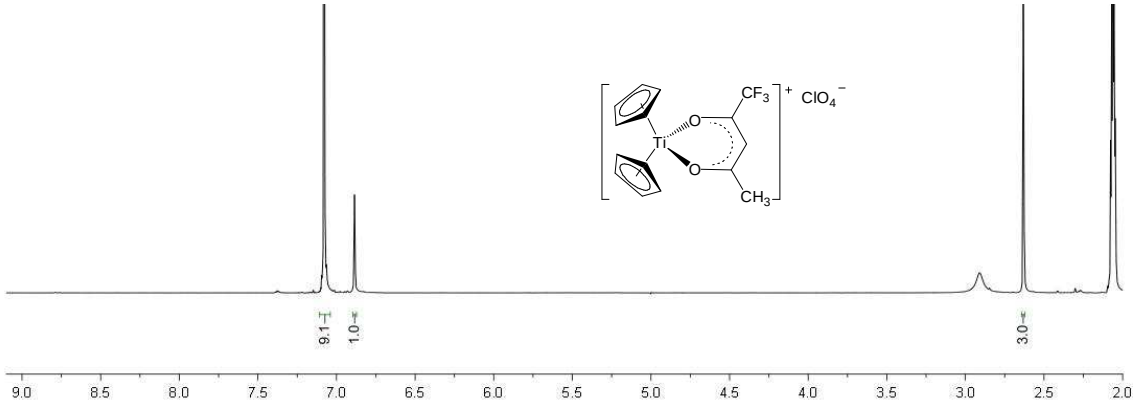

Spectrum 22: **$[TiCp_2(tfth)]^+ClO_4^-$ [4]** **Acetone-d_6**

Bis(η^5-cyclopentadienyl) (trifluorothenoylacetonato-O,O') titanium(IV) perchlorate

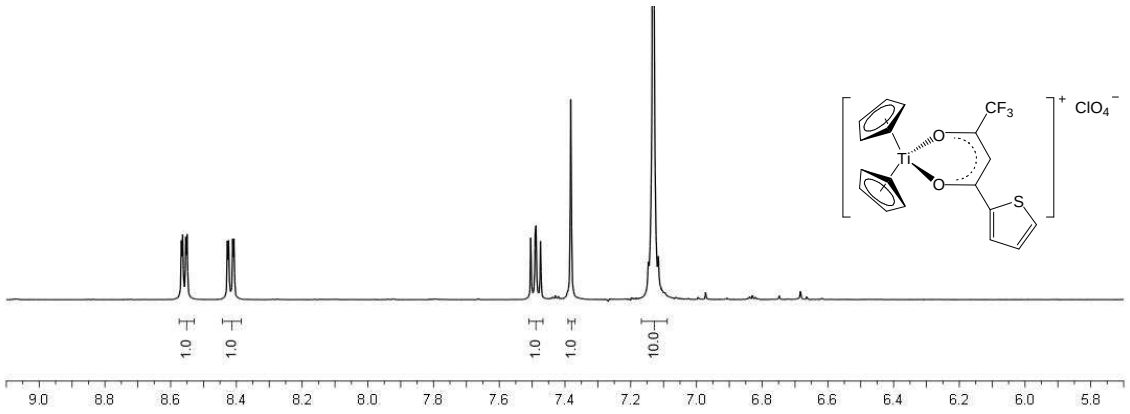

Spectrum 23: **$[TiCp_2(tffu)]^+ClO_4^-$ [5]** **Acetone-d_6**

Bis(η^5-cyclopentadienyl) (trifluorofuroylacetonato-O,O') titanium(IV) perchlorate

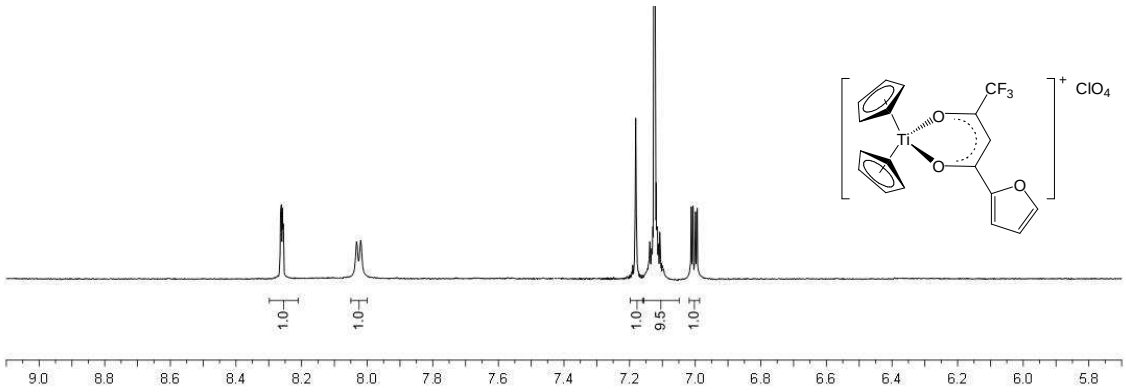

Spectrum 24: **$[TiCp_2(tfba)]^+ClO_4^-$ [6]** **Acetone-d_6**

Bis(η^5-cyclopentadienyl) (trifluorobenzoylacetonato-O,O') titanium(IV) perchlorate

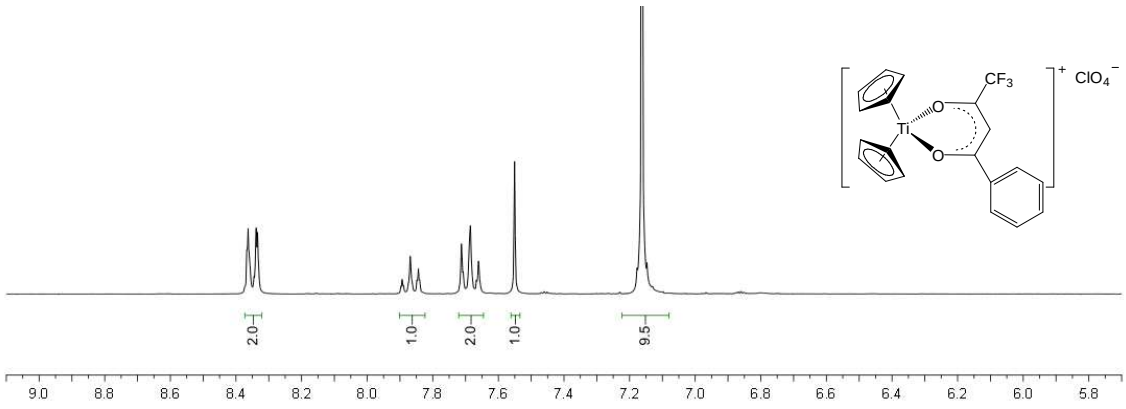

Spectrum 25: **$[TiCp_2(ba)]^+ClO_4^-$ [7]** **Acetone-d_6**

Bis(η^5-cyclopentadienyl) (benzoylacetonato-O,O') titanium(IV) perchlorate

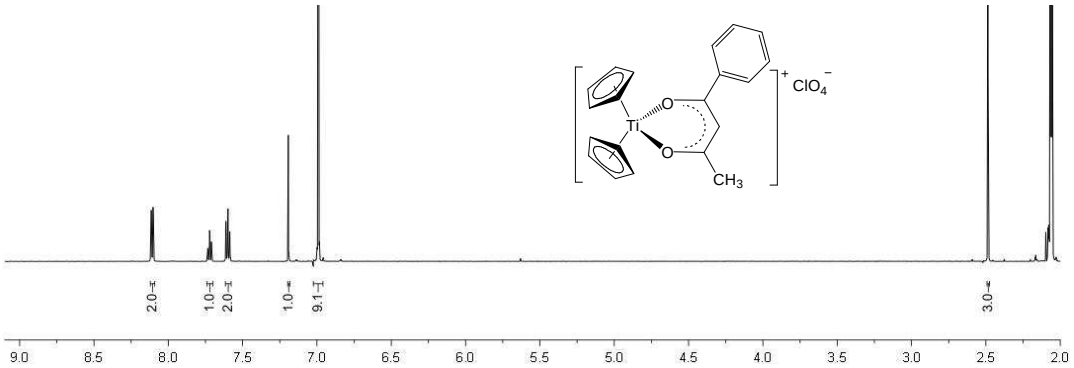

Spectrum 26: **$[TiCp_2(thba)]^+ClO_4^-$ [8]** **Acetone-d_6**

Bis(η^5-cyclopentadienyl) (thenoylbenzoylacetonato-O,O') titanium(IV) perchlorate

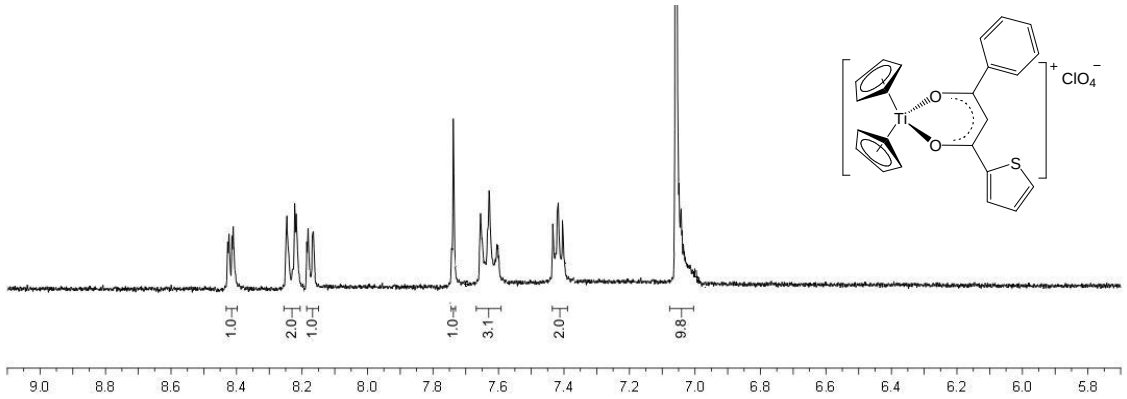

Spectrum 27: **$[TiCp_2(dbm)]^+ClO_4^-$ [9]** **Acetone-d_6**

Bis(η^5-cyclopentadienyl) (dibenzoylmethanato-O,O') titanium(IV) perchlorate

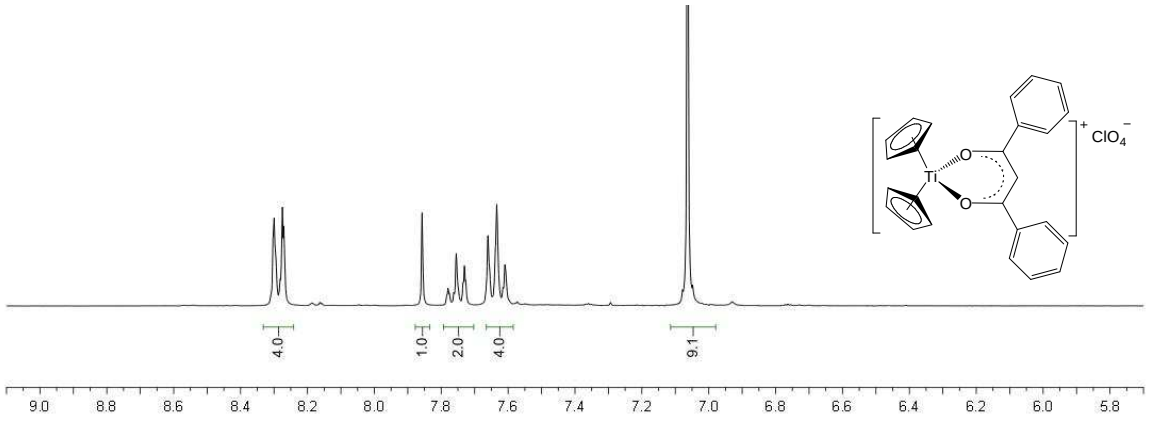

Spectrum 28: **$[TiCp_2(acac)]^+ClO_4^-$ [10]** **Acetone-d_6**

Bis(η^5-cyclopentadienyl) (acetylacetonato-O,O') titanium(IV) perchlorate

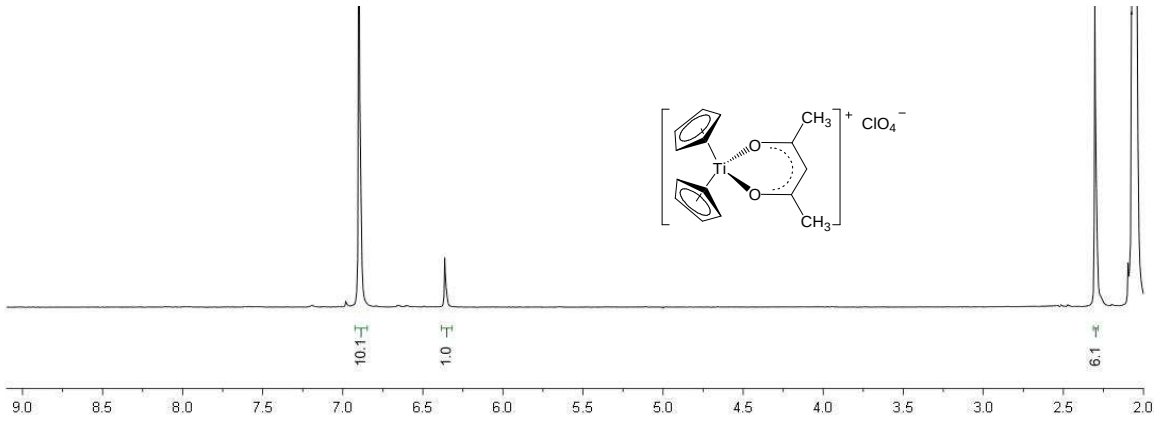

Spectrum 29: **$[TiCp_2(maa)]^+ClO_4^-$ [11]** **Acetone-d_6**

Bis(η^5-cyclopentadienyl) (methylacetylacetonato-O,O') titanium(IV) perchlorate

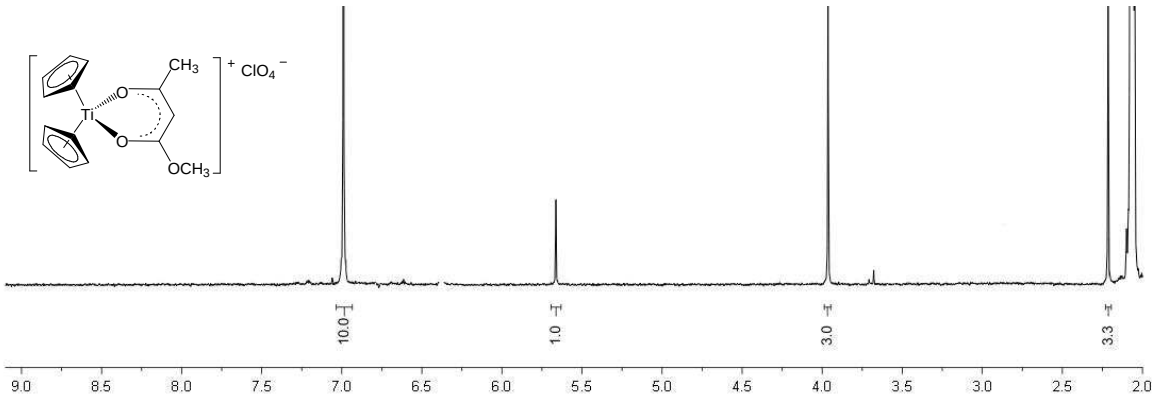

Spectrum 30: **$TiCp_2$(biphen) [12]** **Acetone-d_6**

Bis(η^5-cyclopentadienyl) (biphenolato-O,O') titanium(IV)

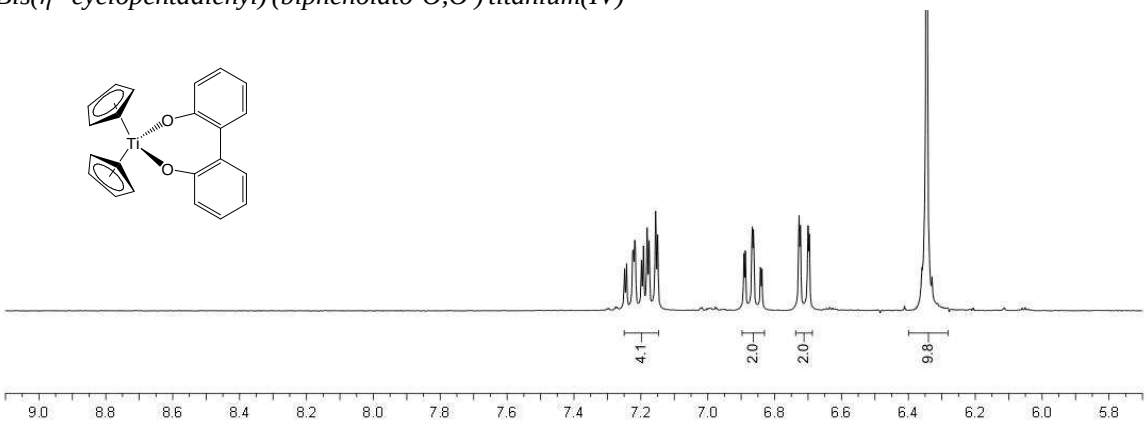

Spectrum 30a: **$TiCp_2$(biphen) [12]** **$CDCl_3$**

Bis(η^5-cyclopentadienyl) (biphenyldiolato-O,O') titanium(IV)

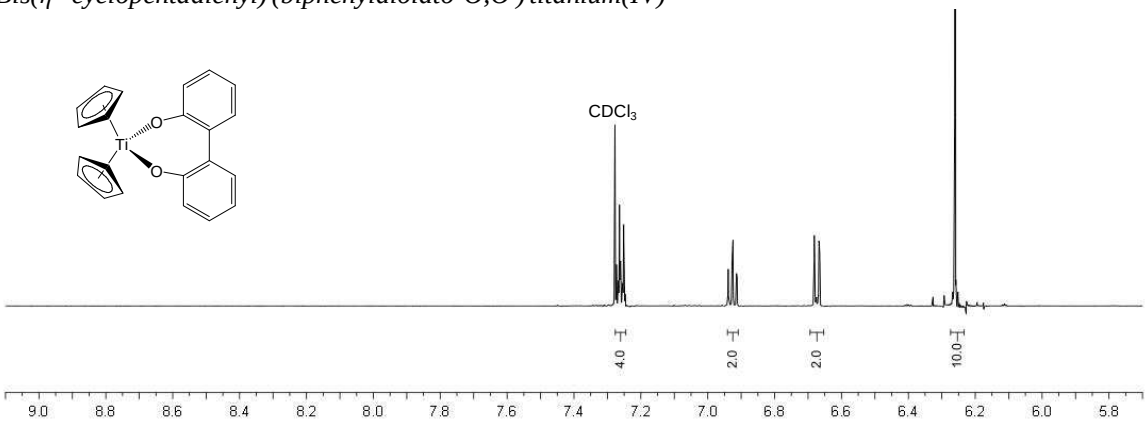

A.3 OCTAHEDRAL Ti(IV) COMPLEXES

Spectrum 31: **$Ti(tfaa)_2Cl_2$ [13]** **$CDCl_3$**

Bis(trifluoroacetylacetonato-O,O') dichloro titanium(IV)

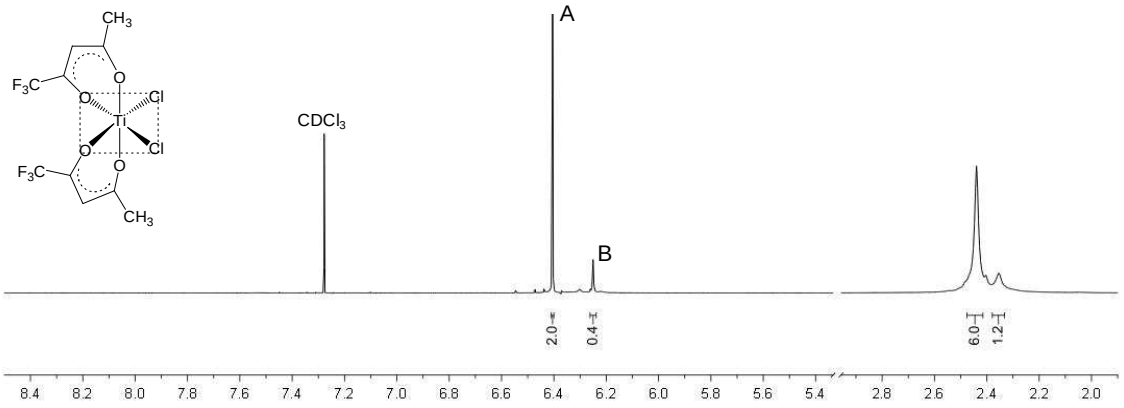

Spectrum 32: **$Ti(hfaa)_2Cl_2$ [14]** **$CDCl_3$**

Bis(hexafluoroacetylacetonato-O,O') dichloro titanium(IV)

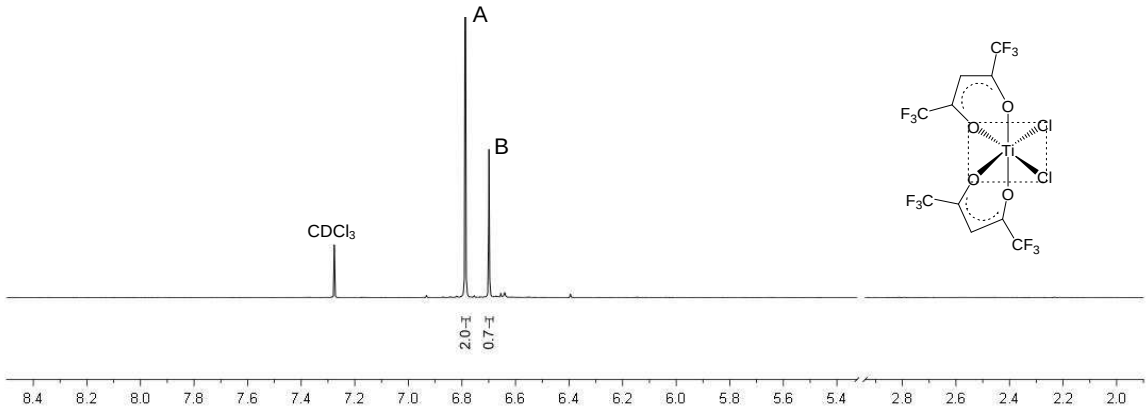

Spectrum 33: **$Ti(tfth)_2Cl_2$ [15]** **$CDCl_3$**

Bis(trifluorothenoylacetonato-O,O') dichloro titanium(IV)

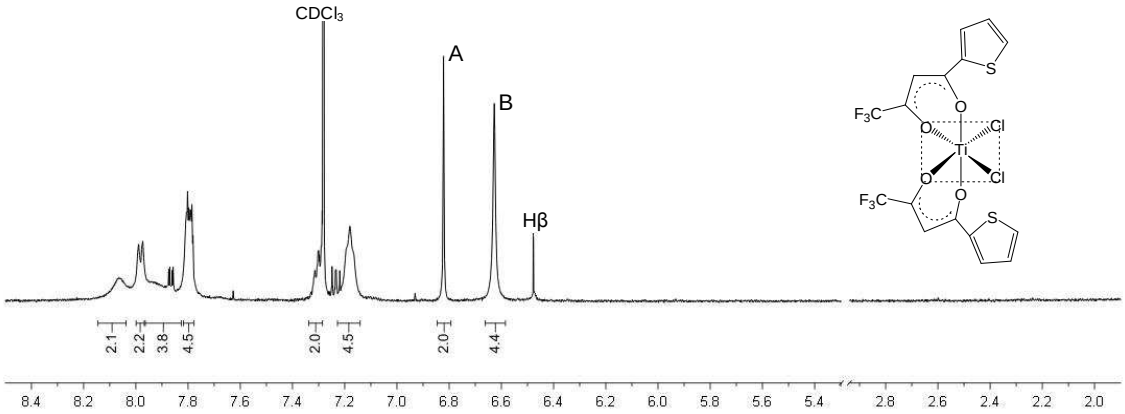

Spectrum 34: **$Ti(tffu)_2Cl_2$ [16]** **$CDCl_3$**

Bis(trifluorofuroylacetonato-O,O') dichloro titanium(IV)

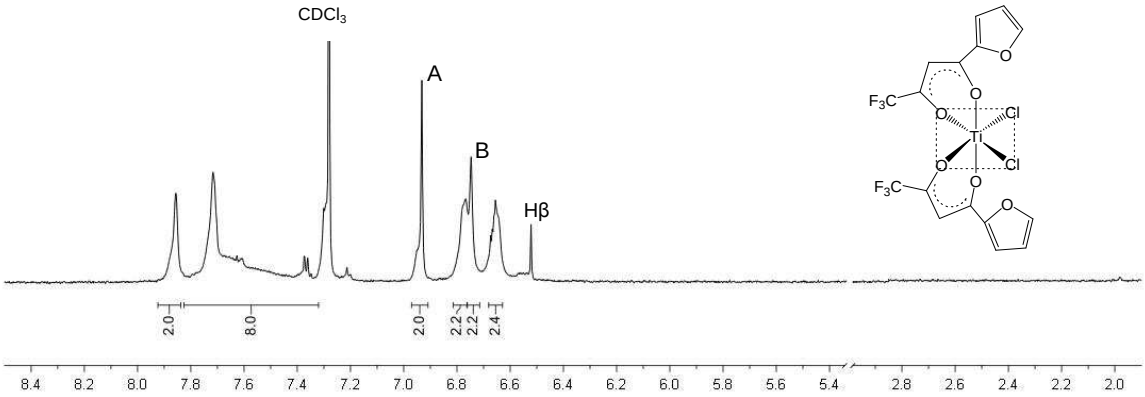

Spectrum 35: **$Ti(tfba)_2Cl_2$ [17]** **$CDCl_3$**

Bis(trifluorobenzoylacetonato-O,O') dichloro titanium(IV)

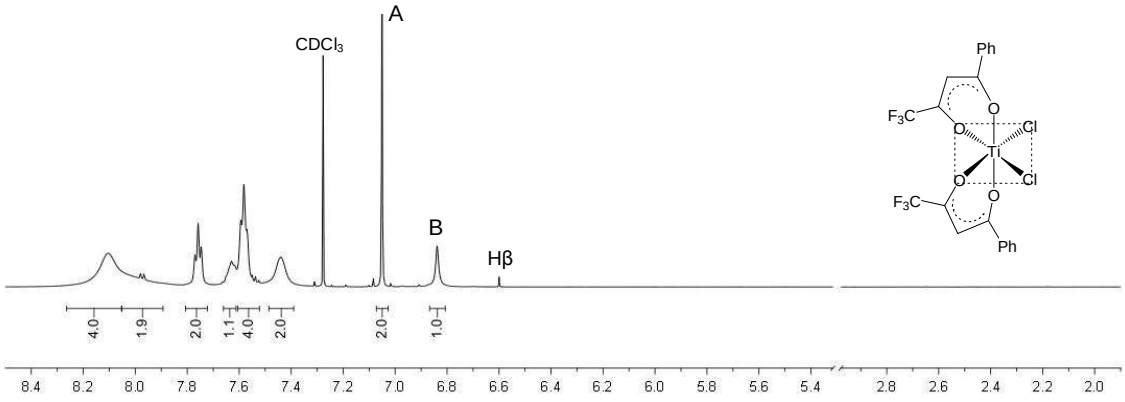

Spectrum 36: **$Ti(tfma)_2Cl_2$ [18]** **$CDCl_3$**

Bis(methyltrifluoroacetonato-O,O') dichloro titanium(IV)

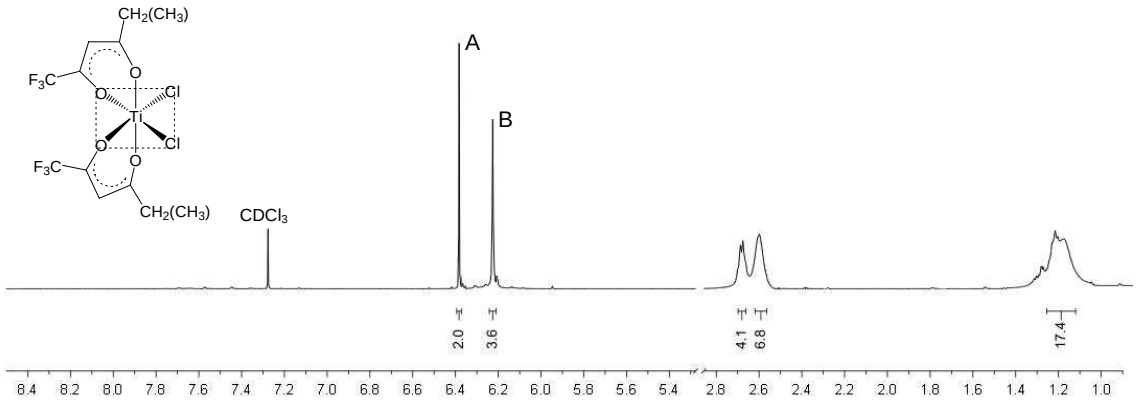

Spectrum 37: **$Ti(tfdma)_2Cl_2$ [19]** **$CDCl_3$**

Bis(dimethyltrifluoroacetonato-O,O') dichloro titanium(IV)

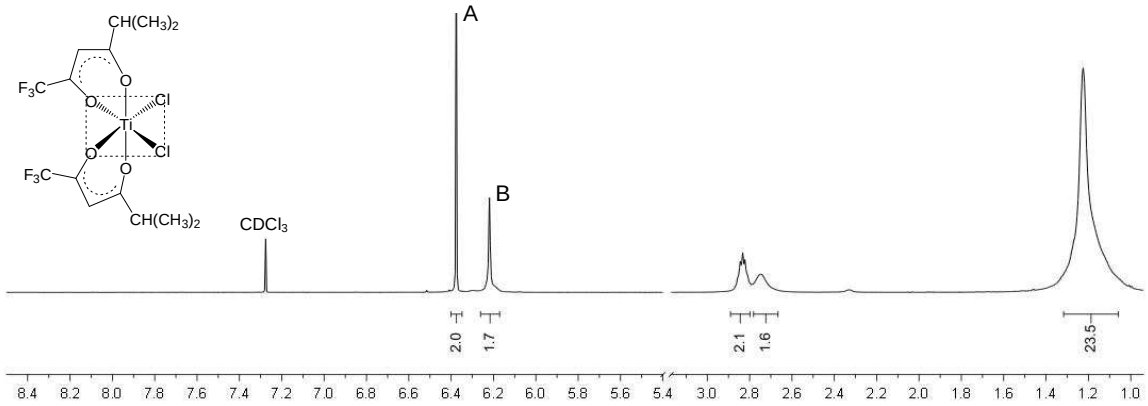

Spectrum 38: **$Ti(tftma)_2Cl_2$ [20]** **$CDCl_3$**

Bis(trimethyltrifluoroacetonato-O,O') dichloro titanium(IV)

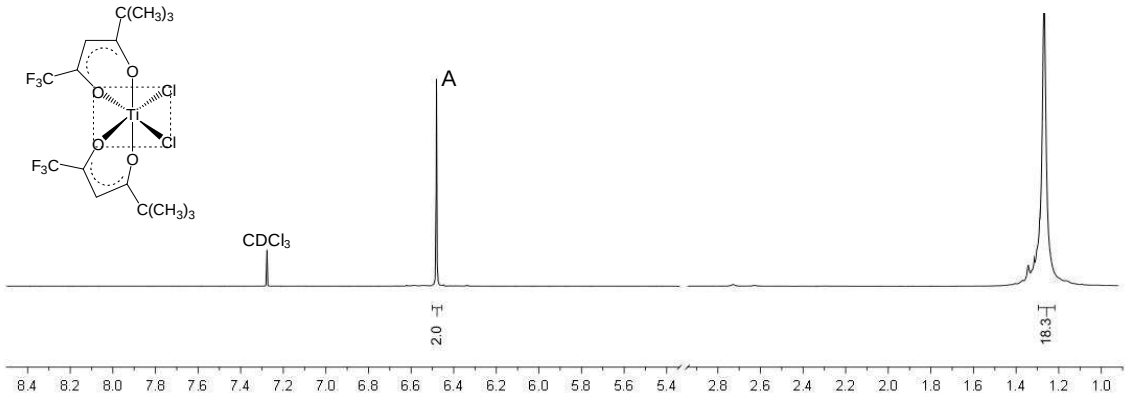

Spectrum 39: **$Ti(ba)_2Cl_2$ [21]** **$CDCl_3$**

Bis(benzoylacetonato-O,O') dichloro titanium(IV)

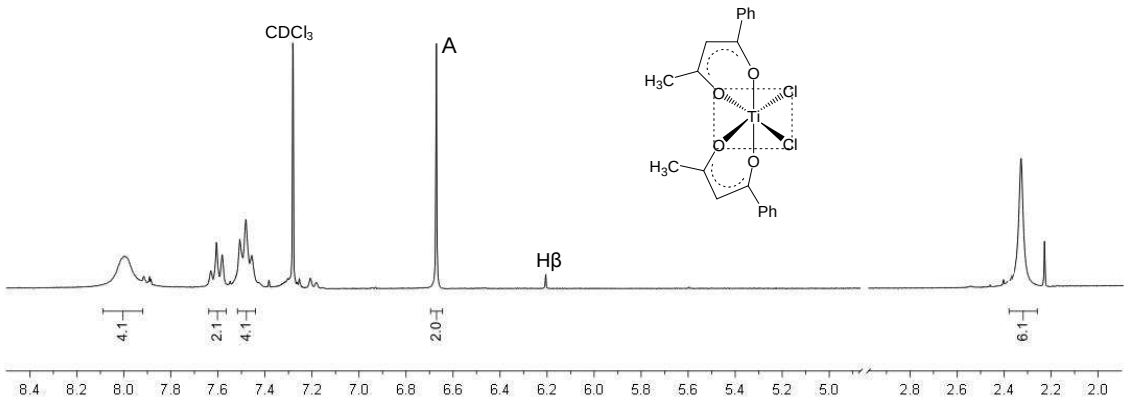

Spectrum 40: **$Ti(dbm)_2Cl_2$ [22]** **$CDCl_3$**

Bis(dibenzoylmethanato-O,O') dichloro titanium(IV)

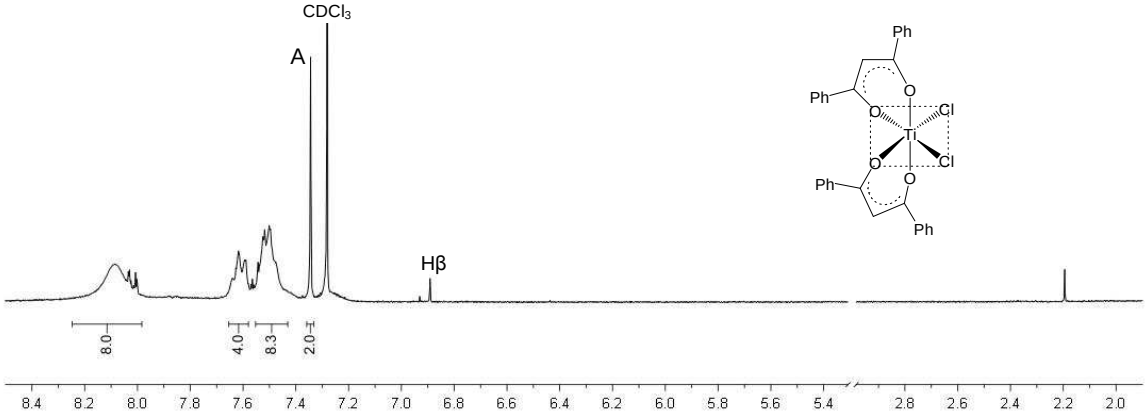

Spectrum 41: **$Ti(acac)_2Cl_2$ [23]** **$CDCl_3$**

Bis(acetylacetonato-O,O') dichloro titanium(IV)

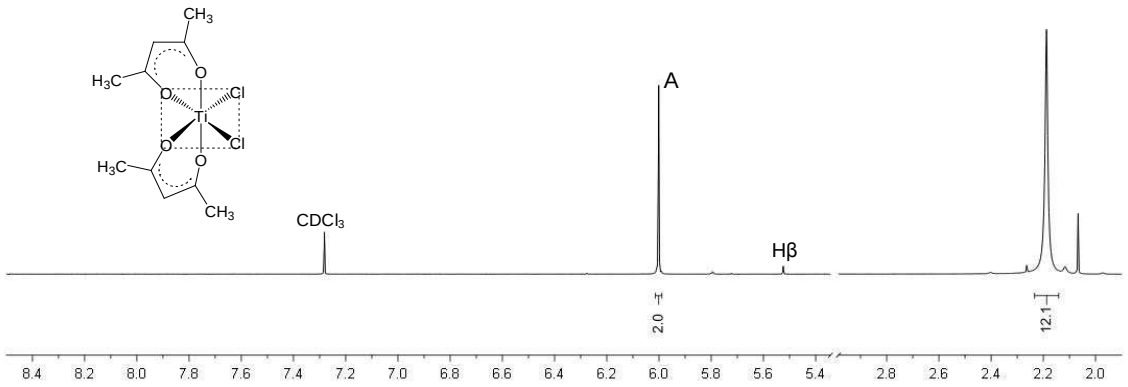

Spectrum 42: **Ti(tfaa)$_2$biphen [24]** **$CDCl_3$**

Bis(trifluoroacetylacetonato-O,O') (biphenyldiolato-O,O') titanium(IV)

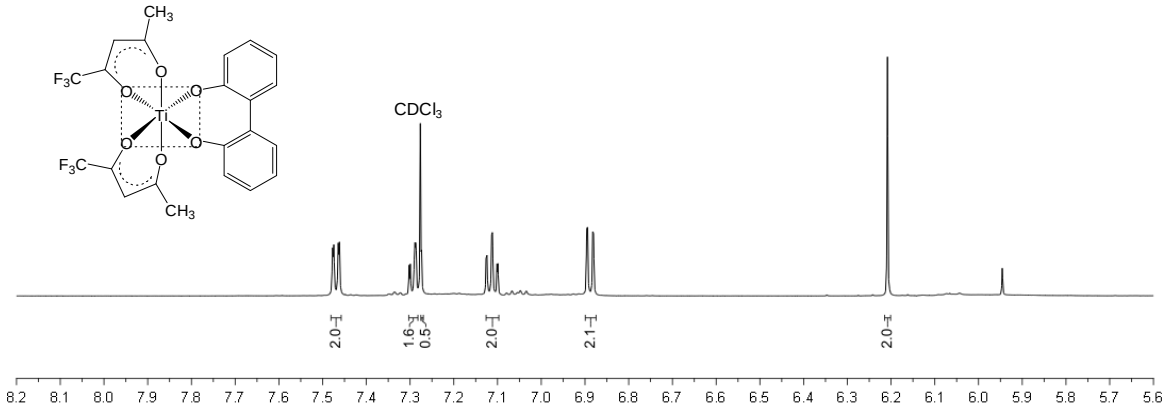

Spectrum 43: **Ti(hfaa)$_2$biphen [25]** **$CDCl_3$**

Bis(hexafluoroacetylacetonato-O,O') (biphenyldiolato-O,O') titanium(IV)

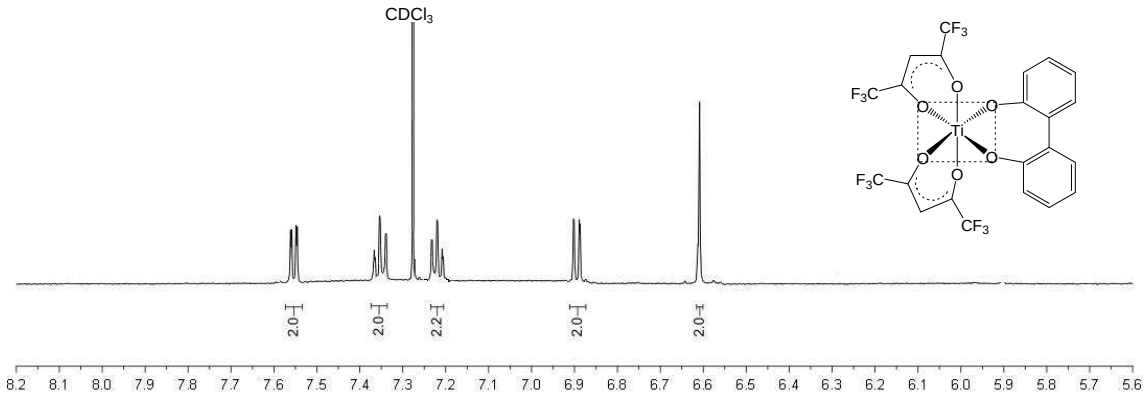

Spectrum 44: **Ti(tfth)$_2$biphen [26]** **$CDCl_3$**

Bis(trifluorothenoylacetonato-O,O') (biphenyldiolato-O,O') titanium(IV)

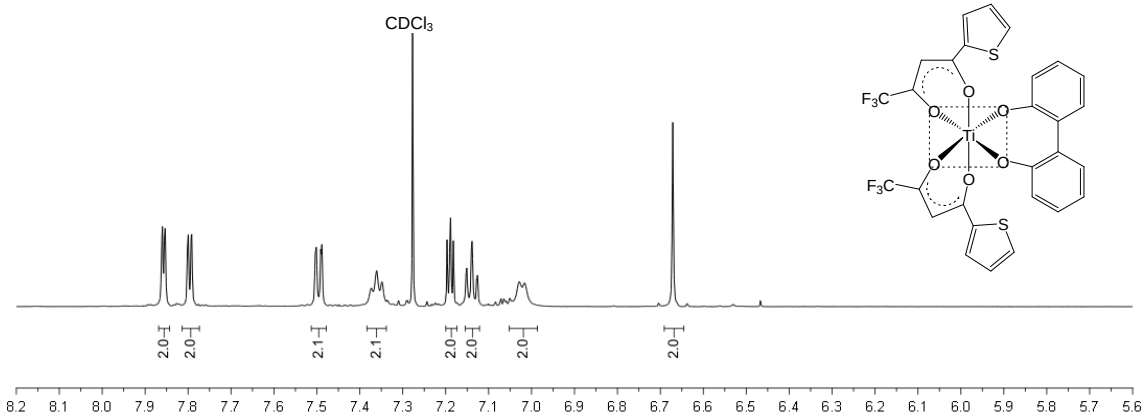

Spectrum 45: **Ti(tffu)$_2$biphen [27]** **$CDCl_3$**

Bis(trifluorofuroylacetonato-O,O') (biphenyldiolato-O,O') titanium(IV)

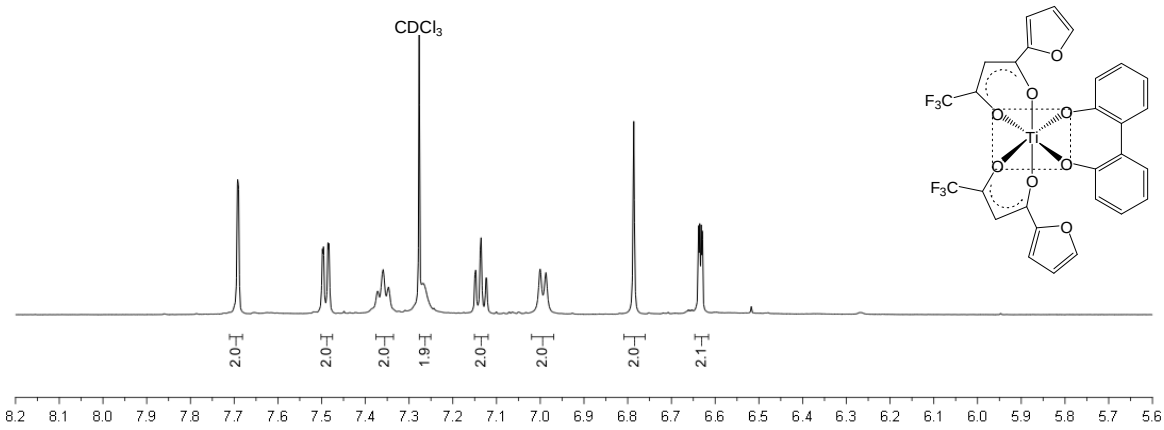

Spectrum 46: **Ti(tfba)$_2$biphen [28]** **$CDCl_3$**

Bis(trifluorobenzoylacetonato-O,O') (biphenyldiolato-O,O') titanium(IV)

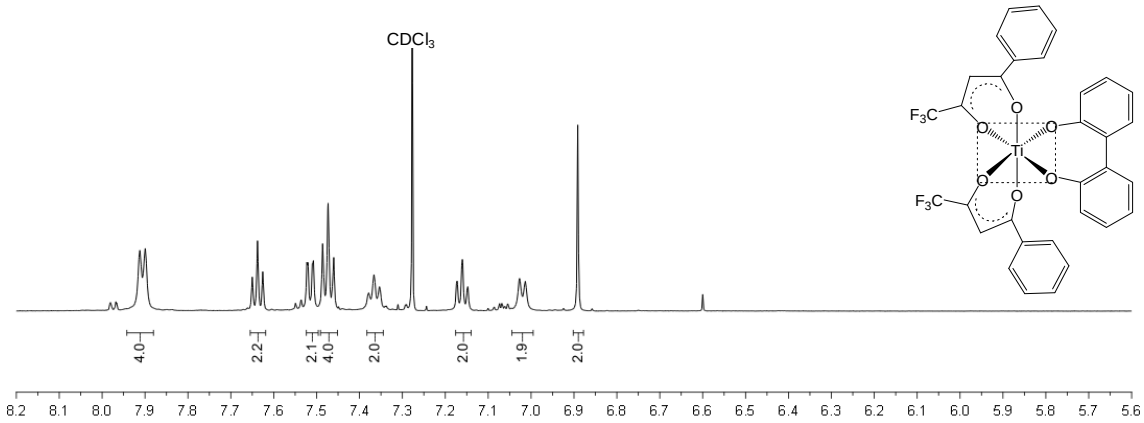

Spectrum 47: **Ti(tfma)$_2$biphen [29]** **$CDCl_3$**

Bis(methyltrifluoroacetonato-O,O') (biphenyldiolato-O,O') titanium(IV)

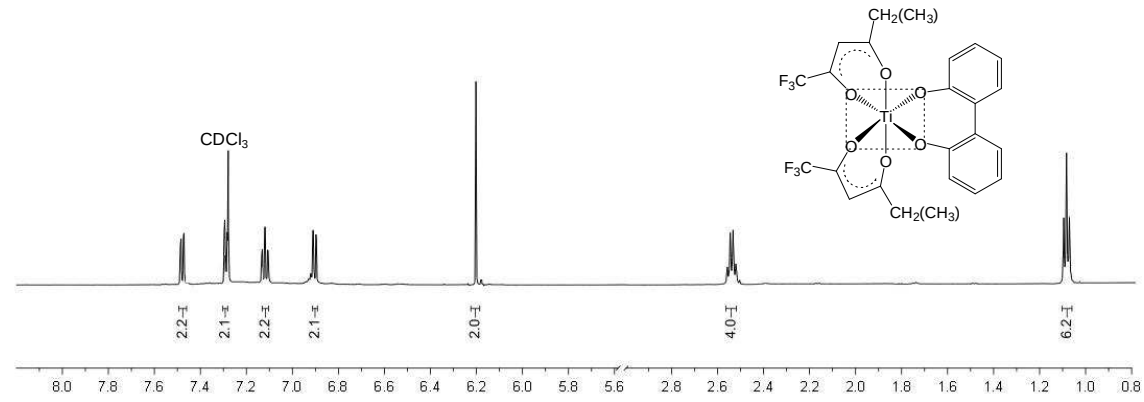

Spectrum 48: **Ti(tfdma)$_2$biphen [30]** **$CDCl_3$**

Bis(dimethyltrifluoroacetonato-O,O') (biphenyldiolato-O,O') titanium(IV)

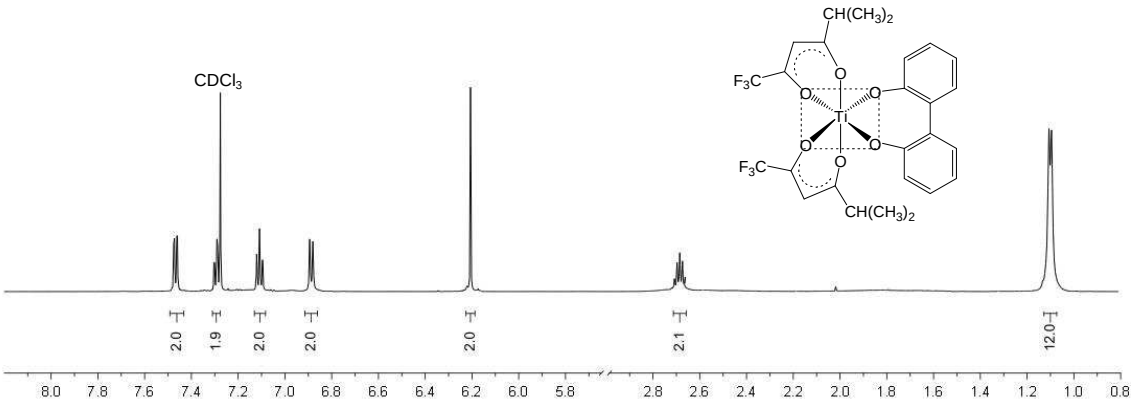

Spectrum 49: **Ti(tftma)$_2$biphen [31]** **$CDCl_3$**

Bis(trimethyltrifluoroacetonato-O,O') (biphenyldiolato-O,O') titanium(IV)

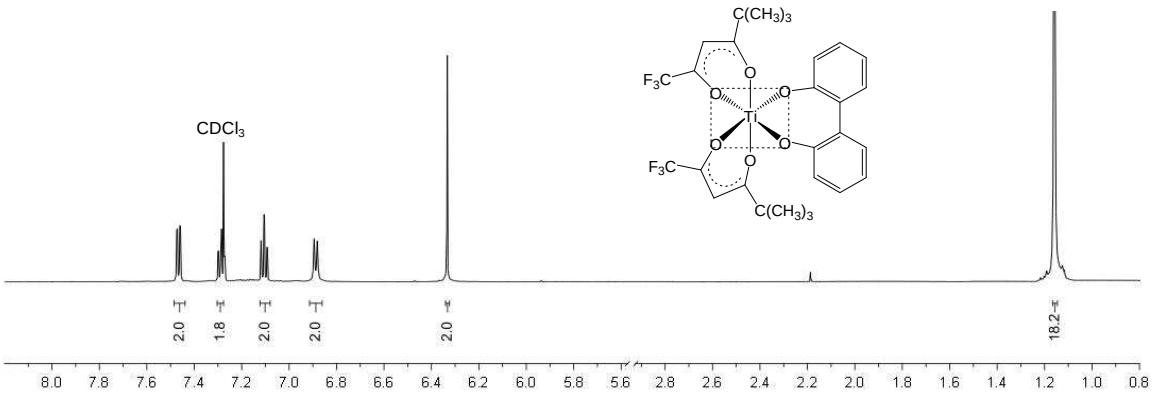

Spectrum 50: **Ti(ba)$_2$biphen [32]** **$CDCl_3$**

Bis(benzoylacetonato-O,O') (biphenyldiolato-O,O') titanium(IV)

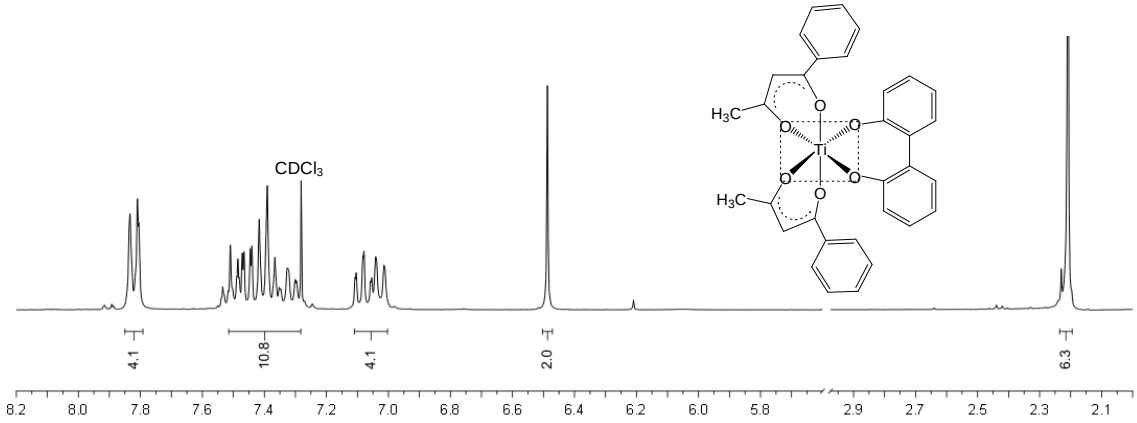

Spectrum 51: **Ti(dbm)$_2$biphen [33]** **$CDCl_3$**

Bis(dibenzoylmethanato-O,O') (biphenyldiolato-O,O') titanium(IV)

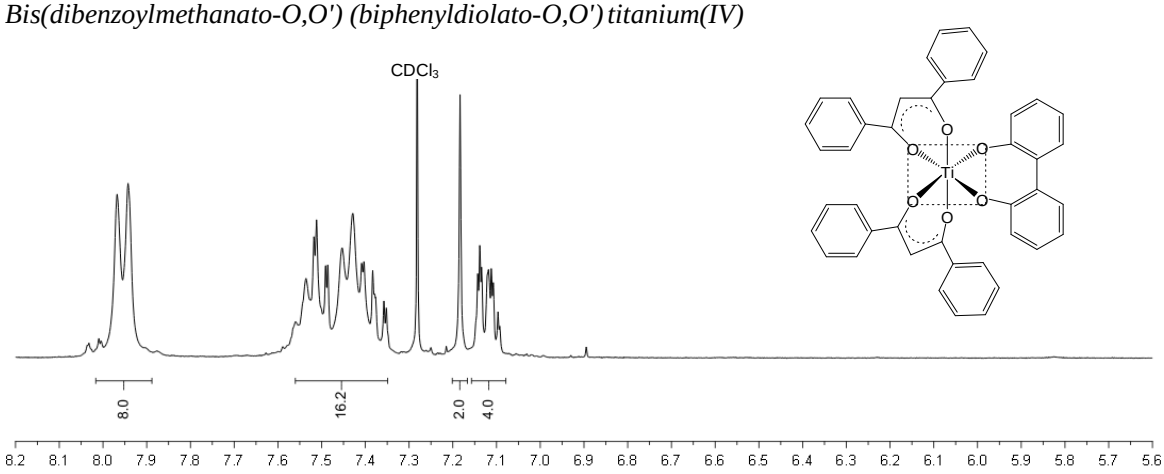

Spectrum 52: **Ti(acac)$_2$cat [34]** **$CDCl_3$**

Bis(acetylacetonato-O,O') (benzyldiolato-O,O') titanium(IV)

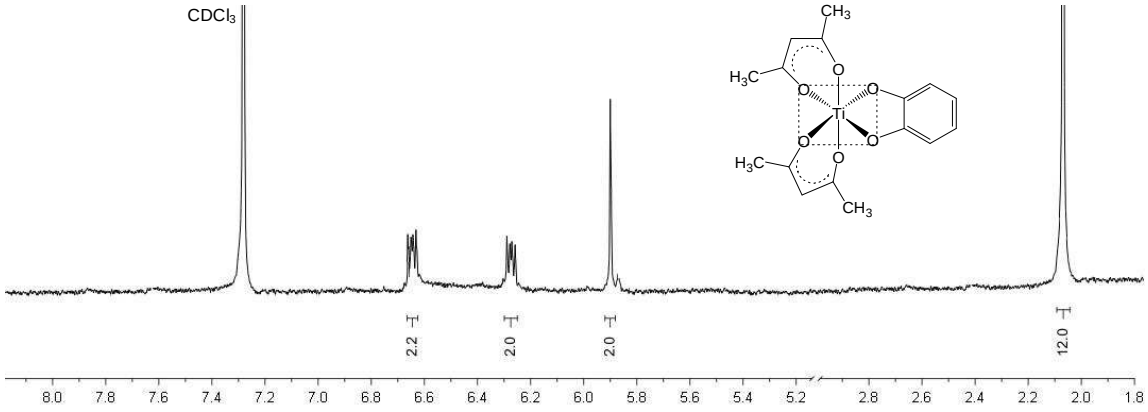

Spectrum 53: **Ti(acac)$_2$naph [35]** **$CDCl_3$**

Bis(acetylacetonato-O,O') (naphthyldiolato-O,O') titanium(IV)

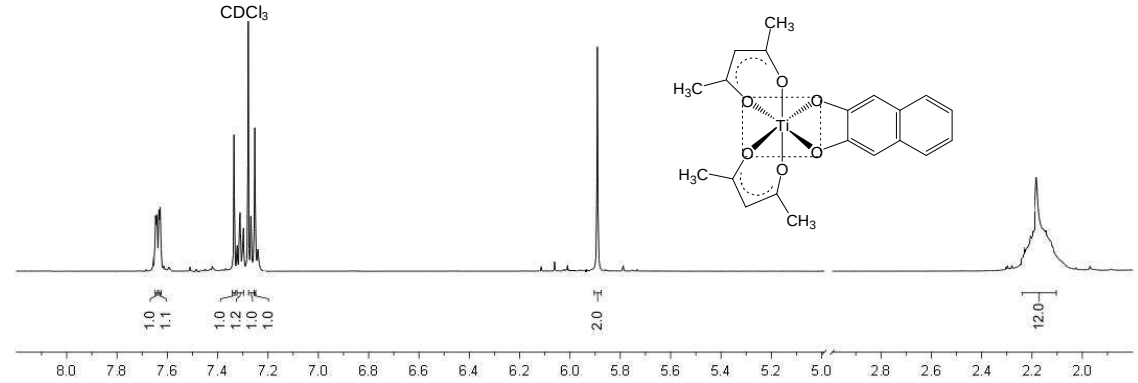

Spectrum 54: **Ti(acac)$_2$biphen [36]** **$CDCl_3$**

Bis(acetylacetonato-O,O') (biphenyldiolato-O,O') titanium(IV)

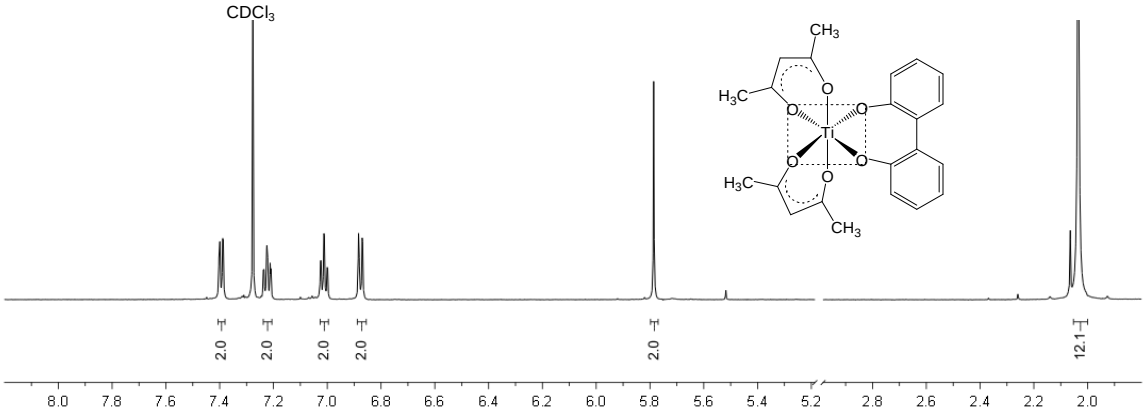

Spectrum 55: **Ti(acac)$_2$binaph [37]** **$CDCl_3$**

Bis(acetylacetonato-O,O') (binaphthyldiolato-O,O') titanium(IV)

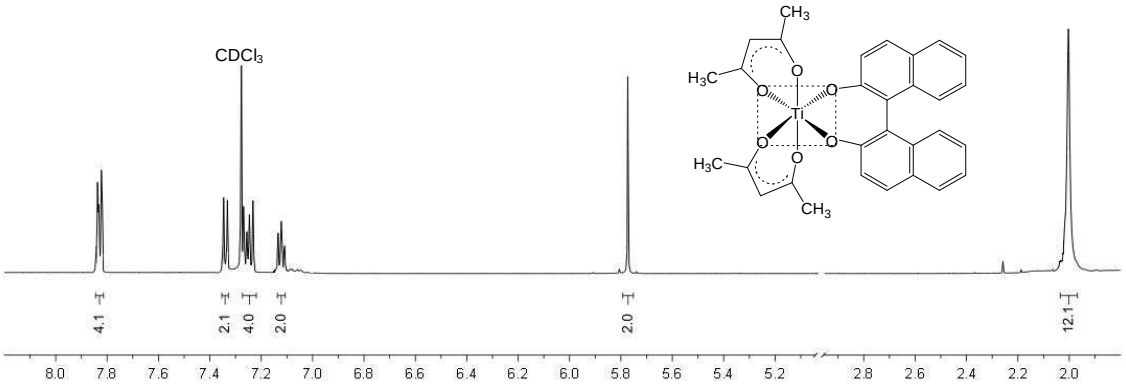

Spectrum 57: **Ti(acac)$_2$mbinaph [39]** **$CDCl_3$**

Bis(acetylacetonato-O,O') (methylenebinaphthyldiolato-O,O') titanium(IV)

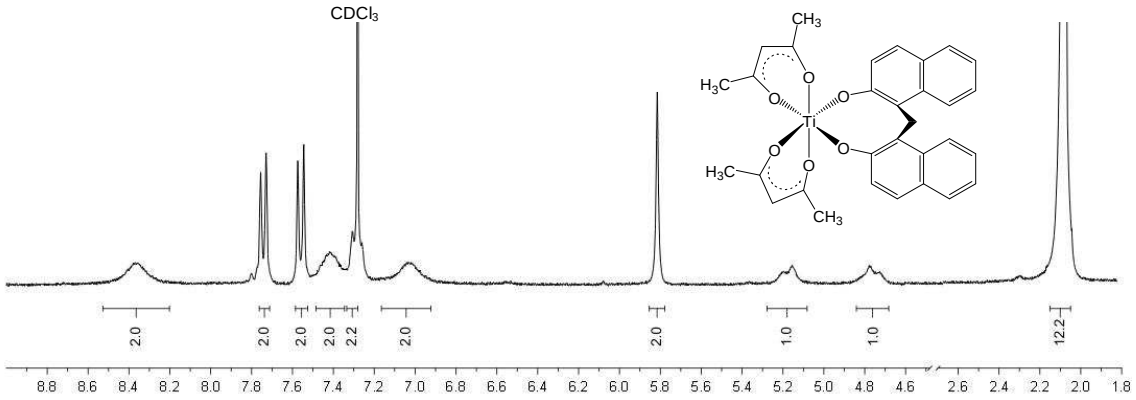

Spectrum 58: **Ti(tfaa)$_2$mbinaph [40]** **$CDCl_3$**

Bis(trifluoroacetylacetonato-O,O') (methylenebinaphthyldiolato-O,O') titanium(IV)

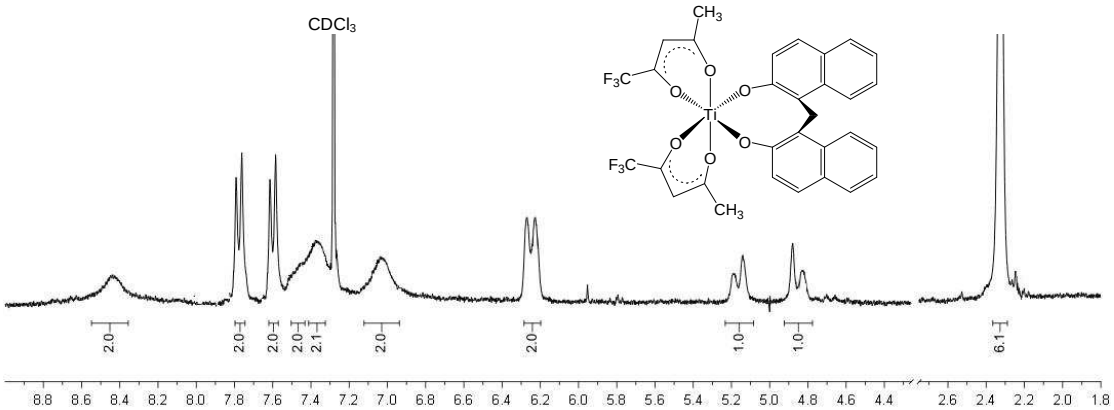

Spectrum 59: **Ti(hfaa)$_2$mbinaph [41]** **$CDCl_3$**

Bis(hexafluoroacetylacetonato-O,O') (methylenebinaphthyldiolato-O,O') titanium(IV)

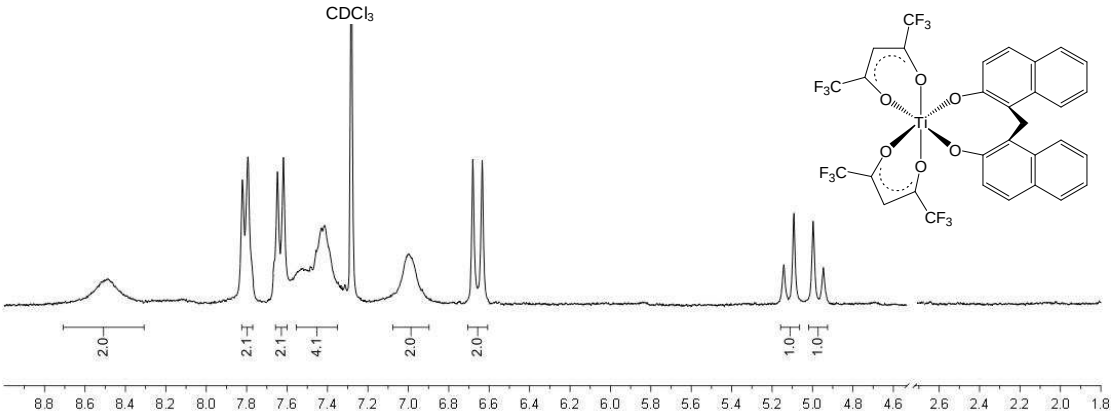

APPENDIX A

B ^{19}F NMR Spectra

B.1 LIGANDS

Spectrum 60: **Hhfaa** (*hexafluoroacetylacetone*) **$CDCl_3$**

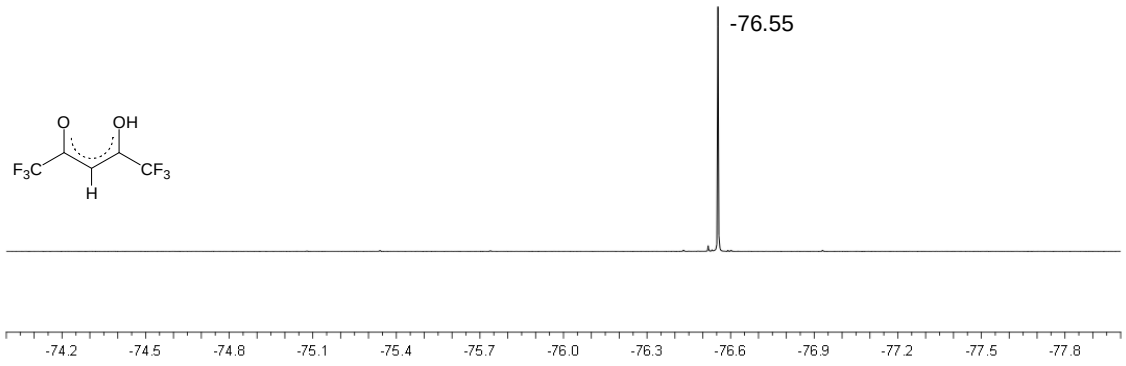

Spectrum 61: **Htfaa** (*trifluoroacetylacetone*) **$CDCl_3$**

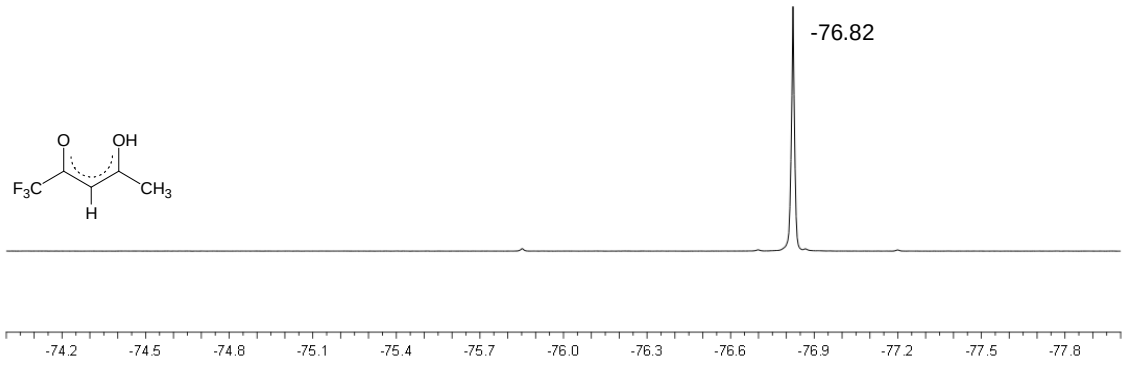

Spectrum 62: **Htfma** (*trifluoromethylacetylacetone*) **$CDCl_3$**

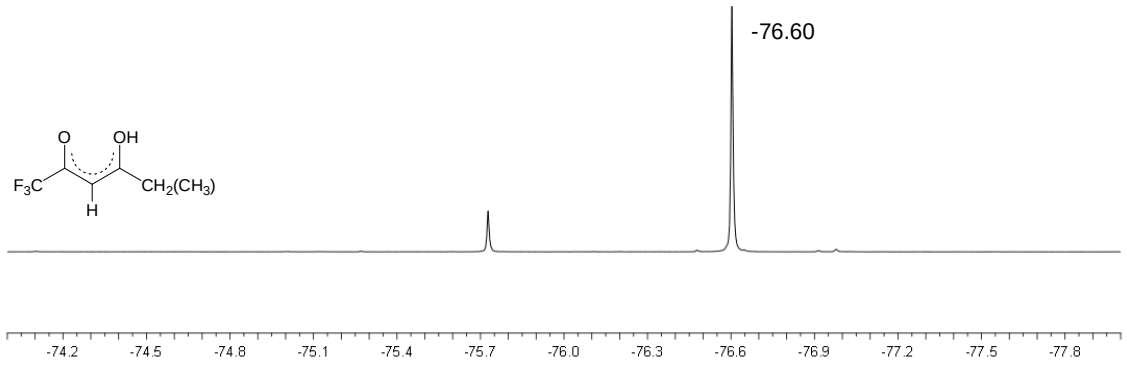

Spectrum 63: **Htfdma** (*trifluorodimethylacetylacetone*) **$CDCl_3$**

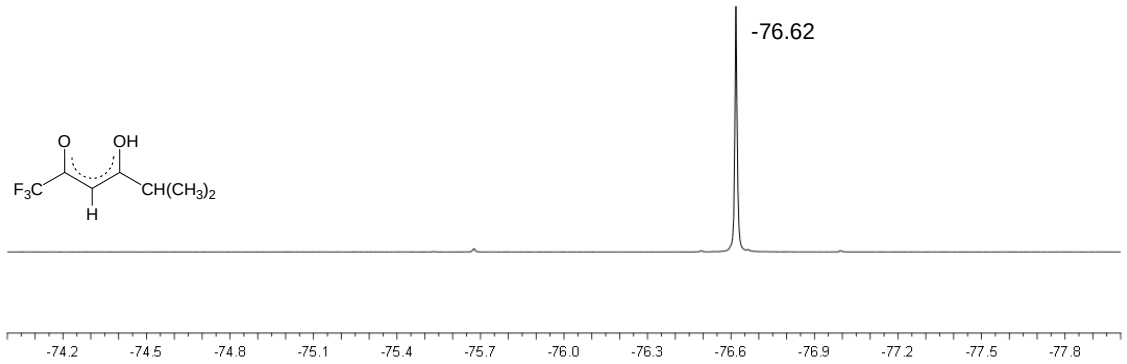

Spectrum 64: **Htftma** (*trifluorotrimethylacetylacetone*) **$CDCl_3$**

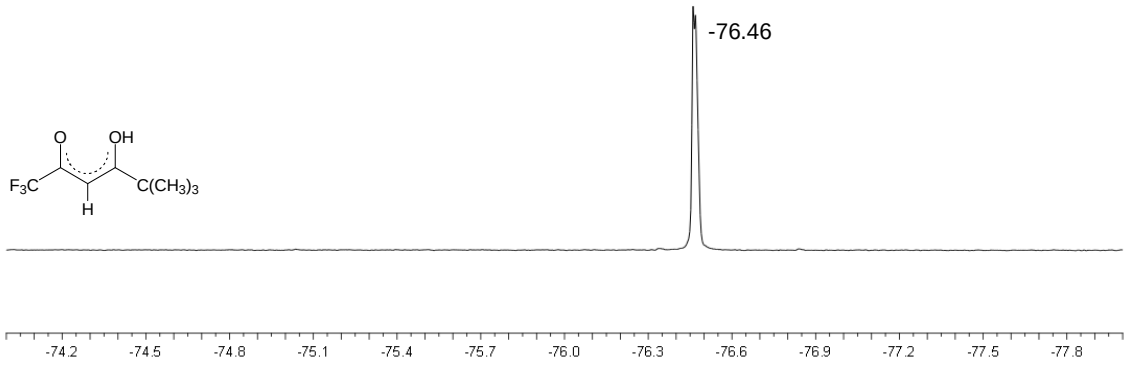

Spectrum 65: **Htfth** (*trifluorothenoylacetone*) **$CDCl_3$**

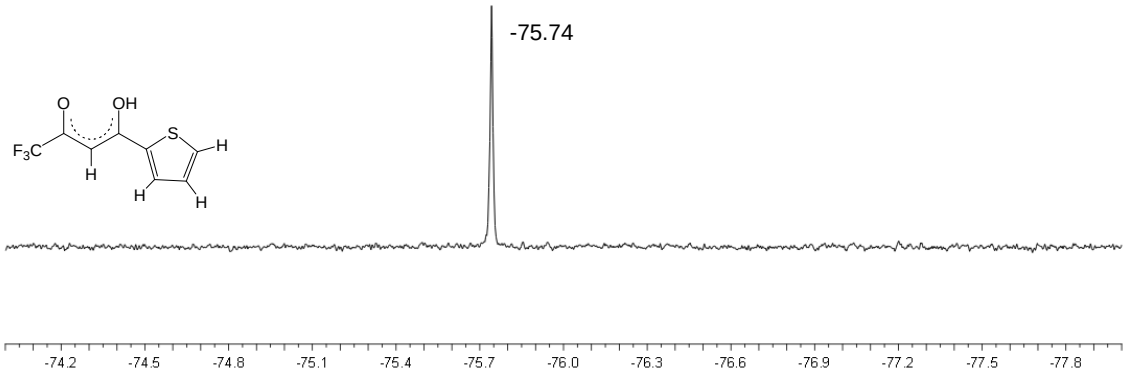

Spectrum 66: **Htffu** (*trifluorofuroylacetone*) **$CDCl_3$**

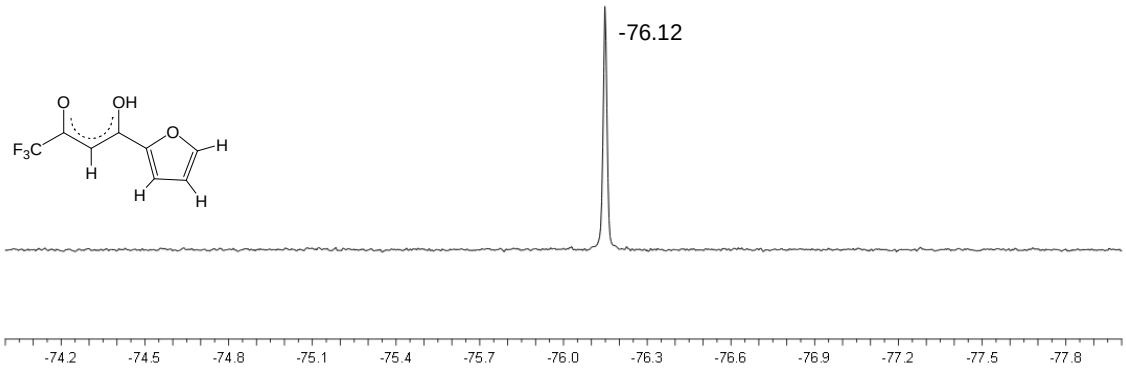

Spectrum 67: **Htfba** (*trifluorobenzoylacetone*) **$CDCl_3$**

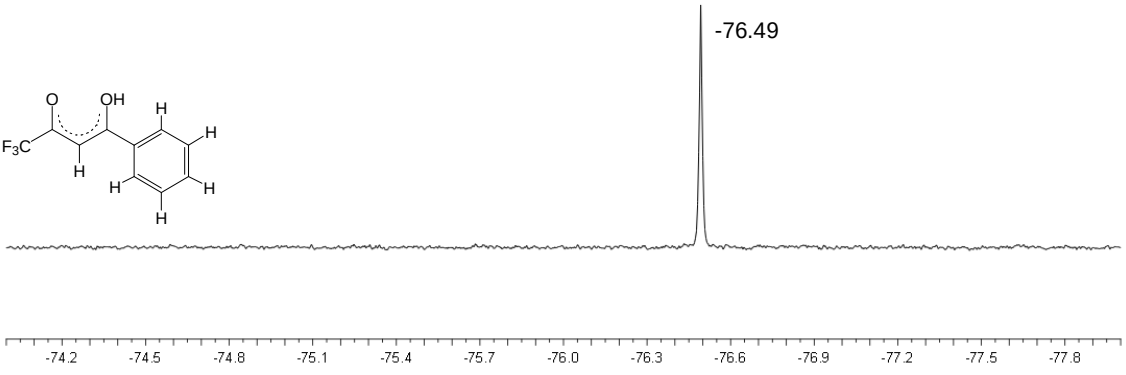

B.2 OCTAHEDRAL Ti(IV) COMPLEXES

Spectrum 68: **$Ti(tfaa)_2Cl_2$ [13]** **$CDCl_3$**

Bis(trifluoroacetylacetonato-O,O') dichloro titatium(IV)

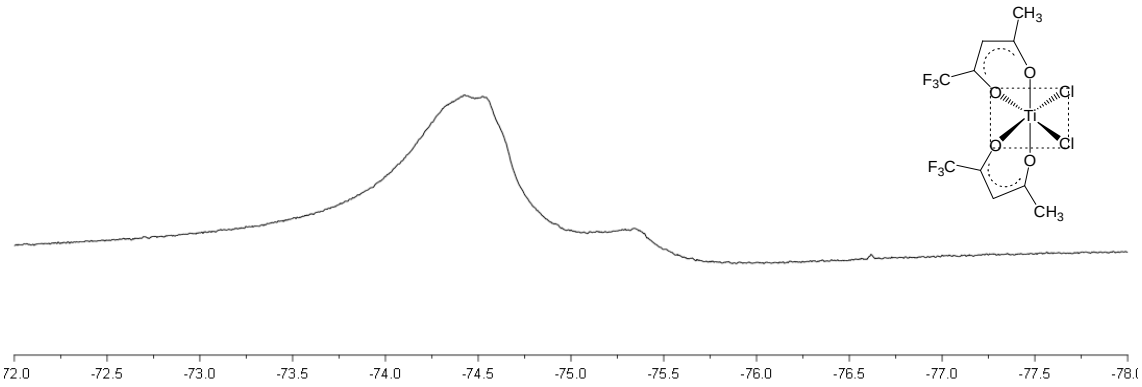

Spectrum 69: **$Ti(hfaa)_2Cl_2$ [14]** **$CDCl_3$**

Bis(hexafluoroacetylacetonato-O,O') dichloro titatium(IV)

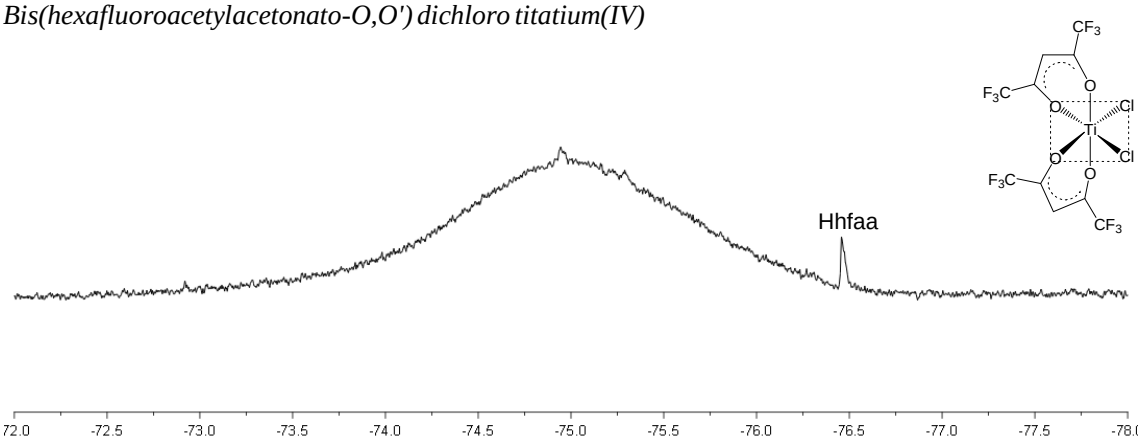

Spectrum 70: **$Ti(tfth)_2Cl_2$ [15]** **$CDCl_3$**

Bis(trifluorothenoylacetonato-O,O') dichloro titatium(IV)

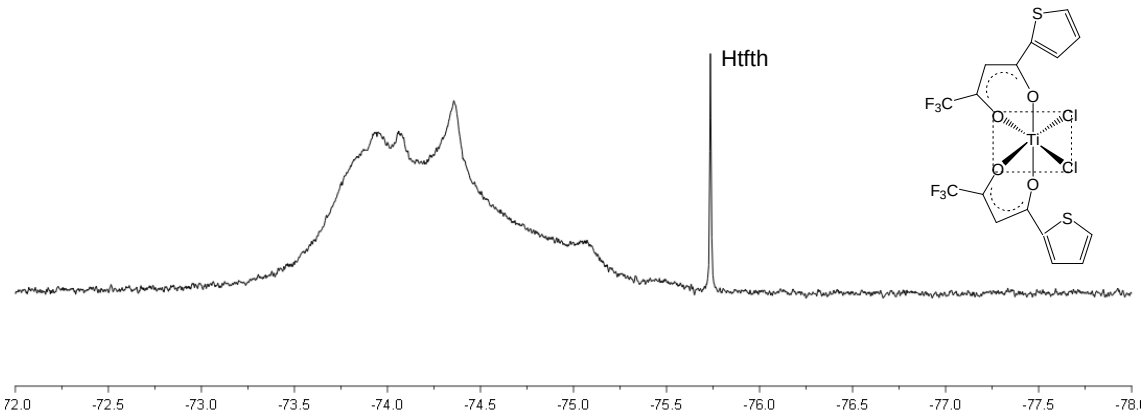

Spectrum 71: **$Ti(tffu)_2Cl_2$ [16]** **$CDCl_3$**

Bis(trifluorofuroylacetonato-O,O') dichloro titatium(IV)

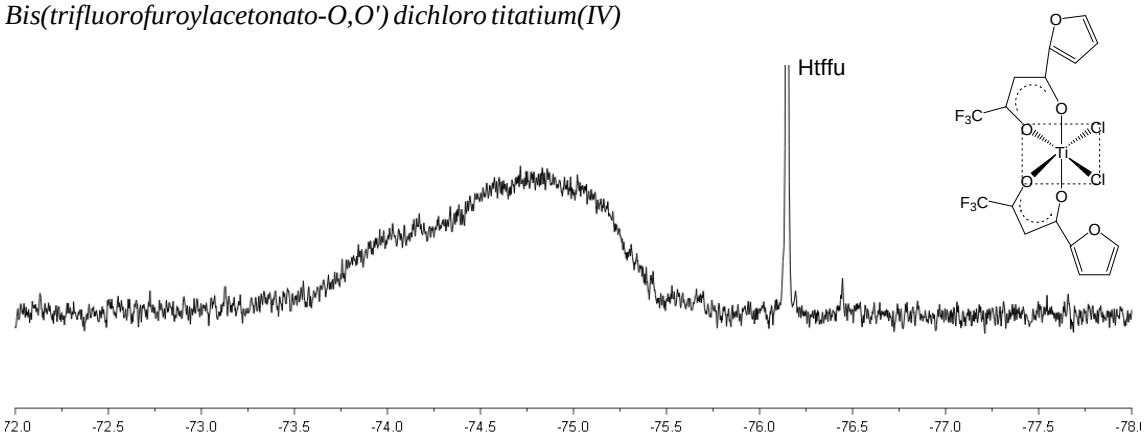

Spectrum 72: **$Ti(tfba)_2Cl_2$ [17]** **$CDCl_3$**

Bis(trifluorobenzoylacetonato-O,O') dichloro titatium(IV)

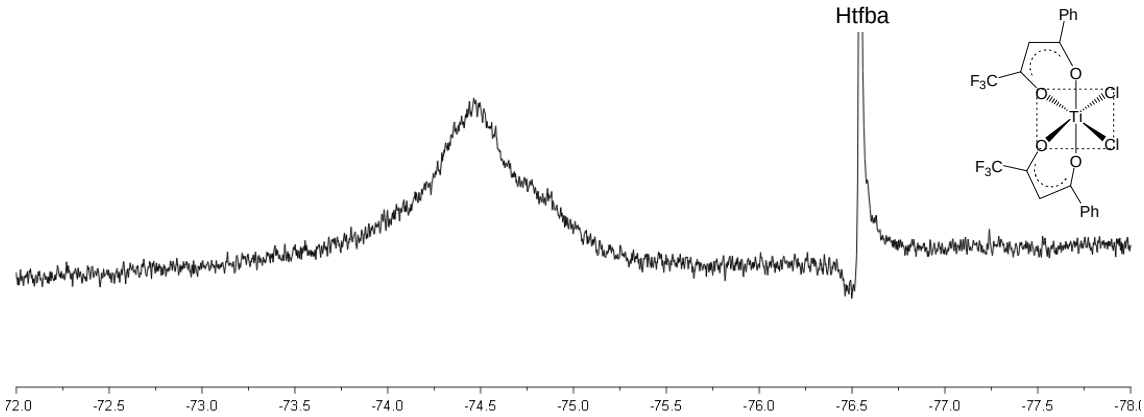

Spectrum 73: **$Ti(tfma)_2Cl_2$ [18]** **$CDCl_3$**

Bis(methyltrifluoroacetonato-O,O') dichloro titatium(IV)

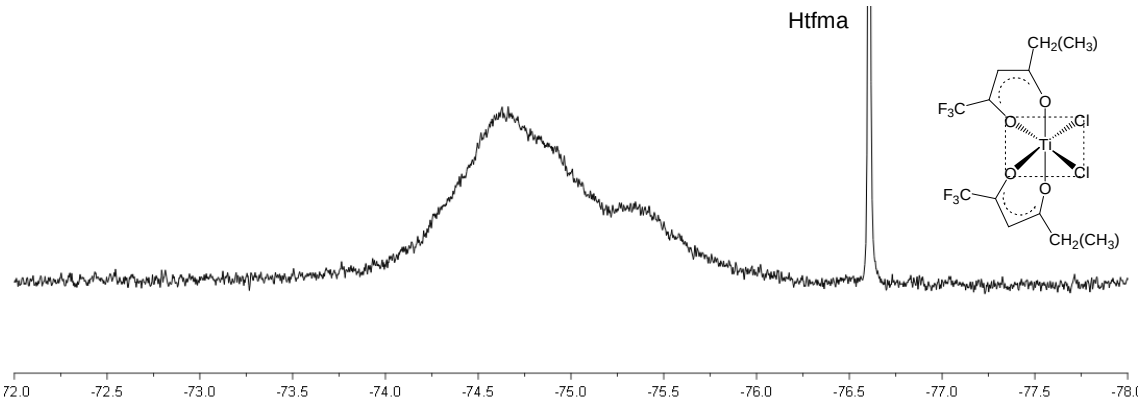

Spectrum 74: **$Ti(tfdma)_2Cl_2$ [19]** **$CDCl_3$**

Bis(dimethyltrifluoroacetonato-O,O') dichloro titatium(IV)

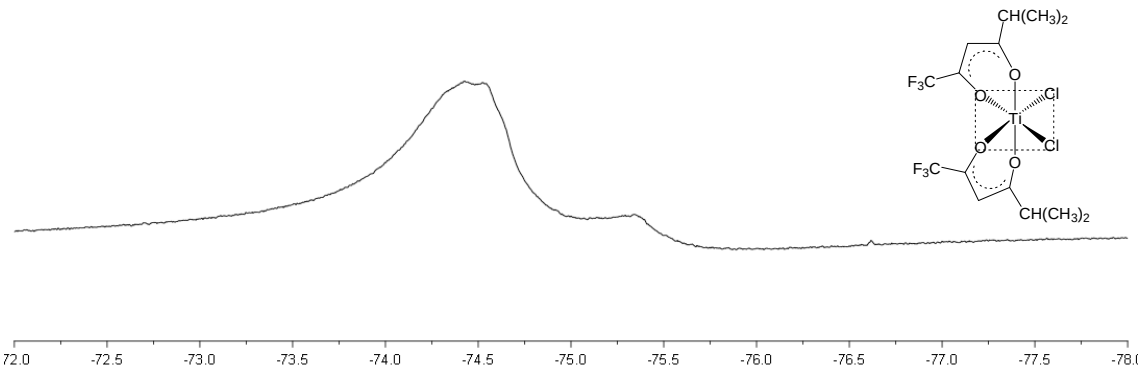

Spectrum 75: **$Ti(tftma)_2Cl_2$ [20]** **$CDCl_3$**

Bis(trimethyltrifluoroacetonato-O,O') dichloro titatium(IV)

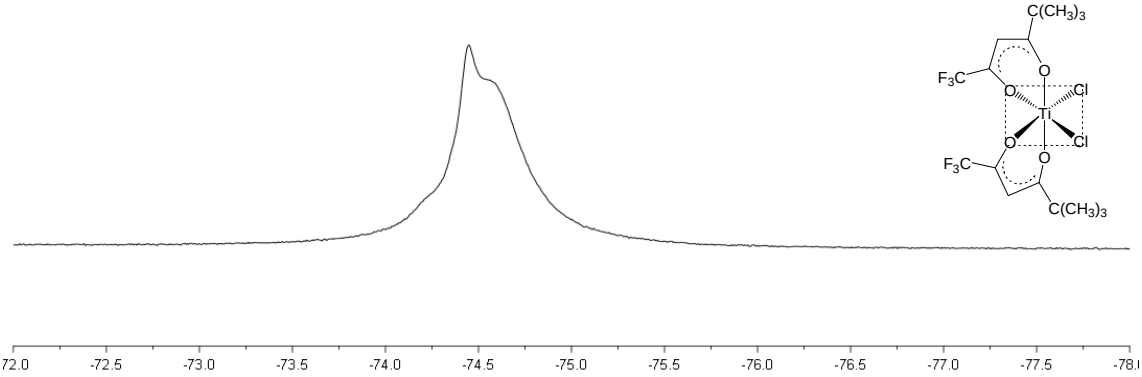

Spectrum 76: **Ti(tfaa)$_2$biphen [24]** **$CDCl_3$**

Bis(trifluoroacetylacetonato-O,O') (biphenyldiolato-O,O') titatium(IV)

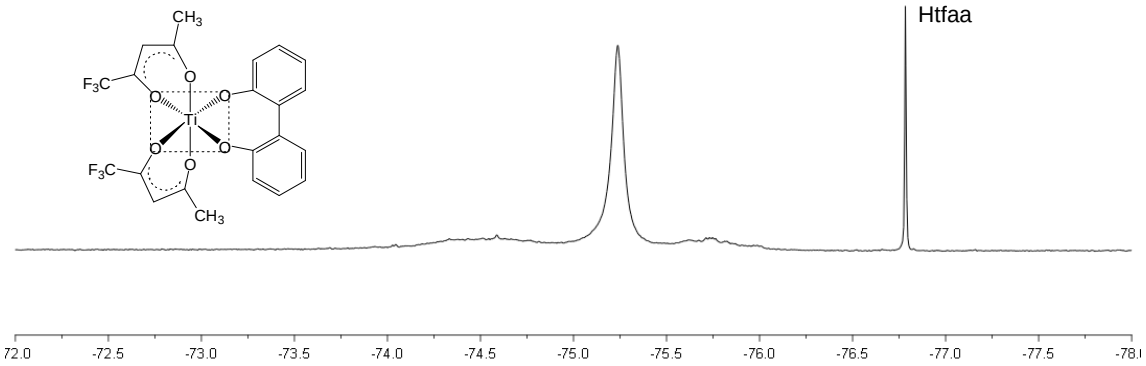

Spectrum 77: **Ti(tfth)$_2$biphen [26]** **$CDCl_3$**

Bis(trifluorothenoylacetonato-O,O') (biphenyldiolato-O,O') titatium(IV)

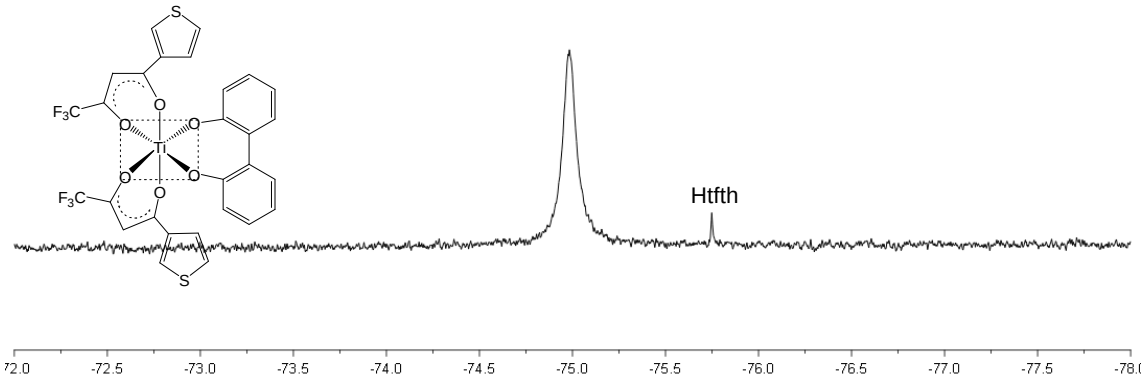

Spectrum 78: **Ti(tffu)$_2$biphen [27]** **$CDCl_3$**

Bis(trifluorofuroylacetonato-O,O') (biphenyldiolato-O,O') titatium(IV)

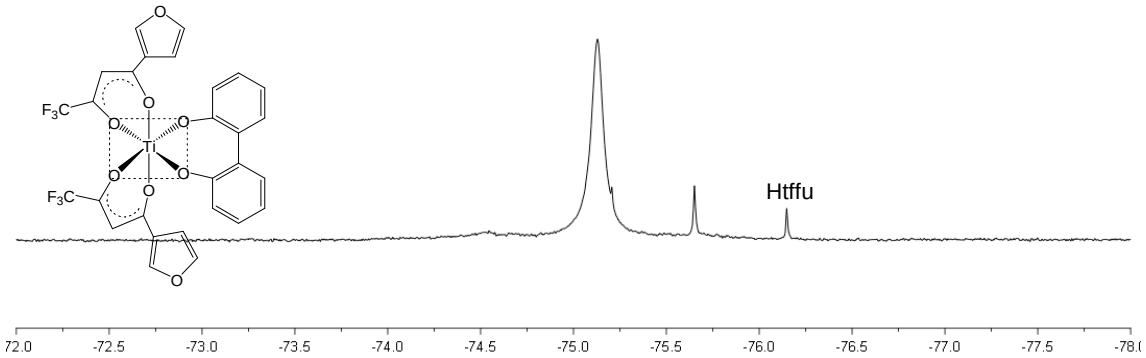

Spectrum 79: **Ti(tfba)$_2$biphen [28]** **$CDCl_3$**

Bis(trifluorobenzoylacetonato-O,O') (biphenyldiolato-O,O') titatium(IV)

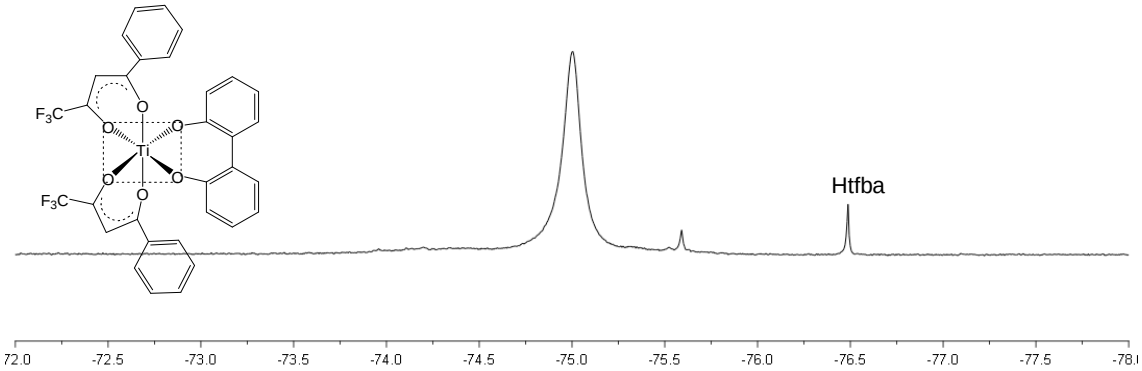

Spectrum 80: **Ti(tfma)$_2$biphen [29]** **$CDCl_3$**

Bis(methyltrifluoroacetonato-O,O') (biphenyldiolato-O,O') titatium(IV)

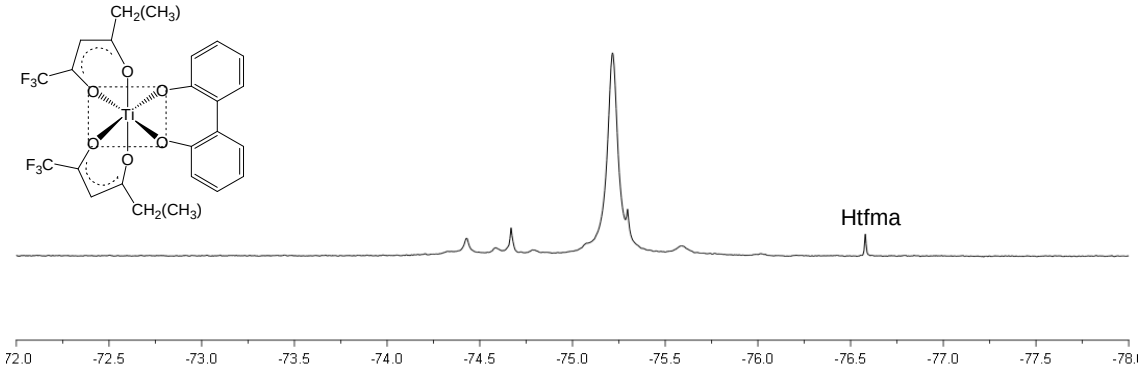

Spectrum 81: **Ti(tfdma)$_2$biphen [30]** **$CDCl_3$**

Bis(dimethyltrifluoroacetonato-O,O') (biphenyldiolato-O,O') titatium(IV)

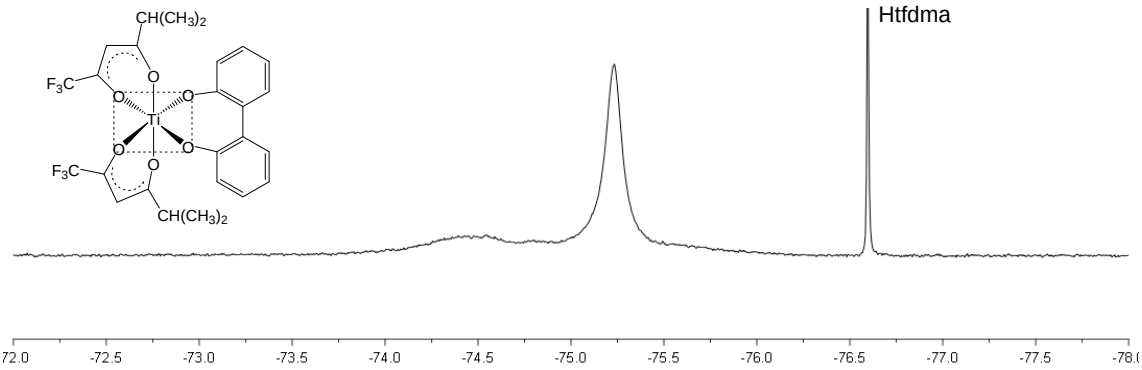

Spectrum 82: **Ti(tftma)$_2$biphen [31]** **$CDCl_3$**

Bis(trimethyltrifluoroacetonato-O,O') (biphenyldiolato-O,O') titatium(IV)

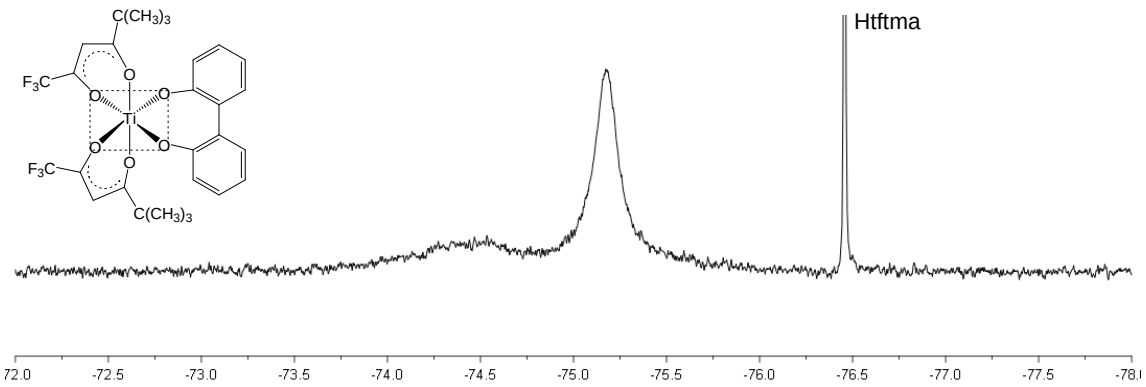

APPENDIX B

C Cyclic Voltammetric Data

C.1 O,O'-DONOR LIGANDS

Table 1 Cyclic voltammetric data (*vs*. Fc/Fc^{+}) for aromatic* β-diketones (Hβ). Measured in 0.1 mol dm^{-3} $[NBu_4][PF_6]/CH_3CN$ on a glassy carbon working electrode at 25 °C. [β] = 3.0 mmol dm^{-3}.

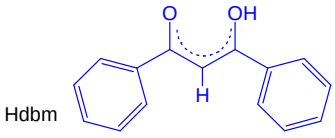

Hdbm

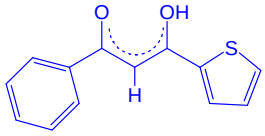

Hthba

v mV s^{-1}	E_{pc} mV	ΔE_p mV	$E^{0'}$ mV	i_{pc} μA	i_{pa}/i_{pc}
Hdbm: **Ph**$COCH_2CO$**Ph**					
100	-1934	71	-1899	51	0.21
200	-1942	82	-1901	75	0.28
300	-1952	98	-1903	94	0.32
500	-1967	123	-1906	124	0.35
1000	-1992	155	-1915	176	0.38
2000	-2027	222	-1916	244	0.40
Hthba: **Ph**$COCH_2CO$**C_4H_3S**					
100	-1884	61	-1854	43	0.27
200	-1891	71	-1856	63	0.34
300	-1896	81	-1856	79	0.38
500	-1903	93	-1857	103	0.43
1000	-1914	110	-1859	147	0.51
2000	-1932	139	-1863	209	0.54

*Aromatic refers to β-diketones with two aromatic side groups.

Table 2 Cyclic voltammetric data (*vs.* Fc/Fc^{+}) for aliphatic* β-diketones (Hβ). Measured in 0.1 mol dm^{-3} $[NBu_4][PF_6]/CH_3CN$ on a glassy carbon working electrode at 25 °C. [β] = 3.0 mmol dm^{-3}.

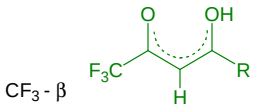

CF3 - β

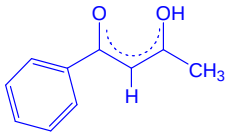

Hba

v mV s^{-1}	E_{pc} mV	i_{pc} μA
Hhfaa: $CF_3COCH_2COCF_3$		
100	-1243	41
200	-1266	57
300	-1282	68
400	-1290	76
500	-1299	84
1000	-1331	113
Htfth: $CF_3COCH_2COC_4H_3S$		
100	-1541	53
200	-1551	76
300	-1560	93
400	-1566	108
500	-1572	121
1000	-1588	169
Htffu: $CF_3COCH_2COC_4H_3O$		
100	-1544	44
200	-1557	63
300	-1569	76
400	-1577	87
500	-1587	97
1000	-1611	136
Htfba: CF_3COCH_2COPh		
100	-1564	60
200	-1576	85
300	-1585	104
400	--	--
500	-1598	134
1000	-1598	186
Htfaa: $CF_3COCH_2COCH_3$		
100	-1851	41
200	-1868	53
300	-1878	64
400	-1888	75
500	-1896	81
1000	-1917	120

v mV s^{-1}	E_{pc} mV	i_{pc} μA
Htfma: $CF_3COCH_2COCH_2(CH_3)$		
100	-1860	55
200	-1876	73
300	-1884	88
400	-1890	99
500	-1896	109
1000	-1928	118
Htfdma: $CF_3COCH_2COCH(CH_3)_2$		
100	-1872	42
200	-1883	60
300	-1898	71
400	-1906	82
500	-1914	89
1000	-1935	123
Htftma: $CF_3COCH_2COC(CH_3)_3$		
100	-1889	42
200	-1900	60
300	-1907	71
400	-1917	81
500	-1925	87
1000	-1937	128
Hba: CH_3COCH_2COPh		
100	-2138	56
200	-2160	77
300	-2173	92
400	-2188	104
500	-2196	114
1000	-2226	153

*Aliphatic refers to β-diketones with either two aliphatic side groups (pure aliphatic) or one aliphatic and one aromatic side group (mixed aliphatic).

Table 3 Cyclic voltammetric data (*vs*. Fc/Fc^+) for biphenol (H_2biphen). Measured in 0.1 mol dm^{-3} $[NBu_4][PF_6]/CH_3CN$ on a glassy carbon working electrode at 25 °C. [H_2biphen] = 3.0 mmol dm^{-3}.

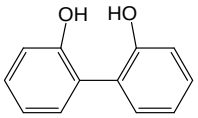

v mV s^{-1}	E_{pc} mV	i_{pc} µA
100	-1934	51
200	-1942	75
300	-1952	94
500	-1967	124
1000	-1992	176
2000	-2027	244

C.2 TETRAHEDRAL Ti(IV) COMPLEXES

Table 4 Cyclic voltammetric data (*vs*. Fc/Fc^+) for Cp_2Ti(biphen). Measured in 0.1 mol dm^{-3} $[NBu_4][PF_6]/CH_3CN$ on a glassy carbon working electrode at 25 °C. [Ti complex] = 2.0 mmol dm^{-3}.

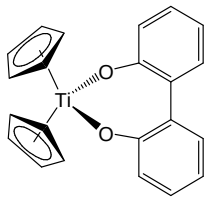

v mV s^{-1}	E_{pc} mV	ΔE_p mV	$E^{0'}$ mV	i_{pc} µA	i_{pa}/i_{pc}
100	-1701[a]	--	--	--	--
200	-1709	79	-1670	36	0.40
300	-1711	81	-1671	56	0.51
400	-1714	84	-1672	76	0.61
500	-1718	91	-1673	93	0.69
1000	-1727	110	-1673	160	0.86

Table 5 Cyclic voltammetric data (*vs.* Fc/Fc^{+}) for $[Cp_2Ti(\beta)]^{+}ClO_4^{-}$ complexes. Measured in 0.1 mol dm^{-3} $[NBu_4][PF_6]/CH_3CN$ on a glassy carbon working electrode at 25 °C. [Ti complex] = 2.0 mmol dm^{-3}.

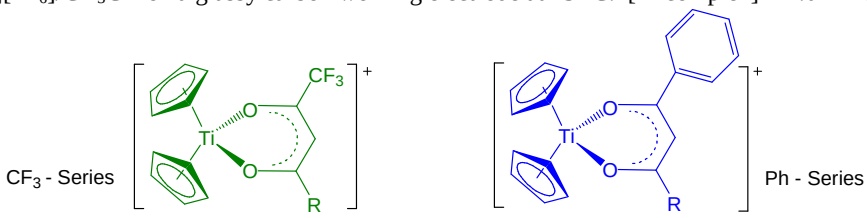

ν mV s^{-1}	Ti^{IV}/Ti^{III} couple					β-diketonanto reduction	
	E_{pc} mV	ΔE_p mV	$E^{0'}$ mV	i_{pc} µA	i_{pa}/i_{pc}	E_{pc} mV	i_{pc} µA
(a) CF_3-Series							
$[Cp_2Ti(tfth)]^{+}$ R = C_4H_3S							
50	-652	67	-619	26	0.86	-1886	25
100	-656	75	-619	39	0.86	-1890	32
150	-661	77	-623	45	0.84	-1898	41
200	-663	85	-621	51	0.82	-1903	47
250	-666	85	-624	56	0.84	-1908	52
$[Cp_2Ti(tffu)]^{+}$ R = C_4H_3O							
50	-655	67	-622	28	0.91	-1908	32
100	-659	70	-624	40	0.90	-1916	42
150	-661	73	-625	48	0.92	-1923	53
200	-664	79	-625	55	0.88	-1928	61
250	-666	81	-626	62	0.86	-1931	68
$[Cp_2Ti(tfba)]^{+}$ R = C_6H_5							
50	-657	72	-621	29	0.97	-1904	31
100	-661	76	-623	41	0.97	-1915	43
150	-666	83	-625	50	0.96	-1923	52
200	-666	87	-623	56	0.98	-1927	59
250	-671	90	-626	61	0.96	-1932	65
$[Cp_2Ti(tfaa)]^{+}$ R = CH_3							
50	-664	74	-627	30	0.95	-2143	22
100	-667	78	-628	41	0.95	-2162	33
150	-670	84	-628	50	0.96	-2177	40
200	-673	90	-628	59	0.96	-2185	47
250	-676	96	-628	67	0.97	-2194	53

ν mV s^{-1}	Ti^{IV}/Ti^{III} couple					β-diketonanto reduction	
	E_{pc} mV	ΔE_p mV	$E^{0'}$ mV	i_{pc} µA	i_{pa}/i_{pc}	E_{pc} mV	i_{pc} µA
(b) Ph-Series							
$[Cp_2Ti(thba)]^+$ R = C_4H_3S							
50	--	--	--	--	--	--	--
100	-869	65	-836	40	0.87	-2305	26
150	-872	70	-837	50	0.87	-2309	36
200	-872	70	-837	58	0.87	-2314	41
250	-874	73	-838	65	0.87	-2317	48
$[Cp_2Ti(dbm)]^+$ R = C_6H_5							
50	-859	67	-825	29	0.87	-2099	28
100	-861	76	-823	41	0.90	-2110	41
150	-865	82	-824	50	0.96	-2118	50
200	-866	82	-825	58	0.96	-2125	60
250	-868	85	-826	64	0.98	-2130	68
$[Cp_2Ti(ba)]^+$ R = CH_3							
50	-878	79	-839	29	1.00	-2295	24
100	-882	84	-840	40	1.00	-2306	40
150	-885	88	-841	47	0.99	-2317	46
200	-887	92	-841	55	0.98	-2323	52
250	-889	96	-841	63	0.98	-2333	59

C.3 OCTAHEDRAL Ti(IV) COMPLEXES

Table 6 Cyclic voltammetric data (*vs.* Fc/Fc^{+}) for $Ti(\beta)_2$(biphen) complexes. Measured in 0.1 mol dm^{-3} $[NBu_4][PF_6]/CH_3CN$ on a glassy carbon working electrode at 25 °C. [Ti complex] = 2.0 mmol dm^{-3}.

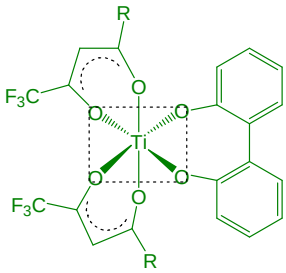

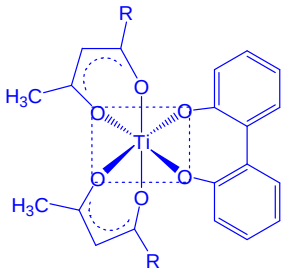

ν mV s^{-1}	**E_{pc}** mV	**ΔE_p** mV	**$E^{0'}$** mV	**i_{pc}** μA	**i_{pa}/i_{pc}**
$Ti(tfba)_2$biphen R = C_6H_5					
50	--	--	--	--	--
100	-991	63	-960	22	0.56
200	-996	75	-959	31	0.59
300	-1000	81	-960	37	0.60
400	-1006	89	-961	43	0.60
500	-1007	92	-961	47	0.60
$Ti(tffu)_2$biphen R = C_4H_3O					
50	-1012	82	-971	17	0.62
100	-1012	83	-971	22	0.66
200	-1014	86	-971	32	0.69
300	-1019	97	-971	39	0.68
400	-1023	103	-972	44	0.67
500	-1027	109	-973	49	0.66
$Ti(tfth)_2$biphen R = C_4H_3S					
50	-1027	74	-990	14	0.85
100	-1028	76	-990	21	0.79
200	-1030	80	-990	28	0.79
300	-1032	83	-991	36	0.77
400	-1036	89	-992	40	0.77
500	-1039	93	-993	45	0.77
$Ti(tfaa)_2$biphen R = CH_3					
50	-1029	89	-985	15	0.66
100	-1030	91	-985	20	0.66
200	-1036	100	-986	26	0.65
300	-1040	107	-987	32	0.64
400	-1046	116	-988	35	0.62
500	-1048	122	-987	38	0.61

ν mV s^{-1}	E_{pc} mV	ΔE_p mV	$E^{0'}$ mV	i_{pc} μA	i_{pa}/i_{pc}
Ti(tfma)$_2$biphe R = CH$_2$(CH$_3$)					
50	--	--	--	--	--
100	-1075	90	-1030	21	0.78
200	-1084	103	-1033	28	0.82
300	-1088	112	-1033	35	0.81
400	-1094	119	-1035	39	0.81
500	-1098	127	-1035	43	0.80
Ti(tfdma)$_2$biphen R = CH(CH$_3$)$_2$					
50	--	--	--	--	--
100	-1076	91	-1031	19	0.60
200	-1083	102	-1032	26	0.60
300	-1091	114	-1034	31	0.60
400	-1099	124	-1037	39	0.59
500	-1104	132	-1038	53	0.58
Ti(tftma)$_2$biphen R = C(CH$_3$)$_3$					
50	-1107	88	-1063	13	0.66
100	-1108	91	-1063	19	0.65
200	-1116	104	-1064	27	0.62
300	-1121	112	-1064	33	0.60
400	-1130	123	-1068	38	0.59
500	-1133	129	-1069	43	0.56
Ti(acac)$_2$biphen R = CH$_3$					
50	-1369	60	-1339	9	0.79
100	-1369	62	-1338	11	0.78
200	-1369	64	-1337	15	0.77
300	-1369	66	-1336	18	0.75
400	-1371	70	-1336	21	0.72
500	-1375	78	-1336	23	0.70
Ti(ba)$_2$biphen R = C$_6$H$_5$					
50	-1386	86	-1343	11	0.94
100	-1387	86	-1344	16	0.94
200	-1393	102	-1344	23	0.96
300	-1401	111	-1346	30	0.95
400	-1408	121	1348	34	0.95
500	-1411	126	-1348	38	0.95

Table 7 Cyclic voltammetric data (*vs.* Fc/Fc^{+}) for $Ti(\beta)_2Cl_2$. Measured in 0.1 mol dm^{-3} $[NBu_4][PF_6]$/ DCE on a glassy carbon working electrode at 25 °C. [Ti complex] = 2.0 mmol dm^{-3}.

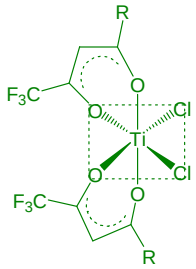

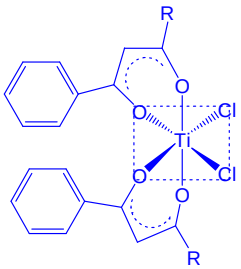

ν mV s^{-1}	**E_{pc}** mV	**ΔE_p** mV	**$E^{0'}$** mV	**i_{pc}** µA	**i_{pa}/i_{pc}**
$Ti(tfba)_2Cl_2$ R = C_6H_5					
100	-418	140	-348	14	0.28
200	-427	159	-348	16	0.24
300	-429	162	-348	16	0.20
400	-441	180	-351	17	0.16
500	-448	189	-354	19	0.10
$Ti(tfaa)_2Cl_2$ R = CH_3					
100	-414	102	-363	16	0.29
$Ti(dbm)_2Cl_2$ R = C_6H_5					
100	-740	117	-682	22	0.71
200	-750	138	-682	27	0.70
300	-758	150	-683	33	0.69
400	-768	166	-685	36	0.66
500	-779	179	-689	41	0.63
1000	-796	207	-692	55	0.53
$Ti(ba)_2Cl_2$ R = CH_3					
100	-775	151	-700	21	0.85
200	-796	186	-703	30	0.83
300	-810	207	-707	34	0.83
400	-821	223	-710	36	0.82
500	-831	238	-712	37	0.82
1000	-850	268	-716	48	0.81